



The
University
Of
Sheffield.

**Understanding the Dynamics and Regulation of Biogenic Volatile
Organic Compound Emissions by Woody Plants**

By:

Nichola Austen

A thesis submitted in partial fulfilment of the requirements for the degree of
Doctor of Philosophy

The University of Sheffield
Faculty of Science
Department of Animal and Plant Sciences

20th December 2016

Abstract

Global vegetation emits over 90% of non-methane volatile organic hydrocarbons into the atmosphere. ~1150 Tg C of isoprene is emitted annually and accounts for 50% of these natural emissions. However, the mechanisms that underpin both the production and regulation of these emissions are currently unknown. It has been hypothesised that isoprene is emitted as a response to extreme heat. Conversely, results of previous studies have demonstrated a decrease in isoprene emissions in plants subjected to elevated carbon dioxide.

This thesis set out to investigate both the independent and interactive effects of extreme temperature and elevated CO₂ on willow plant volatile emissions using both global emissions models and empirical measurements of both gaseous emissions and changes to the plant metabolome. The variability in the magnitude of isoprene emissions from the global emissions models has demonstrated the need for validation of the effects upon the plant metabolome in response to abiotic stresses. Through a full targeted metabolic study, this thesis has demonstrated for the first time that isoprene is produced as a response to elevated temperature in willow. The results of the targeted study have also demonstrated a reallocation of carbon to the non-mevalonate pathway that produces isoprene from other secondary metabolite pathways through the citric acid cycle.

Acknowledgements

This PhD would not have been possible without the help and support of a dedicated, generous, and caring group of people to whom I am eternally grateful. Heartfelt thanks need to be given to the academic and technical support I have received during my studies:

To all of the staff on D floor:

Dr. Heather Walker, thank you for your unremitting patience and support with my foray into the world of analytical chemistry, your indelible knowledge, enthusiasm, and overall moral support during times of panic and stress have been most appreciated.

Professor Mike Burrell, the time that you have taken to help with my experimental design and my subject knowledge have been invaluable. Thank you for your help for all the times that there was a problem with equipment, and for all the times I've popped into your office for a ramble about metabolic pathways.

Dr. Mark Burrell, I promise that I will learn my 10x table one day! Thank you for the technical support, and for the support as a friend through the hard (and good!) times of my PhD.

Gemma Newsome, I am forever grateful for your help and time in making sure things ran as smoothly as possible! Your kind words of encouragement and support have truly helped me to get through this experience.

A special thank you is reserved for Irene Johnson. I couldn't have done this without you. Aside from your patience and time that you have devoted to helping me with the academic side of my work, you have been a friend. Thank you for giving me the shoulder to cry on when I needed it, you saw what a lot of other people didn't. Thank you for giving me the strength to carry on and complete my PhD, I am forever grateful.

Thank you to Dr. Ben Webster for your time and patience in helping me with my experiments. I'll never look at a Lakeland roasting bag the same way again.

To my supervisors, Professor Duncan Cameron and Dr. Gareth Phoenix. Thank you for giving me this incredible opportunity. You've both been there through the

rather large ups and downs of this process and I couldn't have completed this without your support. Thank you for believing in me and bringing my confidence back when I thought that I could not carry on, I am truly honoured to have worked with you both.

A thank you also needs to be given to Professor David Beerling, for giving me the motivation to reach this point.

The continuing support of friends to get me to this point has been incredible: To Emma Bowles, your supportive messages day and night have bolstered me to push on, thank you for your patience and for lending an ear to the ramblings of a stressed student. Your friendship makes me as happy as a clam! To Lee Eales, thank you for being my day to day sounding board, plying me with caffeine, and providing much needed comic relief (at my expense... oooh Betty!) to help me *acquire* this PhD. To Mike Rennison, for helping me get back on my feet and realising that I had the potential all along. To Jacob Nickles, Dr. Chris Hardwick, Dr. Andrew Gray, Dr. Austin Lafferty, Hannah Holbrook, Prof. Duncan Cameron, Dr. Robert Falconer, Alix Riches-Barber, Dr. Richie Louks, Neil Masters, Kate Whiting, Yasmin Badat, and the rest of the Red Deer group for your support and much needed light relief over the years.

To the archaeologists (I'm still an honorary member!): Courtenay-Elle, Martin Huggon, Lenore Thompson, Liam Lee, Ged Poland, Tracy O'Donnell, Samantha Garwood, Hannah Plumer, Kyle Billington, Clare Burke, and Jessie Slater, together and individually you've all been there for me through the years and I am forever grateful for your support.

Thank you to my parents, Judith and Peter. I would have never made it to this point without your incredible support. Thank you for your sacrifices and for believing in me from the beginning. I love you both. Thank you to the rest of my family for the phone calls of support and encouragement, I am lucky to have you all.

Finally, and last but not least, thank you to Dr. Anthony Rennie. I couldn't have done any of this without your never ending support. I'm struggling to find the words to do this justice, so: Thank you for making me happy.

Contents

Abstract	i
Acknowledgements	iii
Contents	v
List of figures	ix
List of tables	xi
Chapter 1: General Introduction	1
1.1 Introduction	1
1.1.1 <i>Climate change</i>	1
1.1.2 <i>Average global temperature increase in the 20th century</i>	2
1.1.3 <i>Atmospheric CO₂ concentration increase in the 20th century</i>	3
1.1.4 <i>Climate change predictions to the year 2100</i>	4
1.2 Global vegetation emissions of Biogenic Volatile Organic Compounds	5
1.2.1 <i>Global vegetation distribution and geography of BVOC emissions</i>	5
1.2.2 <i>Isoprene production</i>	6
1.2.3 <i>BVOC impacts on atmospheric chemistry</i>	7
1.2.4 <i>Climate feedbacks on the terrestrial biosphere</i>	10
1.3 The effect of abiotic stresses on BVOC emissions	12
1.3.1 <i>The effect of increased temperature on BVOCs</i>	14
1.3.2 <i>The effect of increased atmospheric CO₂ concentration on BVOC emissions</i>	15
1.4 Aims and hypotheses	17
1.4.1 <i>Aims and hypotheses of chapter 2</i>	18
1.4.2 <i>Aims and hypotheses of chapter 3</i>	18
1.4.3 <i>Aims and hypotheses of chapter 4</i>	19
Chapter 2: How do CO₂ and Extreme Temperature Interact to Determine the Magnitude of Volatile Organic Carbon Emissions from Woody Plants? A Tandem Theoretical and Empirical Approach	21
2.1 Introduction	21
2.2 Methods	24
2.2.1 <i>Empirical models</i>	24
2.2.1.1 <i>Sheffield Dynamic Global Vegetation Model (SDGVM)</i>	24
2.2.1.2 <i>Model set-up</i>	28
2.2.1.3 <i>Biogenic Volatile Organic Compound Emission Model (BVOCEM)</i>	28
2.2.1.4 <i>Model set-up</i>	30
2.3 Results	31
2.3.1 <i>Empirical modelling results</i>	31
2.4 Discussion	36
2.4.1 <i>Empirical modelling</i>	36
2.5 Empirical approach to BVOC emissions	37
2.5.1 <i>Experiment set up and plant growth</i>	37
2.5.2 <i>Elevated temperature and CO₂ treatment application</i>	38
2.5.3 <i>Plant entrainment</i>	39
2.5.4 <i>Plant harvest</i>	40

2.5.5 <i>Sample elution</i>	40
2.5.6 <i>Leaf surface area</i>	40
2.5.7 <i>Plant biomass</i>	42
2.5.8 <i>Gas-Chromatography Flame Ionisation Detection (GC-FID)</i>	42
2.5.9 <i>Data processing and statistical analysis</i>	43
2.6 Results	44
2.6.1 <i>Measuring isoprene emissions</i>	44
2.6.2 <i>Kovats retention index for each treatment</i>	44
2.6.3 <i>Response of plant biomass to heat shock and CO₂ treatments</i>	44
2.6.4 <i>Isoprene emission in response to heat shock and CO₂ treatments</i>	45
2.6.5 <i>Isoprene emission in response to heat shock and CO₂ treatments in relation to leaf biomass</i>	45
2.6.6 <i>Isoprene emission in response to heat shock and CO₂ treatments in relation to leaf area</i>	48
2.7 Discussion	52
2.7.1 <i>The effect of extreme temperature on woody plant isoprene emissions</i>	52
2.7.2 <i>The effect of elevated CO₂ concentration on woody plant isoprene emissions</i>	54
2.7.3 <i>The effect of the interaction between temperature and CO₂ on woody plant isoprene emissions</i>	55
2.8 Conclusion	56
Chapter 3: The Biochemical Responses of Plant Metabolism to Extreme Temperature and CO₂ in Relation to Leaf Age	58
3.1 Introduction	58
3.2 Materials and methods	61
3.2.1 <i>Experiment set-up and plant growth</i>	61
3.2.2 <i>Elevated temperature and CO₂ treatment application</i>	62
3.2.3 <i>Leaf harvest</i>	62
3.2.3.1 <i>Young leaves</i>	63
3.2.3.2 <i>Mature leaves</i>	63
3.2.4 <i>Plant biomass and leaf surface area</i>	63
3.2.5 <i>Leaf metabolite extraction</i>	64
3.2.6 <i>Matrix-Assisted Laser Desorption/Ionisation Mass Spectrometry Analysis (MALDI-MS) of leaf metabolites</i>	65
3.2.7 <i>Data processing and statistical analysis</i>	65
3.3 Results	70
3.3.1 <i>Unsupervised analysis of metabolic fingerprints by Principal Component Analysis</i>	70
3.3.2 <i>Supervised multivariate analysis of metabolites fingerprints by Orthogonal Partial Least Squares Discriminant Analysis (O2PLS-DA)</i>	75
3.3.3 <i>Supervised multivariate analysis pair-wise comparisons of metabolite fingerprints using Orthogonal Partial Least Squares Discriminant Analysis (OPLS-DA)</i>	80
3.3.4 <i>Identification of metabolic fingerprints</i>	90
3.3.5 <i>Average intensities of % total ion counts of metabolites</i>	96
3.3.6 <i>Statistical significance of treatment interactions on mass bins</i>	100
3.4 Discussion	103
3.4.1 <i>The effect of extreme temperature on plant secondary metabolism</i>	103
3.4.2 <i>The effect of elevated CO₂ concentration on plant secondary metabolism</i>	105
3.4.3 <i>The effect of the interaction between temperature and CO₂ on the plant metabolome</i>	107

3.5 Conclusion	110
Chapter 4: What is the Mechanistic Basis Underpinning the Regulation Volatile Organic Carbon Biosynthesis and Emissions?	111
4.1 Introduction	111
4.2 Materials and methods	112
<i>4.2.1 Experiment set-up and plant growth</i>	<i>112</i>
<i>4.2.2 Elevated temperature and CO₂ treatment application</i>	<i>113</i>
<i>4.2.3 Leaf harvest</i>	<i>114</i>
<i>4.2.4 Leaf metabolite extraction</i>	<i>114</i>
<i>4.2.5 Tandem mass spectrometry (MS/MS) analysis of leaf metabolites</i>	<i>114</i>
<i>4.2.6 Data processing and statistical analysis</i>	<i>116</i>
4.3 Results	117
<i>4.3.1 Identification of plant metabolites using ms/ms</i>	<i>117</i>
<i>4.3.2 Plant secondary metabolism pathway analysis</i>	<i>122</i>
4.4 Discussion	126
<i>4.4.1 The effect of abiotic stresses on plant metabolic pathways</i>	<i>126</i>
4.5 Conclusion	129
Chapter 5: General Discussion	130
5.1 The effect of the interaction between extreme temperature and elevated CO₂ on woody plant isoprene emissions are mitigated	131
5.2 The effect of extreme temperature on plant secondary metabolism is greater than the effect of elevated CO₂	134
5.3 Evidence for the metabolic switch that provides protection for woody plants that have been subjected to both extreme temperature and elevated CO₂	136
5.4 Conclusion	137
Bibliography	139
Appendix	150

Chapter 1: General Introduction

1.1 Introduction

1.1.1 Climate change

Human industrial activity from ~1750 has contributed to a perturbation of the Earth's natural climate system. The Intergovernmental Panel on Climate Change (IPCC, 2007) defines climate change as:

“A change in the state of the climate that can be identified (e.g. using statistical tests) by changes in the mean and/or the variability of its properties, and that persists for an extended period, typically decades or longer. It refers to any change in climate over time, whether due to natural variability or as a result of human activity.”

Observed increases of both average global temperatures and atmospheric carbon dioxide concentrations during the last 250 years are resulting in an increase in the rate that the current climate is changing. These significant changes are having an impact upon both physical and biological systems. Observed responses to climate change in biological systems have been documented on both regional and global scales (Rosenzweig et al., 2008). However, it is important to note that currently, a considerable amount of short-term changes at a local level are caused by factors that are not attributed to climate change (Parmesan & Yohe, 2003), such as land-use change and naturally occurring fluctuations of species. Therefore it is crucial to be able to distinguish between the impacts upon biotic systems that are as a result of more local, short-term driving factors and those that can be ascribed to currently small, systematic trends that will become driving factors of wide spread ecological changes in the future (Parmesan & Yohe, 2003). The difficulty in attributing global climate change to recent,

short-term effects on the biosphere is in disconnecting the driving forces in order to observe and measure their separate parts. In order to fully understand any future changes to the Earth's climate, it is essential to have a comprehensive understanding of the Earth's natural system and the interactions and contributions of these driving forces in order to make predictions of future climate.

1.1.2 Average global temperature increase in the 20th century

Global surface temperatures have increased by approximately 0.2°C per decade over the last 30 years (Hansen et al., 2006). Figure 1 represents the global annual (black line) and five-year mean (red line) mean temperature from 1880-2009 (Hansen et al., 2010) from NASA Goddard Institute for Space Studies Surface Temperature Analysis (GISTEMP).

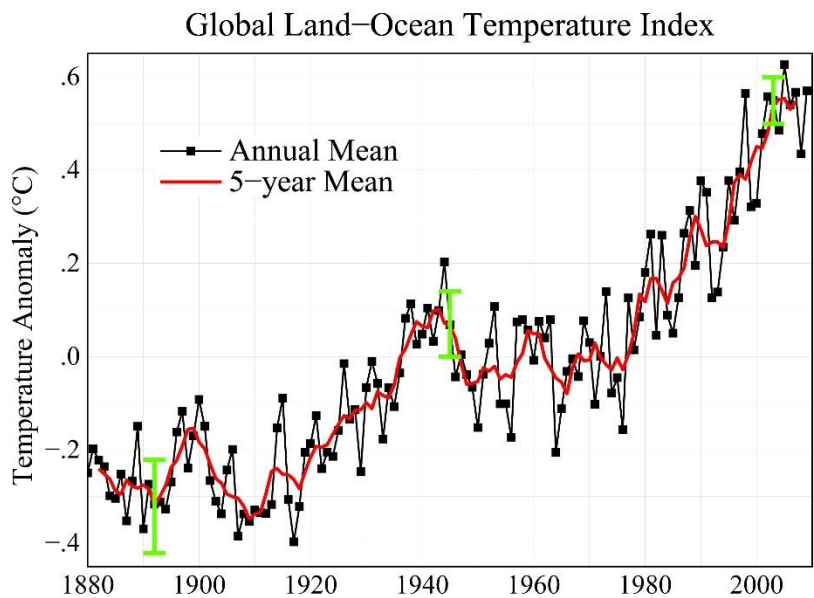


Figure 1.1: Global annual surface temperature relative to 1951-1980 mean temperatures. Green bars are 2σ error estimate of temperature. Taken from Hansen et al., 2010).

Although the majority of warming has occurred during the last 30 years, global average temperatures are overall approximately 1°C warmer than beginning of the last century (Met Office, 2015).

1.1.3 Atmospheric CO₂ concentration increase in the 20th century

Currently, atmospheric CO₂ contributes ~63% of the total radiative forcing that is a result of anthropogenic activity (Raupach et al., 2007). From Pre Industrial (PI) times, the atmospheric concentration has risen from ~280 ppm to currently just over 400 ppm (fig. 1.2). As more gaseous emissions are released into the atmosphere, the dynamics between the processes that can potentially remove CO₂ are going to change (Canadell et al., 2007) and therefore a greater understanding is required of the feedback mechanisms between the atmosphere and the biosphere in order to quantify this dynamic change.

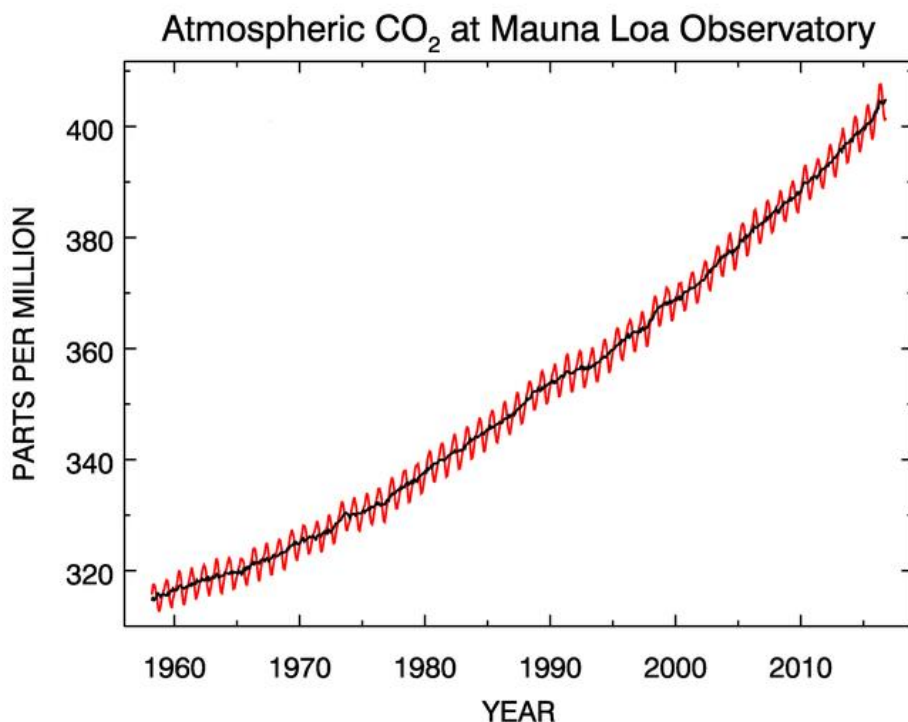


Figure 1.2: Full Mauna Loa CO₂ record of monthly mean atmospheric CO₂ measurements. The CO₂ data (red) is measure as the mole fraction in dry air (ppm). The black curve shows the seasonal correction. (Taken from NOAA/ESRL).

1.1.4 Climate change predictions to the year 2100

With our current understanding of increasing atmospheric CO₂ concentration and subsequent global temperature increase, it is possible to use Earth Systems models to create a range of predictions that represent potential future climate change and the resulting radiative forcing effect. The IPCC fifth assessment report (2014) has set out a new series of climate projections that use a carbon cycle and climate model to infer climate projections (Meinshausen et al., 2011; Moss et al., 2010; Rogelj et al., 2012).

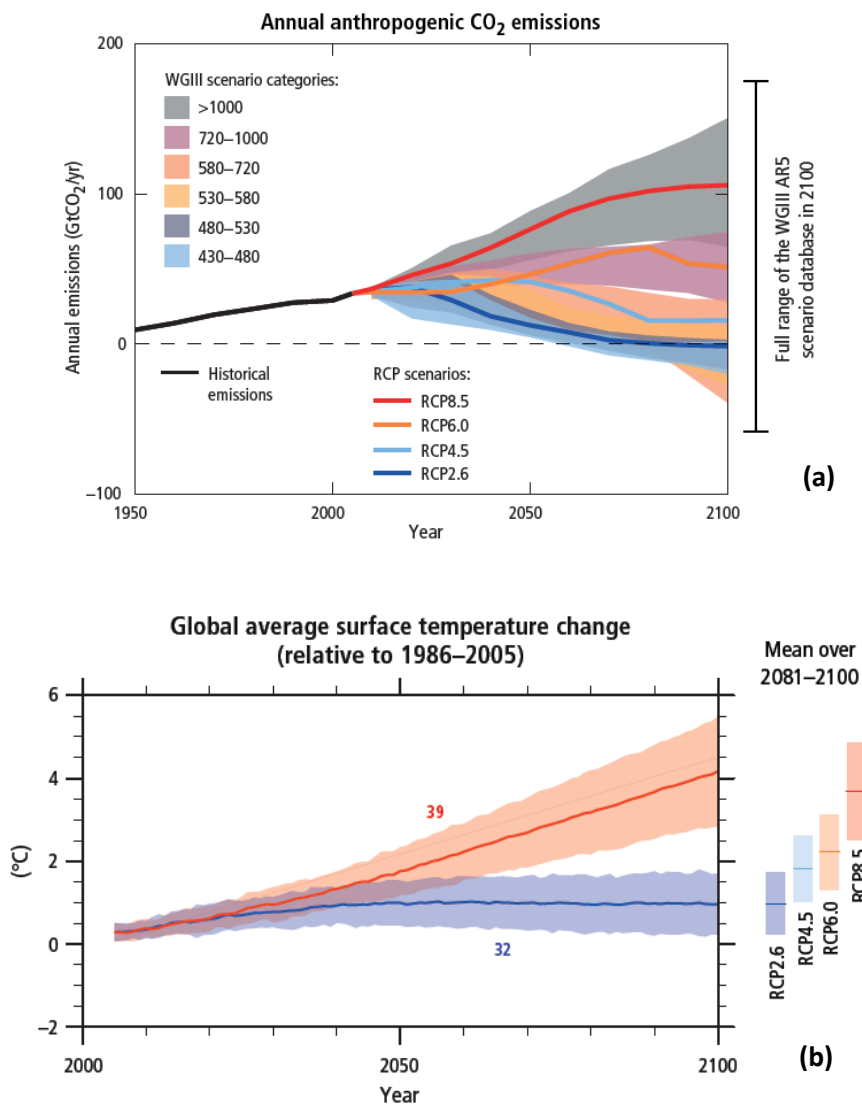


Figure 1.3: Anthropogenic CO₂ emissions (a) and global average temperature increase (b) predictions up to the year 2100 determined by the Representative Concentration Pathways multi-model simulations. Each scenario corresponds to possible future radiative forcing value relative to PI values (W/m²).

Figure 1.3 (a & b respectively) demonstrates the potential increases in both anthropogenic CO₂ emissions and global average temperature up to the year 2100. The Representative Concentration Pathways (RCPs) are a set of concentration trajectories that describe four possible future climate scenarios and their respective radiative forcing as a result of future anthropogenic greenhouse gas emissions that are used to drive climate models (Meinshausen et al., 2011). Although these model scenarios provide some insight into the potential atmospheric CO₂ and temperature increases in the future, there are issues with inconsistencies that have arisen due to a number of different Integrated Assessment Models (IAMs) being used to generate these future scenarios (Meinshausen et al., 2011). Reliance upon these model scenarios is also called into question as a number of the climate models used to generate the data are outdated due to both lack of maintenance and computational costs (Rogelj et al., 2012). As previously stated in section 1.1.1, it is essential to have a comprehensive and up to date understanding of the natural climate system of the Earth before including anthropogenic parameters that will lead to changes in atmosphere-biosphere interactions. In particular, the effects of both increasing CO₂ concentration and temperature need to be assessed not only independently, but also in terms of the impact that the interaction of the two have upon global climate.

1.2 Global Vegetation Emissions of Biogenic Volatile Organic Compounds

1.2.1 Global vegetation distribution and geography of BVOC emissions

Forests, including tropical, boreal, and temperate areas cover approximately 42 million km² of the Earth's surface (Bonan, 2008), the distribution of which is shown in figure 1.4. It has been estimated that annually, global terrestrial vegetation emits

~1150TgC of non-methane, biogenic volatile organic compounds (BVOCs) into the atmosphere (Guenther et al., 1995; Atkinson & Arey, 2003), of which isoprene accounts for ~500 TgC (Guenther et al., 2006) and is the sole focus of this study. This figure accounts for ~90% of all non-methane organic volatiles emitted (Naik et al., 2004). BVOCs not only have a significant impact upon global atmospheric chemistry, but their emission is important functionally for growth, reproduction, and the protection of global vegetation (Peñuelas & Staudt, 2010).



Figure 1.4: The global distribution of forests. Tropical regions are dominated by isoprene emissions and boreal and temperate regions dominated by monoterpenes (Taken from Chamot & Fuller, National Science Foundation, 2008).

1.2.2 Isoprene production

Isoprene (C_5H_8) is the dominant volatile organic species emitted from vegetation and accounts for around 48% of total global BVOC emissions, 75% of these being emitted from tropical trees (Holm et al., 2014). It has been estimated that isoprene is emitted by around 20% of woody plants in both tropical and some temperate regions (Loreto & Fineschi, 2015). Isoprene production is taxonomically broad, with particular

species including *Quercus*, *Populus*, *Salix*, and *Eucalyptus* (Logan et al. 2000; Sharkey et al. 2008). It is more common for fast growing, deciduous trees to emit isoprene, as opposed to slower growing evergreen species that are more prone to emissions of monoterpenes (Sharkey et al., 2008; Loreto & Fineschi, 2015).

Isoprene is produced in and mostly emitted through leaves (Monson et al., 2013). The production of isoprene occurs in the chloroplast of green leaves and is synthesised via the non-mevalonate pathway (2-C-methyl-D-erythritol 4-phosphate/1-deoxy-D-xyulose 5-phosphate pathway (MEP/DOXP)) (Logan et al., 2000). The biosynthesis of isoprene is made at the end of the pathway, where the metabolic intermediate dimethylallyl pyrophosphate (DMAPP) is catalysed by isoprene synthase (IspS) enzyme (Li & Sharkey, 2013). The MEP/DOXP pathway is located downstream of a number of pathways that are associated with central carbon metabolism, including pyruvate, Krebs cycle and glycolysis (Li & Sharkey, 2013). The production of isoprene is as a direct effect of abiotic stresses including light availability and temperature change that can affect the availability of substrate required for isoprene synthesis (Li & Sharkey, 2013). The effects of environmental stresses upon isoprene production are discussed in greater detail in section 1.3.

1.2.3 BVOC Impacts on atmospheric chemistry

It has been well established that BVOCs, and in particular isoprene have a significant impact upon atmospheric chemistry (Claeys et al., 2004; Kroll et al., 2006; Scott et al., 2014). BVOCs are highly volatile and readily photo-oxidised to form more stable vapours through interactions with other species in the atmosphere. The photo-oxidation of isoprene at low levels in the troposphere can lead to the formation of tropospheric ozone (an atmospheric pollutant), and can increase the lifetime of

greenhouse gases such as methane. Through reactions with the OH· radical and NO_x, isoprene can reduce the oxidative capacity of the atmosphere, thus limiting the removal of CH₄ and therefore increasing the greenhouse effect (Kroll et al., 2006).

The low volatility products of isoprene also have the ability to exert a negative radiative forcing effect, therefore impacting upon climate and global temperatures. This can occur through either the process of scattering and absorbing incoming solar radiation (Aerosol Direct Effect), and also through a number of processes that lead to changes in the microphysical properties of clouds and their lifetime (Aerosol Indirect Effects) (Scott et al., 2014). Secondary organic aerosols (SOA) have the potential to grow to cloud condensation nuclei (CCN) sizes (cloud “seeds” which are approximately 0.2µm upon which water vapour condenses) (Claeys et al., 2004) and can increase the Earth’s albedo, thus leading to an increase in diffuse light and therefore a reduction in direct light (Holm et al., 2014). These processes contribute to the global cooling effect of the Earth, thus providing a negation against warming via the greenhouse gas effect.

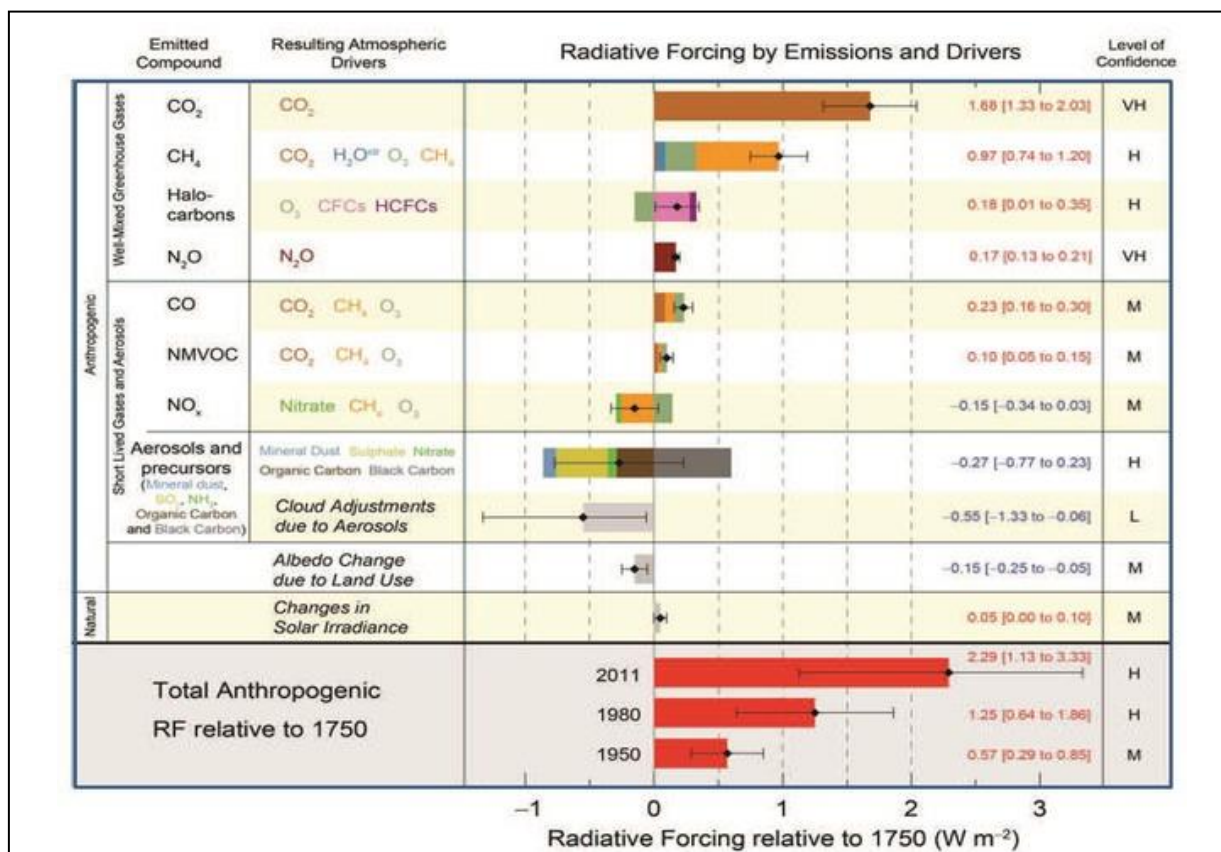


Figure 1.5: Contribution of anthropogenic and natural emissions to the Earth's radiative budget. (Taken from IPCC, 2014)

Figure 1.5 has been compiled by the IPCC physical working group (1, 5th assessment report), regarding the developments in quantification of the impact of increased concentrations of greenhouse gases in the atmosphere and the impact upon the Earth system. Figure 1.5 demonstrates the current level of understanding with regards to the forcing effect that can be exerted by both anthropogenic and natural emissions on the Earth's radiative budget. As demonstrated in figure 1.5, all short-lived gases and aerosol species in the IPCC report are grouped together including both natural (mineral dust) and anthropogenic (black carbon). Although there is an attempt at a quantification of the contribution to changes to cloud microphysics, there is no mention of SOA or their BVOC precursors that, in comparison, are emitted in significantly greater amounts and that have a pivotal role in the formation of clouds that exert a negative forcing. It is

also important to note that the overall confidence level in the data provided for these cloud adjustments is low, with a large range of -1.33 - -0.06 W m^{-2} of the potential contribution to radiative forcing through cloud modification. It is therefore evident that a holistic budget is not feasible when attempting to quantify the separate components of all aerosol species, either primary or secondary. With our current limited understanding of the oxidative chemistry, it is also currently not feasible to categorise BVOC emissions into the sum of their low volatility parts and their role in negating the greenhouse effect. This is due to the large suite of gaseous species that are present in the atmosphere which are emitted from the terrestrial biosphere annually. With these issues in mind, it is clear that there needs to be a compromise when attempting to quantify the complexities of the effects of BVOC emissions upon atmospheric chemistry and the resulting climate feedbacks that occur.

1.2.4 Climate feedbacks on the terrestrial biosphere

It is imperative to remember that, although BVOC emissions make a significant contribution to a negative radiative forcing through their impact upon atmospheric chemistry, fluctuating climate also has an impact upon global vegetation. These interactions can be attributed to a cause and effect type relationship, where increases in temperature and CO_2 lead to increased plant productivity and impact upon emissions. These interactions will be discussed more in depth in chapters 2 and 3.

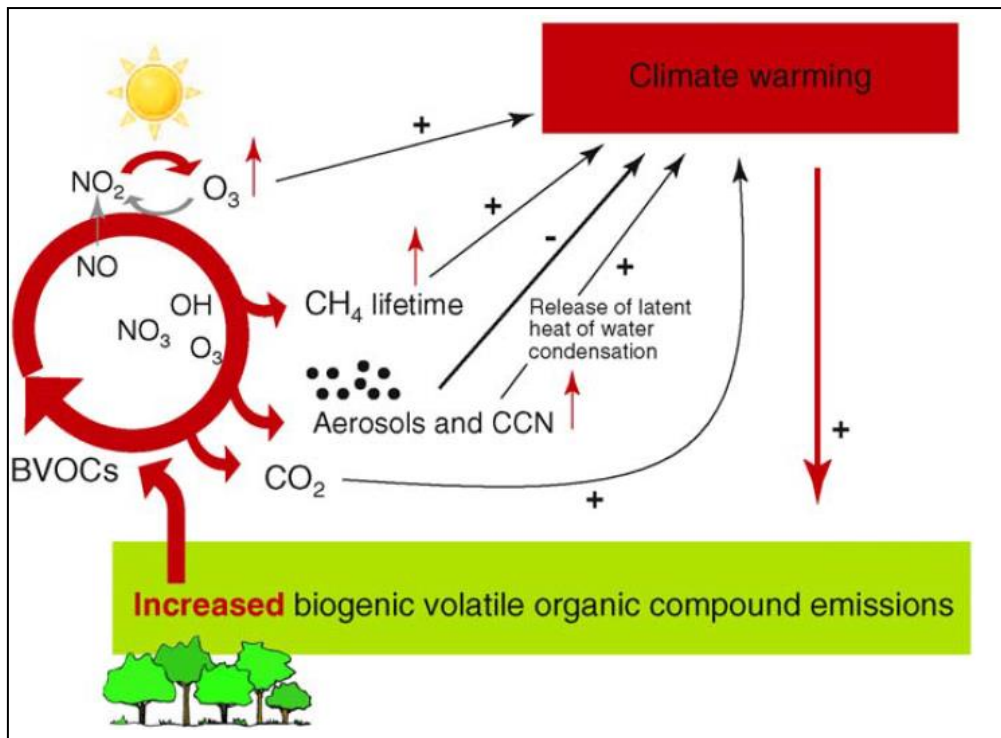


Figure 1.6: Schematic to represent the impact of increased BVOC emissions on atmospheric chemistry (Taken from Peñuelas & Staudt, 2010).

The diagram shown in figure 1.6 demonstrates the interactions between the terrestrial biosphere and the chemistry of the atmosphere. Although biosphere-atmosphere interactions are far more complex than this schematic, the main focus is upon the impact of temperature and CO₂ on global vegetation and the production of BVOCs, and the impact of these biogenic emissions upon atmospheric chemistry and global climate. As discussed earlier, figure 1.6 also demonstrates the interactions of BVOCs with other atmospheric components, particularly NO_x and CH₄. The schematic shows that other than the contribution of aerosols and CCN to a negative radiative forcing, tropospheric ozone, CH₄, water vapour and other atmospheric gaseous species all contribute to climate warming (Peñuelas & Staudt, 2010).

1.3 The Effect of Abiotic Stresses on BVOC Emissions

Although a large amount of work has been dedicated to BVOC emissions and their place within climate science, the fundamental questions surrounding these hydrocarbons remain largely unanswered. The main question that dominates current research is “*what advantage do isoprene emissions provide to the plant?*” (Sharkey et al., 2008). As mentioned previously, isoprene in particular is thought to be produced in response to abiotic stresses exerted upon vegetation, such as an increase in temperature. This idea is supported by the fact that isoprene, unlike other hydrocarbons, is not stored in the plant, but rather released immediately from vegetation that is subject to short-lived temperature fluctuations. Although all plants possess the metabolic pathway for isoprene synthesis, not all plants emit isoprene. It has been shown that in non-emitting plants, there is an absence of the isoprene synthase enzyme (ISPS), that catalyses the reaction with dimethylallyl pyrophosphate and leads to the formation of isoprene at the end of the MEP pathway (Loreto & Fineschi, 2015). It has been suggested therefore that the capacity for plants to emit isoprene has evolved under environmental conditions that have overall favoured perennial vegetation with a seasonal biomass turnover, with relatively short-lived periods of environmental stress, such as deciduous trees (Dani et al., 2014; Loreto & Fineschi, 2015). However, the mechanistic process behind this is still unknown.

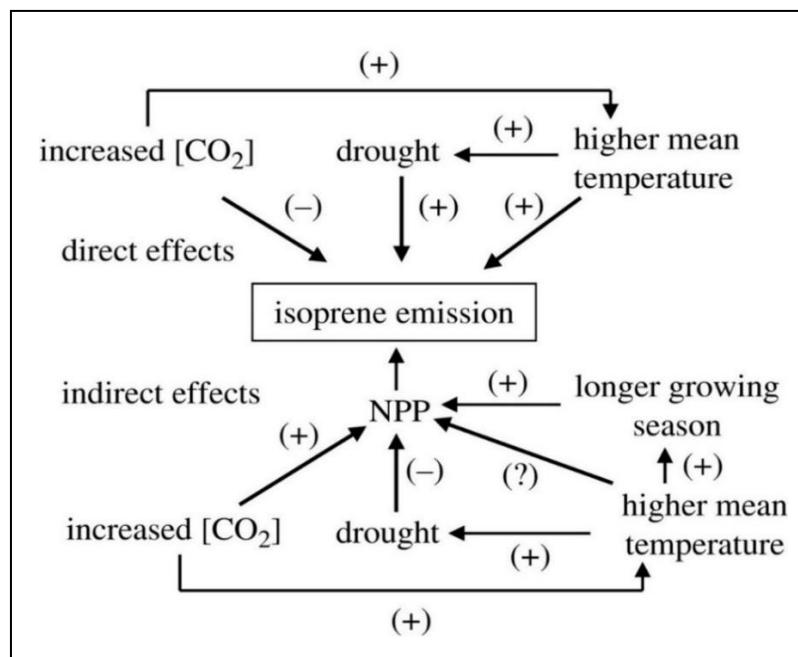


Figure 1.7: Conceptual model representing the direct and indirect effects upon isoprene emission rate. The direct effects are through influences on metabolism and the indirect effects through influences on NPP (taken from Monson et al., 2007).

Figure 1.7 demonstrates these various climatic and environmental effects upon global isoprene emissions. It shows that an increase in temperature impacts isoprene production directly through leaf temperature, and indirectly through photosynthesis. Although it is unclear whether a higher mean temperature increases net primary productivity (NPP), it adds to a longer growing season and therefore greater potential for more emissions to be released. However, an increase in global temperature may also lead to more drought-like conditions that would actually have a negative impact upon NPP and therefore inhibit isoprene production indirectly over a longer period of time. Overall however, figure 1.7 denotes that an average increase in temperature would increase BVOC emissions, both directly through abiotic stress, and indirectly through increased plant productivity. Therefore, due to the sheer volume of annual emissions, and the effect of isoprene upon air quality and global climate and radiative forcing, it is

necessary to attempt to quantify the relative effects within the complex system of biosphere-atmosphere interactions.

1.3.1 The effect of increased temperature on BVOCs

Isoprene emissions are primarily regulated in the leaf by temperature and photosynthetically active radiation (PAR). As isoprene emissions are coupled with photosynthesis, they are only produced during the day. It has been suggested that isoprene is produced as a short term stress response to sudden, extreme, and short-lived increases in temperature. However, the mechanisms behind this response to abiotic stress are unknown, leading to a number of uncertainties in our assumptions around thermotolerance. Although the effects of fluctuating PAR are important in the regulation of isoprene production, they are not the focus of this research. This thesis will instead focus upon the interactive effects of extreme temperature and CO₂ upon *Salix* spp., with a constant diurnal light intensity.

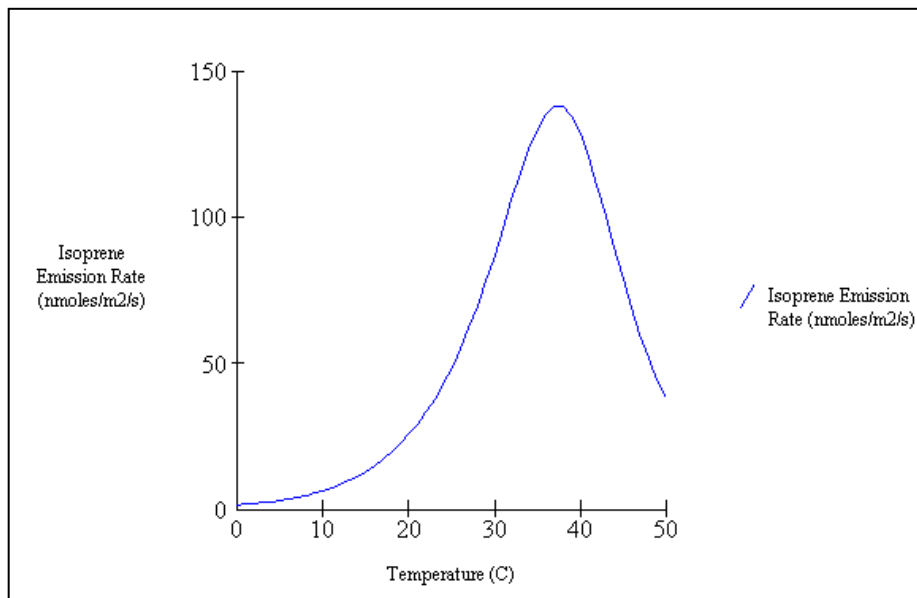


Figure 1.8: Leaf isoprene emission response to leaf temperature model using isoprene emission factors from Guenther et al., 1995. (Taken from WIMOVAC Ltd, 1998).

The top of the canopy is most likely to suffer from heat shock due to high radiant energy fluxes that can lead to large and rapid changes in leaf temperature. When measured, these leaves have been known to emit up to four times the amount of isoprene as those underneath the canopy (Sharkey et al., 2008). Figure 1.8 shows a typical leaf emission response to an increase in temperature. It shows that emissions increase exponentially until around 40°C, where they then decline rapidly. Again, the reason for this sudden drop in emissions is unknown. It has been postulated that isoprene emissions are only produced as a response to short lived stresses, which may explain why low isoprene emitting species are found in areas of prolonged environmental stress, such as arid areas. Vegetation in areas with prolonged levels of stress tend to emit other VOCs including monoterpenes. These emissions account for significantly less of the global BVOC total than isoprene but are still important due to their effects on atmospheric chemistry. Unlike isoprene, which is highly volatile and released immediately after production in the plant leaf, monoterpenes and other VOCs can be stored within the plant and are released depending on temperature (Karl et al., 2009). As with isoprene emissions, the mechanisms that drive the emissions of monoterpenes and other VOCs are still unknown and the thermotolerance hypothesis is currently the generally accepted explanation.

1.3.2 The effect of increased atmospheric CO₂ concentration on BVOCs

As shown in figure 1.8, an increase in leaf temperature drives an increase in isoprene emissions. This is particularly the case for the tropics, where leaves at the top of the canopy have a temperature that can exceed the air temperature by 10°C due to humidity. This leads to a reduction in latent heat loss, therefore driving emissions as a stress response. However, although one would expect to observe an increase in

emissions with an increased CO₂ concentration due to increased plant productivity, it has been shown that an increase in CO₂ will actually suppress isoprene emissions, as demonstrated in figure 1.9.

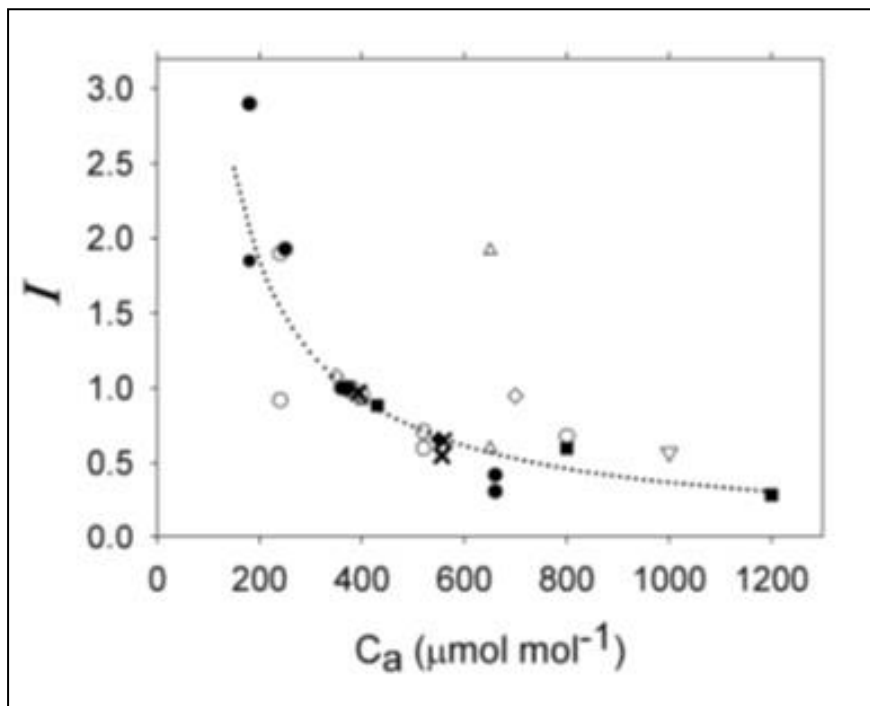


Figure 1.9: Observations of leaf level measurements of isoprene emissions from plants grown in a range of CO₂ concentrations. I= isoprene leaf emission rate, C_a = CO₂ concentrations. (Taken from Young et al., 2009).

It has been suggested that with increasing atmospheric CO₂ concentrations, there will be a de-coupling of isoprene production from photosynthesis. Current research suggests that this decoupling may be linked to competition at the cellular level for isoprene synthesis precursors, towards other reaction pathways as a metabolic control (Young et al., 2009). Although, this hypothesis remains unproven. Observed isoprene emissions over the 21st century have suggested that the competing effects of temperature and CO₂ have been in relative balance (Arneth et al., 2007). The competing effects of these driving factors for all BVOCs have not been fully assessed over a longer time period. Modelling studies that have begun to prescribe a range of future scenarios for isoprene emissions have so far failed to deliver any clear results with confidence (Dani

et al., 2014). It is clear that the current understanding of these effects upon BVOC emissions is still poorly understood and in order to make accurate predictions of future scenarios, more research is required.

1.4 Aims and Hypotheses

The objective of this thesis is to attempt to improve the current understanding of the mechanisms at the cellular level that underpin the production, regulation, and emission of isoprene as a response by woody plants to abiotic stresses. This study has chosen to focus on increasing CO₂ and short-lived extreme temperatures and the response of woody plants to both their independent, and combined interactive effect. This study has chosen to focus on willow. The short rotation coppice hybrid “Terra Nova” (‘LA940140’ x *Salix miyabeana*) (Lindegaard, 2012) was chosen as it is a fast growing, deciduous, woody tree, and also because *Salix* is known to be an isoprene emitting plant. As current volatile organic compound emission models derive their emission rates from canopy level measurements, it is necessary to conduct a number of experiments at the leaf level, and at the cellular level to attempt to reconcile the issues that currently surround the production of isoprene and the interactive effects of abiotic stresses. Furthermore, it is also necessary to investigate the response of different aged leaves to elevated CO₂ and short-lived extreme temperature in order to better understand the response of the plant over time to these stresses. Experiments on both young and mature leaves will provide more information regarding the effects upon plant productivity and what, if any effects these stresses will have upon growth and development.

In order for us to better understand the mechanisms that drive the production and regulation of isoprene emissions from woody plants, a top-down approach from emissions at plant level, through to a targeted metabolic analysis is necessary.

1.4.1 Aims and hypotheses of chapter 2

Firstly, chapter 2 will investigate the emission of isoprene at the leaf level as a response to extreme temperature and elevated CO₂ concentration both independently, and as a combined effect in order to quantify the potential response of the plant to the interaction. The experiment will be conducted through the measurement of isoprene emissions using air entrainment, and the identification and quantification of emissions for each treatment will be analysed using gas chromatography with flame ionisation detection (GC-FID). Therefore this experiment will attempt to answer whether isoprene is emitted as a thermotolerance response, and whether the combined effect of extreme temperature and CO₂ will lead to an increase or decrease in emissions, or whether the two stresses cancel each other out. The following hypotheses have been made:

1. The interactive effects of elevated CO₂ and short-term extreme temperatures will be damped in comparison to the independent effects of both, and will in effect “cancel” each other out.
2. The CO₂ “fertilisation effect” will allow the plant to allocate resources to both plant productivity, and to the synthesis of BVOC emissions thus providing a mechanistic process to explain the mitigation of the interactive effects.

1.4.2 Aims and hypotheses of chapter 3

Following this, chapter 3 investigated the independent and combined effects of abiotic stresses upon the plant metabolome. Through a metabolic profiling study, the

response of the plant metabolome to elevated CO₂ and short-term heat shocks was investigated. Using leaf tissue samples from the same plants subject to the air entrainment experiment, the effects of abiotic stress upon leaf age through the selection of young and mature leaves from each plant were addressed. Both multivariate statistical analyses, and database putative identifications of compounds detected were used to create a metabolic profile for young and mature leaves from the plants that have been subject to the four, two-factorial experiments outlined in chapter 2. This approach was therefore a more holistic approach to plant biochemical responses which focuses on the whole metabolome, rather than just the specific metabolic pathway that regulates the production of isoprene. The following hypotheses have been made:

1. The effect of short-term, extreme heat upon the plant will cause a change to plant secondary metabolism that is not related to the biosynthesis of isoprene but is substrate dependent.
2. An increase in available carbon substrate will allow the plant to “pool” its carbon reserves in mature leaves as a carbon sink.
3. The effect of elevated CO₂ at extreme temperature will be damped as the plant reallocates resources to both isoprene biosynthesis and other secondary metabolic pathways.

1.4.3 Aims and hypotheses of chapter 4

Finally, in chapter 4 a targeted tandem mass spectrometry analysis will be conducted, following the results of the putative identifications of plant secondary metabolism in chapter 3. The response and percentage change of all intermediate metabolites in the MEP/DOXP pathway in response to extreme heat and elevated CO₂ and their combined effects will be investigated. Following the statistical results of

chapter 2, I will also conduct a full metabolic pathway analysis upon the flavonoid biosynthesis pathway, the intermediates of which are produced as a response to abiotic stresses such as temperature and oxidative stress. The percentage change of the intermediates within this pathway will demonstrate the opposite response to those seen in the MEP/DOXP pathway which have been indicated in the untargeted profiling experiment. The following hypotheses have been made:

1. The response of the metabolic intermediates within the MEP/DOXP pathway will increase in abundance relative to the control in plants that have been subject to a heat shock.
2. Subsequently, the intermediates of the flavonoid biosynthesis pathway will demonstrate a down-regulation relative to the control as the allocation of carbon is being reorganised to account for isoprene production
3. Within the flavonoid biosynthesis pathway, there will be a metabolic “switch” that will demonstrate the redistribution of carbon away from the flavonoid pathway into the intermediates that are responsible for isoprene biosynthesis
4. The percentage difference in abundance of MEP/DOXP metabolites that have been subject to the combined treatment will be significantly less than the abundance in metabolites of the plants that were subject to heat stress alone.

Chapter 2: How do CO₂ and Extreme Temperature Interact to Determine the Magnitude of Volatile Organic Carbon Emissions from Woody Plants? A Tandem Theoretical and Empirical Approach.

2.1 Introduction

Biological Volatile Organic Compounds (BVOCs) are emitted by plants under stress, particularly as a result of short-term heat shock where they are believed to play a role in quenching reactive chemical species (Peñuelas & Llusà, 2003). There is a diverse array of BVOCs produced by plants, the relative 'cocktail' of which differs according to vegetation types. What is known however is that the BVOC isoprene is emitted in the greatest amounts on a global scale (Table 2.1).

Table 2.1: The major categories of volatile organic compounds emitted by plant (adapted from Peñuelas & Llusà, 2003).

Chemical species	Estimated annual global emission (10 ¹² g C)	Atmospheric concentrations	Example
Isoprene	175-503	pmol mol ⁻¹ to several nmol mol ⁻¹	N/A
Monoterpenes	127-480	pmol mol ⁻¹	α-pinene, β-pinene,
Other reactive BVOCs	~260	1–3 nmol mol ⁻¹	2-Methyl-3-buten 2-ol, hexenal, acetaldehyde
Other less reactive BVOCs	~260	2–30 nmol mol ⁻¹	Methanol, ethanol, formic acid, acetic acid, acetone
Ethylene	1-20	pmol mol ⁻¹ to several nmol mol ⁻¹	N/A

Moreover, emissions of BVOCs, particularly isoprene and the monoterpenes, may have wider effects on the climate via regulation of the oxidising potential of the troposphere by directly interacting with the hydroxyl radicle (OH·), the principle tropospheric oxidant (Peñuelas & Llusà, 2003). This in turn influences a number of atmospheric processes such as ozone dynamics, carbon monoxide production, and methane oxidation (Peñuelas & Llusà, 2003). Furthermore, recent research suggests a

role for elevated CO₂ in regulation of BVOC emissions by plants (Naik et al., 2004; Sharkey et al., 2008).

Based on this, a number of empirical biogenic emission models such as MEGAN, LPJ-GUESS, and BVOCEM have been developed in order to resolve BVOC fluxes, and to understand their dynamics in the atmosphere in the context of the diversity of global vegetation types and their distribution (Arneth et al., 2011; Guenther et al., 2006; Guenther et al., 2012; Sitch et al., 2003). These emission/flux models are derived from both vegetation classification and distribution models coupled to chemical transport models and consider not only the anthropogenic impact of global BVOC emissions, but also the natural emissions and their combined impact upon atmospheric chemistry (Young et al., 2009). Both MEGAN and its latter derivation BVOCEM are driven by extensive environmental datasets including temperature, photosynthetically active radiation, and CO₂ along with vegetation type distributions derived from dynamic vegetation models in order to generate spatially resolved, predicted values for BVOC emission (Arneth et al., 2011). Moreover, both of these models predict that increases in ambient temperature will induce BVOC emissions, especially isoprene, and secondly, that increasing atmospheric CO₂ will act to suppress BVOC emission (Lathière et al., 2010).

Climate change is associated with both increases in CO₂ and temperature, yet neither MEGAN nor BVOCEM are currently equipped to model this interaction, thus generating further uncertainty in the modelled predictions of BVOC emissions and their spatial patterning. Indeed, past evaluation of these models to determine the extent of agreement across the different modelling platforms used reveals inconsistencies in the modelled predictions when one or more of the driving parameters is changed (Arneth et al., 2011). There are also inconsistencies when the different datasets used to drive each

of the different chemical models are exchanged, leading to either an under or over prediction of annual total BVOC emissions (Arneth et al., 2011).

This is further highlighted by the fact that in current biogenic emission models, including MEGAN, LPJ-GUESS, and BVOCEM, biogenic emissions have been underestimated by up to 50%, particularly for isoprene in tropical regions (Holm et al., 2014) when compared to validation through canopy-level measurements. The major issue that results in discrepancies between the predicted and observed magnitude of BVOC emissions is the driving factors that are inputted into the model, i.e. the mechanistic basis underpinning the induction and emission of BVOCs. Currently, the differences in the driving biophysical parameters are larger than the differences in the emission activity algorithms that constitute the model predictions (Holm et al., 2014).

The central issue confounding accurate prediction of BVOC emissions by models is their limited amounts of mechanistic detail in terms of the regulation of BVOC production *in planta*, and the subsequent feedbacks underpinned by environmental factors such as light, temperature, and CO₂. Some attempts have been made to assign a fixed emission capacity to PFTs in the models, but this has proven difficult because of the variation of emission rates that occur between species or plant functional groups (Arneth et al., 2011). A more detailed understanding of the biochemical pathways responsible for the synthesis of BVOCs is thus urgently needed in order to refine our current models (see Chapter 3).

While canopy level measurements are useful for model validation, they represent coarse-grain data; therefore, to more fully evaluate the accuracy of our current models, it is critical that they are validated relative to finer scale measurements of individual plant-level BVOC emissions, relative to the interactive effects of environmental drivers such as temperature and CO₂.

This chapter will firstly evaluate the dynamical behaviour of current empirical models of BVOC emissions to quantify the magnitude of BVOC emissions, and to understand the drivers for any variability in predictions. Secondly, an experiment-based approach will test the role of CO₂ and heat as drivers of the emission of one such BVOC, isoprene.

2.2 Methods

2.2.1 Empirical models

The following section describes the vegetation model and the emissions model that were used to conduct experiments into the effects of changing temperature and CO₂ upon global vegetation and BVOC emissions.

2.2.1.1 Sheffield Dynamic Global Vegetation Model (SDGVM)

The Sheffield Dynamic Vegetation Model (SDGVM) has been designed in order to simulate the effect of long-term atmospheric changes upon the terrestrial ecosystem. As with all DGVMs, the Sheffield vegetation model calculates the effects of changing climate and atmospheric chemistry upon the distribution of carbon in both the soil and in vegetation. The model also calculates the diversity and potential changes of global vegetation over a given period when exposed to climatic changes, as shown in figure 2.1.

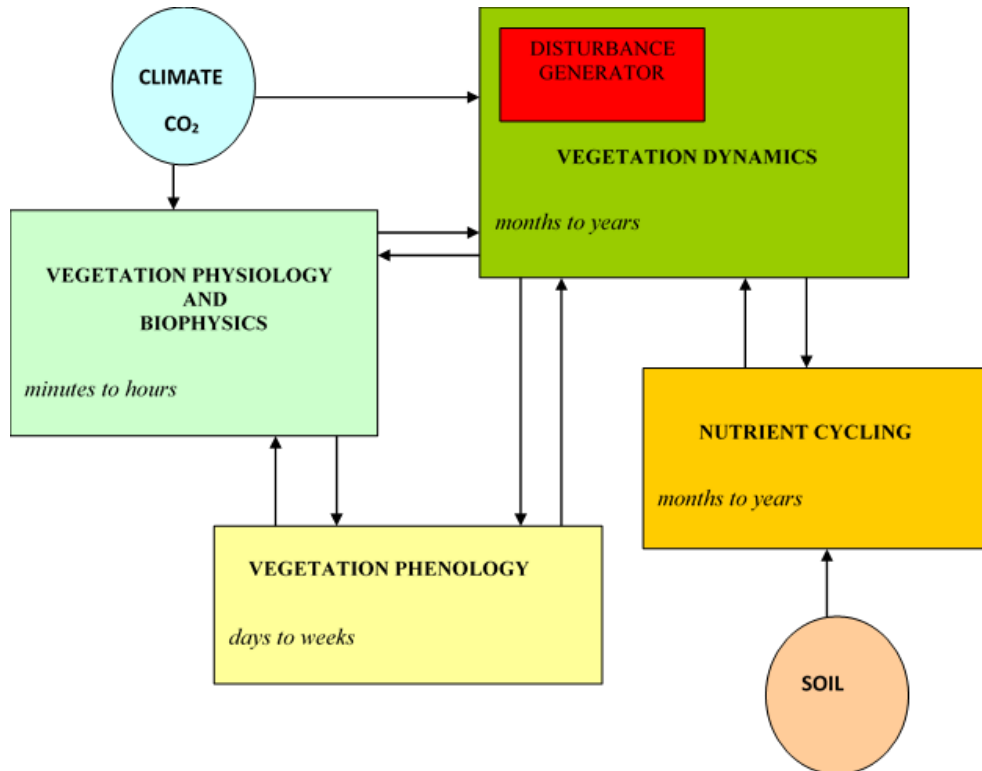


Figure 2.1: Structure of a standard dynamic vegetation model (taken from Cramer et al., 2001)

Table 2.2: Descriptions of the various processes that comprise SDGVM (Adapted from Cramer et al 2001).

Process	SDGVM
Shortest time step	1 day
Photosynthesis	Taken from Farquhar et al. (1980)
Radiation	Beer's law (total vegetation)
Carbon allocation	Annual allocation by demand
Nitrogen uptake	Dependent on soil decomposition and moisture
PFTs	7
Vegetation dynamics	Non-homogeneous area based competition for light
Vegetation establishment	Climatically favoured PFTs establish in proportion to area

SDGVM takes into account a fractional cover of vegetation that is divided into a number of plant functional types (PFTs) (Table 2.3). Table 2.2 shows the various

geochemical and biochemical processes that are taken into account in the model, including the establishment of the seven PFTs in proportion to geographical distribution.

Although SDGVM has specifically been developed for long-term changes to the terrestrial biosphere, it requires some generalisation in order to successfully complete this. The PFTs are grouped according to their geographical location, and whether or not they are deciduous or evergreen, which has an impact upon leaf calculations. The main premise of the model is that it is only the potential vegetation that is calculated. Therefore, there is no parameter or function that accounts for potential changes due to anthropogenic land use. This can be a limiting factor when attempting to accurately make predictions regarding historical, present, and future scenarios. However, for the purpose of this research, it is acceptable to be able to gain a general overview of natural vegetation and its contribution to global BVOC emissions.

Table 2.3: Descriptions of the 7 PFTs that make up the SDGVM fractional cover of vegetation.

PFT number	Description
1	Bare soil
2	Grasses (C ₃)
3	Grasses (C ₄)
4	Fine leaf evergreen trees
5	Deciduous broadleaf trees
6	Fine leaf deciduous trees
7	Broadleaf evergreen trees

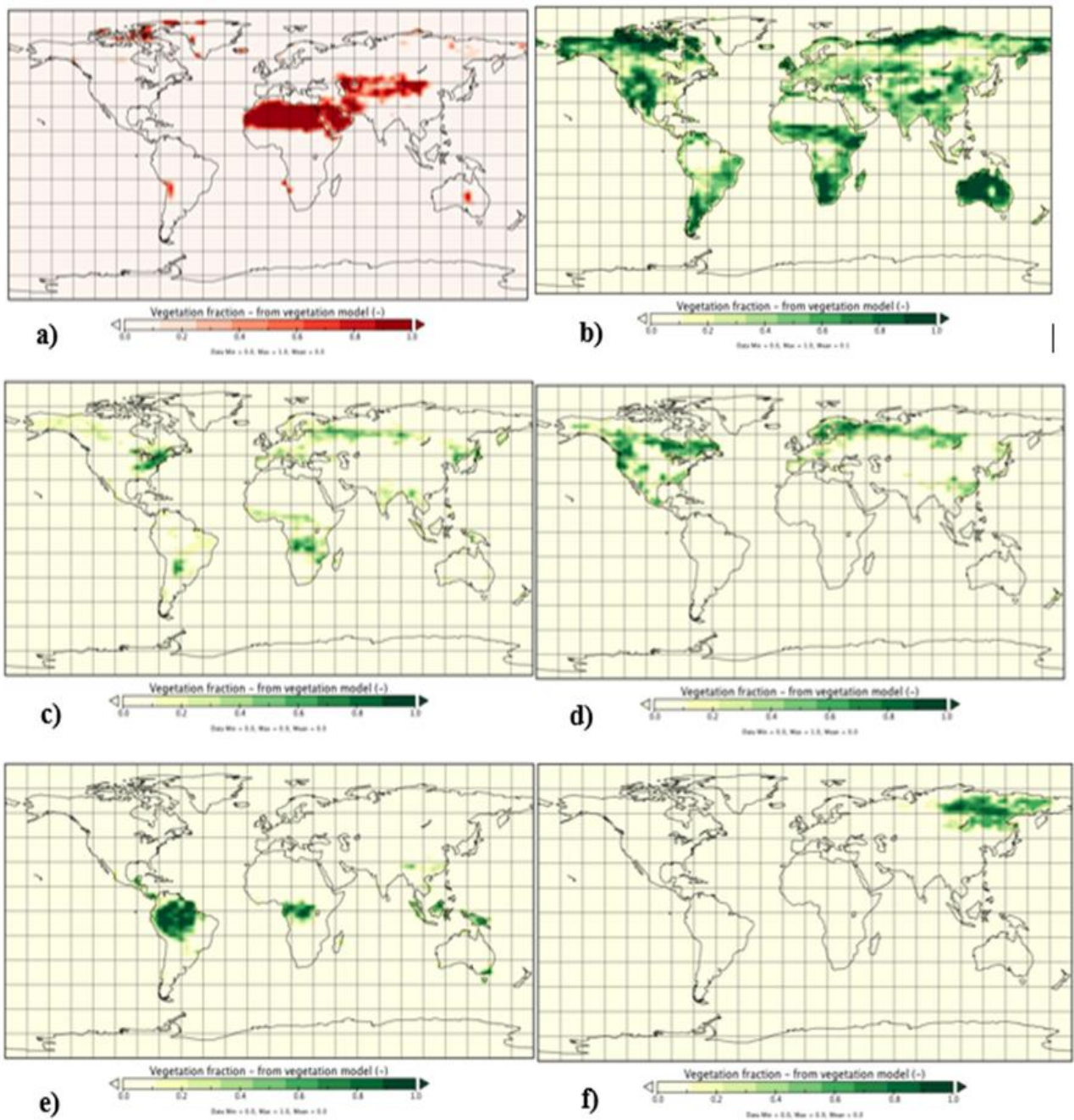


Figure 2.2: Global distribution of plant functional types (PFTs) used as a forcing file to drive BVOCEM for the month of July 1990. A) fraction of bare soil; b) fraction of grasses (C₃ & C₄); c) fine leaf evergreen trees; d) deciduous broadleaf trees; e) fine leaf deciduous trees; f) broadleaf evergreen trees.

Figure 2.2 provides an example of the vegetation fraction for several plant functional types that are generated by SDGVM. Although C₃ grasses are high isoprene emitters, particular focus should be drawn to maps d and e. These fraction of established vegetation in temperate (d), and tropical (e) regions show the distribution of vegetation that are the largest emission sources for isoprene in tropical and temperate regions.

2.2.1.2 Model set up

The model was allocated a 500 year “spin up” randomly selected from 20 years of meteorological data from the Climatic Research Unit (CRU) dataset, therefore allowing the vegetation to attain equilibrium. For each of the fields required for the model, a mean of land only global monthly temperatures was created. SGVM does not take into account sea points as it only calculates terrestrial vegetation. The model was run for the period 1980-2005 at a 1°x1° resolution.

2.2.1.3 Biogenic Volatile Organic Compound Emissions Model (BVOCEM)

The Biogenic Volatile Organic Compound Emission Model (BVOCEM) is an offline emissions scheme that calculates emissions of isoprene and other VOCs from terrestrial vegetation. A number of models have been created to attempt to simulate and quantify the global isoprene flux (Guenther et al., 1995, 2006, 2012). The Model of Emissions of Gases and Aerosols from Nature (MEGAN) defines a number of parameters, including temperature, photosynthetically active radiation, and leaf-level measurements that have been incorporated into the parameters that define BVOCEM.

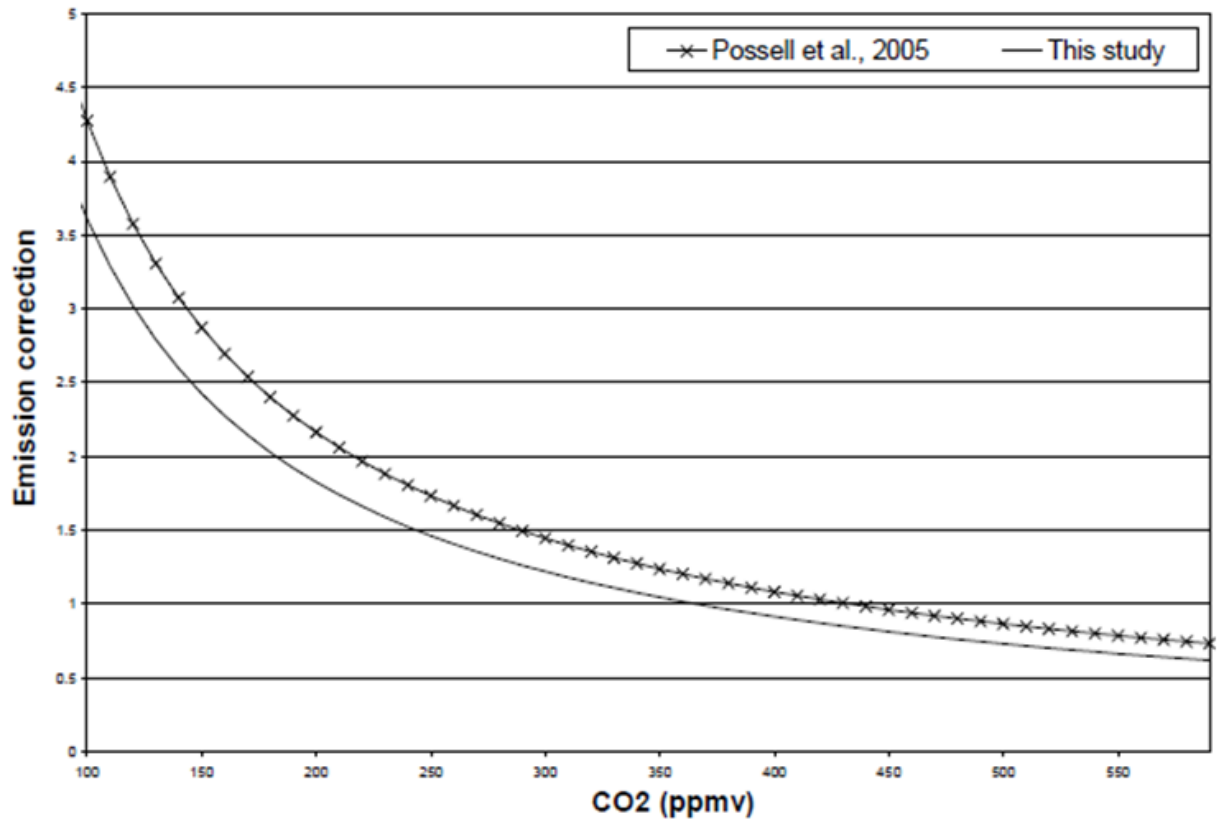


Figure 2.3: Effect of atmospheric CO₂ on isoprene emissions. The black line denotes the function described by Possell et al (2005) and the dotted line is the correction used in BVOCEM (Taken from the BVOCEM user manual).

BVOCEM has made an attempt at integrating the impact of increased atmospheric CO₂ concentration on isoprene emissions. The function proposed by Possell et al (2005) has been used, but with a correction that has normalised the emissions efficiency to 1 for the (then) current day concentration of 366ppm. It is important to note that this function has not been fully reconciled over a long time period and would require further testing to determine the sensitivity of the model to long term changes in atmospheric CO₂ and its impact upon the PFTs within the model.

2.2.1.4 Model set up

Table 2.4: List of parameters that are required by BVOCEM (taken from BVOCEM user guide).

File name	Description	Unit
PAR.nc	Photosynthetically active radiation	$\mu\text{molphot}/\text{m}^2/\text{s}$
tair.nc	Air temperature (2m)	Kelvin
vwc.nc	Volumetric water content	m^3 / m^3
lai.nc	Leaf area index	m^2 / m^2
maxvegetfrac.nc	Vegetation fraction (PFTs)	-
MEGAN_EF_iso_96x73.nc	Isoprene emission factors from Guenther et al. 2006	$\mu\text{g Iso}/ \text{m}^2/\text{h}$

The files needed to drive BVOCEM, as shown in table 2.4, are created from output files from SDGVM. These files were required to be converted into a NetCDF format in order to be read by the model. Pre-prescribed files of photosynthetically active radiation (PAR) and the isoprene emission factors were taken from the work of Guenther et al (2006) and are the same file for each year that BVOCEM were run. The concentration of CO₂ was changed for each year to match the figures shown in the graph (figure 2.3). In order to investigate the effects of CO₂ suppression upon isoprene emissions, CO₂ concentrations were also set at just under ambient (335ppm), ambient (366ppm), and just above ambient (385ppm), and were fixed for the run period. Both the emission factors and the PAR file have a resolution of 2.5°x3.75° and therefore all converted files from SDGVM were scaled to this. Only isoprene emissions in the BVOCEM are calculated using the work from Guenther et al (2006).

2.3 Results

2.3.1 Empirical modelling results

Figure 2.4 shows the variation in predicted isoprene emissions from different models. BVOCEM in particular, is out of the range of more recent estimates of isoprene emissions of 413-600 Tg yr⁻¹ (Arneth et al., 2008; Lathière et al., 2010). Only the MEGAN-MACC, GUESS-ES and BVOCEM models have been run over a long period to look at trends in isoprene emissions. The older version of MEGAN, and POET have been run over the period of a year for biogenic emissions and thus provide limited information for isoprene. Although the emissions for BVOCEM are lower than stated above, the global distribution and pattern that one would expect to see across the globe is shown in figures 2.5 and 2.6. It is therefore likely that one or more parameters will need to be forced in order to predict a result within the range that has been stated in current literature (Arneth et al., 2008). Figure 2.7 does show however, that an increase in atmospheric CO₂ over a 25-year period does suppress isoprene production and therefore lead to a decrease in emissions. However, as stated previously, it has been suggested that currently there is a balancing effect between temperature and CO₂, and therefore there is little change in annual emissions.

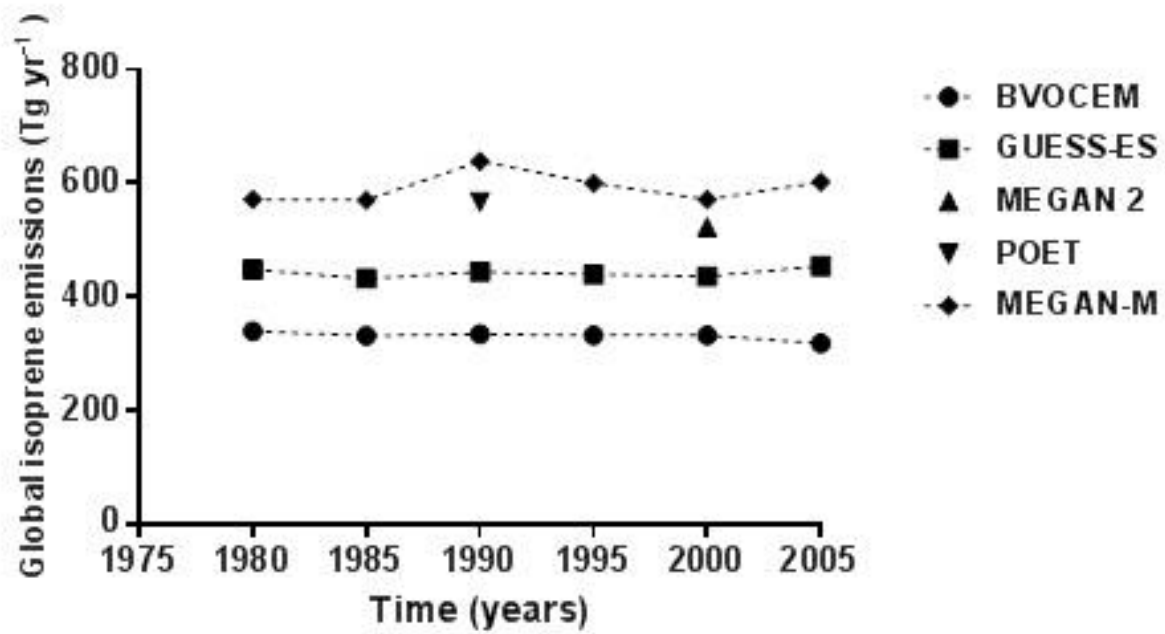


Figure 2.4: Graph of isoprene emissions from 4 global emissions models, and BVOCEM scaled global totals for 5 year intervals (BVOCEM isoprene totals run with variable temperature & CO₂).

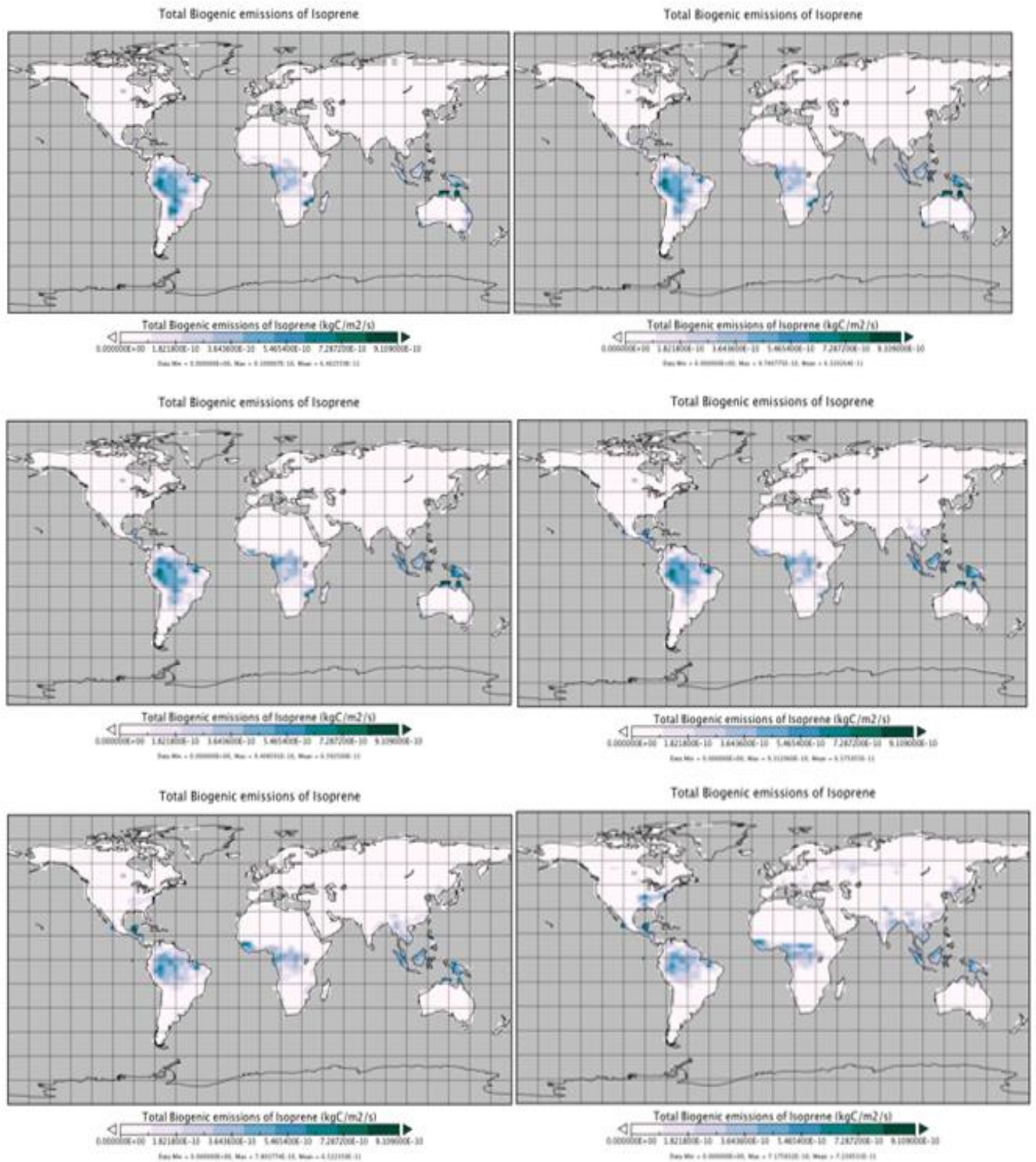


Figure 2.5: Monthly global total isoprene emissions (kg C/m²/s) for all PFTs for the year 1990 (Jan-June), results from BVOCEM (same parameters as figure 2.3).

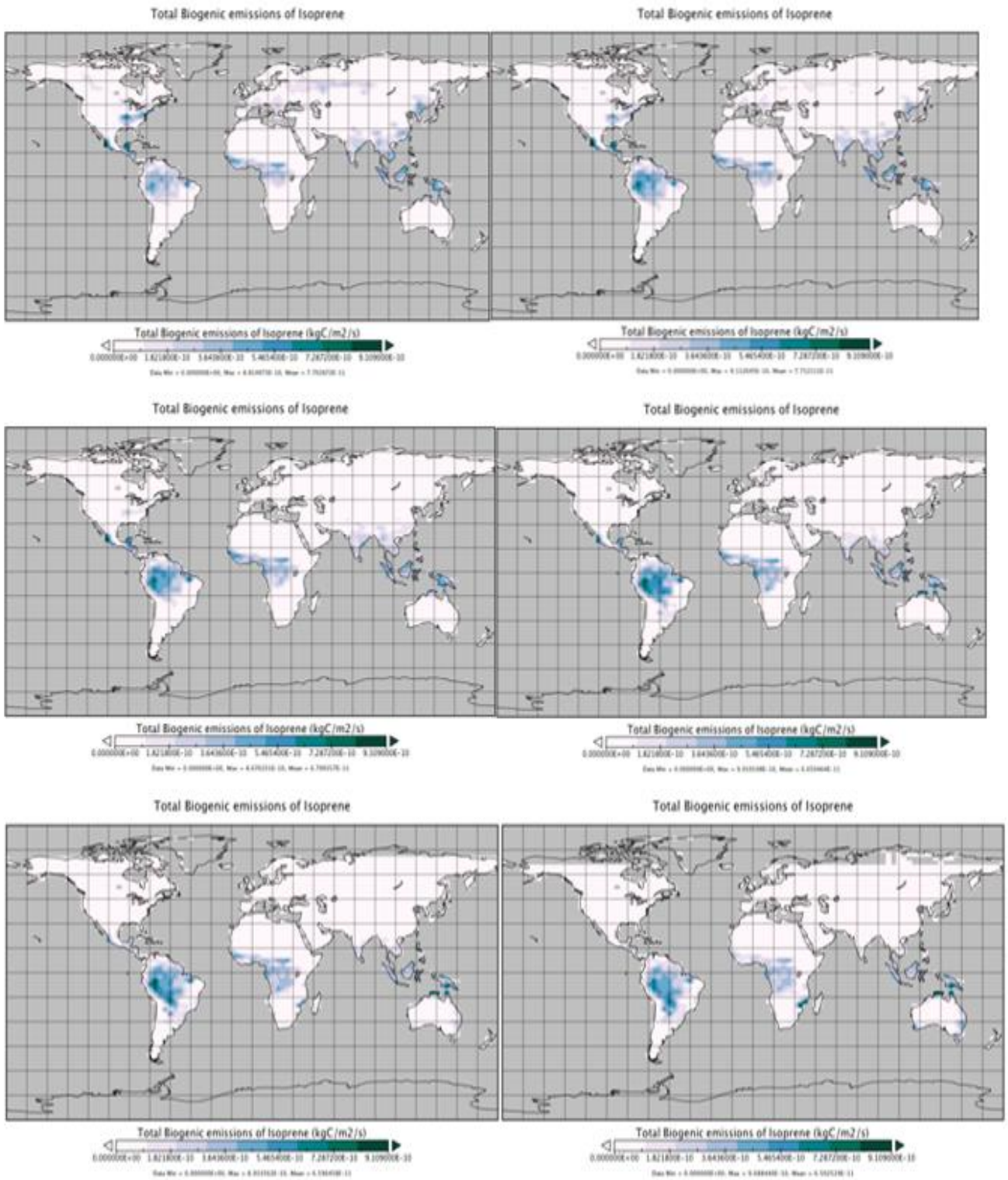


Figure 2.6: Monthly global total isoprene emissions (kg C/m²/s) for all PFTs for the year 1990 (Jul-Dec), results from BVOCEM (same parameters as figure 2.3).

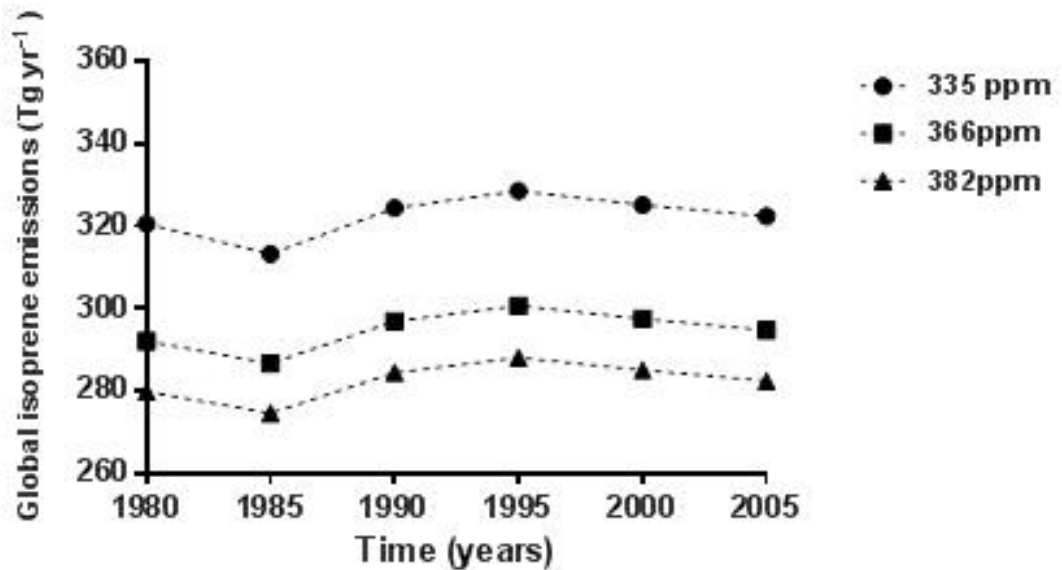


Figure 2.7: Global total emissions of isoprene (Tg yr^{-1}) with 3 fixed CO_2 concentrations generated by BVOCEM.

Figure 2.7 demonstrates the effects of both temperature and CO_2 upon isoprene emissions. By keeping the concentration of CO_2 constant over the same period, and with three model runs of below ambient, ambient, and a higher value of CO_2 it is possible to determine which of the two parameters has a greater effect upon emissions from BVOCEM. It is clear that even a relatively small increase in global CO_2 concentration in the three model runs suppresses isoprene emissions. Although the magnitude of annual global totals are different for each concentration, the directionality over the 25-year period is the same for all three model runs, indicating that variable temperature, as well as CO_2 has a significant impact upon emissions.

2.4 Discussion

2.4.1 Empirical modelling

The modelling results show variability in the magnitude of emissions when compared to the literature, however they do provide striking homology in terms of the patterns of BVOC emissions predicted across the different models. Recent re-evaluation of MEGAN, and the biophysical parameters that drive it, has shown that there a number of uncertainties associated with the model's driving factors. This is relevant as the newer version of MEGAN was developed by Holm et al (2014) from the 2006 paper on which BVOCEM is based. The Holm et al (2014) paper suggests that the greatest variability within the MEGAN model is the calculation of leaf temperature and photosynthetically active radiation (PAR). In tropical regions in particular (where a large amount of isoprene is emitted), both of these driving factors are expected to change as a result of climate change (Holm et al., 2014). The exponential response of isoprene to temperature is extremely sensitive and therefore any increases in air temperature and subsequent increases in leaf temperature will have an effect upon emission rates (Holm et al., 2014). An increase in PAR has been shown to exert the same effect upon isoprene emission rates (Lerdau & Keller, 1997; Holm et al., 2014). As isoprene emissions are driven primarily by these two factors in the model it will be essential to conduct further analysis upon them to attempt to quantify and reconcile the uncertainty within BVOCEM in the future. Although many emission models are built around temperature and PAR parameters (and thus using similar algorithms), the scale, climate, land-use and other important core processes are different. These differences, combined with the gap in current knowledge behind the driving factors of isoprene emission and/or suppression currently lead to a disagreement between the magnitude of isoprene emissions in different global models. Subtle changes in each model may lead to large differences in the driving biophysical parameters, larger than the differences in

the individual algorithms. The simple conclusion that can then be derived following this modelling study is that given the complex feedbacks involved in regulating the biochemical processes that lead to BVOC biosynthesis and emission, it is not sufficient to investigate only the individual regulatory factors/stressors involved in isolation. But rather, that the empirical data used to drive such emission models is developed from a more complex dataset, whereby the regulatory factors are examined in terms of their effects on BVOC emission in factorial combination. This requires a novel, mechanistic approach that differs from previous bottom-up approaches in its attempt to reconcile the effect of abiotic stresses upon isoprene emissions that could therefore drive more accurate modelling results.

The following section of this chapter sets out to test the effects of elevated CO₂ and extreme temperature upon BVOC emissions using an empirical approach. The two experiments using willow (*Salix* spp.) aim to understand the independent and interactive effects of these abiotic stresses upon the production of isoprene.

2.5 Empirical approach to BVOC emissions

2.5.1 Experiment set up and plant growth

32 Willow cuttings of the short rotation coppice hybrid “Terra Nova” (‘LA940140’ x *Salix miyabeana*) (Lindgaard, 2012) were rooted in pots and were filled with John Innes No. 3 potting compost. The cuttings were grown for ten weeks in a controlled environment chamber (see Table 2.5 for environmental parameters) to allow for stems and leaves to establish until the temperature and CO₂ treatments were applied.

Table 2.5: Environmental parameters and time periods for willow growth in controlled environment chamber.

Environmental Parameter	Parameter Values	Time Period
Temperature (day)	20°C	8 hours
Temperature (night)	15°C	16 hours
CO₂	Ambient (~400ppm)	constant
Light	800μmol	8 hours
Humidity	67%	constant

Following the ten-week growth period, four plants were selected at random to be moved into the experimental chamber to acclimate. For 14 days, the four plants were kept in the experimental chamber at either ambient or elevated CO₂ depending on the treatment (see Table 2.6) prior to the application of the temperature treatment. This experiment and set of treatments (Table 2.6) was run twice. For the second experiment, the treatments outlined in Table 2.6 were run in reverse. 16 plants were used for each set of experiments.

2.5.2 Elevated temperature and CO₂ treatment application

After the ten week growth period, the four biological replicates were subject to their prescribed treatments and subsequent air entrainment over an 18 day period. Weeks one and two were kept at the ambient temperature parameters (Table 2.5) for both day and night. Depending on treatment, CO₂ concentrations during these two weeks were either kept at ambient (~400 ppm) or elevated (800 ppm). The heat shock treatment (40°C) (when required for the appropriate treatment) was applied on day 15, else the temperature was kept at the same ambient level until day 18. Table 2.6 shows the parameter values and the time period each was applied for each of the four

treatments. The air entrainment experiment to collect isoprene emissions began at the start of the photoperiod on day 18 and ran for eight hours. The entrainment experiment was repeated, with the treatment application running in opposite order to that shown in Table 2.6.

Table 2.6: Environmental parameters and time periods for treatment application and subsequent entrainment in the controlled environment chamber. Note that the treatments were run in opposite order for the second experiment.

Treatment	Parameter Values		Time Period		
	Temperature	CO ₂	Temperature	CO ₂	Entrainment
1) Hs*eCO ₂	40°C	800ppm	1 photoperiod (8 hours)	constant (19 days)	1 photoperiod (8 hours)
2) eCO ₂	20 °C	800ppm	1 photoperiod (8 hours)	constant (19 days)	1 photoperiod (8 hours)
3) Hs	40°C	Ambient (~400ppm)	1 photoperiod (8 hours)	constant (19 days)	1 photoperiod (8 hours)
4) Control	20 °C	Ambient (~400ppm)	1 photoperiod (8 hours)	constant (19 days)	1 photoperiod (8 hours)

2.5.3 Plant entrainment

On the day prior to the air entrainment experiment for each treatment, the equipment was sterilised and tested to ensure full working order. The 4 Porapak Q adsorbent tubes (70mm length, quartz filter) (Alltech Associates, Lancashire, UK) were eluted with 2ml of hexane solvent and were heated at 120°C overnight to remove any contaminants. Whilst in the oven, charcoal filtered air was pushed through the glass tubes at 700 ml min⁻¹ in order to help with any potential contaminant removal, and to test the air flow. The four polyethylene terephthalate entrainment bags were opened and baked in the oven overnight to remove any contaminants. Aluminium foil that was also

baked overnight was used to wrap the sterilised Porapak tubes prior to the entrainment experiment.

The four plants were encased individually in the polyethylene terephthalate bags (see figure 2.8) and the PTFE tubing and bag was secured using plastic coated wire, without causing damage to the plant's stem. The need for an airtight seal was not necessary due to the difference in flow rates that created a positive pressure to stop any unfiltered air entering the system (Webster et al., 2008). Charcoal filtered air was pumped through each bag at a rate of 700 ml min^{-1} by a KNF (Switzerland) vacuum pump (Model number NMP850KNDC) and was drawn out through an outlet containing the Porapak Q tube at a rate of 400 ml min^{-1} . The Porapak Q tube was also secured in the bag using plastic coated wire. Air entrainment of the four plants began at the start of the photoperiod and ran for 8 hours.

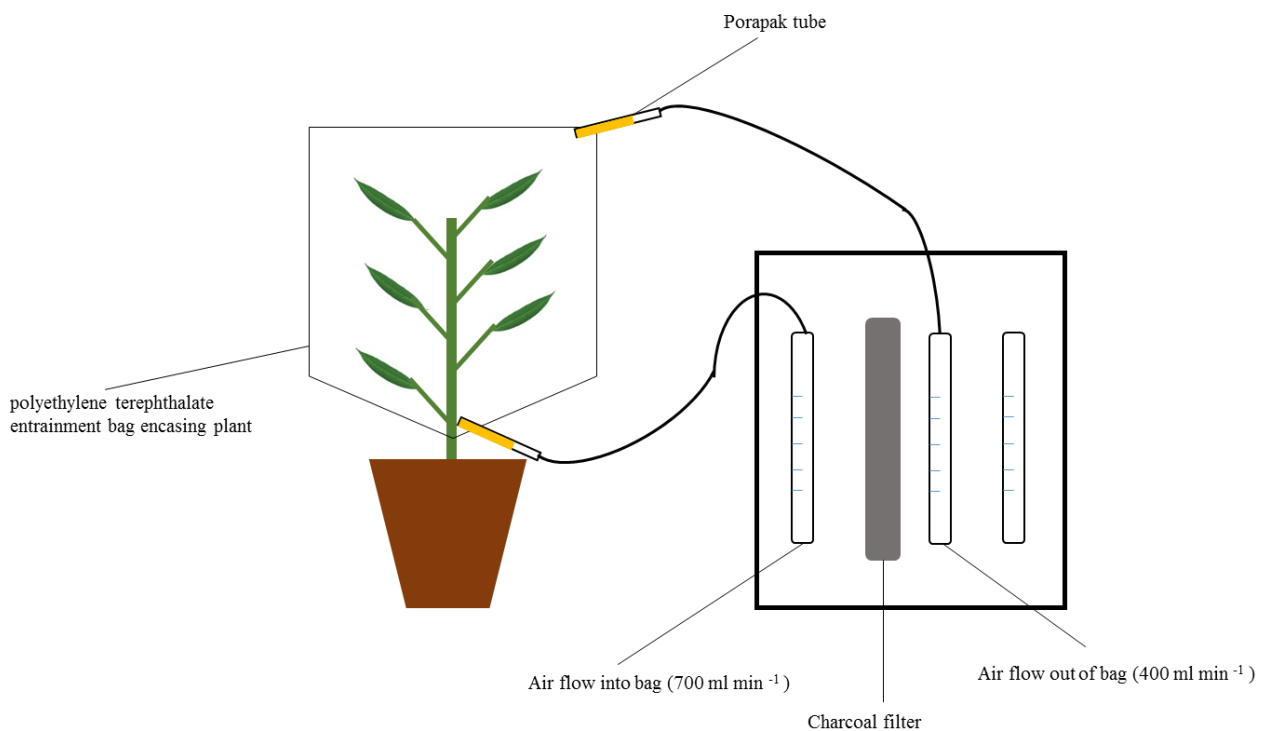


Figure 2.8: Schematic to show the air entrainment experiment set up.

2.5.4 Plant harvest

At the end of the eight-hour air entrainment period, the Porapak Q tubes were removed from the outlet and were individually wrapped in sterilised aluminium foil. Each plant was then cut at the point on the stem where the polyethylene terephthalate entrainment bag had been attached. A young and old leaf sample for each of the four plants were collected for biochemical analyses (see chapter 3: section 3.2.3 for full details of young and old leaf harvest). The plants were stored in individual sample bags and were stored at -80°C in preparation for freeze drying for biomass measurements.

2.5.5 Sample elution

The Porapak Q filter tubes were eluted with 1 ml of hexane solvent into 9 ml glass vials with a PTFE lid (SUPELCO Analytical, USA) to stop evaporation and were stored at -20°C in preparation for gas chromatography (GC) analysis of volatile compounds.

2.5.6 Leaf surface area

The leaf surface area measurement for each plant was calculated using a portable leaf area meter (LI-COR LI-3000C). For all of the leaves from each plant, the area in cm² for each leaf was calculated 3 times and an average was taken and each leaf area was totalled to gain the average leaf area for each plant (see section 2.3.2.5 for statistical results of isoprene emissions from leaf surface area and table A2.1 in the appendix for the leaf area measurements for each plant).

2.5.7 Plant biomass

The separated leaves and stem of each plant sample following leaf area calculation were freeze dried for 5 days and stored in a desiccator prior to the measurement of the dry weights. The total leaves and stem for each plant were weighed (g) in order to calculate the above ground biomass (see section 2.3.2.4 for statistical results of isoprene emissions as a function of leaf biomass and table A2.2 for plant dry weight measurements).

2.5.8 Gas Chromatography-Flame Ionisation Detection (GC-FID)

The eluted solutions were analysed on a PerkinElmer AutoSystem XL GC with an auto ignite FID. A ZB-5 column (30 m x 0.25 i.d., 0.25 µm film thickness) was used. The injection temperature was 200°C with a 2 µl sample injection. The carrier gas was nitrogen. Table 2.7 shows the oven temperature program that was used to analyse the samples. The retention time by analytical standard for the hexane solvent was 2.915. The retention time for the isoprene standards at each concentration was 2.398.

Table 2.7: The oven temperature ramp program for the GC-FID.

Oven Temperature Program	Temperature (°C)
Initial	27°C
Ramp 1	5°C /min to 45°C
Ramp 2	25°C /min to 100°C
Ramp 3	5°C /min to 200°C

2.5.9 Data processing and statistical analysis

A calibration curve was created from the isoprene standard concentrations (nM), and was converted into nanomoles in order to quantify the amount of isoprene present in each of the biological samples. The calibration for each of the standards was calculated using the area of the peak for each analytical standard, and the amount of isoprene found in each standard, expressed as nanomoles.

The same treatments of both experiments were averaged to establish the potential difference in the amount of isoprene emitted by the plants. The percentage difference relative to the control was calculated to show either the increase or decrease of the amount of isoprene in each sample for a given treatment. Isoprene emissions as a function of both leaf dry weight and leaf area according to treatment were also calculated using the same method, and a percentage difference relative to the control for both was also calculated.

A 2-way ANOVA statistical analysis was used to determine whether there was a difference in the quantity of isoprene in the sample in relation to the temperature and CO₂, and the interaction of the two environmental parameters. The same statistical analysis was used to determine if there was any statistical significance when isoprene emissions were calculated as a function of both leaf dry weight and leaf area for each treatment.

2.6 Results

2.6.1 Measuring isoprene emissions

This section sets out the results for the empirical measures of isoprene emission in relation to heat-shock (at 40 °C) and elevated CO₂ (800 ppm).

2.6.2 Kovats retention indices for each treatment

Each biological sample was putatively identified through the Kovats retention index. The average retention times for each of the treatments were found to be 2.39, thus matching the retention index for isoprene from each of the analytical standards.

2.6.3 Response of plant biomass to heat shock and CO₂ treatments

The results of the graph (figure 2.9) and the 2-way ANOVA (Table 2.8), have both demonstrated no significant differences in the dry weight of the above ground biomass as a response to temperature and CO₂, and their interaction.

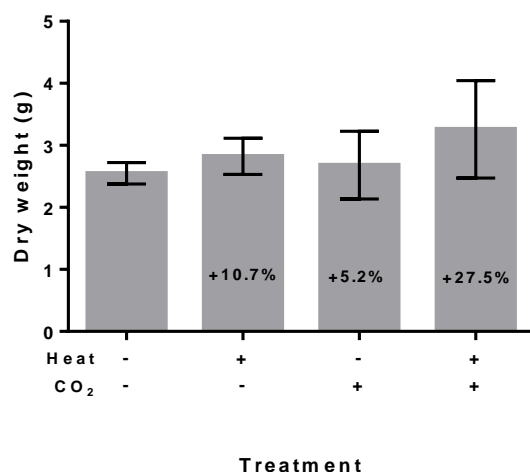


Figure 2.9: Graph to show the above ground biomass (g) for each treatment. Each treatment is an average of the biological replicates for the 2 experiments. The percentage change (\pm) relative to the control is provided. Error bars denote 1 standard deviation (σ).

It has been observed however, that there is an overall trend that shows the control plants have a lower amount of tissue biomass when compared to the other treatments. The plants that have been subjected to the heat shock treatment show a 10.7% increase in above ground biomass relative to the control. A heat shock of 40°C over one photoperiod would not be expected to promote an increase in biomass. It would be expected that the plants that were treated with elevated CO₂ would exhibit greater biomass than a 5.2% increase relative to the control, as the plants were provided with more carbon for energy production. The increase in biomass of the combined Hs**e*CO₂ of 27.5% relative to the control is a large increase when compared to the independent heat shock and elevated CO₂ treatments. The response of plant growth to both the independent, and interactive effects of temperature and CO₂ therefore requires further interrogation. The two-week acclimation period in the controlled environment chamber may not have been long enough to observe a change in plant biomass as a response to treatment, and therefore further work is required to confirm this.

Table 2.8: Results of the 2-way ANOVA statistical significance of above ground biomass (g) of the 4 treatments in relation to temperature, CO₂, and their interaction. DF = degrees of freedom (& associated error); F = F-value; P = P-value (significant if p <0.05).

Treatment	DF	F Value	P Value
Heat	1, 28	0.3	0.587
CO ₂	1, 28	0.21	0.647
CO ₂ *Heat	1, 28	0.09	0.766

2.6.4 Isoprene emission in response to heat shock and CO₂ treatments

The results of the two sets of air entrainment experiments and subsequent GC-FID analysis have shown that there is no statistically significant difference in the effects of temperature, CO₂, and their interaction upon foliar isoprene emissions in this system.

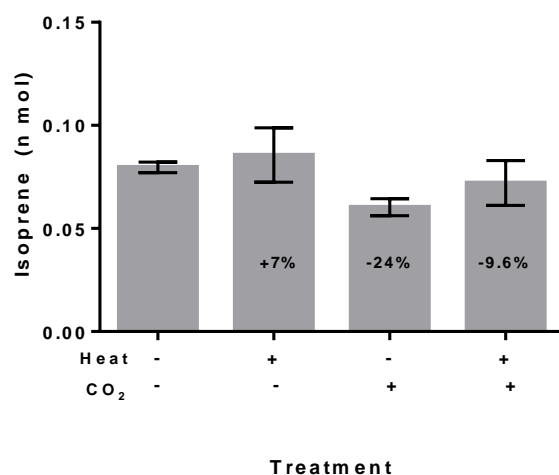


Figure 2.10: Graph to show the amount of isoprene emitted (nmol) as a response by plants to each treatment. Each treatment is an average of the biological replicates for the 2 experiments. The percentage change (\pm) relative to the control is provided. Error bars denote standard error to 1 standard deviation (σ).

Table 2.9 shows the results of the 2-way ANOVA with no significant P-value for heat, CO₂, or their combined effect. However, the percentage difference of each treatment relative to the control shows a difference in isoprene emission (figure 2.10). The percentage increase (albeit small) of 7% of plants subjected to heat shock relative to the control was expected. As demonstrated in figure 1.8 (chapter 1, section 1.3.1), isoprene emissions increase linearly with temperature increase to around 40°C with emissions of isoprene still being produced days after the initial heat shock (Li & Sharkey, 2013). This response to increasing temperature is well documented in the literature (Loreto & Sharkey, 1990; Rasulov et al., 2010; Singaas & Sharkey, 2000). At temperatures above the maximum plant tolerance threshold (over 42°C, as demonstrated in poplar), isoprene emissions decrease to zero (Rasulov et al., 2010; Zimmer et al., 2000). Therefore the decision to exert a 40°C heat shock to the plants was made to ensure isoprene emission without inducing leaf senescence.

Table 2.9: Results of the 2-way ANOVA statistical significance of the amount of isoprene emitted (nmol) in each of the 4 treatments in relation to temperature, CO₂, and their interaction. DF = degrees of freedom (& associated error); F = F-value; P = P-value (significant if p <0.05).

Treatment	DF	F Value	P Value
Heat	1, 17	0.33	0.574
CO ₂	1, 17	0.00	0.997
CO ₂ *Heat	1, 17	0.05	0.821

The decrease in the amount of isoprene emitted by plants that were subject to the elevated CO₂ treatment is also expected. As shown in section 2.2.1.3 (figure 2.3), both studies conducted by Possell et al (2005) and the BVOCEM study show an expected decrease in isoprene emissions at elevated CO₂ concentrations. This is reflected in the marked decrease of 24% (figure 2.10) relative to the control by the plants under the eCO₂ treatment. The results of the meta-analysis in 2.3.1 (figure 2.7) also show that there is a decrease in isoprene emissions as a result of an increase in CO₂ concentration. Even a small increase of 31ppm, and then 16ppm respectively shows a change in the magnitude of global isoprene emissions ranging from ~280 - ~320 Tg yr⁻¹. Although the directionality of the response of isoprene emissions in this study matches previous work, it is the mechanisms that underpin the production and regulation of isoprene at the cellular level that are poorly understood. Chapters 3 and 4 discuss the biochemical responses of the plants to environmental stresses in more detail.

Isoprene emission as a response to the combined Hs**e* CO₂ is surprising however. The percentage decrease of 9.6% of isoprene in relation to the control is less than would be expected. Figure 2.7 shows that under variable temperature (although not as extreme as the heat shock treatment in this study) the effect of changing CO₂ concentrations leads to the variability in isoprene emissions being produced when modelled. Previous work on the effect of elevated atmospheric CO₂ has found that

isoprenoid emissions are either reduced under these conditions (Centritto et al., 2004; Possell et al., 2005; Scholefield et al., 2004), or alternatively has no overall effect upon emissions (Buckley, 2001; Rapparini et al., 2004). The results shown in figure 2.10 suggest that the combined effect of extreme temperature and elevated CO₂ upon the plants may mitigate each other when compared to the independent treatments, but further work would be needed to confirm this as the statistical results in Table 2.9 show that this is not significant.

2.6.5 Isoprene emission in response to heat shock and CO₂ treatments in relation to leaf biomass

The results of the 2-way ANOVA (Table 2.10) show no statistically significant difference for the four treatments and the response of isoprene emissions to them. The results of figure 2.10 show a marked increase in isoprene emissions when calculated as a function of leaf biomass for each treatment. As demonstrated in figure 2.11, the response of isoprene emissions to a heat shock treatment is as expected and shows an increase of 82.7% relative to the control.

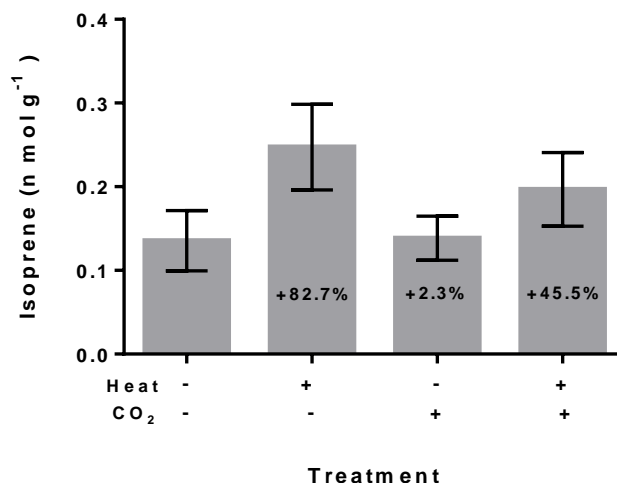


Figure 2.11: Graph to show the amount of isoprene emitted as a function of leaf dry weight (nmol g⁻¹) in relation to each treatment. Each treatment is an average of the biological replicates for the 2 experiments. The percentage change (±) relative to the control is provided. Error bars denote standard error to 1 standard deviation (σ).

The amount of the percentage increase of isoprene emission as a function of dry leaf weight relative to the control is surprising when compared to plant biomass (figure 2.9) and isoprene emissions independent of other factors (figure 2.10) is surprising. The 10.7% increase of biomass in plants subject to a heat shock and the 7% increase in isoprene emission is smaller than the increase in figure 2.11. The increase of isoprene emissions to elevated temperature may be a heat tolerance response. The majority of isoprene emissions from plants are produced in, and come from the leaves, and an increase in temperature will increase plant leaf temperature, thus requiring more isoprene to be released in order to counteract short periods of extreme heat (Sharkey et al., 2008; Siwko et al., 2007).

Unlike figure 2.10 however, there is a slight increase in isoprene emissions (2.3% relative to the control). However, as only foliar biomass was used (the stem was excluded) as plants emit isoprene through their leaves, this may account for why there is an increase in isoprene emission as a response to eCO₂.

The increase in isoprene emissions as a function of dry leaf weight in figure 2.11 (45.5% relative to the control) could be attributed to the higher amount of biomass for plants subject to the combined Hs*eCO₂ treatment seen in figure 2.9. This large increase (compared to the decrease of 9.6% in figure 2.10) could also be attributed to the the fact that isoprene is produced in the plant leaves as opposed to the stem, however there is no statistical significance.

Table 2.10: Results of the 2-way ANOVA statistical significance of the amount of isoprene emitted as a function of dry leaf weight (nmol g⁻¹) of the 4 treatments in relation to temperature, CO₂, and their interaction. DF = degrees of freedom (& associated error); F = F-value; P = P-value (significant if p <0.05).

Treatment	DF	F Value	P Value
Heat	1, 17	0.1	0.304
CO ₂	1, 17	1.13	0.752
CO ₂ *Heat	1, 17	0.27	0.608

2.6.6 Isoprene emission in response to heat shock and CO₂ treatments in relation to leaf area

The results of the 2-way ANOVA in Table 2.11 show that there is no statistically significant difference between the treatments, and their interaction upon isoprene emissions as a function of leaf area.

Table 2.11: Results of the 2-way ANOVA statistical significance of the amount of isoprene emitted as a function of leaf area (nmol cm⁻²) of the 4 treatments in relation to temperature, CO₂, and their interaction. DF = degrees of freedom (& associated error); F = F-value; P = P-value (significant if p <0.05).

Treatment	DF	F Value	P Value
Heat	1, 17	0.3	0.594
CO ₂	1, 17	0.09	0.764
CO ₂ *Heat	1, 17	0.01	0.913

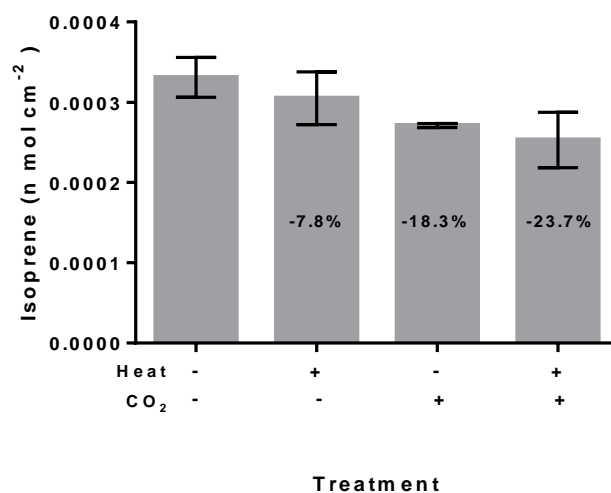


Figure 2.12 Graph to show the amount of isoprene emitted as a function of leaf area (nmol cm⁻²) in relation to each treatment. Each treatment is an average of the biological replicates for the 2 experiments. The percentage change (\pm) relative to the control is provided. Error bars denote standard error to 1 standard deviation (σ).

In contrast to the results reported in section 2.3.2.4, figure 2.12 shows that the amount of isoprene emitted by plants as a response to the treatments shows no increase in emissions as a function of leaf area. The 7.8% reduction in isoprene from plants subject to the heat shock treatment relative to the control is surprising when compared to the results in the preceding sections. Plants subjected to elevated CO₂ demonstrate a reduction in isoprene emission as a function of leaf area (18.3%) which, unlike in figure 2.11, is expected and more similar to the reduction in isoprene emissions that has been shown in figure 2.10.

In contrast to the results of the plants that were subject to the combined Hs*CO₂ in figure 2.10 however, the results for the same treatment in figure 2.12 demonstrate a greater reduction in isoprene emission as a function of leaf area relative to the control (23.7%). As previously discussed, it has been suggested that increases in CO₂ concentration will suppress isoprene emission, and the reduction seen in figure 2.12 would support this.

2.7 Discussion

2.7.1 *The effect of extreme temperature on woody plant isoprene emissions*

The second aim of this chapter was to examine isoprene emissions from woody plants (*Salix* spp.) in response to the independent and interactive effects elevated CO₂ and extreme temperature through a meta-analysis of both global isoprene modelling and a subsequent bottom-up analysis of isoprene emissions at the leaf level.

The results of both the meta-analysis of modelled isoprene emissions, and the results from the air entrainment experiment have revealed some gaps in the current knowledge regarding the variability in the magnitude of isoprene emissions from plants and the mechanisms that regulate the production of isoprene in response to the interactive effects of CO₂ and temperature. It is anticipated however, that the response of the plant to elevated temperature is different to that of the control treatment. In figures 2.11 and 2.12, there is a percentage increase of isoprene emissions relative to the control. As previously discussed in section 2.6.4, an increase in isoprene emissions as a response to short-term, extreme temperatures is well documented in the literature (Rasulov et al., 2010; Sharkey, 2005; Velikova & Loreto, 2005). It has been suggested by Sharkey (2005), that at high temperatures (35°C-40°C) the reduction in the photosynthetic rate of a plant cannot be explained by an increase in photorespiration alone. However, our current understanding of the damage to photosynthetic processes by extreme heat is unclear. Therefore, if the assumption that isoprene provides the plant with protection against damage to photosynthesis, through the quenching of reactive chemical species, our understanding of the mechanistic processes behind this protective capacity are also poorly understood (Sharkey, 2005).

A study by Velikova & Loreto (2005) however, found that in heat stressed plants, the thermotolerance of the plant was reduced if there was an inhibition of

isoprene synthesis. Furthermore, it was found that it was not just the immediate response of the plant to heat stress that provided thermotolerance, but rather that the production of isoprene in response to short-term heat stress allowed for a better recovery of the plant over a period of several days, including the protection of cell membranes (Velikova & Loreto, 2005). This response at the cellular level has also been observed by Sasaki et al (2007) and Siwko et al (2007) who have found that isoprene production stabilises the cell membranes in plant leaves.

It is still unclear however, why isoprene emissions are reduced to zero when temperatures exceed $\sim 45^{\circ}\text{C}$. It has been suggested by Logan et al (2000) and Sasaki et al (2007) it is due to damage to plant enzymes that lead to the production of isoprene. It is possible that extreme temperatures could cause damage to the plant through a reduction in substrate supply and degradation to the synthase enzyme expression, thus causing irreversible damage to the plant at a cellular level. As isoprene synthase is inherently bound to the chloroplast, extreme temperatures above the plants tolerance threshold could lead to enzyme degradation and then cell damage.

The thermotolerance hypothesis could therefore be used to interpret the large increases in isoprene emission as a function of dry leaf weight. The 82.7% increase relative to the control in figure 2.11 shows that the effect upon leaves from elevated temperature is far greater than seen in figure 2.12. It is therefore possible that isoprene in willow is being produced as a defence against cell damage by heat.

It has also been hypothesised by Logan et al (2000) that due to the complexity of biochemistry within the chloroplast, there could be other explanations for the increase in isoprene emissions at elevated temperatures. The 2-C-methyl-D-erythritol 4-phosphate/1-deoxy-D-xyulose 5-phosphate pathway (MEP/DOXP pathway) that produces isoprene in the chloroplast is integrated with a number of other biosynthetic

pathways that regulate plant secondary metabolism through the allocation of carbon via the shikimate pathway and the Calvin cycle. Logan et al (2000) have therefore suggested that the production and emission of carbon-rich isoprene could be a way of maintaining the pools of carbon within the plant for other intermediates of different pathways and therefore isoprene could also be a metabolic regulator for plants.

2.7.2 The effect of elevated CO₂ concentration on woody plant isoprene emissions

The reduction of isoprene emissions in plants subject to elevated CO₂ (figure 2.13) is expected given the current observations in the literature. The results of the meta-analysis (figure 2.4) demonstrate the response of isoprene in the models to difference concentrations of CO₂. Results of global isoprene emissions from models including MEGAN and BVOC-EM, and studies by Centritto et al (2004), Possell et al (2005), and Scholefield et al (2004) have demonstrated a decrease in isoprene emissions as a response to elevated CO₂. More recently, it has been suggested that isoprene emissions are ultimately regulated by the amount of adenosine triphosphate (ATP) that is available rather than through photosynthesis (Rasulov et al., 2016). At elevated CO₂ the electron transport rate of the plant is inhibited in the chloroplast via a number of pathways and therefore isoprene production is suppressed through changes in reductant level (Li & Sharkey, 2013; Rosenstiel et al., 2003; Wilkinson et al., 2009). This is surprising as an increase in CO₂ would provide more carbon to the “fertilisation effect” that enhances photosynthesis and plant productivity (Heald et al., 2009; Körner, 2000). Overall, although there is a consensus that increases in CO₂ lead to an inhibition of isoprene, the mechanisms behind the change are still unknown at the metabolic level and therefore require further interrogation.

2.7.3 *The effect of the interaction between temperature and CO₂ on woody plant isoprene emissions*

It is clear that there are a number of uncertainties associated with the effects of temperature and increased CO₂ concentrations upon isoprene biochemistry. Therefore there is still uncertainty regarding the interactive effects of both upon isoprene production and emission.

The results of the air entrainment experiment to measure isoprene emissions from willow in figure 2.10 have shown that there is a slight reduction in isoprene emission (relative to the control) and would appear that the two environmental parameters mitigate the effects of each other. This small decrease is surprising, as the results from the meta-analysis suggest that even slight changes to the concentration of CO₂ and would lead to isoprene suppression, even with increasing temperatures (figure 2.5). However, from a biochemical perspective, if the plant has more available substrate for energy production, and the biosynthesis of isoprene requires large quantities of carbon, then one would expect to see an increase in emissions. Monson et al (2016) have found that there is an interaction between elevated CO₂ and increased temperatures in oak trees. They have concluded in their study that “*at high CO₂ isoprene emission was still sensitive to temperature, but at high temperature the rate of isoprene emission became insensitive to CO₂*”. The results of this study show that the reduction in isoprene emissions that is seen in the elevated CO₂ treatment is offset by the increase in isoprene emissions as a function of elevated temperature.

The mechanisms behind the apparent 'cancelling out' of the effects of the two stresses is poorly understood and will require further interrogation at the cellular level. Particularly, in relation to the Monson et al (2016) study, we need to address the trade-

off between the sensitivity of each environmental parameter to the other. Detailed analysis of the metabolic regulatory networks that underpin isoprene (and other BVOC) regulation in plants is necessary to attempt to answer the question of energy allocation. Metabolomic profiling provides the necessary information to begin to resolve the regulation of isoprene biosynthesis at the cellular scale and is discussed in detail in chapter 3.

2.8 Conclusion

The results of the meta-analysis and subsequent entrainment experiment demonstrate the need for a greater understanding of the variability in the magnitude of isoprene emissions as a result of the effects of increases in both temperature and CO₂. It is imperative to interrogate the biochemical mechanisms that are responsible for the production and suppression of isoprene as a response to abiotic stresses in order to reconcile the driving parameters of global emission models in the future. The aim of the next chapter will be to investigate the responses of willow plants to abiotic stresses at the cellular level through a metabolic profiling experiment.

Chapter 3: The Biochemical Responses of Plant Metabolism to Extreme Temperature and CO₂ in Relation to Leaf Age.

3.1 Introduction

Understanding the biological controls on plant secondary metabolism in relation to the changing climate is imperative in order to make predictions about potential responses of global vegetation to future climate change. Environmental stress factors such as increasing global temperature, along with an increasing atmospheric CO₂ concentration have an impact upon both plant physiology and phytochemistry (Ahuja et al., 2010). The interaction of these climatic components, and their feedback upon the biosphere are often complex, and non-linear as has been demonstrated in chapter 2. Therefore a more holistic approach is required in order to interrogate the individual components, and their interactions with each other within a complex biological system.

Plant responses to environmental stresses are dynamic and complex (Cramer et al., 2011). The increase in atmospheric CO₂ concentration from 280ppm to just over 400ppm currently has exerted a positive feedback upon average global temperatures leading to a warming of approximately 1°C from preindustrial (PI) times. Although the relationship between an increase in CO₂ and an increase in temperature is logarithmic, the resulting increases of average global temperature from increasing CO₂ will have a significant impact upon global vegetation. The Intergovernmental Panel on Climate Change (IPCC) (2007, 2013) have predicted through a range of best- and worst-case climate scenarios that global temperatures will exceed 1.5°C by the year 2100 from PI times, and that at the current rate of anthropogenic activity, atmospheric CO₂ concentrations could potentially increase up to 800ppm. It is also predicted that extreme weather events, such as floods, droughts and periods of extreme temperature will also increase in frequency as a result of CO₂-induced climate change.

Abiotic stresses (as stated above), such as extreme temperature, as well as environmental factors such as increased CO₂ concentrations, are known to induce dramatic changes in plant secondary metabolism (Edreva et al., 2008; Loreto & Schnitzler, 2010; Ramakrishna & Ravishankar, 2011) and have an effect upon isoprene production as previously discussed in chapters 1 and 2. While CO₂ is considered as a resource (as elevated CO₂ has been shown to increase biomass production and photosynthetic efficiency) (Kainulainen et al. 1998; Mattson et al. 2005; Veteli et al. 2007), CO₂ can also be considered as a stress, with very high concentrations causing dramatic, negative effects on plant physiology (Levine et al., 2008). However, the effect of elevated temperature upon carbon partitioning and plant development is less clear (Paajanen et al. 2011; Veteli et al. 2007) in relation to changes in secondary metabolism as a response to stress.

It is well established that extreme temperatures over 40°C over a long time period (days) can induce leaf senescence (Ahuja et al., 2010; Ramakrishna & Ravishankar, 2011). An increase in temperature will increase the rate of biochemical reactions and thus have an effect upon plant growth and development as resources are allocated to counteract physiological stress (Guy et al., 2008; Ramakrishna & Ravishankar, 2011; Veteli et al. 2007), particularly when these stresses occur at critical developmental stages (Yu et al. 2014). The biochemical response of the plant to acute heat stress at temperatures exceeding those where normal photosynthetic function occurs (>28°C) (Li & Sharkey, 2013) without inducing leaf senescence can be seen when extreme temperature is applied for a short time period experimentally.

One specific example of how phytochemistry responds dramatically to heat lies with the production of biological volatile organic compounds (BVOCs) by some plants, which is enhanced by environmental stress as BVOCs can directly interact with the atmosphere to regulate local climate (see chapter 1, section 1.2.3). It has been

proposed that isoprene emitting plants are generally fast growing, woody plants (e.g. *Salix*) that are not subject to long periods of abiotic stresses such as temperature (Dani et al. 2014; Loreto & Fineschi, 2015). However, in times of increased stress, and especially short-lived extreme temperature fluctuations, the isoprene emission rate can increase to ~50% of carbon that has been fixed by photosynthesis in leaves, and can sometimes exceed the carbon intake of the plant and therefore the rate of isoprene emission decouples from the prevailing rate of photosynthesis (Brilli et al. 2007; Loreto & Fineschi, 2015; Velikova, 2008). Moreover, it has been observed that this decoupling occurs but with no apparent damage to the plants photosystem (Sharkey, 2005). As demonstrated in figure 1.8 in chapter 1, isoprene emission increases exponentially until around 40°C when emissions sharply decline in many plant species (Velikova, 2008). It can then be postulated that there is some benefit to the plant in allocating carbon resources to the production and emission of this hydrocarbon and thus, that isoprene emission has evolved as an advantageous trait for thermotolerance (Peñuelas et al., 2005; Singaas et al., 1997; Sasaki et al., 2007; Velikova & Loreto, 2005). Given the relative energetic costs of producing BVOCs, any up regulation in the biosynthesis of isoprene will undoubtedly restructure plant carbon partitioning with likely knock on effects for secondary metabolism not associated with BVOC synthesis as carbon/energy becomes limiting. It is then an intriguing question as to whether heat shock-induced shifts in plant metabolism are mitigated under the increased carbon fixation conditions that are associated with elevated CO₂. It is therefore necessary to not only assess the responses of plants to abiotic stresses independently, but also as an interactive, dynamic process. In line with these predictions, my empirical measurements of isoprene emission by willow (*Salix spp.*) in Chapter 2 revealed a 24% reduction in isoprene production under elevated CO₂ (at 800 ppm) and a 7% increase in isoprene production as a result of heat shock at 40°C relative to controls (section 2.3.2.3, figure 2.13). The

interactive effects of heat shock and elevated CO₂ however led to a 9.6% reduction in isoprene production, relative to the control. This result is surprising as both elevated CO₂ and extreme temperature have almost cancelled out the effects of each other (with an overall reduction of 7.4% as an interaction relative to the control compared to the independent effects of both). This result therefore suggests that the increase in energy through CO₂ fertilisation is somehow mitigating the dramatic effect upon the allocation of resources to BVOC synthesis that extreme heat has on the plant metabolome. Therefore, if there is available substrate, the assimilated carbon is being allocated to other pathways other than isoprene production. In order to reconcile this result and inform subsequent predictive models for isoprene emission and its subsequent effects on climate, it is essential that we resolve the biochemical mechanisms underpinning these dramatic shifts in isoprene production.

A holistic understanding of interacting effects on plant biochemistry can be achieved through the application of modern metabolomics technologies, which can be defined as “*The systematic study of the unique chemical fingerprints that specific cellular processes leave behind.*” (Daviss, 2005). Through the analysis of plant metabolic profiles, it is possible to not only empirically measure the biochemical changes within a specific plant, but to also determine the relationship of the changes as a systems response to external stresses (Roessner & Bowne, 2009).

This study then examines the interaction of both elevated temperature (heat shock) and CO₂ concentration on the regulation of plant secondary metabolism through an untargeted fingerprint analysis of stress-induced secondary metabolites. Specifically, it can be hypothesised that:

- 1) The effect of short-term increases in temperature will have a detrimental impact upon plant growth and development;

2) That the energetic costs of BVOC biosynthesis under heat shock conditions will restructure plant secondary metabolism and;

3) That elevated CO₂ will reduce the extent to which the plant reorganises its secondary metabolism under heat stress.

3.2 Materials and Methods

3.2.1 Experiment set up and plant growth

Willow cuttings of the short rotation coppice hybrid “Terra Nova” (‘LA940140’ x *Salix miyabeana*) (Lindgaard, 2012) were rooted in pots and were filled with John Innes No. 3 potting compost. The cuttings were grown for 10 weeks in a controlled environment chamber (see Table 3.1 for environmental parameters) to allow for stems and leaves to establish until the temperature and CO₂ treatments were applied.

Table 3.1: Environmental parameters and time periods for willow growth in controlled environment chamber.

Environmental Parameter	Parameter Values	Time Period
Temperature (day)	20°C	8 hours
Temperature (night)	15°C	16 hours
CO₂	Ambient (~400ppm)	constant
Light	800μmol	8 hours
Humidity	67%	constant

Following the 10 week growth period, 4 plants were selected at random to be moved into the experimental chamber to acclimate for 2 weeks prior to the application of the temperature and CO₂ treatments (see section 2.5.1 for a full description of the experimental set up).

3.2.2 Elevated temperature and CO₂ treatment application

The biochemical analysis using untargeted metabolomics was subject to the same temperature and CO₂ treatments (control, elevated CO₂ (eCO₂), heat shocked (Hs), and elevated CO₂ and heat shocked (Hs*eCO₂)) that have been described in chapter 2 and have been outlined for reference in table 3.2 (see section 2.5.2 for a full description of the experimental set up).

Table 3.2: Environmental parameters and time periods for treatment application in controlled environment chamber.

Treatment	Parameter Values		Time Period	
	Temperature	CO ₂	Temperature	CO ₂
Hs*CO ₂	40°C	800ppm	1 photoperiod	constant
eCO ₂	20 °C	800ppm	1 photoperiod	constant
Hs	40°C	Ambient (~400ppm)	1 photoperiod	constant
Control	20 °C	Ambient (~400ppm)	1 photoperiod	constant

3.2.3 Leaf harvest

Representative young and old leaves were collected at the end of the experimental chamber photoperiod on day 4 during treatment week 3. Following the collection of the Poropak tubes for BVOC entrainment (see section 2.4.3-2.4.4.4 for a full description of BVOC entrainment collection) the plants were cut at the point on the stem where the polyethylene terephthalate entrainment bag had been attached. The

plants were stored at -80°C in preparation for freeze drying for leaf area and biomass measurements.

3.2.3.1 *Young leaves*

From each of the 4 plants, a young leaf (the first fully expanded leaf immediately adjacent to the shoot apical meristem) was selected. The young leaves were detached using a scalpel and a 1.5cm sample was cut from the leaf apex. The young leaf samples for each biological replicate (4) of each of the 4 treatments were then flash frozen in liquid nitrogen and were stored at -80°C and subsequently freeze dried ready in preparation for metabolite extraction.

3.2.3.2 *Mature leaves*

From each of the 4 plants a mature leaf that had been enclosed in the polyethylene terephthalate bag was selected. The mature leaves were detached using a sample and a 1cm diameter leaf disc was cut from the lamina. The old leaf for each biological replicate (4) of each of the 4 treatments samples were then flash frozen in liquid nitrogen and were stored at -80°C and subsequently freeze dried ready in preparation for metabolite extraction.

3.2.4 *Plant biomass and leaf surface area*

Leaf surface area measurements for all plants were calculated using a LI-COR LI-3000C portable leaf area meter. For each leaf the area (cm²) was calculated three times and an average was taken (see section 2.2.2.6 for a full description of leaf area calculations and section 2.3.2.5 for the statistical results). The separated leaves and the

stems of all replicates were freeze-dried and then weighed (g) in order to calculate the above ground plant biomass (see section 2.3.2.2 for the statistical results).

3.2.5 *Leaf metabolite extraction*

Plant metabolites for both young and old leaves were extracted using a standard biphasic chloroform/methanol/water extraction (Overly et al., 2005). 2mg of dried leaf sample were ground to a powder using a ball mill and 20µl of MeOH/CHCl₃/H₂O mixture (2:5:1, v/v/v) pre-chilled to -20°C for 15 minutes. The 32 sample tubes were then mixed for 10 seconds using a vortex mixer and were stored on ice for 5 minutes. The samples were mixed again and centrifuged at 14,000 rpm at 4°C for 2 minutes and the resulting supernatants were transferred into a new Eppendorf tubes which were pre-chilled to -20°C. The leaf tissue pellets were re-extracted with 10µl of pre-chilled (-20°C) MeOH/CHCl₃ (1:1, v/v) and were vortexed for 10 seconds. The samples were then stored on ice for 10 minutes. The samples were then spun in a centrifuge (14,000 rpm, 2 minutes, 4°C) and the supernatants were added to the first set of supernatants. The chloroform (organic) phase was separated from the aqueous phase by adding 4µl of chilled and distilled H₂O and 20µl of CHCl₃. To obtain the 2 clear phases (aqueous and organic) the samples were spun in a centrifuge (14,000 rpm, 15 minutes, 4°C). The organic and aqueous phases were then separated into separate tubes and spun again in a centrifuge (14,000 rpm, 2 minutes, 4°C) to ensure good separation of both phases. The samples were then transferred into new tubes and were stored at -80°C ready for analysis.

3.2.6 Matrix-Assisted Laser Desorption/Ionisation Mass Spectrometry Analysis (MALDI-MS) of leaf metabolites

Both aqueous and organic layers of the metabolite extracts were first diluted 1:10 with pure methanol. The polar phases of the metabolite extracts were then analysed on a Waters MALDI Synapt G2-MS in both positive and negative ionisation modes. *Alpha*-Cyano-4-hydroxycinnamic acid (5mg/ml) was used as the matrix in positive mode, as it allows the sample to be readily ionised through the donation of a proton. 9-Aminoacridine (5mg/ml) was used as the matrix in negative mode as it allows the sample to be readily ionised through the loss of a proton. A 2µl volume of the sample/matrix mix was pipetted onto a 96-well target plate and allowed to crystallise. Samples were ionised using an orthogonal MALDI ion source with the laser deployed in a spiral pattern on each spot for one minute. Each sample was analysed in triplicate. Both positive and negative ionisation modes were run using the same method as shown in table 3.3 with nitrogen as the carrier gas.

Table 3.3: MALDI Synapt-G2 method set up for metabolite extraction analysis.

Instrument Parameter	Value
Capillary (kV)	3.00
Sampling Cone (kV)	40
Extraction Cone (kV)	5.00
Source Temperature (°C)	80
Desolvation Gas (L/h)	500
Mass Range (Da)	50-1200
Scan Time (sec)	1.00

3.2.7 Data processing and statistical analysis

Analysis of the effect on above ground biomass in relation to the effects of elevated temperature and CO₂ treatments were conducted using a two-way ANOVA using the statistical software Minitab® version 17 (Minitab Inc., 2010).

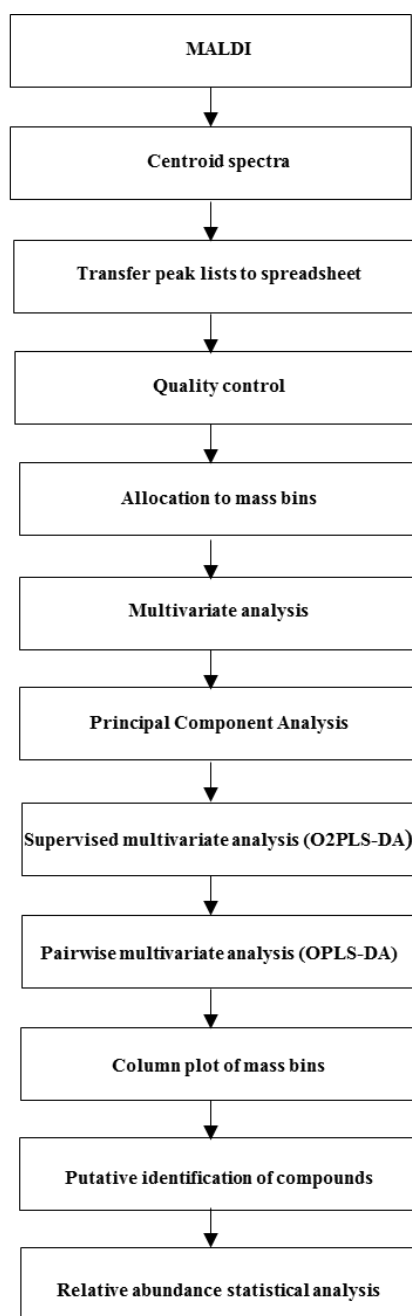


Figure 3.1: Flow chart to demonstrate the step-by-step process of data processing and statistical analysis of plant metabolites.

Figure 3.1 is a flow chart to demonstrate the step-by-step process of processing the raw metabolomics data and subsequent statistical analyses. These processes are described in detail in this section.

The metabolite extract spectral data were centroided and converted into text files to be transferred to a Microsoft Excel spreadsheet using an in-house Visual Basic macro. The conversion of the centroided spectra data to text files was necessary for quality control due to the large amount of data generated. The triplicate runs of each sample were combined to calculate their mean mass to form the metabolite profile for each sample (Overy et al., 2005). The calculation of the masses and the total ion counts (TIC (given as a percentage)) for each replicate were as a result of the following equations:

$$ES+, y < 0.00003x + 0.0033$$

$$ES-, y < 0.00003x + 0.0044 \text{ (Overy et al., 2005)}$$

Where y is the standard deviation and x denotes the mean (of the 3 replicate sample spots (Overy et al., 2005)). This process takes out the most likely false positives and negatives from the full raw data set of TIC by setting a minimum acceptance level for the peak to be included. In order for large quantities of masses to be identified and compared, the data were grouped in mass bins (atomic mass unit) to allow for multivariate analysis of a large data set. Issues in the allocation of mass bins to the correct bin grouping between the two ionisation modes has meant that the data from the negative ionisation mode have been grouped at 0.4 Da, and 0.2 Da for positive ionisation mode data.

Principal Component Analysis (PCA) using the SIMCA (Umetrics) statistical package was conducted to visualise any differences in the metabolite data as an effect of the different temperature and CO₂ treatments. Statistical analyses were conducted on the ion counts of new and old leaf samples in order to calculate the fold changes in identified compounds relative to treatment. PCA is a useful unsupervised, analytical tool as it demonstrates variation within a dataset whilst reducing the dimensionality of

the data (Jandrić et al., 2015; Ringñer, 2008). Through the use of fewer components, it is possible to represent samples with fewer values, thus allowing for samples to be visually represented in order to determine whether there is variation (Ringñer, 2008). As separation was observed between treatments in both positive and negative ionisation modes, it was possible to conduct further multivariate and linear statistical analyses.

Supervised, multivariate analysis was conducted using both orthogonal partial least squares discriminant analysis (OPLS-DA) and O2PLS-DA (which contains an extra component that allows to complete 3 and 4 way analysis) to look at the underlying drivers of variation in metabolite fingerprints between treatments. Through the addition of supervised predicted components, it was possible to complete both pair-wise comparisons (OPLS-DA) and four-way comparisons (O2PLS-DA) of the metabolite samples in relation to treatment.

Mass bins that explained the most variance between treatments following pairwise OPLS-DA interrogation were then displayed in an observation and loadings plot to rank them in order of the proportion of the total variance they explained. The top ranked mass bins for both the aqueous and organic phases in both ionisation modes were then selected to conduct putative compound identification of metabolites. For the purposes of checking the allocation of masses to their correct mass bins, and the corresponding total ion counts in the excel spreadsheet, it was necessary to identify the metabolite masses within each ranked mass bin using MassLynx™ version 41 (Waters). The peak spectra for the mass bin range were centroided in order to establish the detected mass for each biological replicate. It was then possible to compare the spectra to the spreadsheet data to ensure that it had been binned correctly. It was found that for negative mode, it was appropriate to allocate masses to within 0.4 Da, and in positive mode masses were allocated to 0.2 Da. The masses identified within the spectra and the text files with the most intense peaks could then be putatively identified. As no

biological replicates were found to be outliers during the multivariate analysis (no samples can be seen to fall outside of the 95% confidence range of the normal T-squared distribution for multivariate analysis), the detected masses were averaged for the replicates of new, old, and total leaf samples. A table was compiled using online metabolite databases to putatively identify the detected masses for each bin. Accurate (monoisotopic) masses were identified through the Metlin database (Scripps) and Kegg (Pathway Database) through the addition or loss of adduct ions which are detailed in table 3.4. The putatively identified compounds were selected if their error margin of the m/z values were below 40 ppm.

Table 3.4: List of ion adducts used to distinguish accurate masses for both positive and negative ionisation modes.

Mode	Ion Adduct
Positive	+H
	+Na
	+K
Negative	-H

A 2-way ANOVA statistical analysis was used to determine whether either the temperature and/or CO₂ treatments had a significant effect upon the percentage ion counts of the top 10 mass bins for each ionisation mode and metabolite extraction layers. Percentage differences were calculated between new, old and all leaves in relation to the effects of each treatment.

3.3 Results

3.3.1 *Unsupervised analysis of metabolic fingerprints by Principal Component Analysis*

The PCA plots for the metabolite profiles of the aqueous and organic layers in both positive and negative ionisation modes for old and new leaves (see methods for definitions) were considered together to reveal a separation between the control (ambient temperature and ambient CO₂) and other treatments (Hs, eCO₂, and Hs*CO₂) (Figure 3.2a). In negative ionisation mode, there is also some separation in multivariate space between plants exposed to ambient CO₂ compared to eCO₂ treated plants at 20°C. Interestingly, when leaf age is taken into account (figures 3.2b (new leaves) and 3.2c (old leaves)) it is clear that differences in the treatments versus the control as a result of the CO₂ treatment are more pronounced in old leaves as opposed to new leaves. No such separation of eCO₂ old leaves from eCO₂ new leaves was observed when the extracts were analysed in positive ionisation mode. Together, these data strongly imply that abiotic conditions (temperature and CO₂) interact to define the composition of the plant metabolome.

In figures 3.2 and 3.3 there are a small number of biological replicates that can be seen to fall outside of the 95% confidence range of the normal T-squared distribution for multivariate analysis, denoted by the ellipse in the plots. However, interrogation of the raw data in both the mass spectra and the loading plots for each layer and ionisation modes provides no clear explanation that would justify the exclusion of these data from the analysis. This is indicative of variation between the biological replicates of their respective treatments, which is to be expected when conducting experiments on vegetation. At this stage of unsupervised multivariate analysis, the separation of the control from the other three treatments validates the justification of further, supervised interrogation of the data to assess the potential for differences between the effects of

temperature and CO₂ concentrations on the plant metabolome using orthogonal partial least-square discrimination analyses (OPLS-DA and O2PLS-DA).

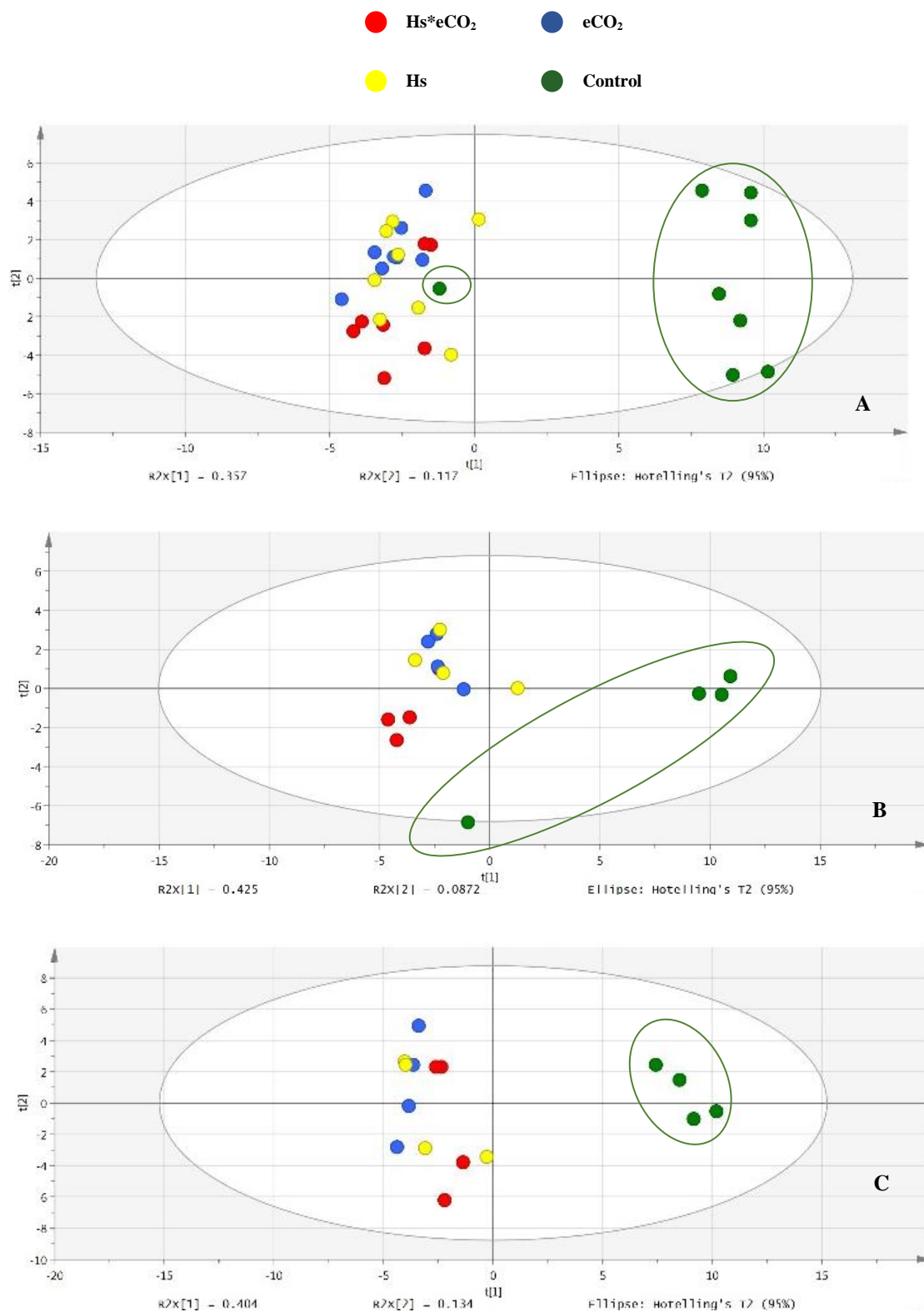


Figure 3.2: Principal Component Analysis plots of the metabolite profiles of young and old leaf samples between the control treatment and temperature and CO₂ treatments. Metabolite profiles of the aqueous layer were analysed in negative ionisation mode. A: All leaves, B: New leaves, C: Old leaves. In each plot the control has been highlighted.

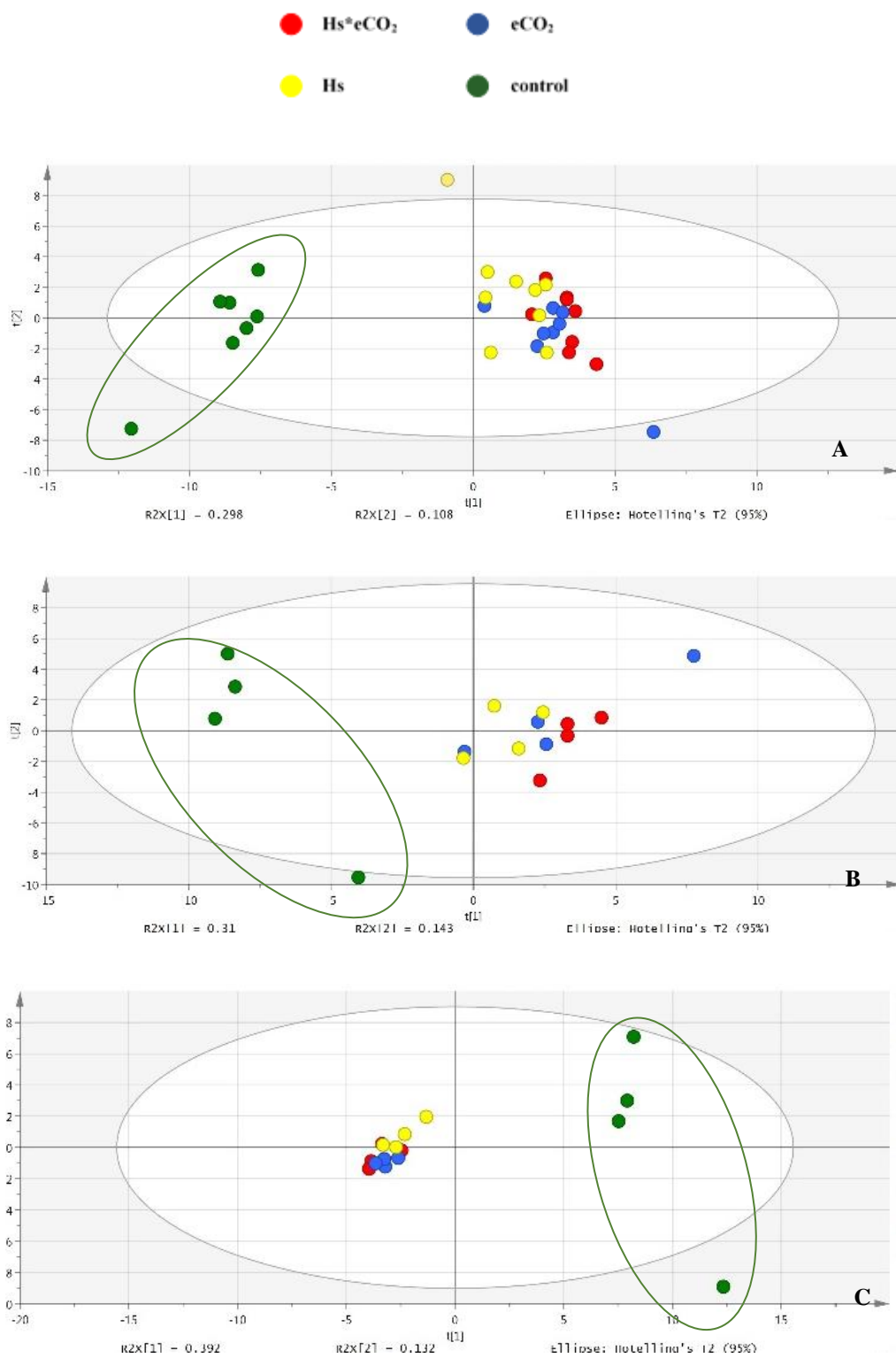


Figure 3.3: Principal Component Analysis plots of metabolite profiles of young and old leaf samples between the control treatment and temperature and CO_2 treatments. Metabolite profiles of the organic layer were analysed in negative ionisation mode. A: All leaves, B: New leaves, C: Old leaves. In each plot the control has been highlighted.

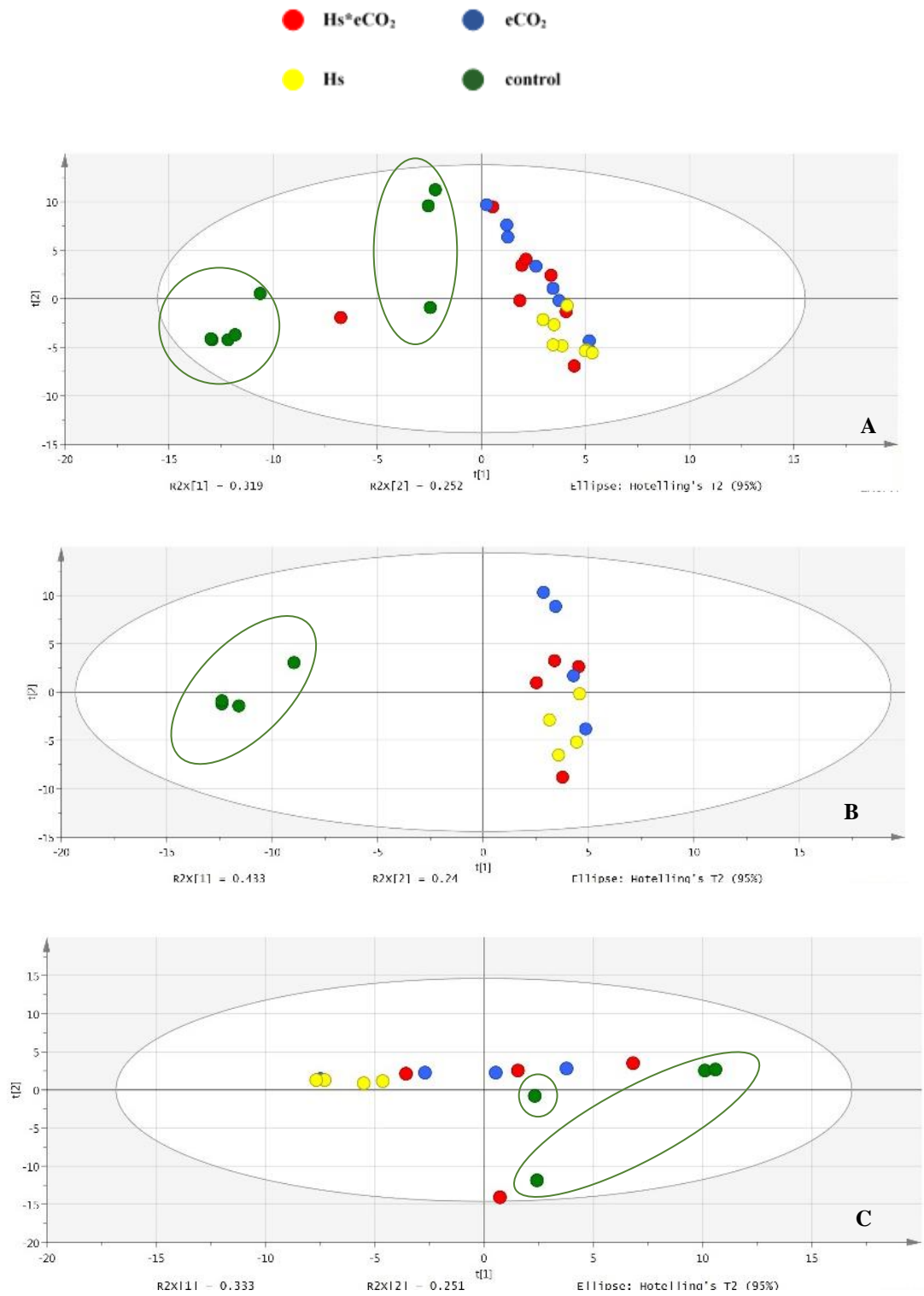


Figure 3.4: Principal Component Analysis plots of metabolite profiles of young and old leaf samples between the control treatment and temperature and CO₂ treatments. Metabolite profiles of the aqueous layer were analysed in positive ionisation mode. A: All leaves, B: New leaves, C: Old leaves. In each plot the control has been highlighted.

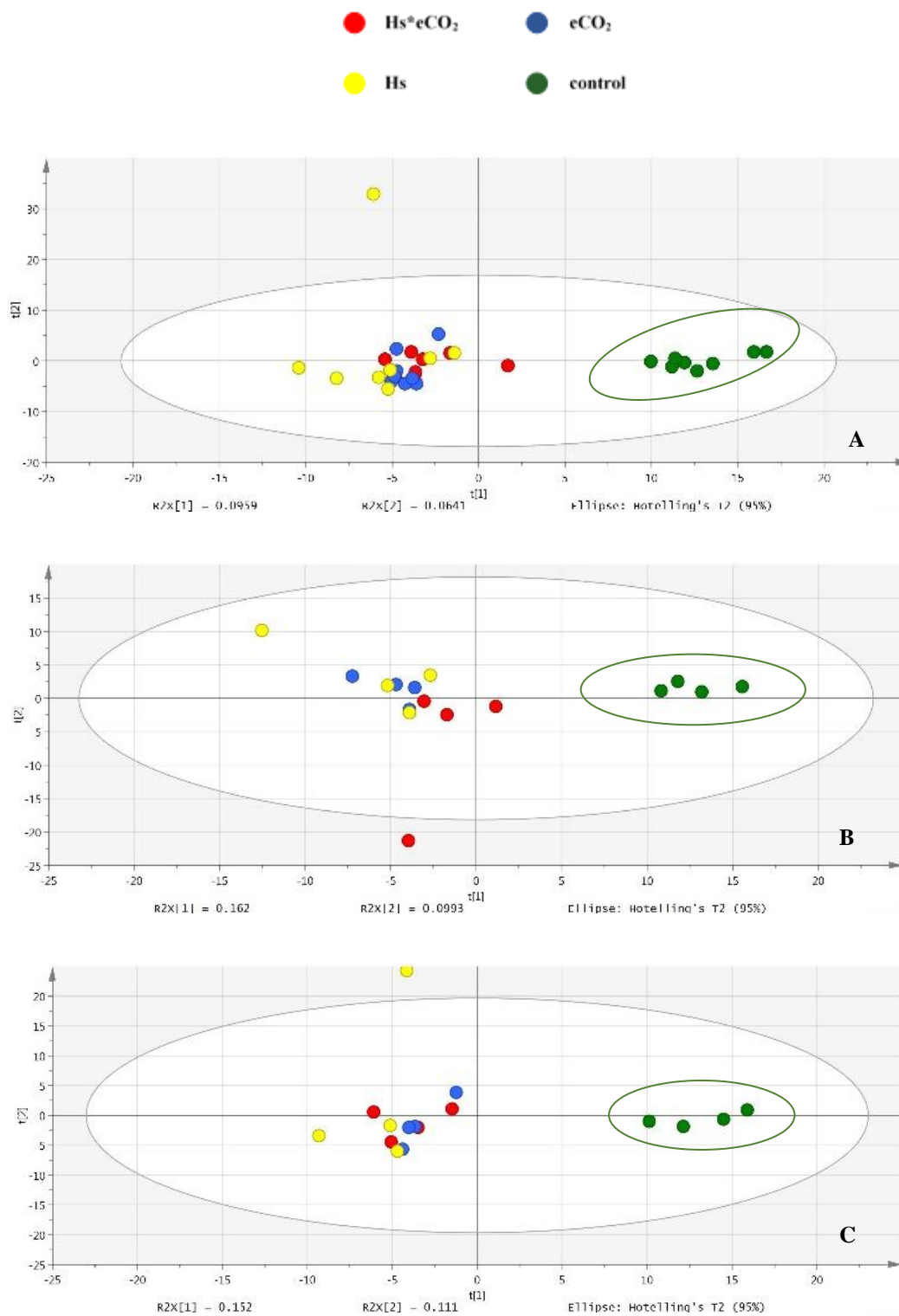


Figure 3.5: Principal Component Analysis plots of metabolite profiles of young and old leaf samples between the control treatment and temperature and CO₂ treatments. Metabolite profiles of the organic layer in positive ionisation mode. A: All leaves, B: New leaves, C: Old leaves. In each plot the control has been highlighted.

3.3.2 *Supervised multivariate analysis of metabolites fingerprints by Orthogonal Partial Least Squares Discriminant Analysis (O2PLS-DA)*

At this stage of unsupervised multivariate analysis, the separation of the control from the other three treatments validates the justification of further, supervised interrogation of the data to assess the potential for difference between the effects of temperature and CO₂ concentrations on the plant metabolome using the discriminant analyses OPLS-DA and O2PLS-DA. Metabolic fingerprints for all treatments (analysed in positive and negative ionisation mode) were subjected to a supervised four way O2PLS-DA multivariate analysis (Figs. 3.6-3.9). The substantial separation between the control and the other treatments is again evident, as it was in the PCA plots. The variation between the biological replicates of the control (with the exception of figure 3.8a, all leaves) is far less than in comparison to the variation that was observed in the PCA plots. The grouping of treatments Hs*eCO₂, eCO₂, and Hs overall is clearer than the unsupervised analyses across all leaves, and young and old leaves (Figs. 3.6a, 3.6b, and 3.6c respectively). Figures 3.6 and 3.9 demonstrate this separation and grouping of the treatments in all three statistical plots. The outlier outside of the 95% confidence range in figure 3.7 (all leaves) has been included as the separation of the samples by leaf age has reconciled the variance between the biological replicates. The response of different leaf ages to changes to the plant metabolome can also be observed, particularly in figures 3.6b and c, 3.7b and c, and 3.9b and c.

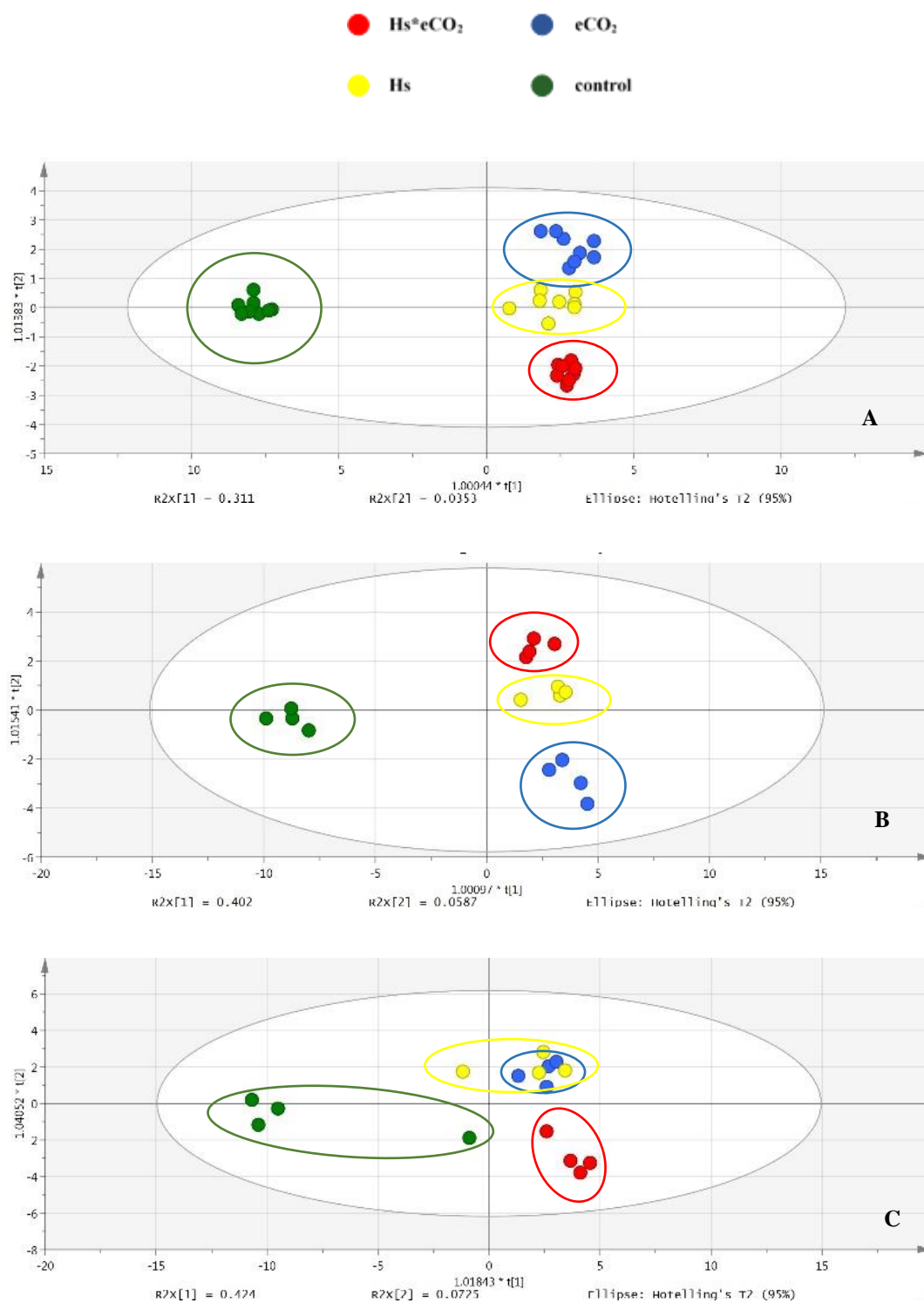


Figure 3.6: Supervised multivariate O2PLS-DA plots of metabolite profiles of young and old leaf samples between the control treatment and temperature and CO₂ treatments. Metabolite profiles of the aqueous layer were analysed in negative ionisation mode. A: All leaves, B: New leaves, C: Old leaves. In each plot the separation between treatments has been highlighted.

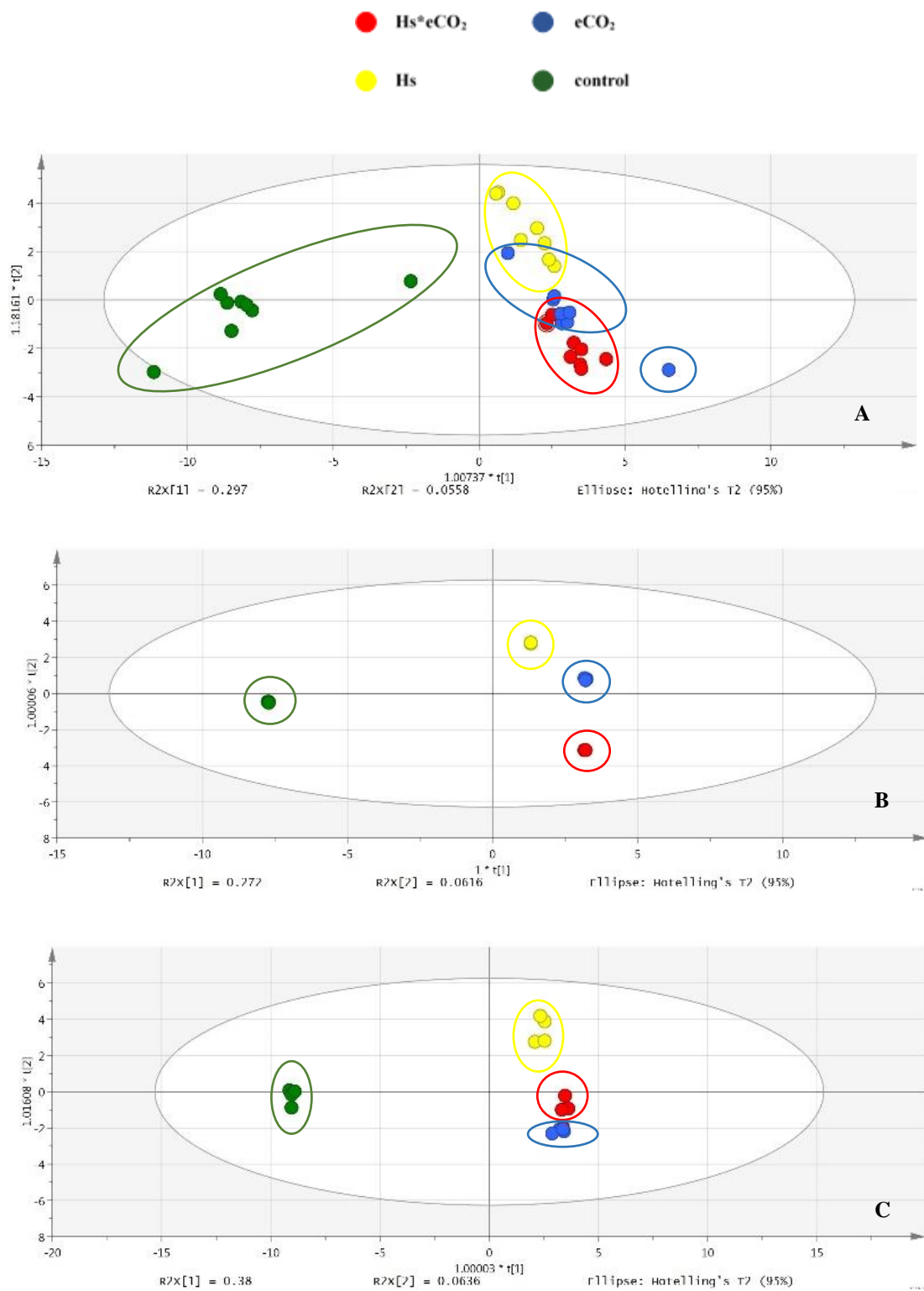


Figure 3.7: Supervised multivariate O2PLS-DA plots of metabolite profiles of young and old leaf samples between the control treatment and temperature and CO₂ treatments. Metabolite profiles of the organic layer were analysed in negative ionisation mode. A: All leaves, B: New leaves, C: Old leaves. In each plot the separation between treatments has been highlighted.

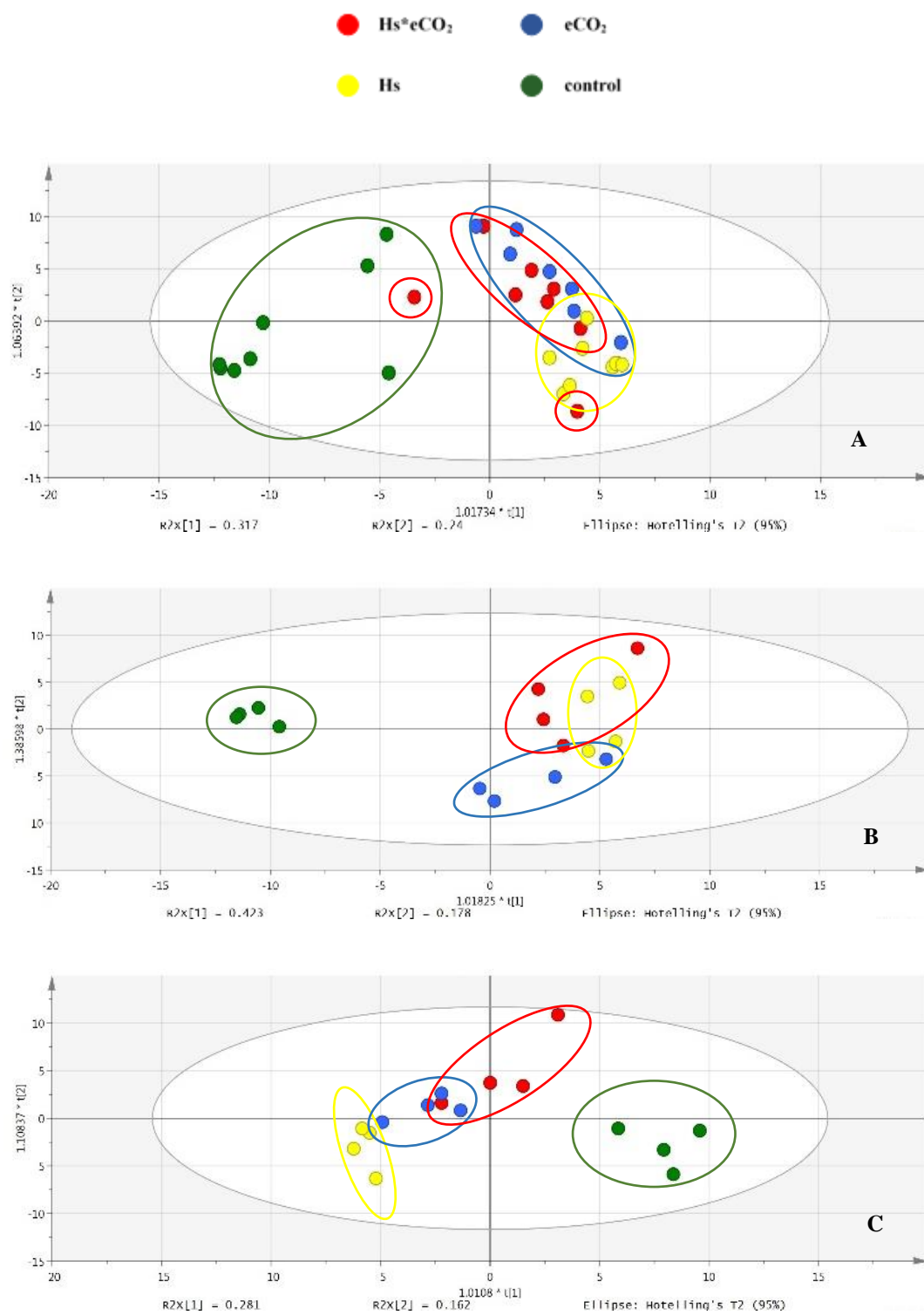


Figure 3.8: Supervised multivariate O2PLS-DA plots of metabolite profiles of young and old leaf samples between the control treatment and temperature and CO₂ treatments. Metabolite profiles of the aqueous layer were analysed in positive ionisation mode. A: All leaves, B: New leaves, C: Old leaves. In each plot the separation between treatments has been highlighted.

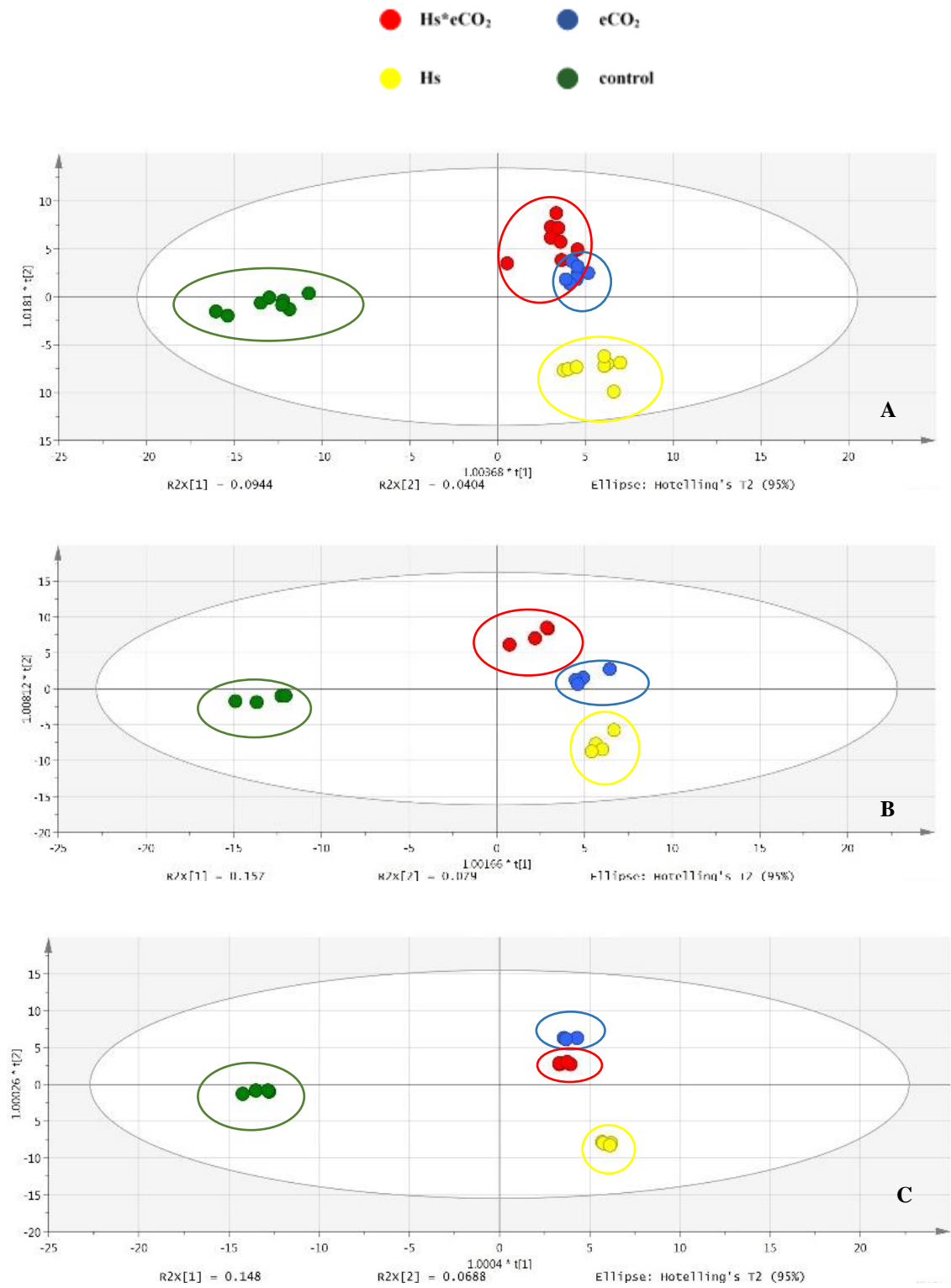


Figure 3.9: Supervised multivariate O2PLS-DA plots of metabolite profiles of young and old leaf samples between the control treatment and temperature and CO₂ treatments. Metabolite profiles of the organic layer were analysed in positive ionisation mode. A: All leaves, B: New leaves, C: Old leaves. In each plot the separation between treatments has been highlighted.

3.3.3 Supervised multivariate analysis pair-wise comparisons of metabolite fingerprints using Orthogonal Partial Least Squares Discriminant Analysis (OPLS-DA)

Supervised multivariate analysis of all treatments versus the control treatment have demonstrated a separation of treatments in multivariate space that is clearer than in the unsupervised multivariate analyses. The separation of the control from the other three treatments, and the separation of the three treatments from each other validates the justification for further interrogation of the data. In order to evaluate the effects of temperature and CO₂ concentrations on the plant metabolome, it was necessary to conduct pairwise analyses on treatments using orthogonal partial least square discrimination analysis (OPLS-DA) to compare the treatments against one another to look at separation in multivariate space to assess potential differences. Table 3.5 shows the combination of analyses for all treatments, with increasing complexity in the interrogation of the effects of temperature and/or CO₂ concentrations for aqueous layer samples run in negative ionisation mode. The results of the four pairwise comparisons are displayed in figures 3.10-3.13.

Table 3.5: Table of the pairwise comparisons of treatments to show the effect of temperature and CO₂ as independent and combined environmental parameters

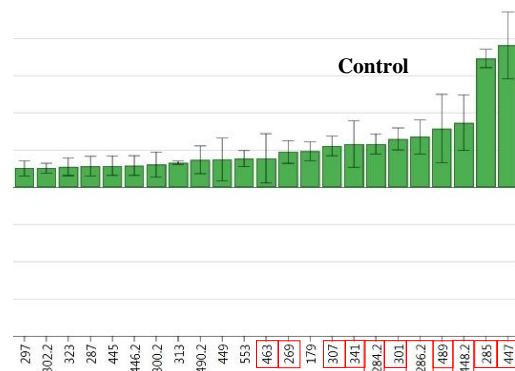
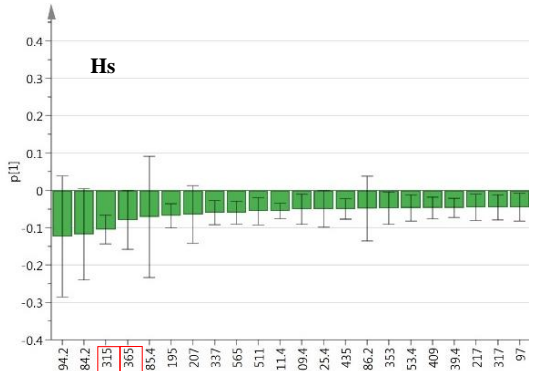
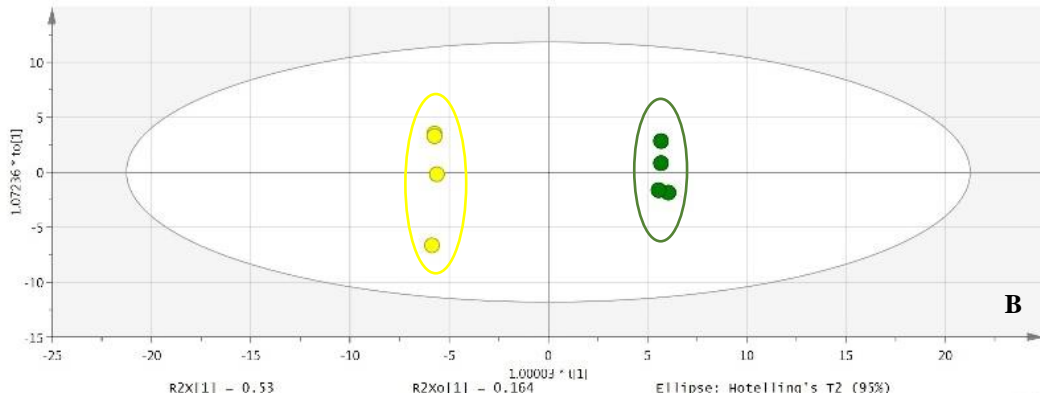
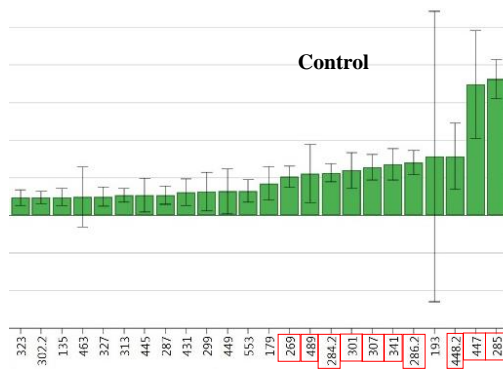
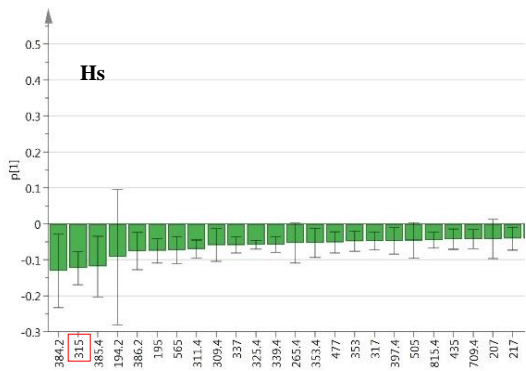
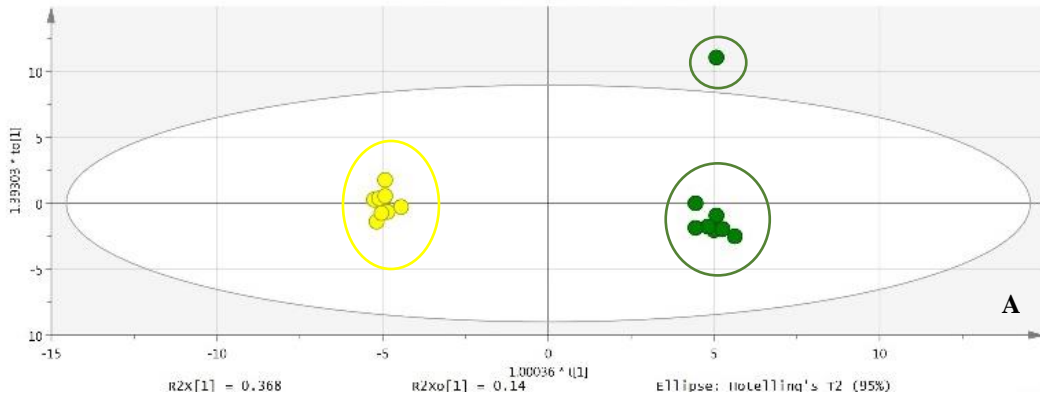
Treatment	Treatment parameters	Comparison
Hs vs control	400ppm/40°C vs 400ppm/20°C	Effect of temperature vs control
eCO ₂ vs control	800ppm/20°C vs 400ppm/20°C	Effect of CO ₂ vs control
Hs*eCO ₂ vs eCO ₂	800ppm/40°C vs 800ppm/20°C	Effect of temperature at elevated CO ₂
Hs*eCO ₂ vs Hs	800ppm/40°C vs 400ppm/40°C	Effect of CO ₂ at extreme temperature

Increasing complexity of statistical interrogation of treatments

The aqueous layer in negative ionisation mode has been chosen to demonstrate the pairwise separation between the four treatments as an example that is representative of both organic and aqueous layers and both ionisation modes. All other pairwise comparisons of the OPLS-DA statistical plots can be found in figures A3.1-A3.12 in the appendix.

As was found in the four way supervised O2PLS-DA plots, a biological replicate of the control treatment falls outside the 95% confidence range in figures 3.10 and 3.11. However, the variation between the biological replicates for the control with the exception of this one replicate are far less than exhibited in the unsupervised multivariate analysis. Figures 3.10 and 3.11 demonstrate that there is a substantial separation between Hs, eCO₂, and the control respectively in the pairwise comparisons as demonstrated previously in both the PCA and O2PLS-DA plots. The response of different leaf ages in relation to changes to the plant metabolome can also be observed in figures 3.10b and c, and 3.11b and c.

● Hs ● Control



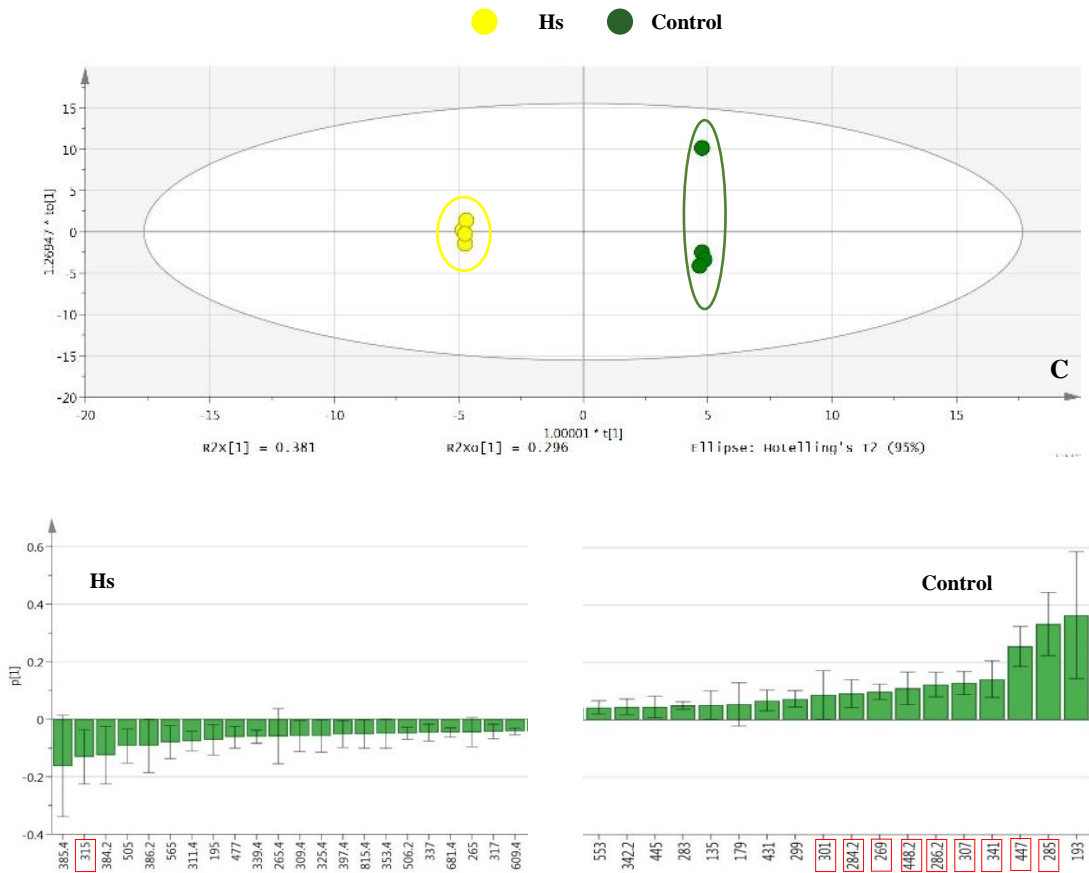
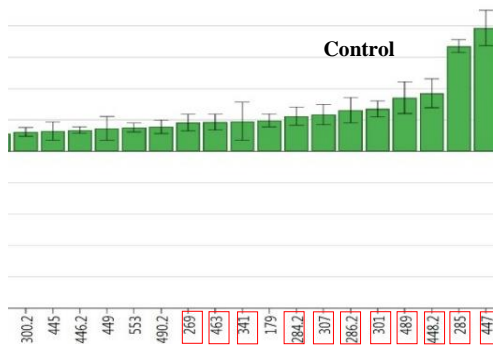
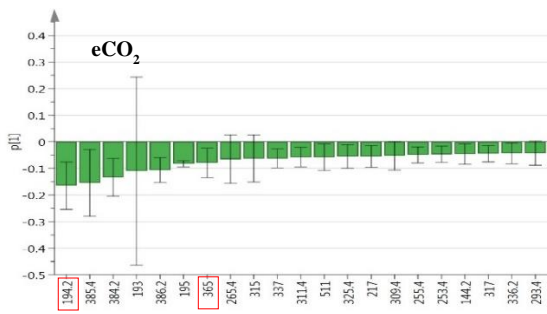
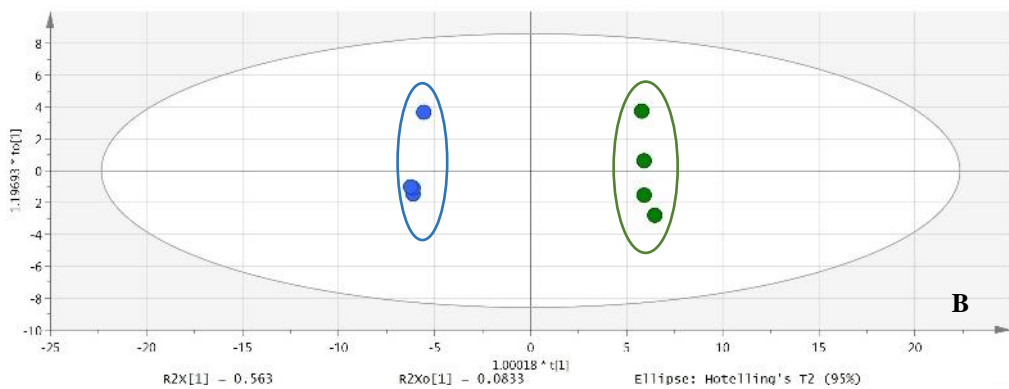
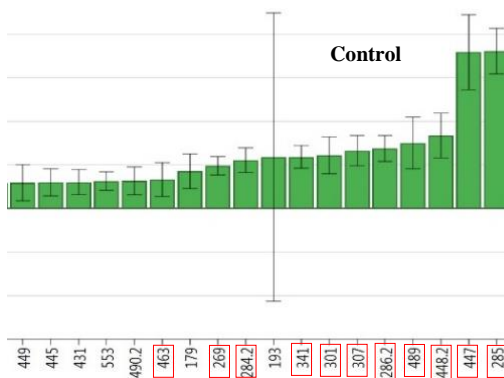
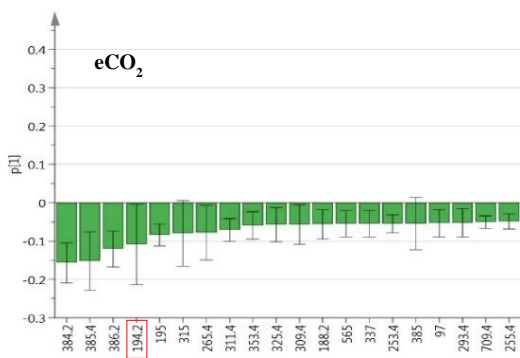
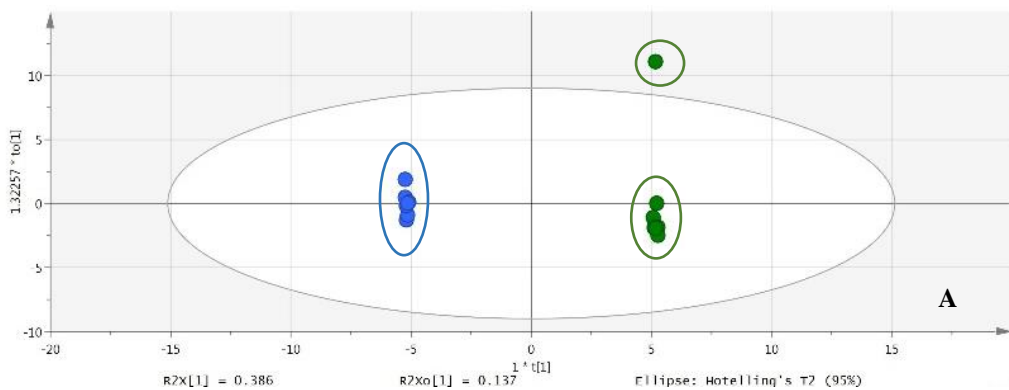


Figure 3.10: Supervised multivariate OPLS-DA plots of pair-wise comparisons of the metabolite profiles of treatments Hs & control. Metabolite profiles of the aqueous layer were analysed in negative ionisation mode. A: All leaves, B: New leaves, C: Old leaves. The corresponding loadings plots underneath each OPLS-DA plot demonstrate the discriminant mass bins (highlighted in red) associated with each treatment in the pair-wise comparison for all, new, and old leaves.

● eCO₂ ● Control



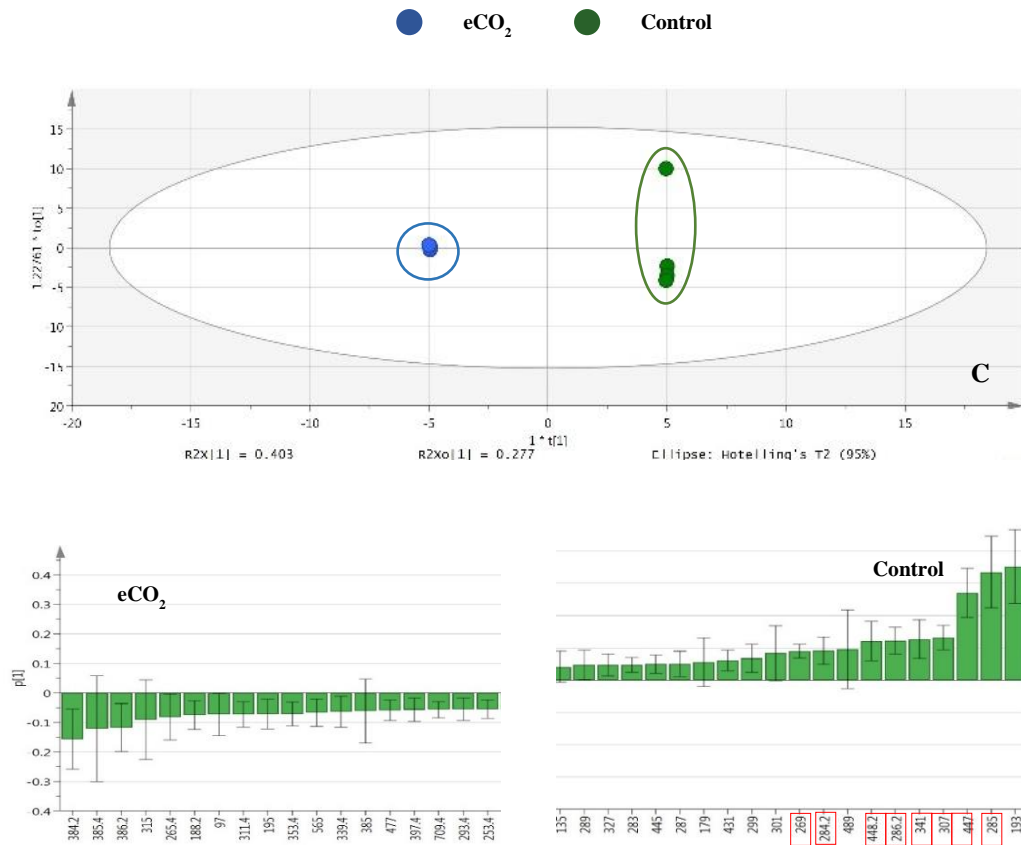
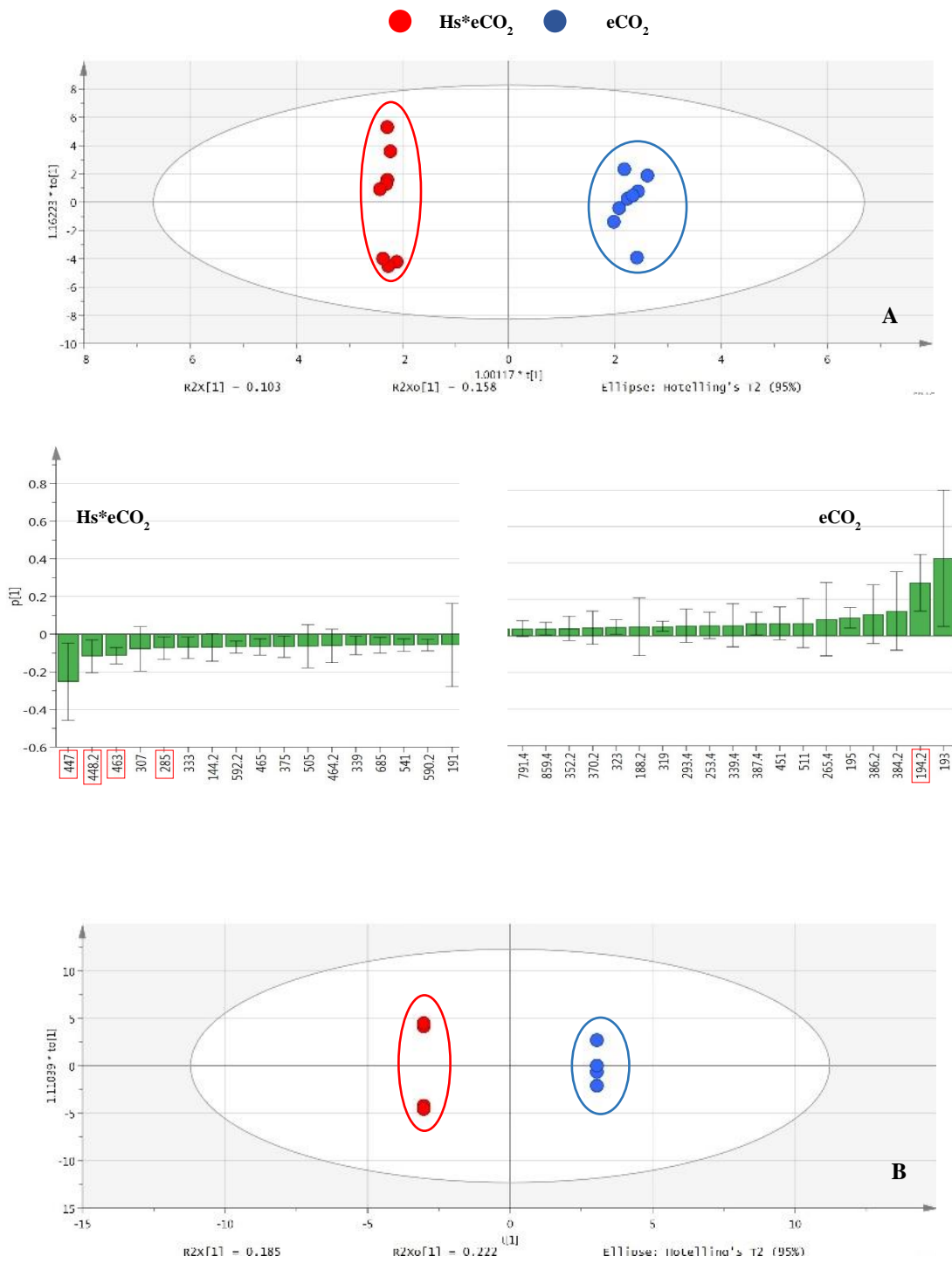


Figure 3.11: Supervised multivariate OPLS-DA plots of the pair-wise comparisons of the metabolite profiles of treatments eCO_2 & control. Metabolite profiles of the aqueous layer were analysed in negative ionisation mode. A: All leaves, B: New leaves, C: Old leaves. The corresponding loadings plots underneath each OPLS-DA plot demonstrate the discriminant mass bins (highlighted in red) associated with each treatment in the pair-wise comparison for all, new, and old leaves.

Figures 3.12 and 3.13 denote the increasing complexity of multivariate interrogation between Hs^*eCO_2 and eCO_2 , and Hs^*eCO_2 vs Hs respectively. The variation of biological replicates in multivariate space for each of the treatments is greater than in the previous pairwise comparisons. This is to be expected as the interactions of the abiotic stresses will subject a change to the plant metabolome that is different to the effect of the stresses independently of one another. The observation of changes to the metabolome are less clear than in the previous pairwise comparisons,

which is unsurprising given that an increase in CO₂ concentration and extreme temperature exert competing effects upon plant growth.



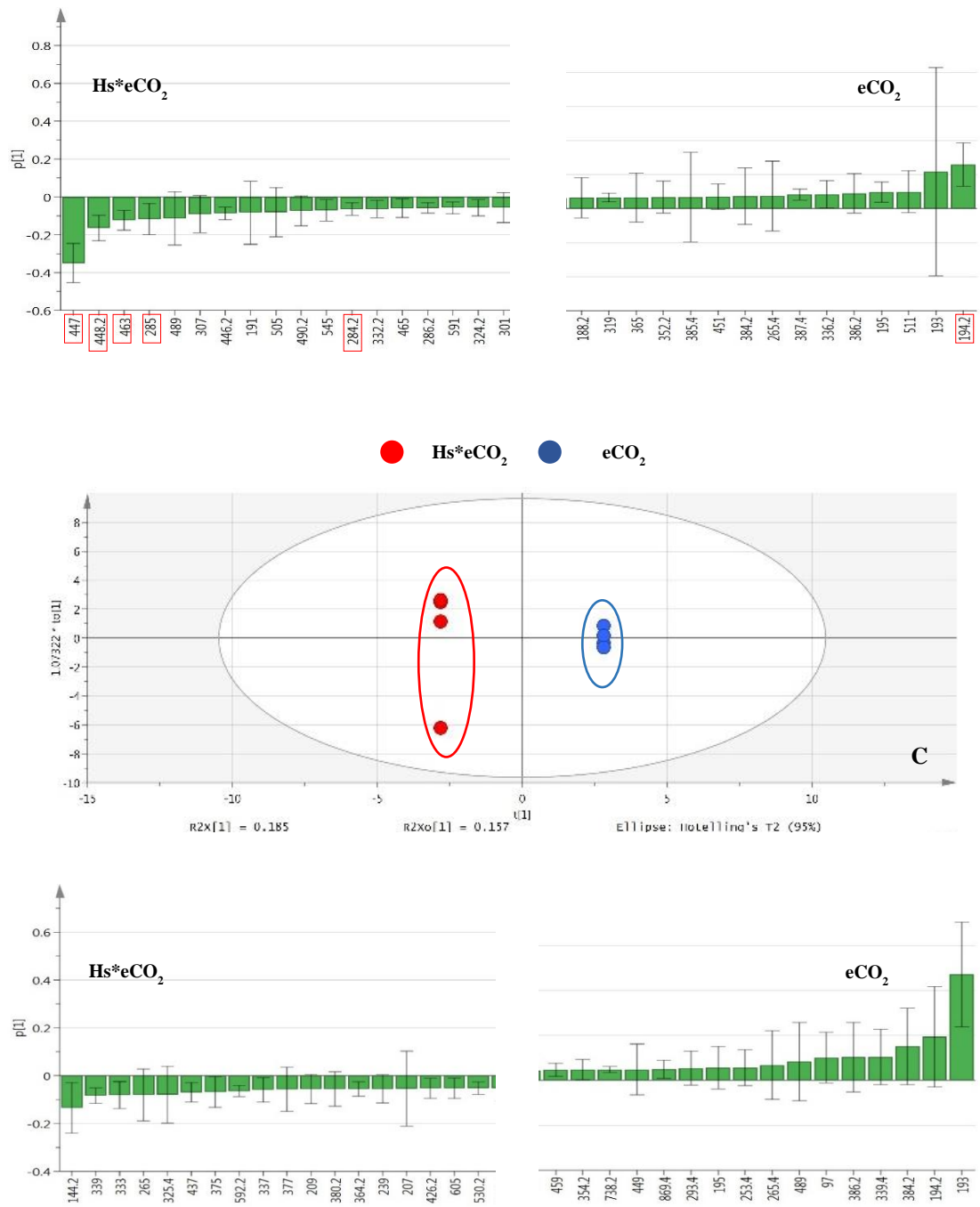
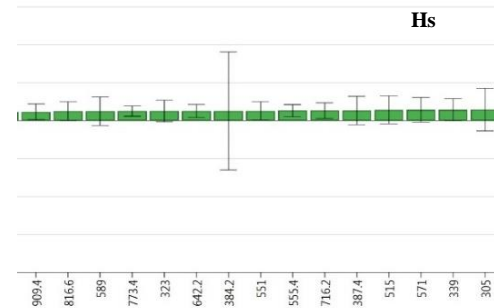
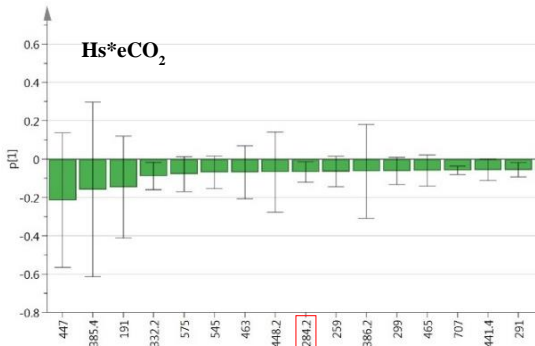
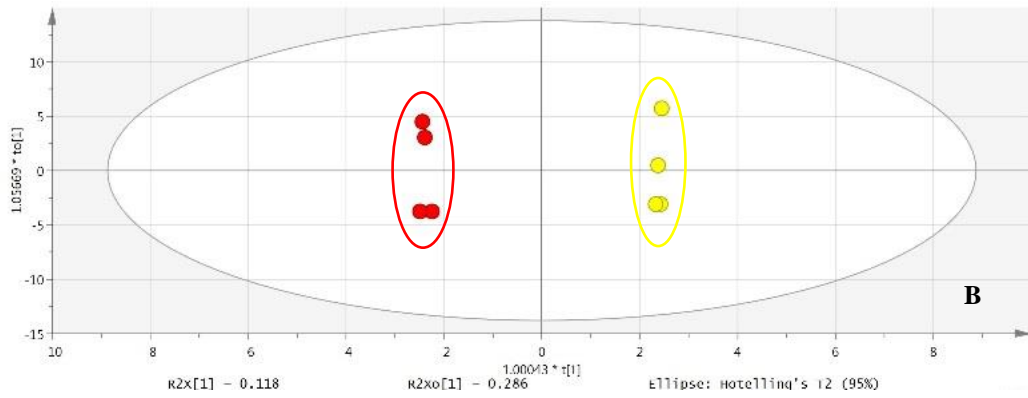
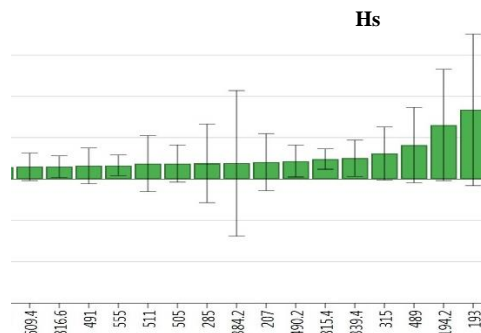
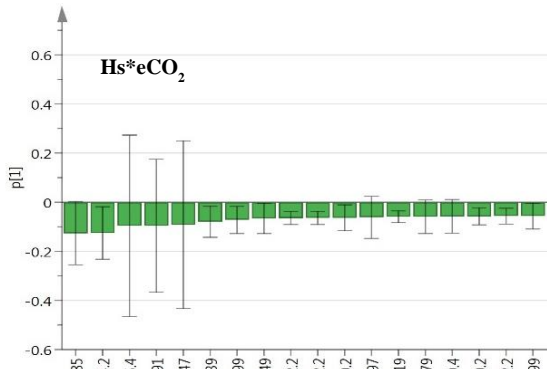
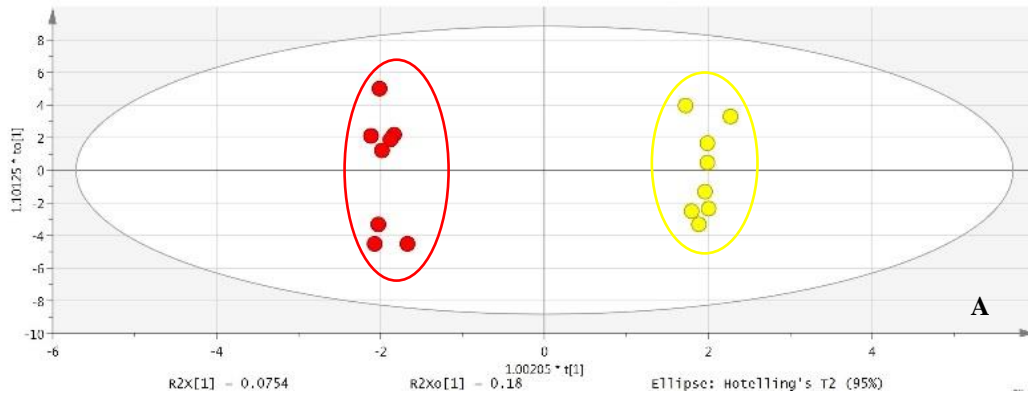


Figure 3.12: Supervised multivariate OPLS-DA plots of the pair-wise comparisons of the metabolite profiles of treatments Hs*eCO₂ & eCO₂. Metabolite profiles of the aqueous layer were analysed in negative ionisation mode. A: All leaves, B: New leaves, C: Old leaves. The corresponding loadings plots underneath each OPLS-DA plot demonstrate the discriminant mass bins (highlighted in red) associated with each treatment in the pair-wise comparison for all, new, and old leaves.

● Hs*eCO₂ ● Hs



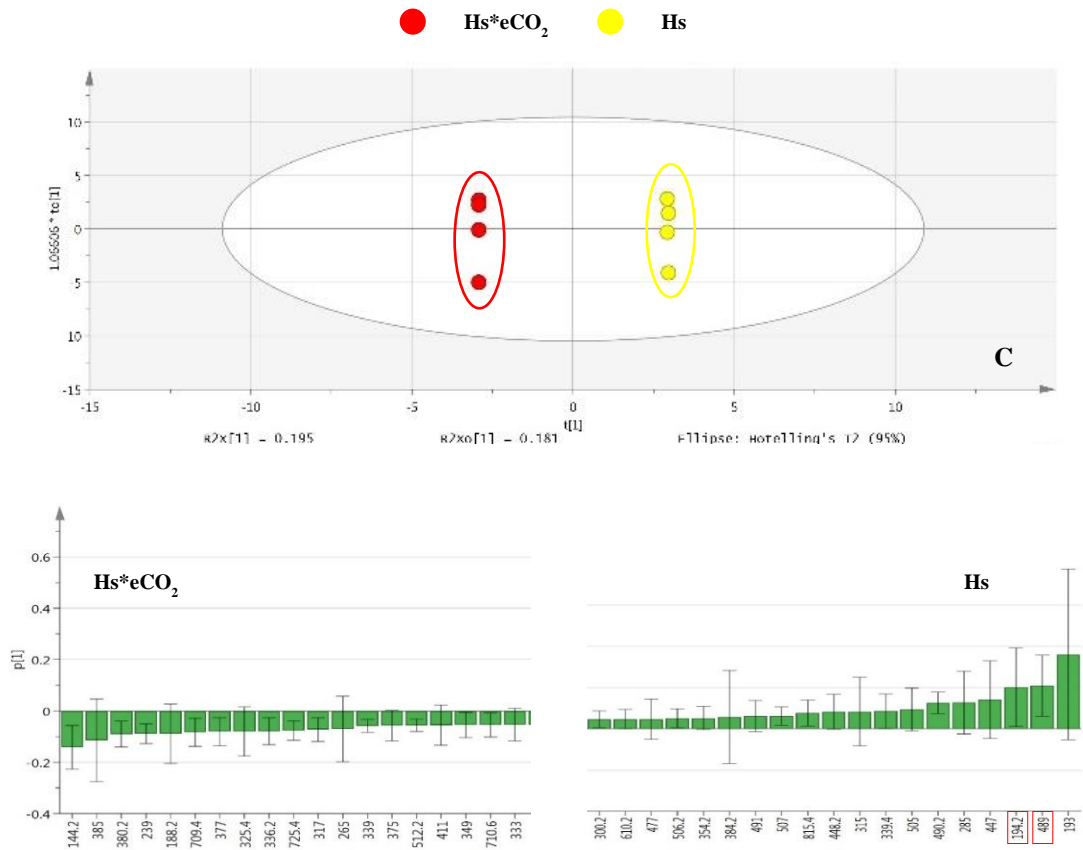


Figure 3.13: Supervised multivariate OPLS-DA plots of the pair-wise comparisons of the metabolite profiles of treatments Hs*CO₂ & Hs. Metabolite profiles of the aqueous layer were analysed in negative ionisation mode. A: All leaves, B: New leaves, C: Old leaves. The corresponding loadings plots underneath each OPLS-DA plot demonstrate the discriminant mass bins (highlighted in red) associated with each treatment in the pair-wise comparison for all, new, and old leaves.

3.3.4 Identification of metabolic fingerprints

For each layer and ionisation mode, the top mass bins (m/z) that were shown by the statistical analyses in the pairwise comparison to be responsible for the separation between treatments in the metabolomic fingerprints were selected. Within each bin, several masses were detected and putatively identified. For several bins, more than one compound was identified and assigned due to the difference in the monoisotopic masses of compounds being smaller than the binning size (0.4Da for negative mode and 0.2Da for positive mode). Table 3.6 demonstrates an overview of the mass bins and their corresponding detected masses that were putatively identified for the aqueous layer in negative mode. Tables A3.1-3.4 in the appendix show the comprehensive tables of putatively identified compounds for the mass bins from the aqueous positive mode, and both organic negative and positive modes. A larger number of discriminating mass bins were found in negative ionisation mode. The most frequently represented chemical groups were flavones, glucosides, flavonoids, and phenylpropanoids. These chemical groups suggest that the metabolic pathways that potentially have been affected by the extreme temperature and elevated CO₂ concentration treatments were the pathway responsible for flavonoid biosynthesis, including the phenylpropanoid, anthocyanin and flavone/flavonol pathways.

Table 3.6: Discriminant mass bins and their associated detected and accurate masses. The putatively identified compounds, their chemical groups, and the associated pathways are displayed. An error in parts per million is included to show the putative compounds' variation from the detected mass (aqueous layer analysed in negative ESI mode).

Bin	Detected Mass	Standard error	Accurate Mass	Δ ppm	Name	Chemical Formula	Chemical group	Pathway
194.2	194.1057	0.000718505	195.1137	39	6-hydroxypseudooxynicotine	C ₁₀ H ₁₅ N ₂ O ₂	Ketone	Nicotinate metabolism
	194.1051	0.000619476	195.1131					
	194.1060	0.000826419	195.1140					
	194.1048	0.000830944	195.1128					
	194.1059	0.000935665	195.1139					
	194.1105	0.001394184	195.113	30	Glucosaminic acid D-Glucose oxime	C ₆ H ₁₃ NO ₆	Glucosinolate	Pentose Phosphate
	194.0729	0.000439282	195.0809					
194.0766	0.002208223	195.0846	2	2-(3-pyridyl)-Benzimidazole	C ₁₂ H ₉ N ₃	Indole	Tryptophan metabolism	
			29	Damascenone	C ₁₀ H ₁₃ NO ₃	Ketone	Shikimate biosynthesis	
269	269.0861	0.000526189	270.094	15	Isomedicarpin Strobopinin Vignafuran	C ₁₆ H ₁₄ O ₄	Flavonoid Flavonone Flavonoid	Flavonoid biosynthesis
	269.0844	0.006887069	270.0924	9				
	269.0864	0.001046049	270.0943	16				
	269.0894	0.002254163	270.0974	7	Apigenin Demethyltexasin	C ₁₅ H ₁₀ O ₅	Flavone Flavonoid Flavonoid	
	269.0799	0.0054946	270.0878					
	269.0879	0.00065228	270.0959	22				
	269.0356	0.000204252	270.0436	36	Sulfuretin			
	269.0359	0.000403113	270.0439	35				
284.2	284.0745	0.000207289	285.0824	11	Buchananine	C ₁₂ H ₁₅ NO ₇	Alkaloid	Pyridine alkaloid biosynthesis
	284.0736	0.00062149	285.0816	13				
	284.0776	0.002355446	285.0856	0				
	284.0745	0.000178536	285.0824	11				
	284.0736	0.000585769	285.0815	14				
	284.0748	0.000693722	285.0828	9				
	284.0224	0.00030078	285.0304					
	284.0228	0.000633813	285.0307					

Table 3.6: Continued

285	285.0826	0.000174553	286.0905	20	Gummiferol Carajuron (-)-Nissolin Kushenin Nissicarpin Calythropsin	C ₁₅ H ₁₀ O ₆	Flavonoid Anthocyanin Flavonoid Isoflavonoid Flavonoid Chalcone Flavone Flavonol Anthocyanin Flavonol Isoflavone Flavone	Flavonoid biosynthesis
	285.0824	0.000477461	286.0903					
	285.0829	0.000201556	286.0908					
	285.0831	0.000151554	286.091					
	285.0829	0.000188331	286.0909					
	285.0826	0.000108253	286.0906					
	285.0404	0.001483661	286.0484					
285.0365	0.002904845	286.0445	14					
286.2	286.0862	0.000296595	287.0942	24	Volkenin Tetraphyllin B Rutaecarpine	C ₁₂ H ₁₇ NO ₇	Glucoside Glycosyl Alkaloid	Anthocyanin biosynthesis Glycogen synthesis Tryptophan metabolism
	286.0865	0.000427931	287.0945	20				
	286.0873	0.000403887	287.0953	19				
	286.0876	0.000204252	287.0956	25				
	286.0860	0.000477624	287.0940	24				
	286.0862	3.53553E-05	287.0942					
	286.0347	0.000422788	287.0427					
286.0352	0.001036445	287.0432						
301	301.0786	0.000408312	302.0866	22	Haematoxylin Hesperetin Homoeriodictyol	C ₁₆ H ₁₄ O ₆	Phenol Flavonone Flavonone	Flavonoid biosynthesis
	301.0766	0.000136931	302.0846	14				
	301.0784	0.000127475	302.0864	22				
	301.0792	0.000143069	302.0872	15				
	301.0764	0.000178098	302.0844	2				
	301.0781	0.000303109	302.0861	33	Quercetin Morin Delphinidin Isoetin Herbacetin	C ₁₅ H ₁₀ O ₇	Flavonol Flavonol Anthocyanin Flavone Flavonol	
	301.0253	0.000482668	302.0333	34				
	301.0250	0.000764853	302.0330					

Table 3.6: Continued

307	307.1258	0.000408312	308.1338	32	Glutathione Allamandin	C ₁₀ H ₁₆ N ₃ O ₆ S ₁ C ₁₅ H ₁₆ O ₇	Thiol Terpenoid	Glutathione biosynthesis Terpenoid biosynthesis
	307.1259	0.000136931	308.1339					
	307.1267	0.000127475	308.1347					
	307.1268	0.000143069	308.1347					
	307.1268	0.000178098	308.1347					
	307.1261	0.000303109	308.1342					
	307.0724	0.000482668	308.0804					
	307.0721	0.000764853	308.0801					
315	315.0129	0.000225	316.0209	2	Lettowianthine	C ₁₉ H ₁₁ NO ₄	Alkaloid	Alkaloid biosynthesis
	315.0126	0	316.0209					
	314.9351	0.022553641	315.9431					
	314.9869	0.043206756	315.9431					
	314.9351	0.022618093	315.9431					
	314.9087	7.5E-05	315.9166					
	315.0544	0.003970103	316.0624					
	314.9989	0.036619539	316.0068					
341	341.1546	0.000207289	342.1626	11 26 18 35 28 16 33	(±)-pavine Magnoflorine	C ₂₀ H ₂₄ N ₁ O ₄	Alkaloid Alkaloid	Isoquinoline alkaloid biosynthesis Isoquinoline alkaloid biosynthesis
	341.1558	0.000583631	342.16375					
	341.1557	0.000219018	342.1637					
	341.1556	0.000143614	342.1635					
	341.1586	0.002112019	342.1665					
	341.1539	0.001644118	342.1618					
	341.0968	0.000429207	342.1047					
	341.0976	0.001096586	342.1056					
					Glucocaffeic acid	C ₁₅ H ₁₈ O ₉ C ₁₉ H ₁₈ O ₆ C ₁₂ H ₂₂ O ₁₁	Glycoside Carbonyl Carbohydrate	Maltose degradation
					Dulxanthone A			
					Maltose			

Table 3.6: Continued

365	365.1033	6.49519E-05	366.1113	0	Derrubone Glycyrol Glycyrrhizaisoflavone B Wampetin Salicin 6-phosphate Arnottin II	C ₂₁ H ₁₈ O ₆	Isoflavone Glycerin Isoflavone Furocoumarin Glycoside Benzofuran	Flavonoid biosynthesis Galactose metabolism Flavonoid biosynthesis Phenylpropanoid metabolism Glycolysis / Gluconeogenesis/Phosphotransferase system (PTS) Phenylpropanoid metabolism	
	365.1031	0.000358818	366.1111						
	365.1039	0.000296595	366.1119						
	365.1038	0.000387903	366.1118						
	365.1035	0.000389511	366.1115						
	365.1034	0.000134048	366.1114						
	365.054	0.006458328	366.062						28
365.060	0.009780433	366.0682	34						
385	385.19665	0.001184536	386.2046	4	Pterxyin Isosamidin Samidin Peucenidin	C ₂₁ H ₂₂ O ₇	Phenylpropanoid	Shikimate pathway	
	385.19575	0.000490376	386.2035						
	385.19725	0.000493077	386.2052						
	385.196625	0.000450521	386.2046						
	385.196625	0.000865574	386.2046						
	385.19495	0.00071807	386.2029						
	385.131225	0.000362931	386.1392						
385.131025	0.000483962	386.139	4						
447	447.1484	0.000365718	448.1564	39	Dichotosin kaempferol Astragalin Quercetin Oroboside Isoorientin Orientin Luteolin Scutellarein Fisetin Herbacetin Carthamone Maritimein Naringenin	C ₂₃ H ₂₈ O ₉	Glucosyloxy flavan Glucoside Glucoside Glycoside Glycoside Glucoside Flavone Flavone Flavone Glucoside Flavonoid Chalcone Phenol Flavonone	Flavonoid biosynthesis	
	447.1476	0.000296859	448.1555						
	447.1482	0.000174553	448.1562						
	447.1486	0.000250936	448.1566						
	447.1487	0.000856866	448.1567						
	447.1479	0.000304908	448.1559						
	447.0956	0.000343466	448.1036						
	447.0869	0.004589186	448.0949						
									5
									14

Table 3.6: Continued

448.2	448.15062	0.000134048	449.1586					
	448.1504	0.000262202	449.1584					
	448.1511	0.000201556	449.159					
	448.1509	0.000262202	449.1589					
	448.1508	0.000243349	449.1588					
	448.1503	5.44862E-05	449.1582					
	448.0901	0.003807127	449.0981	28	Glucosquerellin Cyanidin 7-glucoside	C ₁₄ H ₂₇ NO ₉ S ₃ C ₂₁ H ₂₁ O ₁₁	Glucosinolate Flavonoid	Glucosinolate biosynthesis Anthocyanin biosynthesis
448.0842	0.002275687	449.0922	24					
463	463.141675	0.000397453	464.1496	36	Hesperetin 7-O- glucoside	C ₂₂ H ₂₄ O ₁₁	Flavonoid	Flavonoid biosynthesis Sequiterpenoid biosynthesis
	463.142525	0.000198037	464.1505	22	Diffutin Enhydrin	C ₂₃ H ₂₈ O ₁₀	Flavan Sequiterpene	
	463.143575	0.000530772	464.1515	20				
	463.14355	0.000147902	464.1515	20				
	463.141725	0.000717962	464.1497	24				
	463.141775	0.000720568	464.1497	24				
	463.0728	0.000671751	464.0808	33	Quercimeritrin Myricitrin	C ₂₁ H ₂₀ O ₁₂	Flavonoid	
463.0716	0.000594112	464.0796	35	Gossypetin 8- rhamnoside				
489	489.1609	0.00032476	490.1689		Demethylalangsideside	C ₂₄ H ₂₉ NO ₁₀	Alkaloid	Isoquinoline alkaloid biosynthesis
	489.1605	0.000246221	490.1685					
	489.1613	0.000219374	490.1692					
	489.1615	0.000190394	490.1695	6				
	489.1614	489.161425	490.1694					
	489.1615	7.5E-05	490.1692					
	489.0975	0.004257695	490.1055	12				
489.1117	0.013123518	490.1197						

3.3.5 Average intensities of % total ion counts of metabolites

Prior to the two-way ANOVA, the average intensities of the putatively identified mass bins were calculated for each layer and ionisation mode. Table 3.7 shows the percentage ion count and corresponding statistical significance for each mass bin which have been separated into new and old leaves as well as an average representation for all leaves across replicates in each treatment for the aqueous layer in negative mode. Tables A3.5-3.7 in the appendix show the aqueous layer in positive mode and the organic layer in both modes. The graphs of the average intensities of the discriminatory mass bins demonstrate a change in the percentage total ion count between the control treatment and the three elevated treatments through both up and down regulation of secondary metabolites.

Mass bins 315 and 385 demonstrate this difference in their relative abundances through up regulation of secondary metabolites compared to the control, with a slightly greater increase of %TIC being seen in young leaves. In table 3.6 these mass bins have been putatively assigned to both alkaloid biosynthesis and the shikimate pathway respectively. It can be seen in table 3.7 that the increase in the relative abundances of these mass bins can be attributed to the plants that were exposed to elevated CO₂ treatments. This is not unexpected given that these secondary metabolites and the synthesis of essential amino acids are known to be directly related to, an increase in photosynthesis (Foyer et al., 2000). However, an increase in photosynthetic efficiency of the plants was not measured in this experiment.

Discrimination of relative abundances were not found overall when leaf age was taken into account between the secondary metabolites that exhibited down regulation in relation to the control treatment. Both young and old leaves demonstrate average

intensities almost identical to the relative abundance of all leaves for each treatment. The discriminant mass bins that demonstrate a decrease in relative abundances of all treatments except the control can be attributed to secondary metabolites that are intermediates within flavonoid biosynthesis. Although surprising, this find is not unprecedented in the literature and will be discussed in more detail in the discussion section (3.4.2).

Table 3.7: Total % ion count of discriminatory mass bins (m/z) for aqueous layer in negative mode for all leaves, new leaves, and old leaves. Error bars denote standard error to 1 standard deviation (σ).

m/z	All Leaves	New Leaves	Old Leaves
194.2			
269			
284.2			
285			
286.2			
301			

Table 3.7: Continued.

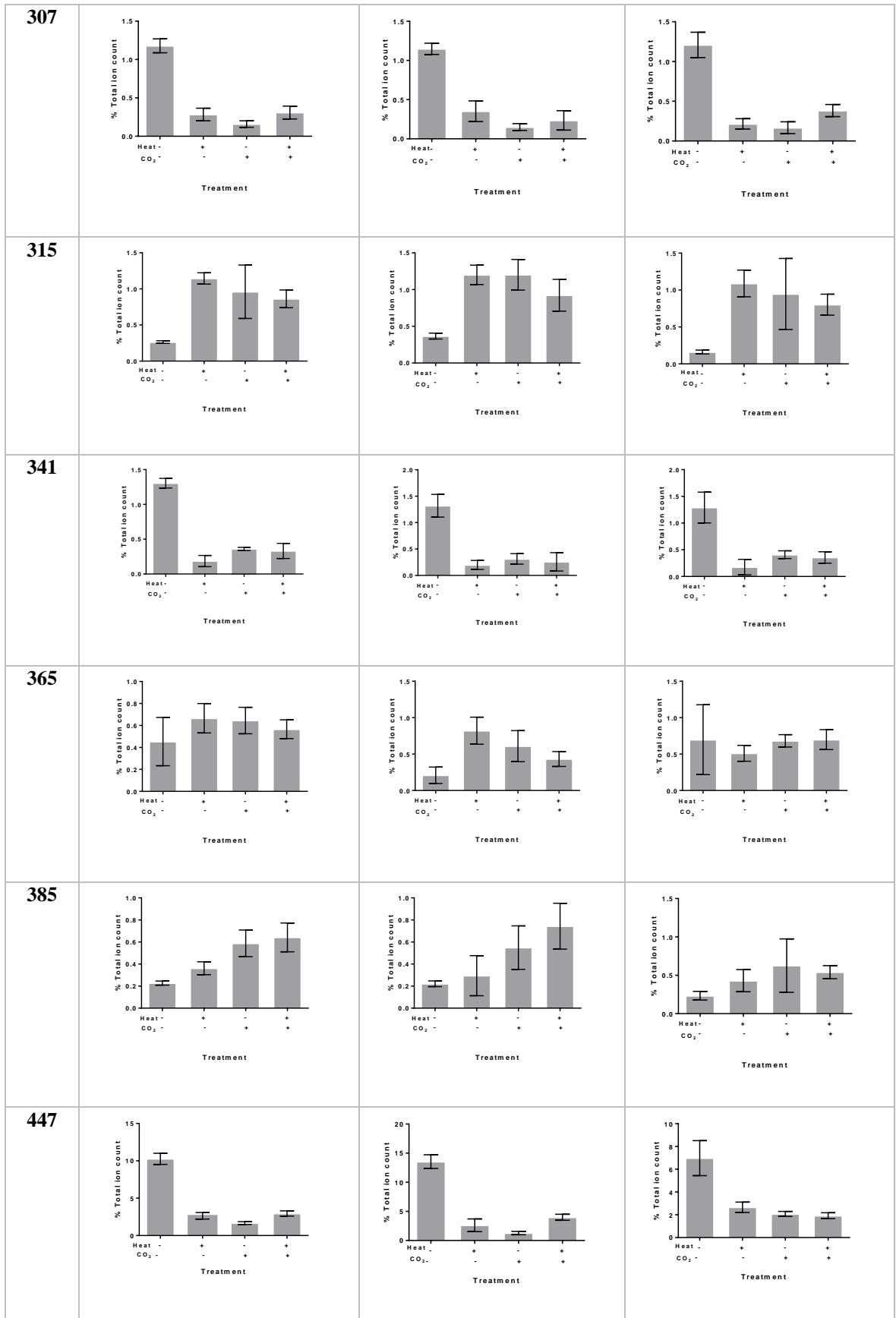
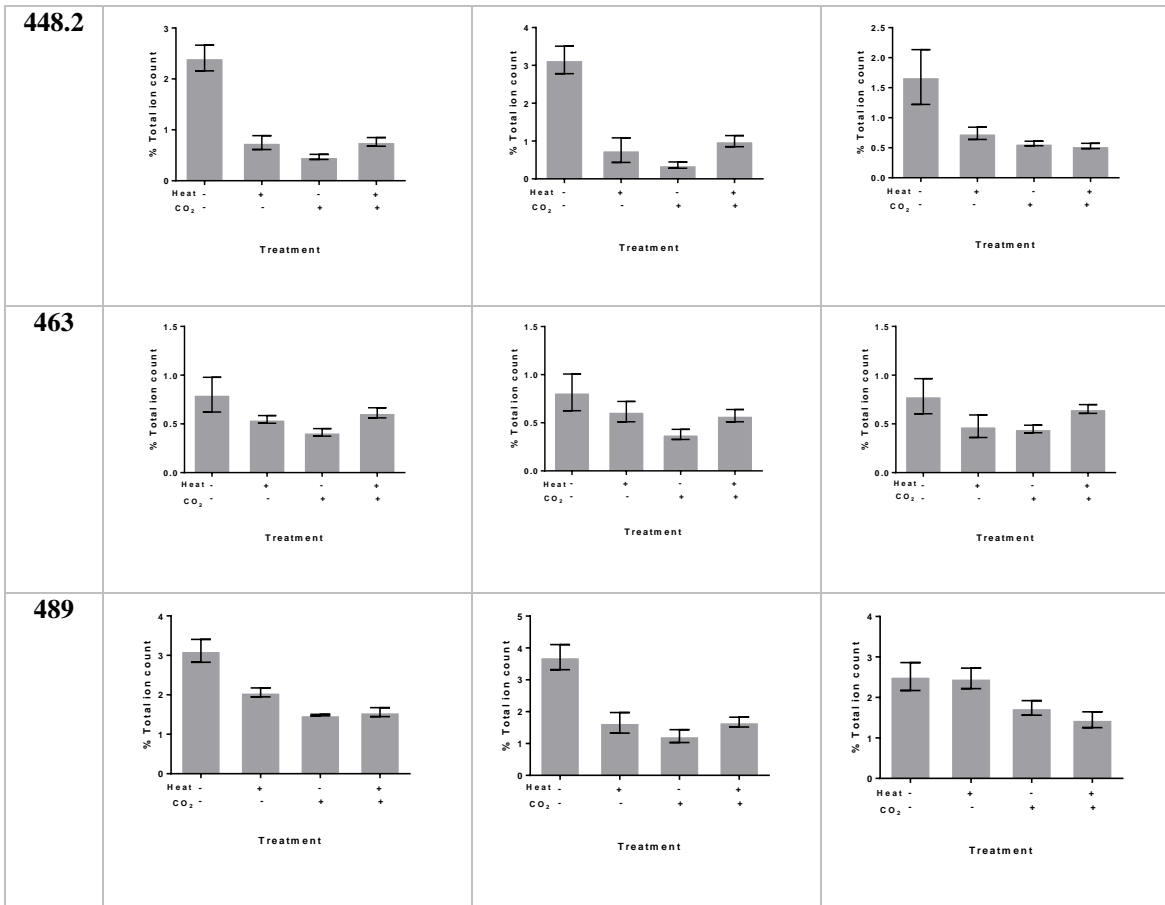


Table 3.7: Continued.



3.3.6 Statistical significance of treatment interactions on mass bins

Tables 3.8, 3.9, and 3.10 show the statistical significance of the average intensities of the mass bins in relation to the effect of CO₂ concentration, temperature and the interaction of both (please see tables A-3.8-3.16 in the appendix for negative aqueous and the organic layer in both modes) for all, new, and old leaves respectively. Although the mass bins chosen were deemed statistically significant through the supervised multivariate analysis, it is necessary to determine the significance of each bin using a two-way ANOVA with subsequent pairwise comparisons for each treatment. Overall there is agreement that there is a statistically significant difference between treatments, particularly for the pairwise comparisons of the effect of a heat

spike applied to elevated CO₂ (Hs*eCO₂ vs eCO₂) and the effect of increased CO₂ to extreme temperature (Hs*eCO₂ vs Hs), which can be observed especially in new leaves. There is also a statistically significant difference between the elevated treatments (Hs*eCO₂) and the control (ambient) which is to be expected as these two treatments differ in their parameters the most.

Table 3.8: Results of two-way ANOVA statistical significance for all leaves of % ion count intensities of the 3 treatments different to the control, and their interaction for the discriminatory mass bins for aqueous layer, negative ionisation mode. DF = degrees of freedom (& associated error); F = F-value; P = P-value (significant if p <0.05 (shown in bold)). Arrows denote up or down regulation relative to the control treatment.

M/Z		CO ₂			Heat			CO ₂ *Heat		
		DF	F	P	DF	F	P	DF	F	P
194.2	↑	1, 12	0.03	0.871	1, 12	0.33	0.575	1, 12	9.69	0.009
269	↓	1, 12	37.23	<0.001	1, 12	39.47	<0.001	1, 12	39.89	<0.001
284.2	↓	1, 12	29.24	<0.001	1, 12	24.36	<0.001	1, 12	30.79	<0.001
285	↓	1, 12	51.87	<0.001	1, 12	43.25	<0.001	1, 12	46.63	<0.001
286.2	↓	1, 12	29.27	<0.001	1, 12	25.02	<0.001	1, 12	28.47	<0.001
301	↓	1, 12	26.03	<0.001	1, 12	16.76	0.001	1, 12	21.91	0.001
307	↓	1, 12	41.91	<0.001	1, 12	23.48	<0.001	1, 12	46.26	<0.001
315	↑	1, 12	3.87	0.073	1, 12	1.08	0.319	1, 12	6.04	0.030
341	↓	1, 12	26.99	0.000	1, 12	55.54	<0.001	1, 12	50.04	<0.001
365	↑	1, 12	0.10	0.761	1, 12	0.20	0.661	1, 12	0.97	0.344
385	↑	1, 12	11.58	0.005	1, 12	1.01	0.335	1, 12	0.18	0.675
447	↓	1, 12	75.42	<0.001	1, 12	44.28	<0.001	1, 12	87.38	<0.001
448.2	↓	1, 12	40.4	<0.001	1, 12	20.3	0.001	1, 12	41.59	<0.001
463	↓	1, 12	2.72	0.125	1, 12	0.08	0.785	1, 12	5.52	0.037
489	↓	1, 12	40.74	<0.001	1, 12	8.65	0.012	1, 12	11.48	0.005

Table 3.9: Results of two-way ANOVA statistical significance for new leaves of % ion count intensities of new leaves for the 3 treatments different to the control, and their interaction for the discriminatory mass bins for aqueous layer, negative ionisation mode. DF = degrees of freedom (& associated error); F = F-value; P = P-value (significant if p <0.05 (shown in bold)). Arrows denote up or down regulation relative to the control treatment.

M/Z		CO ₂			Heat			CO ₂ *Heat		
		DF	F	P	DF	F	P	DF	F	P
194.2	↑	1,12	5.49	0.037	1,12	7.11	0.021	1,12	8.00	0.015
269	↓	1,12	17.61	0.001	1,12	16.94	0.001	1,12	46.96	<0.001
284.2	↓	1,12	42.67	<0.001	1,12	51.44	<0.001	1,12	117.11	<0.001
285	↓	1,12	297.3	<0.001	1,12	314.4	<0.001	1,12	726.4	<0.001
286.2	↓	1,12	15.72	0.002	1,12	19.44	0.001	1,12	43.77	<0.001
301	↓	1,12	29.36	<0.001	1,12	25.36	<0.001	1,12	66.68	<0.001
307	↓	1,12	9.37	0.01	1,12	5.86	0.032	1,12	19.51	0.001
315	↑	1,12	7.22	0.021	1,12	6.6	0.026	1,12	11.03	0.007
341	↓	1,12	3.94	0.073	1,12	4.88	0.049	1,12	11.46	0.006
365	↑	1,12	5.38	0.039	1,12	3.61	0.082	1,12	6.04	0.03
385	↑	1,12	1.12	0.311	1,12	0.34	0.57	1,12	0.34	0.73
447	↓	1,12	30.73	<0.001	1,12	36.5	<0.001	1,12	63.44	<0.001
448.2	↓	1,12	15.93	0.002	1,12	20.01	0.001	1,12	34.2	<0.001
463	↓	1,12	0.92	0.356	1,12	2.57	0.135	1,12	2.87	0.116
489	↓	1,12	7.93	0.016	1,12	10.76	0.007	1,12	19.46	0.001

Table 3.10: Results of two-way ANOVA statistical significance for old leaves of % ion count intensities of old leaves for the 3 treatments different to the control, and their interaction for the discriminatory mass bins for aqueous layer, negative ionisation mode. DF = degrees of freedom (& associated error); F = F-value; P = P-value (significant if p <0.05 (shown in bold)). Arrows denote up or down regulation relative to the control treatment.

M/Z		CO ₂			Heat			CO ₂ *Heat		
		DF	F	P	DF	F	P	DF	F	P
194.2	↑	1,12	3.71	0.078	1,12	3.43	0.089	1,12	2.34	0.152
269	↓	1,12	5.72	0.034	1,12	5.61	0.036	1,12	12.78	0.004
284.2	↓	1,12	3.46	0.088	1,12	3.78	0.076	1,12	7.76	0.016
285	↓	1,12	2.71	0.126	1,12	3.12	0.103	1,12	7.93	0.016
286.2	↓	1,12	3.77	0.076	1,12	4.11	0.065	1,12	9.58	0.009
301	↓	1,12	1.09	0.317	1,12	1.56	0.236	1,12	3.27	0.096
307	↓	1,12	18.56	0.001	1,12	19.88	0.001	1,12	35.78	<0.001
315	↑	1,12	2.59	0.133	1,12	2.08	0.175	1,12	4.04	0.068
341	↓	1,12	5.14	0.043	1,12	3.4	0.09	1,12	9.38	0.01
365	↑	1,12	0.23	0.641	1,12	0.07	0.792	1,12	0.16	0.701
385	↑	1,12	0.08	0.786	1,12	0.35	0.562	1,12	0.52	0.484
447	↓	1,12	1.74	0.212	1,12	2.39	0.148	1,12	6.44	0.026
448.2	↓	1,12	0.85	0.375	1,12	1.32	0.273	1,12	3.63	0.081
463	↓	1,12	3.85	0.073	1,12	4.17	0.064	1,12	5.33	0.04
489	↓	1,12	2.53	0.138	1,12	0.45	0.513	1,12	0.24	0.635

3.4 Discussion

3.4.1 *The effect of extreme temperature on plant secondary metabolism*

The aim of this chapter was to examine the regulation of plant secondary metabolites in response to the independent and interactive effects of elevated CO₂ and extreme temperature through an untargeted fingerprint analysis.

The metabolic response of the plant to elevated temperature is different to that of the control treatment and can be seen in figure 3.10 in section 3.3.3. The clear separation between the different treatments is observed in both new and old leaves in the pairwise multivariate analysis. The significant differences of the two treatments is also evident in the changes in the relative abundances of the discriminant mass bins (table 3.7) where overall there is a reduction in the abundance of the most discriminatory masses (with exception to mass bins 194.2, 315, and 385) in heat shocked plants relative to the control. Putative identification of the most discriminatory masses that were reduced in the heat shock treatment revealed them to be associated with the flavonoid biosynthesis pathway. Down regulation of flavonoids by the heat treatment is surprising as they are known to be produced in response to environmental stress, for example, the synthesis of Quercetin-3-*O*-glycoside and Luteolin-7-*O*-glycoside is induced by ultraviolet radiation as precursors to defensive pigment biosynthesis (Brunetti, et al, 2013, Fini et al, 2011), while apigenin-7-*O*-glycoside and kaempferol-3-*O*-glycoside are produced as an antioxidant response to reactive oxygen species (ROS) in periods of oxidative stress (Brunetti et al, 2013).

The suppression of the anthocyanin biosynthetic pathway in putatively identified discriminant mass bins 205, 381, 448.2, and 489 is comparable to observations in the literature, however the mechanisms that lead to a decrease in anthocyanin concentration

as a response to elevated heat shock are still poorly understood (Mori et al., 2007). The suppression of anthocyanin concentration at elevated temperatures has been observed in a number of plant species including apple (Ubi et al. 2006), orange (Lo Piero et al. 2005), and red wine grape (Mori et al. 2007). In particular the concentrations of Cyanidin 3-glucoside and Delphinidin 3-glucoside were markedly reduced in red wine grapes that had been subjected to temperatures over 35°C (Mori et al. 2007), which has been a confirmed observation in this study, particularly in putatively identified mass bins 205 and 381. The result of the suppression of anthocyanin species such as Cyanidin 3-glucoside and Delphinidin 3-glucoside as a result of elevated temperature is not unprecedented, but is poorly understood (Mori et al., 2007). However this has been established on a number of occasions as a response to elevated CO₂, and there is evidence that this occurs due to an increase in substrate availability and allocation of resources, and will be discussed in depth in the next section.

As discussed previously, it is unexpected that there is a suppression of the flavonoids as a response to elevated temperature as they are known to be produced in response to abiotic stresses. In particular, the production of secondary metabolites with antioxidant properties in plants suffering from temperature stress is widely discussed within the literature (Akula & Ravishankar, 2011; Paajanen et al. 2011; Treutter, 2006; Viteli et al. 2007). The ability of the flavonoids in particular to scavenge atmospheric free radicals and reduce the effect of ROS upon the plant has been observed at the cellular level (Agati et al. 2012; Pietta, 2000; Procházková et al. 2011). It has therefore been postulated that the same should happen in cases of extreme temperature (prior to the onset of leaf senescence), due to plant sensitivity in response to short-lived stress. However, particularly in the studies of Paajanen et al (2011), and Veteli et al (2002; 2007), it would appear that overall there is a reduction in the concentration of phenolic

compounds that are part of the flavonoid and anthocyanin pathways e.g. Quercetin and Kaempferol 7-*O*-glucoside (Treutter, 2006) as a response to elevated temperature.

However, isoprene also has the ability to recycle free radicals and other ROS that could potentially cause oxidative stress to the plant (Wolfertz et al. 2003). As isoprene is costly for the plant to produce in the allocation of carbon substrate away from respiration to volatile organic compound production, it could be the case that the plant is allocating resources to the production and emission of a secondary metabolite that has both antioxidant and thermotolerance properties. Therefore although expensive, the short-term gain against short-lived heat stress is biochemically viable and beneficial to the plant. As both the terpenoid biosynthesis pathway and the flavonoid biosynthesis pathway share pyruvic acid following the conversion of glucose through the glycolysis pathway from the citric acid cycle, it would make sense to have some sort of 'directional switch' as a result of substrate competition, where the available substrate is allocated to the more appropriate and immediate resource in times of short-lived abiotic stress. This has been observed by Loreto & Sharkey (1993) who found that short-term isoprene emission concentration increases positively correlate with increases in adenosine triphosphate (ATP) in leaves in times of short-term heat stress.

3.4.2 The effect of elevated CO₂ concentration on plant secondary metabolism

An increase in atmospheric CO₂ concentration is known to promote a positive response in C₃ plant species in terms of photosynthesis and biomass gains, including *Salix pp.* Paajanen et al (2011) observed that in willow, an increase in CO₂ concentration not only increased plant biomass, but also had an opposite effect to temperature on phenolic compound concentrations. Plants grown at elevated CO₂ concentrations exhibit less of a change to their biochemistry than those subjected to

periods of extreme heat (Ramakrishna & Ravishankar, 2011, Taub, 2010). This is demonstrated in the relative abundance of plant metabolites in the discriminant mass bins shown in table 3.7. Putatively identified discriminant mass bins 194.2, 315, and 385 demonstrate an up-regulation of amino acid compounds in all treatments when compared to the control. Discriminant mass bin 365 was found to show significant differences between treatments in new leaves (see table 3.9 for P values), particularly in the up-regulation of putatively identified phenolic compounds including Salicin 6-phosphate as a result of an increase in CO₂ concentration when compared to the control treatment.

Although it has not been putatively identified in the aqueous layer in negative ionisation mode, there is evidence that the up-regulation of the shikimate, tryptophan, alkaloid and pentose phosphate pathways is as a result of, and linked by the intermediate Phosphoenolpyruvic acid (PEP). Amino acid compounds including glucosaminic acid, maltose, and pterxyin within these biosynthetic pathways can also be seen in all of the putatively identified mass bin table 3.6 and in the appendix (A3.7-A3.10). PEP has a significant role as an intermediate in the biosynthesis of glucose via the gluconeogenic pathway and citric acid cycle (TCA), as its metabolism leads to pyruvate and ATP transfer, and can be used for the biosynthesis of phenolic compounds through the shikimate pathway and thus facilitate carbon fixation (Dizengremel et al. 2012; Kaling et al. 2014; Trowbridge et al. 2011). Li et al (2008) have also found that an increase in CO₂ leads to an observed increase in the diversity of plant secondary metabolites. They found that, at elevated CO₂, there was an increase in cell growth in young leaves when compared with ambient air. The results of this study have observed an increase in the relative abundance of secondary metabolites associated with the shikimate pathway and glycolysis in young leaves compared to the control. This study parallels with those of Ainsworth et al (2006) and Li et al (2008) in that the observation

of glucose, galactose and maltose compounds increase as a response to elevated CO₂. The increase in glycolysis intermediates are required for PEP formation and metabolism, therefore providing a flux of substrate into the citric acid cycle for the biosynthesis of secondary metabolites and energy production (Ainsworth et al 2008). This adds strength to the idea that an increase in CO₂ concentration is leading to an increase in carbon partitioning in the plant and therefore providing an up-regulation in secondary metabolites. The same conclusion has been drawn by Viteli et al (2007) that elevated CO₂ concentrations are contributing to an increase in carbon-rich secondary metabolites.

The discriminant mass bins showing up-regulation when compared to the control reveal that there is variability between the relative abundance of key metabolites in response to eCO₂ and the Hs treatments for both new and old leaves. This would therefore imply that plants that are subjected to elevated levels of CO₂ are subject to higher rates of photosynthetic efficiency, thus leading to more carbon partitioning and an increase in plant biomass and a reduction in water loss through a decrease in stomatal conductance (Hikosaka et al., 2005, Lammertsma et al., 2011, Taub, 2010). These physiological and chemical processes that occur as a result of an increase in CO₂ are therefore not exerting the same level of stress upon the plant as extreme temperature and therefore would not require a drastic change to the allocation of carbon needed to support secondary metabolism, and in particular, those secondary metabolites that are associated with stress mitigation.

3.4.3 The effect of the interaction between temperature and CO₂ on the plant metabolome

If extreme heat can induce an increase in energy-expensive secondary metabolites such as terpenoids, and elevated CO₂ concentrations lead to an increases in

the metabolic intermediates of energy generating processes such as glycolysis then these two environmental factors have the potential to directly influence each other via substrate competition, which should be reflected by wholesale changes in the metabolome. Specifically, does either heat stress and elevated CO₂ represent a more dominant regulator of metabolism, or would the two mitigate each other in their interaction i.e. the extra energy resulting from elevated CO₂ has the potential to lessen the trade off in terms of plant resource partitioning between the terpenoid and flavonoid pathways? From this, it can be predicted that the flavonoids suppressed under the heat shock treatment will increase in relative terms under the combined heat shock and elevated CO₂ treatment, as elevated CO₂ is providing more resources to the net carbon budget of the plant. Therefore, the trade off in terms of allocation to the production of either flavonoids or terpenoids is less pronounced. This hypothesis is partially supported by my data as there is a significant interaction between CO₂ and heat shock (Tables 3.8, 3.9, and 3.10) for discriminant mass bin numbers 284.2, 286.2, 301, 307, 341, 447, 448.2, 463, and 489 (putatively identified as the flavonoids). In this case, the relative abundances of these masses are higher in the CO₂*heat shock treatment than in the heat shock treatment alone, although these differences are not dramatic in terms of their magnitude when old and new leaves are looked at together.

The response of isoprene emission to extreme temperature would increase and therefore redirect the available carbon to the production of terpenoid species that potentially increase a plant's thermotolerance. The response of young leaves to extreme temperature is unsurprising as they are a carbon sink as they require more carbon for growth and development. Therefore the lack of significant discriminant mass bins in old leaves is also unsurprising as the carbon fixed as a result of increased photosynthetic efficiency due to CO₂ fertilisation would be allocated to an increased sink strength in new leaves. This theory has also been postulated by Farrar & Williams (1991), and

Peñuelas & Estiarte (1998). Both studies have led to the conclusion that the decrease in plant concentrations of secondary metabolites is as a result of the carbon sink in new leaves (Zvereva & Kozlov, 2006).

The results of this study have therefore confirmed the hypotheses that the 1) the effect of short-term extreme heat stress will have a detrimental effect upon plant function and development through the loss of fixed carbon; and 2) that when plants are subjected to both elevated temperature and CO₂, the resulting impact upon the plant metabolome from elevated temperature is greater than the effect of elevated CO₂, particularly in young leaves.

Following this, chapter 4 will further investigate the biochemical responses of plant metabolism to extreme temperature and elevated CO₂. Using tandem mass spectrometry, the production and regulation of metabolite intermediates from both the flavonoid and non-mevalonate (MEP) (metabolic pathway of isoprenoid biosynthesis) pathways will be assessed. Through the quantification of compound fragmentation patterns and their metabolic flux in relation to treatment, the mechanistic basis underpinning the allocation and redirection of carbon to isoprene biosynthesis in leaves will be investigated.

3.5 Conclusion

This study demonstrates the need for more complex analysis of interactions of abiotic stresses than previously conducted. Although it is necessary to understand the mechanisms behind environmental factors as independent stresses, a more rigorous approach is required to understand the complex nature of the interactions of temperature, and CO₂ and their effect upon leaf age and the plant metabolome. This is particularly pertinent when attempting to reconcile environmental parameters within predictive Earth Systems models for use in future climate feedback predictions.

Chapter 4: What is the Mechanistic Basis Underpinning the Regulation of Volatile Organic Carbon Biosynthesis and Emissions?

4.1 Introduction

The biochemical mechanisms underpinning the production of the volatile isoprene have, until relatively recently, been equivocal. The 2-C-methyl-D-erythritol 4-phosphate/1-deoxy-D-xylulose 5-phosphate (MEP/DOXP) metabolic pathway responsible for isoprene production was only discovered within the last 20 years (Rohmer, 1999). Previously, it was thought that isoprene was produced through the mevalonate pathway, as through this pathway isopentenyl pyrophosphate (IPP) and dimethylallyl pyrophosphate (DMAPP) are produced and are the precursors to isoprenoid biosynthesis (Hunter, 2007). It has been well established in the literature that isoprene emissions increase when the plant is subject to short-term heat stress, thus suggesting that isoprene is produced as a thermotolerance response to abiotic stress (Holopainen, 2013). In chapter 2 it was demonstrated that isoprene emissions showed a trend towards an increase when plants were subjected to a 40°C heat shock, and that isoprene emissions demonstrated a decreasing trend when plants were subjected to elevated CO₂ concentrations. However, it was the mitigation of the interaction of these two abiotic stresses that produced the most interesting results. Following this discovery, it was then possible in chapter 3 to conduct an untargeted fingerprint analysis of the secondary metabolism of willow to investigate the biochemical effects of these stresses, both independently and their combined interaction. The putative identification of a number of secondary metabolites suggested that substrate was being allocated away from certain pathways in times of heat stress. Therefore it is necessary to conduct a further investigation to assess the response of the secondary metabolome, and in particular the MEP/DOXP pathway, in order to quantify the isoprene precursors in the leaf tissue samples that have been subjected to the various treatments.

This study investigates the biochemical mechanisms that underpin the regulation of isoprene biosynthesis and subsequent emission. Through a targeted analysis using tandem mass spectrometry, several key plant secondary metabolites that are precursors to the biosynthesis of isoprene will be identified. Furthermore, following the identification through fragmentation patterns, it will be possible to conduct a full pathway analysis of both the flavonoid and MEP/DOXP metabolic pathways to determine the effects of abiotic stresses upon stress-induced secondary metabolites. Specifically it can be hypothesised that:

- 1) All metabolites in the flavonoid biosynthesis pathway will demonstrate suppression;
- 2) In heat shocked plants, there will be a significant up-regulation of intermediates along the MEP/DOXP pathway relative to the control treatment as isoprene production increases, demonstrated through a change in percentage total ion count of each metabolite.

4.2 Materials & Methods

4.2.1 Experiment set up and plant growth

Cuttings of the willow hybrid “Terra Nova” (‘LA940140’ x *Salix miyabeana*) (Lindegaard, 2012) were rooted in pots filled with John Innes No. 3 potting compost. The cuttings were grown to the same specifications (table 4.1) as described in chapters 2 and 3 for 10 weeks before the temperature and CO₂ treatments were applied (see sections 2.5.2 and 3.2 for full descriptions of the experimental set up). The leaf samples used for the tandem mass spectrometry identification were the same extraction samples that were used in chapter 3.

Table 4.1: Environmental parameters and time periods for willow growth in controlled environment chamber.

Environmental Parameter	Parameter Values	Time Period
Temperature (day)	20°C	8 hours
Temperature (night)	15°C	16 hours
CO₂	Ambient (~400ppm)	constant
Light	800µmol	8 hours
Humidity	67%	constant

4.2.2 Elevated temperature and CO₂ treatment application

The biochemical analysis using targeted metabolomics was subject to the same temperature and CO₂ treatments (control, elevated CO₂ (eCO₂), heat shocked (Hs), and elevated CO₂ and heat shocked (Hs*eCO₂)) that have been described in chapter 2, (section 2.5.2) and for the untargeted metabolomics in chapter 3 (section 3.2). Table 4.2 outlines the treatments for reference.

Table 4.2: Environmental parameters and time periods for treatment application in controlled environment chamber.

Treatment	Parameter Values		Time Period	
	Temperature	CO₂	Temperature	CO₂
Hs*CO ₂	40°C	800ppm	1 photoperiod	constant
eCO ₂	20 °C	800ppm	1 photoperiod	constant
Hs	40°C	Ambient (~400ppm)	1 photoperiod	constant
Control	20 °C	Ambient (~400ppm)	1 photoperiod	constant

4.2.3 Leaf harvest

From each of the four plants, a representative young (the first fully expanded leaf immediately adjacent to the shoot apical meristem) and mature leaf was selected (see section 3.2.3.1 & 3.2.3.2 for full descriptions of leaf harvest) at the end of the photoperiod of the treatment application day. The leaf samples from each plant were then flash frozen in liquid nitrogen and were stored at -80°C and then freeze dried in order to be prepared for metabolite biphasic extraction. Leaf surface area measurements were calculated using a LI-COR LI-3000C portable leaf area meter and given as cm² (see section 2.2.2.6 for a full description of leaf area calculations and section 2.3.2.5 for the statistical results). The separated leaves and stems of each plant were weighed (g) following freeze drying to calculate the above ground plant biomass (see section 2.3.2.2 for the statistical results).

4.2.4 Leaf metabolite extraction

Plant metabolites for both young and mature leaf samples were extracted using a standard biphasic chloroform/methanol/water extraction (Overy et al., 2005). 2mg of each young and mature dried leaf sample were weighed and then extracted into their polar phases (see section 3.2.5 for a full description of the leaf metabolite extraction method). Following the extraction the samples were stored at -80°C in preparation for tandem mass spectrometry analysis.

4.2.5 Tandem mass spectrometry (MS/MS) analysis of leaf metabolites

Both the aqueous and organic layers of the metabolite extracts were diluted 1:10 with pure methanol. The polar phases of the metabolite extracts were then analysed in

negative ionisation mode on an Applied Biosystems/MDS Sciex QSTAR Elite quadrupole time-of-flight (QTOF) mass spectrometer using liquid chromatography tandem mass spectrometry (LC/MS/MS) with a turbospray electrospray head. Each sample was injected at a volume of 2µl through a borosilicate capillary NanoES emitter (Thermo Scientific, Hertfordshire) with a flow rate of 10µl/min. Table 4.4 shows the instrument settings for each of the optimised standards of the intermediates that were then used to analyse each sample.

Table 4.3: List of metabolite intermediates for the flavonoid and terpenoid pathways.

Flavonoid Biosynthesis	Terpenoid Backbone Biosynthesis
Apigenin	Dimethylallyl pyrophosphate (DMAPP)
Cyanidin	Geranyl pyrophosphate (GPP)
Luteolin	Isopentenyl pyrophosphate (IPP)
Quercetin	2-C-Methyl-D-erythritol 4-phosphate (MEP)

In order to identify the molecule fragmentation patterns of interest, the samples were compared with fragmentation patterns of standards that were analysed under the same conditions. Following the results of chapter 3, 4 intermediates from the flavonoid metabolic pathway were chosen, along with 4 intermediates from the 2-C-methyl-D-erythritol 4-phosphate/1-deoxy-D-xylulose 5-phosphate (MEP/DOXP) metabolic pathway to be analysed using tandem mass spectrometry. A list of the intermediates can be found in table 4.3.

Table 4.4: QTOF LC/MS/MS instrument settings following optimisation for each metabolite intermediate.

Instrument Settings	Apigenin	Cyanidin	Luteolin	Quercetin	Dimethylallyl diphosphate	Geranyl diphosphate	Isopentenyl diphosphate	2-C-Methyl-erythritol 4-phosphate
TOF masses (Da)	100-280	100-340	100-300	100-310	100-260	100-325	100-250	100-225
Declustering potential	-120.00	-120.00	-120.00	-120.00	-120.00	-120.00	-120.00	-120.00
Focusing potential	-265.00	-265.00	-265.00	-265.00	-265.00	-265.00	-265.00	-265.00
Collision energy	-40.00	-47.00	-40.00	-38.00	-25.00	-25.00	-32.00	-31.00
Collision gas	Nitrogen	Nitrogen	Nitrogen	Nitrogen	Nitrogen	Nitrogen	Nitrogen	Nitrogen
Collisionally activated dissociation (CAD)	7.00	4.00	3.00	4.00	4.00	4.00	3.00	6.00
Curtain gas (CUR)	20.00	20.00	20.00	20.00	20.00	20.00	20.00	20.00
Ion Spray Voltage (IS)	-1500.00	-1500.00	-1500.00	-1500.00	-1500.00	-1500.00	-1800.00	-1800.00

4.2.6 Data processing and statistical analysis

Analysis of the analytical standards and tissue extract samples fragmentation patterns were conducted using Analyst QS 2.0 (Applied Biosystems) software to generate a spectra of the total ion count (TIC) for each sample (see section 4.3.1 for the results of the fragmentation pattern identifications).

Following the identification of metabolites in the plant samples from the fragmentation patterns, a full pathway analysis of both the flavonoid and MEP/DOXP biosynthesis pathways was conducted. The changes in percentage total ion count of each metabolic intermediate for each pathway was calculated relative to the control treatment. The raw metabolite spectral data for both aqueous and organic phases in negative ESI mode were processed using the same in-house Visual Basic macro that has been outlined in chapter 2, section 3.2.7. The triplicate runs of each sample from the

MALDI-MS analysis were combined to calculate their mean mass to create a metabolite profile for each sample (Overy et al., 2005).

Analysis of the change in percentage total ion count relative to the control were conducted using a two-way ANOVA and subsequent post-hoc Tukey HSD test using the statistical software Minitab® version 17 (Minitab Inc., 2010). In order to visually represent the changes along the pathway more clearly, the changes according to treatment have been displayed in a schematic of each pathway for each polar phase and ESI mode. Significant differences as a result of the Tukey HSD test have been denoted by an asterisk.

4.3 Results

4.3.1 Identification of plant metabolites using ms/ms

Through tandem mass spectrometry analysis, the compounds outlined in table 4.3 have been identified. The four intermediates of the flavonoid biosynthesis pathway, and the four intermediates of the MEP/DOXP pathway were identified through comparison with analytical standard solutions. The flavonoid pathway intermediates were chosen as a result of the findings of flavonoid suppression in chapter 3 (section 3.3.5). The intermediates from the MEP/DOXP pathway were chosen as they are the metabolic precursors to the production of isoprene. Figure 4.1 demonstrates the fragmentation pattern for apigenin, an intermediate metabolite in the flavonoid pathway, A) denotes the fragmentation pattern of the standard through optimisation of the instrument (see table 4.3 for instrument settings), and B) shows the fragmentation pattern of apigenin from a young leaf sample from the elevated CO₂ treatment, in its

organic phase. The parent ion can be seen on the right side of the spectra with values of 269.1096 and 269.1134 in spectra A) and B) respectively. The accurate mass for apigenin is 270.053 and the spectra shows the loss of a hydrogen adduct due to being run in negative ionisation mode. Fragmentation patterns of all of the identified compounds in the leaf tissue samples and the analytical standards can be found in the appendix in figures A4.1-4.9 in the appendix.

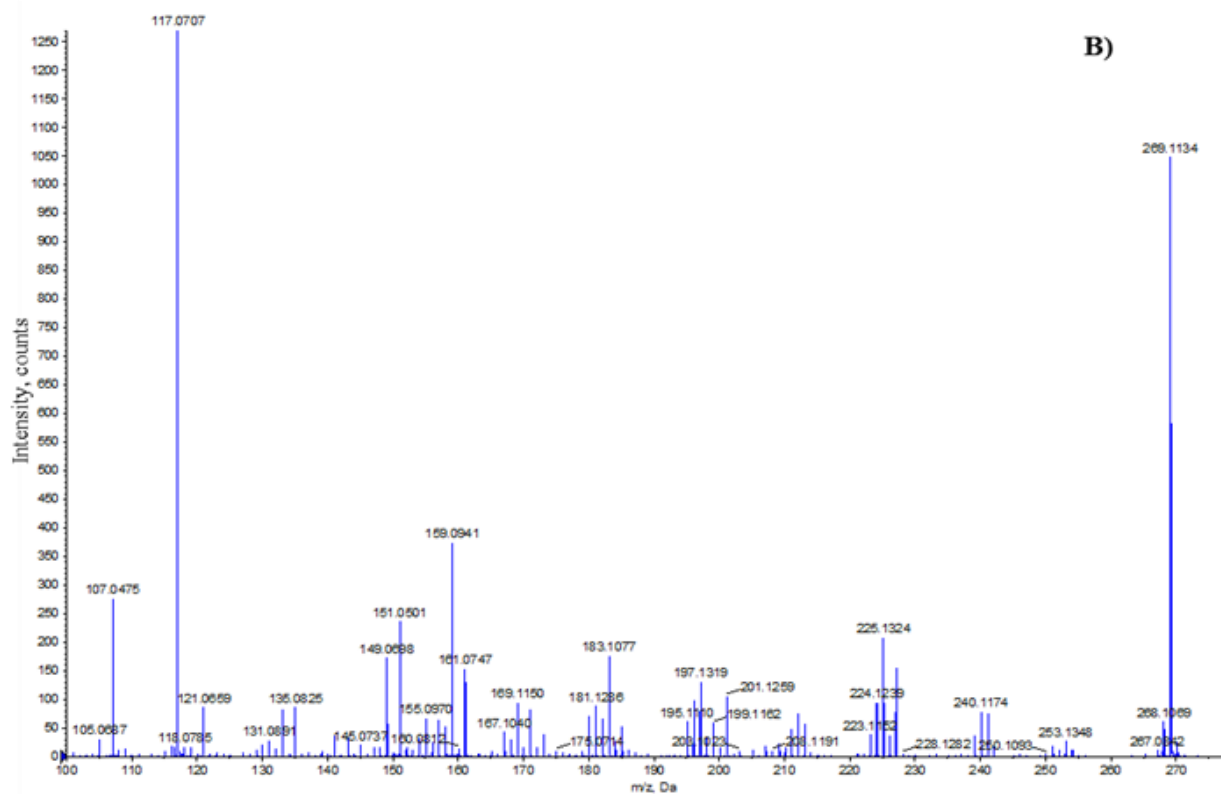
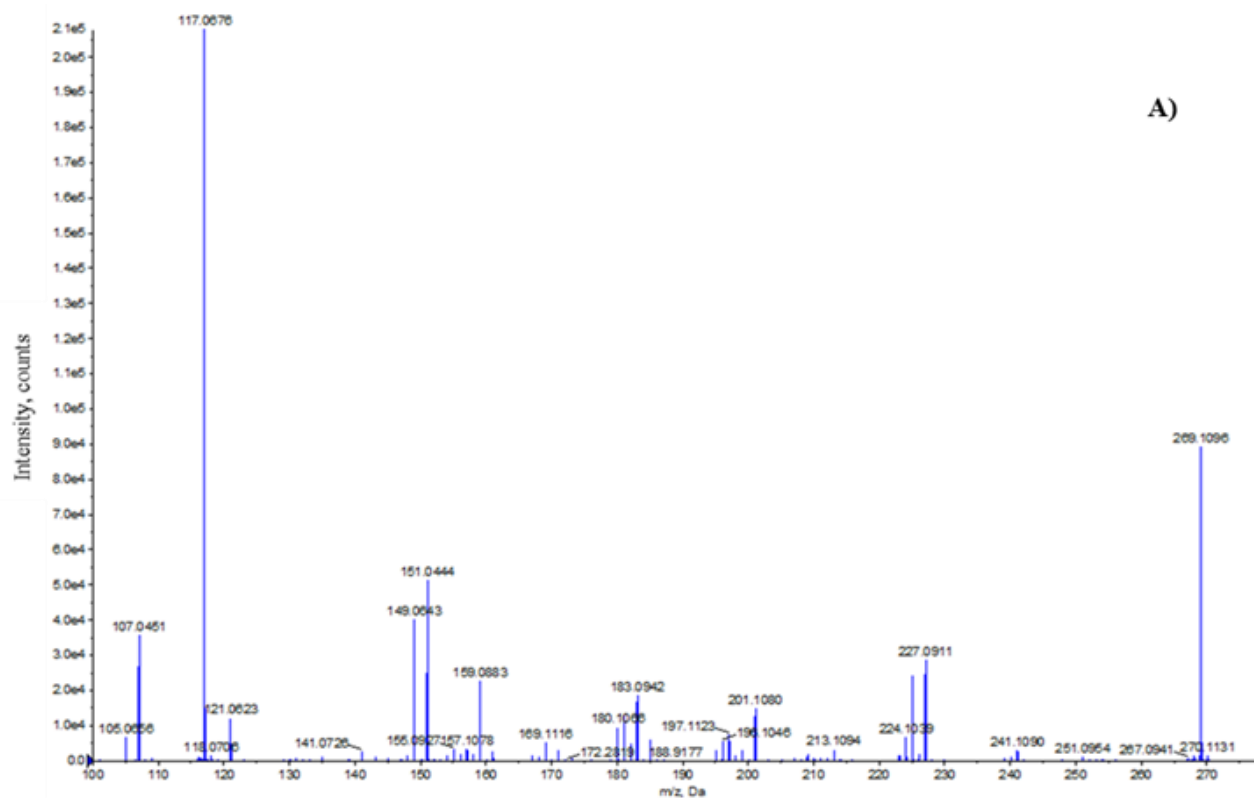


Figure 4.1: MS/MS fragmentation pattern of apigenin analysed in negative ESI mode. A) Apigenin in standard solution. B) Apigenin in eCO₂ sample, new leaf, organic polar phase.

Figure 4.2 is an example of the identification of a metabolite from the MEP/DOXP pathway. 2-C-Methyl-D-erythritol 4-phosphate (MEP) is an intermediate at the beginning of the pathway and a direct precursor to isoprene production. Part A) shows the fragmentation pattern of the analytical standard, and part B) shows the presence of MEP in a tissue sample of a mature leaf subject to the heat shock treatment in its aqueous polar phase. The parent ion for MEP in A) is 215.0855, and in part B) the mass of the parent ion is the same. The monoisotopic mass of MEP is 216.0399 and the parent ion again represents the loss of a hydrogen adduct as both the analytical standard and the sample were analysed in negative ionisation mode.

As shown in the appendix (A4.1-4.9), the 8 intermediates from both pathways were confirmed in almost all of the young and mature leaf tissue samples.

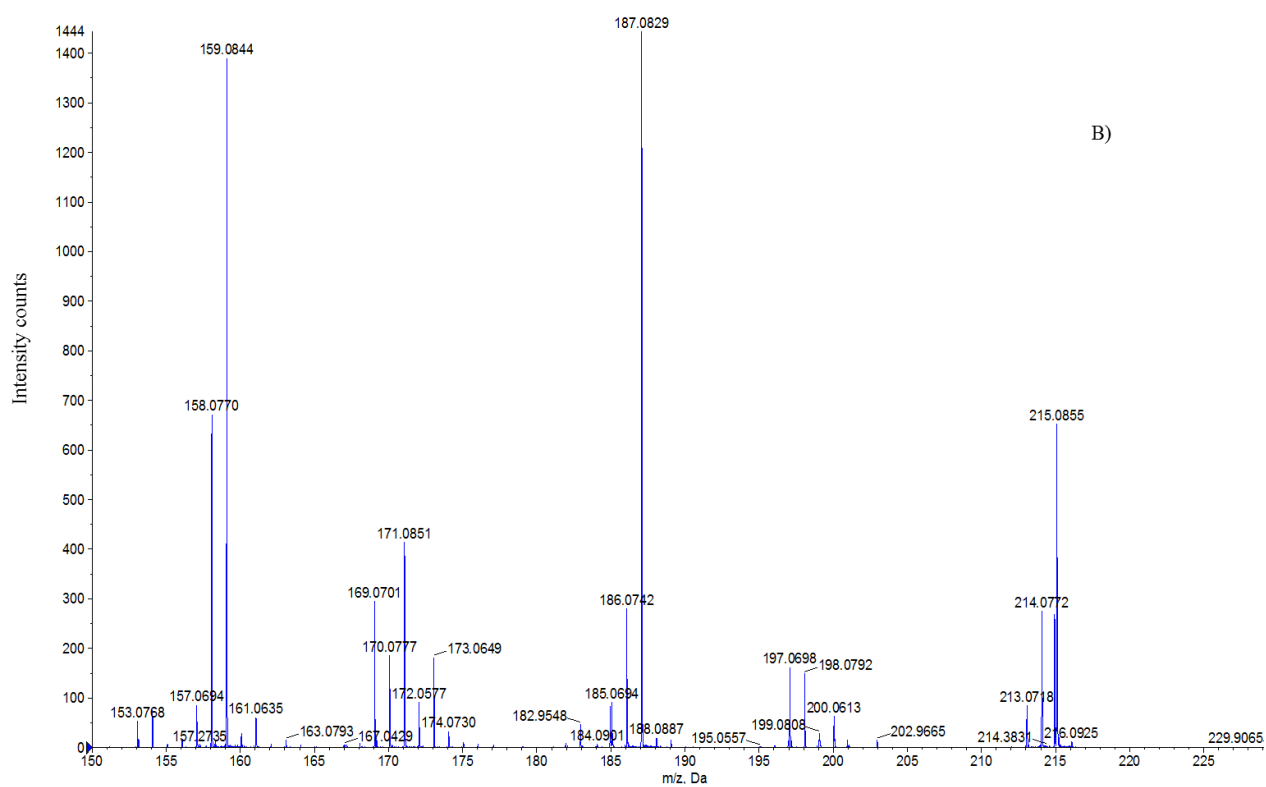
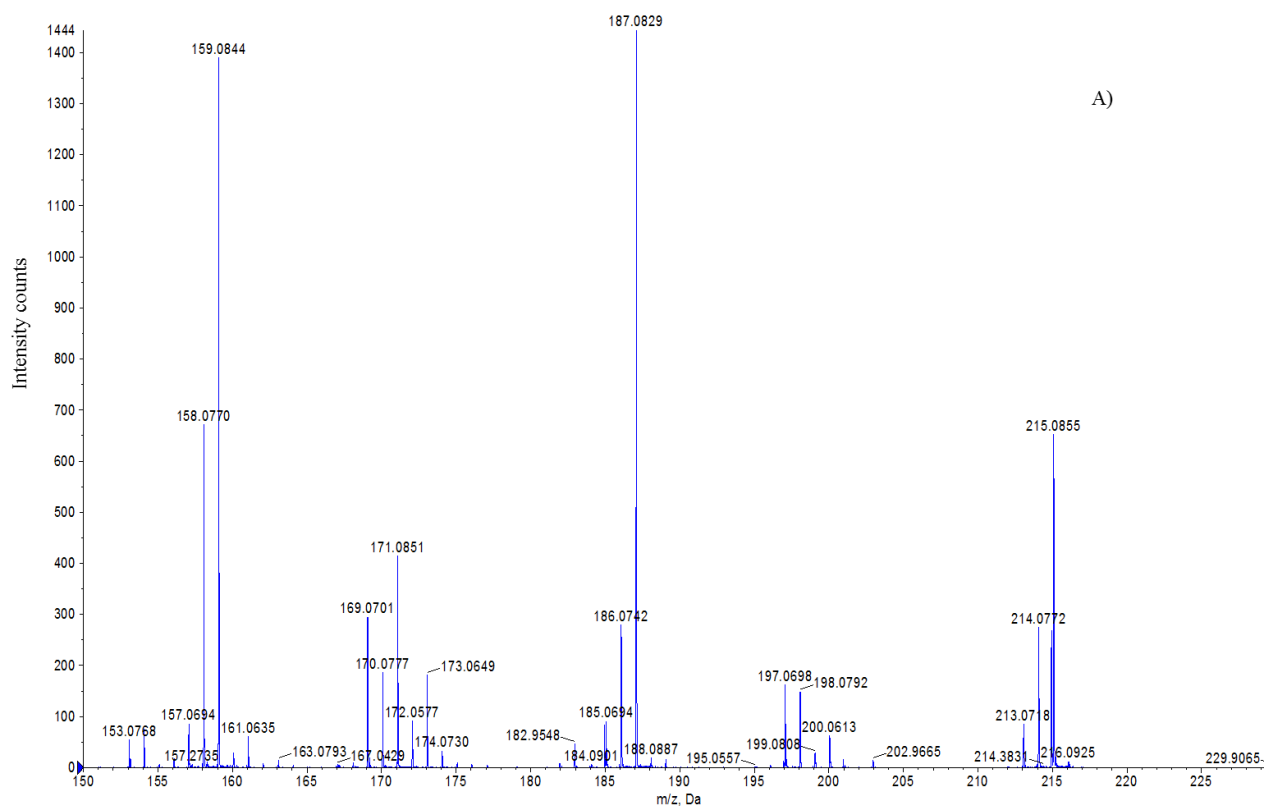


Figure 4.2: MS/MS fragmentation pattern of 2-C-methyl-D-erythritol 4-phosphate (MEP) analysed in negative ESI mode. A) 2-C-methyl-D-erythritol 4-phosphate (MEP) in standard solution. B) 2-C-methyl-D-erythritol 4-phosphate (MEP) in heat shock treatment, mature leaf, aqueous polar phase.

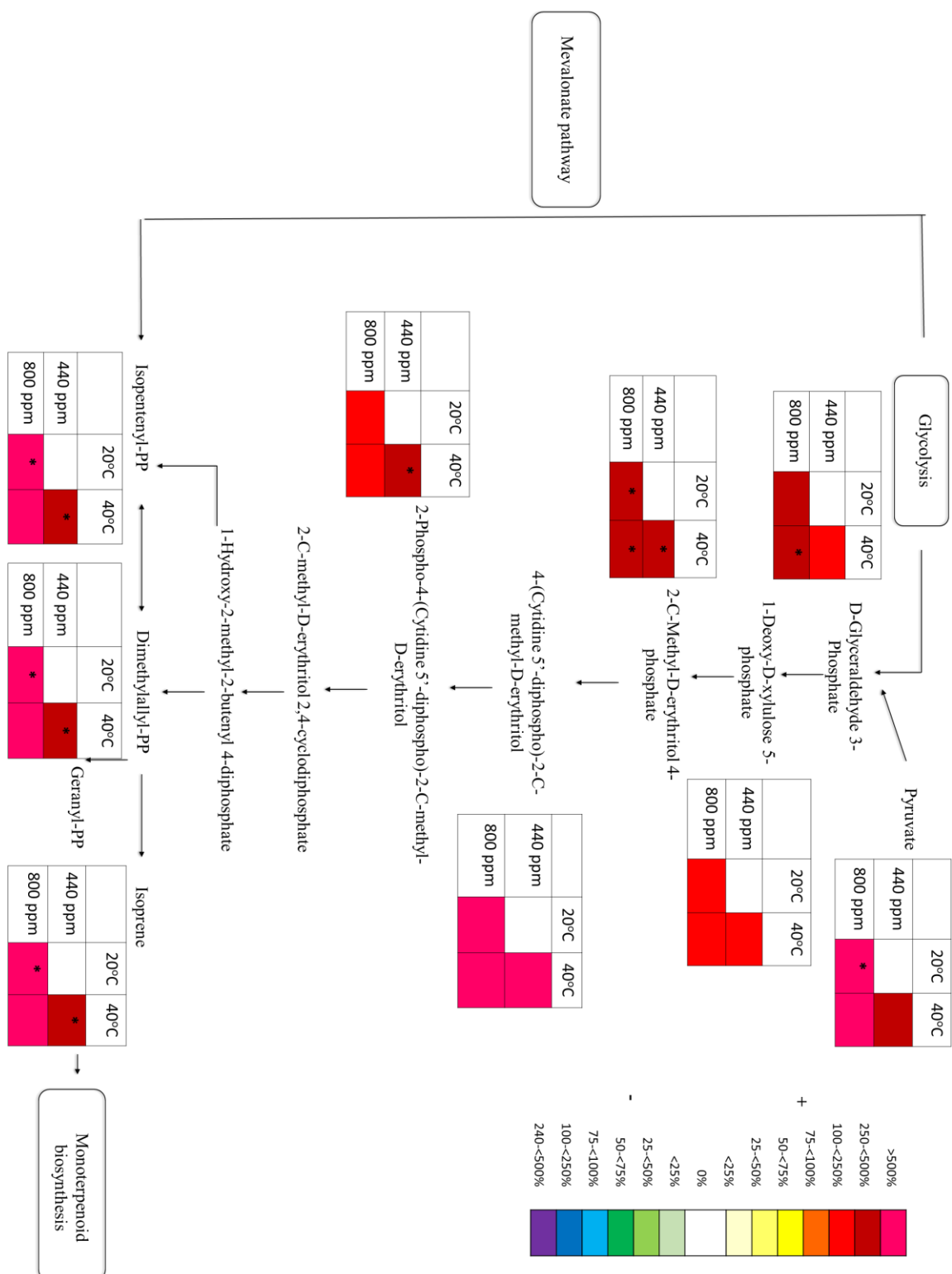
4.3.2 *Plant secondary metabolism pathway analysis*

Following the identification and confirmation of several intermediates in both the flavonoid and MEP/DOXP pathways (table 4.3) through fragmentation patterns compared to analytical standards, a full pathway analysis could be undertaken. Figure 4.3 shows a simplified sketch of the flavonoid biosynthesis pathway and the intermediates that have been identified through tandem ms/ms. Intermediates in the flavonoid pathway that are precursors to the four identified metabolites are also shown in the diagram. However, these have not been confirmed through ms/ms, but have been putatively identified using the data from the untargeted metabolomic analysis and putative identification tables from chapter 3 (table 3.6 and tables A3.1-3.4 in the appendix).

The results of the change in percentage total ion count of the abundance of each intermediate matches the results of table 3.7 in chapter 3. The mass bins that demonstrated a down-regulation of compounds relative to the control that can be found within the flavonoid biosynthesis pathway match the change in %TIC of each metabolite that was analysed. The asterisks in the boxes show differences that are significant. Apart from dihydroquercetin and cinnamoyl-CoA, all of the intermediates show significant differences between treatments when compared to the control. Leucocyanidin has not been included as this metabolite could not be identified in the raw spectra data from the untargeted analyses. The up-regulation of p-coumaroyl-CoA for each treatment when compared to the control is of interest as all other intermediates (with the exception of cinnamoyl-CoA) in the pathway demonstrate suppression in figure 4.3. However, a number of enzymes that are found in different secondary metabolic pathways use p-coumaroyl-CoA. This intermediate is required for phenylpropanoid biosynthesis is used by transferase enzymes in the shikimate pathway for amino acid biosynthesis. It can therefore be postulated that the suppression of metabolites that are up-stream in the flavonoid biosynthesis pathway is as a result of p-coumaroyl-CoA and cinnamoyl-CoA being allocated to other pathways, such as the phenylpropanoid of shikimate pathways, but further work would be required to confirm this. A CO₂ isotope labelling study would need to be conducted to assess the potential different sources of carbon allocation within plant secondary metabolites (Funk, et al., 2004 & Schnitzler, et al., 2004).

Figure 4.4 shows a simplified sketch of the MEP/DOXP pathway. The boxes demonstrate the percentage differences in the abundance of the metabolites in the pathway for each treatment relative to the control. Overall there is an up-regulation of each of the intermediates when compared to the control. Both MEcPP and HMB-PP in

the pathway could not be identified from the raw spectra data from the untargeted analyses and have therefore not been included.



There is however, no suppression of the metabolites in the MEP/DOXP pathway that were subject to the elevated CO₂ treatment. Given our current understanding about the inhibition of isoprene production (see trend demonstrated in figure 1.9) at increased atmospheric CO₂ concentrations, one would expect there to be a more marked down-regulation when compared to the control and the heat shock treatments. Plants that were subject to the elevated CO₂ treatment have shown a significant difference when compared to the control in the production and up-regulation of pyruvate. This is unsurprising given that pyruvate provides ATP to cells through the citric acid cycle and therefore an increase in substrate will provide more ATP for plant secondary metabolic pathways. Following the results of chapter 2, where statistical analyses demonstrated the mitigation of the interaction between elevated CO₂ and a heat shock, it is to be expected that the precursors to isoprene emission do not exhibit a statistically significant difference as a result of the combined treatment when compared to the control. Isopentenyl-PP, Dimethylallyl-PP (and Geranyl-PP, the precursor to monoterpenoid biosynthesis) all show statistically significant increases as a result of the independent effects of elevated CO₂ and a heat shock.

4.4 Discussion

4.4.1 The effect of abiotic stresses on plant metabolic pathways

The aim of this chapter was to both identify and further investigate the MEP/DOXP and flavonoid biosynthesis pathway to assess the production and regulation of isoprene emissions in response to changes in CO₂ and temperature through the use of tandem ms/ms. Through the identification of intermediates within the pathway that have been outlined in table 4.4, a full pathway analysis was conducted to investigate the metabolites within each pathway.

It has been demonstrated that intermediates within the MEP/DOXP pathway were identified in plants that were subject to heat shock treatment. Figure 4.2 shows the fragmentation patterns of both an analytical standard of the MEP intermediate, and the same fragmentation pattern that was identified in the tissue sample of a young leaf. In figures A4.1-4.8 in the appendix the various spectra demonstrate that the intermediates of the MEP pathway can be found in almost all of the leaf tissue samples for all treatments. It is also unsurprising, following the results of chapter 2 and 3, that the metabolic response of the plant to elevated temperature is different to that of the control treatment. The up-regulation of all of the intermediates in the MEP/DOXP pathway (except for MEcPP and HMB-PP which could not be identified), and the significant differences for heat shocked plants compared to the control are in line with the literature, and as discussed in chapter 2, suggest that the production of isoprene through the MEP/DOXP pathway is a thermotolerance response.

The response of the intermediates in the flavonoid biosynthesis pathway follow the same pattern of suppression that have been demonstrated in chapter 3. The putative identification and abundance of flavonoid metabolites in figure 4.3 (with the exception of cinnamoyl-CoA and p-coumaroyl-CoA) show a substantial down-regulation when compared with the control treatment. These results match those of Behnke et al (2010), who reported that there is a down-regulation of phenolic biosynthesis in poplar trees that were subjected to elevated temperature. This down regulation can be seen in the variation of the number of carbon atoms between cinnamoyl-CoA and p-coumaroyl-CoA, and the other intermediates within the flavonoid pathway. A loss of 15 carbon atoms at the point of down regulation indicates that the carbon is being allocated elsewhere. The consistency of 15 carbon atoms in the flavonoid intermediates such as Naringenin ($C_{15}H_{12}O_5$) show that that pathway behaves as a “closed loop”, and that therefore the carbon that is required for isoprene biosynthesis is being allocated from a

different carbon pool within the plant. There is evidence in the literature that isoprene is synthesised from a number of different carbon sources (Funk et al., 2004), and that pyruvate and phosphoenolpyruvate (PEP) in particular could be a feasible route into the chloroplast for the isoprene biosynthesis (Banerjee & Sharkey, 2014). As demonstrated in figure 4.4, there is an up regulation of pyruvate that feeds directly into the MEP pathway, which suggests that it is recently photosynthesised carbon that has been transported from the Calvin-Benson cycle. However, unlike the large number of carbon atoms in the precursors to the flavonoid pathway, pyruvate only has 3 carbon atoms. As isoprene is constructed from 5 carbon units, there must be a secondary regulation point within the pathway where extra carbon can be transported for isoprene biosynthesis. Methylerythritol 2,4-cyclodiphosphate (MEcPP) has 5 carbon units in contrast to the 3 in pyruvate, and the enzymatic reactions of the former, 4-(Cytidine 5'-diphospho)-2-C-methyl-D-erythritol (CDP-ME) and the latter, 2-Phospho-4-(cytidine 5'-diphospho)-2-C-methyl-D-erythritol (CDP_MEP) enzymes contain more carbon units (14) than any other of the intermediates within the MEP pathway. As both of these enzymes synthesise with ATP in order to form MEcPP, it can be suggested that this metabolite has an important regulatory function within the pathway. MEcPP is a known antioxidant (Banerjee & Sharkey, 2014) in times of high oxidative stress, which would account for the investment of extra carbon units for its production. However as stated above, MEcPP was not present in the putative identification of metabolites using percentage total ion count, and further work would need to be conducted in order to determine this function in *Salix* spp. Although it has been found in ¹³C labelling experiments that 77% of recently fixed carbon in heat stressed plants comes from pyruvate (Funk et al., 2004), the exact source of pyruvate is not clearly understood (Banerjee & Sharkey, 2014) and requires further interrogation through labelling experiments.

As previously discussed in the results of chapter 3, suppression of phenolic compounds occurs at high temperatures, most likely as a result of the degradation of both the flavonoids and the anthocyanins (Behnke et al., 2010; Dela et al., 2003). Due to both the antioxidant nature of isoprene, and the ability of isoprene to protect the plant cell membrane (as does lignin as a result of flavonoid biosynthesis), it can be conferred that though it is cost intensive to produce isoprene, the benefits far outweigh the energetic cost and therefore substrate would be allocated away from other pathways for the biosynthesis of isoprene (Wahid et al., 2012).

4.5 Conclusion

This targeted, quantitative study demonstrates the effect that increased isoprene production has upon plant secondary metabolism. The identification of several intermediates in both the MEP/DOXP and flavonoid pathways confirms the putative identifications from chapter 3, and provides an explanation for the biochemical mechanisms that underpin the regulation of BVOC biosynthesis in willow when subject to abiotic stresses. However, as previously stated, more work needs to be conducted in order to fully understand the allocation of carbon into the MEP pathway through pyruvate and/or PEP, thus leading to a comprehensive understanding of MEP metabolic regulation. Confirmation of this would therefore provide an empirical, mechanistic basis for isoprene emissions that could then be scaled up for use in global emissions models (Banerjee & Sharkey, 2014).

Chapter 5: General Discussion

Anthropogenically induced climate change in the last two centuries is contributing to observable changes to the Earth's natural climate system. Increases in atmospheric CO₂ concentration and subsequent global average temperature have occurred at a rate that cannot be explained by natural climatic processes alone. Current research that is aiming to understand the human-induced changes to climate faces the challenge of attempting to quantify the complexities of the climate system. However, when looking at the effects of climate change from a global perspective, it is necessary to attempt to understand not only the driving factors of climate change, but also their interaction and feedback onto the biosphere (Heyder et al., 2011).

It is not just the feedback onto the terrestrial biosphere that is important, but also the feedback of responses of the terrestrial biosphere that have an impact upon global climate. The exchange of gases between the biosphere and atmosphere (depending on the chemical species) have the ability to mitigate the greenhouse warming effect to an extent (Arnth et al., 2010). Terrestrial plants emit approximately 400-600Tg C of one such volatile, isoprene, annually, which can lead to the formation of secondary organic aerosol and exert a negative radiative forcing through their direct and indirect effects in the atmosphere (Scott et al., 2014). However, quantification of the effects of these emissions is still a relatively new science. Global emissions and chemical transport models have been developed to attempt to infer predictions regarding future emissions in response to changing climate, but there are still a number of issues with the accuracy of these (Pacifico et al., 2009). What is also currently unclear is what the driving forces are that determine isoprene production and regulation. With the discovery of the MEP/DOXP metabolic pathway in isoprene-emitting plants in the last twenty years, research has focused upon the biochemical responses of global vegetation to abiotic stresses through metabolomic studies. Currently there is limited knowledge regarding

the mechanisms that underpin the production and regulation of isoprene at a cellular level in response to abiotic stresses. Moreover, most research has focused upon one aspect of changing climate, such as temperature, rather than attempting to increase the complexity of the effects of climate change on vegetation.

With respect to this, the aim of this PhD was therefore to hierarchically investigate the mechanisms that control the regulation and production of isoprene in woody trees from both leaf and plant level emissions through to a targeted study of plant metabolism. This thesis has increased our current understanding of the response of plant secondary metabolism as a response to the interactive effects of elevated CO₂ and extreme temperature. It has provided evidence that current global emissions models cannot reconcile the effect of elevated CO₂ concentration upon isoprene emissions, and further provided evidence that the interaction of the two stresses in effect cancels each other out. Furthermore, this work has shown that there is a carbon allocation trade-off within the plant at times of increased stress, and that at both elevated CO₂ and extreme temperature, substrate availability allows for a reorganisation of plant secondary metabolism that demonstrates the physiological justification for BVOC production without causing damage to the plant during times of short-lived stresses at temperatures up to 40°C.

5.1 The effect of the interaction between extreme temperature and elevated CO₂ on woody plant isoprene emissions are mitigated

Willow plants that were exposed to both elevated CO₂ and extreme temperature treatments demonstrated a slight reduction in isoprene emissions when compared to the other treatments and the control (see chapter 2). This indicates that when isoprene-emitting plants are subject to a combined effect of abiotic stresses, the independent

effects of both that are known to have an effect on isoprene emissions are mitigated. It has been well documented in the literature that isoprene emissions increase when plants are exposed to short-lived extreme heat (Rasulov et al., 2010; Sharkey, 2005; Velikova & Loreto, 2005). The results of chapter 2 agree with the current literature as the plants that were exposed to 40°C heat shock showed a 7% increase when compared to the control treatment. The current explanation for the increase in isoprene emissions in plants as a response to short-lived heat stress is the thermotolerance hypothesis (Peñuelas & Llusià, 2004; Sharkey et al., 2008). This hypothesis has merit given that 1) all plants exhibit heat-tolerance mechanisms such as heat shock proteins and therefore isoprene production may be another adaptation in order to cope with abiotic stress, and 2) there must be some benefit to the plant as the cost of isoprene production is so energetically expensive that evolution would rapidly select against the trait in the absence of such a fitness enhancement, particularly in geographical locations such as arid environments or those with long term extreme temperatures. Further to this, plants subject to temperatures higher than ~45°C demonstrate a large decrease in isoprene emissions that is most likely as a result of enzyme degradation and damage to the plant at the cellular level, ultimately leading to plant senescence. Although plants were not subject to temperatures higher than 40°C in this study, the increase in comparison to the plants at ambient (20°C) temperatures suggest that there is a causal effect of temperature upon isoprene production.

Currently it is unclear in the literature whether elevated CO₂ concentration either decreases, or has little effect upon isoprene emission. The response of the plant is dependent on environment, geographical setting and the species type (Peñuelas & Llusià, 2003) or indeed genotype. In this study however, the results of the air entrainment experiment have shown that plants that were subject to elevated CO₂ showed a 24% decrease in isoprene production relative to the control plants. Given

what is currently known about the effect of increases in carbon upon plant productivity and biomass, and that isoprene production requires up to 50% of a plant's stored carbon, one could therefore infer that an increase in CO₂ would lead to an increase in isoprene emissions. However, the results of both the meta-analysis and the air entrainment study (chapter 2) have shown that isoprene has been both modelled and measured to show a decrease in emissions. This also gives strength to the thermotolerance hypothesis as the driver behind isoprene emissions as it can be suggested that the plant is storing the additional substrate for rapid isoprene biosynthesis under times of stress. This parallels plant responses to disease pressure where, an interaction with a pathogen can leave a plant in a metabolically 'primed' state such that it can more rapidly and more strongly initiate its defences in the case of a subsequent attack (Cameron et al. 2013).

Therefore the pertinent question is what will happen when plants are subjected to both elevated CO₂ and extreme temperature? Following the results of the meta-analysis, isoprene emissions have been predicted to decrease substantially with even slight changes to the concentration of CO₂, even when temperature increases. Hence the 9.6% decrease in isoprene emissions in plants that were subject to both stresses was surprising. It can thus be suggested that increases in CO₂ are dampening the effects of extreme heat, but that ultimately isoprene production is more sensitive to the effects of temperature than it is CO₂. What is still unknown however is whether this effect is evident in all isoprene emitting plants, or whether this is specific to willow, or even cultivar specific. If further investigations found this to be a universal response by isoprene emitting species, it can therefore be inferred that the response of plants to predicted future climate change will be a reduction in isoprene emissions than compared to the current rate, thus decreasing the mitigation effect of the interactions of BVOCs in the atmosphere and the contribution to a negative radiative forcing.

5.2 The effect of extreme temperature on plant secondary metabolism is greater than the effect of elevated CO₂

The results of chapter 3 have demonstrated that when plants are subjected to extreme heat, their secondary metabolism is altered through the reallocation of carbon substrate when compared to the control treatment, and along with plants subject to the elevated CO₂ treatment. When the plants were subject to both elevated CO₂ and temperature, I showed that the resulting impact upon the plant metabolome is more similar to the response to temperature rather than that to the effect of CO₂.

The suppression of the flavonoid and anthocyanin biosynthesis pathways in plants that have been exposed to elevated temperatures is surprising. As discussed in the previous section, there are a number of heat tolerance mechanisms that are present in plants and the flavonoid pathway is responsible for having antioxidant properties that protect the plant against increases in sunlight irradiance and temperature. Isoprene has both thermotolerance and antioxidant properties. Given that both the MEP/DOXP pathway and the flavonoid biosynthesis pathway both share pyruvic acid as a source of carbon, it can be inferred that substrate is being allocated to the MEP/DOXP pathway instead of to other secondary metabolites. Although some studies have suggested that the flavonoids may be favoured over isoprene for their antioxidant properties (Owen & Peñuelas, 2005), the results of chapter 2 and 3 suggest that isoprene emissions is more parsimonious as a response to heat. As discussed in the previous section, isoprene production is energetically expensive and therefore there needs to be a trade-off in terms of the allocation of energy to different metabolic pathways in order for the plant to be protected against heat stress. This interpretation is strengthened by the results of the air entrainment experiment (chapter 2) as isoprene emissions increase with an increase in temperature.

The evidence for a thermotolerance response at the biochemical level is also strengthened by the current knowledge of the evolution of isoprene emitting capacity and the taxonomical and geographical distribution of species that produce BVOCs. Isoprene emissions are produced by fast growing perennial plants such as willow and poplar (Loreto & Fineschi, 2015). As these plants grow quickly in summer, they are therefore subject to rapid variations in temperature that could have an effect upon their photosynthetic rate. Therefore instead of utilising heat shock proteins or secondary metabolites such as the flavonoids that protect against oxidative stress, plants may have favoured a short-term, expensive yet effective method of dealing with short-term stresses (Loreto & Fineschi, 2015), such as the production of isoprene.

Although isoprene emissions decrease with an increase in CO₂, at the cellular level, it can be seen that carbon is being allocated to other pathways in plant secondary metabolism that promote plant productivity. Although the results of the above ground biomass measurements did not reveal any significance in plant growth in samples that were exposed to elevated CO₂ levels, the up-regulation of the shikimate, tryptophan, alkaloid and pentose phosphate pathways shows that carbon is being allocated to promote plant growth. It can therefore be suggested that if plants were grown in elevated CO₂ conditions from planting, there would be an increase in biomass in contrast to those grown in ambient CO₂ conditions. The biochemical intermediates that have been putatively identified as being up-regulated in relation to the control are those that are directly involved in the conversion and storage of energy via the citric acid cycle. Old leaves in particular have been demonstrated to be a carbon sink, which suggests that the plant is storing carbon in chemical forms that could be rapidly utilised in times of heat stress for isoprene production.

Plants that have been subject to an increase in carbon substrate, but have also been subjected to heat stress show that there is a significant interaction between the two

abiotic stresses. It has been shown that in young leaves, the response of the plant metabolome to the interactive effects of both elevated CO₂ and extreme temperature is greater than in mature leaves. This is because the carbon sink that has been demonstrated in mature leaves is providing a carbon source for the young leaves that are more susceptible to heat stress and thus will be producing more isoprene. As there is more carbon substrate available, in times of short-term heat stress isoprene can be produced and emitted whilst the plant's photosynthetic ability is not compromised and therefore the plant is protected. Therefore more work needs to be conducted to assess the allocation of carbon through the citric acid cycle into pyruvate to look for the metabolic "switch" that can allow the plant to divert carbon whilst maintaining normal photosynthetic function at temperatures greater than 28°C.

5.3 Evidence for the metabolic switch that provides protection for woody plants that have been subjected to both extreme temperature and elevated CO₂

In chapter 4, the results of the targeted metabolic analysis have confirmed the hypotheses that were put forward in chapter 3. There is evidence of a metabolic switch that is able to allocate carbon to the MEP/DOXP pathway for isoprene production, therefore causing a suppression of other secondary metabolic pathways such as the flavonoid biosynthesis pathway. The identification through tandem ms/ms of the intermediates of both the flavonoid and MEP/DOXP pathways have confirmed that the putative identifications made in chapter 3 show that temperature induces the greatest response in plants. The up-regulation of the intermediate p-coumaroyl-CoA within the flavonoid pathway would suggest that this is where substrate is being diverted and allocated to a different pathway. As discussed previously, both the flavonoid biosynthesis pathway and the MEP/DOXP share pyruvic acid as an intermediate, and it

may be the case that through the shikimate pathway carbon is being redirected to isoprene production. Further investigation needs to be carried out on the intermediates that derive from the citric acid cycle, including pyruvate, PEP and intermediates within the shikimate pathway in order to confirm this. Carbon budgeting (chapter 4) shows that there is an up regulation of pyruvate that feeds directly into the MEP pathway, suggesting that recently photosynthesised carbon from the Calvin-Benson cycle has been transported to this pathway. This however requires further identification as other experiments have not identified the source of carbon from pyruvate in heat stressed plants.

5.4 Conclusion

This PhD thesis has enhanced our current understanding of the effect of abiotic stresses on willow secondary metabolism and isoprene regulation and production. Thus, in relation to the effects of future climate change upon global vegetation, the results of this thesis demonstrate the need for more detailed biochemical processes to be incorporated into current global volatile organic compound emissions models. The variability in the magnitude of isoprene emissions in global models is due to a lack of understanding of the biochemical mechanisms that regulate the production of isoprene through the MEP pathway and the carbon costs to the plant through allocation to different metabolic pathways. Further research into the carbon trade-off between pathways and the allocation of recently assimilated carbon from the Calvin-Benson cycle will provide more information regarding the effect of elevated CO₂ on plant productivity and isoprene production, especially when combined with the thermotolerance response of vegetation under stress from extreme temperature. There is however, a need for further investigative work into whether the metabolic changes in

isoprene emitting plants are cultivar-specific, or whether these responses are general for all isoprene emitting species when subjected to both elevated temperature and CO₂. Moreover, it is essential to further investigate the potential metabolic switch in woody plants hinted at by this research and subsequent carbon allocation to different pathways that effect the production and regulation of not only isoprene emission, but other secondary metabolites that are associated with plant stress. Subsequently it will then be possible to investigate the response of woody plants to abiotic stress at the forest level, rather than on a plant-by-plant basis that can then be scaled up to enhance current isoprene emissions rates that are used by global emissions models currently.

Bibliography

Agati, G., Azzarello, E., Pollastri, S., and Tattini, M., 2012. Flavonoids as antioxidants in plants: location and functional significance. *Plant Science*. Vol. 196. pp. 67-76.

Ahuja, I., de Vos, R. C H., Bones, A. M., and Hall, R. D., 2010. Plant molecular stress responses face climate change. *Trends in Plant Science*. Vol. 15 (12). pp. 664-681.

Ainsworth, E. A., Rogers, A., Vodkin, L. O., Walter, A., and Schurr, U., 2006. The effects of elevated CO₂ concentration on soybean gene expression. An analysis of growing and mature leaves. *Plant Physiology*. Vol.142. pp. 135-147.

Akula, R., and Ravishankar, G. A., 2011. Influence of abiotic stress signals on secondary metabolites in plants. *Plant Signaling and Behavior*. Vol. 6 (11). pp. 1720-1731.

Arneth, A., Miller, P. A., Scholze, M., Hickler, T., Schurgers, G., Smith, B., and Prentice, I. C., 2007. CO₂ inhibition of global terrestrial isoprene emissions: Potential implications for atmospheric chemistry. *Geophysical Research Letters*. Vol. 34 (18). DOI: 10.1029/2007GL030615

Arneth, A., Monson, R. K., Schurgers, G., Niinemets, Ü., and Palmer, P. I., 2008. Why are estimates of global terrestrial isoprene emissions so similar (and why is this not so for monoterpenes)? *Atmospheric Chemistry and Physics*. Vol. 8. pp. 4605-4620.

Arneth, A., Sitch, S., Bondeau, A., Butterbach-Bahl, K., Foster, P., Gedney, N., de Noblet-Ducoudré, N., Prentice, I. C., Sanderson, M., Thonicke, K., Wania, R., and Zaehle, S., 2010. From biota to chemistry and climate: towards a comprehensive description of trace gas exchange between the biosphere and atmosphere. *Biogeosciences*. Vol. 7. pp. 121-149.

Arneth, A., Schurgers, G., Lathiere, J., Duhl, T., Beerling, D. J., Hewitt, C. N., Martin, M., and Guenther, A., 2011. Global terrestrial isoprene emission models: sensitivity to variability in climate and vegetation. *Atmospheric Chemistry and Physics*. Vol. 11. pp. 8037-8052.

Atkinson, R., and Arey, J., 2003. Gas-phase tropospheric chemistry of biogenic organic compounds: a review. *Atmospheric Environment*. Vol 37 (2). pp. 197-219.

Banerjee, A., and Sharkey, T. D., 2014. Methylerythritol 4-phosphate (MEP) pathway metabolic regulation. *Natural Product Reports*. Vol. 31. pp. 1043-1055.

Behnke, A., Kaiser, A., Zimmer, I., Brüggemann, N., Janz, D., Polle, A., Hampp, R., Hänsch, R., Popko, J., Schmitt-Koplin, P., Ehlting, B., Rennenberg, H., Barta, C., Loreto, F., Schnitzler, J., 2010. RNAi-mediated suppression of isoprene emission in poplar transiently impacts phenolic metabolism under high temperature and high light intensities: a transcriptomic and metabolomic analysis. *Plant Molecular Biology*. Vol. 74. pp. 61-75.

- Bonan, G. B., 2008. Forests and Climate Change: Forcings, Feedbacks, and the Climate Benefits of Forests. *Science*. Vol. 320. pp. 1444-1449.
- Brilli, F., Barta, C., Fortunati, A., Lerda, M., Loreto, F., Centritto, M., 2007. Response of isoprene emission and carbon metabolism to drought in white poplar (*Populus alba*) saplings. *New Phytologist*. Vol. 175. pp. 244-254.
- Brunetti, C., Di Ferdinando, M., Fini, A., Pollastri, S., and Tattini, M. 2013. Flavonoids as antioxidants and developmental regulators: relative significance in plants and humans. *International Journal of Molecular Sciences*. Vol. 14. pp. 3540-3555.
- Buckley, P. T., 2001. Isoprene emissions from a Florida scrub oak species grown in ambient and elevated carbon dioxide. *Atmospheric Environment*. Vol. 35. pp. 631-634.
- Cameron, D. D., Neal, A. L., van Wees, S. C. M., and Ton, J., 2013. Mycorrhiza-induced resistance: more than the sum of its parts? *Trends in Plant Science*. Vol. 18 (10). pp. 539-545.
- Canadell, J. G., Le Quéré, C., Raupach, M. R., Field, C. B., Buitenhuis, E. T., Ciais, P., Conway, T. J., Gillett, N. P., Houghton, R. A., and Marland, G., 2007. Contributions to accelerating atmospheric CO₂ growth from economic activity, carbon intensity, and efficiency of natural sinks. *Proceedings of the National Academy of Science*. Vol. 104 (47). pp. 18866-18870.
- Centritto, M., Nascetti, P., and Petrilli, L., 2004. Profiles of isoprene emission and photosynthetic parameters in hybrid poplar exposed to free-air CO₂ enrichment. *Plant Cell and Environment*. Vol. 27. pp. 403-412.
- Chamot, J. A., and Fuller, N. R., 2008. Forests and Climate Change: What's their role in Global Warming? [Online] Available at: <http://www.ucar.edu/news/features/forests/>. [Accessed: 14th July 2015].
- Claeys, M., Graham, B., Vas, G., Wang, W., Vermeylen, R., Pashynska, V., Cafmeyer, J., Guyon, P., Andreae, M. O., Artaxo, P., and Maenhaut, W., 2004. Formation of secondary organic aerosols through photooxidation of isoprene. *Science*. Vol. 303. pp. 1173-1176.
- Climatic Research Unit: University of East Anglia. Jones, P., Harpham, C., Osborn, R., and Salmon, M., 2014. Temperature. [Online]. Available from: <http://www.cru.uea.ac.uk/cru/data/temperature/>. [Accessed 24th August 2015].
- Cramer, G. R., Urano, K., Delrot, S., Pezzotti, M., and Shinozaki, K., 2011. Effects of abiotic stress on plants: a systems biology perspective. *BMC Plant Biology*. Vol. 11. pp. 1-14.
- Cramer, W., Bondeau, A., Woodward, I., F., Prentice, C. I., Betts, R. A., Brovkin, V., Cox, P. M., Fisher, V., Foley, J. A., Friend, A. D., Kuckarik, C., Lomas, M. R., Ramankutty, N., Sitch, S., Smith, B., White, A., and Young-Molling, C., 2001. Global response of terrestrial ecosystem structure and function to CO₂ and climate change: results from six dynamic global vegetation models. *Global Change Biology*. Vol. 7. pp. 357-373.

Dani, K. G., Jamie, I. M., Prentice, I. C. and Atwell, B. J., 2014. Evolution of isoprene emission capacity in plants. *Trends in Plant Science*. Vol. 19 (7). pp. 439-446.

Daviss, B., 2005. Growing pains for metabolomics. *The Scientist*. Vol. 19 (8). pp. 25-28.

Dela, G., Or, E., Ovadia, R., Nissim-Levi, A., Weiss, D., Oren-Shamir, M., 2003. Changes in anthocyanin concentration and composition in 'Jaguar' rose flower due to transient high-temperature conditions. *Plant Science*. Vol. 164. pp. 333-340.

Dizengremel, P., Vaultier, M.-N., Le Thiec, D., Cabané, M., Bagard, M., Gérard, D., Gérard, J., Dghim, A. A., Richet, N., Afif, D., Pireaux, J.-C., Hazenfratz-Sauder, M.-P., and Jolivet, Y., 2012. Phosphoenolpyruvate is at the crossroads of leaf metabolic responses to ozone stress. *New Phytologist*. Vol. 195. pp. 512-517.

Earth System Research Laboratory. Tans, P., and Keeling, R., (2015). Trends in Atmospheric Carbon Dioxide. [Online] Available from: ftp://aftp.cmdl.noaa.gov/products/trends/co2/co2_annmean_mlo.txt. [Accessed 24th August 2015].

Edreva, A., Velikova, V., Tsonev, T., Dagnon, S., Gürel, A., Aktaş, L., and Gesheva, E., 2008. Stress-protective role of secondary metabolites: diversity of functions and mechanisms. *General and Applied Plant Physiology*. Vol. 34. pp. 67-78.

Farquhar, G. D., von Caemmerer, S., and Berry, J. A., 1980. A biochemical model of photosynthetic CO₂ assimilation in leaves of C₃ species. *Planta*. Vol. 149. pp. 78-90.

Farrar, J. F., and Williams, M. L., 1991. The effects of increased atmospheric carbon dioxide and temperature on carbon partitioning, source-sink relations and respiration. *Plant, Cell, and Environment*. Vol. 14. pp. 819-830.

Fini, A., Brunetti, C., Di Ferdinando, M., Ferrini, F., and Tattini, M. 2011. Stress-induced flavonoid biosynthesis and the antioxidant machinery of plants. *Plant Signalling and Behaviour*. Vol. 6 (5). pp. 709-711.

Foyer, C. H., Ferrario-Méry, S., & Huber, S. C., 2000. Regulation of carbon fluxes in the cytosol: coordination of sucrose synthesis, nitrate reduction and organic acid and amino acid biosynthesis. In R. C. Leegood, T. D. Sharkey, & S. V. Caemmerer (Eds). *Photosynthesis: Physiology and Metabolism*. New York: Kluwer Academic Publishers. pp. 177-203.

Funk, J. L., Mak, J. E., and Lerdau, M. T., 2004. Stress-induced changes in carbon sources for isoprene production in *Populus deltoides*. *Plant, Cell, and Environment*. Vol. 27. pp. 747-755.

Guenther, A., Hewitt, C. N., Erickson, D., Fall, R., Geron, C., Graedel, T., Harley, P., Klinger, L., Lerdau, M., McKay, W. A., Pierce, T., Scholes, B., Steinbrecher, R., Tallamraju, R., Taylor, J., and Zimmerman, P., 1995. A global model of natural

volatile organic compound emissions. *Journal of Geophysical Research*. Vol. 100. pp. 8873- 8892.

Guenther, A., Karl, T., Harley, P., Wiedinmyer, C., Palmer, P. I., and Geron, C., 2006. Estimates of Global Terrestrial Isoprene Emissions using MEGAN (Models of Emissions of Gases and Aerosols from Nature). *Atmospheric Chemistry and Physics Discussions*. Vol. 6 (1). pp. 107-173.

Guenther, A. B., Jiang, X., Heald, C. L., Sakulyanontvittaya, T., Duhl, T., Emmons, L. K., and Wang, X., 2012. The Model of Emissions of Gases and Aerosols from Nature version 2.1 (MEGAN2.1): an extended and updated framework for modelling biogenic emissions. *Geoscientific Model Development*. Vol 5. pp. 1471-14952.

Guy, C., Kaplan, F., Kopka, J., Selbig, J., and Hinch, D. K., 2008. Metabolomics of temperature stress. *Physiologia Plantarum*. Vol132. pp. 220-235.

Hansen, J., Sato, M., Ruedy, R., Lo, K., Lea, D. W., and Medina-Elizade, M., 2006. Global Temperature Change. *Proceedings of the National Academy of Science*. Vol. 103 (39). pp. 14288-14293.

Hansen, J., Ruedy, R., Sato, M., and Lo, K., 2010. Global surface temperature change. *Review of Geophysics*. RG4004.

Heald, C. L., Wilkinson, M. J., Monson, R. K., Alo, C. A., Wang, G., and Guenther, A., 2009. Response of isoprene emission to ambient CO₂ changes and implications for global budgets. *Global Change Biology*. Vol. 15. pp. 1127-1140.

Heyder, U., Schaphoff, S., Gerten, D., and Lucht, W., 2011. Risk of severe climate change impact on the terrestrial biosphere. *Environmental Research Letters*. Vol. 6. pp. 1-8.

Hikosaka, K., Onoda, Y., Kinugasa, T., Nagashima, H., Anten, N. P. R., and Hirose, T., 2005. Plant responses to CO₂ concentration at different scales: leaf, whole plant, canopy, and population. *Ecological Research*. Vol. 20. pp. 243-253.

Holm J. A., Jardine, K., Guenther, A. B., Chambers, J. Q., and Tribuzy, E., 2014. Evaluation of MEGAN-CLM parameter sensitivity to predictions of isoprene emissions from an Amazonian rainforest. *Atmospheric Chemistry and Physics Discussions*. Vol 14. pp. 23995-24041.

Holopainen, J. K., 2013. Loss of isoprene-emitting capacity: deleterious for trees? *Tree Physiology*. Vol. 33. pp. 559-561.

Hunter, W. N., 2007. The Non-mevalonate pathways of isoprenoid precursor biosynthesis. *The Journal of Biological Chemistry*. Vol. 282 (30). pp. 21573-21577.

IPCC, 2007: Climate Change 2007: *Synthesis Report. Contribution of Working Groups I, II and III to the Fourth Assessment Report of the Intergovernmental Panel on*

Climate Change [Core Writing Team, Pachauri, R.K and Reisinger, A. (Eds.)]. IPCC, Geneva, Switzerland.

IPCC, 2013: *Climate Change 2013: The Physical Science Basis. Contribution of Working Group I to the Fifth Assessment Report of the Intergovernmental Panel on Climate Change*. T. F. Stocker, D. Qin, G. K. Plattner, M. Tignor, S.K. Allen, J. Boschung, A. Nauels, Y. Xia, V. Bex and P.M. Midgley (Eds). Cambridge University Press, United Kingdom and New York, USA.

IPCC, 2014: *Climate Change 2014: Synthesis Report. Contribution of Working Groups I, II, and III to the Fifth Assessment Report of the Intergovernmental Panel on Climate Change*. R. K. Pachauri, and L. A. Meyer (Eds). Cambridge University Press, United Kingdom and New York, USA.

Jandrić, Z., Haughey, S. A., Frew, R. D., McComb, K., Galvin-King, P., Elliott, C. T., and Cannavan, A., 2015. Discrimination of honey of different floral origins by a combination of various chemical parameters. *Food Chemistry*. Vol. 189. pp. 52-59.

Kainulainen, P., Holopainen, J. K., and Holopainen, T., 1998. The influence of elevated CO₂ and O₃ concentrations on Scots pine needles: changes in starch and secondary metabolites over three exposure years. *Oecologia*. Vol. 114. pp. 455-460.

Kaling, M., Kanawati, B., Ghirado, A., Albert, A., Winkler, J. B., Heller, W., Barta, C., Loreto, F., Schmitt-Kopplin, P., and Schnitzler, J.-P., 2014. UV-B mediated metabolic rearrangements in poplar by non-targeted metabolomics. *Plant, Cell and Environment*. Vol. 38 (5). pp. 1-13.

Karl, M., Guenther, A., Köble, R., Leip, A., and Seufert, G., 2009. A new European plant-specific emission inventory of biogenic volatile organic compounds for use in atmospheric transport models. *Biogeosciences*. Vol. 6. pp. 1059-1087.

Kegg Pathway Database. Available at:
<http://www.genome.jp/kegg/pathway.html> (Accessed 14th September 2016).

Körner, C., 2000. Biosphere responses to CO₂ enrichment. *Ecological Applications*. Vol. 10. pp. 1590-1619.

Kroll, J. H., Ng, N. L., Murphy, S. M., Flagan, R. C., and Seinfeld, J. H., 2006. Secondary organic aerosol formation from isoprene photooxidation. *Environmental Science and Technology*. Vol. 40. pp. 1869-1877.

Lammertsma, E. I., de Boer, H. J., Dekker, S. C., Dilcher, D. L., Lotter, A. F., and Wagner-Cremer, F., 2011. Global CO₂ rise leads to reduced maximum stomatal conductance in Florida vegetation. *Proceedings of the National Academy of Science*. Vol. 108 (10). pp. 4035-4040.

Lathièrè, J., Hewitt, C. N., and Beerling, D. J., 2010. Sensitivity of isoprene emissions from the terrestrial biosphere to 20th century changes in atmospheric CO₂ concentration, climate and land use. *Global Biogeochemical cycles*. Vol. 24 (1). pp. GB1004.

Lerdau, M., and Keller, M., 1997. Controls on isoprene emission from trees in a subtropical dry forest. *Plant, Cell, and Environment*. Vol. 20. pp. 469-578.

Levine, L. H., Kasahara, H., Kopka, J., Erban, A., Fehrl, I., Kaplan, F., Zhao, W., Littell, R. C., Guy, C., Wheeler, R., Sager, J., Mills, A., Levine, H. G., 2008. Physiologic and metabolic responses of wheat seedlings to elevated and super-elevated carbon dioxide. *Advances in Space Research*. Vol. 42. pp. 1917-1928.

Li, P., Ainsworth, E. A., Leakey, A. D. B., Ulanov, A., Lozovaya, V., Ort, D. R., and Bohnert, H. J., 2008. *Arabidopsis* transcript and metabolite profiles: ecotype-specific responses to open air elevated [CO₂]. *Plant, Cell and Environment*. Vol. 31. pp. 1673-1687.

Li, Z., and Sharkey, T. D., 2013. Molecular and pathway controls on biogenic volatile organic compound emissions. In Niinemets, Ü., and Monson, R. K., (eds) *Biology, controls and models of tree volatile organic compounds*. London: Springer. pp. 119-151.

Lindegaard, K., 2012. Willow Varietal Identification Guide. *Agriculture and Food Development Authority*. B. Caslin, J. Finnan, and A. McCracken (Eds).

Lo Piero, A. R., Puglisi, I., Rapisarda, P., and Petrone, G., 2005. Anthocyanins accumulation and related gene expression in red orange fruit induced by low temperature storage. *Journal of Agricultural Food and Chemistry*. Vol. 53. pp. 9083-9088.

Logan, B. A., Monson, R. K., and Potosnak, M. J., 2000. Biochemistry and physiology of foliar isoprene production. *Trends in Plant Science*. Vol. 5 (11). pp. 477-481.

Loreto, F., and Fineschi, S., 2015. Reconciling functions and evolution of isoprene emission in higher plants. *New Phytologist*. Vol. 206. pp. 578-582.

Loreto, F., and Schnitzler, J-P., 2010. Abiotic stresses and induced BVOCs. *Trends in Plant Science*. Vol. 15 (3). pp. 154-166.

Loreto, F., and Sharkey, T. D., 1990. A gas-exchange study of photosynthesis and isoprene emissions in *Quercus rubra*. *Planta*. Vol. 182. pp. 523-531.

Loreto, F., and Sharkey, T. D., 1993. On the relationship between isoprene emission and photosynthetic metabolites under different environmental conditions. *Planta*. Vol. 189. pp. 420-424.

Mattson W. J., Julkunen-Tiitto, R., Herms, D. A., and Larsson, S., 2005. CO₂ enrichment and carbon partitioning to phenolics: Do plant responses accord better with the protein competition or the growth-differentiation balance models? *Oikos*. Vol. 111 (2). pp. 337-347.

Meinshausen, M., Smith, S. J., Calvin, K., Daniel, J. S., Kainuma, M. L. T., Lamarque, J-F., Matsumoto, K., Montzka, S. A., Raper, S. C. B., Riahi, K., Thomson, A., Velders, G. J. M., and van Vuuren, D. P. P., 2011. The RCP greenhouse gas

concentrations and their extensions from 1765 to 2300. *Climatic Change*. Vol. 109. pp. 213-241.

Met Office. Global climate in context as the world approaches 1°C above pre-industrial for the first time. [Online]. University of East Anglia: Met Office. 2016. Available at: <http://www.metoffice.gov.uk/research/news/2015/global-average-temperature-2015>. [Last accessed 06/08/17].

Minitab Inc., 2010. "Analyzing Data". *Getting Started with Minitab 17*. pp. 24.

Monson, R. K., Trahan, N., Rosenstiel, T. N., Veres, P., Moore, D., Wilkinson, M., Norby, R. J., Volder, A., Tjoelker, M. G., Briske, D. D., Karnosky, D. F., and Fall, R., 2007. Isoprene Emission from Terrestrial Ecosystems in Response to Global Change: the Gap between Models and Observations. *Philosophical Transactions of the Royal Society A*. Vol 365. pp. 1677-1695.

Monson, R. K., Jones, R. T., Rosenstiel, T. N., and Schnitzler, J.-P., 2013. Why only some plants emit isoprene. *Plant Cell and Environment*. Vol. 36. pp. 503-516.

Monson, R. K., Neice, A. A., Trahan, N. A., Shiach, I., McCorkel, J. T., and Moore, D. J. P., 2016. Interactions between temperature and intercellular CO₂ concentration in controlling lead isoprene emission rates. *Plant Cell and Environment*. Vol. 39. pp. 2404-2413.

Mori, K., Goto-Yamamoto, N., Kitayama, M., and Hashizume, K., 2007. Loss of anthocyanins in red-wine grape under high temperature. *Journal of Experimental Biology*. Vol. 58 (8). pp. 1935-1945.

Moss, R. H., Edmonds, J. A., Hibbard, K. A., Manning, M. R., Rose, S. K., van Vuuren, D. P., Carter, T. R., Emori, S., Kainuma, M., Kram, T., Meehl, G. A., Mitchell, J. F. B., Nakicenovic, N., Riahi, K., Smith, S. J., Stouffer, R. J., Thomson, A. M., Weyant, J. P., and Wilbanks, T. J., 2010. The next generation of scenarios for climate change research and assessment. *Nature*. Vol. 463. pp. 747-756.

Naik, V., Delire, C., and Wuebbles, D. J., 2004. Sensitivity of Global Biogenic Isoprenoid Emissions to Climate Variability and Atmospheric CO₂. *Journal of Geophysical Research: Atmospheres*. Vol 109. D06301.

National Oceanic and Atmospheric Administration: *Trends in Atmospheric carbon dioxide: Full Mauna Loa CO₂ record*. USA: Earth System Research Laboratory: Global Monitoring Division. Available at: <http://www.esrl.noaa.gov/gmd/ccgg/trends/full.html>. [Accessed 10th November 2016.]

Overy, S. A., Walker, H. J., Malone, S., Howard, T. P., Baxter, C. J., Sweetlove, L. J., Hill, S. A., and Quick, P. W., 2005. Application of metabolite profiling to the identification of traits in a population of tomato introgression lines. *Journal of Experimental Botany*. Vol. 56. pp. 287-296.

- Owen, S., and Peñuelas, J., 2005. Opportunistic emissions of volatile isoprenoids. *Trends in Plant Science*. Vol. 10. pp. 42-426.
- Paajanen, E., Julkunen-Titto, R., Nybakken, L., Petrelius, M., Tegelberg, R., Pusenius, J., Rousi, M., and Kellomäki, S., 2011. Dark-leaved willow (*Salix myrsinifolia*) is resistant to three-factor (elevated CO₂, temperature and UV-B-radiation) climate change. *New Phytologist*. Vol. 190. pp. 161-168.
- Pacifico, F., Harrison, S. P., Jones, C. D., and Sitch, S., 2009. Isoprene emissions and climate. *Atmospheric Environment*. Vol. 43. pp. 6121-6135.
- Parmesan, C., and Yohe, G., 2003. A globally coherent fingerprint of climate change impacts across natural systems. *Nature*. Vol. 42. pp. 37-42.
- Peñuelas, J., Estiarte, M., 1998. Can elevated CO₂ affect secondary metabolism and ecosystem function? *Trends in Ecology and Evolution*. Vol. 13. pp. 20-24.
- Peñuelas, J., and Llusà, J., 2003. BVOCs: plant defense against climate warming? *Trends in Plant Science*. Vol. 8 (3). pp. 105-109.
- Peñuelas, J., and Llusà, J., 2004. Plant VOC emissions: making use of the unavoidable. *Trends in Ecology and Evolution*. Vol. 19 (8). pp. 402-404.
- Peñuelas, J., Llusà, J., Asensio, D., and Munné-Bosch, S., 2005. Linking isoprene with plant thermotolerance, antioxidants and monoterpene emissions. *Plant, Cell and Environment*. Vol. 28. pp. 278-286.
- Peñuelas, J., and Staudt, M., 2010. BVOCs and global change. *Trends in Plant Science*. Vol. 15 (3). pp. 133-144.
- Pietta, P.-G., 2000. Flavonoids as antioxidants. *Journal of Natural Produce*. Vol. 63. pp. 1035-1042.
- Possell, M., Hewitt, N. C., and Beerling, D., J., 2005. The Effects of Glacial Atmospheric CO₂ Concentrations and Climate on Isoprene Emissions by Vascular Plants. *Global Change Biology*. Vol. 11 (1). pp. 60-69.
- Procházková, D., Boušà, I., and Wilhelmová, N., 2011. Antioxidant and prooxidant properties of flavonoids. *Fitoterapia*. Vol. 82 (4). pp. 513-523.
- Ramakrishna, A., and Ravishankar, G. A., 2011. Influence of abiotic stress signals on secondary metabolites in plants. *Plant Signalling and Behaviour*. Vol. 6 (11). pp. 1720-1731.
- Rapparini, F., Baraldi, R., Miglietta, F., 2004. Isoprenoid emission in trees of *Quercus pubescens* and *Quercus ilex* with lifetime exposure to naturally high CO₂ environment. *Plant Cell and Environment*. Vol. 27. pp. 381-391.
- Rasulov, B., Hüve, K., Bichele, I., Laisk, A., and Niinemets, Ü., 2010. Temperature response of isoprene emissions in vivo reflects a combined effect of

substrate limitations and isoprene synthase activity: A kinetic analysis. *Plant Physiology*. Vol. 154. pp. 1558-1570.

Rasulov, B., Talts, E., and Niinemets, Ü., 2016: In press. Spectacular oscillations in plant isoprene emission under transient conditions explain the enigmatic CO₂ response. *Plant Physiology*. Vol 172. pp. 2275-2285.

Raupach, M. R., Marland, G., Ciais, P., Le Quéré, C., Canadell, J. G., Klepper, G., and Field, G. B., 2007. Global and regional drivers of accelerating CO₂ emissions, *Proceedings of the National Academy of Science*. Vol. 104 (24). pp. 10288-10293.

Ringñer, M., 2008. What is principal component analysis? *Nature Biotechnology*. Vol. 26. pp. 303-304.

Roessner, U., and Bowne, J., 2009. What is metabolomics all about? *Biotechniques*. Vol. 46 (5). pp. 363-365.

Rogelj, J., Meinshausen, M., and Knutti, R., 2012. Global warming under old and new scenarios using IPCC climate sensitivity range estimates. *Nature Climate Change*. Vol. 2. pp. 248-253.

Rohmer, M., 1999. The discovery of a mevalonate-independent pathway for isoprenoid biosynthesis in bacteria, algae and higher plants. *Natural Product Reports*. Vol. 16. pp. 565-574.

Rosenstiel, T. N., Potosnak, M. J., Griffin, K. L., Fall, R., and Monson, R. K., 2003. Increased CO₂ uncouples growth from isoprene emission in an agriforest ecosystem. *Nature*. Vol. 421. pp. 256-259.

Rosenzweig, C., Karoly, D., Vicarelli, M., Neofotis, P., Wu, Q., Casassa, G., Menzel, A., Root, T. L., Estrella, N., Seguin, B., Tryjanowski, P., Liu, C., Rawlins, S., and Imeson, A., 2008. Attributing physical and biological impacts to anthropogenic climate change. *Nature*. Vol 453. pp. 353-358.

Sasaki, K., Saito, T., Lämsä, M., Oksman-Caldentey, K.-M., Suzuki, M., Ohyama, K., Muranaka, T., Ohara, K., and Yazaki, K., 2007. Plants utilise isoprene emission as a thermotolerance mechanism. *Plant Cell Physiology*. Vol. 48 (9). pp. 1254-1262.

Schnitzler, J., Graus, M., Kreuzwieser, J., Heizmann, U., Rennenberg, H., Wisthaler, A., and Hansel, A., 2004. Contribution of different carbon sources to isoprene biosynthesis in poplar leaves. *Plant Physiology*. Vol. 135. pp. 152-160.

Scholefield, P. A., Doick, K. J., and Herbert, B. M. J., 2004. Impact of rising CO₂ on emissions of volatile organic compounds: isoprene emission from *Phragmites australis* growing at elevated CO₂ in a natural carbon dioxide spring. *Plant Cell and Environment*. Vol. 27. pp. 393-401.

Scott, C. E., Rap, A., Spracklen, D. V., Forster, P. M., Carslaw, K. S., Mann, G. W., Pringle, K. J., Kivekäs, N., Kulmala, M., Lihavainen, H., and Tunved, P., 2014. The

direct and indirect radiative effects of biogenic secondary organic aerosol. *Atmospheric Chemistry and Physics*. Vol. 14. pp. 447-470.

Scripps Center for Metabolomics. Metlin: Metabolite Search. Available at: <https://metlin.scripps.edu/index.php> (Accessed: 14th September 2016).

Sharkey, T. D., 2005. Effects of moderate heat stress on photosynthesis: importance of thylakoid reactions, rubisco deactivation, reactive oxygen species, and thermotolerance provided by isoprene. *Plant, Cell and Environment*. Vol. 28. pp. 269-277.

Sharkey, T. D., Wiberley, A. E., and Donohue, A. R., 2008. Isoprene Emission from Plants: Why and How. *Annals of Botany*. Vol. 101. pp. 5-18.

Singsaas, E. L., Lerdau, M., Winter, K., and Sharkey, T. D., 1997. Isoprene increases thermotolerance of isoprene-emitting species. *Plant Physiology*. Vol. 115. pp. 1413-1420.

Singsaas, E. L., and Sharkey, T. D., 2000. The effects of high temperature on isoprene synthesis in oak leaves. *Plant Cell and Environment*. Vol. 23. pp. 751-757.

Sitch, S., Smith, B., Prentice, I. C., Arneth, A., Bondeau, A., Cramer, W., Kaplan, J. O., Levis, S., Lucht, W., Sykes, M. T., Thonicke, K., and Venevsky, S., 2003. Evaluation of ecosystem dynamics, plant geography and terrestrial carbon cycling in the LPJ dynamic global vegetation model. *Global Change Biology*. Vol. 9. pp. 161-185.

Siwko, M. E., Marrink, S. J., de Vries, A. H., Kozubek, A., Schoot Uiterkamp, A. J. M., and Mark, A. E., 2007. Does isoprene protect plant membranes from thermal heat shock? A molecular dynamics study. *Biochimica et Biophysica Acta* 1768. pp. 198-206.

Taub, D. R., 2010. Effects of rising atmospheric concentrations of carbon dioxide on plants. *Nature Education Knowledge*. Vol. 3 (10). pp. 21.

Treutter, D., 2006. Significance of flavonoids in plant resistance: a review. *Environmental Chemistry Letters*. Vol. 4. pp. 147-157.

Trowbridge, A. M., Asensio, D., Eller, A. S. D., Way, D. A., Wilkinson, M. J., Schnitzler, J.-P., Jackson, R. B., and Monson, R. K., 2012. Contribution of various carbon sources toward isoprene biosynthesis in poplar leaves mediated by altered atmospheric CO₂ conditions. *PLoS ONE*. Vol. 7 (2). e32387.

Ubi, B. W., Honda, C., Bessbo, H., Kondo, S., Wada, M., Kobayashi, S., Moriguchi, T., 2006. Expression analysis of anthocyanin biosynthesis genes in apple skin: effect of UV-B and temperature. *Plant Science*. Vol. 170. pp. 571-578.

Velikova, V., 2008. Isoprene as a tool for plant protection against abiotic stresses. *Journal of Plant Interactions*. Vol. 3 (1). pp. 1-15.

- Velikova, V., and Loreto, F., 2005. On the relationship between isoprene emission and thermotolerance in *Phragmites australis* leaves exposed to high temperatures and during the recovery from heat stress. *Plant, Cell and Environment*. Vol. 28. pp. 318-327.
- Veteli, T. O., Kuokkanen, K., Julkunen-Tiitto, R., Roininen, H., and Tahvanainen, J., 2002. Effects of elevated CO₂ and temperature on plant growth and herbivore defensive chemistry. *Global Change Biology*. Vol. 8. pp. 1240-1252.
- Veteli, T. O., Mattson, W. J., Niemelä, P., Julkunen-Tiitto, R., Kellomäki, S., Kuokkanen, K., and Lavola, A., 2007. Do elevated temperature and CO₂ generally have counteracting effects on phenolic phytochemistry of boreal trees? *Journal of Chemical Ecology*. Vol. 33. pp. 287-296.
- Wahid, A., Farooq, M., Hussain, I., Rasheed, R., and Galani, S., 2012. Responses and management of heat stress in plants. In *Environmental Adaptations and Stress Tolerance of Plants in the Era of Climate Change*. P. Ahmad, and M. N. V. Prasad (eds). Springer: New York, Dordrecht, Heidelberg, London.
- Webster, B., Bruce, T., Dufour, S., Birkemeyer, C., Birkett, M., Hardie, J., and Pickett, J., 2008. Identification of volatile compounds used in host location by the black bean aphid, *Aphis fabae*. *Journal of Chemical Ecology*. Vol. 34. pp. 1153-1161.
- Wilkinson, M. J., Monson, R. K., Trahan, N., Lee, S., Brown, E., Jackson, R. B., Polley, H. W., Fay, P. A., and Fall, R., 2009. Leaf isoprene emission rate as a function of atmospheric CO₂ concentration. *Global Change Biology*. Vol. 15. pp. 1189-1200.
- WIMOVAC ltd, 1998. *Model of Volatile Hydrocarbon Emission*. [Online] Available from: https://www.staffs.ac.uk/assets/harvard_quick_guide_tcm44-47797.pdf. [Accessed: 20th April 2015].
- Wolfertz, M., Sharkey, T. D., Boland, W., Kühnemann, F., Yeh, S., and Weise, S. E., 2003. Biochemical regulation of isoprene emission. *Plant, Cell, and Environment*. Vol. 26 (8). pp. 1357-1364.
- Young, P. J., Arneth, A., Schurgers, G., Zeng, G., and Pyle, J. A., 2009. The CO₂ inhibition of terrestrial isoprene significantly affects future ozone predictions. *Atmospheric Chemistry and Physics*. Vol. 9. pp. 2793-2803.
- Yu, E., Fan, C., Yang, Q., Li, X., Wan, B., Dong, Y., Wang, X., and Zhou, Y., 2014. Identification of heat responsive genes in *Brassica napus* Siliques at the seed-filling stage through transcriptional profiling. *PLoS ONE*. Vol. 9 (7). pp. e101914.
- Zimmer, W., Brüggermann, N., Emeis, S., Giersch, C., Lehning, A., Steinbrecher, R., and Schnitzler, J. P., 2000. Process-based modelling of isoprene emission by oak leaves. *Plant Cell and Environment*. Vol. 23. pp. 585-595.
- Zvereva, E. L., and Kozlov, M. V., 2006. Consequences of simultaneous elevation of carbon dioxide and temperature for plant-herbivore interactions: a metaanalysis. *Global Change Biology*. Vol. 12. pp. 27-41.

Appendix

Table A2.1: The average leaf area measurements for each of the biological replicates for the four treatments and two sets of experiments (cm²).

Hs*eCO ₂ 1(1) average(cm ²)	Hs*eCO ₂ 2 (1) average(cm ²)	Hs*eCO ₂ 3 (1) average(cm ²)	Hs*eCO ₂ 4 (1) average(cm ²)	eCO ₂ 1 (1) average(cm ²)	eCO ₂ 2 (1) average(cm ²)	eCO ₂ 3 (1) average (cm ²)	eCO ₂ 4 (1) average (cm ²)
2.3967	3.75	2.693	2.09	2.623	1.557	1.73	1.653
21.367	25.24	26.61	19.59	14.58	13.07	21.9433	13.083
17.96	21.4067	25.523	18.013	17.66	10.32	5.0033	28.417
7.15	11.22	0.5167	0.2567	8.4567	11.973	22.6033	29.16
13.37	11.467	1.67	1.173	1.28	11.8167	6	16.757
13.78	12.39	0.8867	3.513	16.773	11.43	5.54	22.887
11.72	1.91	12.6167	1.99	0.47	12.38	1.6067	22.323
9.41	1.3	7.887	2.473	12.123	11.337	3.3367	15.573
15.41	7.24	14.967	2.067	20.323	10.903	3.28	14.96
8.5	14.477	15.473	3.66	9.8467	9.87	5.8833	17.7
9.557	19.57	11.523	32.23	27.6	6.23	17.923	6.4367
17.76	21.573	9.5	31.43	2.743	9.4	26.543	12.81
11.803	12.373	11.98	29.1267	20.737	15.093	4.18	15.46
15.713	16.19	10.04	29.7133	14.373	11.677	1.3133	10.367
14.9	20.803	7.796	32.083	10.05	11.53	0.6533	11.857
11.993	13.44	12.273	32.233	20.84		22.65	5.617
8.24	11.973	13.913	30.6133	6.083		27.043	7.687
13.056	19.237	19.887	31.31	12.897		18.51	9.9973
16.88	22.48	18.053	34.677			26.81	4.277
7.893	21.4933	10.377	27.01			17.13	10.007
8.12	23.876	12.4	25.153			18.12	6.6
6.35		19.72	25.02				10.03
12.2233		15.643	22.323				7.277
10.603		7.86	32.87				11.533
11.24		5.813	23.14				12.25
8.14		4.78	23.93				
10.143		9.356	28.1067				
		4.906					
		7.56					
		5.143					

Table A2.1: Continued.

Hs 1 (1) average(cm ²)	Hs 2 (1) average(cm ²)	Hs 3 (1) average(cm ²)	Hs 4 (1) average(cm ²)	Control 1 (1) average (cm ²)	Control 2 (1) average (cm ²)	Control 3 (1) average (cm ²)	Control 4 (1) average(cm ²)
0.6467	1.04	1.733	3.183	0.5977	0.563	1.683	1.127
25.71	22.3033	25.033	15.913	12.9933	15.4	23.43	13.32
16.65	1.94	30.08	25.44	2.837	4.69	8.723	21.123
15.4067	3.07	21.28	24.23	16.257	14.713	5.507	20.803
12.843	27.263	27.03	23.877	13.02	3.237	8.5867	18.7467
19.91	9.67	26.697	18.237	11.707	5.8	12.457	18.7467
21.8867	16.98	6.43	33.443	5.483	5.927	14.813	1.743
19.8167	27.73	30.25	24.483	11.133	9.6067	19.85	15.113
30.83	20.61	31.1633	19.137	19.417	8.82	17.277	14.4167
21.4067	31.59	31.4633	8.687	12.843	13.6633	11.77	11.37
10.6567	37.94	29.947	4.36	12.573	8.603	5.03	11.673
5.183	24.03	30.137	7.627	6.643	10.143	13.58	9.89
16.253	35.567	24.82	10.573	4.83	10.03	6.447	17.813
13.84	23.8		24.857	4.863	5.233	4.593	10.147
3.42	12.123		15.087	3.5867	1.9767	4.76	4.83
	28.653		14.277	3.4967	7.44	8.36	14.463
	31.843			1.563	12.3967	7.79	17.717
	4.4			5.9867	11.9533	5.84	7.67
	1.03			5.523	11.8167	21.54	11.43
	0.9067			6.32	1.75	16.13	
				20.84	4.5267	2.58	
				8.297	5.373	3.67	
				11.14	3.4033	6.71	
				17.137	4.667	2.55	
				14.77	8.7633		
				10.7167	21.067		
				21.123	6.873		
				5.983			
				7.133			

Table A2.1: Continued.

Control 1 (2) average(cm ²)	Control 2 (2) average(cm ²)	Control 3 (2) average(cm ²)	Control 4 (2) average (cm ²)	Hs 1 (2) average (cm ²)	Hs 2 (2) average (cm ²)	Hs 3 (2) average (cm ²)	Hs 4 (2) average (cm ²)
1.74	0.99	0.59	0.7	0.987	0.497	0.94	0.573
16.34	13.263	20.54	18.607	16.7	16.43	17.203	13.88
1.233	2.5	3.637	14.653	9.807	1.22	1.443	11.1867
13.59	1.177	8.78	6.903	5.447	1.693	1.0267	18.817
23.92	1.567	12.587	2.99	4.59	14.44	0.1377	19.243
10.213	1.963	9.803	7.287	18.893	13.77	0.697	5.133
9.05	7.977	7.147	3.497	16.123	11.01	1.573	14.407
5.057	5.297	6.623	8.987	22.187	6.46	1.473	7.643
4.863	14.533	19.107	20.143	1.613	1.563	2.563	22.397
15.457	16.297	10.393	16.713	16.773	1.26	3.357	13.32
12.257	6.867	7.227	11.92	6.77	14.847	9.213	19.92
6.87	5.397	8.203	16.8	8.49	11.73	2.03	19.78
18.637	11.47	13.413	15.49	12.35	8.42	4.77	5.64
18.44	13.2	14.927	13.317	10.413	11.32	0.937	2.117
4.43	12.71	18.613	14.33	10.033	9.14	3.417	1.3
2.547	8.67	18.497	17.89	11.593	11.687	2.63	0.73
13.35	5.2	11.997	12.46	12.507	3.167	1.203	3.943
8.81	9.1	14.34	12.71	15.85	17.35	15.337	16.877
13.123	2.22	17.227	19.9		18.57	3.687	12.2
17.853	13.31	21.287	22.623		7.4767	3.557	15.7
2.26	7.237		25.057		3.483	2.733	9.607
1.47	7.613		17.01		14.47	10.18	6.67
16.61	15.81		20.543		9.807	12.55	
8.957					20.83	20.373	
14.353					19.66	13.517	
12.63					18.83	6.237	
						16.213	
						9.257	
						6.97	
						18.74	
						15.37	
						7.75	
						6.163	
						6.233	
						11.737	
						4.92	
						3.963	

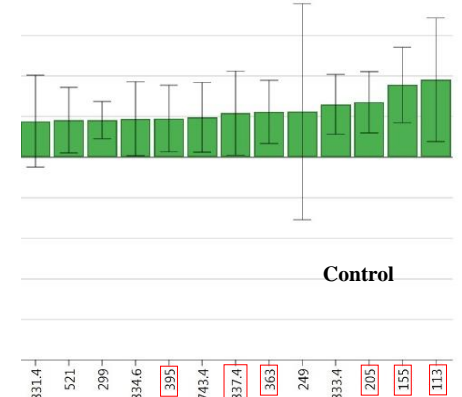
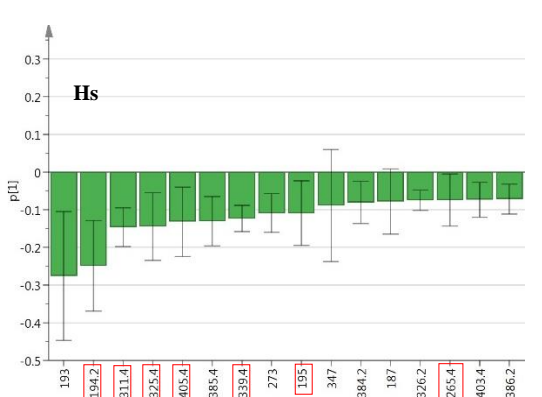
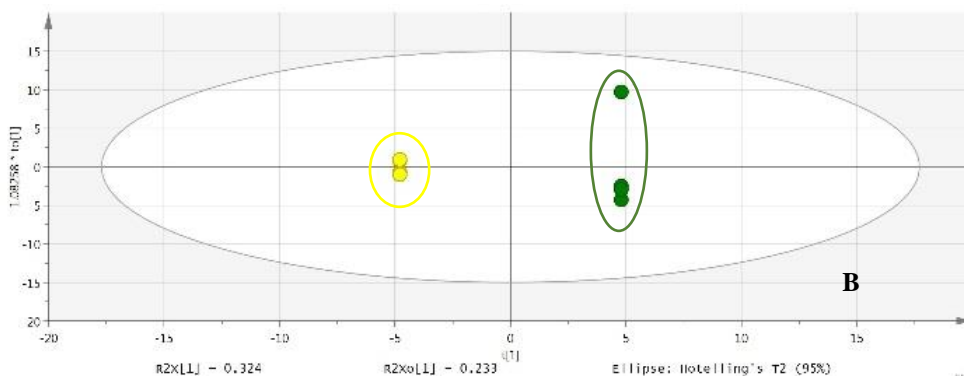
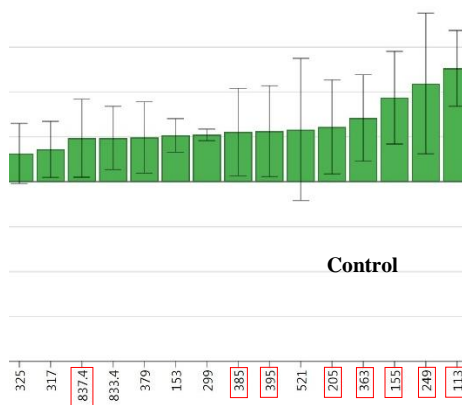
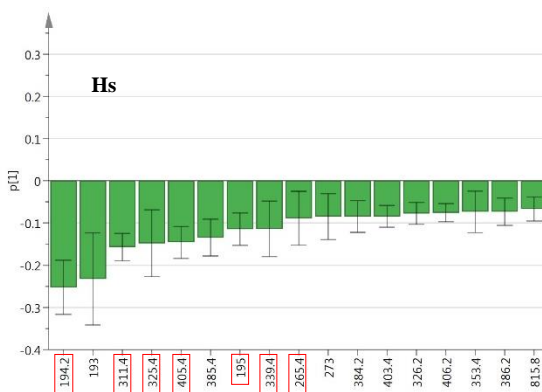
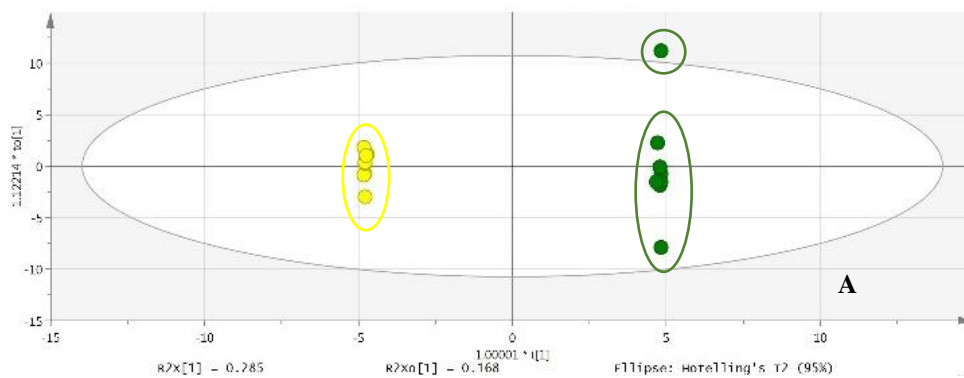
Table A2.1: Continued.

eCO ₂ 1 (2) average (cm ²)	eCO ₂ 2 (2) average (cm ²)	eCO ₂ 3 (2) average (cm ²)	eCO ₂ 4 (2) average (cm ²)	Hs 1 (2) average (cm ²)	Hs 2 (2) average (cm ²)	Hs 3 (2) average (cm ²)	Hs 4 (2) average (cm ²)
1.563	0.527	0.713	1.74	1.2	1.18	0.903	1.913
18.823	10.187	18.6	19.623	16.79	18.447	19.75	21.2233
0.77	0.533	11.16	6.563	2.54	1.19	3.833	23.3167
14.97	1.05	13.547	1.27	4.177	7.893	12.103	18.787
12.71	12.287	17.807	20	7.227	17.837	7.647	4.07
2.783	2.203	19.463	0.357	1.76	8.56	6.44	15.17
8.963	3.537	24.817	6.43	8.353	2.607	1.06	18.42
14.39	4.587	19.63	13.37	13.72	6.307	12.35	14.957
7.877	13.893	7.087	0.603	6.43	13.15	7.993	16.706
3.5233	2.793	17.57	6.223	9.38	16.803	8.52	23.223
11.043	3.74	1.557	2.09	15.53	9.757	5.34	12.157
8.863	1.083	1.167	11.327	3.017	5.52	2.803	7.07
14.523	14.567	3.943	12.74	1.547	2.433	4.1867	6.97
7.553	7.553	1.807	7.903	9.357	8.52	17.47	12.58
14.47	14.47	1.95	9.4	3.57	4.563	5.737	16.68
17.313	17.313	5.343	12.09	9.727	10.103	4.24	11.453
10.613	10.643	11.21	5.67	0.993	7.3067	1.123	11.44
14.17	14.17	11.9	11.88	11.73		6.567	18.323
12.567	12.57	14.307	10.937	16.89		9.627	17.01
		3.67	8.98			8.46	13.37
		8.55	11.467			11.317	17.2
			16.74				16.97
			5.747				15.597
			11.17				16.48

Table A2.2: Dry weight of leaves, stems, and the totals (mg) for the biological replicates and for the two sets of experiments.

Treatment	Leaves (mg)	Stem (mg)	Total (mg)
Hs*eCO ₂ 1(1)	1.68	1.72	3.4
Hs*eCO ₂ 2(1)	1.74	1.36	3.1
Hs*eCO ₂ 3(1)	1.96	1.68	3.64
Hs*eCO ₂ 4(1)	5.09	3.08	8.17
eCO ₂ 1 (1)	1.063	1.02	2.623
eCO ₂ 2 (1)	0.983	0.76	1.743
eCO ₂ 3 (1)	2.383	1.48	3.863
eCO ₂ 4 (1)	4.103	1.9	6.003
Hs 1 (1)	1.343	2.1	3.443
Hs 2 (1)	2.363	1.24	3.603
Hs 3 (1)	2.203	1.57	3.773
Hs 4 (1)	1.923	1.36	3.283
Control 1 (1)	2.373	0.68	3.053
Control 2 (1)	1.673	0.46	2.133
Control 3 (1)	6.68	0.48	1.863
Control 4 (1)	1.693	0.45	2.143
Control 1 (2)	7.14	1.08	2.923
Control 2 (2)	1.593	0.85	2.443
Control 3 (2)	6.92	1	2.623
Control 4 (2)	2.233	0.98	3.213
Hs 1 (2)	1.093	0.56	1.653
Hs 2 (2)	1.743	0.77	2.513
Hs 3 (2)	1.503	1.03	2.533
Hs 4 (2)	1.123	0.65	1.773
eCO ₂ 1 (2)	1.253	0.82	2.073
eCO ₂ 2 (2)	0.873	0.61	1.483
eCO ₂ 3 (2)	1.133	0.87	2.006
eCO ₂ 4 (2)	1.033	0.63	1.663
Hs*eCO ₂ 1(2)	0.563	1	1.563
Hs*eCO ₂ 2(2)	0.463	0.92	1.383
Hs*eCO ₂ 3(2)	0.363	0.93	1.293
Hs*eCO ₂ 4(2)	2.363	1.16	3.523

● Hs ● Control



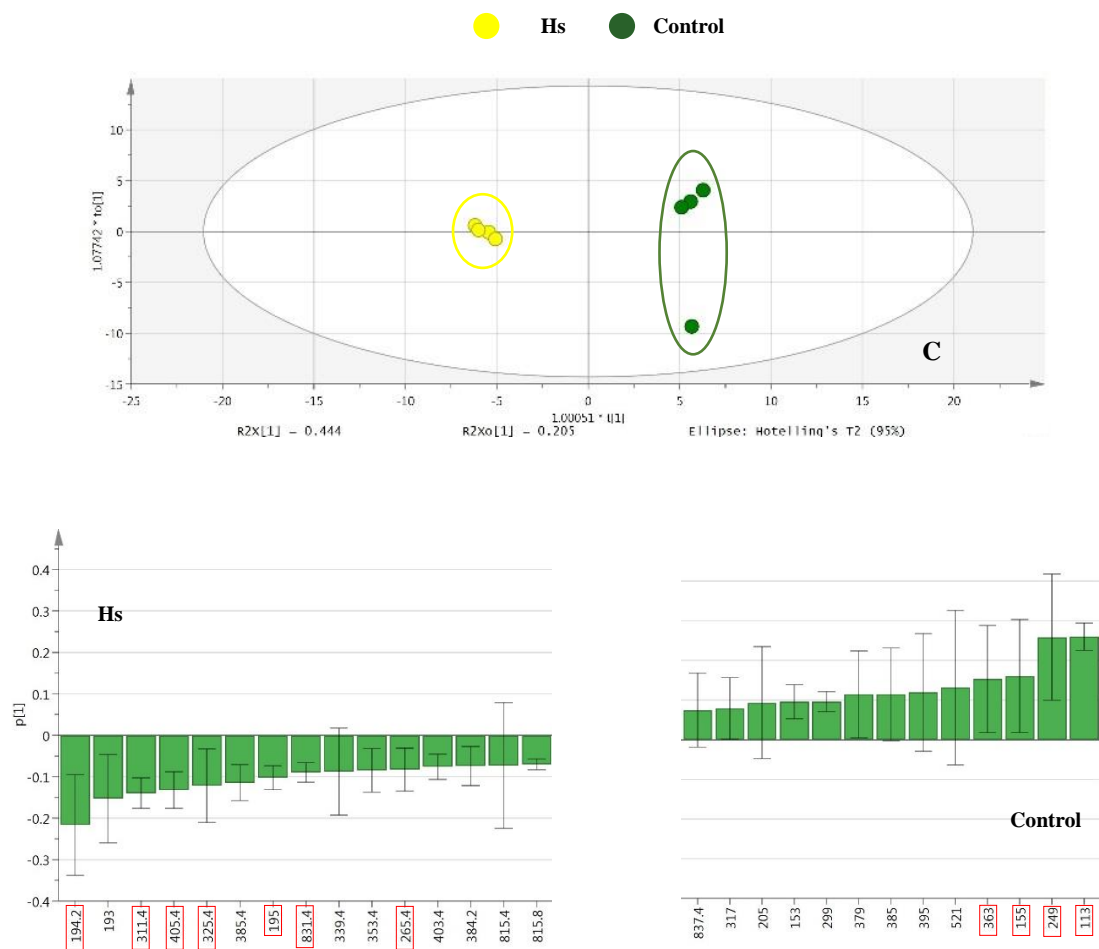
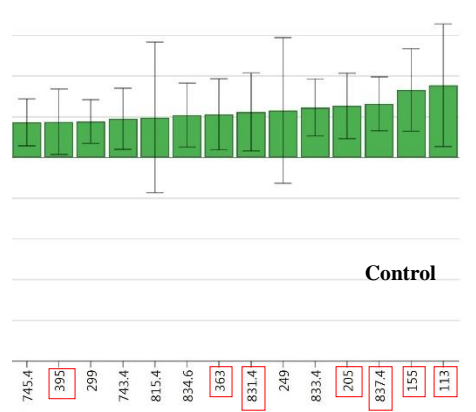
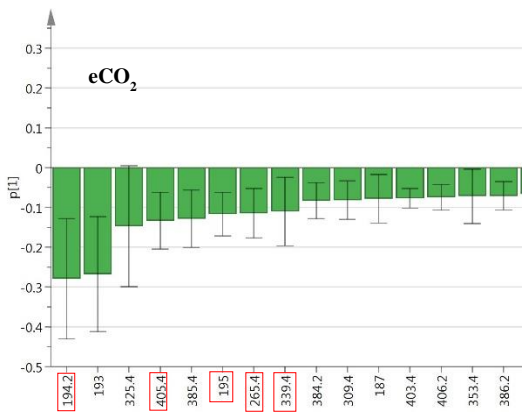
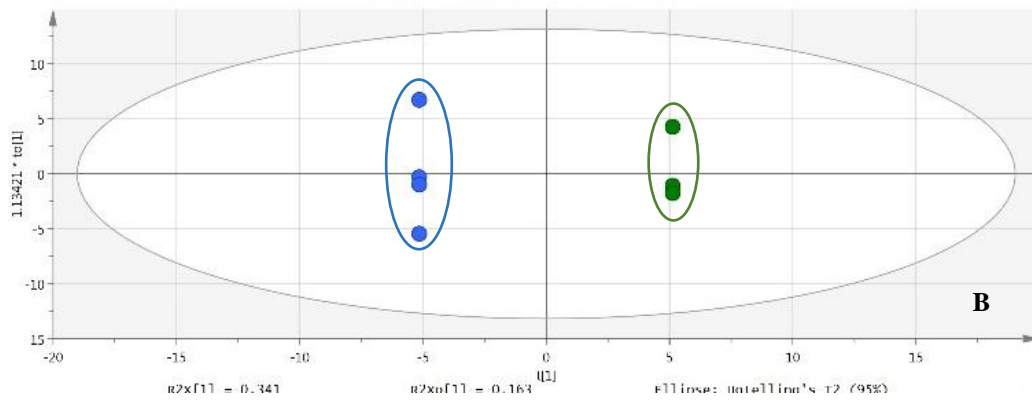
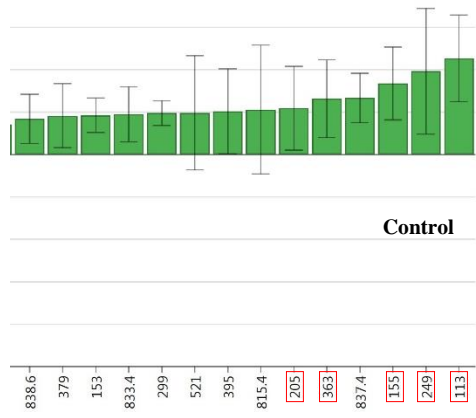
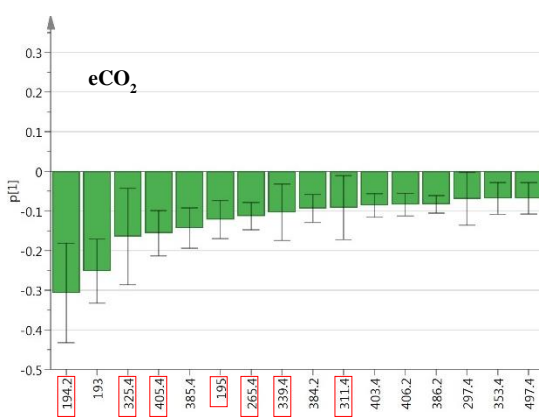
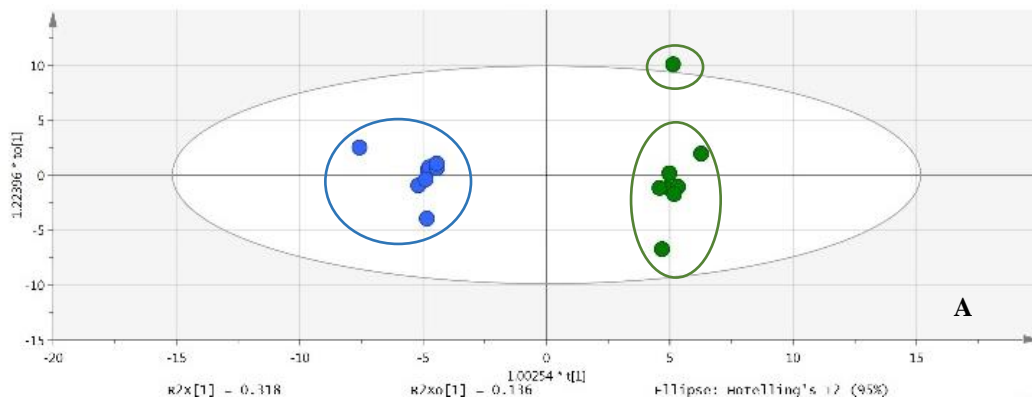


Figure A3.1: Supervised multivariate OPLS-DA plots of pair-wise comparisons of the metabolite profiles of treatments Hs & control. Metabolite profiles of the organic layer were analysed in negative ionisation mode. A: All leaves, B: New leaves, C: Old leaves. The corresponding loadings plots underneath each OPLS-DA plot demonstrate the discriminant mass bins associated with each treatment in the pair-wise comparison for all, new, and old leaves.

● eCO₂ ● Control



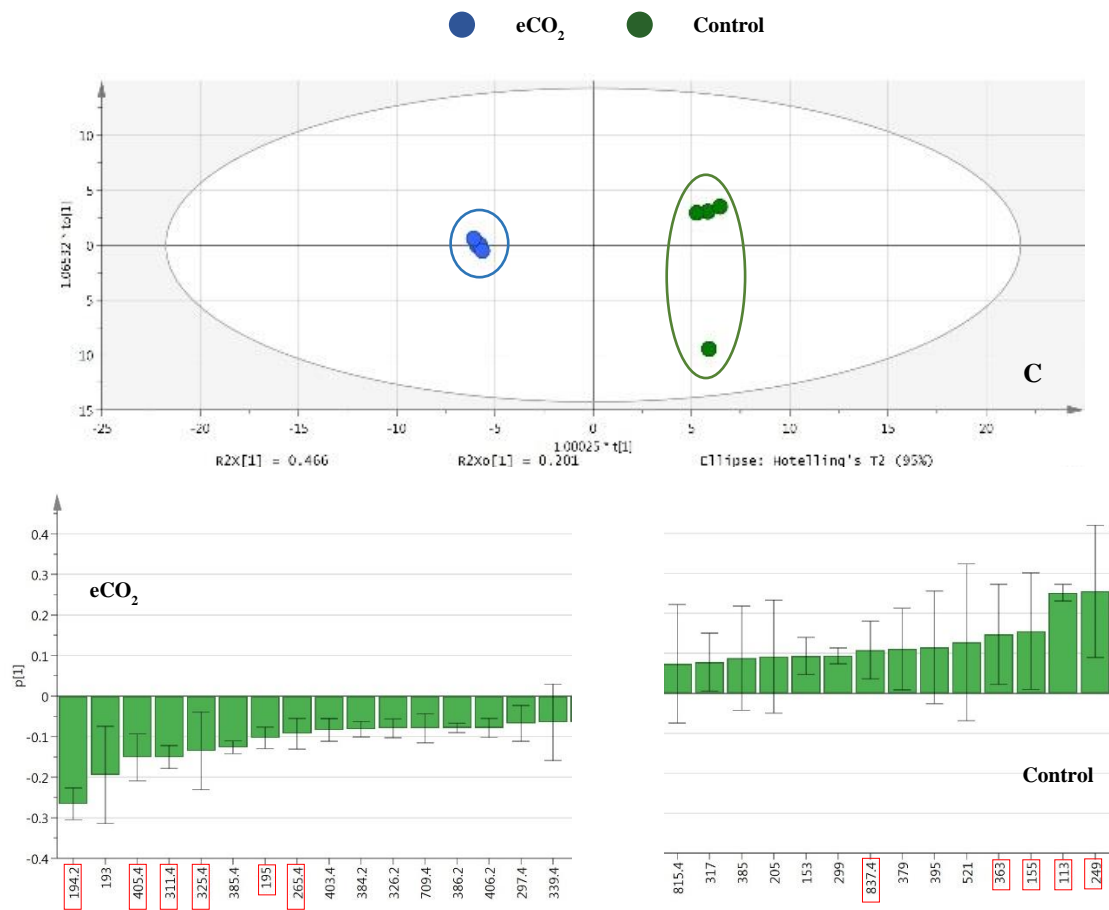
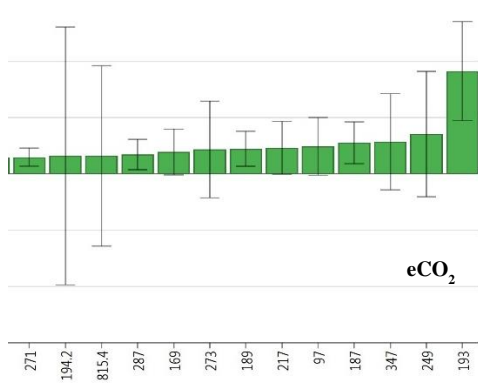
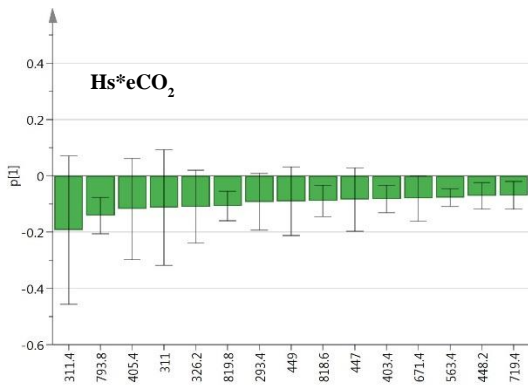
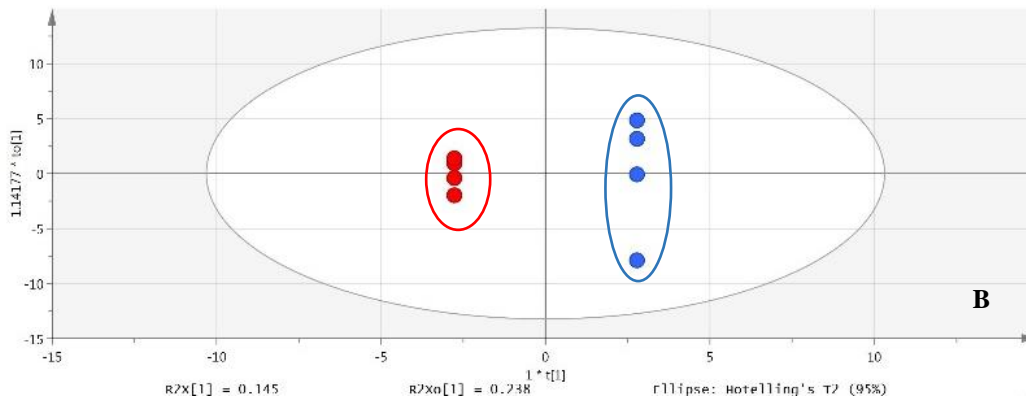
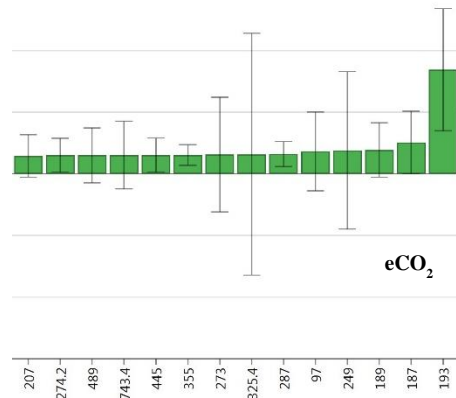
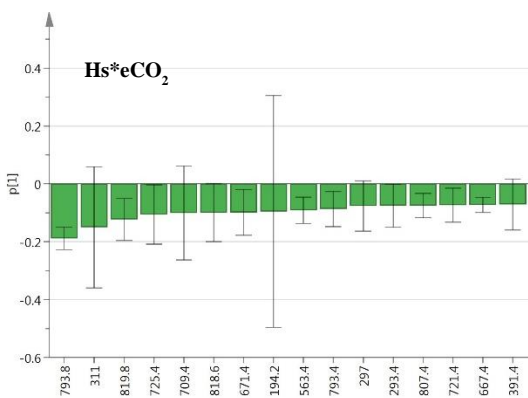
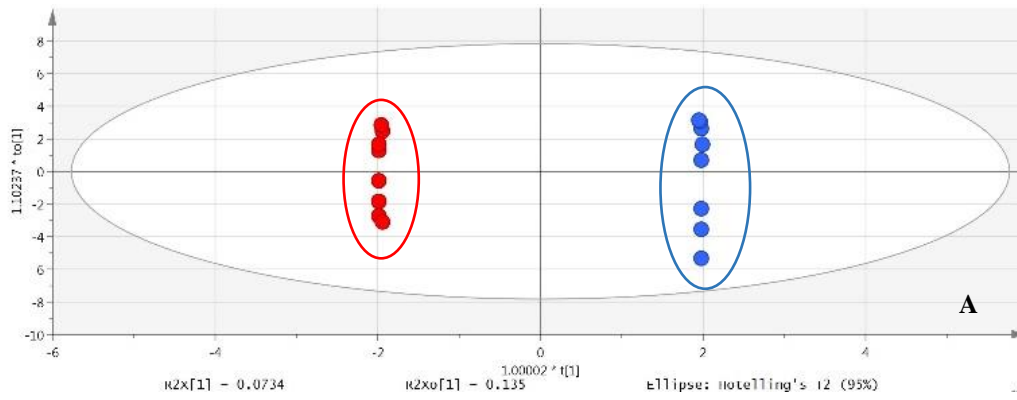


Figure A3.2: Supervised multivariate OPLS-DA plots of the pair-wise comparisons of the metabolite profiles of treatments eCO₂ & control. Metabolite profiles of the organic layer were analysed in negative ionisation mode. A: All leaves, B: New leaves, C: Old leaves. The corresponding loadings plots underneath each OPLS-DA plot demonstrate the discriminant mass bins associated with each treatment in the pair-wise comparison for all, new, and old leaves.

● **Hs*eCO₂** ● **eCO₂**



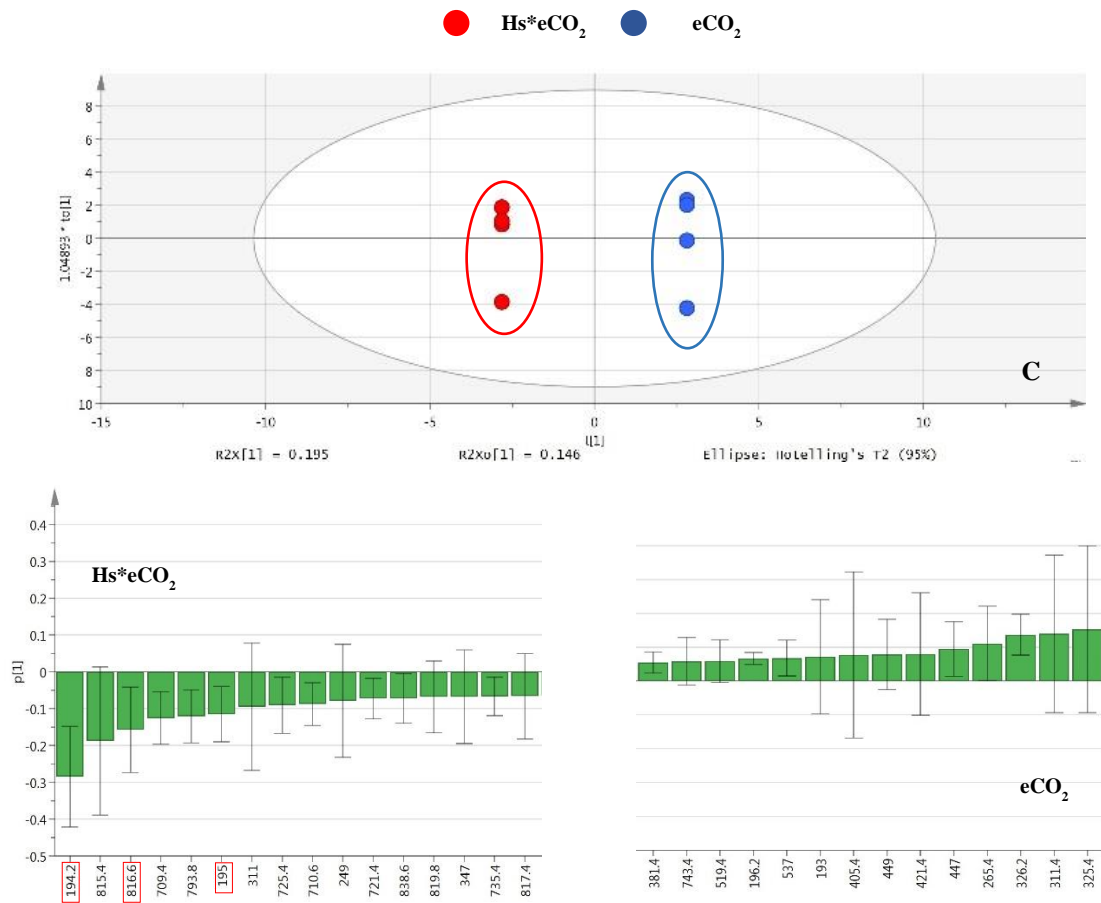
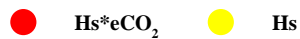
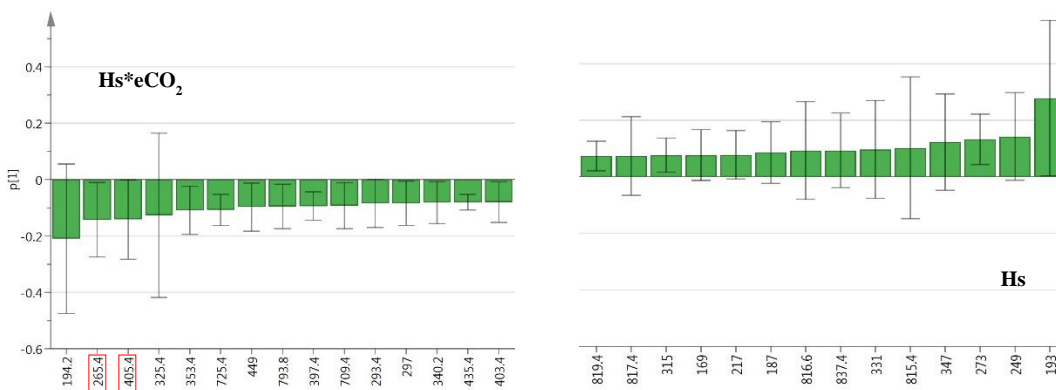
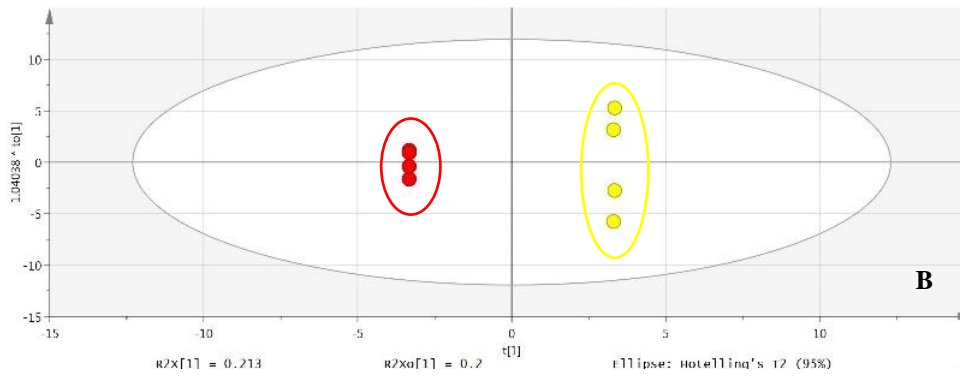
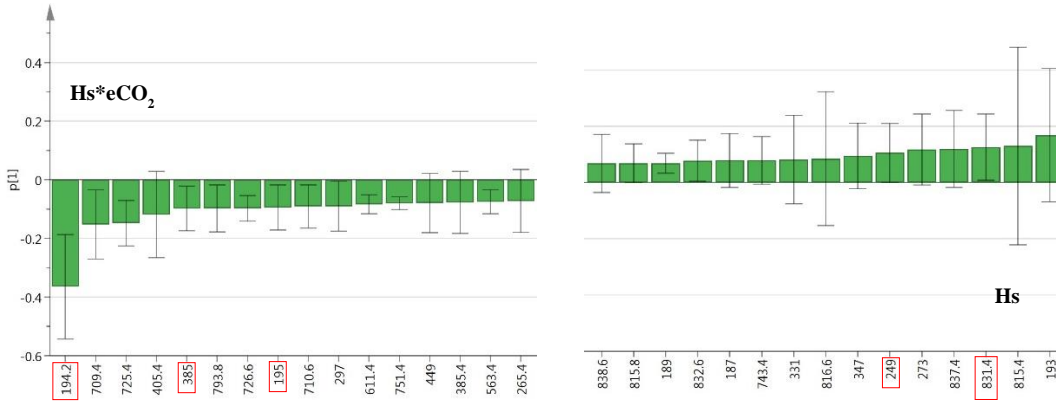
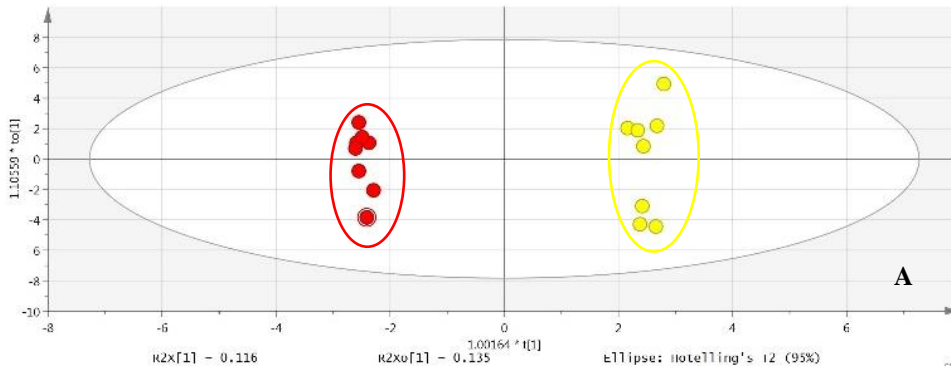


Figure A3.3: Supervised multivariate OPLS-DA plots of the pair-wise comparisons of metabolite profiles of treatments $Hs*eCO_2$ & eCO_2 . Metabolite profiles of the organic layer were analysed in negative ionisation mode. A: All leaves, B: New leaves, C: Old leaves. The corresponding loadings plots underneath each OPLS-DA plot demonstrate the discriminant mass bins associated with each treatment in the pair-wise comparison for all, new, and old leaves.





● Hs*eCO₂ ● Hs

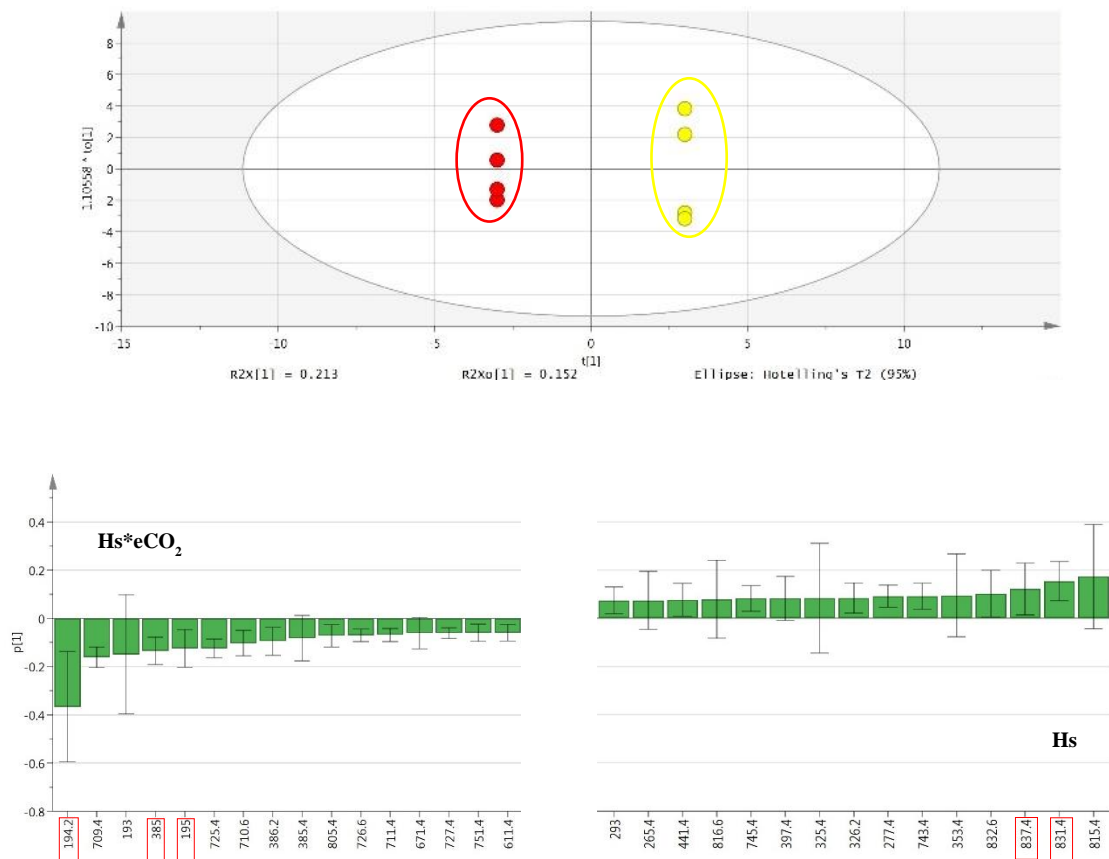
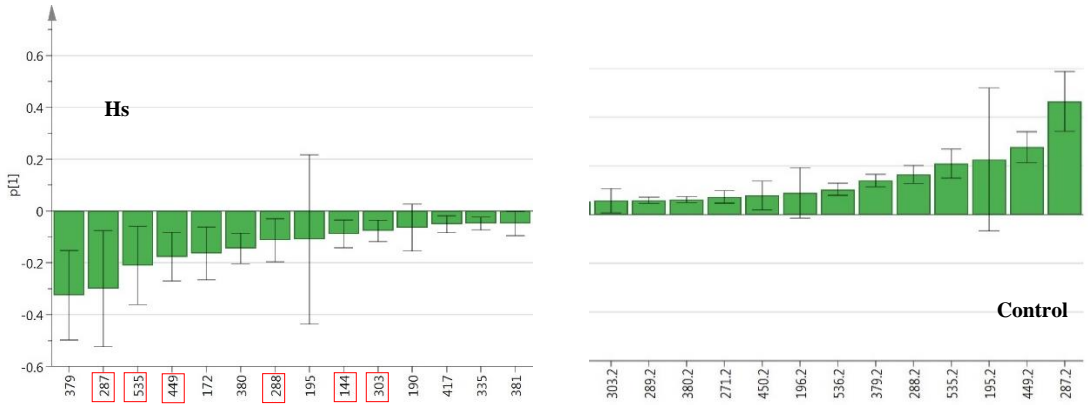
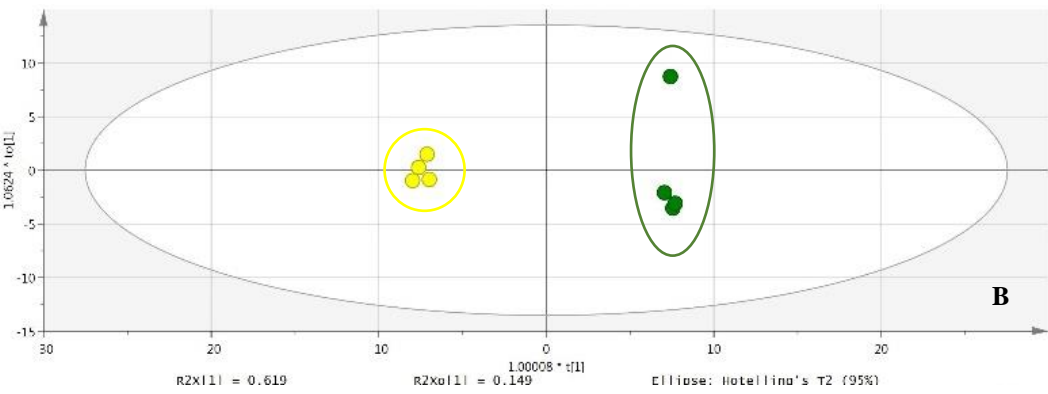
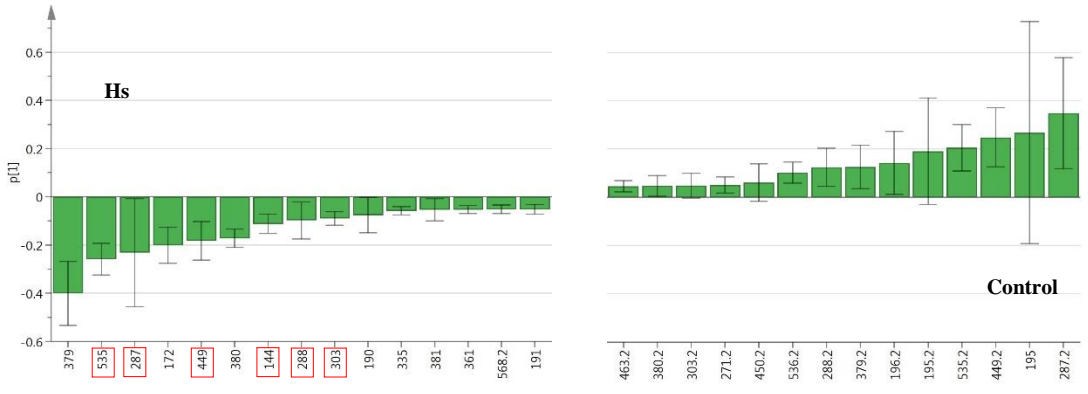
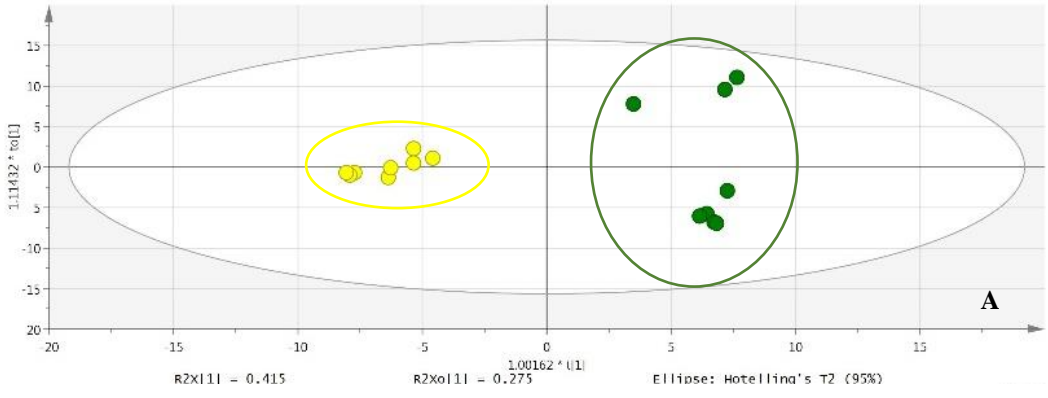


Figure A3.4: Supervised multivariate OPLS-DA plots of the pair-wise comparisons of metabolite profiles of treatments Hs*CO₂ & Hs. Metabolite profiles of the organic layer were analysed in negative ionisation mode. A: All leaves, B: New leaves, C: Old leaves. The corresponding loadings plots underneath each OPLS-DA plot demonstrate the discriminant mass bins associated with each treatment in the pair-wise comparison for all, new, and old leaves.

● Hs ● Control



● Hs ● Control

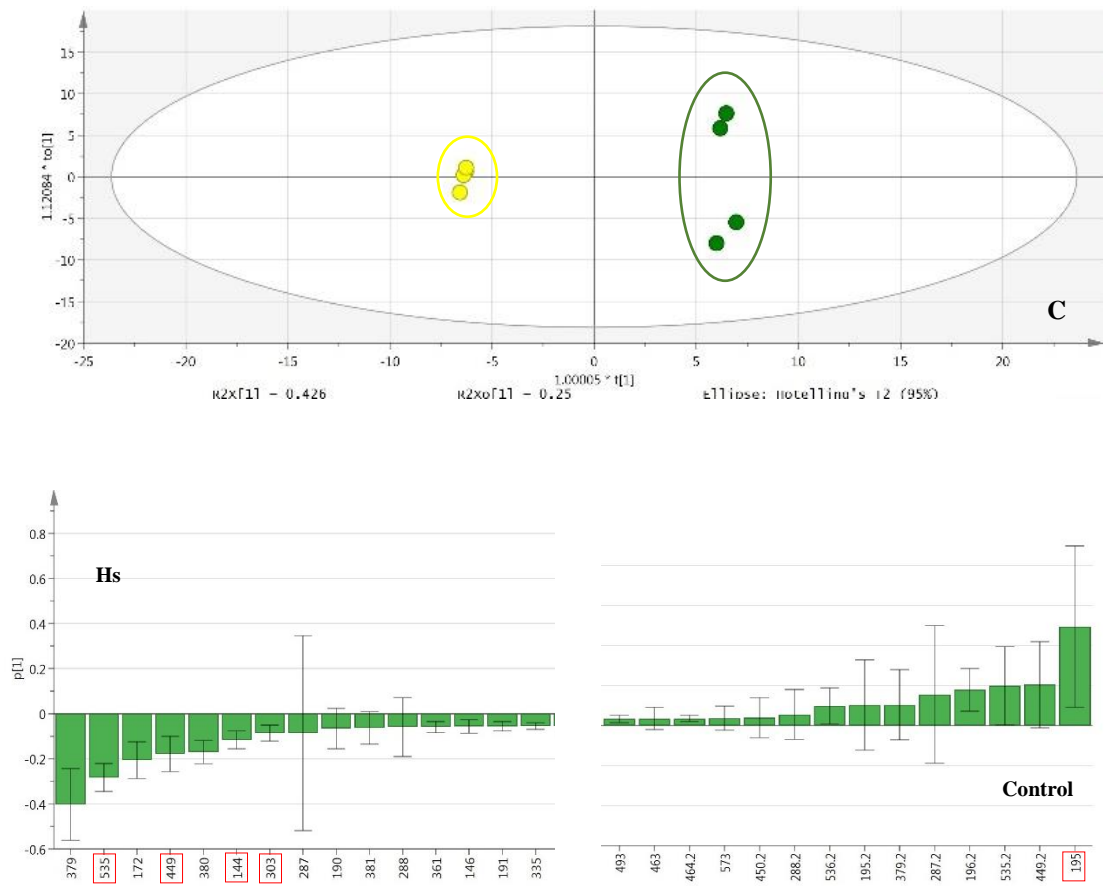
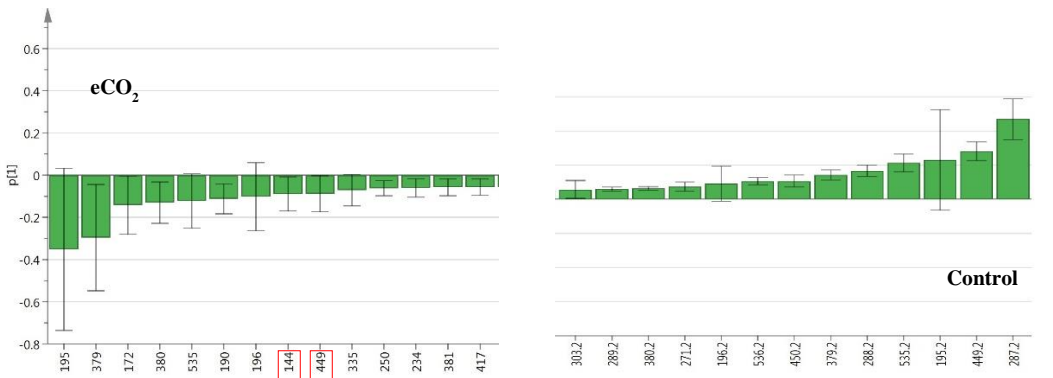
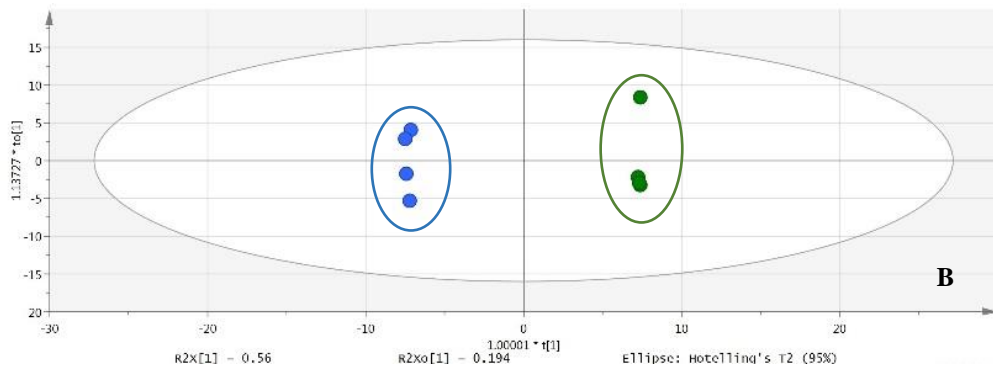
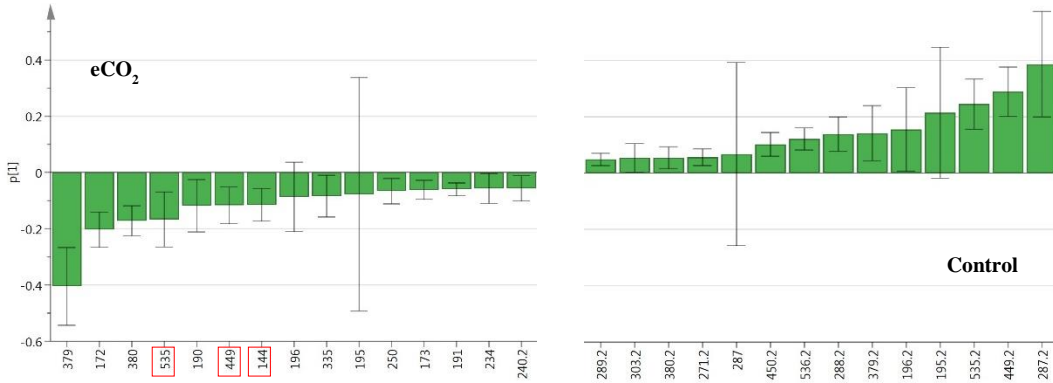
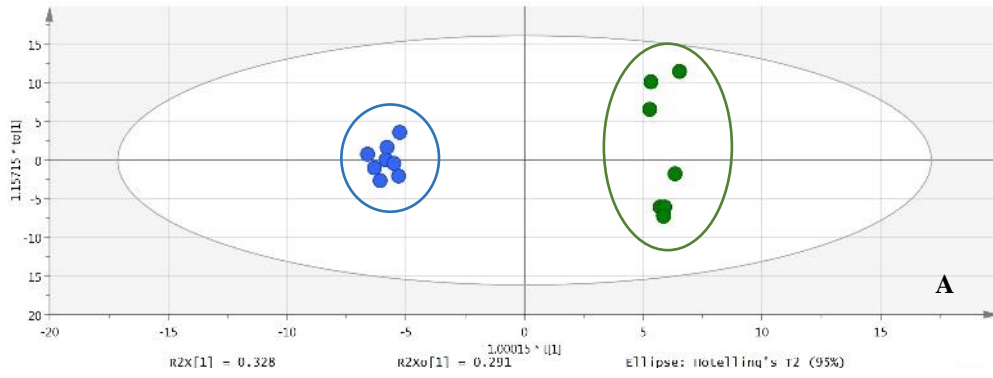


Figure A3.5: Supervised multivariate OPLS-DA plots of the pair-wise comparisons of metabolite profiles of treatments Hs & control. Metabolite profiles of the aqueous layer were analysed in positive ionisation mode. A: All leaves, B: New leaves, C: Old leaves. The corresponding loadings plots underneath each OPLS-DA plot demonstrate the discriminant mass bins associated with each treatment in the pair-wise comparison for all, new, and old leaves.

● eCO₂ ● Control



● eCO_2 ● Control

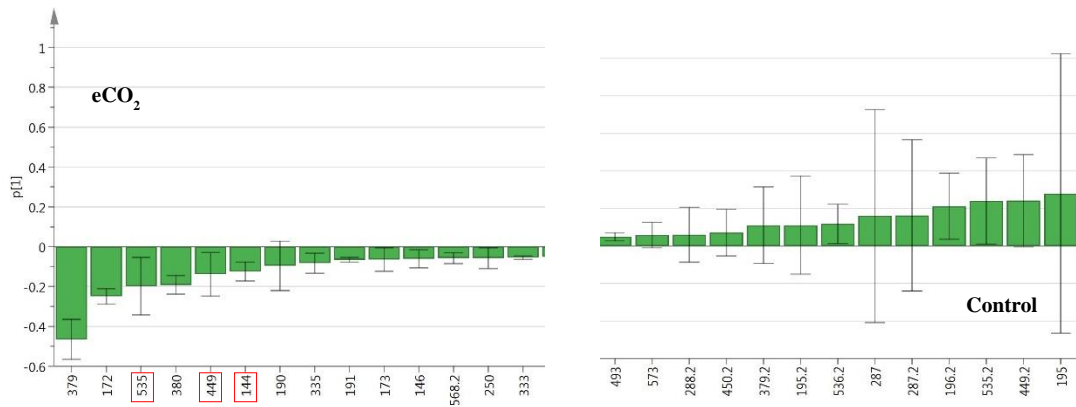
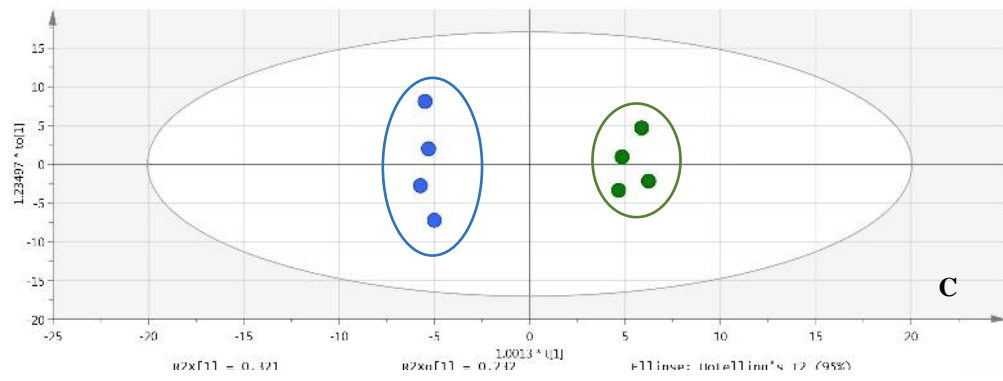
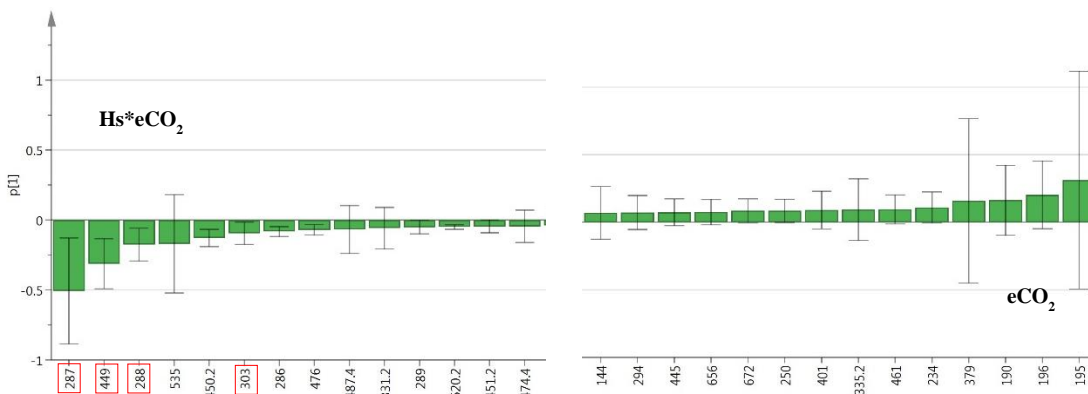
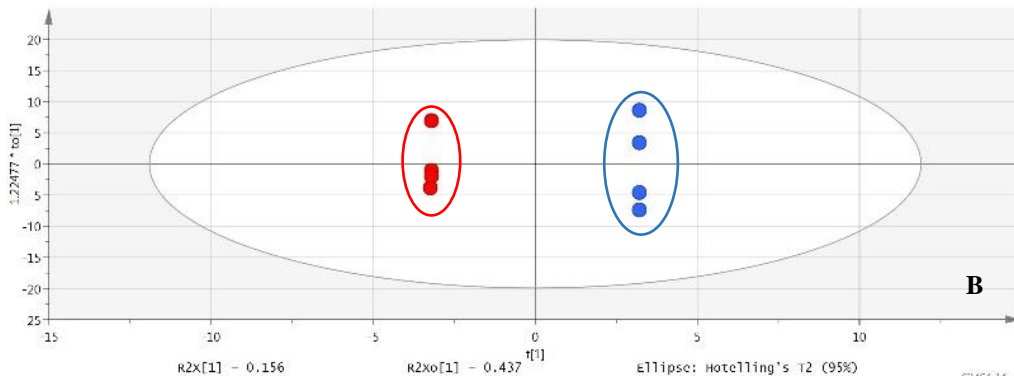
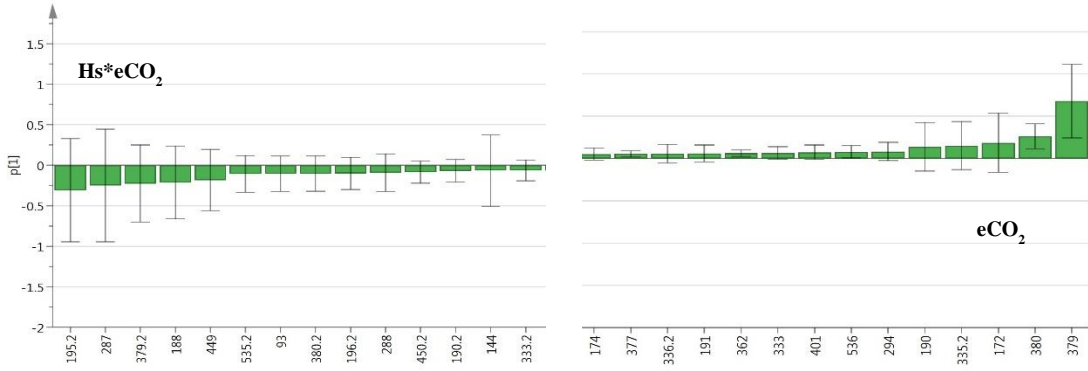
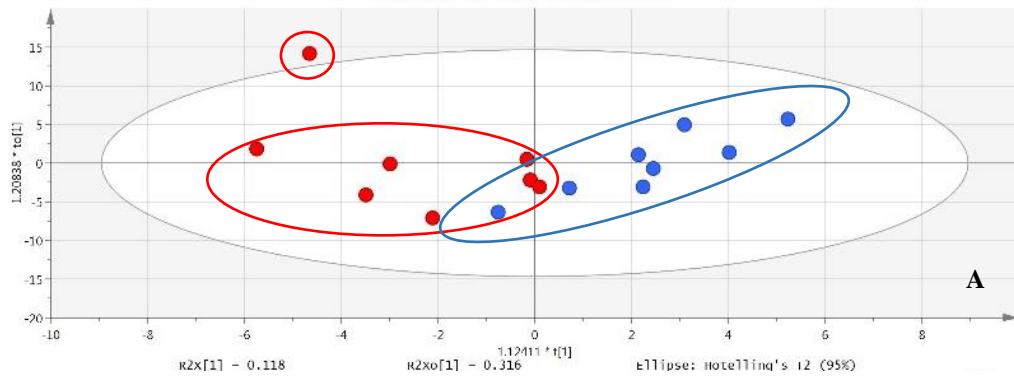


Figure A3.6: Supervised multivariate OPLS-DA plots of the pair-wise comparisons of metabolite profiles of treatments eCO₂ & control. Metabolite profiles of the aqueous layer in positive ionisation mode. A: All leaves, B: New leaves, C: Old leaves. The corresponding loadings plots underneath each OPLS-DA plot demonstrate the discriminant mass bins associated with each treatment in the pair-wise comparison for all, new, and old leaves.

● Hs*eCO₂ ● eCO₂



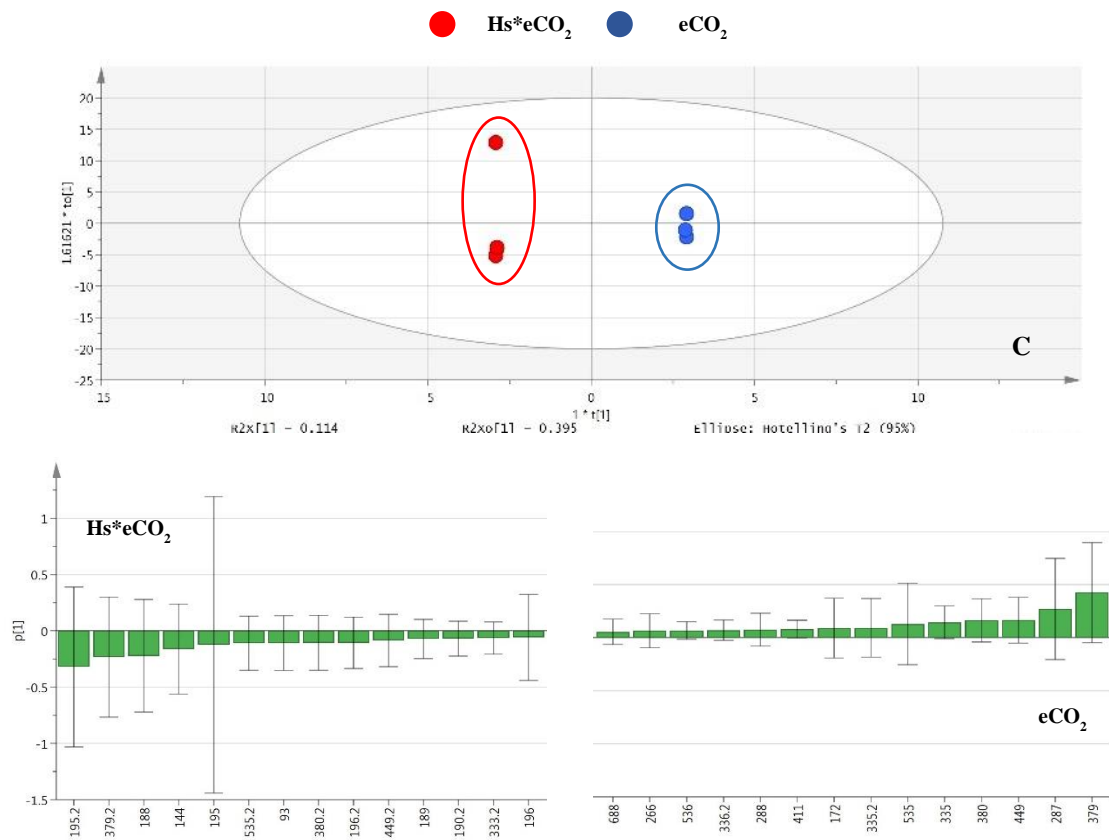
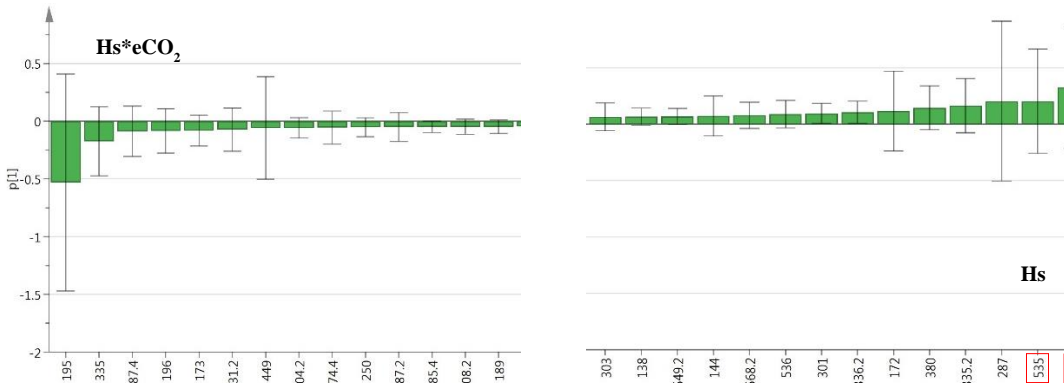
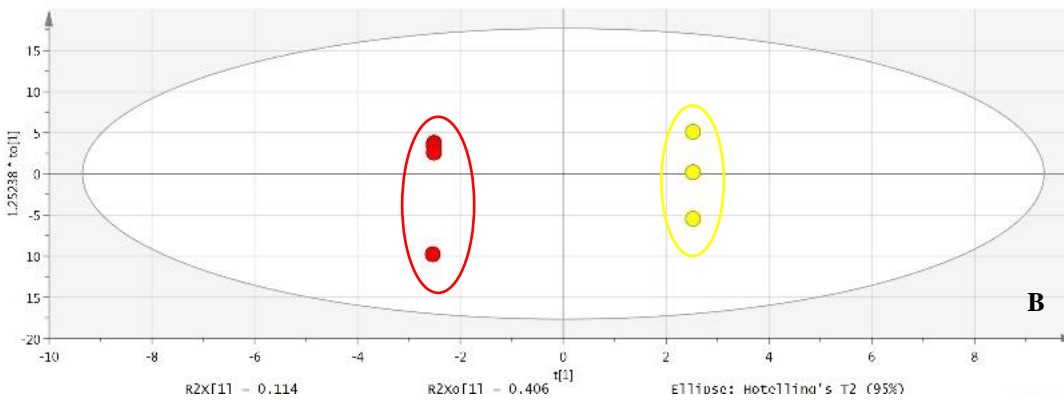
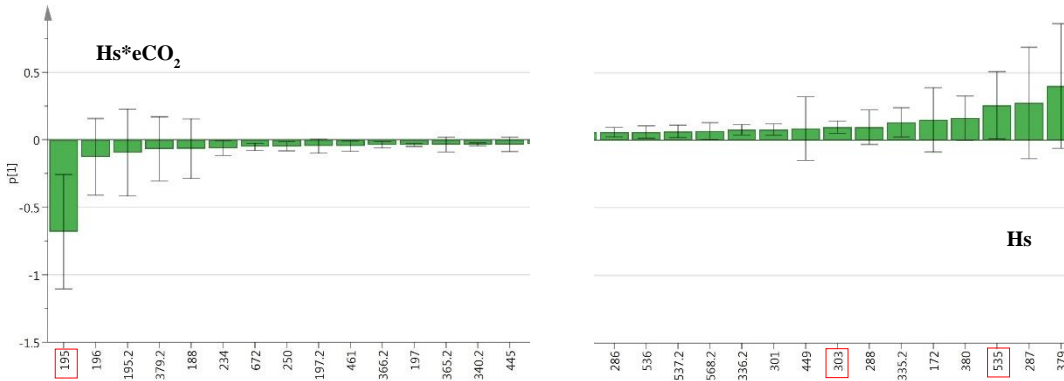
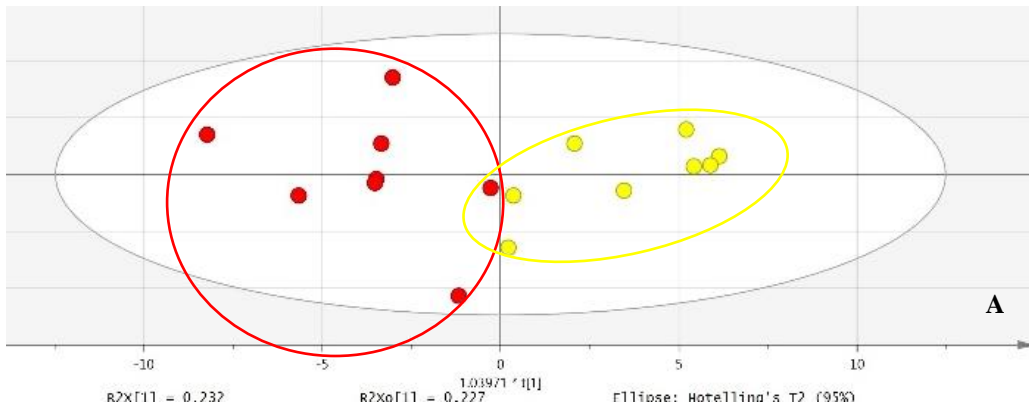


Figure A3.7: Supervised multivariate OPLS-DA plots of the pair-wise comparisons of the metabolite profiles of treatments Hs^*eCO_2 & eCO_2 . Metabolite profiles of the aqueous layer were analysed in positive ionisation mode. A: All leaves, B: New leaves, C: Old leaves. The corresponding loadings plots underneath each OPLS-DA plot demonstrate the discriminant mass bins associated with each treatment in the pair-wise comparison for all, new, and old leaves.

● Hs^*eCO_2 ● Hs



● Hs*eCO₂ ● Hs

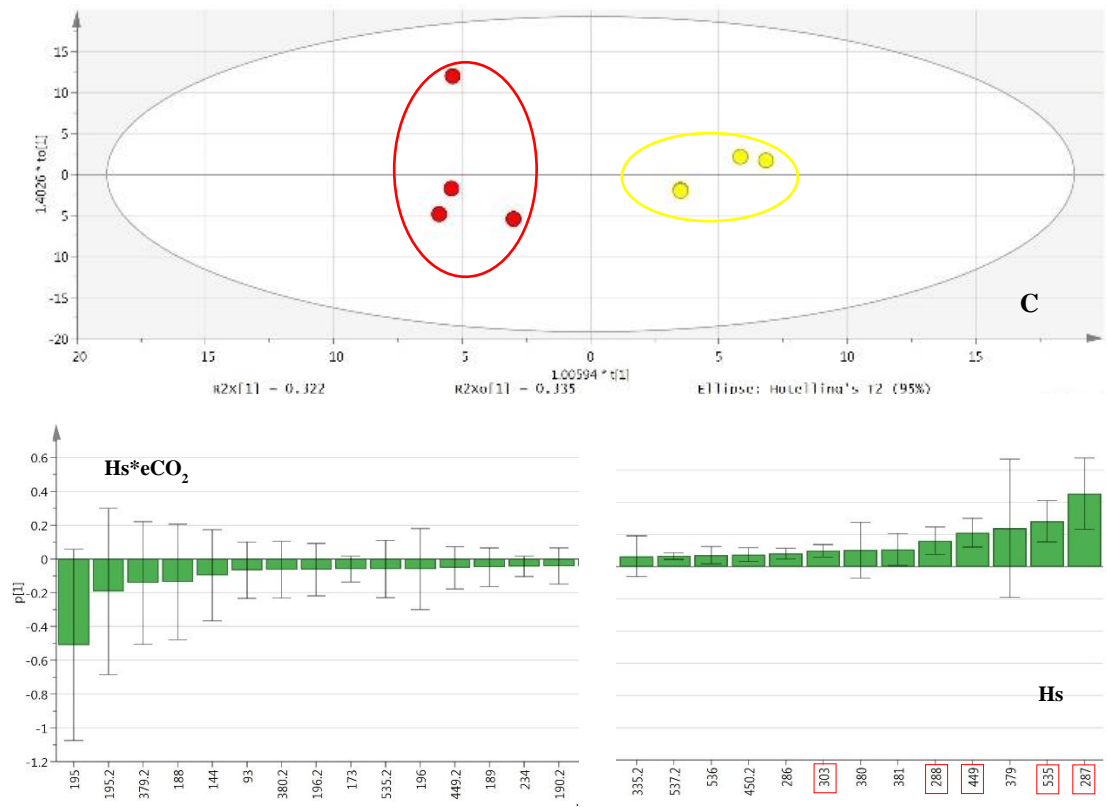
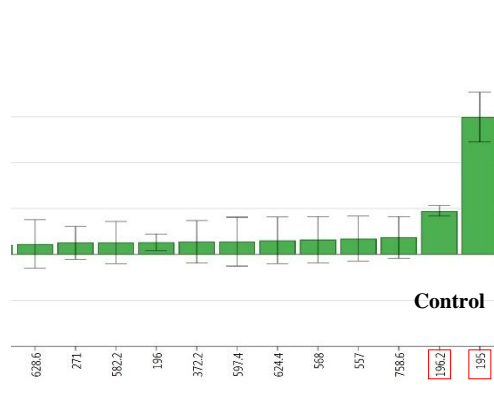
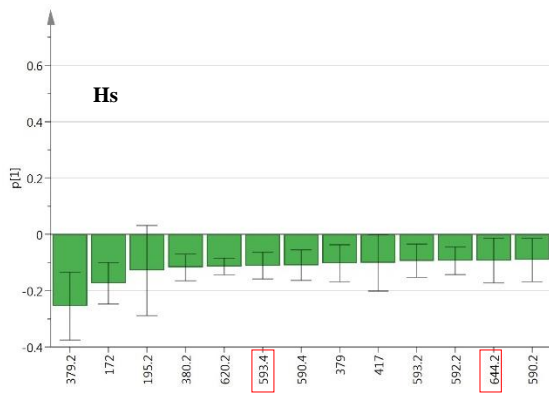
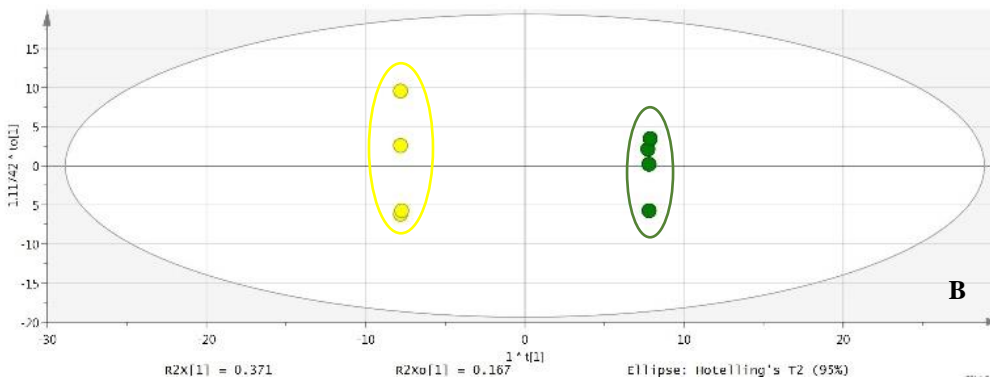
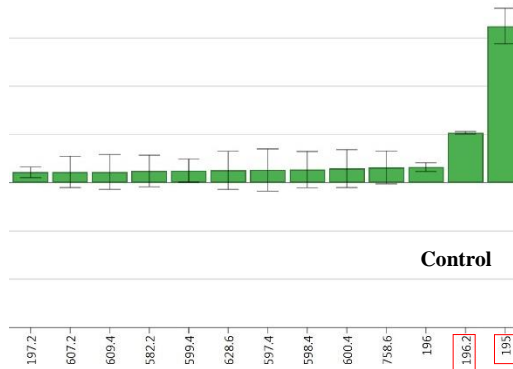
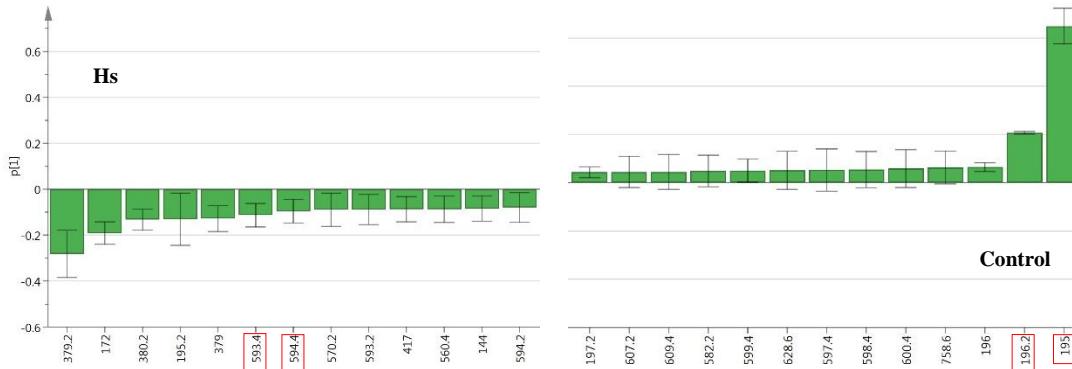
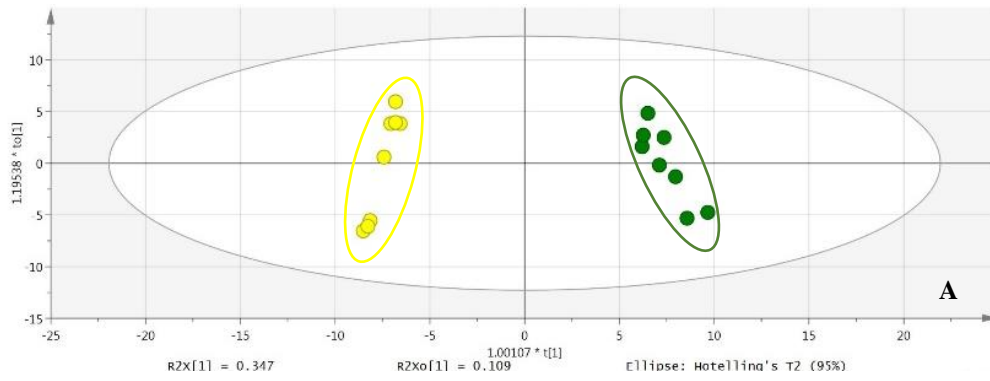


Figure A3.8: Supervised multivariate OPLS-DA plots of the pair-wise comparisons of metabolite profiles of treatments Hs*CO₂ & Hs. Metabolite profiles of the aqueous layer were analysed in positive ionisation mode. A: All leaves, B: New leaves, C: Old leaves. The corresponding loadings plots underneath each OPLS-DA plot demonstrate the discriminant mass bins associated with each treatment in the pair-wise comparison for all, new, and old leaves.

● Hs ● Control



● Hs ● Control

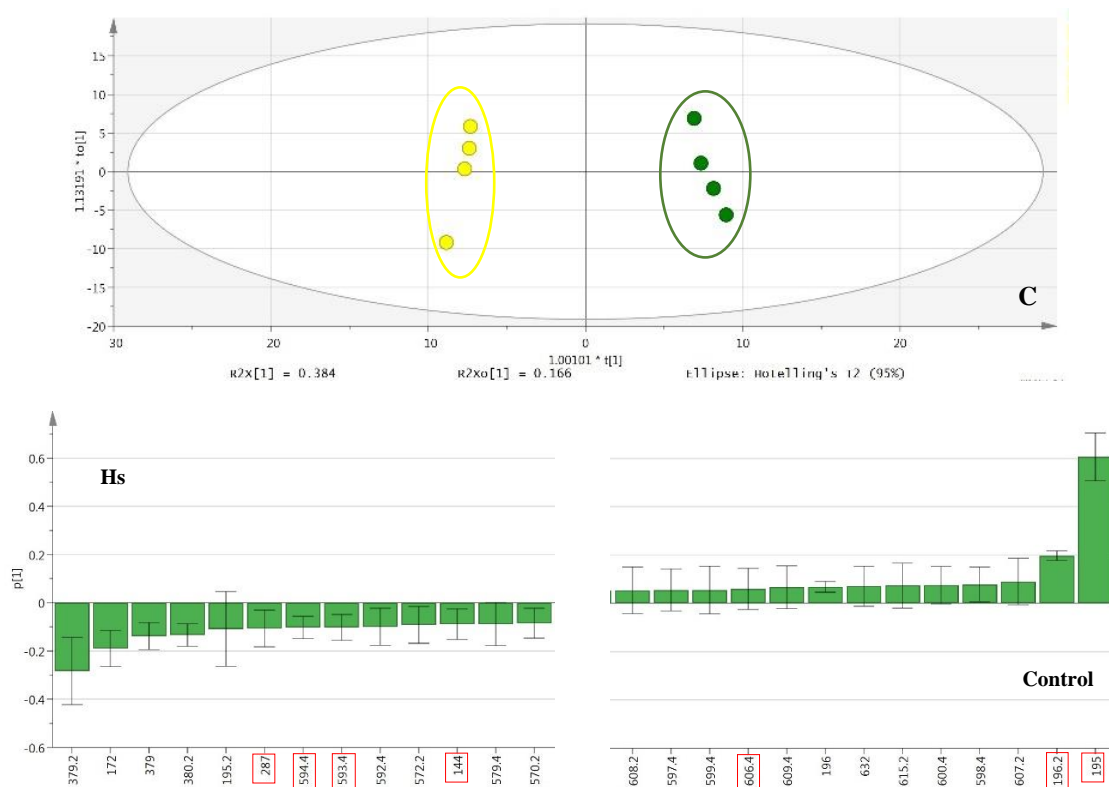
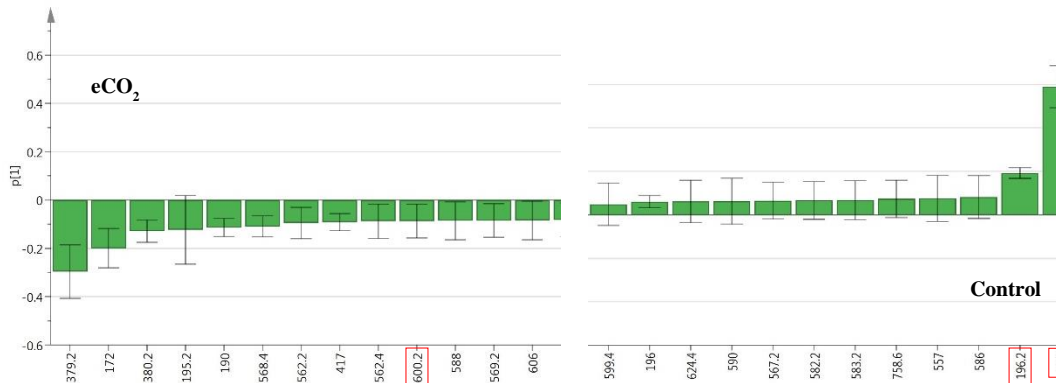
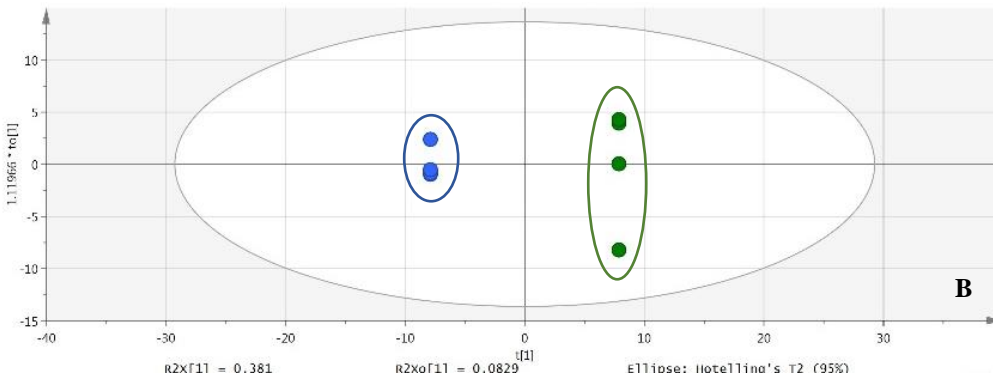
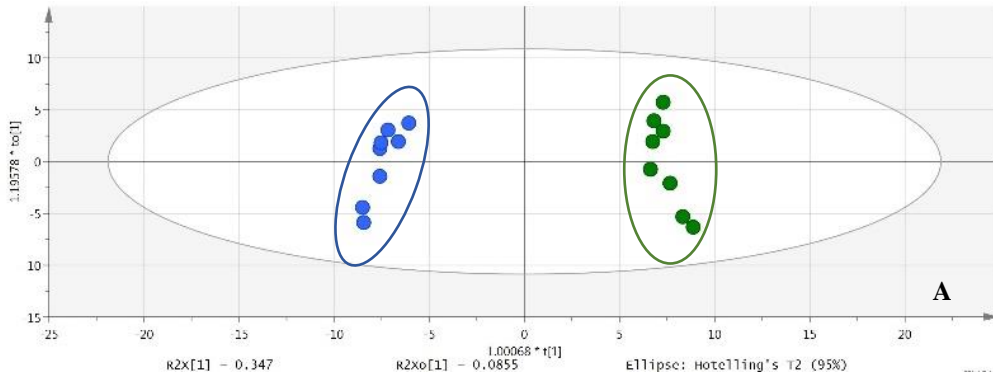


Figure A3.9: Supervised multivariate OPLS-DA plots of the pair-wise comparisons of the metabolite profiles of treatments Hs & control. Metabolite profiles of the organic layer were analysed in positive ionisation mode. A: All leaves, B: New leaves, C: Old leaves. The corresponding loadings plots underneath each OPLS-DA plot demonstrate the discriminant mass bins associated with each treatment in the pair-wise comparison for all, new, and old leaves.



● eCO_2 ● Control

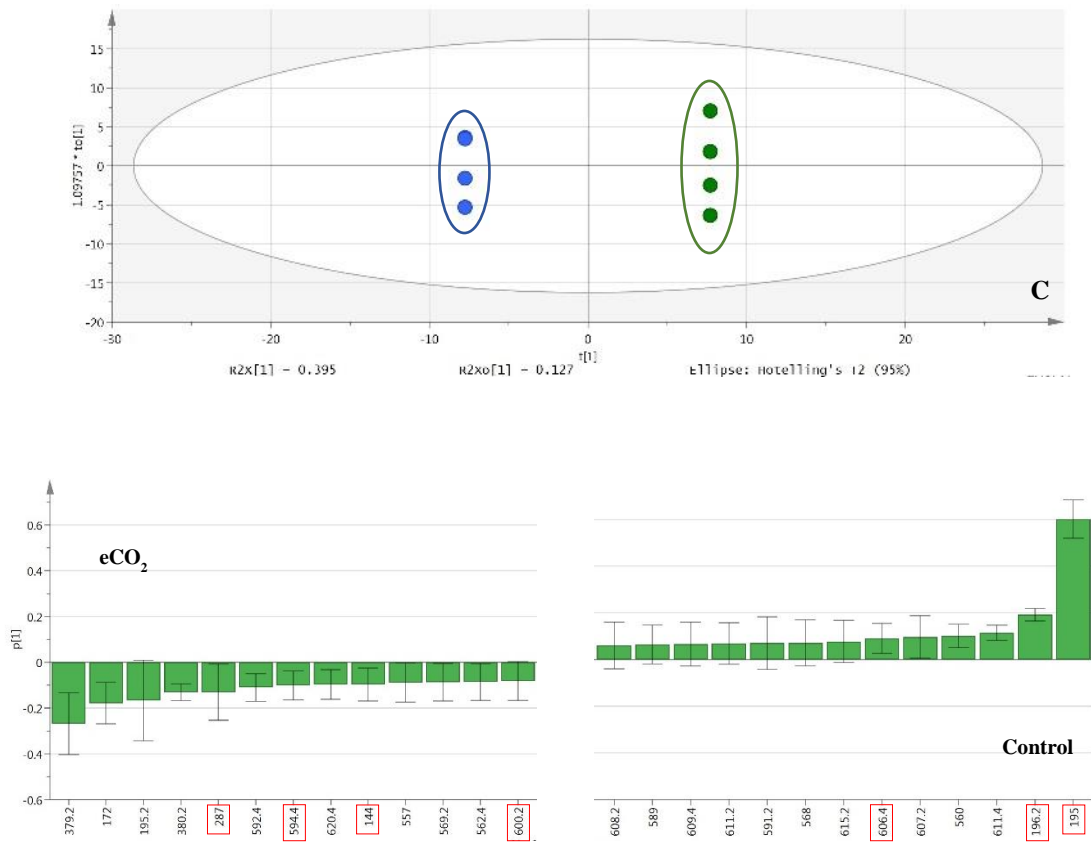
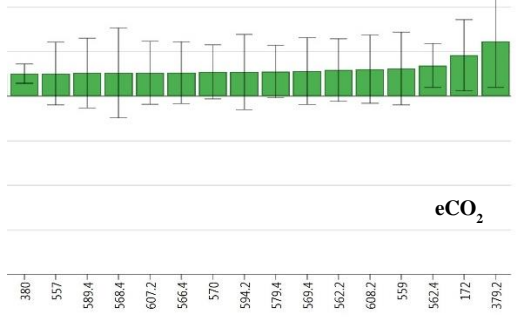
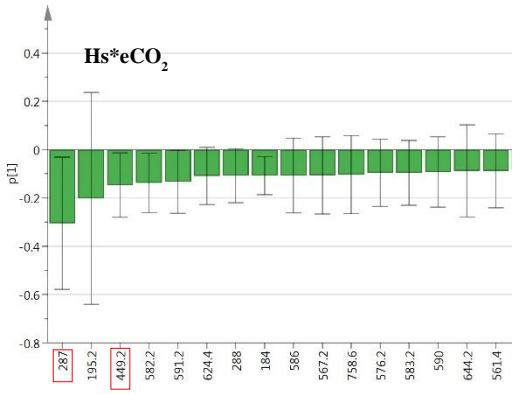
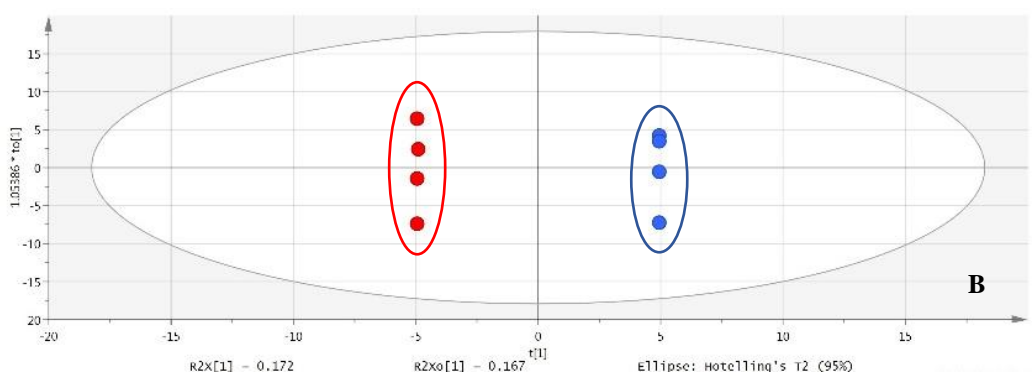
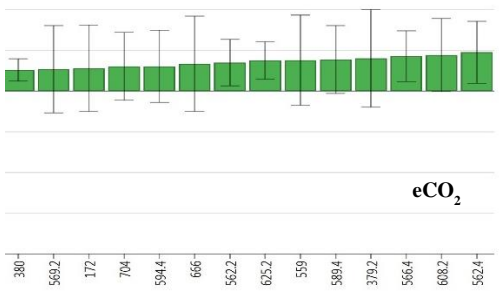
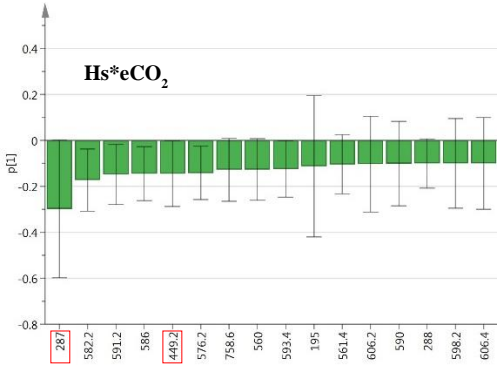
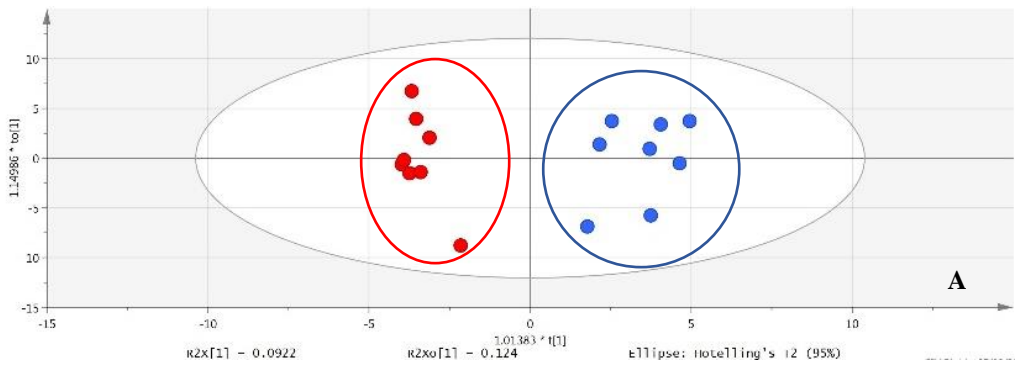


Figure A3.10 Supervised multivariate OPLS-DA plots of the pair-wise comparisons of the metabolite profiles of treatments eCO_2 & control. Metabolite profiles of the organic layer were analysed in positive ionisation mode. A: All leaves, B: New leaves, C: Old leaves. The corresponding loadings plots underneath each OPLS-DA plot demonstrate the discriminant mass bins associated with each treatment in the pair-wise comparison for all, new, and old leaves.

● $Hs*eCO_2$ ● eCO_2



● Hs*eCO₂ ● eCO₂

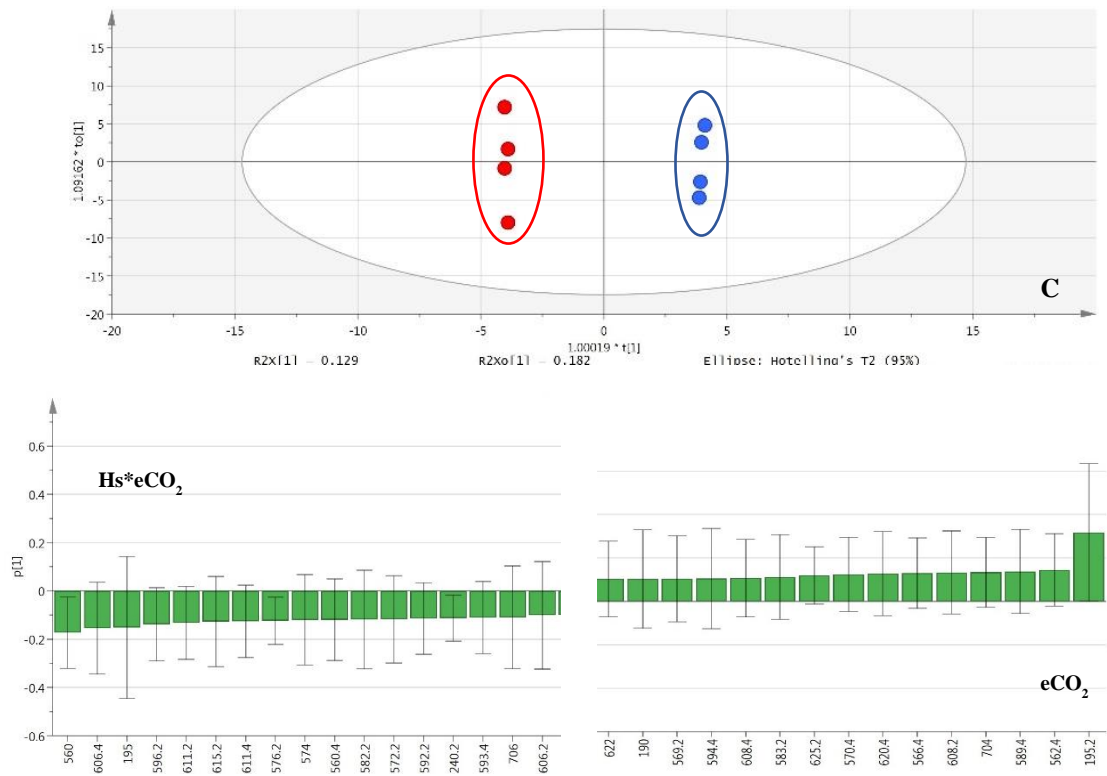
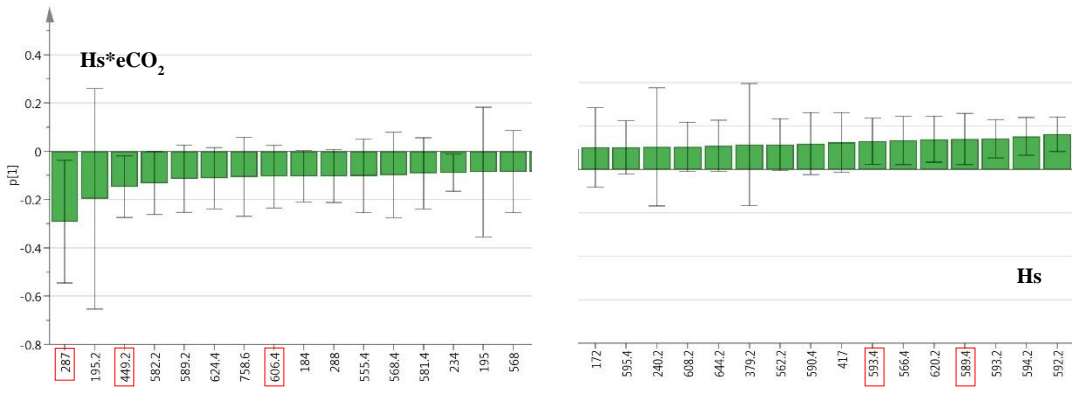
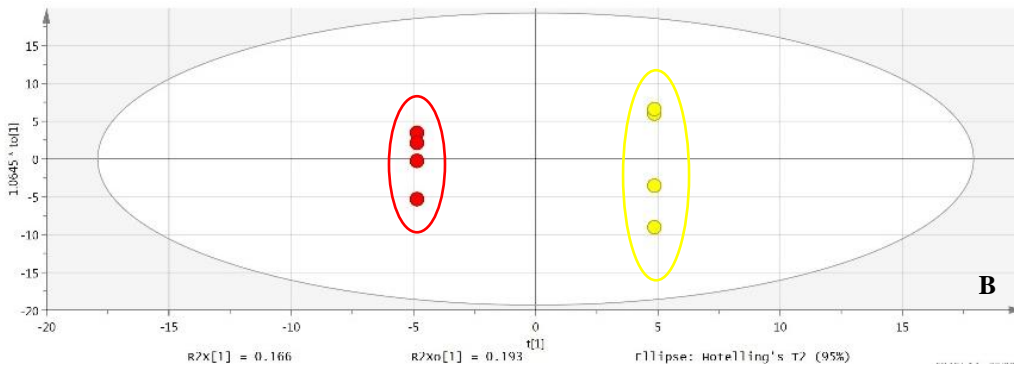
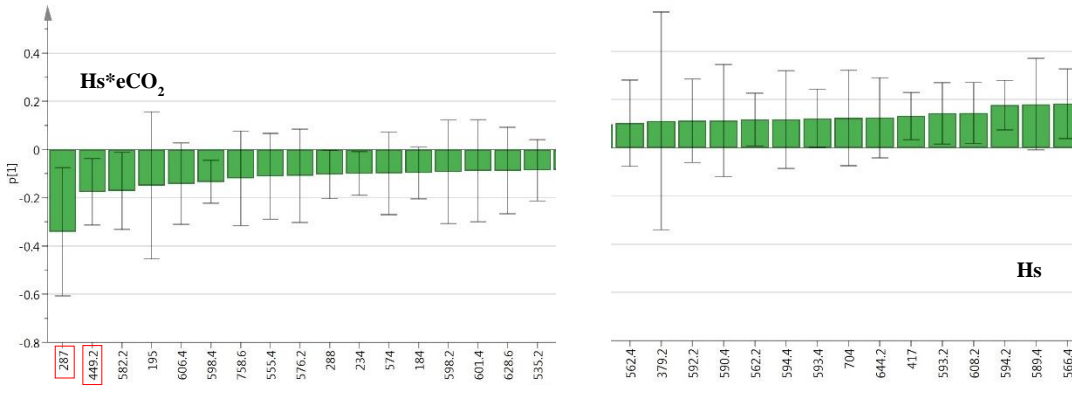
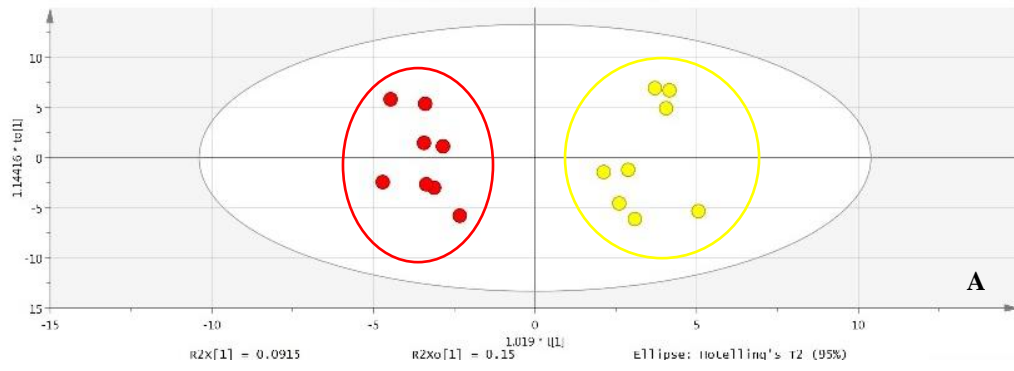


Figure A3.11: Supervised multivariate OPLS-DA plots of the pair-wise comparisons of the metabolite profiles of treatments Hs*eCO₂ & eCO₂. Metabolite profiles of the organic layer were analysed in positive ionisation mode. A: All leaves, B: New leaves, C: Old leaves. The corresponding loadings plots underneath each OPLS-DA plot demonstrate the discriminant mass bins associated with each treatment in the pair-wise comparison for all, new, and old leaves.

● Hs*eCO₂ ● Hs



● $Hs \cdot eCO_2$ ● Hs

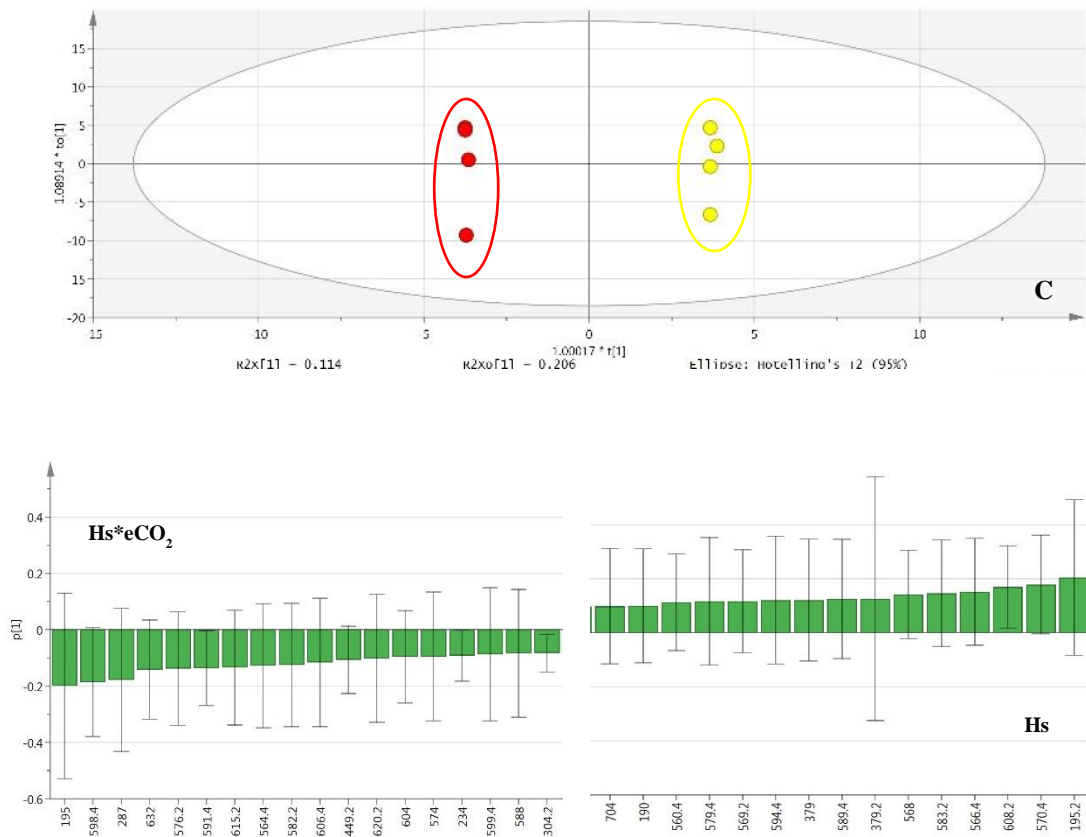


Figure A3.12: Supervised multivariate OPLS-DA plots of the pair-wise comparisons of the metabolite profiles of treatments Hs*CO₂ & Hs. Metabolite profiles for the organic layer were analysed in positive ionisation mode. A: All leaves, B: New leaves, C: Old leaves. The corresponding loadings plots underneath each OPLS-DA plot demonstrate the discriminant mass bins associated with each treatment in the pair-wise comparison for all, new, and old leaves.

Table A3.1: Discriminant mass bins and their associated detected and accurate masses. The putatively identified compounds, their chemical groups, and the associated pathways are displayed. An error in parts per million is included to show the putative compounds' variation from the detected mass (aqueous layer analyzed in negative ESI mode).

Bin	Detected Mass	Standard error	Treatment	Accurate Mass	Appm	Name	Chemical Formula	Chemical group	Pathway
447	447.1484	0.000365718	ANL	448.1564	39	Dichotosin	C ₂₃ H ₂₈ O ₉	glucosyloxy flavan	flavonoid biosynthesis
		0.000296859	ALD	448.1555	39	Dichotosin	C ₂₃ H ₂₈ O ₉	glucosyloxy flavan	flavonoid biosynthesis
	447.14755								
	447.148225	0.000174553	BNL	448.156225	39	Dichotosin	C ₂₃ H ₂₈ O ₉	glucosyloxy flavan	flavonoid biosynthesis
	447.148575	0.000250936	BLD	448.156575	39	Dichotosin	C ₂₃ H ₂₈ O ₉	glucosyloxy flavan	flavonoid biosynthesis
	447.148725	0.000856866	CNL	448.156725	39	Dichotosin	C ₂₃ H ₂₈ O ₉	glucosyloxy flavan	flavonoid biosynthesis
	447.147925	0.000304908	CLD	448.155925	39	Dichotosin	C ₂₃ H ₂₈ O ₉	glucosyloxy flavan	flavonoid biosynthesis
	447.095625	0.000343466	DNL	448.103625	5	kaempferol 7-O-glucoside	C ₂₁ H ₁₉ O ₁₁	glucoside	kaempferol glycoside biosynthesis/flavonoid biosynthesis
	Kaempferol 3-O-β-D-galactoside (Trifolin)					C ₂₁ H ₂₀ O ₁₁	galactoside	Flavonone/Flavonol biosynthesis	
	Astragalgin					C ₂₁ H ₂₀ O ₁₁	glucoside	Flavonol biosynthesis	
	Naringenin-4'-O-β-D-Glucuronide					C ₂₁ H ₂₀ O ₁₁	flavonone	Flavonol biosynthesis	
	Naringenin-7-O-β-D-Glucuronide					C ₂₁ H ₂₀ O ₁₁	flavonone	Flavonol biosynthesis	
	Cyanidin 3-O-galactoside					C ₂₁ H ₂₀ O ₁₁	anthocyanin	Anthocyanin biosynthesis/flavonoid biosynthesis	
	Quercitrin					C ₂₁ H ₂₀ O ₁₁	glycoside	Flavonol biosynthesis	
	Aureusidin 6-O-glucoside					C ₂₁ H ₂₀ O ₁₁	glucoside	Flavonoid biosynthesis	
	Orobo 8-C-glucoside					C ₂₁ H ₂₀ O ₁₁	glucoside	Flavonoid biosynthesis	
	Luteolin 7-O-glucoside					C ₂₁ H ₂₀ O ₁₁	flavonone	Flavonone/Flavonol biosynthesis	
	6-C-Glucosylorobol					C ₂₁ H ₂₀ O ₁₁	flavonoid	Flavonoid biosynthesis	
	Oroboside					C ₂₁ H ₂₀ O ₁₁	glucoside	Flavonoid biosynthesis	
	Cyanidin 5-O-glucoside					C ₂₁ H ₂₀ O ₁₁	anthocyanin	Anthocyanin biosynthesis	
petunidin-3-O-arabinoside	C ₂₁ H ₂₀ O ₁₁					anthocyanin	Anthocyanin biosynthesis		
7-O-β-D-Glucopyranoside	C ₂₁ H ₂₀ O ₁₁					flavonol	Flavonoid biosynthesis		
5,7,2',6'-Tetrahydroxyflavone 2'-O-glucoside	C ₂₁ H ₂₀ O ₁₁					flavanol	Flavonoid biosynthesis		
Isoorientin	C ₂₁ H ₂₀ O ₁₁					flavone	Flavonoid biosynthesis		
Orientin	C ₂₁ H ₂₀ O ₁₁					flavone	Flavonoid biosynthesis		
Isorhamnetin 3-α-L-arabinofuranoside	C ₂₁ H ₂₀ O ₁₁					flavonol	Flavonoid biosynthesis		
Distichin	C ₂₁ H ₂₀ O ₁₁					flavanol	Flavonoid biosynthesis		
Isorhamnetin 3-xyloside	C ₂₁ H ₂₀ O ₁₁	flavone	Flavonoid biosynthesis						
Luteolin 5-glucoside	C ₂₁ H ₂₀ O ₁₁	flavanol	Flavonoid biosynthesis						

						Luteolin 7-glucoside	C21H20O11	flavone	Flavonoid biosynthesis
						Luteolin 7-galactoside	C21H20O11	flavone	Flavonone/Flavonol biosynthesis
						Luteolin 3'-glucoside	C21H20O11	flavone	Flavonone/Flavonol biosynthesis
						Luteolin 4'-glucoside	C21H20O11	flavone	Flavonone/Flavonol biosynthesis
						Scutellarein 6-glucoside	C21H20O11	flavone	Flavonone/Flavonol biosynthesis
						Scutellarein 7-glucoside	C21H20O11	flavone	Flavonone/Flavonol biosynthesis
						6-Hydroxyluteolin 5-rhamnoside	C21H20O11	flavone	Flavonone/Flavonol biosynthesis
						6-Hydroxyluteolin 7-rhamnoside	C21H20O11	flavone	Flavonone/Flavonol biosynthesis
						6-Hydroxyluteolin 6-rhamnoside	C21H20O11	flavone	Flavonone/Flavonol biosynthesis
						6-C-Galactosylisoscuteallarein	C21H20O11	flavone	Flavonone/Flavonol biosynthesis
						Isoscuteallarein 7-glucoside	C21H20O11	glucoside	Flavonoid biosynthesis
						Fisetin 8-C-glucoside	C21H20O11	glucoside	Flavonoid biosynthesis
						Fisetin 3-glucoside	C21H20O11	glucoside	Flavonoid biosynthesis
						Fisetin 7-glucoside	C21H20O11	glucoside	Flavonoid biosynthesis
						Fisetin 4'-glucoside	C21H20O11	glucoside	Flavonoid biosynthesis
						Datiscanin	C21H20O11	glucoside	Flavonoid biosynthesis
						6-C-Glucopyranosylkaempferol	C21H20O11	glucoside	kaempferol glycoside biosynthesis
						8-C-beta-D-Glucopyranosylkaempferol	C21H20O11	flavone	Flavonone/Flavonol biosynthesis
						Kaempferol 3-alpha-D-galactoside	C21H20O11	galactoside	Flavonone/Flavonol biosynthesis
						Kaempferol 7-alloside	C21H20O11	glycoside	Flavonone/Flavonol biosynthesis
						Kaempferol 7-galactoside	C21H20O11	glycoside	Flavonone/Flavonol biosynthesis
						Kaempferol 4'-glucoside	C21H20O11	glucoside	Flavonoid biosynthesis
						8-C-Methylquercetin 3-xyloside	C21H20O11	glycoside	Flavonone/Flavonol biosynthesis
						Quercetin 7-rhamnoside	C21H20O11	glycoside	Flavonol biosynthesis
						Rhamnetin 3-alpha-L-arabinofuranoside	C21H20O11	flavonol	Flavonol biosynthesis
						Rhamnetin 3-alpha-L-arabinopyranoside	C21H20O11	flavonol	Flavonol biosynthesis
						Quercetin 3-methyl ether 3'-xyloside	C21H20O11	flavinoid	Flavonoid biosynthesis
						Herbacetin 7-rhamnoside	C21H20O11	flavinoid	Flavonoid biosynthesis
						Herbacetin 8-rhamnoside	C21H20O11	flavinoid	Flavonoid biosynthesis

						Carthamone	C21H20O11	Chalcone	Flavonoid biosynthesis
						Maritimein	C21H20O11	Phenol	Flavonoid biosynthesis
						Maritimetin 7-glucoside	C21H20O11	glucoside	Flavonoid biosynthesis
						Cernuoside	C21H20O11	glucoside	Flavonoid biosynthesis
						Dihydrobaicalein 7-O-glucuronide	C21H20O11	glucuronide	Flavonoid biosynthesis
						Dihydronorwogonin 7-O-glucuronide	C21H20O11	glucuronide	Flavonoid biosynthesis
						8-C-Glucosylorobol	C21H20O11	glucosyl	Flavonoid biosynthesis
447.08695	0.004589186	DLD	448.09495	14		Naringenin-4'-O- β -D-Glucuronide	C21H20O11	Flavonone	Flavonol biosynthesis
				14		Naringenin-7-O- β -D-Glucuronide	C21H20O11	Flavonone	Flavonol biosynthesis
				14		kaempferol 7-O-glucoside	C21H19O11	Glucoside	kaempferol glycoside biosynthesis
				14		Cyanidin 3-O-galactoside	C21H20O11	Anthocyanin	Anthocyanin biosynthesis
				14		Quercitrin	C21H20O11	Flavonol	Flavonol biosynthesis
				14		Aureusidin 6-O-glucoside	C21H20O11	Aurone	
				14		Astragalin	C21H20O11		Flavonol biosynthesis
				14		Luteolin 7-O-glucoside	C21H20O11	Flavonone	Flavonone/Flavonol biosynthesis
				14		8-C-Glucosylorobol	C21H20O11	Glucosyl	
				14		Kaempferol 3-O- β -D-galactoside (Trifolin)	C21H20O11		
				14		6-C-Glucosylorobol	C21H20O11		
				14		Cyanidin 5-O-glucoside	C21H20O11		
				14		Orobol 7-O-glucoside	C21H20O11		
				14		petunidin-3-O-arabinoside	C21H20O11		
				14		5,7,2',6'-Tetrahydroxyflavone 2'-O-glucoside	C21H20O11		
				14		5,7,3',4'-Tetrahydroxy-4-phenylcoumarin 5-O-glucoside	C21H20O11		
				14		7,3',4',5'-Tetrahydroxyflavone 7-glucoside	C21H20O11		
				14		Isoorientin	C21H20O11		
				14		Orientin	C21H20O11		
				14		6-C-Galactosylisoscutearein	C21H20O11		
				14		Isorhamnetin 3-xyloside	C21H20O11		
				14		Luteolin 5-glucoside	C21H20O11		
				14		Luteolin 7-glucoside	C21H20O11		
				14		Luteolin 7-galactoside	C21H20O11		
				14		Luteolin 3'-glucoside	C21H20O11		
				14		Luteolin 4'-glucoside	C21H20O11		
				14		Scutellarein 6-glucoside	C21H20O11		
				14		Scutellarein 7-glucoside	C21H20O11		
				14		6-Hydroxyluteolin 5-rhamnoside	C21H20O11		
				14		6-Hydroxyluteolin 7-rhamnoside	C21H20O11		
				14		6-Hydroxyluteolin 6-rhamnoside	C21H20O11		
				14		Fisetin 8-C-glucoside	C21H20O11		

Flavonone/Flavonol biosynthesis

					14	Fisetin 3-glucoside	C21H20O11		
					14	Fisetin 7-glucoside	C21H20O11		
					14	Fisetin 4'-glucoside	C21H20O11		
					14	Datiscanin	C21H20O11		
					14	6-C-Glucopyranosylkaempferol	C21H20O11		
					14	8-C-beta-D-Glucopyranosylkaempferol	C21H20O11		
					14	Kaempferol 3-alpha-D-galactoside	C21H20O11		
					14	Kaempferol 7-alloside	C21H20O11		
					14	Kaempferol 7-galactoside	C21H20O11		
					14	Kaempferol 4'-glucoside	C21H20O11		
					14	8-C-Methylquercetin 3-xyloside	C21H20O11		
					14	Quercetin 7-rhamnoside	C21H20O11		
					14	Rhamnetin 3-alpha-L-arabinofuranoside	C21H20O11		
					14	Rhamnetin 3-alpha-L-arabinopyranoside	C21H20O11		
					14	Quercetin 3-methyl ether 3'-xyloside	C21H20O11		
					14	Herbacetin 7-rhamnoside	C21H20O11		
					14	Herbacetin 8-rhamnoside	C21H20O11		
					14	Carthamone	C21H20O11		
					14	Maritimein	C21H20O11		
					14	Maritimetin 7-glucoside	C21H20O11		
					14	Cernuoside	C21H20O11		
					14	Aureusin	C21H20O11		
					14	Dihydrobaicalein 7-O-glucuronide	C21H20O11		
					14	Dihydronorwogonin 7-O-glucuronide	C21H20O11		
	194.1057	0.000718505	ANL	195.1137		N/A			
	194.1051	0.000619476	ALD	195.1131	39	N-Benzylidene	C ₁₄ H ₁₃ N		
	194.106025	0.000826419	BNL	195.114025		6-hydroxypseudooxynicotine	C ₁₀ H ₁₅ N ₂ O ₂	ketone	Nicotine Degredation
194.2									
	194.104775	0.000830944	BLD	195.112775	39	N-Benzylidene	C ₁₄ H ₁₃ N		
						6-hydroxypseudooxynicotine	C ₁₀ H ₁₅ N ₂ O ₂	ketone	Nicotine Degredation
	194.105975	0.000935665	CNL	195.113975		6-hydroxypseudooxynicotine	C ₁₀ H ₁₅ N ₂ O ₂	ketone	Nicotine Degredation
	194.105	0.001394184	CLD	195.113		6-hydroxypseudooxynicotine	C ₁₀ H ₁₅ N ₂ O ₂	ketone	Nicotine Degredation
	194.072975		DNL	195.080975		6-hydroxymethyl-7,8-dihydropterin	C ₁₀ H ₁₅ N ₂ O ₂	Pteridine	6-hydroxymethyl-dihydropterin diphosphate biosynthesis I
					30	Glucosaminic acid	C ₆ H ₁₃ NO ₆		Pentose phosphate pathway
					30	D-Glucose oxime	C ₆ H ₁₃ NO ₆	glucosinolate	glucosinolate biosynthesis
					23	2-Amino-4-hydroxy-6-(hydroxymethyl)-7,8-dihydropteridine	C ₇ H ₉ N ₅ O ₂		
					2	2-(3-pyridyl)-Benzimidazole	C ₁₂ H ₉ N ₃		

	194.0766	0.002208223	DLD	195.0846	2	2-(3-pyridyl)-Benzimidazole	C12H9N3		
					29	Damascenine	C10H13NO3	ketone	shikimate biosynthesis
	448.150625	0.000134048	ANL	449.1586		N/A			
	448.1504	0.000262202	ALD	449.1584		N/A			
	448.15105	0.000201556	BNL	449.159		N/A			
	448.1509	0.000262202	BLD	449.1589		N/A			
448.2	448.150825	0.000243349	CNL	449.1588		N/A			
	448.150275	5.44862E-05	CLD	449.1582		N/A			
	448.090125	0.003807127	DNL	449.0981	28	Glucosquerellin	C14H27NO9S3	Glucosinolate	glucosinolate biosynthesis
					28	6-(Methylthio)hexyl glucosinolate	C14H27NO9S3		
					24	Cyanidin 3-galactoside	C21H21O11		
					24	Cyanidin 7-glucoside	C21H21O11		
					24	Cyanidin 4'-glucoside	C21H21O11		
	448.0842	0.002275687	DLD	449.0922	28	Glucosquerellin	C14H27NO9S3	Glucosinolate	
					28	6-(Methylthio)hexyl glucosinolate	C14H27NO9S3		
					24	Cyanidin 3-galactoside	C21H21O11	Glucosinolate	glucosinolate biosynthesis
					24	Cyanidin 7-glucoside	C21H21O11	Glucosinolate	glucosinolate biosynthesis
					24	Cyanidin 4'-glucoside	C21H21O11	Glucosinolate	glucosinolate biosynthesis
	285.082575	0.000174553	ANL	286.0905	20	Gummiferol	C16H14O5		
					20	Brazilin	C16H14O5		
					20	Carajuron	C16H14O5	anthocyanin	Flavonoid biosynthesis
					20	Peltogynan	C16H14O5	anthocyanin	Flavonoid biosynthesis
					20	3'-Hydroxydihydroformononetin	C16H14O5	isoflavonone	Flavonoid biosynthesis
					20	Vestitone	C16H14O5	isoflavonone	Flavonoid biosynthesis
					20	Dihydrobiochanin A	C16H14O5	isoflavonone	Flavonoid biosynthesis
					20	(-)-Nissolin	C16H14O5	flavonoid	Flavonoid biosynthesis
				20	Vesticarpan	C16H14O5	isoflavonoid	Flavonoid biosynthesis	
				20	Kushenin	C16H14O5	isoflavonoid	Flavonoid biosynthesis	
				20	(6aR,11aR)-3,8-Dihydroxy-9-methoxypterocarpan	C16H14O5	flavonoid	Flavonoid biosynthesis	
				20	Nissicarpan	C16H14O5	flavonoid	Flavonoid biosynthesis	
				20	4-Hydroxymedicarpin	C16H14O5	flavonoid	Flavonoid biosynthesis	
				20	Melilotocarpan B	C16H14O5	flavonoid	Flavonoid biosynthesis	
				20	Desmocarpan	C16H14O5	flavonoid	Flavonoid biosynthesis	
				20	6a-Hydroxymedicarpin	C16H14O5	flavonoid	Flavonoid biosynthesis	
				20	6a-Hydroxyisomedicarpin	C16H14O5	flavonoid	Flavonoid biosynthesis	
				20	Claussequinone	C16H14O5	isoflavonone	Flavonoid biosynthesis	
				20	Sepiol	C16H14O5	flavonoid	Flavonoid biosynthesis	
				20	Hagin C	C16H14O5	flavonoid	Flavonoid biosynthesis	

				20	Homobutein	C16H14O5	polyphenol	phenyl propanoid pathway
				20	3,2',4'-Trihydroxy-4-methoxychalcone	C16H14O5	chalcone	Flavonoid biosynthesis
				20	Sappanchalcone	C16H14O5	chalcone	Flavonoid biosynthesis
				20	Calythropsin	C16H14O5	chalcone	Flavonoid biosynthesis
				20	Kukulkanin B	C16H14O5	chalcone	Flavonoid biosynthesis
				20	2,2',4'-Trihydroxy-6'-methoxychalcone	C16H14O5	chalcone	Flavonoid biosynthesis
				20	2',4',6'-Trihydroxy-4-methoxychalcone	C16H14O5	chalcone	Flavonoid biosynthesis
				20	Helichrysetin	C16H14O5	flavonoid	Flavonoid biosynthesis
				20	Neosakuranetin	C16H14O5	chalcone	Flavonoid biosynthesis
				20	Licodione 2'-methyl ether	C16H14O5	chalcone	Flavonoid biosynthesis
				20	2',6',beta-Trihydroxy-4'-methoxychalcone	C16H14O5	chalcone	Flavonoid biosynthesis
				20	2',4',beta-Trihydroxy-6'-methoxychalcone	C16H14O5	chalcone	Flavonoid biosynthesis
				20	Licochalcone B	C16H14O5	chalcone	Flavonoid biosynthesis
				20	Linderone	C16H14O5	chalcone	Flavonoid biosynthesis
				20	2',4'-Dihydroxy-3,4-methylenedioxydihydrochalcone	C16H14O5	chalcone	Flavonoid biosynthesis
				20	3'-Formyl-2',4',6'-trihydroxydihydrochalcone	C16H14O5	chalcone	Flavonoid biosynthesis
				20	5,6-Dihydroxy-4'-methoxyflavanone	C16H14O5	flavonone	Flavonoid biosynthesis
				20	Dihydroechioidinin	C16H14O5	flavonone	Flavonoid biosynthesis
				20	Poriol	C16H14O5	flavonone	Flavonoid biosynthesis
				20	3-Methylnaringenin	C16H14O5	flavonoid	Flavonoid biosynthesis
				20	Isosakuranetin	C16H14O5	flavonone	Flavonoid biosynthesis
				20	Naringenin 5-methyl ether	C16H14O5	flavonone	Flavonoid biosynthesis
				20	Sakuranetin	C16H14O5	flavonone	Flavonoid biosynthesis
				20	Dihydrooxylin A	C16H14O5	flavonone	Flavonoid biosynthesis
				20	Dihydrowogonin	C16H14O5	flavonone	Flavonoid biosynthesis
				20	5,8-Dihydroxy-7-methoxyflavanone	C16H14O5	flavonone	Flavonoid biosynthesis
				20	Sainfuran	C16H14O5	polyphenol	phenyl propanoid pathway
				20	2',4'-Dihydroxy-5,6-dimethoxy-2-phenylbenzofuran	C16H14O5	flavonoid	Flavonoid biosynthesis
				20	Pterofuran	C16H14O5	flavonoid	Flavonoid biosynthesis
				20	Isopterofuran	C16H14O5	flavonoid	Flavonoid biosynthesis
				20	2,7-Dihydroxy-4'-methoxyisoflavanone	C16H14O5	flavonoid	Flavonoid biosynthesis
				20	(-)-Vestitone	C16H14O5	isoflavone	Flavonoid biosynthesis
				20	Moracin A	C16H14O5	flavonoid	Flavonoid biosynthesis
				20	Quinquangulin	C16H14O5		
				20	Oxypeucedanin	C16H14O5		
				20	Phyllodulcin	C16H14O5	polyphenol	phenylpropanoid pathway
				20	Moracin B	C16H14O5	flavonoid	Flavonoid biosynthesis
				20	Heliannone C	C16H14O5		
				20	Moracin F	C16H14O5	flavonoid	Flavonoid biosynthesis
				20	(R)-Pabulenol	C16H14O5		

				20	(-)-5,7-Dihydroxy-3-(4-hydroxybenzyl)-4-chromanone	C16H14O5	homoisoflavonoid	Flavonoid biosynthesis
285.082375	0.000477461	ALD	286.0903	20	Gummiferol	C16H14O5	homoisoflavonoid	Flavonoid biosynthesis
				20	Brazilin	C16H14O5	homoisoflavonoid	Flavonoid biosynthesis
				20	Carajuron	C16H14O5	homoisoflavonoid	Flavonoid biosynthesis
285.082375				20	Peltogynan	C16H14O5	homoisoflavonoid	Flavonoid biosynthesis
				20	3'-Hydroxydihydroformononetin	C16H14O5	homoisoflavonoid	Flavonoid biosynthesis
				20	Vestitone	C16H14O5	homoisoflavonoid	Flavonoid biosynthesis
				20	Dihydrobiochanin A	C16H14O5	homoisoflavonoid	Flavonoid biosynthesis
				20	(-)-Nissolin	C16H14O5	homoisoflavonoid	Flavonoid biosynthesis
				20	Vesticarpan	C16H14O5	homoisoflavonoid	Flavonoid biosynthesis
				20	Kushenin	C16H14O5	homoisoflavonoid	Flavonoid biosynthesis
				20	(6aR,11aR)-3,8-Dihydroxy-9-methoxypterocarpan	C16H14O5	homoisoflavonoid	Flavonoid biosynthesis
				20	Nissicarpan	C16H14O5	homoisoflavonoid	Flavonoid biosynthesis
				20	4-Hydroxymedicarpin	C16H14O5	homoisoflavonoid	Flavonoid biosynthesis
				20	Melilotocarpin B	C16H14O5	homoisoflavonoid	Flavonoid biosynthesis
				20	Desmocarpan	C16H14O5	homoisoflavonoid	Flavonoid biosynthesis
				20	6a-Hydroxymedicarpin	C16H14O5	homoisoflavonoid	Flavonoid biosynthesis
				20	6a-Hydroxyisomedicarpin	C16H14O5	homoisoflavonoid	Flavonoid biosynthesis
				20	Claussequinone	C16H14O5	homoisoflavonoid	Flavonoid biosynthesis
				20	Sepiol	C16H14O5	homoisoflavonoid	Flavonoid biosynthesis
				20	Haginin C	C16H14O5	homoisoflavonoid	Flavonoid biosynthesis
				20	Homobutein	C16H14O5	homoisoflavonoid	Flavonoid biosynthesis
				20	3,2',4'-Trihydroxy-4-methoxychalcone	C16H14O5	homoisoflavonoid	Flavonoid biosynthesis
				20	Sappanchalcone	C16H14O5	homoisoflavonoid	Flavonoid biosynthesis
				20	Calythropsin	C16H14O5	homoisoflavonoid	Flavonoid biosynthesis
				20	Kukulkanin B	C16H14O5	homoisoflavonoid	Flavonoid biosynthesis
				20	2,2',4'-Trihydroxy-6'-methoxychalcone	C16H14O5	homoisoflavonoid	Flavonoid biosynthesis
				20	2',4',6'-Trihydroxy-4-methoxychalcone	C16H14O5	homoisoflavonoid	Flavonoid biosynthesis
				20	Helichrysetin	C16H14O5	homoisoflavonoid	Flavonoid biosynthesis
				20	Neosakuranetin	C16H14O5	homoisoflavonoid	Flavonoid biosynthesis
				20	Licodione 2'-methyl ether	C16H14O5	homoisoflavonoid	Flavonoid biosynthesis
				20	2',6',beta-Trihydroxy-4'-methoxychalcone	C16H14O5	homoisoflavonoid	Flavonoid biosynthesis
				20	2',4',beta-Trihydroxy-6'-methoxychalcone	C16H14O5	homoisoflavonoid	Flavonoid biosynthesis
				20	Licochalcone B	C16H14O5	homoisoflavonoid	Flavonoid biosynthesis
				20	Linderone	C16H14O5	homoisoflavonoid	Flavonoid biosynthesis
				20	2',4'-Dihydroxy-3,4-methylenedioxydihydrochalcone	C16H14O5	homoisoflavonoid	Flavonoid biosynthesis
				20	3'-Formyl-2',4',6'-trihydroxydihydrochalcone	C16H14O5	homoisoflavonoid	Flavonoid biosynthesis
				20	5,6-Dihydroxy-4'-methoxyflavanone	C16H14O5	homoisoflavonoid	Flavonoid biosynthesis
				20	Dihydroechioidinin	C16H14O5	homoisoflavonoid	Flavonoid biosynthesis
				20	Poriol	C16H14O5	homoisoflavonoid	Flavonoid biosynthesis
				20	3-Methylnaringenin	C16H14O5	homoisoflavonoid	Flavonoid biosynthesis
				20	Isosakuranetin	C16H14O5	homoisoflavonoid	Flavonoid biosynthesis

				20	Naringenin 5-methyl ether	C16H14O5	homioisoflavonoid	Flavonoid biosynthesis
				20	Sakuranetin	C16H14O5	homioisoflavonoid	Flavonoid biosynthesis
				20	Dihydrooroxilin A	C16H14O5	homioisoflavonoid	Flavonoid biosynthesis
				20	Dihydrowogonin	C16H14O5	homioisoflavonoid	Flavonoid biosynthesis
				20	5,8-Dihydroxy-7-methoxyflavanone	C16H14O5	homioisoflavonoid	Flavonoid biosynthesis
				20	Sainfuran	C16H14O5	homioisoflavonoid	Flavonoid biosynthesis
				20	2',4'-Dihydroxy-5,6-dimethoxy-2-phenylbenzofuran	C16H14O5	homioisoflavonoid	Flavonoid biosynthesis
				20	Pterofuran	C16H14O5	homioisoflavonoid	Flavonoid biosynthesis
				20	Isopterofuran	C16H14O5	homioisoflavonoid	Flavonoid biosynthesis
				20	2,7-Dihydroxy-4'-methoxyisoflavanone	C16H14O5	homioisoflavonoid	Flavonoid biosynthesis
				20	(-)-Vestitone	C16H14O5	homioisoflavonoid	Flavonoid biosynthesis
				20	Moracin A	C16H14O5	homioisoflavonoid	Flavonoid biosynthesis
				20	Quinquangulin	C16H14O5	homioisoflavonoid	Flavonoid biosynthesis
				20	Oxypeucedanin	C16H14O5	homioisoflavonoid	Flavonoid biosynthesis
				20	Phylodulcin	C16H14O5	homioisoflavonoid	Flavonoid biosynthesis
				20	Moracin B	C16H14O5	homioisoflavonoid	Flavonoid biosynthesis
				20	Asperxanthone	C16H14O5	homioisoflavonoid	Flavonoid biosynthesis
				20	Heliannone C	C16H14O5	homioisoflavonoid	Flavonoid biosynthesis
				20	Moracin F	C16H14O5	homioisoflavonoid	Flavonoid biosynthesis
				20	(R)-Pabulenol	C16H14O5	homioisoflavonoid	Flavonoid biosynthesis
				20	(-)-5,7-Dihydroxy-3-(4-hydroxybenzyl)-4-chromanone	C16H14O5	homioisoflavonoid	Flavonoid biosynthesis
285.08285	0.000201556	BNL	286.0908	20	Gummiferol	C16H14O5	homioisoflavonoid	Flavonoid biosynthesis
				20	Brazilin	C16H14O5	homioisoflavonoid	Flavonoid biosynthesis
				20	Carajuron	C16H14O5	homioisoflavonoid	Flavonoid biosynthesis
				20	Peltogynan	C16H14O5	homioisoflavonoid	Flavonoid biosynthesis
				20	3'-Hydroxydihydroformononetin	C16H14O5	homioisoflavonoid	Flavonoid biosynthesis
				20	Vestitone	C16H14O5	homioisoflavonoid	Flavonoid biosynthesis
				20	Dihydrobiochanin A	C16H14O5	homioisoflavonoid	Flavonoid biosynthesis
				20	(-)-Nissolin	C16H14O5	homioisoflavonoid	Flavonoid biosynthesis
				20	Vesticarpan	C16H14O5	homioisoflavonoid	Flavonoid biosynthesis
				20	Kushenin	C16H14O5	homioisoflavonoid	Flavonoid biosynthesis
				20	(6aR,11aR)-3,8-Dihydroxy-9-methoxypterocarpan	C16H14O5	homioisoflavonoid	Flavonoid biosynthesis
				20	Nissicarpin	C16H14O5	homioisoflavonoid	Flavonoid biosynthesis
				20	4-Hydroxymedicarpin	C16H14O5	homioisoflavonoid	Flavonoid biosynthesis
				20	Melilotocarpan B	C16H14O5	homioisoflavonoid	Flavonoid biosynthesis
				20	Desmocarpan	C16H14O5	homioisoflavonoid	Flavonoid biosynthesis
				20	6a-Hydroxymedicarpin	C16H14O5	homioisoflavonoid	Flavonoid biosynthesis
				20	6a-Hydroxyisomedicarpin	C16H14O5	homioisoflavonoid	Flavonoid biosynthesis
				20	Clausequinone	C16H14O5	homioisoflavonoid	Flavonoid biosynthesis
				20	Sepiol	C16H14O5	homioisoflavonoid	Flavonoid biosynthesis
				20	Haginin C	C16H14O5	homioisoflavonoid	Flavonoid biosynthesis
				20	Homobutein	C16H14O5	homioisoflavonoid	Flavonoid biosynthesis

				20	3,2',4'-Trihydroxy-4-methoxychalcone	C16H14O5	homioisoflavonoid	Flavonoid biosynthesis	
				20	Sappanchalcone	C16H14O5	homioisoflavonoid	Flavonoid biosynthesis	
				20	Calythropsin	C16H14O5	homioisoflavonoid	Flavonoid biosynthesis	
				20	Kukulkanin B	C16H14O5	homioisoflavonoid	Flavonoid biosynthesis	
				20	2,2',4'-Trihydroxy-6'-methoxychalcone	C16H14O5	homioisoflavonoid	Flavonoid biosynthesis	
				20	2',4',6'-Trihydroxy-4-methoxychalcone	C16H14O5	homioisoflavonoid	Flavonoid biosynthesis	
				20	Helichrysetin	C16H14O5	homioisoflavonoid	Flavonoid biosynthesis	
				20	Neosakuranetin	C16H14O5	homioisoflavonoid	Flavonoid biosynthesis	
				20	Licodione 2'-methyl ether	C16H14O5	homioisoflavonoid	Flavonoid biosynthesis	
				20	2',6',beta-Trihydroxy-4'-methoxychalcone	C16H14O5	homioisoflavonoid	Flavonoid biosynthesis	
				20	2',4',beta-Trihydroxy-6'-methoxychalcone	C16H14O5	homioisoflavonoid	Flavonoid biosynthesis	
				20	Licochalcone B	C16H14O5	homioisoflavonoid	Flavonoid biosynthesis	
				20	Linderone	C16H14O5	homioisoflavonoid	Flavonoid biosynthesis	
				20	2',4'-Dihydroxy-3,4-methylenedioxydihydrochalcone	C16H14O5	homioisoflavonoid	Flavonoid biosynthesis	
				20	3'-Formyl-2',4',6'-trihydroxydihydrochalcone	C16H14O5	homioisoflavonoid	Flavonoid biosynthesis	
				20	5,6-Dihydroxy-4'-methoxyflavanone	C16H14O5	homioisoflavonoid	Flavonoid biosynthesis	
				20	Dihydroechioidinin	C16H14O5	homioisoflavonoid	Flavonoid biosynthesis	
				20	Poriol	C16H14O5	homioisoflavonoid	Flavonoid biosynthesis	
				20	3-Methylnaringenin	C16H14O5	homioisoflavonoid	Flavonoid biosynthesis	
				20	Isosakuranetin	C16H14O5	homioisoflavonoid	Flavonoid biosynthesis	
				20	Naringenin 5-methyl ether	C16H14O5	homioisoflavonoid	Flavonoid biosynthesis	
				20	Sakuranetin	C16H14O5	homioisoflavonoid	Flavonoid biosynthesis	
				20	Dihydrooxylin A	C16H14O5	homioisoflavonoid	Flavonoid biosynthesis	
				20	Dihydrowogonin	C16H14O5	homioisoflavonoid	Flavonoid biosynthesis	
				20	5,8-Dihydroxy-7-methoxyflavanone	C16H14O5	homioisoflavonoid	Flavonoid biosynthesis	
				20	Sainfuran	C16H14O5	homioisoflavonoid	Flavonoid biosynthesis	
				20	2',4'-Dihydroxy-5,6-dimethoxy-2-phenylbenzofuran	C16H14O5	homioisoflavonoid	Flavonoid biosynthesis	
				20	Pterofuran	C16H14O5	homioisoflavonoid	Flavonoid biosynthesis	
				20	Isopterofuran	C16H14O5	homioisoflavonoid	Flavonoid biosynthesis	
				20	2,7-Dihydroxy-4'-methoxyisoflavanone	C16H14O5	homioisoflavonoid	Flavonoid biosynthesis	
				20	(-)-Vestitone	C16H14O5	homioisoflavonoid	Flavonoid biosynthesis	
				20	Moracin A	C16H14O5	homioisoflavonoid	Flavonoid biosynthesis	
				20	Quinquangulin	C16H14O5	homioisoflavonoid	Flavonoid biosynthesis	
				20	Oxypeucedanin	C16H14O5	homioisoflavonoid	Flavonoid biosynthesis	
				20	Phyllodulcin	C16H14O5	homioisoflavonoid	Flavonoid biosynthesis	
				20	Moracin B	C16H14O5	homioisoflavonoid	Flavonoid biosynthesis	
				20	Asperxanthone	C16H14O5	homioisoflavonoid	Flavonoid biosynthesis	
				20	Heliannone C	C16H14O5	homioisoflavonoid	Flavonoid biosynthesis	
				20	Moracin F	C16H14O5	homioisoflavonoid	Flavonoid biosynthesis	
				20	(R)-Pabulenol	C16H14O5	homioisoflavonoid	Flavonoid biosynthesis	
				20	(-)-5,7-Dihydroxy-3-(4-hydroxybenzyl)-4-chromanone	C16H14O5	homioisoflavonoid	Flavonoid biosynthesis	
285	285.083075	0.000151554	BLD	286.091	20	Gummiferol	C16H14O5	homioisoflavonoid	Flavonoid biosynthesis

				20	Brazilin	C16H14O5	homoisoflavonoid	Flavonoid biosynthesis
				20	Carajuron	C16H14O5	homoisoflavonoid	Flavonoid biosynthesis
				20	Peltogynan	C16H14O5	homoisoflavonoid	Flavonoid biosynthesis
				20	3'-Hydroxydihydroformononetin	C16H14O5	homoisoflavonoid	Flavonoid biosynthesis
				20	Vestitone	C16H14O5	homoisoflavonoid	Flavonoid biosynthesis
				20	Dihydrobiochanin A	C16H14O5	homoisoflavonoid	Flavonoid biosynthesis
				20	(-)-Nissolin	C16H14O5	homoisoflavonoid	Flavonoid biosynthesis
				20	Vesticarpan	C16H14O5	homoisoflavonoid	Flavonoid biosynthesis
				20	Kushenin	C16H14O5	homoisoflavonoid	Flavonoid biosynthesis
				20	(6aR,11aR)-3,8-Dihydroxy-9-methoxypterocarpan	C16H14O5	homoisoflavonoid	Flavonoid biosynthesis
				20	Nissicarpan	C16H14O5	homoisoflavonoid	Flavonoid biosynthesis
				20	4-Hydroxymedicarpin	C16H14O5	homoisoflavonoid	Flavonoid biosynthesis
				20	Melilotocarpan B	C16H14O5	homoisoflavonoid	Flavonoid biosynthesis
				20	Desmocarpan	C16H14O5	homoisoflavonoid	Flavonoid biosynthesis
				20	6a-Hydroxymedicarpin	C16H14O5	homoisoflavonoid	Flavonoid biosynthesis
				20	6a-Hydroxyisomedicarpin	C16H14O5	homoisoflavonoid	Flavonoid biosynthesis
				20	Claussequinone	C16H14O5	homoisoflavonoid	Flavonoid biosynthesis
				20	Sepiol	C16H14O5	homoisoflavonoid	Flavonoid biosynthesis
				20	Haginin C	C16H14O5	homoisoflavonoid	Flavonoid biosynthesis
				20	Homobutein	C16H14O5	homoisoflavonoid	Flavonoid biosynthesis
				20	3,2',4'-Trihydroxy-4-methoxychalcone	C16H14O5	homoisoflavonoid	Flavonoid biosynthesis
				20	Sappanchalcone	C16H14O5	homoisoflavonoid	Flavonoid biosynthesis
				20	Calythropsin	C16H14O5	homoisoflavonoid	Flavonoid biosynthesis
				20	Kukulkanin B	C16H14O5	homoisoflavonoid	Flavonoid biosynthesis
				20	2,2',4'-Trihydroxy-6'-methoxychalcone	C16H14O5	homoisoflavonoid	Flavonoid biosynthesis
				20	2',4',6'-Trihydroxy-4-methoxychalcone	C16H14O5	homoisoflavonoid	Flavonoid biosynthesis
				20	Helichrysetin	C16H14O5	homoisoflavonoid	Flavonoid biosynthesis
				20	Neosakuranetin	C16H14O5	homoisoflavonoid	Flavonoid biosynthesis
				20	Licodione 2'-methyl ether	C16H14O5	homoisoflavonoid	Flavonoid biosynthesis
				20	2',6',beta-Trihydroxy-4'-methoxychalcone	C16H14O5	homoisoflavonoid	Flavonoid biosynthesis
				20	2',4',beta-Trihydroxy-6'-methoxychalcone	C16H14O5	homoisoflavonoid	Flavonoid biosynthesis
				20	Licochalcone B	C16H14O5	homoisoflavonoid	Flavonoid biosynthesis
				20	Linderone	C16H14O5	homoisoflavonoid	Flavonoid biosynthesis
				20	2',4'-Dihydroxy-3,4-methylenedioxydihydrochalcone	C16H14O5	homoisoflavonoid	Flavonoid biosynthesis
				20	3'-Formyl-2',4',6'-trihydroxydihydrochalcone	C16H14O5	homoisoflavonoid	Flavonoid biosynthesis
				20	5,6-Dihydroxy-4'-methoxyflavanone	C16H14O5	homoisoflavonoid	Flavonoid biosynthesis
				20	Dihydrochoidinin	C16H14O5	homoisoflavonoid	Flavonoid biosynthesis
				20	Poriol	C16H14O5	homoisoflavonoid	Flavonoid biosynthesis
				20	3-Methylnaringenin	C16H14O5	homoisoflavonoid	Flavonoid biosynthesis
				20	Isosakuranetin	C16H14O5	homoisoflavonoid	Flavonoid biosynthesis
				20	Naringenin 5-methyl ether	C16H14O5	homoisoflavonoid	Flavonoid biosynthesis
				20	Sakuranetin	C16H14O5	homoisoflavonoid	Flavonoid biosynthesis
				20	Dihydroroxylin A	C16H14O5	homoisoflavonoid	Flavonoid biosynthesis

				20	Dihydrowogonin	C16H14O5	homoisoflavonoid	Flavonoid biosynthesis
				20	5,8-Dihydroxy-7-methoxyflavanone	C16H14O5	homoisoflavonoid	Flavonoid biosynthesis
				20	Sainfuran	C16H14O5	homoisoflavonoid	Flavonoid biosynthesis
				20	2',4'-Dihydroxy-5,6-dimethoxy-2-phenylbenzofuran	C16H14O5	homoisoflavonoid	Flavonoid biosynthesis
				20	Pterofuran	C16H14O5	homoisoflavonoid	Flavonoid biosynthesis
				20	Isopteroferan	C16H14O5	homoisoflavonoid	Flavonoid biosynthesis
				20	2,7-Dihydroxy-4'-methoxyisoflavanone	C16H14O5	homoisoflavonoid	Flavonoid biosynthesis
				20	(-)-Vestitone	C16H14O5	homoisoflavonoid	Flavonoid biosynthesis
				20	Moracin A	C16H14O5	homoisoflavonoid	Flavonoid biosynthesis
				20	Quinquangulin	C16H14O5	homoisoflavonoid	Flavonoid biosynthesis
				20	Oxypeucedanin	C16H14O5	homoisoflavonoid	Flavonoid biosynthesis
				20	Phyllodulcin	C16H14O5	homoisoflavonoid	Flavonoid biosynthesis
				20	Moracin B	C16H14O5	homoisoflavonoid	Flavonoid biosynthesis
				20	Asperxanthone	C16H14O5	homoisoflavonoid	Flavonoid biosynthesis
				20	Heliannone C	C16H14O5	homoisoflavonoid	Flavonoid biosynthesis
				20	Moracin F	C16H14O5	homoisoflavonoid	Flavonoid biosynthesis
				20	(R)-Pabulenol	C16H14O5	homoisoflavonoid	Flavonoid biosynthesis
				20	(-)-5,7-Dihydroxy-3-(4-hydroxybenzyl)-4-chromanone	C16H14O5	homoisoflavonoid	Flavonoid biosynthesis
285.082975	0.000188331	CNL	286.0909	20	Gummiferol	C16H14O5	homoisoflavonoid	Flavonoid biosynthesis
				20	Brazilin	C16H14O5	homoisoflavonoid	Flavonoid biosynthesis
				20	Carajuron	C16H14O5	homoisoflavonoid	Flavonoid biosynthesis
				20	Peltogynan	C16H14O5	homoisoflavonoid	Flavonoid biosynthesis
				20	3'-Hydroxydihydroformononetin	C16H14O5	homoisoflavonoid	Flavonoid biosynthesis
				20	Vestitone	C16H14O5	homoisoflavonoid	Flavonoid biosynthesis
				20	Dihydrobiochanin A	C16H14O5	homoisoflavonoid	Flavonoid biosynthesis
				20	(-)-Nissolin	C16H14O5	homoisoflavonoid	Flavonoid biosynthesis
				20	Vesticarpan	C16H14O5	homoisoflavonoid	Flavonoid biosynthesis
				20	Kushenin	C16H14O5	homoisoflavonoid	Flavonoid biosynthesis
				20	(6aR,11aR)-3,8-Dihydroxy-9-methoxypterocarpan	C16H14O5	homoisoflavonoid	Flavonoid biosynthesis
				20	Nissicarpin	C16H14O5	homoisoflavonoid	Flavonoid biosynthesis
				20	4-Hydroxymedicarpin	C16H14O5	homoisoflavonoid	Flavonoid biosynthesis
				20	Melilotocarpin B	C16H14O5	homoisoflavonoid	Flavonoid biosynthesis
				20	Desmocarpan	C16H14O5	homoisoflavonoid	Flavonoid biosynthesis
				20	6a-Hydroxymedicarpin	C16H14O5	homoisoflavonoid	Flavonoid biosynthesis
				20	6a-Hydroxyisomedicarpin	C16H14O5	homoisoflavonoid	Flavonoid biosynthesis
				20	Clausequinone	C16H14O5	homoisoflavonoid	Flavonoid biosynthesis
				20	Sepiol	C16H14O5	homoisoflavonoid	Flavonoid biosynthesis
				20	Haginin C	C16H14O5	homoisoflavonoid	Flavonoid biosynthesis
				20	Homobutein	C16H14O5	homoisoflavonoid	Flavonoid biosynthesis
				20	3,2',4'-Trihydroxy-4-methoxychalcone	C16H14O5	homoisoflavonoid	Flavonoid biosynthesis
				20	Sappanchalcone	C16H14O5	homoisoflavonoid	Flavonoid biosynthesis
				20	Calythropsin	C16H14O5	homoisoflavonoid	Flavonoid biosynthesis

				20	Kukulkanin B	C16H14O5	homioisoflavonoid	Flavonoid biosynthesis
				20	2,2',4'-Trihydroxy-6'-methoxychalcone	C16H14O5	homioisoflavonoid	Flavonoid biosynthesis
				20	2',4',6'-Trihydroxy-4-methoxychalcone	C16H14O5	homioisoflavonoid	Flavonoid biosynthesis
				20	Helichrysetin	C16H14O5	homioisoflavonoid	Flavonoid biosynthesis
				20	Neosakuranetin	C16H14O5	homioisoflavonoid	Flavonoid biosynthesis
				20	Licodione 2'-methyl ether	C16H14O5	homioisoflavonoid	Flavonoid biosynthesis
				20	2',6',beta-Trihydroxy-4'-methoxychalcone	C16H14O5	homioisoflavonoid	Flavonoid biosynthesis
				20	2',4',beta-Trihydroxy-6'-methoxychalcone	C16H14O5	homioisoflavonoid	Flavonoid biosynthesis
				20	Licochalcone B	C16H14O5	homioisoflavonoid	Flavonoid biosynthesis
				20	Linderone	C16H14O5	homioisoflavonoid	Flavonoid biosynthesis
				20	2',4'-Dihydroxy-3,4-methylenedioxydihydrochalcone	C16H14O5	homioisoflavonoid	Flavonoid biosynthesis
				20	3'-Formyl-2',4',6'-trihydroxydihydrochalcone	C16H14O5	homioisoflavonoid	Flavonoid biosynthesis
				20	5,6-Dihydroxy-4'-methoxyflavanone	C16H14O5	homioisoflavonoid	Flavonoid biosynthesis
				20	Dihydroechioidinin	C16H14O5	homioisoflavonoid	Flavonoid biosynthesis
				20	Poriol	C16H14O5	homioisoflavonoid	Flavonoid biosynthesis
				20	3-Methylnaringenin	C16H14O5	homioisoflavonoid	Flavonoid biosynthesis
				20	Isosakuranetin	C16H14O5	homioisoflavonoid	Flavonoid biosynthesis
				20	Naringenin 5-methyl ether	C16H14O5	homioisoflavonoid	Flavonoid biosynthesis
				20	Sakuranetin	C16H14O5	homioisoflavonoid	Flavonoid biosynthesis
				20	Dihydroroxylin A	C16H14O5	homioisoflavonoid	Flavonoid biosynthesis
				20	Dihydrowogonin	C16H14O5	homioisoflavonoid	Flavonoid biosynthesis
				20	5,8-Dihydroxy-7-methoxyflavanone	C16H14O5	homioisoflavonoid	Flavonoid biosynthesis
				20	Sainfuran	C16H14O5	homioisoflavonoid	Flavonoid biosynthesis
				20	2',4'-Dihydroxy-5,6-dimethoxy-2-phenylbenzofuran	C16H14O5	homioisoflavonoid	Flavonoid biosynthesis
				20	Pterofuran	C16H14O5	homioisoflavonoid	Flavonoid biosynthesis
				20	Isopterofuran	C16H14O5	homioisoflavonoid	Flavonoid biosynthesis
				20	2,7-Dihydroxy-4'-methoxyisoflavanone	C16H14O5	homioisoflavonoid	Flavonoid biosynthesis
				20	(-)-Vestitone	C16H14O5	homioisoflavonoid	Flavonoid biosynthesis
				20	Moracin A	C16H14O5	homioisoflavonoid	Flavonoid biosynthesis
				20	Quinquangulin	C16H14O5	homioisoflavonoid	Flavonoid biosynthesis
				20	Oxypeucedanin	C16H14O5	homioisoflavonoid	Flavonoid biosynthesis
				20	Phyllodulcin	C16H14O5	homioisoflavonoid	Flavonoid biosynthesis
				20	Moracin B	C16H14O5	homioisoflavonoid	Flavonoid biosynthesis
				20	Asperxanthone	C16H14O5	homioisoflavonoid	Flavonoid biosynthesis
				20	Heliannone C	C16H14O5	homioisoflavonoid	Flavonoid biosynthesis
				20	Moracin F	C16H14O5	homioisoflavonoid	Flavonoid biosynthesis
				20	(R)-Pabulenol	C16H14O5	homioisoflavonoid	Flavonoid biosynthesis
				20	(-)-5,7-Dihydroxy-3-(4-hydroxybenzyl)-4-chromanone	C16H14O5	homioisoflavonoid	Flavonoid biosynthesis
285.082625	0.000108253	CLD	286.0906	20	Gummiferol	C16H14O5	homioisoflavonoid	Flavonoid biosynthesis
				20	Brazilin	C16H14O5	homioisoflavonoid	Flavonoid biosynthesis
				20	Carajuron	C16H14O5	homioisoflavonoid	Flavonoid biosynthesis
				20	Peltogynan	C16H14O5	homioisoflavonoid	Flavonoid biosynthesis

				20	3'-Hydroxydihydroformononetin	C16H14O5	homioisoflavonoid	Flavonoid biosynthesis
				20	Vestitone	C16H14O5	homioisoflavonoid	Flavonoid biosynthesis
				20	Dihydrobiochanin A	C16H14O5	homioisoflavonoid	Flavonoid biosynthesis
				20	(-)-Nissolin	C16H14O5	homioisoflavonoid	Flavonoid biosynthesis
				20	Vesticarpan	C16H14O5	homioisoflavonoid	Flavonoid biosynthesis
				20	Kushenin	C16H14O5	homioisoflavonoid	Flavonoid biosynthesis
				20	(6aR,11aR)-3,8-Dihydroxy-9-methoxypterocarpan	C16H14O5	homioisoflavonoid	Flavonoid biosynthesis
				20	Nissicarpin	C16H14O5	homioisoflavonoid	Flavonoid biosynthesis
				20	4-Hydroxymedicarpin	C16H14O5	homioisoflavonoid	Flavonoid biosynthesis
				20	Melilotocarpan B	C16H14O5	homioisoflavonoid	Flavonoid biosynthesis
				20	Desmocarpin	C16H14O5	homioisoflavonoid	Flavonoid biosynthesis
				20	6a-Hydroxymedicarpin	C16H14O5	homioisoflavonoid	Flavonoid biosynthesis
				20	6a-Hydroxyisomedicarpin	C16H14O5	homioisoflavonoid	Flavonoid biosynthesis
				20	Claussequinone	C16H14O5	homioisoflavonoid	Flavonoid biosynthesis
				20	Sepiol	C16H14O5	homioisoflavonoid	Flavonoid biosynthesis
				20	Hagin C	C16H14O5	homioisoflavonoid	Flavonoid biosynthesis
				20	Homobutein	C16H14O5	homioisoflavonoid	Flavonoid biosynthesis
				20	3,2',4'-Trihydroxy-4-methoxychalcone	C16H14O5	homioisoflavonoid	Flavonoid biosynthesis
				20	Sappanchalcone	C16H14O5	homioisoflavonoid	Flavonoid biosynthesis
				20	Calythropsin	C16H14O5	homioisoflavonoid	Flavonoid biosynthesis
				20	Kukulkanin B	C16H14O5	homioisoflavonoid	Flavonoid biosynthesis
				20	2,2',4'-Trihydroxy-6'-methoxychalcone	C16H14O5	homioisoflavonoid	Flavonoid biosynthesis
				20	2',4',6'-Trihydroxy-4-methoxychalcone	C16H14O5	homioisoflavonoid	Flavonoid biosynthesis
				20	Helichrysetin	C16H14O5	homioisoflavonoid	Flavonoid biosynthesis
				20	Neosakuranetin	C16H14O5	homioisoflavonoid	Flavonoid biosynthesis
				20	Licodione 2'-methyl ether	C16H14O5	homioisoflavonoid	Flavonoid biosynthesis
				20	2',6',beta-Trihydroxy-4'-methoxychalcone	C16H14O5	homioisoflavonoid	Flavonoid biosynthesis
				20	2',4',beta-Trihydroxy-6'-methoxychalcone	C16H14O5	homioisoflavonoid	Flavonoid biosynthesis
				20	Licochalcone B	C16H14O5	homioisoflavonoid	Flavonoid biosynthesis
				20	Linderone	C16H14O5	homioisoflavonoid	Flavonoid biosynthesis
				20	2',4'-Dihydroxy-3,4-methylenedioxydihydrochalcone	C16H14O5	homioisoflavonoid	Flavonoid biosynthesis
				20	3'-Formyl-2',4',6'-trihydroxydihydrochalcone	C16H14O5	homioisoflavonoid	Flavonoid biosynthesis
				20	5,6-Dihydroxy-4'-methoxyflavanone	C16H14O5	homioisoflavonoid	Flavonoid biosynthesis
				20	Dihydroechioidinin	C16H14O5	homioisoflavonoid	Flavonoid biosynthesis
				20	Poriol	C16H14O5	homioisoflavonoid	Flavonoid biosynthesis
				20	3-Methylnaringenin	C16H14O5	homioisoflavonoid	Flavonoid biosynthesis
				20	Isosakuranetin	C16H14O5	homioisoflavonoid	Flavonoid biosynthesis
				20	Naringenin 5-methyl ether	C16H14O5	homioisoflavonoid	Flavonoid biosynthesis
				20	Sakuranetin	C16H14O5	homioisoflavonoid	Flavonoid biosynthesis
				20	Dihydrooxylin A	C16H14O5	homioisoflavonoid	Flavonoid biosynthesis
				20	Dihydrowogonin	C16H14O5	homioisoflavonoid	Flavonoid biosynthesis
				20	5,8-Dihydroxy-7-methoxyflavanone	C16H14O5	homioisoflavonoid	Flavonoid biosynthesis
				20	Sainfuran	C16H14O5	homioisoflavonoid	Flavonoid biosynthesis

				20	2',4'-Dihydroxy-5,6-dimethoxy-2-phenylbenzofuran	C16H14O5	homoisoflavonoid	Flavonoid biosynthesis
				20	Pterofuran	C16H14O5	homoisoflavonoid	Flavonoid biosynthesis
				20	Isopterofuran	C16H14O5	homoisoflavonoid	Flavonoid biosynthesis
				20	2,7-Dihydroxy-4'-methoxyisoflavanone	C16H14O5	homoisoflavonoid	Flavonoid biosynthesis
				20	(-)-Vestitone	C16H14O5	homoisoflavonoid	Flavonoid biosynthesis
				20	Moracin A	C16H14O5	homoisoflavonoid	Flavonoid biosynthesis
				20	Quinquangulin	C16H14O5	homoisoflavonoid	Flavonoid biosynthesis
				20	Oxypeucedanin	C16H14O5	homoisoflavonoid	Flavonoid biosynthesis
				20	Phyllodulcin	C16H14O5	homoisoflavonoid	Flavonoid biosynthesis
				20	Moracin B	C16H14O5	homoisoflavonoid	Flavonoid biosynthesis
				20	Asperxanthone	C16H14O5	homoisoflavonoid	Flavonoid biosynthesis
				20	Heliannone C	C16H14O5	homoisoflavonoid	Flavonoid biosynthesis
				20	Moracin F	C16H14O5	homoisoflavonoid	Flavonoid biosynthesis
				20	(R)-Pabulenol	C16H14O5	homoisoflavonoid	Flavonoid biosynthesis
				20	(-)-5,7-Dihydroxy-3-(4-hydroxybenzyl)-4-chromanone	C16H14O5	homoisoflavonoid	Flavonoid biosynthesis
285.0404	0.001483661	DNL	286.0484	0	Luteolin	C15H10O6	flavone	Flavonoid biosynthesis
				0	Kaempferol	C15H10O6	flavonol	Flavonoid biosynthesis
				0	Cyanidin	C15H10O6	anthocyanidin	Flavonoid biosynthesis
				0	Fisetin	C15H10O6	flavonol	Flavonoid biosynthesis
				0	Aurantidin	C15H10O6	anthocyanidin	Flavonoid biosynthesis
				0	Baptigenin	C15H10O6	isoflavone	Flavonoid biosynthesis
				0	7,8,2',4'-Tetrahydroxyisoflavone	C15H10O6	isoflavone	Flavonoid biosynthesis
				0	Orobol	C15H10O6	isoflavone	Flavonoid biosynthesis
				0	2'-Hydroxygenistein	C15H10O6	isoflavone	Flavonoid biosynthesis
				0	6-Hydroxygenistein	C15H10O6	isoflavone	Flavonoid biosynthesis
				0	7,3',4',5'-Tetrahydroxyflavone	C15H10O6	isoflavone	Flavonoid biosynthesis
				0	5,7,2',5'-Tetrahydroxyflavone	C15H10O6	isoflavone	Flavonoid biosynthesis
				0	5,7,2',6'-Tetrahydroxyflavone	C15H10O6	isoflavone	Flavonoid biosynthesis
				0	5,7,2',3'-Tetrahydroxyflavone	C15H10O6	isoflavone	Flavonoid biosynthesis
				0	Norartocarpetin	C15H10O6	flavone	Flavonoid biosynthesis
				0	Scutellarein	C15H10O6	flavone	Flavonoid biosynthesis
				0	Isoscutellarein	C15H10O6	flavone	Flavonoid biosynthesis
				0	3,7,8,4'-Tetrahydroxyflavone	C15H10O6	isoflavone	Flavonoid biosynthesis
				0	Datiscetin	C15H10O6	isoflavone	Flavonoid biosynthesis
				0	6-Hydroxygalangin	C15H10O6	flavonol	Flavonoid biosynthesis
				0	8-Hydroxygalangin	C15H10O6	flavonol	Flavonoid biosynthesis
				0	Maritimetin	C15H10O6	phenol	phenyl propanoid biosynthesis
				0	Aureusidin	C15H10O6	aurone	Flavonoid biosynthesis
				0	6-Demethoxycapillarisin	C15H10O6	flavonoid	Flavonoid biosynthesis
285.03645	0.002904845	DLD	286.04445	14	Luteolin	C15H10O6	flavone	Flavonoid biosynthesis
				14	Kaempferol	C15H10O6	flavonol	Flavonoid biosynthesis

					14	Cyanidin	C15H10O6	anthocyanidin	Flavonoid biosynthesis
					14	Fisetin	C15H10O6	flavonol	Flavonoid biosynthesis
					14	Aurantininidin	C15H10O6	anthocyanidin	Flavonoid biosynthesis
					14	Baptigenin	C15H10O6	isoflavone	Flavonoid biosynthesis
					14	7,8,2',4'-Tetrahydroxyisoflavone	C15H10O6	isoflavone	Flavonoid biosynthesis
					14	Orobol	C15H10O	isoflavone	Flavonoid biosynthesis
					14	2'-Hydroxygenistein	C15H10O6	isoflavone	Flavonoid biosynthesis
					14	6-Hydroxygenistein	C15H10O6	isoflavone	Flavonoid biosynthesis
					14	7,3',4',5'-Tetrahydroxyflavone	C15H10O6	isoflavone	Flavonoid biosynthesis
					14	5,7,2',5'-Tetrahydroxyflavone	C15H10O6	isoflavone	Flavonoid biosynthesis
					14	5,7,2',6'-Tetrahydroxyflavone	C15H10O6	isoflavone	Flavonoid biosynthesis
					14	5,7,2',3'-Tetrahydroxyflavone	C15H10O6	isoflavone	Flavonoid biosynthesis
					14	Norartocarpetin	C15H10O6	isoflavone	Flavonoid biosynthesis
					14	Scutellarein	C15H10O6	flavone	Flavonoid biosynthesis
					14	Isoscutellarein	C15H10O6	flavone	Flavonoid biosynthesis
					14	3,7,8,4'-Tetrahydroxyflavone	C15H10O6	isoflavone	Flavonoid biosynthesis
					14	Datisctin	C15H10O6	isoflavone	Flavonoid biosynthesis
					14	6-Hydroxygalangin	C15H10O6	flavonol	Flavonoid biosynthesis
					14	8-Hydroxygalangin	C15H10O6	flavonol	Flavonoid biosynthesis
					14	Maritimetin	C15H10O6	phenol	phenylpropanoid biosynthesis
					14	Aureusidin	C15H10O6	aurone	Flavonoid biosynthesis
					14	6-Demethoxycapillarisin	C15H10O6	flavonoid	Flavonoid biosynthesis
489	489.160925	0.00032476	ANL	490.168925	6	Demethylalangiside	C24H29NO10	alkaloid	Isoquinoline alkaloid biosynthesis
					6	Demethylisoalangiside	C24H29NO10	alkaloid	Isoquinoline alkaloid biosynthesis
	489.16055	0.000246221	ALD	490.16855	6	Demethylalangiside	C24H29NO10	alkaloid	Isoquinoline alkaloid biosynthesis
					6	Demethylisoalangiside	C24H29NO10	alkaloid	Isoquinoline alkaloid biosynthesis
	489.16125	0.000219374	BNL	490.16925	6	Demethylalangiside	C24H29NO10	alkaloid	Isoquinoline alkaloid biosynthesis
					6	Demethylisoalangiside	C24H29NO10	alkaloid	Isoquinoline alkaloid biosynthesis
	489.1615	0.000190394	BLD	490.1695	6	Demethylalangiside	C24H29NO10	alkaloid	Isoquinoline alkaloid biosynthesis
					6	Demethylisoalangiside	C24H29NO10	alkaloid	Isoquinoline alkaloid biosynthesis
	489.161425	489.161425	CNL	490.169425	6	Demethylalangiside	C24H29NO10	alkaloid	Isoquinoline alkaloid biosynthesis
				6	Demethylisoalangiside	C24H29NO10	alkaloid	Isoquinoline alkaloid biosynthesis	

	489.16145	7.5E-05	CLD	490.16945	6	Demethylalangiside	C24H29NO10	alkaloid	Isoquinoline alkaloid biosynthesis
					6	Demethylisoalangiside	C24H29NO10	alkaloid	Isoquinoline alkaloid biosynthesis
	489.097525	0.004257695	DNL	490.105525	12	Cyanidin 3-(6"-acetyl-galactoside)	C23H23O12	anthocyanidin	Flavonoid biosynthesis
					12	Cyanidin 3-(4-acetylglucoside)	C23H23O12	anthocyanidin	Flavonoid biosynthesis
	489.111725	0.013123518	DLD	490.119725	12	Cyanidin 3-(6"-acetyl-galactoside)	C23H23O12	anthocyanidin	Flavonoid biosynthesis
					12	Cyanidin 3-(4-acetylglucoside)	C23H23O12	anthocyanidin	Flavonoid biosynthesis
315	315.01295	0.000225	ANL	316.02095		N/A			
	315.0126	0	ALD	316.02095		N/A			
	314.935075	0.022553641	BNL	315.943075		N/A			
	314.9869	0.043206756	BLD	315.943075		N/A			
	314.93505	0.022618093	CNL	315.94305		N/A			
	314.90865	7.5E-05	CLD	315.91665		N/A			
	315.054375	0.003970103	DNL	316.062375	2	Lettowianthine	C19H11NO4		
314.99885	0.036619539	DLD	316.00685		N/A				
307	307.125825	0.000408312	ANL	308.133825		N/A			
	307.1259	0.000136931	ALD	308.1339		N/A			
	307.1267	0.000127475	BNL	308.1347		N/A			
	307.126775	0.000143069	BLD	308.134775		N/A			
	307.126775	0.000178098	CNL	308.134775		N/A			
	307.12615	0.000303109	CLD						
	307.072375	0.000482668	DNL	308.080375	32	glutathione	C10H16N3O6S1		glutathione-ascorbate cycle
					32	Allamandin	C15H16O7	isoprenoid	Isoprenoid biosynthesis
					32	4R,5R,6S-Trihydroxy-2-hydroxymethyl-2-cyclohexen-1-one 6-(2-hydroxy-6-methylbenzoate)	C15H16O7	benzenoid	
	307.0721	0.000764853	DLD	308.0801	32	glutathione	C10H16N3O6S1		
				32	Allamandin	C15H16O7	isoprenoid	Isoprenoid biosynthesis	
				32	4R,5R,6S-Trihydroxy-2-hydroxymethyl-2-cyclohexen-1-one 6-(2-hydroxy-6-methylbenzoate)	C15H16O7			
301	301.078625	0.000408312	ANL	302.086625	22	Haematoxylin	C16H14O6	phenol	
					22	Hesperetin	C16H14O6	flavonone	flavonoid biosynthesis
					22	4,2',4',6'-Tetrahydroxy-3-methoxychalcone	C16H14O6	phenylpropanoid	phenylpropanoid biosynthesis

				22	3,4,3',4'-Tetrahydroxy-2-methoxychalcone	C ₁₆ H ₁₄ O ₆	phenylpropanoid	phenylpropanoid biosynthesis
				22	Homoeriodictyol	C ₁₆ H ₁₄ O ₆	flavonone	flavonoid biosynthesis
				22	2,5,7-trihydroxy-4'-methoxyisoflavanone	C ₁₆ H ₁₃ O ₆	isoflavone	isoflavonoid biosynthesis
				22	carthamidin-7-methyl ether	C ₁₆ H ₁₄ O ₆	flavonone	flavonoid biosynthesis
				22	<i>cis</i> -(-)-7,2'-dihydroxy-4',5'-methylenedioxyisoflavanol	C ₁₆ H ₁₄ O ₆	sioflavonol	pisatin biosynthesis/pterocarpan biosynthesis/maackiain biosynthesis
301.07655	0.000136931	ALD	302.08455	14	4,2',4',6'-Tetrahydroxy-3-methoxychalcone	C ₁₆ H ₁₄ O ₆	flavonone	flavonoid biosynthesis
				14	3,4,3',4'-Tetrahydroxy-2-methoxychalcone	C ₁₆ H ₁₄ O ₆	phenylpropanoid	phenylpropanoid biosynthesis
				14	Haematoxylin	C ₁₆ H ₁₄ O ₆	phenylpropanoid	phenylpropanoid biosynthesis
				14	Hesperetin	C ₁₆ H ₁₄ O ₆	flavonone	flavonoid biosynthesis
				14	Homoeriodictyol	C ₁₆ H ₁₄ O ₆	isoflavone	isoflavonoid biosynthesis
				14	2,5,7-trihydroxy-4'-methoxyisoflavanone	C ₁₆ H ₁₃ O ₆	flavonone	flavonoid biosynthesis
				14	carthamidin-7-methyl ether	C ₁₆ H ₁₄ O ₆	flavonone	flavonoid biosynthesis
				14	<i>cis</i> -(-)-7,2'-dihydroxy-4',5'-methylenedioxyisoflavanol	C ₁₆ H ₁₄ O ₆	sioflavonol	pisatin biosynthesis/pterocarpan biosynthesis/maackiain biosynthesis
301.0784	0.000127475	BNL	302.0864	22	4,2',4',6'-Tetrahydroxy-3-methoxychalcone	C ₁₆ H ₁₄ O ₆	flavonone	flavonoid biosynthesis
				22	3,4,3',4'-Tetrahydroxy-2-methoxychalcone	C ₁₆ H ₁₄ O ₆	phenylpropanoid	phenylpropanoid biosynthesis
				22	Haematoxylin	C ₁₆ H ₁₄ O ₆	phenylpropanoid	phenylpropanoid biosynthesis
				22	Hesperetin	C ₁₆ H ₁₄ O ₆	flavonone	flavonoid biosynthesis
				22	Homoeriodictyol	C ₁₆ H ₁₄ O ₆	isoflavone	isoflavonoid biosynthesis
				22	2,5,7-trihydroxy-4'-methoxyisoflavanone	C ₁₆ H ₁₃ O ₆	flavonone	flavonoid biosynthesis
				22	carthamidin-7-methyl ether	C ₁₆ H ₁₄ O ₆	flavonone	flavonoid biosynthesis
				22	<i>cis</i> -(-)-7,2'-dihydroxy-4',5'-methylenedioxyisoflavanol	C ₁₆ H ₁₄ O ₆	sioflavonol	pisatin biosynthesis/pterocarpan biosynthesis/maackiain biosynthesis
301.0792	0.000143069	BLD	302.0872	24	4,2',4',6'-Tetrahydroxy-3-methoxychalcone	C ₁₆ H ₁₄ O ₆	flavonone	flavonoid biosynthesis
				24	3,4,3',4'-Tetrahydroxy-2-methoxychalcone	C ₁₆ H ₁₄ O ₆	phenylpropanoid	phenylpropanoid biosynthesis

				24	Haematoxylin	C16H14O6	phenylpropanoid	phenylpropanoid biosynthesis
				24	Hesperetin	C16H14O6	flavonone	flavonoid biosynthesis
				24	Homoeriodictyol	C16H14O6	isoflavone	isoflavonoid biosynthesis
				24	2,5,7-trihydroxy-4'-methoxyisoflavanone	C16H13O6	flavonone	flavonoid biosynthesis
				24	carthamidin-7-methyl ether	C ₁₆ H ₁₄ O ₆	flavonone	flavonoid biosynthesis
				24	<i>cis</i> -(-)-7,2'-dihydroxy-4',5'-methylenedioxyisoflavanol	C ₁₆ H ₁₄ O ₆	sioflavonol	pisatin biosynthesis/pterocarpan biosynthesis/maackiain biosynthesis
301.076375	0.000178098	CNL	302.084375	15	4,2',4',6'-Tetrahydroxy-3-methoxychalcone	C16H14O6	flavonone	flavonoid biosynthesis
				15	3,4,3',4'-Tetrahydroxy-2-methoxychalcone	C16H14O6	phenylpropanoid	phenylpropanoid biosynthesis
				15	Haematoxylin	C16H14O6	phenylpropanoid	phenylpropanoid biosynthesis
				15	Hesperetin	C16H14O6	flavonone	flavonoid biosynthesis
				15	Homoeriodictyol	C16H14O6	isoflavone	isoflavonoid biosynthesis
				15	2,5,7-trihydroxy-4'-methoxyisoflavanone	C16H13O6	flavonone	flavonoid biosynthesis
				15	carthamidin-7-methyl ether	C ₁₆ H ₁₄ O ₆	flavonone	flavonoid biosynthesis
				15	<i>cis</i> -(-)-7,2'-dihydroxy-4',5'-methylenedioxyisoflavanol	C ₁₆ H ₁₄ O ₆	sioflavonol	pisatin biosynthesis/pterocarpan biosynthesis/maackiain biosynthesis
301.078075	0.000303109	CLD		20	Haematoxylin	C16H14O6	phenylpropanoid	phenylpropanoid biosynthesis
				20	Hesperetin	C16H14O6	flavonone	flavonoid biosynthesis
				20	4,2',4',6'-Tetrahydroxy-3-methoxychalcone	C16H14O6	flavonone	flavonoid biosynthesis
				20	3,4,3',4'-Tetrahydroxy-2-methoxychalcone	C16H14O6	phenylpropanoid	phenylpropanoid biosynthesis
				20	Homoeriodictyol	C16H14O6	isoflavone	isoflavonoid biosynthesis
				20	2,5,7-trihydroxy-4'-methoxyisoflavanone	C16H13O6	flavonone	flavonoid biosynthesis
				20	carthamidin-7-methyl ether	C ₁₆ H ₁₄ O ₆	flavonone	flavonoid biosynthesis
				20	<i>cis</i> -(-)-7,2'-dihydroxy-4',5'-methylenedioxyisoflavanol	C ₁₆ H ₁₄ O ₆	sioflavonol	pisatin biosynthesis/pterocarpan biosynthesis/maackiain biosynthesis
301.025275	0.000482668	DNL	302.033275	33	Quercetin	C15H10O7	flavonol	flavonoid biosynthesis
				33	Morin	C15H10O7	flavonol	flavonoid biosynthesis
				33	Delphinidin	C15H10O7	anthocyanidin	flavonoid biosynthesis

				33	HIERACIN	C15H10O7	glycoside	flavonoid biosynthesis
				33	Isoetin	C15H10O7	flavone	flavonoid biosynthesis
				33	6-Hydroxyluteolin	C15H10O7	flavone	flavonoid biosynthesis
				33	Hypolaetin	C15H10O7	flavone	flavonoid biosynthesis
				33	Robinetin	C15H10O7	flavone	flavonoid biosynthesis
				33	6-Hydroxykaempferol	C15H10O7	glucoside	flavonoid biosynthesis
				33	Herbacetin	C15H10O7	flavonol	flavonoid biosynthesis
				33	Bracteatin	C15H10O7	glucoside	flavonoid biosynthesis
				33	2'-Hydroxypseudobaptigenin	C15H10O7	isoflavone	flavonoid biosynthesis
301.025025	0.000764853	DLD	302.033025	34	Quercetin	C15H10O7	flavonol	flavonoid biosynthesis
				34	Morin	C15H10O7	flavonol	flavonoid biosynthesis
				34	Delphinidin	C15H10O7	anthocyanidin	flavonoid biosynthesis
				34	HIERACIN	C15H10O7	glycoside	flavonoid biosynthesis
				34	Isoetin	C15H10O7	flavone	flavonoid biosynthesis
				34	6-Hydroxyluteolin	C15H10O7	flavone	flavonoid biosynthesis
				34	Hypolaetin	C15H10O7	flavone	flavonoid biosynthesis
				34	Robinetin	C15H10O7	flavone	flavonoid biosynthesis
				34	6-Hydroxykaempferol	C15H10O7	glucoside	flavonoid biosynthesis
				34	Herbacetin	C15H10O7	flavonol	flavonoid biosynthesis
				34	Bracteatin	C15H10O7	glucoside	flavonoid biosynthesis
				34	2'-Hydroxypseudobaptigenin	C15H10O7	isoflavone	flavonoid biosynthesis
365.103325	6.49519E-05	ANL	366.111325	0	Derrubone	C21H18O6	isoflavone	flavonoid biosynthesis
				0	Glycyrol	C21H18O6		
				0	Glycyrrhizaisoflavone B	C21H18O6	isoflavone	flavonoid biosynthesis
				0	Wampetin	C21H18O6		
				0	7(8)-dihydrojusticidin B	C21H18O6	phenylpropanoid	diphyllin biosynthesis/justicidin B biosynthesis
365.1031	0.000358818	ALD	366.1111	0	Derrubone	C21H18O6	N/A	N/A
				0	Glycyrol	C21H18O6	N/A	N/A
				0	Glycyrrhizaisoflavone B	C21H18O6	N/A	N/A
				0	Wampetin	C21H18O6	N/A	N/A
				0	7(8)-dihydrojusticidin B	C21H18O6	N/A	N/A
365.103975	0.000296595	BNL	366.111975	0	Derrubone	C21H18O6	N/A	N/A
				0	Glycyrol	C21H18O6	N/A	N/A
				0	Glycyrrhizaisoflavone B	C21H18O6	N/A	N/A
				0	Wampetin	C21H18O6	N/A	N/A
				0	7(8)-dihydrojusticidin B	C21H18O6	N/A	N/A
365.103775	0.000387903	BLD	366.111775	0	Derrubone	C21H18O6	N/A	N/A

				0	Glycyrol	C21H18O6	N/A	N/A
				0	Glycyrrhizaisoflavone B	C21H18O6	N/A	N/A
				0	Wampetin	C21H18O6	N/A	N/A
				0	7(8)-dihydrojusticidin B	C21H18O6	N/A	N/A
365.103475	0.000389511	CNL	366.111475	0	Derrubone	C21H18O6	N/A	N/A
				0	Glycyrol	C21H18O6	N/A	N/A
				0	Glycyrrhizaisoflavone B	C21H18O6	N/A	N/A
				0	Wampetin	C21H18O6	N/A	N/A
				0	7(8)-dihydrojusticidin B	C21H18O6	N/A	N/A
365.103375	0.000134048	CLD	366.111375	0	Derrubone	C21H18O6	N/A	N/A
				0	Glycyrol	C21H18O6	N/A	N/A
				0	Glycyrrhizaisoflavone B	C21H18O6	N/A	N/A
				0	Wampetin	C21H18O6	N/A	N/A
				0	7(8)-dihydrojusticidin B	C21H18O6	N/A	N/A
365.054	0.006458328	DNL	366.062	9	1-(5'-Phosphoribosyl)-5-formamido-4-imidazolecarboxamide	C10H15N4O9P	N/A	N/A
				28	Salicin 6-phosphate	C13H19O10P	glycoside	Glycolysis / Gluconeogenesis/Phosphotransferase system (PTS)
				34	Arnottin II	C20H14O7	benzofuran	
365.06025	0.009780433	DLD	366.06825	27	1-(5'-Phosphoribosyl)-5-formamido-4-imidazolecarboxamide	C10H15N4O9P		Biosynthesis of plant secondary metabolites
				11	Salicin 6-phosphate	C13H19O10P	glycoside	Glycolysis / Gluconeogenesis/Phosphotransferase system (PTS)
				17	Arnottin II	C20H14O7		
286.086225		ANL	287.094225	24	Volkenin	C12H17NO7	glucoside	N/A
				24	Tetraphyllin B	C12H17NO7	glycosyl	N/A
286.08645		ALD	287.09445	24	Volkenin	C12H17NO7	glucoside	N/A
				24	Tetraphyllin B	C12H17NO7	glycosyl	N/A
286.08725		BNL	287.09525	20	Volkenin	C12H17NO7	glucoside	N/A
				20	Tetraphyllin B	C12H17NO7	glycosyl	N/A
				39	Rutaecarpine	C18H13N3O	glucoside	N/A
286.087625		BLD	287.095625	19	Volkenin	C12H17NO7	glycosyl	N/A
				19	Tetraphyllin B	C12H17NO7	glucoside	N/A
				38	Rutaecarpine	C18H13N3O	glycosyl	N/A
286.08605		CNL	287.09405	25	Volkenin	C12H17NO7	glucoside	N/A
				25	Tetraphyllin B	C12H17NO7	glycosyl	N/A

	286.0862		CLD	287.0942	24	Volkenin	C12H17NO7	glucoside	N/A
					24	Tetraphyllin B	C12H17NO7	glycosyl	N/A
	286.0347		DNL	287.0427		N/A			
	286.035225		DLD	287.043225		N/A			
341	341.154625		ANL	342.1626		(±)-pavine	C20H24N1O4	alkaloid	N/A
						magnoflorine	C20H24N1O4	alkaloid	N/A
	341.15575		ALD	342.16375		(±)-pavine	C20H24N1O4	alkaloid	N/A
						magnoflorine	C20H24N1O4	alkaloid	N/A
	341.155725		BNL	342.1637		(±)-pavine	C20H24N1O4	alkaloid	N/A
						magnoflorine	C20H24N1O4	alkaloid	N/A
	341.15555		BLD	342.1635		(±)-pavine	C20H24N1O4	alkaloid	N/A
						magnoflorine	C20H24N1O4	alkaloid	N/A
	341.15855		CNL	342.1665		(±)-pavine	C20H24N1O4	alkaloid	N/A
						magnoflorine	C20H24N1O4	alkaloid	N/A
	341.15385		CLD	342.1618		(±)-pavine	C20H24N1O4	alkaloid	N/A
						magnoflorine	C20H24N1O4	alkaloid	N/A
	341.096775		DNL	342.1047	26	Caffeic acid 3-glucoside	C15H18O9	glucoside	
					26	1-Caffeoyl-beta-D-glucose	C15H18O9	glucoside	
					26	Glucocaffeic acid	C15H18O9	carbonyl	
					18	Dulxanthone A	C19H18O6	carbonyl	
					18	Dulxanthone D	C19H18O6	carbonyl	
					35	Sucrose	C12H22O11	carbohydrate	sucrose metabolism
					35	Maltose	C12H22O11	carbohydrate	maltose degradation
					35	Epimelibiose	C12H22O11	galactose	Galactose metabolism
					35	Galactinol (1-α-d-galactosyl-myo-inositol)	C12H22O11	glycosyltransferases	Galactose metabolism
					35	Melibiose	C12H22O11		melibiose metabolism
					35	Cellobiose	C12H22O11		Starch and sucrose metabolism/Phosphotransferase system (PTS)
					35	Laminaribiose	C12H22O11	glucosyl	
					35	Nigerose (Sakebiose)	C12H22O11	glucosyl	
					35	Gentiobiose	C12H22O11	carbohydrate	
					35	Sophorose	C12H22O11	glucosyl	
					35	Mannobiose	C12H22O11	carbohydrate	
				35	Glucinol	C12H22O11			
				35	D-(+)-Cellobiose	C12H22O11	glucosyl	Starch and sucrose metabolism/Phosphotransferase system (PTS)	
				35	Isomaltose	C12H22O11	carbohydrate		
				35	Levanbiose	C12H22O11			
				28	Caffeic acid 3-glucoside	C15H18O9			

	341.0976		DLD	342.1056	28	1-Caffeoyl-beta-D-glucose	C15H18O9		
					28	Glucocaffeic acid	C15H18O9		
					16	Dulxanthone A	C19H18O6		
					16	Dulxanthone D	C19H18O6		
					33	Sucrose	C12H22O11		
					33	Maltose	C12H22O11		
					33	Epimelibiose	C12H22O11		
					33	Galactinol (1- α -d-galactosyl-myo-inositol)	C12H22O11		
					33	Melibiose	C12H22O11		
					33	Cellobiose	C12H22O11		
					33	Laminaribiose	C12H22O11		
					33	Nigerose (Sakebiose)	C12H22O11		
					33	Gentiobiose	C12H22O11		
					33	Sophorose	C12H22O11		
					33	Mannobiose	C12H22O11		
					33	Glucinol	C12H22O11		
					33	D-(+)-Cellobiose	C12H22O11		
					33	Isomaltose	C12H22O11		
					33	Levanbiose	C12H22O11		
284.2	284.074475		ANL	285.0824	11	Buchananine	C12H15NO7	alkaloid	
	284.0736		ALD	285.0816	13	Buchananine	C12H15NO7	alkaloid	
	284.07765		BNL	285.0856	0	Buchananine	C12H15NO7	alkaloid	
	284.07445		BLD	285.0824	11	Buchananine	C12H15NO7	alkaloid	
	284.07355		CNL	285.0815	14	Buchananine	C12H15NO7	alkaloid	
	284.0748		CLD	285.0828	9	Buchananine	C12H15NO7	alkaloid	
	284.022425		DNL	285.0304		N/A			
	284.022775		DLD	285.0307		N/A			
269.08605			ANL	270.094	15	2'-O-methylisiquiritigenin	C16H14O4	chalcone	flavonoid biosynthesis
					15	(-)-Medicarpin	C16H14O4	flavonoid	Isoflavonoid biosynthesis
					15	Isomedicarpin	C16H14O4	flavonoid	Isoflavonoid biosynthesis
					15	Isoliquiritigenin 2'-methy ether	C16H14O4	chalcone	flavonoid biosynthesis
					15	Isoliquiritigenin 4'-methyl ether	C16H14O4	chalcone	flavonoid biosynthesis
					15	Strobopinin	C16H14O4	flavonone	flavonoid biosynthesis
					15	Vignafuran	C16H14O4	flavonoid	Isoflavonoid biosynthesis
	269.084425		ALD	270.0924	9	2'-O-methylisiquiritigenin	C16H14O4		
					9	(-)-Medicarpin	C16H14O4		
					9	Isomedicarpin	C16H14O4		
				9	Isoliquiritigenin 2'-methy ether	C16H14O4			
				9	Isoliquiritigenin 4'-methyl ether	C16H14O4			

269				9	Strobopinin	C16H14O4		
				9	Vignafuran	C16H14O4		
	269.086375	BNL	270.0943	16	2'-O-methylisoliquiritigenin	C16H14O4		
				16	(-)-Medicarpin	C16H14O4		
				16	Isomedicarpin	C16H14O4		
				16	Isoliquiritigenin 2'-methy ether	C16H14O4		
				16	Isoliquiritigenin 4'-methyl ether	C16H14O4		
				16	Strobopinin	C16H14O4		
				16	Vignafuran	C16H14O4		
	269.0894	BLD	270.0974	16	2'-O-methylisoliquiritigenin	C16H14O4		
	269.07985	CNL	270.0878	7	2'-O-methylisoliquiritigenin	C16H14O4		
				7	(-)-Medicarpin	C16H14O4		
				7	Isomedicarpin	C16H14O4		
				7	Isoliquiritigenin 2'-methy ether	C16H14O4		
				7	Isoliquiritigenin 4'-methyl ether	C16H14O4		
				7	Strobopinin	C16H14O4		
				7	Vignafuran	C16H14O4		
	269.087925	CLD	270.0959	22	2'-O-methylisoliquiritigenin	C16H14O4		
				22	(-)-Medicarpin	C16H14O4		
				22	Isomedicarpin	C16H14O4		
				22	Isoliquiritigenin 2'-methy ether	C16H14O4		
				22	Isoliquiritigenin 4'-methyl ether	C16H14O4		
				22	Strobopinin	C16H14O4		
				22	Vignafuran	C16H14O4		
	269.035625	DNL	270.0436	36	7,8,4'-trihydroxyflavone	C15H10O5	glucoside	flavonoid biosynthesis
				36	Pelargonidin	C15H10O5	anthocyanidin	flavonoid biosynthesis
				36	Apigenin	C15H10O5	flavone	flavonoid biosynthesis
				36	Genistein	C15H10O5	isoflavone	flavonoid biosynthesis
				36	Emodin	C15H10O5	hydroxyanthraquinone	
				36	2-Hydroxychrysophanol	C15H10O5	hydroxyanthraquinone	
				36	Baicalein	C15H10O5	flavone	flavonoid biosynthesis
				36	Galangin	C15H10O5	flavonol	flavonoid biosynthesis
				36	3'-Hydroxydaidzein	C15H10O5	isoflavone	flavonoid biosynthesis
				36	2'-Hydroxydaidzein	C15H10O5	isoflavone	flavonoid biosynthesis
				36	Demethyltaxasin	C15H10O5	flavonoid	flavonoid biosynthesis
				36	Norwogonin	C15H10O5	flavone	flavonoid biosynthesis
				36	Resokaempferol	C15H10O5	flavonoid	flavonoid biosynthesis
				36	Sulfuretin	C15H10O5	flavonoid	flavonoid biosynthesis
				36	Lucidin	C15H10O5	Anthraquinone	
				36	Morindone	C15H10O5	Anthraquinone	
				36	Purpurin 1-methyl ether	C15H10O5	quinone	
				36	Islandicin	C15H10O5	Anthraquinone	
269.0359	DLD	270.0439	35	7,8,4'-trihydroxyflavone	C15H10O5			

				35	Pelargonidin	C15H10O5		
				35	Apigenin	C15H10O5		
				35	Genistein	C15H10O5		
				35	Emodin	C15H10O5		
				35	2-Hydroxychrysophanol	C15H10O5		
				35	Baicalin	C15H10O5		
				35	Galangin	C15H10O5		
				35	3'-Hyoxydaidzein	C15H10O5		
				35	2'-Hyoxydaidzein	C15H10O5		
				35	Demethyltaxasin	C15H10O5		
				35	Norwogonin	C15H10O5		
				35	Resokaempferol	C15H10O5		
				35	Sulfuretin	C15H10O5		
				35	Lucidin	C15H10O5		
				35	Morindone	C15H10O5		
				35	Purpurin 1-methyl ether	C15H10O5		
				35	Islandicin	C15H10O5		
385	385.19665	ANL	386.2046		N/A			
	385.195575	ALD	386.2035		N/A			
	385.19725	BNL	386.2052		N/A			
	385.196625	BLD	386.2046		N/A			
	385.196625	CNL	386.2046		N/A			
	385.19495	CLD	386.2029		N/A			
	385.131225	DNL	386.1392	4	Pteryxin	C21H22O7	Phenylpropanoid	Phenylpropanoid biosynthesis
				4	Isosamidin	C21H22O7	Phenylpropanoid	Phenylpropanoid biosynthesis
				4	Peucenidin	C21H22O7	Phenylpropanoid	Phenylpropanoid biosynthesis
				4	Samidin	C21H22O7	Phenylpropanoid	Phenylpropanoid biosynthesis
	385.131025	DLD	386.139	4	Pteryxin	C21H22O7	Phenylpropanoid	Phenylpropanoid biosynthesis
				4	Isosamidin	C21H22O7	Phenylpropanoid	Phenylpropanoid biosynthesis
				4	Peucenidin	C21H22O7	Phenylpropanoid	Phenylpropanoid biosynthesis
			4	Samidin	C21H22O7	Phenylpropanoid	Phenylpropanoid biosynthesis	
463	463.141675	ANL	464.1496	36	Hesperetin 7-O-glucoside	C22H24O11	flavonoid	flavonoid biosynthesis
				36	Hesperetin 5-O-glucoside	C22H24O11	flavonoid	flavonoid biosynthesis
	463.142525	ALD	464.1505	22	p-nitrophenyl-β-D-cellobioside	C18H25N1O13	glycolase	
				22	Diffutin	C23H28O10	flavan	flavonoid biosynthesis

				22	Enhydrin	C23H28O10	Sesquiterpenoids	Sesquiterpenoid biosynthesis
				22	Glaucolide A	C23H28O10	Sesquiterpenoids	Sesquiterpenoid biosynthesis
463.143575	BNL	464.1515		20	p-nitrophenyl- β -D-cellobioside	C18H25N1O13		
				20	Diffutin	C23H28O10		
				20	Enhydrin	C23H28O10		
				20	Glaucolide A	C23H28O10		
463.14355	BLD	464.1515		20	p-nitrophenyl- β -D-cellobioside	C18H25N1O13		
				20	Diffutin	C23H28O10		
				20	Enhydrin	C23H28O10		
				20	Glaucolide A	C23H28O10		
463.141725	CNL	464.1497		24	p-nitrophenyl- β -D-cellobioside	C18H25N1O13		
				24	Diffutin	C23H28O10		
				24	Enhydrin	C23H28O10		
				24	Glaucolide A	C23H28O10		
463.141775	CLD	464.1497		24	p-nitrophenyl- β -D-cellobioside	C18H25N1O13		
				24	Diffutin	C23H28O10		
				24	Enhydrin	C23H28O10		
				24	Glaucolide A	C23H28O10		
463.0728	DNL	464.0808		33	Quercimeritrin	C21H20O12	flavonoid	flavonoid biosynthesis
				33	Myricitrin	C21H20O12	flavonoid	flavonoid biosynthesis
				33	Gossypetin 8-rhamnoside	C21H20O12	flavonoid	flavonoid biosynthesis
				33	Quercetin 3-O-glucoside	C21H20O12	flavone	flavone/flavonol biosynthesis
				33	Delphinidin 3-O-glucoside	C21H20O12	anthocyanin	flavonoid biosynthesis
				33	Quercetin 3- β -D-glucoside	C21H20O12	flavonoid	flavonoid biosynthesis
				33	Quercetin 3-galactoside	C21H20O12	flavonoid	flavonoid biosynthesis
				33	Quercetin 4'-glucoside	C21H20O12	flavonoid	flavonoid biosynthesis
				33	quercetin 7-O-glucoside	C21H20O12	flavonoid	flavonoid biosynthesis
463.071675	DLD	464.0796		35	quercetin 7-O-glucoside	C21H20O12	flavonoid	flavonoid biosynthesis
				35	Quercimeritrin	C21H20O12		
				35	Myricitrin	C21H20O12		
				35	Gossypetin 8-rhamnoside	C21H20O12		
				35	Quercetin 3-O-glucoside	C21H20O12		
				35	Delphinidin 3-O-glucoside	C21H20O12		
				35	Quercetin 3- β -D-glucoside	C21H20O12		
				35	Quercetin 3-galactoside	C21H20O12		
				35	Quercetin 4'-glucoside	C21H20O12		

Table A 3.2: Discriminant mass bins and their associated detected and accurate masses. The putatively identified compounds, their chemical groups, and the associated pathways are displayed. An error in parts per million is included to show the putative compounds' variation from the detected mass (aqueous layer analyzed in positive ESI mode).

Bin	Treatment	Detected mass	Adduct	Accurate mass	Δ ppm	Compound	Chemical formula	Chemical Group	Chemical Pathway	
195	ANL	195.0851	H	196.0931	6	QUEBRACHITOL	C7H14O6	cyclitol	N/A	
					6	D-Glucoside	C7H14O6	glycoside	N/A	
	ALD	195.0851			6	3-O-Methyl-myo-inositol	C7H14O6	inositol	Inositol phosphate metabolism	
					6	1-O-Methyl-myo-inositol	C7H14O6	inositol	Inositol phosphate metabolism	
	BNL	195.0851			6	D-4-O-Methyl-myo-inositol	C7H14O6	inositol	Inositol phosphate metabolism	
					6	4-O-Methyl-myo-inositol	C7H14O6	inositol	Inositol phosphate metabolism	
					6	Sequoyitol	C7H14O6	cyclitol	N/A	
					6	D-Pinitol	C7H14O6	cyclitol	N/A	
					6	L-Pinitol	C7H14O6	cyclitol	N/A	
				Na	218.0749		N/A			
				K	234.1834		N/A			
	BLD	195.0851								
				H	196.0982	19	QUEBRACHITOL	C7H14O6	cyclitol	N/A
	CNL	195.0851				19	D-Glucoside	C7H14O6	glycoside	N/A
						19	3-O-Methyl-myo-inositol	C7H14O6	inositol	Inositol phosphate metabolism
	CLD	195.0851				19	1-O-Methyl-myo-inositol	C7H14O6	inositol	Inositol phosphate metabolism
						19	D-4-O-Methyl-myo-inositol	C7H14O6	inositol	Inositol phosphate metabolism
						19	4-O-Methyl-myo-inositol	C7H14O6	inositol	Inositol phosphate metabolism
						19	Sequoyitol	C7H14O6	cyclitol	N/A
						19	D-Pinitol	C7H14O6	cyclitol	N/A
					19	L-Pinitol	C7H14O6	cyclitol	N/A	
					13	Caffeine	C8H10N4O2			
			Na	218.08		N/A				

	DNL	195.0902								
	DLD	195.0902	K	234.1885		N/A				
535	ANL	535.0832	H	536.0912		N/A				
	ALD	535.0832	Na	558.073		N/A				
	BNL	535.0832	K	574.1815		N/A				
	BLD	535.0832								
	CNL	535.0832								
	CLD	535.0832								
	DNL	535.1001	H	536.1081	15	Luteolin 7-O-(6''-malonylglucoside)	C24H22O14	flavone		
					15	Cyanidin 3-O-(6-O-malonyl-β-D-glucoside)	C24H22O14	anthocyanidin		
			Na	558.0899						
			K	574.1984		dalcochinin-8'-O-β-glucoside	C29H34O12	isoflavone		
						tetrahydropteroyl di-L-glutamate	C24H27N8O9			
		DLD	535.095	H	536.103	24	Luteolin 7-O-(6''-malonylglucoside)	C24H22O14		
					24	Cyanidin 3-O-(6-O-malonyl-β-D-glucoside)	C24H22O14			
						558.0848	dalcochinin-8'-O-β-glucoside	C29H34O12		
						tetrahydropteroyl di-L-glutamate	C24H27N8O9			
			K	574.1933						
	ANL	287.0439	H	288.0519	38	Luteolin	C15H10O6	flavone		
					38	Kaempferol	C15H10O6	flavonol		
					38	Cyanidin	C15H10O6	anthocyanidin		
					38	Fisetin	C15H10O6	flavonol		
					38	Baptigenin	C15H10O6	isoflavone		
					38	Orobol	C15H10O6	isoflavone		

287				38	2'-Hydroxygenistein	C15H10O6	isoflavone	
				38	6-Hydroxygenistein	C15H10O6	isoflavone	
				38	Norartocarpetin	C15H10O6	flavone	
				38	Scutellarein	C15H10O6	flavone	
				38	Isoscutellarein	C15H10O6	flavone	
				38	Datiscetin	C15H10O6	flavonol	
				38	Maritimetin	C15H10O6	aurone	
				38	Aureusidin	C15H10O6	aurone	
					naringenin dibenzoylmethane tautomer	C15H11O6	flavone	
					2-amino-4,5-dihydroxy-6-oxo-7-(phosphoxy)heptanoate	C7H12N1O9P1		
					2',3,4,4',6'-pentahydroxychalcone	C15H12O6	chalcone	
					Terbufos	C9H21O2P1S3		
					(2S)-eriodictyol	C15H11O6	flavonone	
					2-hydroxynaringenin	C15H11O6	flavone	
					(-)-dihydrokaempferol	C15H12O6	flavonoid	
					9-hydroxyrubrofusarin	C15H12O6		
	ALD	287.0439	Na	317.0337				
	BNL	287.0439	K	326.1422	3	5-Hydroxyindoleacetyl glycine	C12H12N2O4	
	BLD	287.0439						
	CNL	287.0439						
CLD	287.0439							
DNL	287.051	H	288.059	13	Luteolin	C15H10O6		
				13	Kaempferol	C15H10O6		
DLD	287.051	H		13	Cyanidin	C15H10O6		
				13	Fisetin	C15H10O6		
				13	Baptigenin	C15H10O6		

				13	Orobol	C15H10O6		
				13	2'-Hydroxygenistein	C15H10O6		
				13	6-Hydroxygenistein	C15H10O6		
				13	Norartocarpetin	C15H10O6		
				13	Scutellarein	C15H10O6		
				13	Isoscutellarein	C15H10O6		
				13	Datisctetin	C15H10O6		
				13	Maritimetin	C15H10O6		
				13	Aureusidin	C15H10O6		
					naringenin dibenzoylmethane tautomer	C15H11O6		
					2-amino-4,5-dihydroxy-6-oxo-7-(phosphoxy)heptanoate	C7H12N1O9P1		
					2',3,4,4',6'-pentahydroxychalcone	C15H12O6		
					Terbufos	C9H21O2P1S3		
					(2S)-eriodictyol	C15H11O6		
					2-hydroxynaringenin	C15H11O6		
					(-)-dihydrokaempferol	C15H12O6		
					9-hydroxyrubrofusarin	C15H12O6		
		Na	317.0408					
		K	326.1493	3	5-Hydroxyindoleacetyl glycine	C12H12N2O4		
449	ANL	449.085	450.093	37	Glucobrassicin	C16H20N2O9S2	glucosinolate	
	ALD	449.085	472.0748					
	BNL	449.085	488.1833	32	Sumatrol	C23H22O7		
				32	Toxicarol	C23H22O7		
	BLD	449.085		32	Tephrosin	C23H22O7		
				32	Lactupicrin	C23H22O7		
				32	12a-Hydroxyrotenone	C23H22O7	Rotenone	

CNL	449.085							
CLD	449.085							
DNL	449.0998	450.1078	17	Kaempferol 7-O-glucoside	C21H20O11	flavonol		
			17	Quercitrin	C21H20O11			
			17	Aureusidin 6-O-glucoside	C21H20O11	aurone		
			17	Astragalin	C21H20O11	flavonol		
			17	Luteolin 7-O- β -D-glucoside	C21H20O11	flavone		
			17	Kaempferol 3-O- β -D-galactoside	C21H20O11	flavonol		
			17	Cyanidin 5-O-glucoside	C21H20O11	anthocyanidin		
			17	6-C-Galactosylluteolin	C21H20O11	flavonoid		
			17	8-C-Galactosylluteolin	C21H20O11	flavonoid		
			17	Scutellarein 7-glucoside	C21H20O11	flavone		
			17	Carthamone	C21H20O11	chalcone		
			17	Chrysanthemine	C21H20O11	anthocyanidin		
				2',3,4,4',6'-pentahydroxychalcone 4'-O- β -D-glucoside	C21H22O11	chalcone		
		472.0896		N/A				
		488.1981	0	Sumatrol	C23H22O7			
			0	Toxicarol	C23H22O7			
			0	Tephrosin	C23H22O7			
			0	Lactupicrin	C23H22O7			
			0	12a-Hydroxyrotenone	C23H22O7			
DLD	449.0975	450.1055	24	Kaempferol 7-O-glucoside	C21H20O11			
			23	Quercitrin	C21H20O11			

				23	Aureusidin 6-O-glucoside	C21H20O11		
				23	Astragalín	C21H20O11		
				23	Luteolin 7-O-β-D-glucoside	C21H20O11		
				23	Kaempferol 3-O-β-D-galactoside	C21H20O11		
				23	Cyanidin 5-O-glucoside	C21H20O11		
				23	6-C-Galactosylluteolin	C21H20O11		
				23	8-C-Galactosylluteolin	C21H20O11		
				23	Scutellarein 7-glucoside	C21H20O11		
				23	Carthamone	C21H20O11		
				23	Chrysanthemín	C21H20O11		
				23	2',3,4,4',6'-pentahydroxychalcone 4'-O-β-D-glucoside	C21H22O11		
		472.0873			N/A			
		488.1958		4	Sumatrol	C23H22O7		
				4	Toxicarol	C23H22O7		
				4	Tephrosin	C23H22O7		
				4	Lactupicrin	C23H22O7		
				4	12a-Hydroxyrotenone	C23H22O7		
	ANL	144.0401	145.0481					
			167.0299					
	ALD	144.0401	183.1384					
	BNL	144.0401						
	BLD	144.0401						
	CNL	144.0401						
	CLD	144.0401						
	DNL	144.0441	145.0521	145.0561	5-methylthiopentanitrile oxide	C6H11N1O1S1		

144				25	(-)-5-(2-Propenyl)-2-oxazolidinethione	C6H9NOS		
				25	Raphanusamide	C6H9NOS		
	DLD	144.0441	183.1424					
196	ANL	196.0879	197.0959	32	Glucosaminic acid	C6H13NO6		
				32	D-Glucose oxime	C6H13NO6		
	ALD	196.0879		25	2-Amino-4-hydroxy-6-(hydroxymethyl)-7,8-dihydropteridine	C7H9N5O2		
	BNL	196.0879						
	BLD	196.0879	219.0777		N/A			
			235.1862		N/A			
	CNL	196.0879						
	CLD	196.0879						
	DNL	196.0929	197.1009		N/A			
	DLD	196.0929	235.1912		N/A			
288	ANL	288.0448	289.0528		N/A			
			311.0346		N/A			
	ALD	288.0448	327.1431		(S)-scoulerine	C19H21N1O4		
	BNL	288.0448						
	BLD	288.0448						
	CNL	288.0448						
	CLD	288.0448						
	DNL	288.0518	289.0598	39	Indoleglycerol phosphate	C11H14NO6P		
			311.0416	39	Furofoline I	C16H11NO3	alkaloid	
	DLD	288.0518	327.1501		(S)-scoulerine	C19H21N1O4		
ANL	303.0377	304.0457		N/A				

303			326.0275		N/A		
	ALD	303.0377	342.136		Coniferin	C16H22O8	
	BNL	303.0377					
	BLD	303.0377					
	CNL	303.0377					
	CLD	303.0377					
	DNL	303.0451	304.0531		taxifolin	C15H12O7	flavononol
					eriodictyol dibenzoylmethane tautomer	C10H12N2O7P1	
					(+)-taxifolin	C15H12O7	flavononol
					(+)-epitaxifolin	C15H12O7	taxifolin
					(2S)-dihydrotricetin	C15H12O7	
					2-hydroxyeriodictyol	C15H12O7	flavonone
				15	Quercetin	C15H10O7	
				15	Morin	C15H10O7	flavonol
				15	Delphinidin	C15H10O7	flavonol
				15	HIERACIN	C15H10O7	tricetin
				15	Isoetin	C15H10O7	flavonol
				15	6-Hydroxyluteolin	C15H10O7	flavonol
				15	Hypolaetin	C15H10O7	flavone
				15	Robinetin	C15H10O7	flavonol
			15	6-Hydroxykaempferol	C15H10O7	flavonol	
			15	Herbacetin	C15H10O7	flavonol	
			15	Bracteatin	C15H10O7	aurone	
			15	2'-Hydroxypseudobaptigenin	C15H10O7		
DLD	303.0451	342.1434		Coniferin	C16H22O8		

Table A3.3: Discriminant mass bins and their associated detected and accurate masses. The putatively identified compounds, their chemical groups, and the associated pathways are displayed. An error in parts per million is included to show the putative compounds' variation from the detected mass (organic layer analyzed in negative ESI mode).

Bin	Treatment	Detected mass	Accurate mass	Δ ppm	Name	chemical formula	chemical group	pathway
	ANL	194.0976	195.1056					
	ALD	194.0976	195.1056					
	BNL	194.0976	195.1056					
	BLD	194.0976	195.1056					
	CNL	194.0976	195.1056					
	CLD	194.0976	195.1056					
	DNL	194.0524	195.0604	33	Dopaquinone	C9H9NO4		Tyrosine metabolism
				33	Leucodopachrome	C9H9NO4		Tyrosine metabolism
	DLD	194.0524	195.0604	33	1,2-Epoxy-3-(p-Nitrophenoxy)propane	C9H9NO4		
					β-oxo-L-tyrosine	C9H8N1O4		
				leucodopachrome	C9H8N1O4			
405.4	ANL	405.3178	406.3258					
	ALD	405.3178	406.3258					
	BNL	405.3178	406.3258					
	BLD	405.3178	406.3258					
	CNL	405.3178	406.3258					
	CLD	405.3178	406.3258					
	DNL	405.252	406.26					
	DLD	405.2498	406.2578					
			36	Ardisianone	C24H38O5	quinone	ubiquinone biosynthesis	
249	ANL	249.08395	250.09195	14	2-(5'-Methylthio)pentylmalic acid	C10H18O5S	glucosinolate	glucosinolate biosynthesis
				14	3-(5'-Methylthio)pentylmalic acid	C10H18O5S	glucosinolate	glucosinolate biosynthesis
				32	Flindersiachromone	C17H14O2	flavone	flavonoid biosynthesis

	ALD	248.8872	249.8952					
	BNL	248.8872	249.8952					
	BLD	249.078775	250.086775	33	Methoxybrassitin	C12H14N2O2S	Acyl group	glucosinolate biosynthesis
				6	2-(5'-Methylthio)pentylmalic acid	C10H18O5S	glucosinolate	glucosinolate biosynthesis
				6	3-(5'-Methylthio)pentylmalic acid	C10H18O5S	glucosinolate	glucosinolate biosynthesis
	CNL	248.8872	249.8952					
	CLD	248.8872	249.8952					
	DNL	248.9532	249.9612					
	DLD	248.9532	249.9612					
325.4	ANL	325.23165	326.23965	20	AVOCADYNE ACETATE	C19H34O4	Fatty alcohol	
	ALD	325.229675	326.237675	27	AVOCADYNE ACETATE	C19H34O4	Fatty alcohol	
	BNL	325.2277	326.2357	32	AVOCADYNE ACETATE	C19H34O4	Fatty alcohol	
	BLD	325.2277	326.2357	32	AVOCADYNE ACETATE	C19H34O4	Fatty alcohol	
	CNL	325.2277	326.2357	32	AVOCADYNE ACETATE	C19H34O4	Fatty alcohol	
	CLD	325.2277	326.2357	32	AVOCADYNE ACETATE	C19H34O4	Fatty alcohol	
	DNL	325.1767	326.1847		N/A			
	DLD	325.1767	326.1847		N/A			
195	ANL	195.0985	196.1065		N/A			
	ALD	195.0985	196.1065		N/A			
	BNL	195.0985	196.1065		N/A			
	BLD	195.0985	196.1065		N/A			
	CNL	195.0985	196.1065		N/A			
	CLD	195.0985	196.1065		N/A			
	DNL	195.0593	196.0673		N/A			
	DLD	195.0593	196.0673	35	orsellinic acid	C10H12O4	Aromatic polyketide	chalcone synthase

				35	acetosyringone	C10H12O4	phenol	N/A
				35	XANTHOXYLIN	C10H12O4	methoxyphenol	N/A
				35	Atraric acid	C10H12O4	phenol	N/A
837.4	ANL	837.5573	838.5653		N/A			
	ALD	837.56365	838.57165		N/A			
	BNL	837.5668	838.5748		N/A			
	BLD	837.5573	838.5653		N/A			
	CNL	837.5573	838.5653		N/A			
	CLD	837.5573	838.5653		N/A			
	DNL	837.45645	838.46445	34	Talinumoside I	C43H66O16	prenol lipids	N/A
	DLD	837.453275	838.461275	34	Talinumoside I	C43H66O16	prenol lipids	N/A
311.4	ANL	311.212	312.22		N/A			
	ALD	311.212	312.22		N/A			
	BNL	311.212	312.22		N/A			
	BLD	311.212	312.22		N/A			
	CNL	311.212	312.22		N/A			
	CLD	311.212	312.22		N/A			
	DNL	311.160175	312.168175	16	triptophenolide	C20H24O3	diterpenoid	terpenoid biosynthesis
				16	Jatrophone	C20H24O3	diterpenoid	terpenoid biosynthesis
	DLD	311.160175	312.168175		N/A			
339.4	ANL	339.2458	340.2538	37	Plastoquinone 3	C23H32O2	oxidative phosphorylation	
	ALD	339.2458	340.2538		N/A			
	BNL	339.2458			N/A			
	BLD	339.2458	340.2538		N/A			
	CNL	339.2458	340.2538		N/A			
	CLD	339.2458	340.2538		N/A			
	DNL	339.217875	340.225875		N/A			

	DLD	339.191675	340.199675		N/A			
385	ANL	385.1927	386.2007	15	Corchoionol C 9-glucoside	C19H30O8	terpenoid glycoside	N/A
				15	Citroside A	C19H30O8	Glycosyl	
					O-methylandrocymbine	C22H28N1O5	Isoquinoline alkaloid biosynthesis/Biosynthesis of alkaloids derived from shikimate pathway	
	ALD	385.197	386.205	26	Corchoionol C 9-glucoside	C19H30O8	terpenoid glycoside	N/A
				26	Citroside A	C19H30O8	Glycosyl	
					O-methylandrocymbine	C22H28N1O5	Isoquinoline alkaloid biosynthesis/Biosynthesis of alkaloids derived from shikimate pathway	
	BNL	385.197	386.205		N/A			
					O-methylandrocymbine	C22H28N1O5	Isoquinoline alkaloid biosynthesis/Biosynthesis of alkaloids derived from shikimate pathway	
	BLD	385.19485	386.20285	20	Corchoionol C 9-glucoside	C19H30O8	terpenoid glycoside	N/A
				20	Citroside A	C19H30O8	Glycosyl	
					O-methylandrocymbine	C22H28N1O5	Isoquinoline alkaloid biosynthesis/Biosynthesis of alkaloids derived from shikimate pathway	
	CNL	385.1927	386.2007	15	Corchoionol C 9-glucoside	C19H30O8	terpenoid glycoside	N/A
				15	Citroside A	C19H30O8	Glycosyl	
	CLD	385.1927	386.2007	15	Corchoionol C 9-glucoside	C19H30O8	terpenoid glycoside	N/A
				15	Citroside A	C19H30O8	Glycosyl	
					O-methylandrocymbine	C22H28N1O5	Isoquinoline alkaloid biosynthesis/Biosynthesis of alkaloids derived from shikimate pathway	
	DNL	384.9225	385.9305		N/A			
	DLD	384.9225	385.9305		N/A			
363	ANL	363.149925	364.1579	13	Gibberellin A8	C19H24O7	diterpenoid	diterpenoid biosynthesis
				13	Vernomygdin	C19H24O7	sesquiterpenoid	sesquiterpenoid biosynthesis
				13	Zexbrevin B	C19H24O7	sesquiterpenoid	sesquiterpenoid biosynthesis
				13	(7R*,8R*)-3-Methoxy-3',4,7,9,9'-pentahydroxy-8,4'-oxyneolignan	C19H24O7	lignan glycoside	N/A

	ALD	363.1416	364.1496	9	Gibberellin A8	C19H24O7	diterpenoid	diterpenoid biosynthesis
				9	Vernomygdin	C19H24O7	sesquiterpenoid	sesquiterpenoid biosynthesis
				9	Zexbrevin B	C19H24O7	sesquiterpenoid	sesquiterpenoid biosynthesis
				9	(7R*,8R*)-3-Methoxy-3',4,7,9,9'-pentahydroxy-8,4'-oxyneolignan	C19H24O7	lignan glycoside	N/A
	BNL	363.1374	364.1454	20	Gibberellin A8	C19H24O7	diterpenoid	diterpenoid biosynthesis
				20	Vernomygdin	C19H24O7	sesquiterpenoid	sesquiterpenoid biosynthesis
				20	Zexbrevin B	C19H24O7	sesquiterpenoid	sesquiterpenoid biosynthesis
				20	(7R*,8R*)-3-Methoxy-3',4,7,9,9'-pentahydroxy-8,4'-oxyneolignan	C19H24O7	lignan glycoside	N/A
	BLD	363.124925	364.1329					
	CNL	363.095725	364.1037	22	Justicidin B	C21H16O6	lignan	phenylpropanoid biosynthesis
	CLD	363.14575	364.1537	2	Gibberellin A8	C19H24O7	diterpenoid	diterpenoid biosynthesis
				2	Vernomygdin	C19H24O7	sesquiterpenoid	sesquiterpenoid biosynthesis
				2	Zexbrevin B	C19H24O7	sesquiterpenoid	sesquiterpenoid biosynthesis
				2	(7R*,8R*)-3-Methoxy-3',4,7,9,9'-pentahydroxy-8,4'-oxyneolignan	C19H24O7	lignan glycoside	N/A
	DNL	363.1627	364.1707	24	11-Methoxy-vinorine	C22H24N2O3	alkaloid	indole alkaloid biosynthesis
	DLD	362.9292	363.9372		N/A			
113	ANL	113.03955	114.0475	11	heptan-2-one	C7H14O	ketone	N/A
	ALD	113.050025	114.058		N/A			
	BNL	113.060475	114.0684		N/A			

	BLD	113.06745	114.0754		N/A			
	CNL	113.0407	114.0487		N/A			
	CLD	113.051825	114.0598		N/A			
	DNL	112.9828	113.9908		acetylenedicarboxylate	C4O4	amino acid	pyruvate metabolism
	DLD	112.9828	113.9908		N/A			
155	ANL	155.02915	156.0371		6-hydroxy-2-cyclohexenone-carboxylate	C7H7O4	glycoside	phenylpropanoid biosynthesis
					N-methylethanolamine phosphate	C3H9N1O4P1	phosphate	Glycerophospholipid metabolism
	ALD	155.04005	156.04805		N/A			
	BNL	155.04005	156.04805		N/A			
	BLD	155.085	156.093		N/A			
	CNL	154.988325	155.9963		N/A			
	CLD	155.01965	156.0276		N/A			
	DNL	154.9698	155.9778		N/A			
	DLD	154.9698	155.9778		N/A			
265.4	ANL	265.18945	266.1974	10	APHYLLIC ACID	C15H26N2O2	alkaloid	
	ALD	265.193	266.201	3	APHYLLIC ACID	C15H26N2O2		
	BNL	265.193	266.201	3	APHYLLIC ACID	C15H26N2O2		
	BLD	265.187675	266.1956	17	APHYLLIC ACID	C15H26N2O2		
	CNL	265.1859	266.1939	23	APHYLLIC ACID	C15H26N2O2		
	CLD	265.1859	266.1939	23	APHYLLIC ACID	C15H26N2O2		
	DNL	265.1399	266.1479	19	Borreline	C17H18N2O	Indole	N/A
	DLD	265.1399	266.1479	17	Rugosal A	C15H22O4	sesquiterpenoid	sesquiterpenoid biosynthesis
205	ANL	205.0172	206.0252		N/A			
	ALD	205.0172	206.0252		N/A			
	BNL	205.0172	206.0252		N/A			
	BLD	205.0172	206.0252		N/A			

	CNL	205.0172	206.0252		N/A		
	CLD	205.0172	206.0252		N/A		
	DNL	204.9644	205.9724		N/A		
	DLD	204.9644	205.9724		N/A		
	ALD	831.5792	832.5872		N/A		
	BNL	831.582325	832.5903		N/A		
	BLD	831.582325	832.5903		N/A		
	CNL	831.5792	832.5872		N/A		
	CLD	831.5792	832.5872		N/A		
	DNL	831.4724	832.4807		N/A		
	DLD	831.4724	832.4807		N/A		
816.6	ANL	816.580575	817.588575		N/A		
	ALD	816.580575	817.588575		N/A		
	BNL	816.580575	817.588575		N/A		
	BLD	816.580575	817.588575		N/A		
	CNL	816.580575	817.588575		N/A		
	CLD	816.580575	817.588575		N/A		
	DNL	816.4779	817.4859		N/A		
	DLD	816.474775	817.482775		N/A		
395	ANL	395.136925	396.144925		N/A		
	ALD	395.123875	396.131875		N/A		
	BNL	395.11735	396.12535		N/A		
	BLD	395.09995	396.10795		N/A		
	CNL	395.128225	396.136225		N/A		
	CLD	395.128225	396.136225		N/A		
	DNL	395.09995	396.10795		N/A		
	DLD	394.876275	395.884275		N/A		

Table A3.4: Discriminant mass bins and their associated detected and accurate masses. The putatively identified compounds, their chemical groups, and the associated pathways are displayed. An error in parts per million is included to show the putative compounds' variation from the detected mass (organic layer analyzed in positive ESI mode).

Bin	Treatment	Detected mass		Accurate mass	Appm	Compound	Chemical formula	Chemical group	Pathway	
195	ANL	195.0878	H	196.0958	37	Phenanthrene-9,10-oxide	C14H10O			
					37	9-Hydroxyphenanthrene	C14H10O			
	ALD	195.0878			37	Phenanthrene-1,2-oxide	C14H10O			
					37	1-Phenanthrol	C14H10O			
	BNL	195.0878			7	QUEBRACHITOL	C7H14O6			
					7	D-Glucoside	C7H14O6			
	BLD	195.0878			7	3-O-Methyl-myo-inositol	C7H14O6			
					7	1-O-Methyl-myo-inositol	C7H14O6			
	CNL	195.0878			7	D-4-O-Methyl-myo-inositol	C7H14O6			
					7	Methyl beta-D-glucopyranoside	C7H14O6			
	CLD	195.0878			7	Sequoyitol	C7H14O6			
					7	D-Pinitol	C7H14O6			
					7	L-Pinitol	C7H14O6			
				Na	218.0776	7	DESOXYPEGANINE	C11H12N2		
				K	234.1861					
	DNL	195.027066 7	H	196.0351			3,4-dihydroxyphenylpyruvate	C9H7O5		
							(2E,4Z,5E)-2-hydroxy-7-oxo-(2-oxoethylidene)hepta-2,5-dienoate	C9H7O5		
							2-hydroxy-4-[(1E)-3-oxoprop-1-en-1-yl]-2H-pyran-6-carboxylate	C9H7O5		
							(2E,4Z,6E)-5-formyl-2-hydroxy-8-oxoocta-2,4,6-trienoate	C9H7O5		
							arabidopyl alcohol	C9H7O5		
						2-hydroxy-3-[(1E)-3-oxoprop-1-en-1-yl]-2H-pyran-6-carboxylate	C9H7O5			
						iso-arabidopyl alcohol	C9H7O5			
	195.0902	Na	218.0169	3		3-Dehydroshikimic acid	C7H8O5			
				3		2-Hydroxyhepta-2,4-dienedioate	C7H8O5			

				3	2-Oxohept-3-enedioate	C7H8O5		
				3	5-Dehydroshikimate	C7H8O5		
		K	234.1254	4	1,2,4-Triazole-3-alanine	C5H8N4O2		
				24	3-Indoleacetonitrile	C10H8N2		
DLD	195.0902	H	196.0982	19	QUEBRACHITOL	C7H14O6		
				19	D-Glucoside	C7H14O6		
				19	3-O-Methyl-myo-inositol	C7H14O6		
				19	1-O-Methyl-myo-inositol	C7H14O6		
				19	D-4-O-Methyl-myo-inositol	C7H14O6		
				19	Methyl beta-D-glucopyranoside	C7H14O6		
				19	Sequoyitol	C7H14O6		
				19	D-Pinitol	C7H14O6		
				19	L-Pinitol	C7H14O6		
		Na	218.08					
		K	234.1885					
287	ANL	287.0544	H	288.0624	2	Luteolin	C15H10O6	Flavonoid biosynthesis
					2	Kaempferol	C15H10O6	
					2	Cyanidin	C15H10O6	
					2	Fisetin	C15H10O6	
					2	Orobol	C15H10O6	
					2	2'-Hydroxygenistein	C15H10O6	
					2	6-Hydroxygenistein	C15H10O6	
					2	Norartocarpetin	C15H10O6	
					2	Scutellarein	C15H10O6	
					2	Isoscutellarein	C15H10O6	

				2	Datisctin	C15H10O6	
				2	6-Hydroxygalangin	C15H10O6	
				2	8-Hydroxygalangin	C15H10O6	
				2	Maritimetin	C15H10O6	
				2	Aureusidin	C15H10O6	
					naringenin dibenzoylmethane tautomer	C15H11O6	
					2,4',5,7-tetrahydroxyisoflavanone	C15H12O6	
ALD	287.0544				dalbergoidin	C15H11O6	
					2,6,7,4'-tetrahydroxyisoflavanone	C15H12O6	
BNL	287.0544				2-[hydroperoxy(4-hydroxyphenyl)methyl]-6-hydroxy-1-benzofuran-3-one	C15H12O6	
					(2S)-eriodictyol	C15H11O6	
BLD	287.0544				2-hydroxynaringenin	C15H11O6	
					(-)-dihydrokaempferol	C15H12O6	
					(+)-dihydrokaempferol	C15H12O6	
		Na	310.0442		N/A		
		K	326.1527		N/A		
CNL	287.0544						
CLD	287.0544						
DNL	287.051	H	288.059	13	Luteolin	C15H10O6	Flavonoid biosynthesis
				13	Kaempferol	C15H10O6	
				13	Cyanidin	C15H10O6	
				13	Fisetin	C15H10O6	
				13	Orobol	C15H10O6	
				13	2'-Hydroxygenistein	C15H10O6	
				13	6-Hydroxygenistein	C15H10O6	
				13	Norartocarpetin	C15H10O6	

				13	Scutellarein	C15H10O6		
				13	Isoscutellarein	C15H10O6		
				13	Datisctin	C15H10O6		
				13	6-Hydroxygalangin	C15H10O6		
				13	8-Hydroxygalangin	C15H10O6		
				13	Maritimetin	C15H10O6		
				13	Aureusidin	C15H10O6		
					naringenin dibenzoylmethane tautomer	C15H11O6		
					2,4',5,7-tetrahydroxyisoflavanone	C15H12O6		
					dalbergioidin	C15H11O6		
					2,6,7,4'-tetrahydroxyisoflavanone	C15H12O6		
					2-[hydroperoxy(4-hydroxyphenyl)methyl]-6-hydroxy-1-benzofuran-3-one	C15H12O6		
					(2S)-eriodictyol	C15H11O6		
					2-hydroxynaringenin	C15H11O6		
					(-)-dihydrokaempferol	C15H12O6		
					(+)-dihydrokaempferol	C15H12O6		
		Na	310.0408		N/A			
	DLD	287.051	K	326.1493	28	5-Hydroxyindoleacetyl glycine	C12H12N2O4	
593.4	ANL	593.374925	H	594.3829	10	agavoside A	C33H52O9	
					10	nuatigenin 3-beta-D-glucopyranoside	C33H52O9	
					17	Santiaguine	C38H48N4O2	
			Na	616.3647		N/A		
			K	632.4732		caldariellaquinol	C39H68O2S2	
		593.4556	H	594.4636		N/A		
			Na	616.4454	38	Zeaxanthin	C40H58O2	
					23	Dihydrospheroidene/ Methoxyneurosporene	C41H62O	

		K	632.5539		N/A		
ALD	593.386235	H	594.3942	29	agavoside A	C33H52O9	
				29	nuatigenin 3-beta-D-glucopyranoside	C33H52O9	
				2	Santiaguine	C38H48N4O2	
		Na	616.376		N/A		
		K	632.4845		N/A		
BNL	593.37225	H	594.3803	6	agavoside A	C33H52O9	
				6	nuatigenin 3-beta-D-glucopyranoside	C33H52O9	
				21	Santiaguine	C38H48N4O2	
		Na	616.3621		N/A		
		K	632.4706		caldariellaquinol	C39H68O2S2	
	593.3989	H	594.4069	23	Santiaguine	C38H48N4O2	
		Na	616.3887		N/A		
		K	632.4972	21	1'-Hydroxy- γ -carotene/ 1'-OH- γ -Carotene/ (Carotenoid B)	C40H58O	
				21	Demethylspheroidene/ (Demethylated spheroidene)	C40H58O	
	593.4521	H	594.4601		N/A		
		Na	616.4419	32	Zeaxanthin	C40H58O2	
				28	Dihydrospheroidene/ Methoxyneurosporene	C41H62O	
		K	632.5504		N/A		
BLD	593.3536	H	594.3616		caldariellaquinol	C39H68O2S2	
		Na	616.3434		N/A		
		K	632.4519	39	Demethylspheroidene/ (Demethylated spheroidene)	C40H58O	
				39	1'-Hydroxy- γ -carotene/ 1'-OH- γ -Carotene/ (Carotenoid B)	C40H58O	
	593.45475	H	594.4628		N/A		
		Na	616.4446	36	Zeaxanthin	C40H58O2	

				24	Dihydrospheroidene/ Methoxyneurosporene	C41H62O		
		K	632.5531		N/A			
CNL	593.38555	H	594.3936	28	agavoside A	C33H52O9		
				28	nuatigenin 3-beta-D-glucopyranoside	C33H52O9		
				1	Santiaguine	C38H48N4O2		
		Na	616.3754		N/A			
		K	632.4839		caldariellaquinol	C39H68O2S2		
	593.437866 7	H	594.4459		N/A			
		Na	616.4277	8	Zeaxanthin	C40H58O2		
		K	632.5362		N/A			
	593.4627	H	594.4707		N/A			
		Na	616.4525	11	Dihydrospheroidene/ Methoxyneurosporene	C41H62O		
		K	632.561		N/A			
CLD	593.366925	H	594.3749	2	agavoside A	C33H52O9		
				2	nuatigenin 3-beta-D-glucopyranoside	C33H52O9		
				30	Santiaguine	C38H48N4O2		
		Na	616.3567		N/A			
		K	632.4652		caldariellaquinol	C39H68O2S2		
					N/A			
	593.455633 3	H	594.4636		N/A			
		Na	616.4454	38	Zeaxanthin	C40H58O2		
				23	Dihydrospheroidene/ Methoxyneurosporene	C41H62O		
		K	632.5539		N/A			
DNL	593.370975	H	594.379	4	agavoside A	C33H52O9		
				4	nuatigenin 3-beta-D-glucopyranoside	C33H52O9		

				23	Santiaguine	C38H48N4O2		
		Na	616.3608		N/A			
		K	632.4693		caldariellaquinol	C39H68O2S2		
					N/A			
DLD	593.365675	H	594.3737	4	agavoside A	C33H52O9		
				4	nuatigenin 3-beta-D-glucopyranoside	C33H52O9		
				32	Santiaguine	C38H48N4O2		
		Na	616.3555		N/A			
		K	632.464		caldariellaquinol	C39H68O2S2		
	593.4614	H	594.4694		N/A			
		Na	616.4512	13	Dihydrospheroidene/ Methoxyneurosporene	C41H62O		
		K	632.5597		N/A			
568.2	ANL	568.1276	H	569.1356	N/A			
			Na	591.1174	N/A			
			K	607.2259	N/A			
	ALD	568.1354	H	569.1434	N/A			
			Na	591.1252	N/A			
			K	606.2337	N/A			
	BNL	568.1328	H	569.1408	N/A			
			Na	591.1226	N/A			
			K	607.2311	N/A			
	568.2136	H	569.2216		N/A			
			Na	591.2034	15	Dihydrozeatin-9-N-glucoside-O-glucoside	C22H35N5O11	
			K	607.3119		N/A		
	568.27095	H	569.279		N/A			
			Na	591.2608		N/A		
			K	607.3693		N/A		

BLD	568.1328	H	569.1408			N/A		
		Na	591.2051			N/A		
		K	607.2311			N/A		
	568.215333 3	H	569.2593			N/A		
		Na	591.2051	12	Dihydrozeatin-9-N-glucoside-O-glucoside	C22H35N5O11		
		K	607.3136			N/A		
	568.2814	H	569.2894			N/A		
		Na	591.2712			N/A		
		K	607.3797			N/A		
CNL	568.1302	H	569.1382			N/A		
		Na	591.12			N/A		
		K	607.2285			N/A		
	568.229233 3	H	569.2372			N/A		
		Na	591.219	11	Dihydrozeatin-9-N-glucoside-O-glucoside	C22H35N5O11		
		K	607.3275			N/A		
	568.2709	H	569.2789			N/A		
		Na	591.2607			N/A		
		K	607.3692			N/A		
CLD	568.1302	H	569.1382			N/A		
		Na	591.12			N/A		
		K	607.2285			N/A		
	568.21957	H	569.2276			N/A		
		Na	591.2094	5	Dihydrozeatin-9-N-glucoside-O-glucoside	C22H35N5O11		
		K	607.3179			N/A		
	568.2709	H	569.2789			N/A		

		Na	591.2607			N/A		
		K	601.3692			N/A		
	DNL	568.1235	H	569.1315		N/A		
			Na	591.1133		N/A		
			K	607.2218		N/A		
		568.2173	H	569.2253		N/A		
			Na	591.2071	9	Dihydrozeatin-9-N-glucoside-O-glucoside	C22H35N5O11	
			K	607.3156		N/A		
	DLD	568.1183	H	569.1263		N/A		
			Na	591.1081		N/A		
			K	607.2166		N/A		
		568.23295	H	569.241		N/A		
			Na	591.2228	18	Dihydrozeatin-9-N-glucoside-O-glucoside	C22H35N5O11	
			K	607.3313		N/A		
196.2	ANL	196.131875	H	197.1399		N/A		
			Na	219.1217		N/A		
			K	235.2302		N/A		
	ALD	196.128825	H	197.1368		N/A		
			Na	219.1186	21	(R)-pantothenate	C9H16N1O5	
			K	235.2271		N/A		
	BNL	196.134	H	197.142		N/A		
			Na	219.1238		N/A		
			K	235.2323		N/A		
		196.171725	H	197.1797		N/A		
			Na	219.1615		N/A		
			K	235.27		N/A		
	BLD	196.134925	H	197.1429		N/A		

		Na	219.1247		N/A		
		K	235.2332		N/A		
	196.174775	H	197.1828		N/A		
		Na	219.1646		N/A		
		K	235.2731		N/A		
	196.21	H	197.218		N/A		
		Na	219.1998		N/A		
		K	235.3083		N/A		
CNL	196.131875	H			N/A		
		Na			N/A		
		K			N/A		
	196.1671	H			N/A		
		Na			N/A		
		K			N/A		
	196.1947	H			N/A		
		Na			N/A		
		K			N/A		
CLD	196.134925	H			N/A		
		Na			N/A		
		K			N/A		
	196.184466 7	H			N/A		
		Na			N/A		
		K			N/A		
	196.24365	H			N/A		
		Na			N/A		
		K			N/A		
DNL	196.149575	H			N/A		

			Na				N/A		
			K				N/A		
		196.223566 7	H				N/A		
			Na				N/A		
			K				N/A		
		196.2766	H				N/A		
			Na				N/A		
			K				N/A		
DLD		196.155675	H				N/A		
			Na				N/A		
			K				N/A		
		196.2889	H				N/A		
			Na				N/A		
			K				N/A		
449.2	ANL	449.107	H	450.115	1	Naringenin-4'-O-β-D-Glucuronide	C21H20O11		
					1	Naringenin-7-O-β-D-Glucuronide	C21H20O11		
					1	KAEMPFEROL-7-O-GLUCOSIDE	C21H20O11		
					1	Idaein	C21H20O11		
					1	Quercitrin	C21H20O11		
					1	Astragalin	C21H20O11		
					1	Aureusidin 6-O-glucoside	C21H20O11		
					1	Luteolin 7-O-β-D-glucoside	C21H20O11		
					1	Kaempferol 3-O-β-D-galactoside	C21H20O11		
					1	Cyanidin 5-O-glucoside	C21H20O11		
					1	Isoorientin	C21H20O11		
					1	Orientin	C21H20O11		
					1	Fisetin 8-C-glucoside	C21H20O11		

				1	Datiscanin	C21H20O11		
				1	Carthamone	C21H20O11		
				1	Maritimein	C21H20O11		
				1	Chrysanthemin	C21H20O11		
				450.1162	8C-glucosyl-2-hydroxynaringenin	C21H21O11		
		Na	472.0968	450.1162	6C-glucosyl-2-hydroxynaringenin	C21H21O11		
				450.1162	2-[hydroperoxy-(4-glucosyl-hydroxyphenyl)methyl]-6-hydroxy-1-benzofuran-3-on	C21H21O11		
		K	488.2053	16	Toxicarol	C23H22O7		
				16	Tephrosin	C23H22O7		
ALD	449.107	H		16	Lactupicrin	C23H22O7		
		Na		16	12a-Hydroxyrotenone	C23H22O7		
		K		30	Bruceine D	C20H26O9		
BNL	449.107	H			N/A			
		Na			N/A			
		K			N/A			
BLD	449.107	H			N/A			
		Na			N/A			
		K			N/A			
	449.24595	H	450.254		N/A			
		Na	472.2358		N/A			
		K	488.3443		N/A			
CNL	449.107				N/A			
	449.1811	H	450.1891	32	Lonchocarpenin	C27H28O6		
					2-cis,6-trans,10-trans-geranylgeranyl diphosphate	C20H33O7P2		
					(2Z,6Z,10E)-tetraprenyl diphosphate	C20H33O7P2		
					geranylgeranyl diphosphate	C20H33O7P2		

					terpentedienyl diphosphate	C20H33O7P2		
					(13E)-labda-7,13-dien-15-yl diphosphate	C20H33O7P2		
					(+)-copalyl diphosphate	C20H33O7P2		
					9α-copalyl diphosphate	C20H33O7P2		
					(-)-ent-copalyl diphosphate	C20H33O7P2		
		Na	472.1709	6	Abscisic acid glucose ester	C21H30O9		
		K	488.2794	19	Vismione D	C25H30O5		
				27	Forskolin	C22H34O7		
				27	Nigakilhemiacetal A	C22H34O7		
	449.2274	H	450.2354	23	Jodrellin A	C24H32O8		
		Na	472.2172		N/A			
		K	488.3257		N/A			
	449.2737	H	450.2817		N/A			
		Na	472.2635		N/A			
		K	488.372		N/A			
CLD	449.107				N/A			
	449.245933 3	H	450.2539		N/A			
		Na	472.2357		N/A			
		K	488.3442		N/A			
DNL	449.1044	H	450.1124	7	Naringenin-4'-O-β-D-Glucuronide	C21H20O11		
				7	Naringenin-7-O-β-D-Glucuronide	C21H20O11		
				7	KAEMPFEROL-7-O-GLUCOSIDE	C21H20O11		
				7	Idaein	C21H20O11		
				7	Quercitrin	C21H20O11		
				7	Astragalin	C21H20O11		
				7	Aureusidin 6-O-glucoside	C21H20O11		
				7	Luteolin 7-O-β-D-glucoside	C21H20O11		

				7	Kaempferol 3-O-β-D-galactoside	C21H20O11		
				7	Cyanidin 5-O-glucoside	C21H20O11		
				7	Isoorientin	C21H20O11		
				7	Orientin	C21H20O11		
				7	Fisetin 8-C-glucoside	C21H20O11		
				7	Datiscanin	C21H20O11		
				7	Carthamone	C21H20O11		
				7	Maritimein	C21H20O11		
				7	Chrysanthemine	C21H20O11		
					8C-glucosyl-2-hydroxynaringenin	C21H21O11		
					6C-glucosyl-2-hydroxynaringenin	C21H21O11		
					2-[hydroperoxy-(4-glucosyl-hydroxyphenyl)methyl]-6-hydroxy-1-benzofuran-3-on	C21H21O11		
		Na	472.0942		N/A			
		K	488.2027	10	Toxicarol	C23H22O7		
				10	Tephrosin	C23H22O7		
				10	Lactupicrin	C23H22O7		
				10	12a-Hydroxyrotenone	C23H22O7		
				36	Bruceine D	C20H26O9		
					N/A			
	449.2272	H	450.2352	22	Jodrellin A	C24H32O8		
		Na	472.217		N/A			
		K	488.3255		N/A			
	449.25735	H	450.2654		N/A			
		Na	472.2472		N/A			
		K	488.3557		N/A			
DLD	449.1044				N/A			

		449.2133	H		38	Lonchocarpenin	C27H28O6		
	ANL	589.3624	H		30	Echinenone/ (Myxoxanthin)	C40H54O		
	ALD	589.462325				N/A			
	BNL	589.345625				N/A			
		589.4252	H		21	Anhydrorhodovibrin	C41H58O		
		589.4438	H		9	Anhydrorhodovibrin	C41H58O		
		589.4968				N/A			
	BLD	589.3403				N/A			
		589.4544				N/A			
	CNL	589.4119				N/A			
	CLD	589.366825	H		23	Echinenone/ (Myxoxanthin)	C40H54O		
			H		23	OH-Chlorobactene	C40H54O		
	DNL	589.371666 7	H		15	Echinenone/ (Myxoxanthin)	C40H54O		
			H		15	OH-Chlorobactene	C40H54O		
		589.3575	H		39	Echinenone/ (Myxoxanthin)	C40H54O		
			H		39	OH-Chlorobactene	C40H54O		
		589.4106				N/A			
	DLD	589.350466 7				N/A			
600.2	ANL	600.1379				N/A			
	ALD	600.191425				N/A			
		600.2343				N/A			
	BNL	600.172675				N/A			
		600.25035				N/A			
	BLD	600.166466 7				N/A			
		600.2664				N/A			
	CNL	600.17535				N/A			

		600.252133 3				N/A			
	CLD	600.187833 3				N/A			
		600.23425				N/A			
	DNL	600.195833 3				N/A			
		600.2563				N/A			
	DLD	600.22775				N/A			
628	ANL	628.055075	H		17	GDP-Man		C16H25N5O16P2	
			H		17	GDP-L-galactose		C16H25N5O16P2	
			H		17	GDP-L-gulose		C16H25N5O16P2	
			H		17	GDP-glucose		C16H25N5O16P2	
			H		33	UDP-2-acetamido-4-dehydro-2,6-dideoxyglucose		C17H25N3O16P2	
			H		33	UDP-2-acetamido-2,6-dideoxy-beta-L-arabino-hexos-4-ulose		C17H25N3O16P2	
			H		15	ADP-Mannose		C16H25N5O15P2	
			H		15	GDP-6-deoxy-D-mannose		C16H25N5O15P2	
			H		15	GDP-6-deoxy-D-talose		C16H25N5O15P2	
			H		15	GDP-L-fucose		C16H25N5O15P2	
			H		15	ADP-glucose		C16H25N5O15P2	
			H		15	Adenosine Diphosphate Glucose		C16H25N5O15P2	
			H		15	Guanosine diphosphofucose		C16H25N5O15P2	
	ALD	628.05235	H		22	GDP-Man		C16H25N5O16P2	
			H		22	GDP-L-galactose		C16H25N5O16P2	
			H		22	GDP-L-gulose		C16H25N5O16P2	
			H		22	GDP-glucose		C16H25N5O16P2	
			H		29	UDP-2-acetamido-4-dehydro-2,6-dideoxyglucose		C17H25N3O16P2	

		H		29	UDP-2-acetamido-2,6-dideoxy-beta-L-arabino-hexos-4-ulose	C17H25N3O16P2		
		H		11	ADP-Mannose	C16H25N5O15P2		
		H		11	GDP-6-deoxy-D-mannose	C16H25N5O15P2		
		H		11	GDP-6-deoxy-D-talose	C16H25N5O15P2		
		H		11	GDP-L-fucose	C16H25N5O15P2		
		H		11	ADP-glucose	C16H25N5O15P2		
		H		11	Adenosine Diphosphate Glucose	C16H25N5O15P2		
		H		11	Guanosine diphosphofucose	C16H25N5O15P2		
BNL	628.0551				N/A			
BLD	628.0551				N/A			
CNL	628.0551				N/A			
CLD	628.0578	H		13	GDP-Man	C16H25N5O16P2		
		H		13	GDP-L-galactose	C16H25N5O16P2		
		H		13	GDP-L-gulose	C16H25N5O16P2		
				13	GDP-glucose	C16H25N5O16P2		
				37	UDP-2-acetamido-4-dehydro-2,6-dideoxyglucose	C17H25N3O16P2		
				37	UDP-2-acetamido-2,6-dideoxy-beta-L-arabino-hexos-4-ulose	C17H25N3O16P2		
				19	ADP-Mannose	C16H25N5O15P2		
				19	GDP-6-deoxy-D-mannose	C16H25N5O15P2		
				19	GDP-6-deoxy-D-talose	C16H25N5O15P2		
				19	GDP-L-fucose	C16H25N5O15P2		
				19	ADP-glucose	C16H25N5O15P2		
				19	Adenosine Diphosphate Glucose	C16H25N5O15P2		
				19	Guanosine diphosphofucose	C16H25N5O15P2		
DNL	628.056975				N/A			
DLD	628.05145			23	GDP-Man	C16H25N5O16P2		
				23	GDP-L-galactose	C16H25N5O16P2		
				23	GDP-L-gulose	C16H25N5O16P2		

				23	GDP-glucose	C16H25N5O16P2		
				27	UDP-2-acetamido-4-dehydro-2,6-dideoxyglucose	C17H25N3O16P2		
				27	UDP-2-acetamido-2,6-dideoxy-beta-L-arabino-hexos-4-ulose	C17H25N3O16P2		
				9	ADP-Mannose	C16H25N5O15P2		
				9	GDP-6-deoxy-D-mannose	C16H25N5O15P2		
				9	GDP-6-deoxy-D-talose	C16H25N5O15P2		
				9	GDP-L-fucose	C16H25N5O15P2		
				9	ADP-glucose	C16H25N5O15P2		
				9	Adenosine Diphosphate Glucose	C16H25N5O15P2		
				9	Guanosine diphosphofucose	C16H25N5O15P2		
606.4	ANL	606.352375			N/A			
		606.373			N/A			
		606.46275			N/A			
	ALD	606.351925			N/A			
		606.4089			N/A			
		606.4843			N/A			
	BNL	606.3389		38	Taxine B	C33H45NO8		
		606.326833 3			N/A			
		606.4735			N/A			
	BLD	606.3685			N/A			
		606.4304			N/A			
	CNL	606.38195			N/A			
		606.43045			N/A			
		606.4735			N/A			
	CLD	606.3362			N/A			
		606.414275			N/A			
		606.495			N/A			

	DNL	606.349275				N/A		
		606.4544				N/A		
	DLD	606.40505				N/A		
557.2	ANL	557.2052			33	7-Dehydrologanin tetraacetate	C25H32O14	
					33	Deutzioside pentaacetate	C25H32O14	
					17	punaglandin 1	C27H37ClO10	
					31	11-Hydroxyiridodial glucoside pentaacetate	C26H36O13	
					10	3,4,7-Trihydroxy-5-methoxy-8-prenylflavan 7-O-beta-D-glucopyranoside	C27H34O11	
					10	Undulatone	C27H34O11	
					10	Arctiin	C27H34O11	
					10	Forsythin	C27H34O11	
					10	Myricatomentoside II	C27H34O11	
					25	all-trans-pentaprenyl diphosphate	C25H44O7P2	
					25	Geranylarnesyl diphosphate	C25H44O7P2	
		557.2672			24	Ingenol 3,20-dibenzoate	C34H36O7	
					26	Pyropheophorbide a	C33H34N4O3	
	ALD	557.1794			12	7-Dehydrologanin tetraacetate	C25H32O14	
					12	Deutzioside pentaacetate	C25H32O14	
					29	Dalpanin	C26H30O12	
					35	Undulatone	C27H34O11	
					35	Myricatomentoside II	C27H34O11	
					39	Gossypol	C30H30O8	
					1	Provincialin	C27H34O10	
	BNL	557.2052			33	7-Dehydrologanin tetraacetate	C25H32O14	
					33	Deutzioside pentaacetate	C25H32O14	
					31	11-Hydroxyiridodial glucoside pentaacetate	C26H36O13	
					31	8-epi-11-Hydroxyiridodial glucoside pentaacetate	C26H36O13	

			10	Undulatone	C27H34O11		
			10	Myricatomentoside II	C27H34O11		
			25	all-trans-pentaprenyl diphosphate	C25H44O7P2		
			25	Geranylarnesyl diphosphate	C25H44O7P2		
	557.2672		24	Ingenol 3,20-dibenzoate	C34H36O7		
BLD	557.1846		26	Pyropheophorbide a	C33H34N4O3		
			3	7-Dehydrologanin tetraacetate	C25H32O14		
			3	Deutzioside pentaacetate	C25H32O14		
			38	Dalpanin	C26H30O12		
			26	Undulatone	C27H34O11		
			26	Myricatomentoside II	C27H34O11		
			11	Provincialin	C27H34O10		
CNL	557.22065		3	11-Hydroxyiridodial glucoside pentaacetate	C26H36O13		
			3	8-epi-11-Hydroxyiridodial glucoside pentaacetate	C26H36O13		
			38	Undulatone	C27H34O11		
			38	Myricatomentoside II	C27H34O11		
			2	all-trans-pentaprenyl diphosphate	C25H44O7P2		
			2	Geranylarnesyl diphosphate	C25H44O7P2		
			15	7-Dehydrologanin tetraacetate	C25H32O14		
CLD	557.1949		15	Deutzioside pentaacetate	C25H32O14		
			7	Undulatone	C27H34O11		
	557.2465		7	Myricatomentoside II	C27H34O11		
			29	Provincialin	C27H34O10		
	557.2465		10	Pyropheophorbide a	C33H34N4O3		
DNL	557.2759						
DLD	557.1623		36	Phellamurin	C26H30O11		

Table A3.5: Total % ion count of discriminatory mass bins (m/z) for organic layer in negative mode for all leaves, new leaves, and old leaves. Error bars denote standard error to 1 standard deviation (σ).

m/z	All Leaves	New Leaves	Old Leaves
113			
155			
194.2			
195			
205			
249			
265.4			

Table A3.5: Continued.

<i>m/z</i>	All Leaves	New Leaves	Old Leaves
311.4			
325.4			
339.4			
363			
385			
395			
405.4			

Table A3.5: Continued.

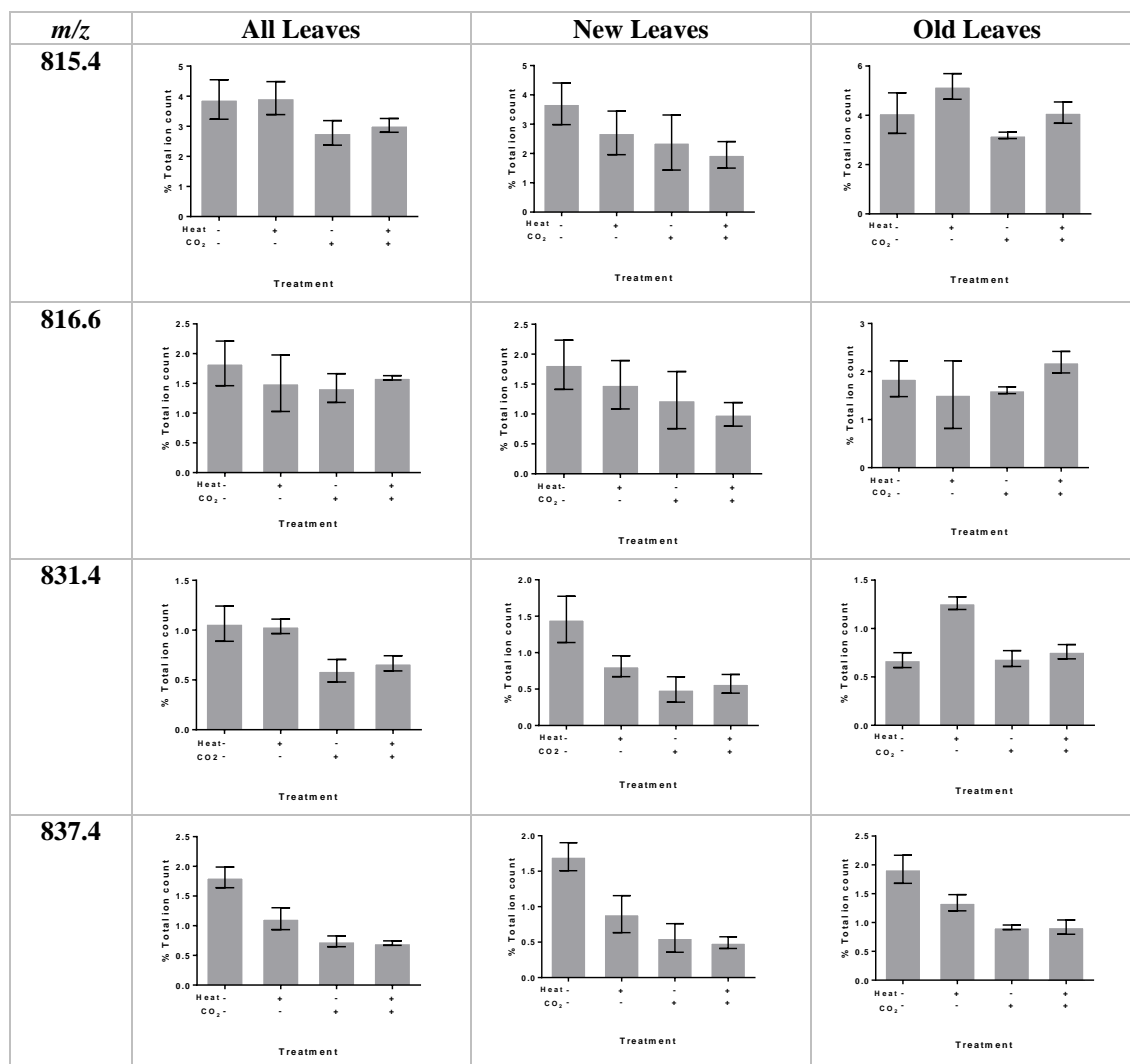
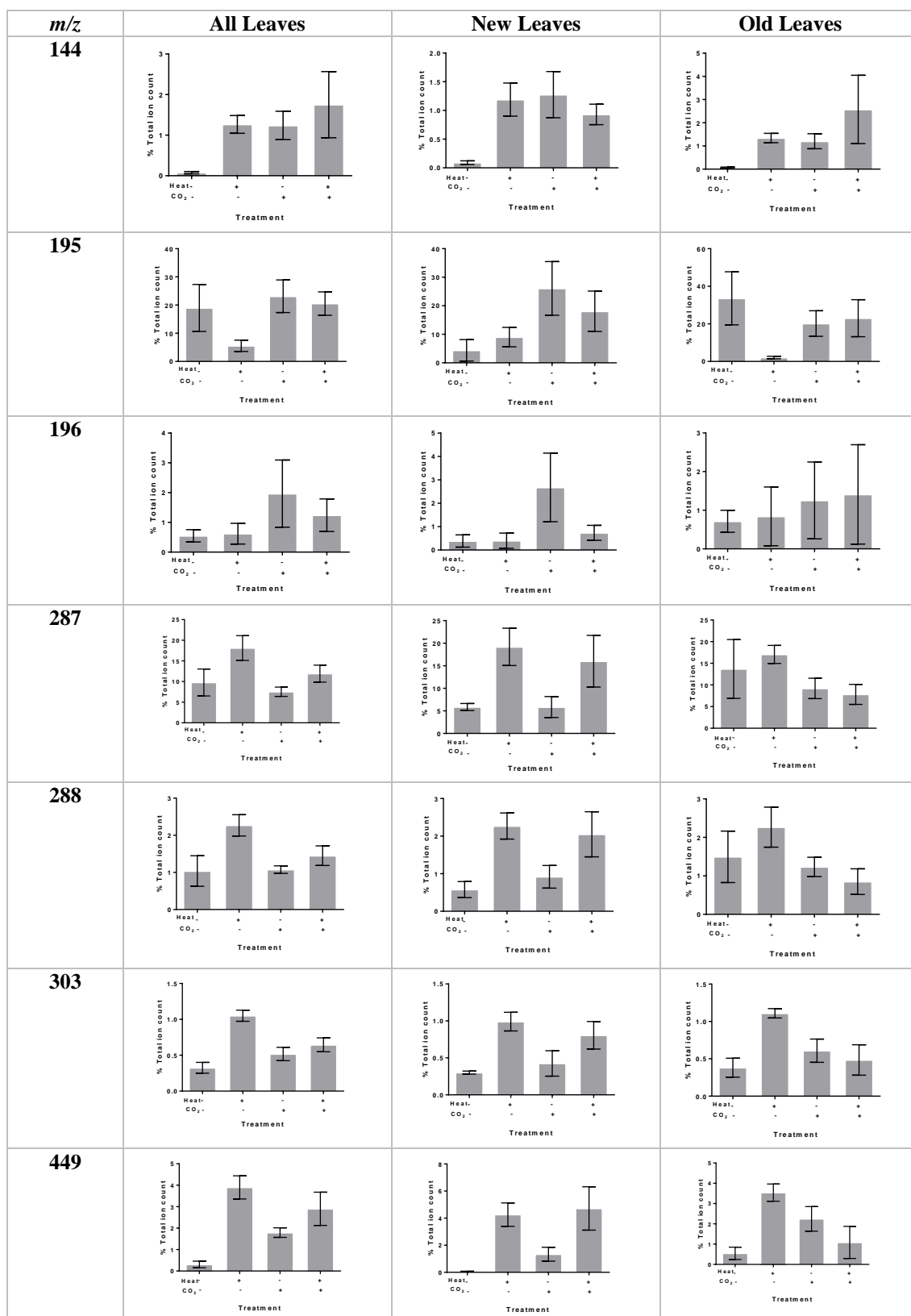


Table A3.6: Total % ion count of discriminatory mass bins (m/z) for aqueous layer in positive mode for all leaves, new leaves, and old leaves. Error bars denote standard error to 1 standard deviation (σ).



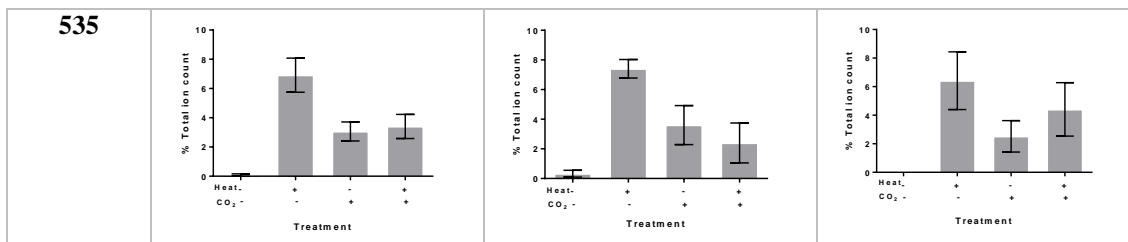


Table A3.6: Continued.

Table A3.7: Total % ion count of discriminatory mass bins (m/z) for organic layer in positive mode for all leaves, new leaves, and old leaves. Error bars denote standard error to 1 standard deviation (σ).

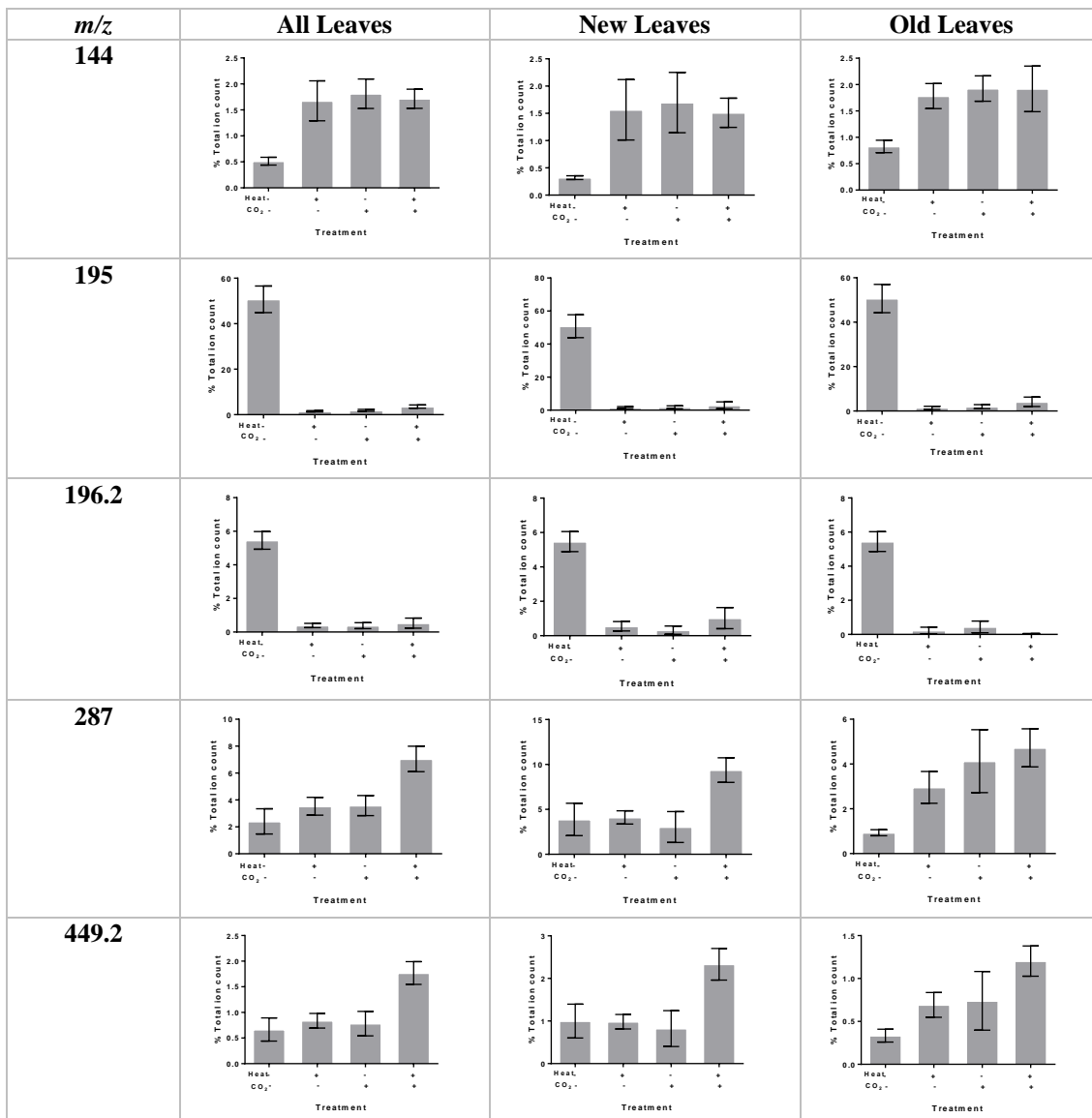


Table A3.7 Continued.

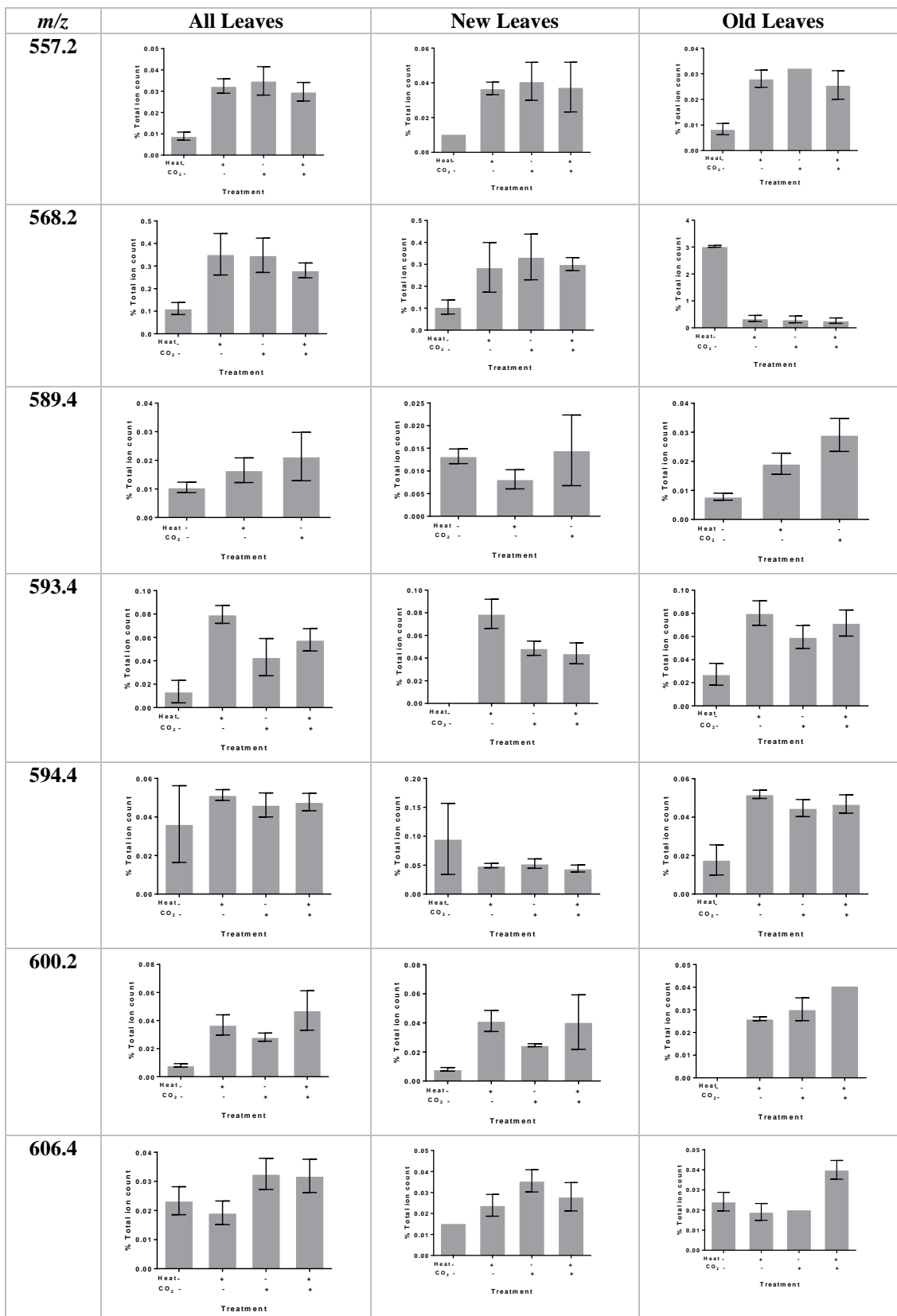


Table A3.7 Continued.

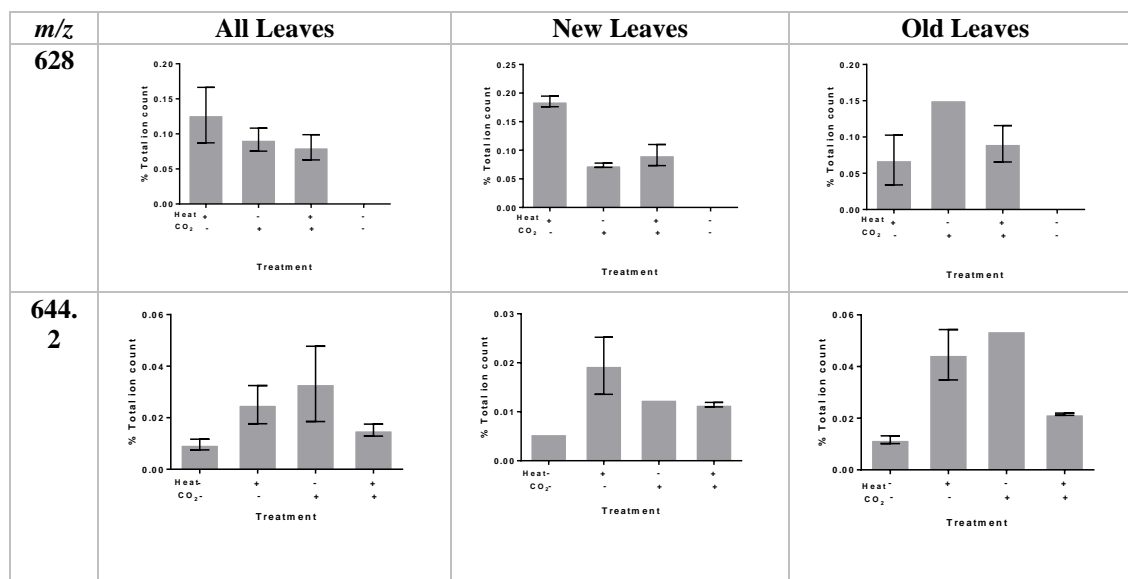


Table A3.8: Results of two-way ANOVA statistical significance of % ion count intensities of the 4 treatments (all leaves) and their pairwise comparisons for the discriminatory mass bins for organic layer, negative ionisation mode. DF = degrees of freedom (& associated error); F = F-value; P = P-value (significant if p < 0.05).

M/Z	CO ₂			Heat			CO ₂ *Heat		
	DF	F	P	DF	F	P	DF	F	P
113	1, 12	56.13	<0.001	1, 12	56.39	<0.001	1, 12	56.27	<0.001
155	1, 12	7.46	0.018	1, 12	7.46	0.018	1, 12	7.44	0.018
194.2	1, 12	39.61	<0.001	1, 12	10.5	0.007	1, 12	5.73	0.034
195	1, 12	29.18	<0.001	1, 12	15.09	0.002	1, 12	9.33	0.01
205	1, 12	4.25	0.062	1, 12	4.01	0.068	1, 12	4.05	0.067
249	1, 12	7.78	0.016	1, 12	6.59	0.025	1, 12	5.19	0.042
265.4	1, 12	12.07	0.005	1, 12	2.69	0.127	1, 12	5.42	0.038
311.4	1, 12	12.94	0.004	1, 12	9.97	0.008	1, 12	8.87	0.012
325.4	1, 12	12.36	0.004	1, 12	0.56	0.467	1, 12	6.96	0.022
339.4	1, 12	2.97	0.111	1, 12	0.00	0.992	1, 12	1.35	0.269
363	1, 12	22.14	0.001	1, 12	21.9	0.001	1, 12	20.99	0.001
385	1, 12	1.19	0.297	1, 12	5.28	0.04	1, 12	4.03	0.068
395	1, 12	11.04	0.006	1, 12	11.44	0.005	1, 12	10.5	0.007
405.4	1, 12	6.66	0.024	1, 12	2.27	0.158	1, 12	4.12	0.065
815.4	1, 12	4.28	0.061	1, 12	0.09	0.768	1, 12	0.04	0.836
816.6	1, 12	0.25	0.627	1, 12	0.06	0.81	1, 12	0.6	0.454
831.4	1, 12	12.94	0.004	1, 12	0.04	0.843	1, 12	0.18	0.675
837.4	1, 12	29.91	<0.001	1, 12	7.14	0.02	1, 12	5.97	0.031

Table A3.9: Results of two-way ANOVA statistical significance of % ion count intensities of the 4 treatments (new leaves) and their pairwise comparisons for the discriminatory mass bins for organic layer, negative ionisation mode. DF = degrees of freedom (& associated error); F = F-value; P = P-value (significant if $p < 0.05$).

<i>M/Z</i>	CO₂			Heat			CO₂*Heat		
	DF	F	P	DF	F	P	DF	F	P
113	1,12	3.15	0.110	1,12	3.16	0.109	1,12	3.17	0.109
155	1,12	6.79	0.026	1,12	6.75	0.027	1,12	6.74	0.027
194.2	1,12	11.49	0.005	1,12	1.73	0.213	1,12	3.41	0.09
195	1,12	8.68	0.012	1,12	2.56	0.136	1,12	5.40	0.039
205	1,12	9.02	0.011	1,12	8.70	0.012	1,12	8.74	0.012
249	1,12	2.89	0.115	1,12	2.16	0.167	1,12	0.32	0.58
265.4	1,12	2.65	0.142	1,12	0.22	0.649	N/A	N/A	N/A
311.4	1,12	0.07	0.792	1,12	4.06	0.079	1,12	0.00	0.960
325.4	1,12	4.13	0.073	1,12	0.10	0.759	1,12	0.83	0.385
339.4	1,12	1.79	0.213	1,12	0.09	0.768	1,12	1.36	0.274
363	1,12	5.84	0.034	1,12	5.65	0.037	1,12	5.08	0.046
385	1,12	0.71	0.415	1,12	4.27	0.061	1,12	1.21	0.293
395	1,12	4.09	0.068	1,12	4.31	0.062	1,12	3.87	0.075
405.4	1,12	3.02	0.108	1,12	1.56	0.235	1,12	1.56	0.236
815.4	1,12	1.99	0.184	1,12	0.93	0.354	1,12	0.15	0.703
816.6	1,12	1.96	0.186	1,12	0.55	0.474	1,12	0.02	0.904
831.4	1,12	8.6	0.013	1,12	1.89	0.195	1,12	3.07	0.105
837.4	1,12	15.5	0.002	1,12	4.97	0.046	1,12	3.59	0.082

Table A3.10: Results of two-way ANOVA statistical significance of % ion count intensities of the 4 treatments (old leaves) and their pairwise comparisons for the discriminatory mass bins for organic layer, negative ionisation mode. DF = degrees of freedom (& associated error); F = F-value; P = P-value (significant if $p < 0.05$).

<i>M/Z</i>	CO₂			Heat			CO₂*Heat		
	DF	F	P	DF	F	P	DF	F	P
113	1,12	924.81	<0.000	1,12	927.78	<0.000	1,12	924.59	<0.000
155	1,12	20.39	0.001	1,12	20.41	0.001	1,12	20.37	0.001
194.2	1,12	66.59	<0.000	1,12	26.1	<0.000	1,12	3.65	0.080
195	1,12	52.26	<0.000	1,12	40.45	<0.000	1,12	6.87	0.022
205	1,12	1.77	0.210	1,12	1.65	0.226	1,12	1.62	0.230
249	1,12	9.31	0.010	1,12	8.29	0.014	1,12	9.67	0.009
265.4	1,12	0.10	0.755	1,12	0.11	0.744	1,12	13.23	0.007
311.4	1,12	12.97	0.006	1,12	5.29	0.047	1,12	12.88	0.006
325.4	1,12	1.41	0.265	1,12	0.17	0.688	1,12	3.75	0.085
339.4	1,12	7.31	0.024	1,12	0.02	0.898	1,12	11.24	0.008
363	1,12	5.96	0.033	1,12	6.04	0.032	1,12	5.91	0.033
385	1,12	0.93	0.354	1,12	3.6	0.082	1,12	3.98	0.069
395	1,12	3.34	0.093	1,12	3.44	0.089	1,12	3.25	0.097
405.4	1,12	6.80	0.023	1,12	0.33	0.579	1,12	2.67	0.128
815.4	1,12	3.36	0.092	1,12	3.47	0.087	1,12	0.02	0.884
816.6	1,12	0.27	0.610	1,12	0.09	0.768	1,12	1.21	0.292
831.4	1,12	10.63	0.007	1,12	19.55	0.0001	1,12	12.08	0.005
837.4	1,12	21.28	0.001	1,12	3.48	0.087	1,12	3.56	0.084

Table A3.11: Results of two-way ANOVA statistical significance of % ion count intensities of the 4 treatments (all leaves) and their pairwise comparisons for the discriminatory mass bins for aqueous layer positive ionisation mode. DF = degrees of freedom (& associated error); F = F-value; P = P-value (significant if p <0.05).

<i>M/Z</i>	CO₂			Heat			CO₂*Heat		
	DF	F	P	DF	F	P	DF	F	P
144	1, 12	3.26	0.096	1, 12	3.47	0.087	1, 12	0.55	0.473
195	1, 12	2.96	0.111	1, 12	2.07	0.176	1, 12	0.95	0.349
196	1, 12	2.39	0.148	1, 12	0.25	0.629	1, 12	0.36	0.557
287	1, 12	2.83	0.118	1, 12	6.43	0.026	1, 12	0.62	0.447
288	1, 12	1.83	0.201	1, 12	7.78	0.016	1, 12	2.22	0.162
303	1, 12	1.52	0.241	1, 12	24.44	<0.001	1, 12	12	0.005
449	1, 12	0.25	0.629	1, 12	23.02	<0.001	1, 12	6.41	0.026
535	1, 12	0.11	0.742	1, 12	20.85	0.001	1, 12	17.04	0.001

Table A3.12: Results of two-way ANOVA statistical significance of % ion count intensities of the 4 treatments (new leaves) and their pairwise comparisons for the discriminatory mass bins for aqueous layer positive ionisation mode. DF = degrees of freedom (& associated error); F = F-value; P = P-value (significant if p <0.05).

<i>M/Z</i>	CO₂			Heat			CO₂*Heat		
	DF	F	P	DF	F	P	DF	F	P
144	1,12	3.07	0.105	1,12	2.04	0.179	1,12	7.47	0.018
195	1,12	5.74	0.034	1,12	0.07	0.796	1,12	0.97	0.343
196	1,12	2.84	0.118	1,12	1.53	0.240	1,12	1.57	0.234
287	1,12	0.18	0.679	1,12	9.87	0.008	1,12	0.18	0.680
288	1,12	0.02	0.881	1,12	12.86	0.004	1,12	0.51	0.490
303	1,12	0.04	0.845	1,12	12.03	0.005	1,12	1.00	0.338
449	1,12	0.84	0.379	1,12	16.09	0.002	1,12	0.18	0.675
535	1,12	0.01	0.913	1,12	3.37	0.100	1,12	1.00	0.343

Table A3.13: Results of two-way ANOVA statistical significance of % ion count intensities of the 4 treatments (old leaves) and their pairwise comparisons for the discriminatory mass bins for aqueous layer positive ionisation mode. DF = degrees of freedom (& associated error); F = F-value; P = P-value (significant if p <0.05).

<i>M/Z</i>	CO₂			Heat			CO₂*Heat		
	DF	F	P	DF	F	P	DF	F	P
144	1,12	2.43	0.145	1,12	3.03	0.107	1,12	0.00	0.954
195	1,12	0.17	0.691	1,12	2.40	0.148	1,12	3.44	0.088
196	1,12	0.63	0.441	1,12	0.12	0.738	1,12	0.04	0.844
287	1,12	3.07	0.105	1,12	0.06	0.806	1,12	0.37	0.556
288	1,12	3.16	0.101	1,12	0.17	0.689	1,12	1.49	0.245
303	1,12	1.84	0.200	1,12	4.24	0.062	1,12	8.48	0.013
449	1,12	0.45	0.514	1,12	2.64	0.130	1,12	13.60	0.003
535	1,12	0.51	0.493	1,12	5.83	0.036	1,12	11.57	0.007

Table A3.14: Results of two-way ANOVA statistical significance of % ion count intensities of the 4 treatments (all leaves) and their pairwise comparisons for the discriminatory mass bins for organic layer, positive ionisation mode. DF = degrees of freedom (& associated error); F = F-value; P = P-value (significant if $p < 0.05$).

<i>M/Z</i>	CO₂			Heat			CO₂*Heat		
	DF	F	P	DF	F	P	DF	F	P
144	1, 12	6.69	0.024	1, 12	4.23	0.062	1, 12	5.91	0.032
195	1, 12	62.1	<0.001	1, 12	64.2	<0.001	1, 12	73.49	<0.001
196.2	1, 12	59.12	<0.001	1, 12	58.76	<0.001	1, 12	66.08	<0.001
287	1, 12	7.94	0.015	1, 12	7.61	0.017	1, 12	1.97	0.186
449.2	1, 12	6.14	0.029	1, 12	7.53	0.018	1, 12	3.73	0.077
557.2	1, 12	0.92	0.357	1, 12	3.63	0.081	1, 12	0.04	0.836
568.2	1, 12	1.69	0.218	1, 12	1.89	0.195	1, 12	5.93	0.031
589.4	1, 12	0.44	0.52	1, 12	1.83	0.201	1, 12	2.93	0.113
593.4	1, 12	0.12	0.733	1, 12	13.19	0.003	1, 12	5.3	0.04
594.4	1, 12	0.09	0.774	1, 12	0.59	0.456	1, 12	0.4	0.541
600.2	1, 12	0.37	0.553	1, 12	2.52	0.138	1, 12	4.42	0.057
606.4	1, 12	1.97	0.186	1, 12	0.01	0.913	1, 12	1.54	0.238
628	1, 12	0.14	0.717	1, 12	6.72	0.024	1, 12	4.21	0.063
644.2	1, 12	0.00	0.974	1, 12	1.18	0.299	1, 12	1.6	0.229

Table A3.15: Results of two-way ANOVA statistical significance of % ion count intensities of the 4 treatments (new leaves) and their pairwise comparisons for the discriminatory mass bins for organic layer, positive ionisation mode. DF = degrees of freedom (& associated error); F = F-value; P = P-value (significant if $p < 0.05$).

<i>M/Z</i>	CO₂			Heat			CO₂*Heat		
	DF	F	P	DF	F	P	DF	F	P
144	1,12	2.55	0.136	1,12	1.63	0.226	1,12	2.99	0.109
195	1,12	42.55	<0.000	1,12	43.43	<0.000	1,12	47.78	<0.000
196.2	1,12	25.83	<0.000	1,12	21.08	0.001	1,12	37.29	<0.000
287	1,12	2.27	0.158	1,12	5.00	0.045	1,12	4.32	0.060
449.2	1,12	2.76	0.123	1,12	4.45	0.057	1,12	4.64	0.052
557.2	1,12	1.01	0.362	1,12	0.55	0.492	1,12	0.91	0.383
568.2	1,12	2.34	0.155	1,12	0.87	0.371	1,12	1.81	0.206
589.4	1,12	0.03	0.873	1,12	0.44	0.544	N/A	N/A	N/A
593.4	1,12	5.35	0.054	1,12	0.06	0.813	N/A	N/A	N/A
594.4	1,12	0.52	0.498	1,12	0.68	0.442	1,12	0.32	0.591
600.2	1,12	2.91	0.139	1,12	12.16	0.013	1,12	1.55	0.259
606.4	1,12	1.92	0.215	1,12	0.00	0.959	1,12	0.85	0.393
628	1,12	15.09	0.030	1,12	0.54	0.515	N/A	N/A	N/A
644.2	1,12	0.00	0.953	1,12	0.79	0.416	1,12	1.06	0.350

Table A3.16: Results of two-way ANOVA statistical significance of % ion count intensities of the 4 treatments (old leaves) and their pairwise comparisons for the discriminatory mass bins for organic layer, positive ionisation mode. DF = degrees of freedom (& associated error); F = F-value; P = P-value (significant if p <0.05).

<i>M/Z</i>	CO₂			Heat			CO₂*Heat		
	DF	F	P	DF	F	P	DF	F	P
144	1,12	4.13	0.067	1,12	2.45	0.146	1,12	2.51	0.141
195	1,12	45.34	<0.000	1,12	47.50	<0.000	1,12	56.67	<0.000
196.2	1,12	54.94	<0.000	1,12	64.25	<0.000	1,12	47.23	<0.000
287	1,12	7.65	0.017	1,12	2.14	0.169	1,12	0.64	0.441
449.2	1,12	4.81	0.049	1,12	3.87	0.073	1,12	0.06	0.807
557.2	1,12	3.59	0.117	1,12	1.47	0.280	1,12	5.25	0.071
568.2	1,12	0.29	0.601	1,12	0.78	0.398	1,12	1.76	0.214
589.4	1,12	10.91	0.021	1,12	3.87	0.106	N/A	N/A	N/A
593.4	1,12	0.94	0.358	1,12	7.04	0.026	1,12	2.77	0.130
594.4	1,12	4.03	0.070	1,12	11.02	0.007	1,12	8.61	0.014
600.2	1,12	2.08	0.245	1,12	1.18	0.356	N/A	N/A	N/A
606.4	1,12	1.86	0.215	1,12	1.38	0.278	1,12	3.98	0.086
628	1,12	0.14	0.746	1,12	0.67	0.499	N/A	N/A	N/A
644.2	1,12	0.50	0.552	1,12	0.00	0.959	1,12	6.95	0.119

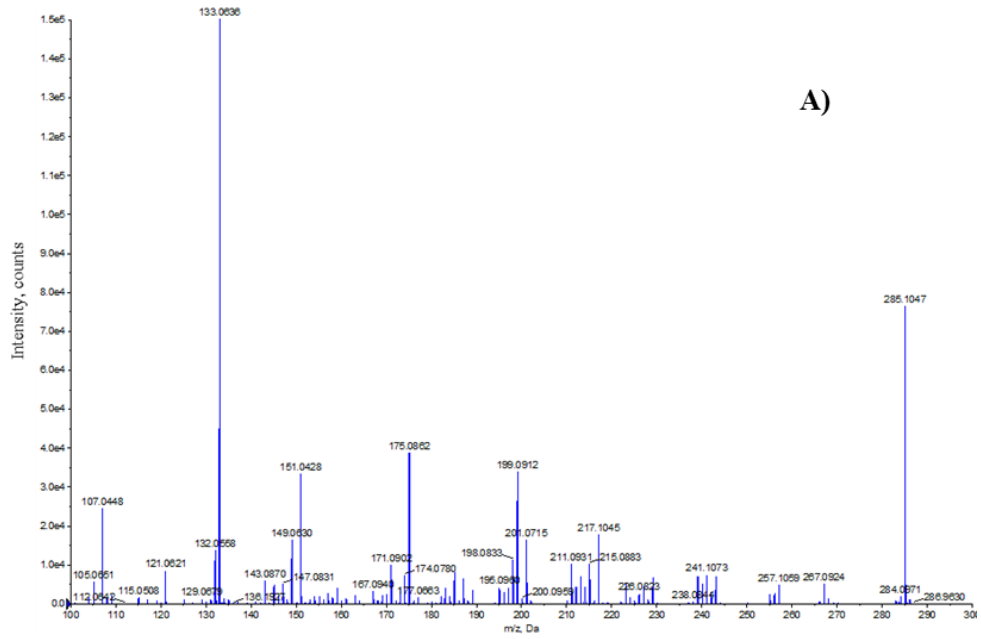


Figure A4.1: A) Luteolin standard in solution analysed in negative ESI mode. B) Cyanidin standard in solution analysed in negative ESI mode. C) Quercetin standard in solution analysed in negative ESI mode. D) DMAPP standard in solution analysed in negative ESI mode. E) GPP standard in solution analysed in negative ESI mode. F) IPP standard in solution analysed in negative ESI mode.

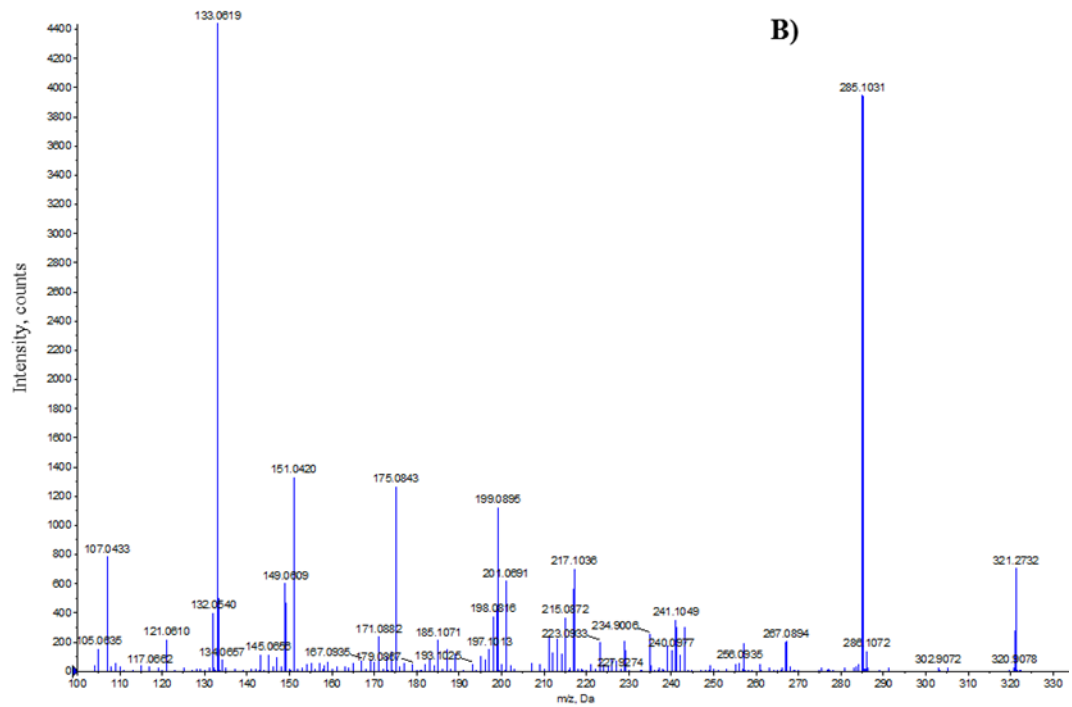


Figure 4.1: Continued.

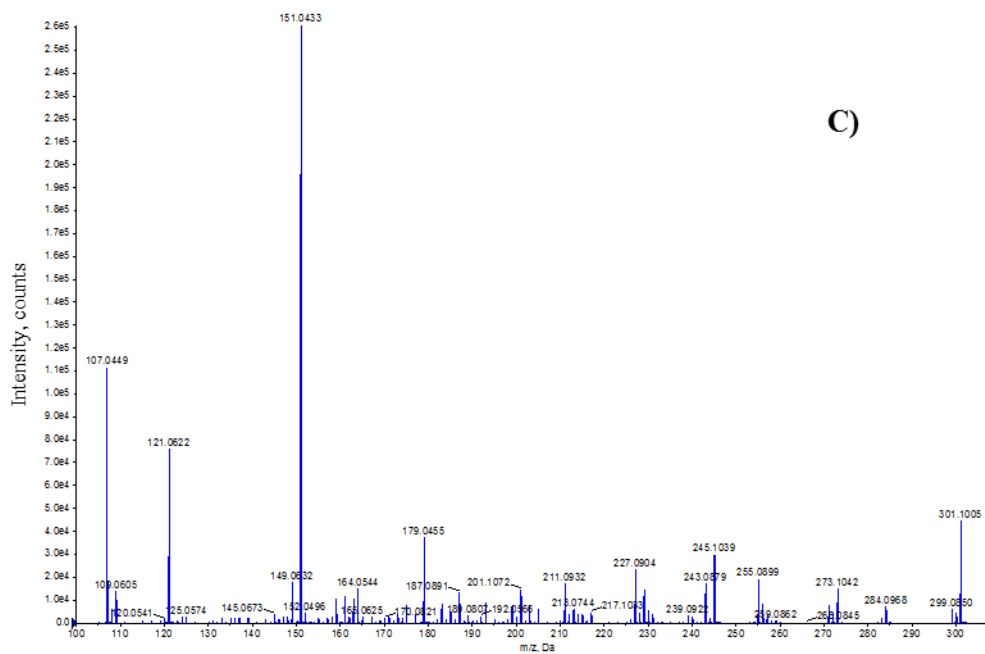


Figure 4.1: Continued.

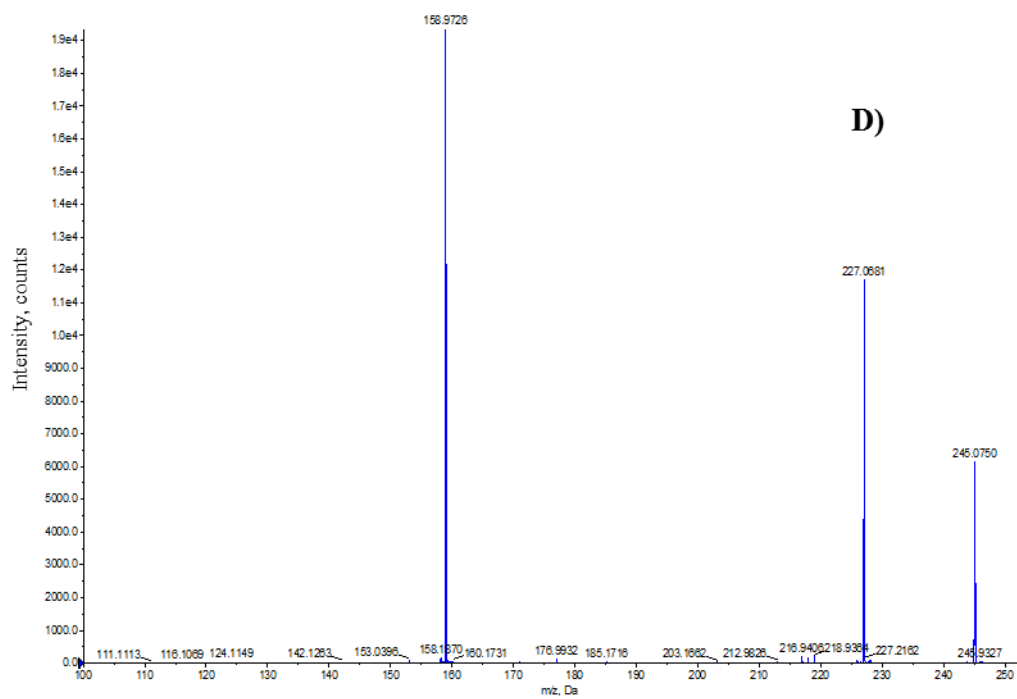


Figure 4.1: Continued.

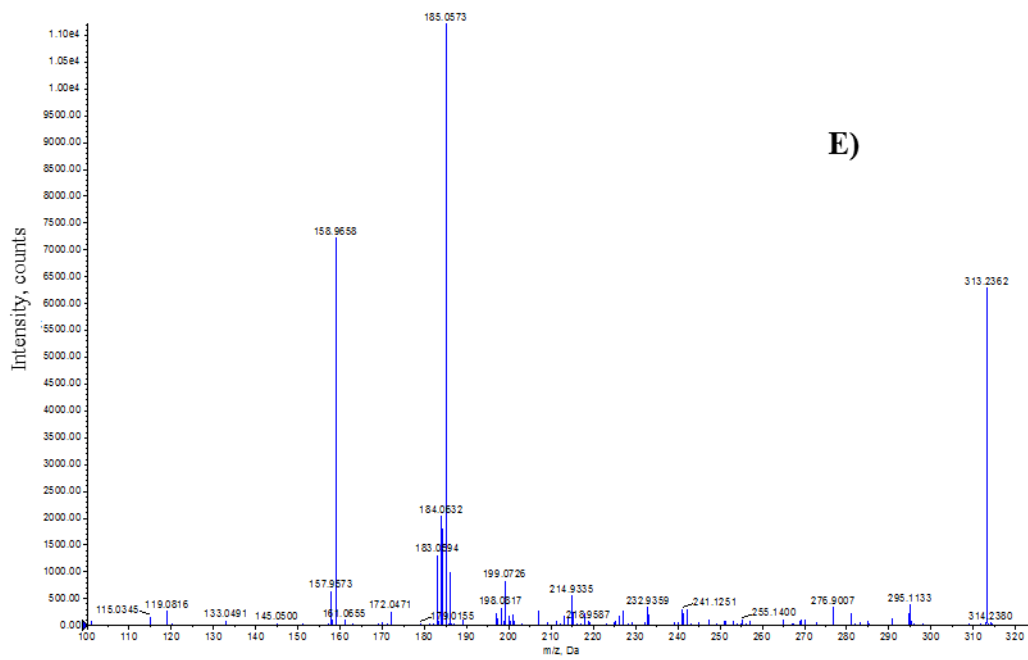


Figure 4.1: Continued.

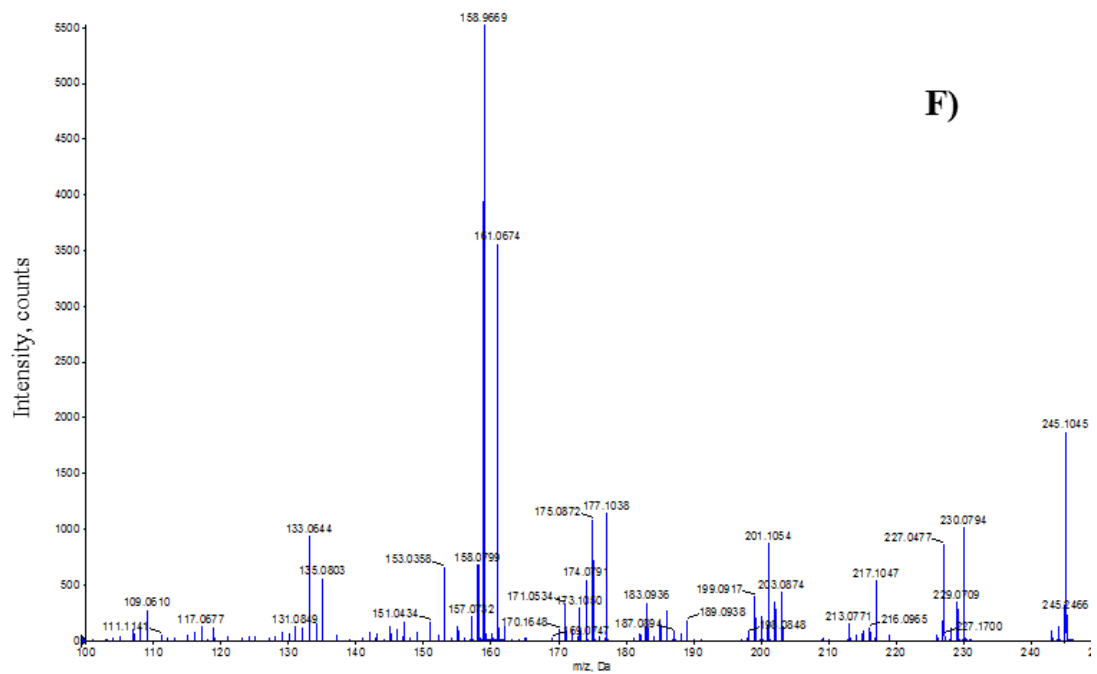


Figure 4.1: Continued.

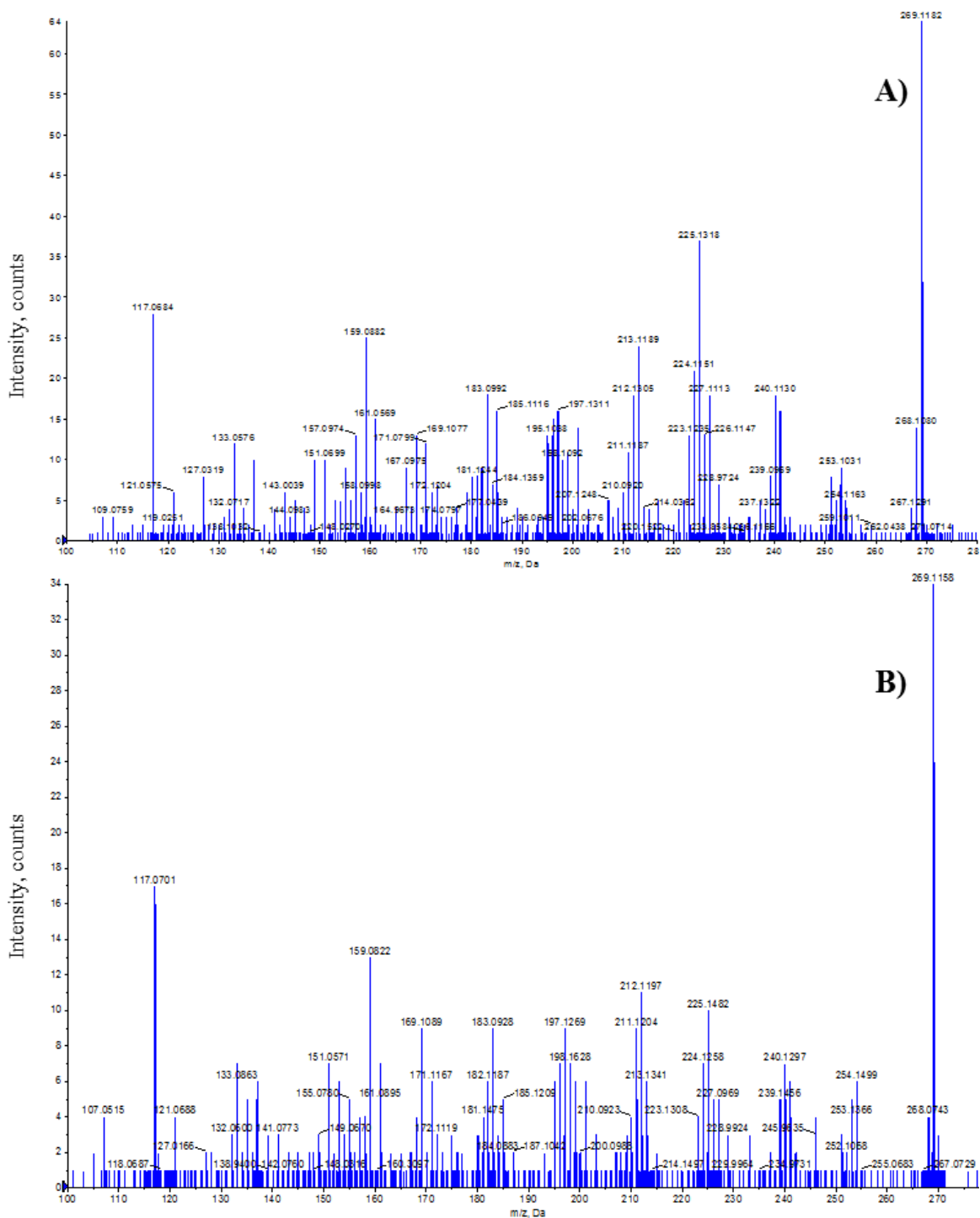


Figure A4.2: MS/MS fragmentation pattern of Apigenin analysed in negative ESI mode. A) Apigenin in heat shock & eCO₂ treatment, mature leaf, aqueous polar phase. B) Apigenin in heat shock & eCO₂ treatment, mature leaf, organic polar phase. C) Apigenin in heat shock treatment & eCO₂, new leaf, aqueous polar phase. D) Apigenin in heat sock & eCO₂ treatment, new leaf, organic polar phase. E) Apigenin in eCO₂ treatment, mature leaf, aqueous polar phase. F) Apigenin in eCO₂ treatment, mature leaf, organic polar phase. G) Apigenin in eCO₂ treatment, new leaf, aqueous polar phase. H) Apigenin in heat shock treatment, mature leaf, aqueous polar phase. I) Apigenin in heat shock treatment, mature leaf, organic polar phase. J) Apigenin in heat shock treatment, new leaf, aqueous polar phase. K) Apigenin in heat shock treatment, new leaf, organic polar phase. L) Apigenin in control treatment, mature leaf, aqueous polar phase. M) Apigenin in control treatment, mature leaf, organic polar phase. N) Apigenin in control treatment, new leaf, aqueous polar phase. O) Apigenin in control treatment, new leaf, organic polar phase.

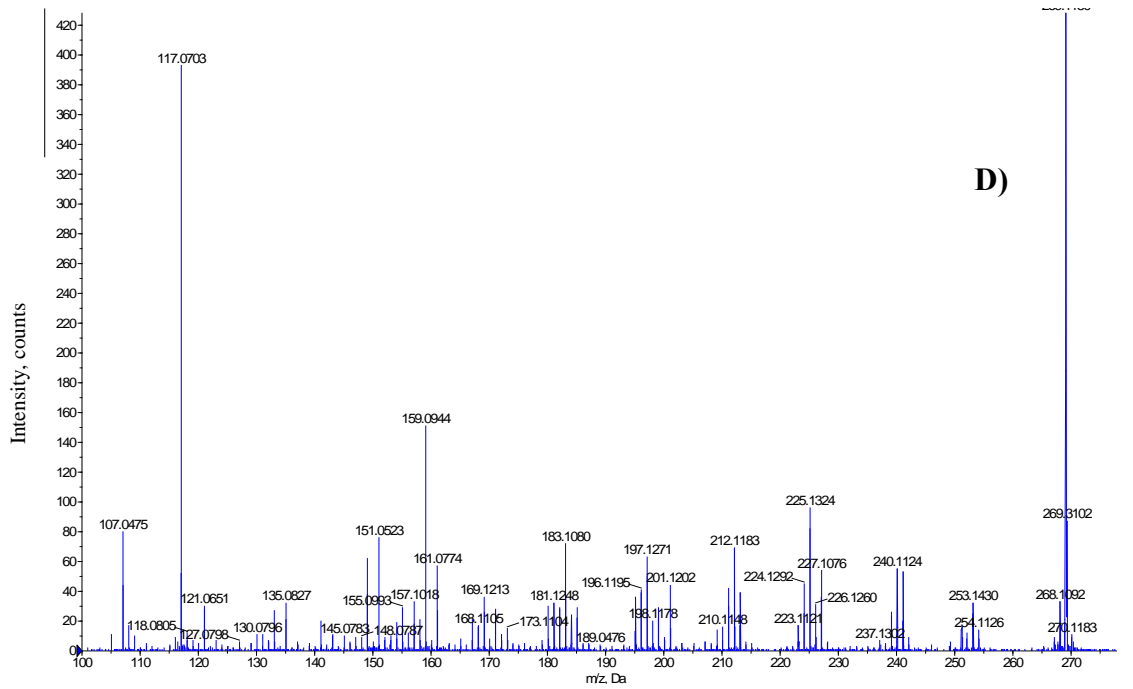
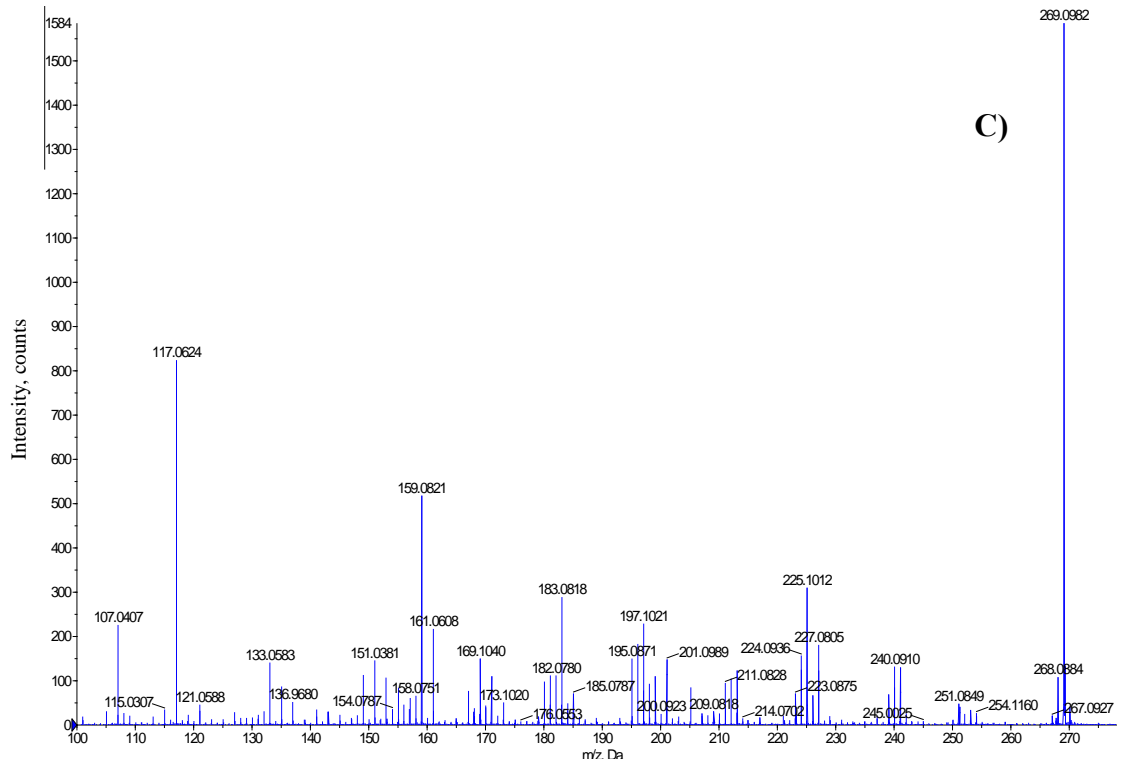


Figure 4.2: Continued.

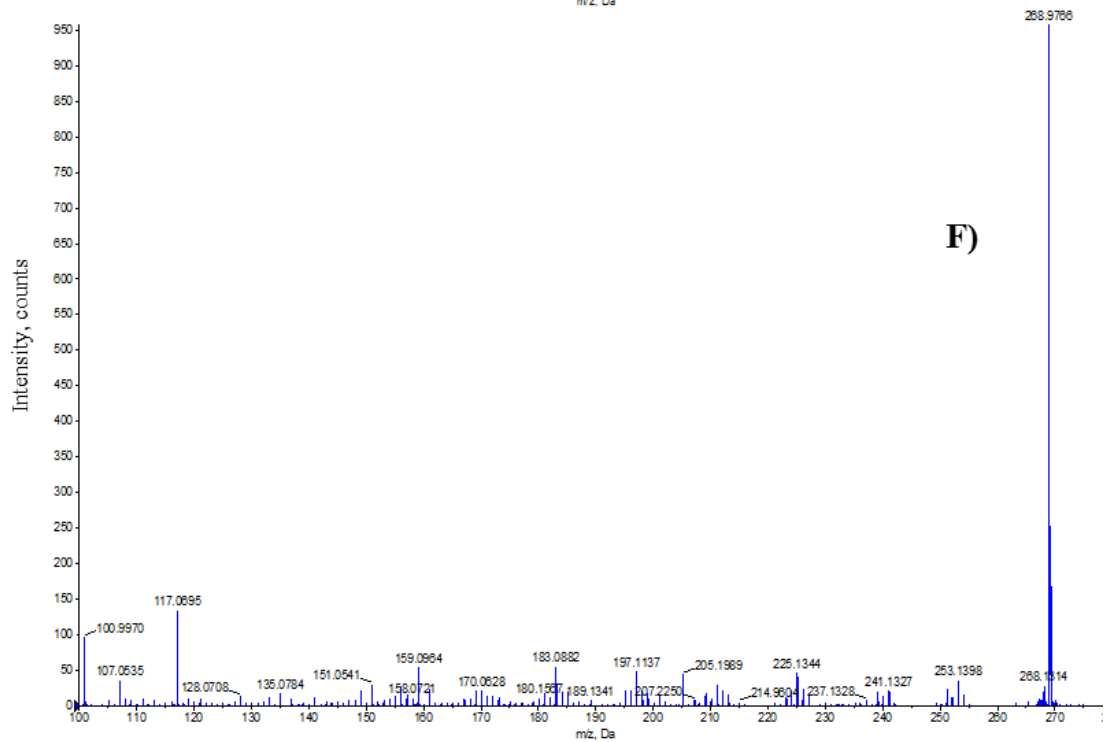
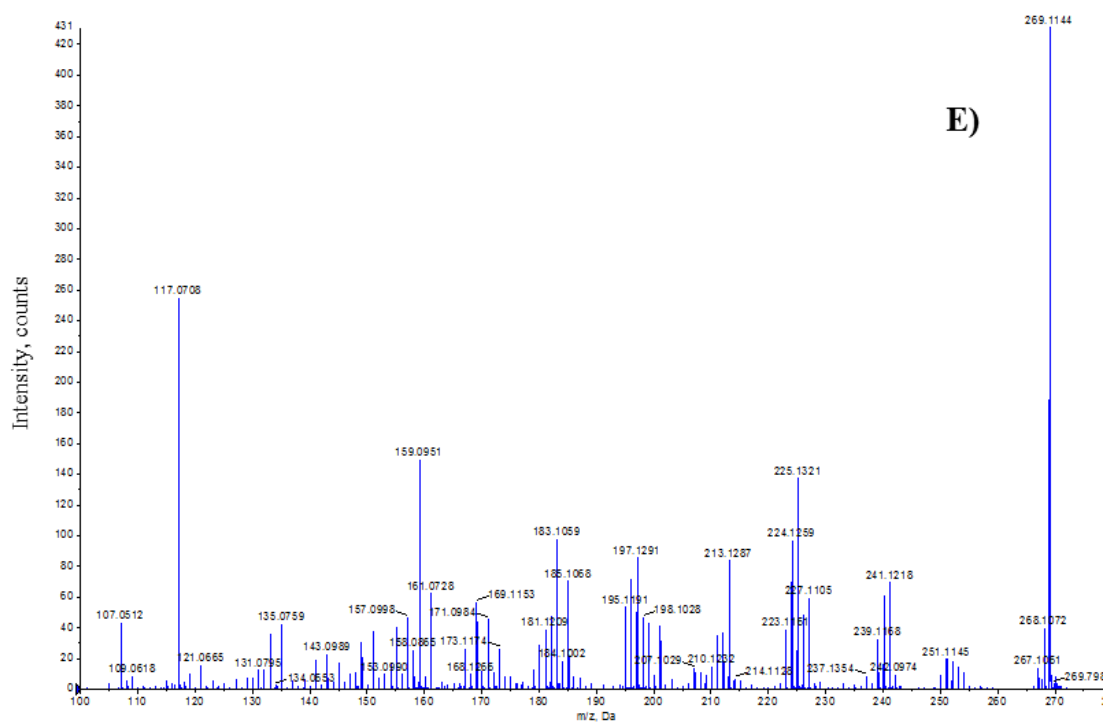


Figure 4.2: Continued.

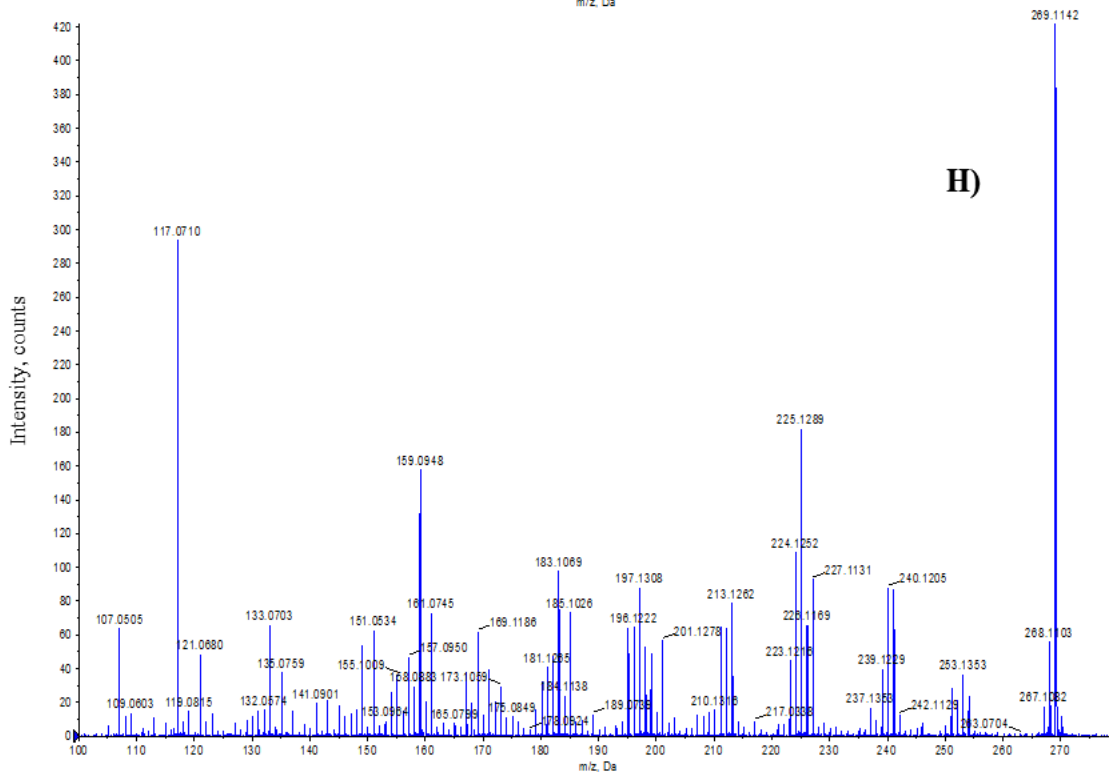
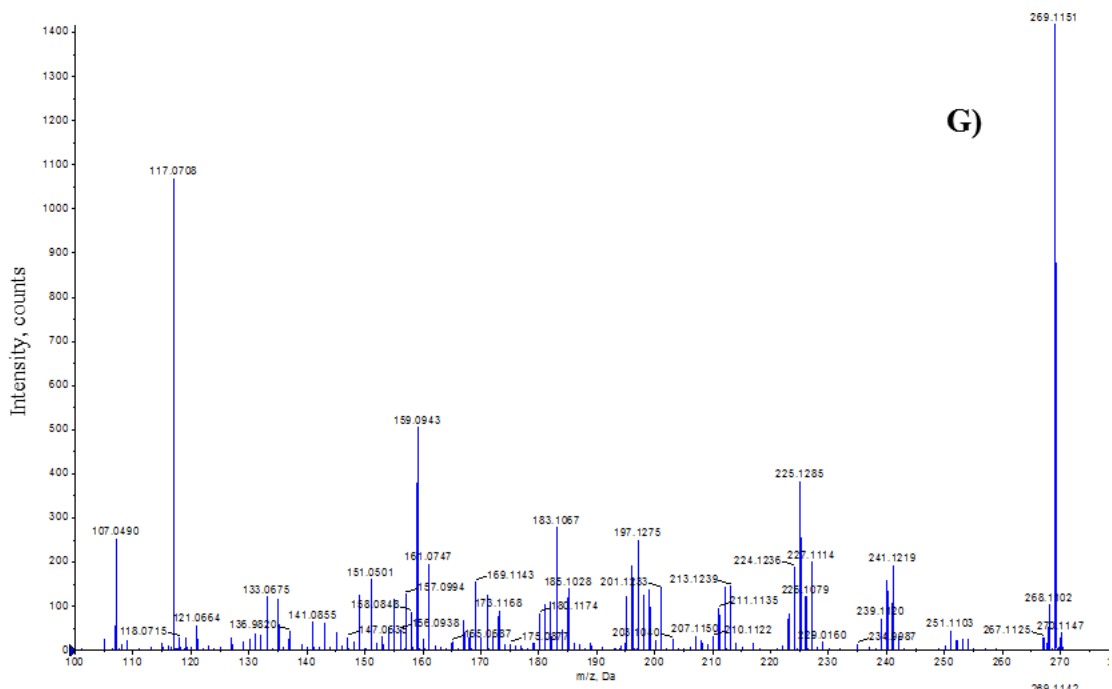


Figure 4.2: Continued.

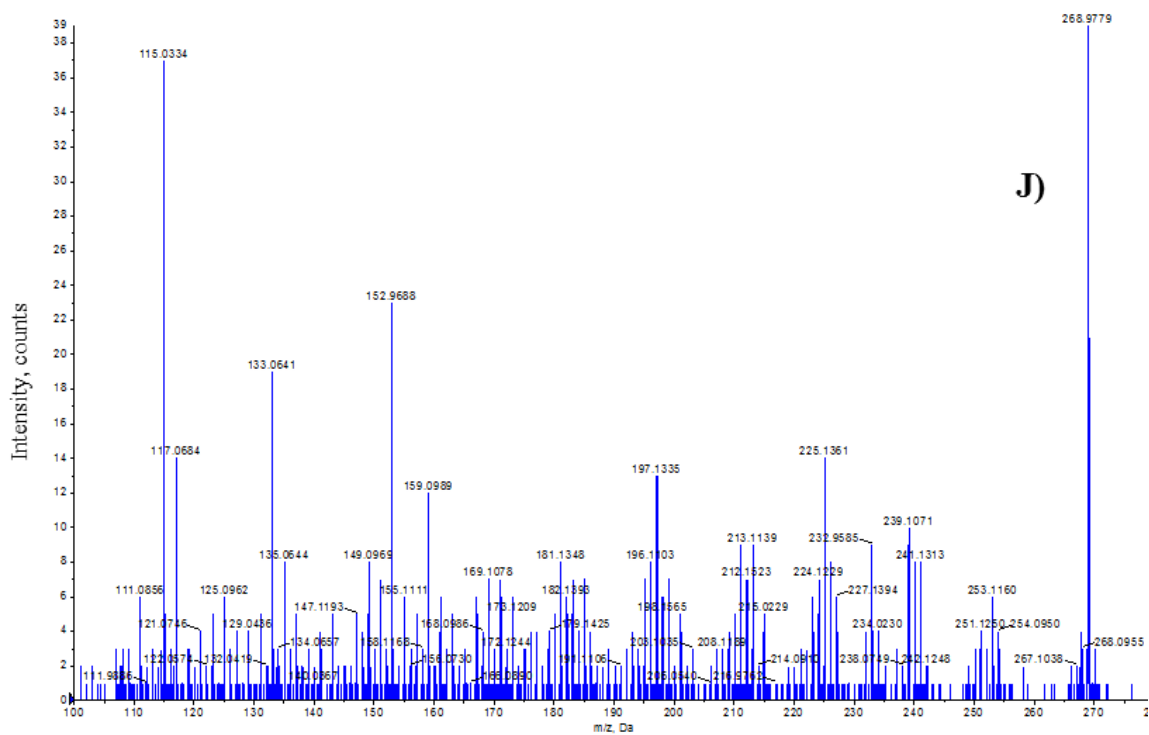
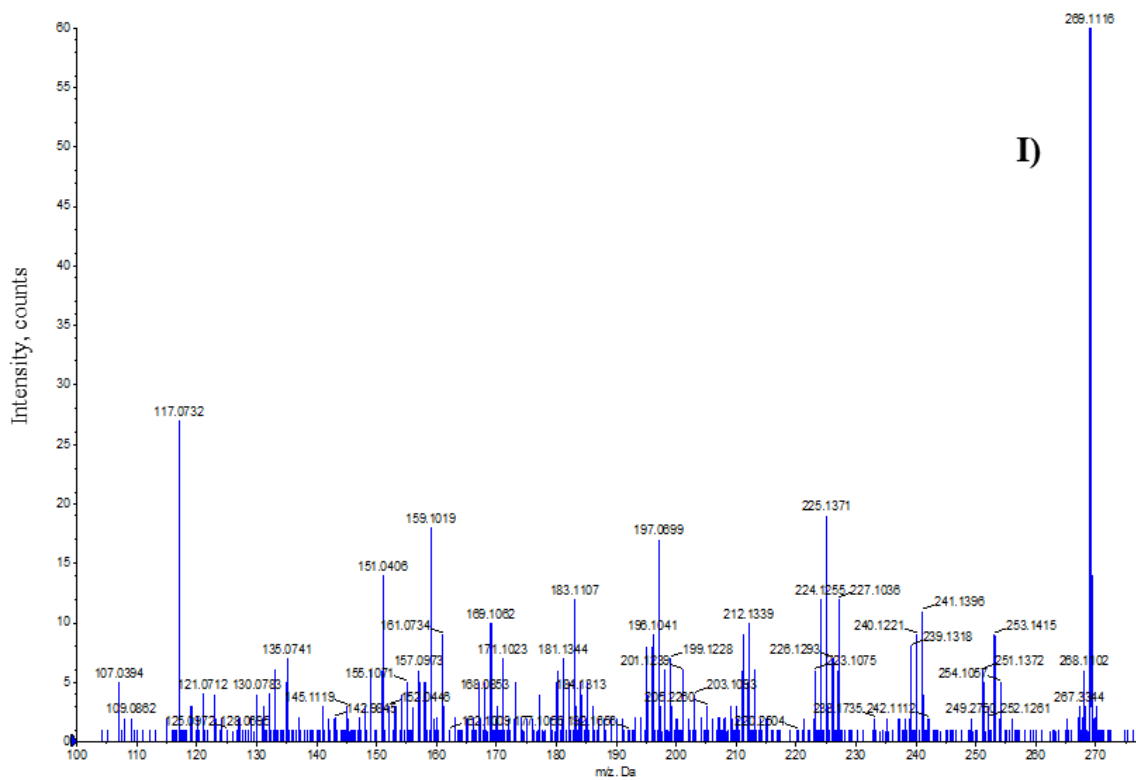


Figure 4.2: Continued.

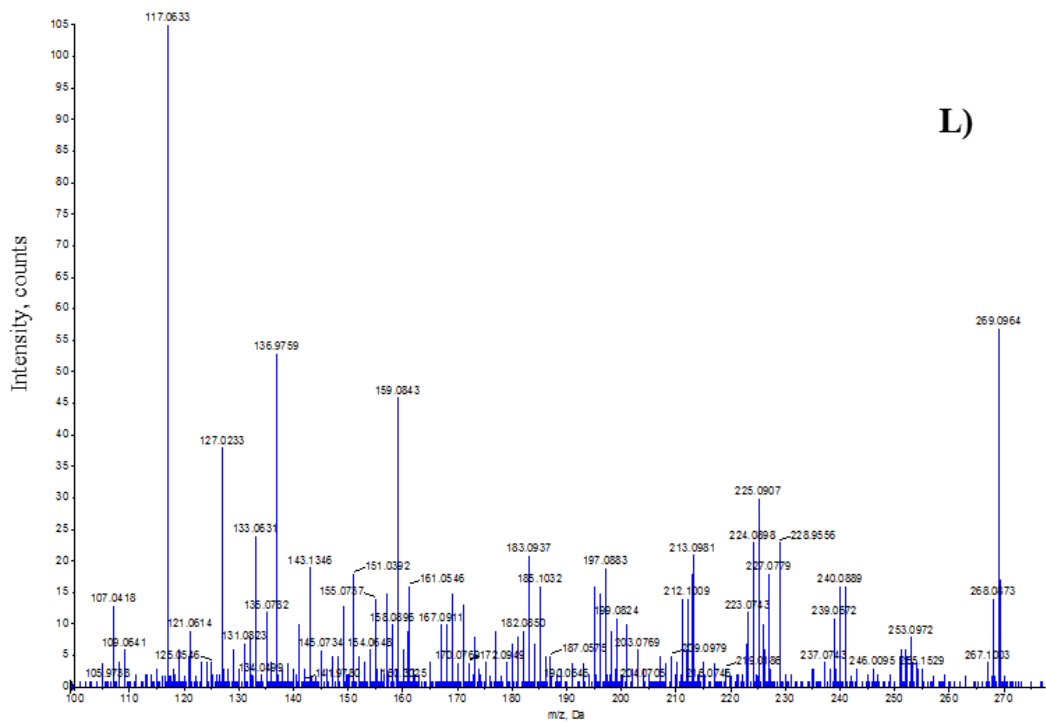
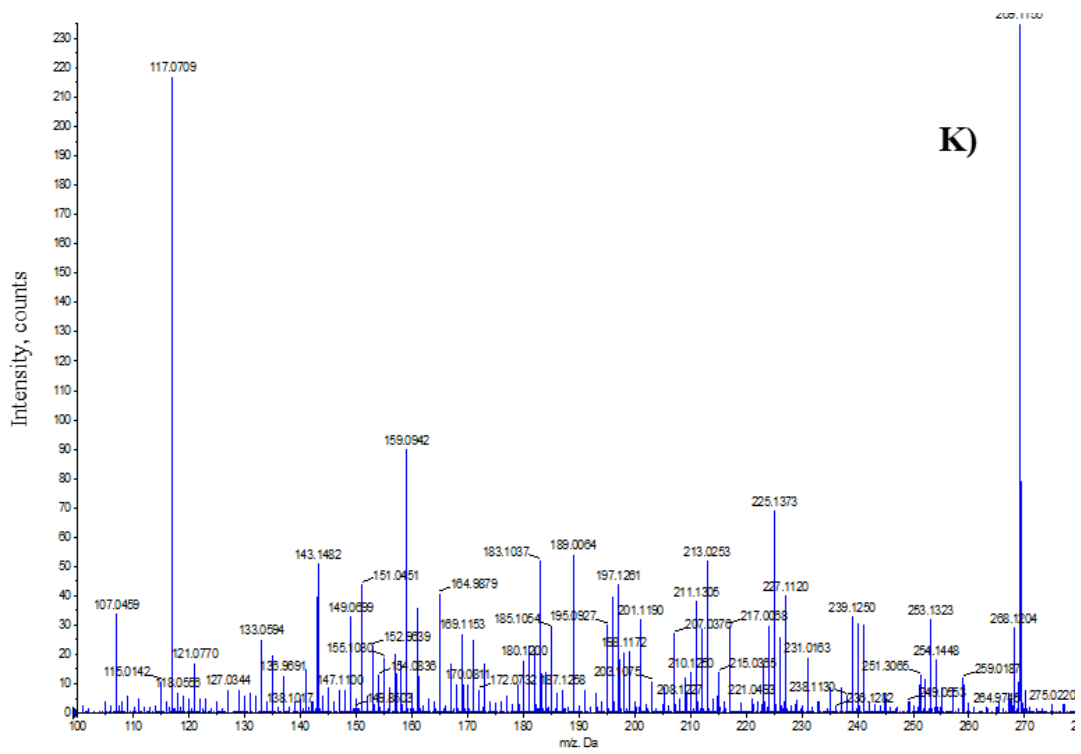
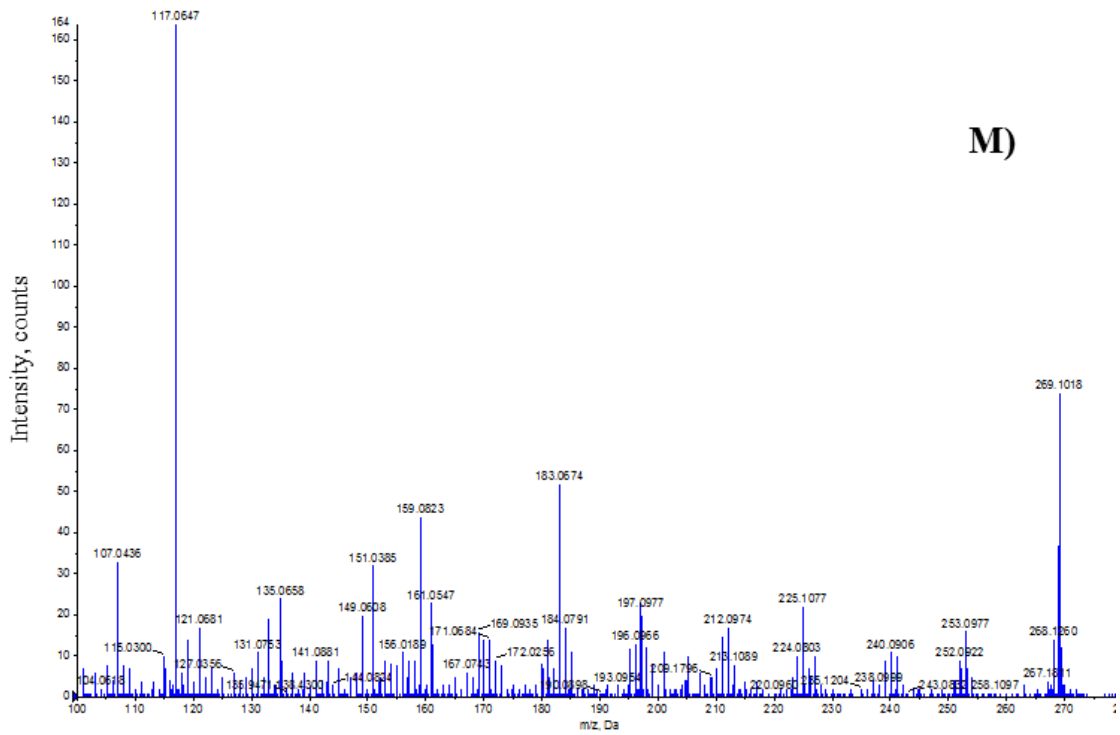
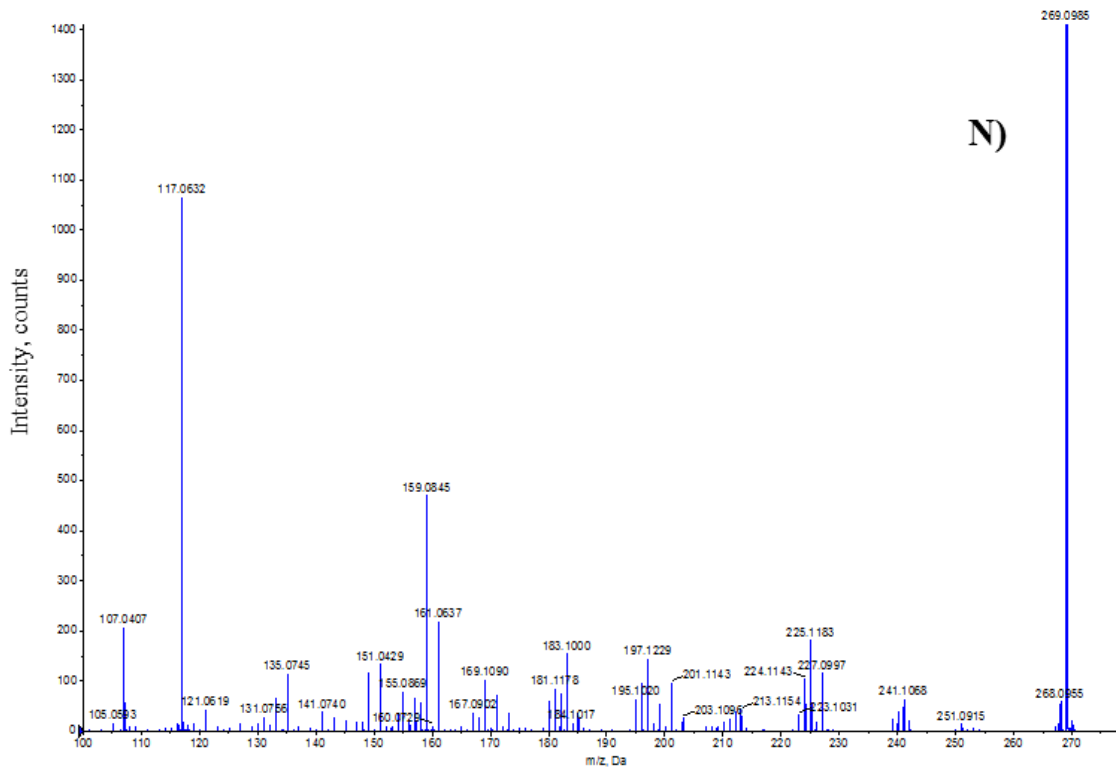


Figure 4.2: Continued.



M)



N)

Figure 4.2: Continued.

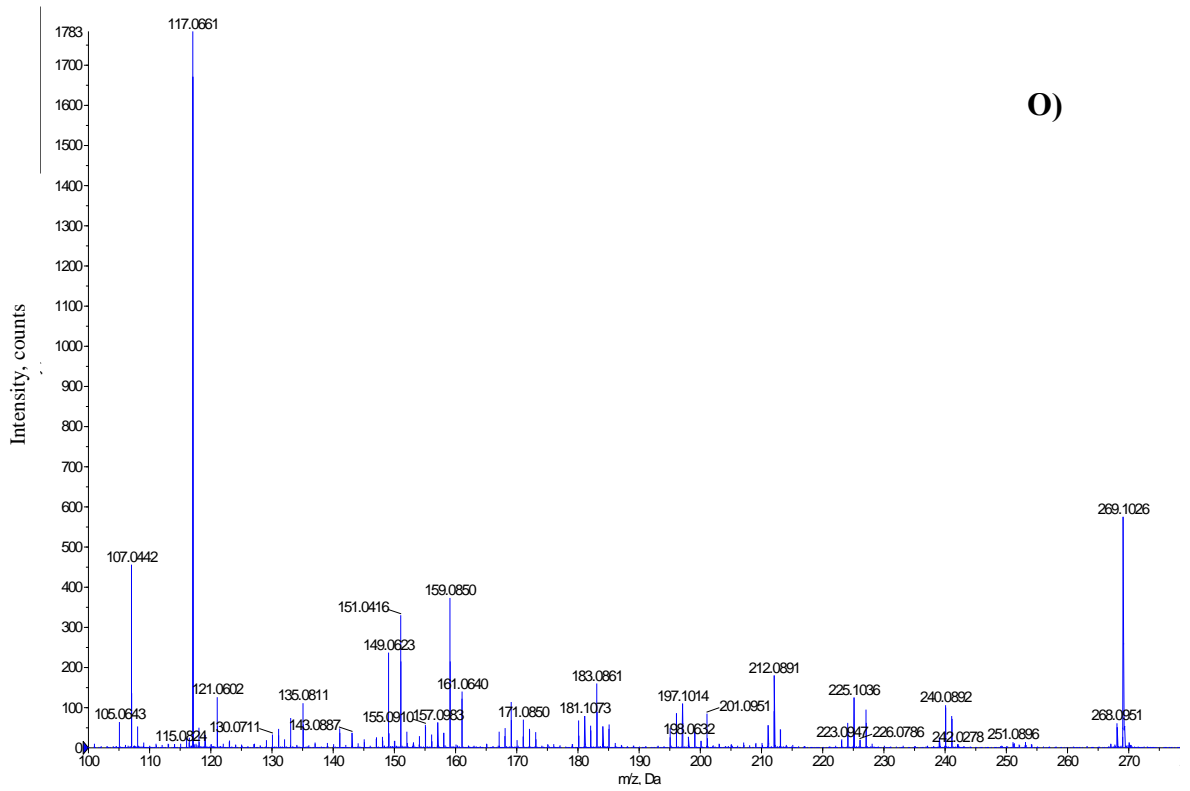


Figure 4.2: Continued.

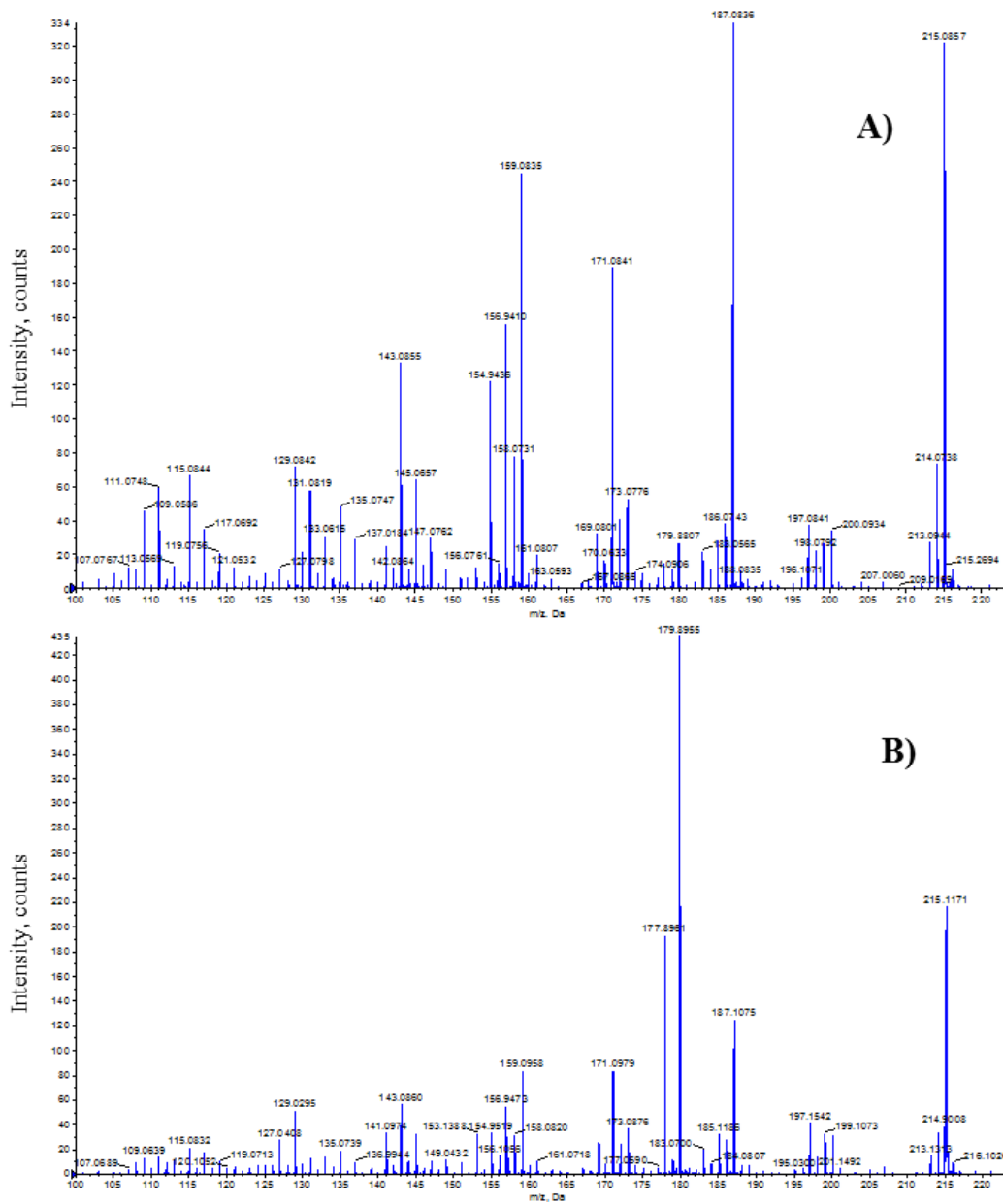


Figure A4.3: MS/MS fragmentation pattern of MEP analysed in negative ESI mode. A) MEP in heat shock & eCO₂ treatment, mature leaf, aqueous polar phase. B) MEP in heat shock & eCO₂ treatment, mature leaf, organic polar phase. C) MEP in heat shock treatment & eCO₂, new leaf, aqueous polar phase. D) MEP in heat sock & eCO₂ treatment, new leaf, organic polar phase. E) MEP in eCO₂ treatment, mature leaf, aqueous polar phase. F) MEP in eCO₂ treatment, mature leaf, organic polar phase. G) MEP in eCO₂ treatment, new leaf, aqueous polar phase. H) MEP in eCO₂ treatment, new leaf, organic polar phase. I) MEP in heat shock treatment, mature leaf, organic polar phase. J) MEP in heat shock treatment, new leaf, aqueous polar phase. K) MEP in heat shock treatment, new leaf, organic polar phase. L) MEP in control treatment, mature leaf, aqueous polar phase. M) MEP in control treatment, mature leaf, organic polar phase. N) MEP in control treatment, new leaf, aqueous polar phase. O) MEP in control treatment, new leaf, organic polar phase.

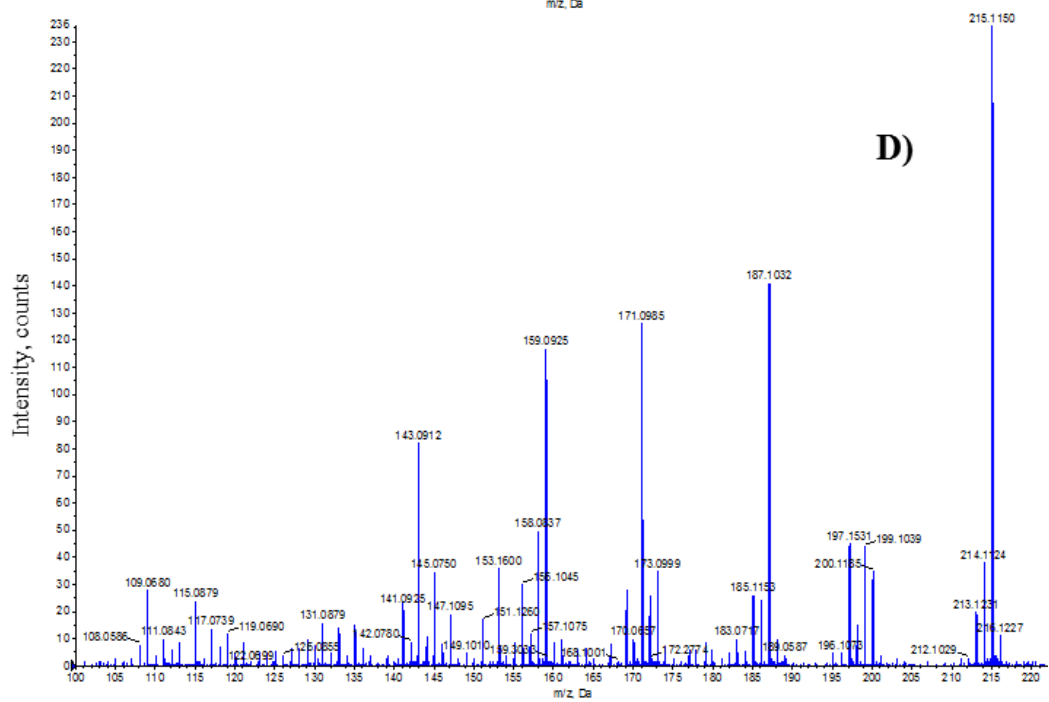
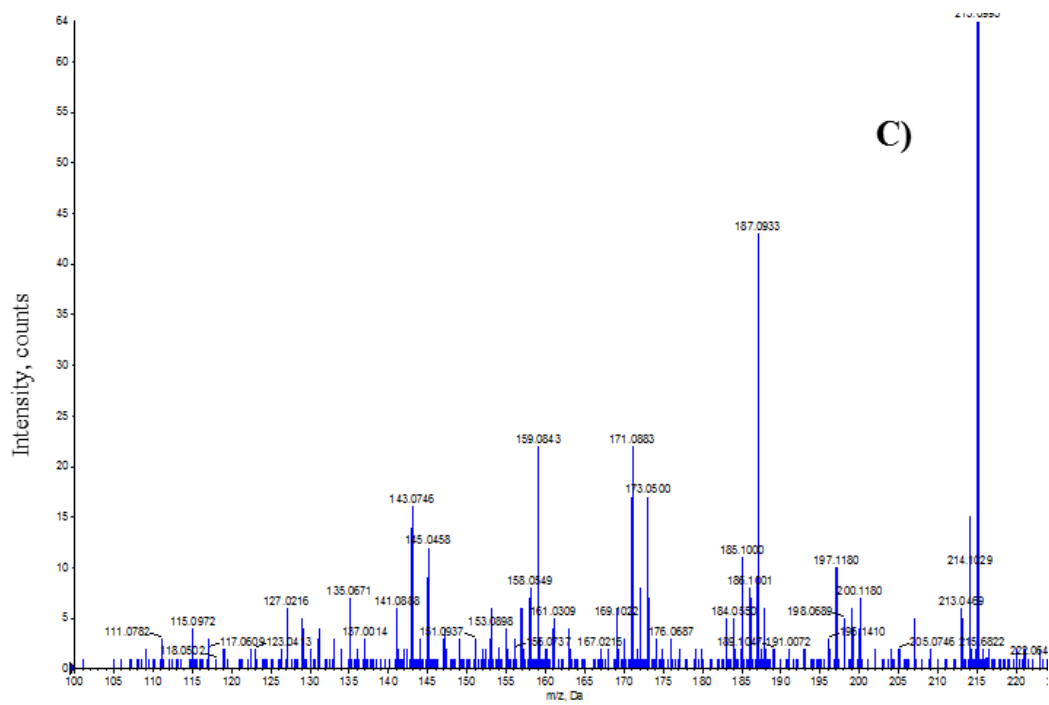


Figure 4.3: Continued.

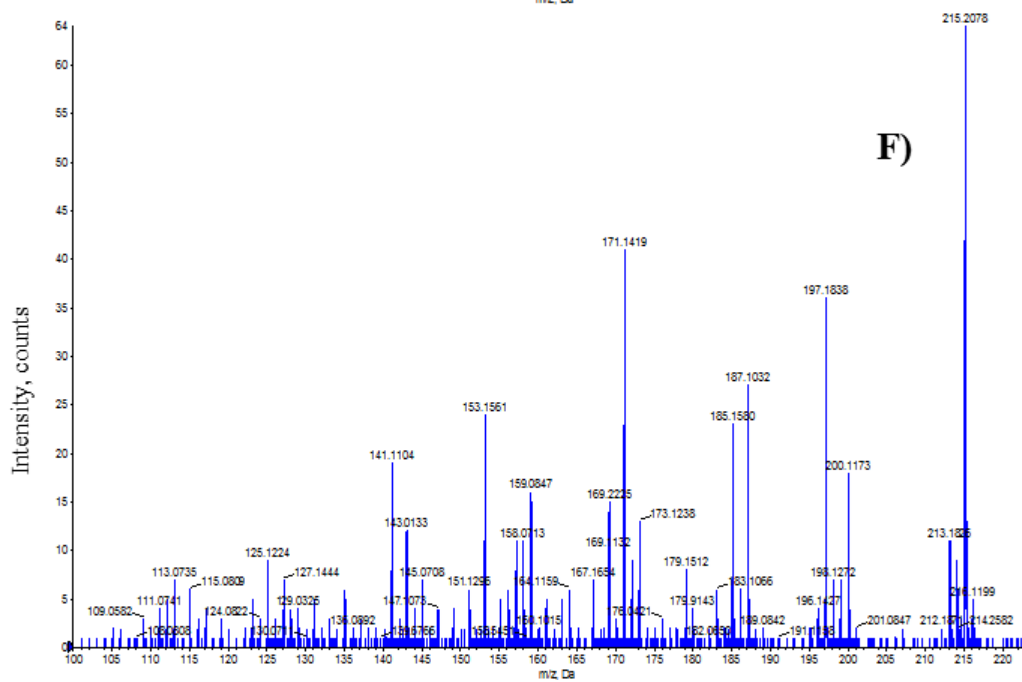
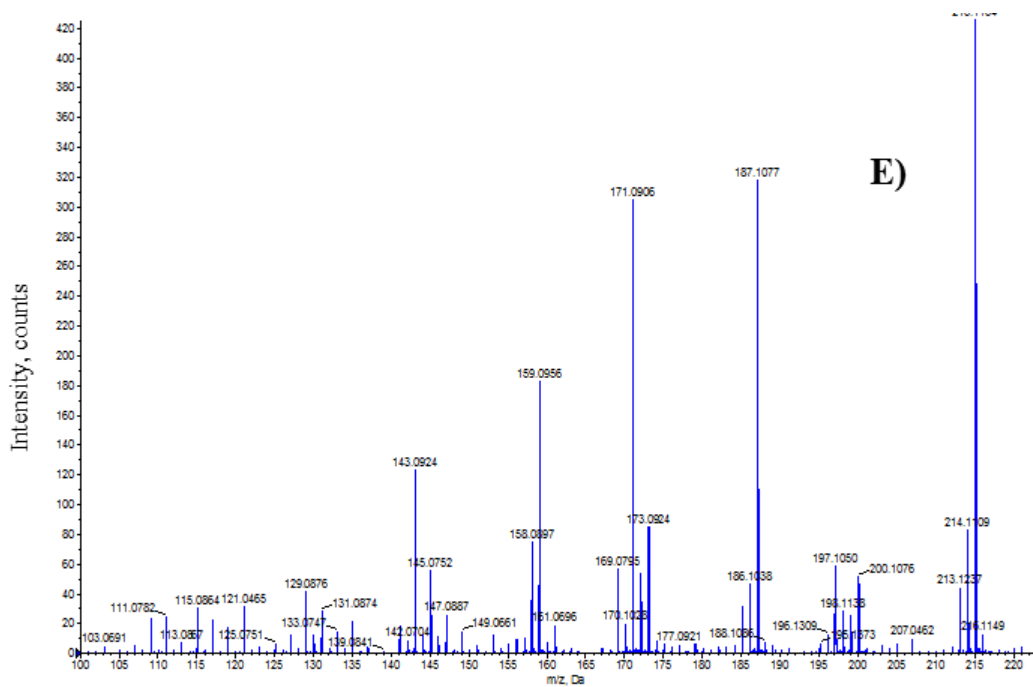


Figure 4.3: Continued.

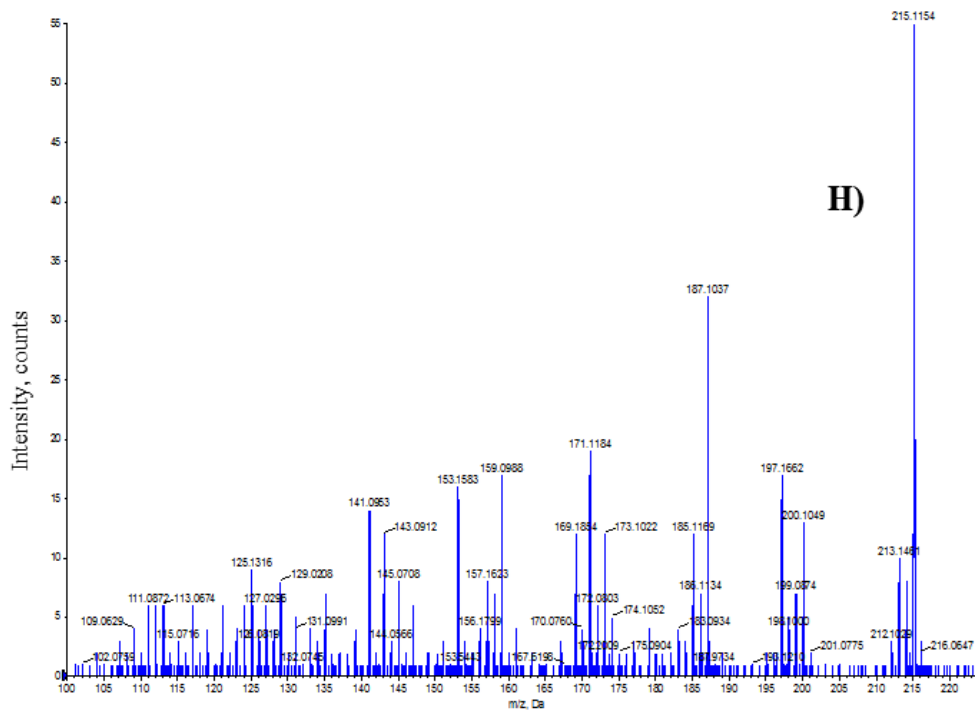
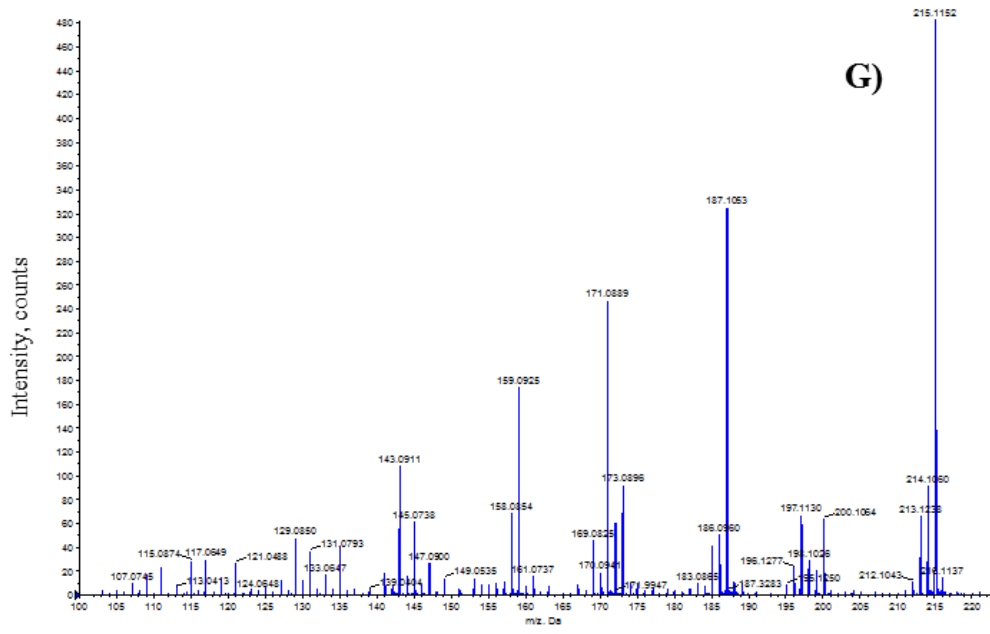


Figure 4.3: Continued.

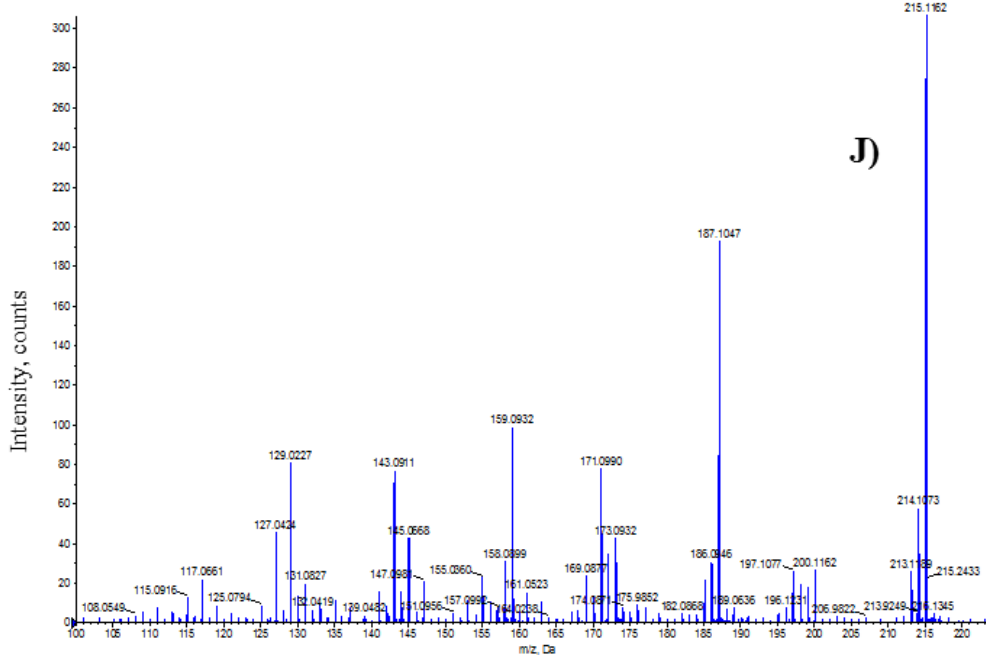
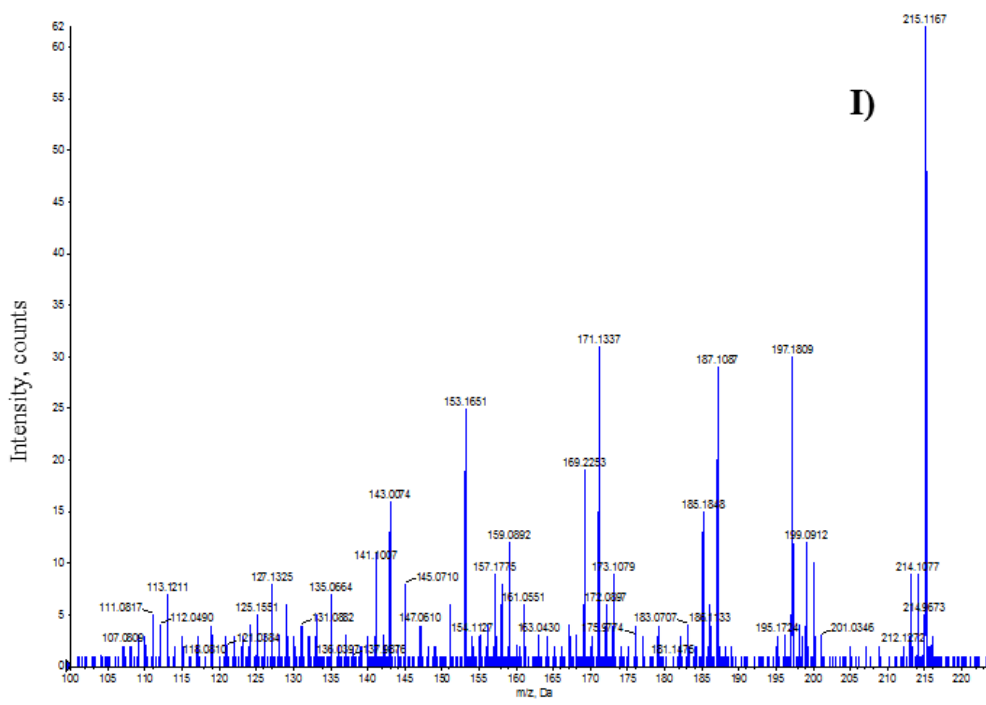


Figure 4.3: Continued.

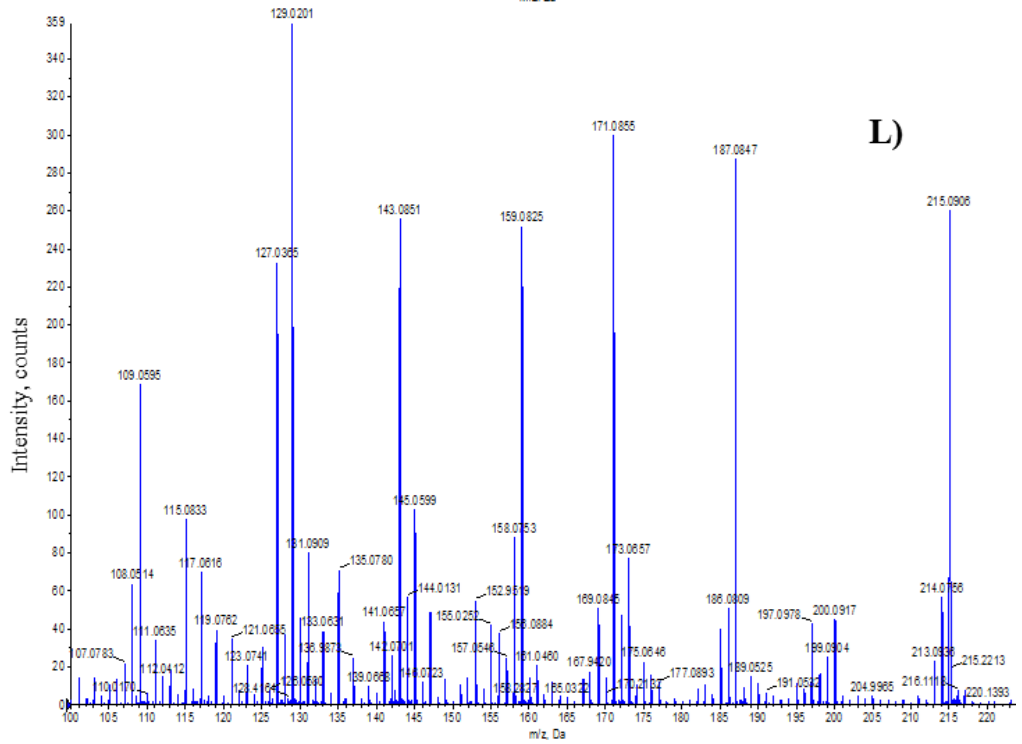
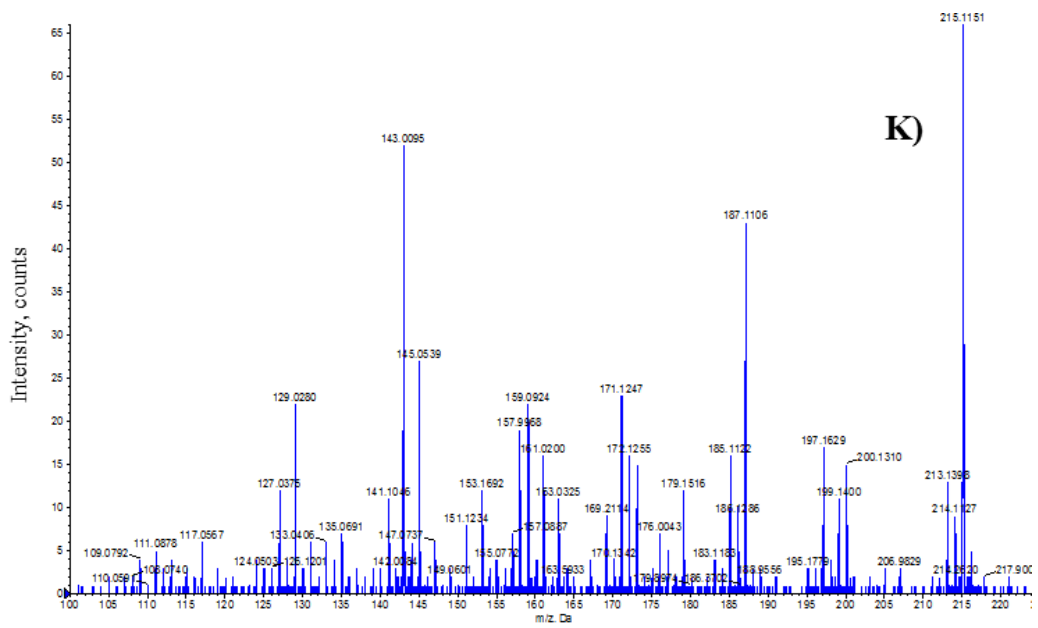


Figure 4.3: Continued.

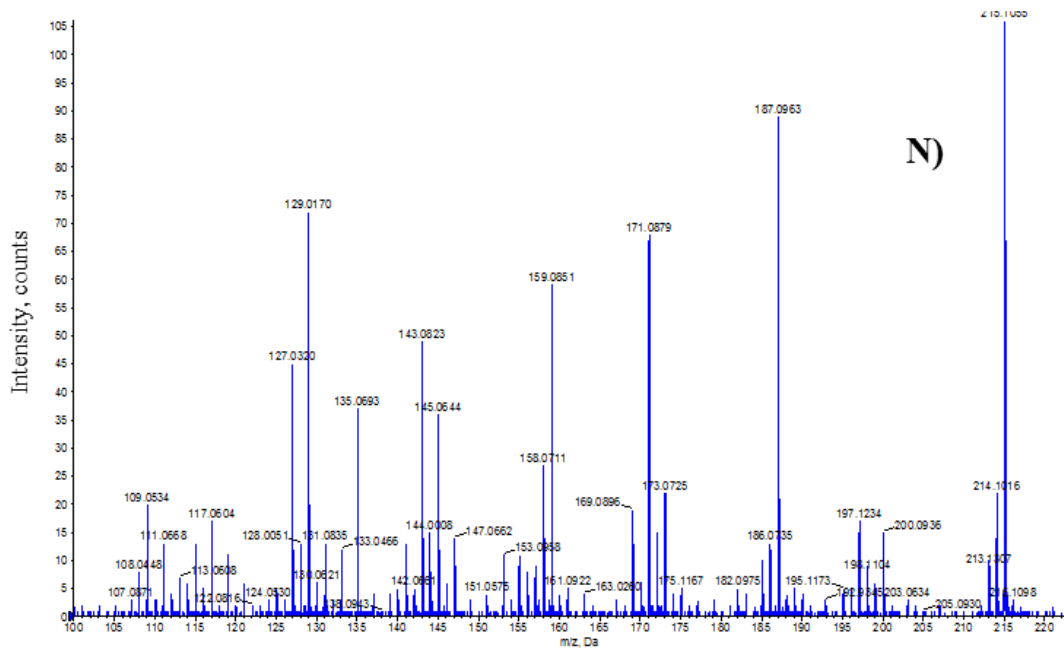
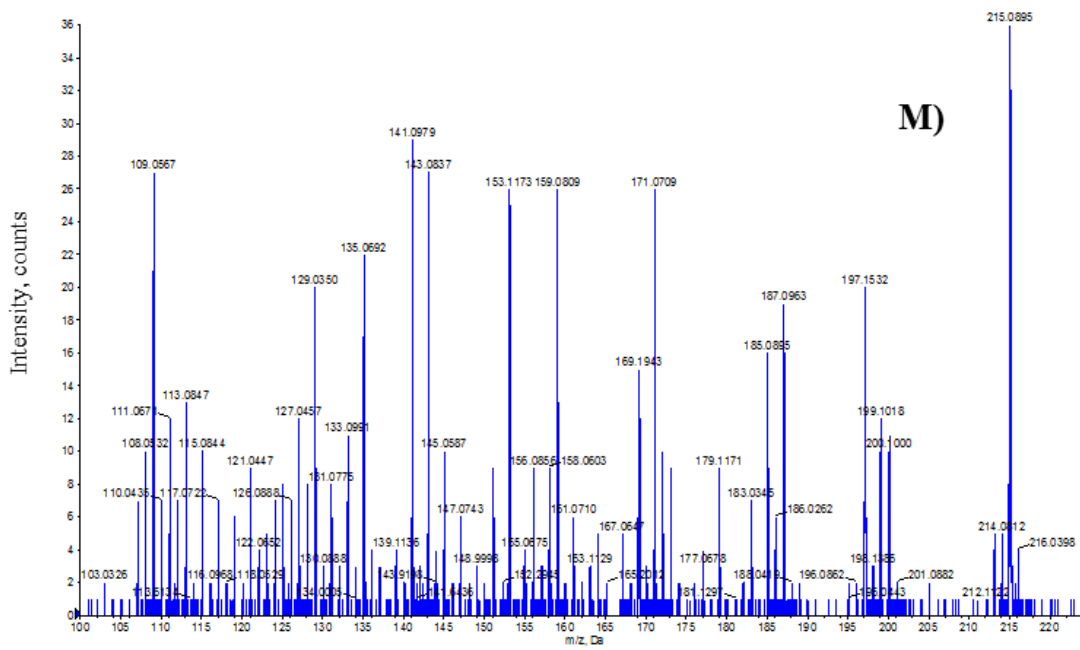


Figure 4.3: Continued.

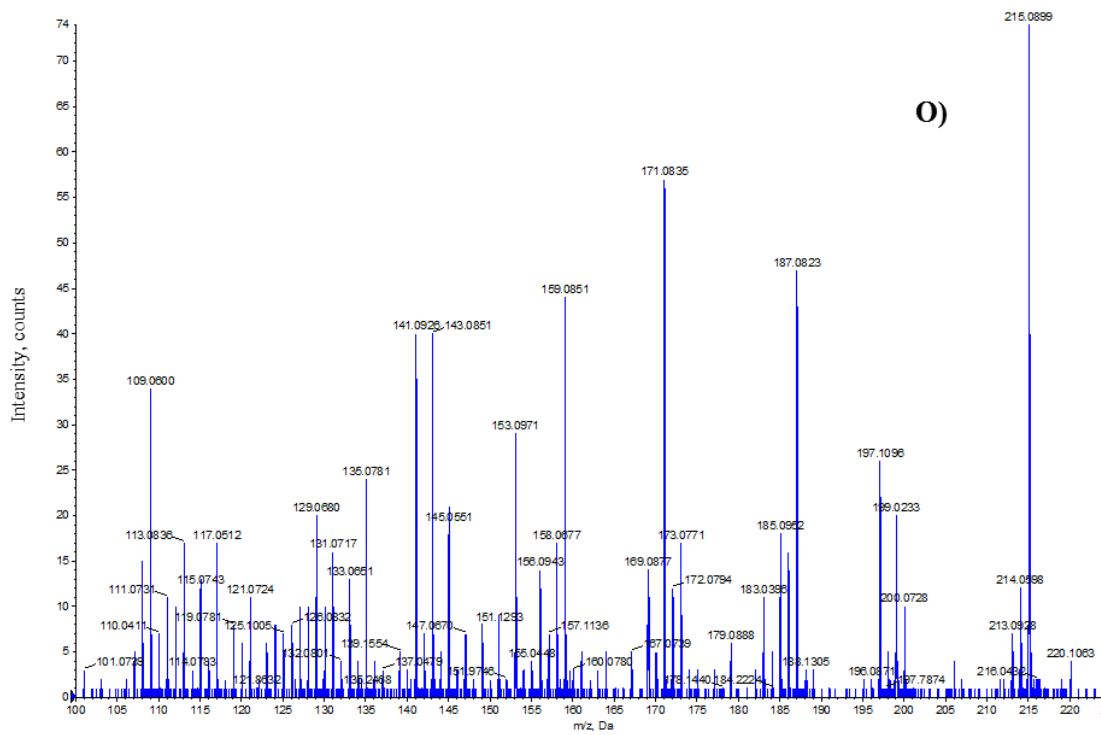


Figure 4.3: Continued.

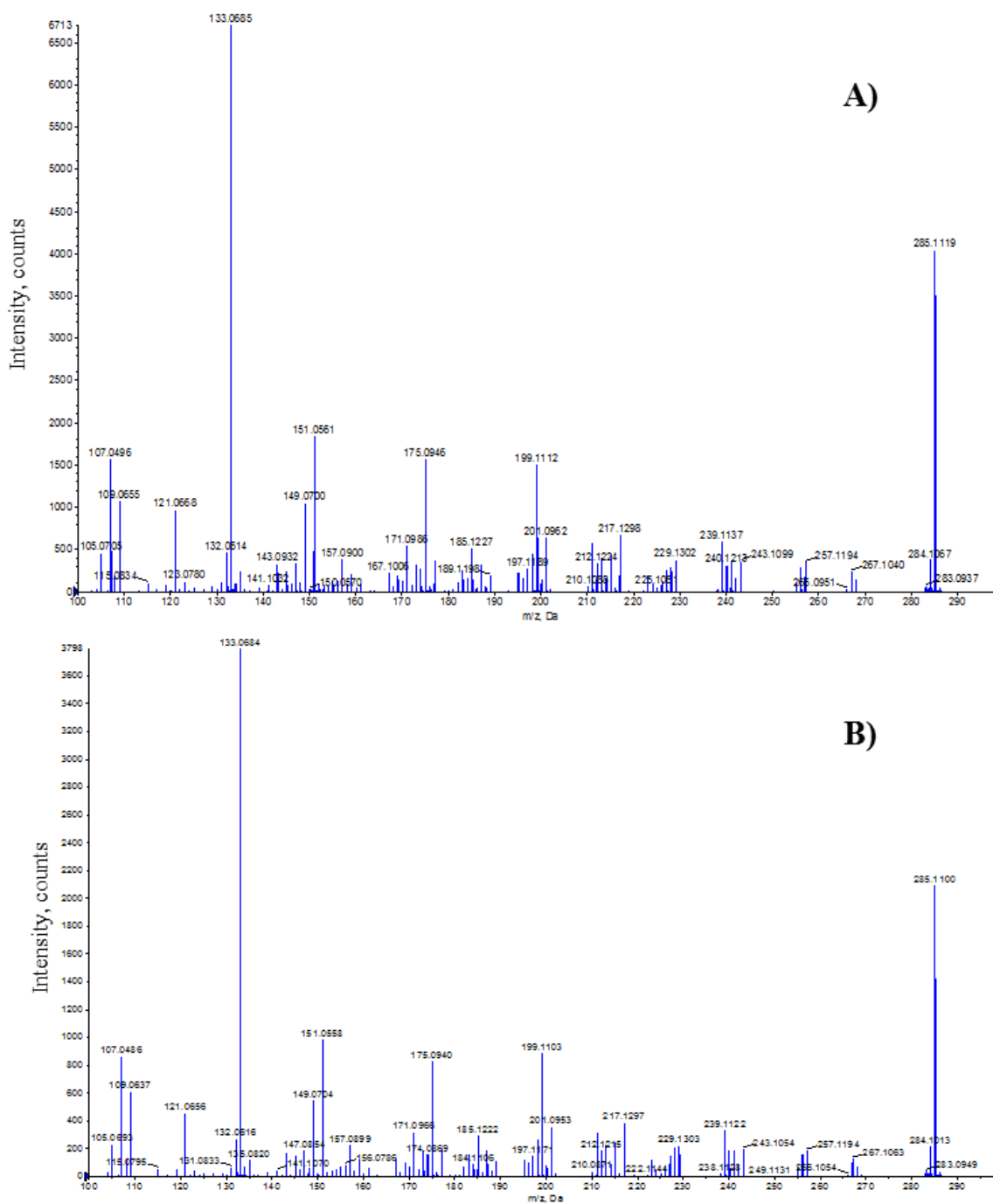


Figure A4.4: MS/MS fragmentation pattern of Luteolin analysed in negative ESI mode. A) Luteolin in heat shock & eCO₂ treatment, mature leaf, aqueous polar phase. B) Luteolin in heat shock & eCO₂ treatment, mature leaf, organic polar phase. C) Luteolin in heat shock treatment & eCO₂, new leaf, aqueous polar phase. D) Luteolin in heat sock & eCO₂ treatment, new leaf, organic polar phase. E) Luteolin in eCO₂ treatment, mature leaf, aqueous polar phase. F) Luteolin in eCO₂ treatment, mature leaf, organic polar phase. G) Luteolin in eCO₂ treatment, new leaf, aqueous polar phase. H) Luteolin in eCO₂ treatment, new leaf, organic polar phase. I) Luteolin in heat shock treatment, mature leaf, organic polar phase. J) Luteolin in heat shock treatment, mature leaf, organic polar phase. K) Luteolin in heat shock treatment, new leaf, aqueous polar phase. L) Luteolin in heat shock treatment, new leaf, organic polar phase. M) Luteolin in control treatment, mature leaf, aqueous polar phase. N) Luteolin in control treatment, mature leaf, organic polar phase. O) Luteolin in control treatment, new leaf, aqueous polar phase. P) Luteolin in control treatment, new leaf, organic polar phase. Q) Luteolin standard.

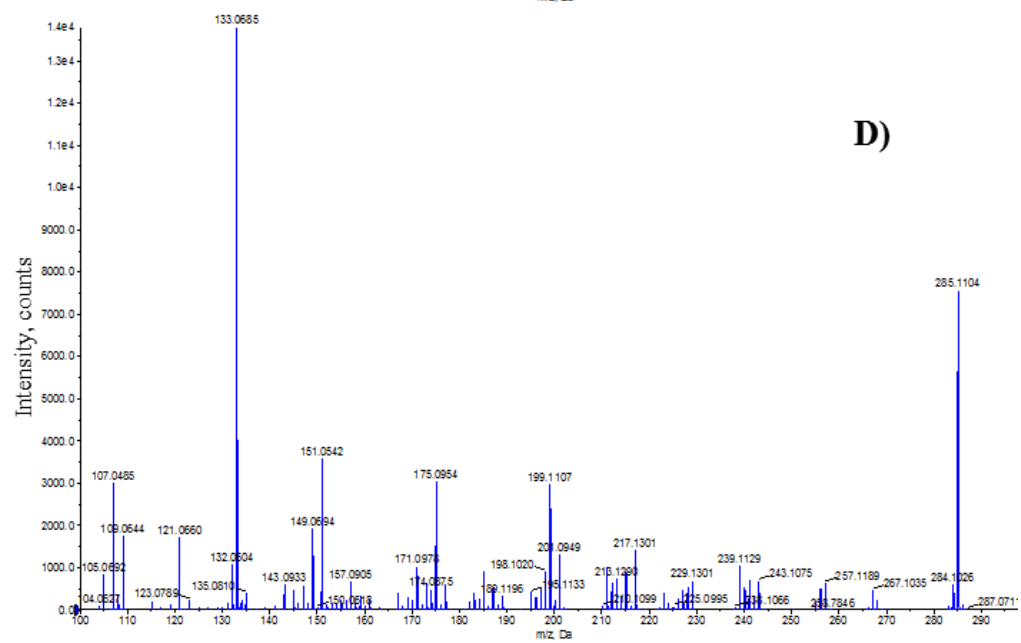
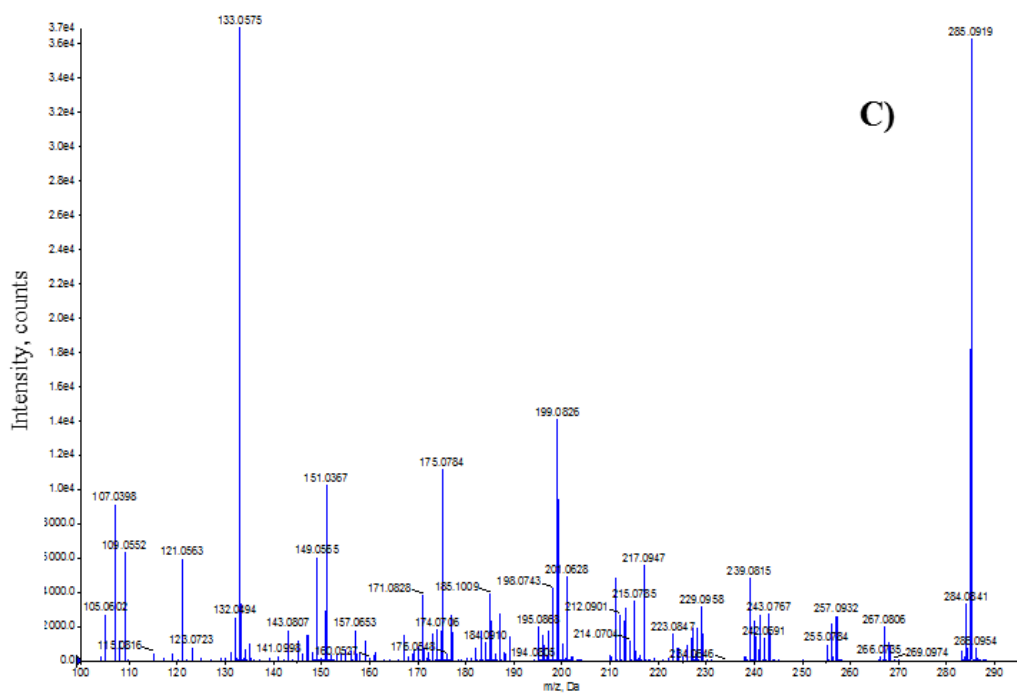
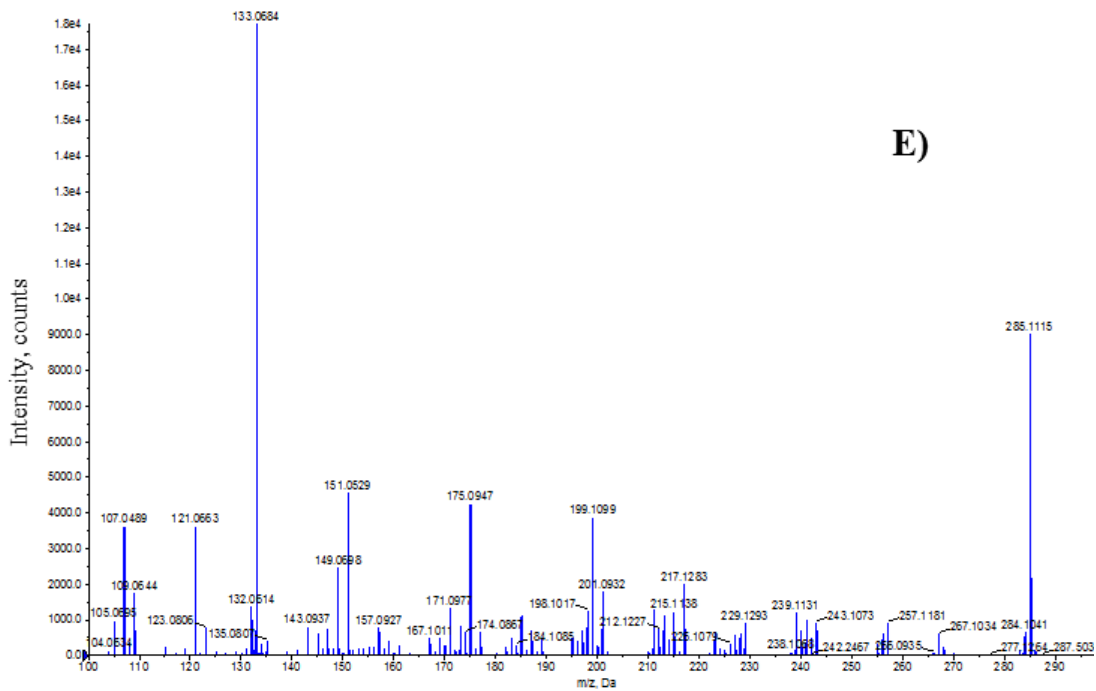
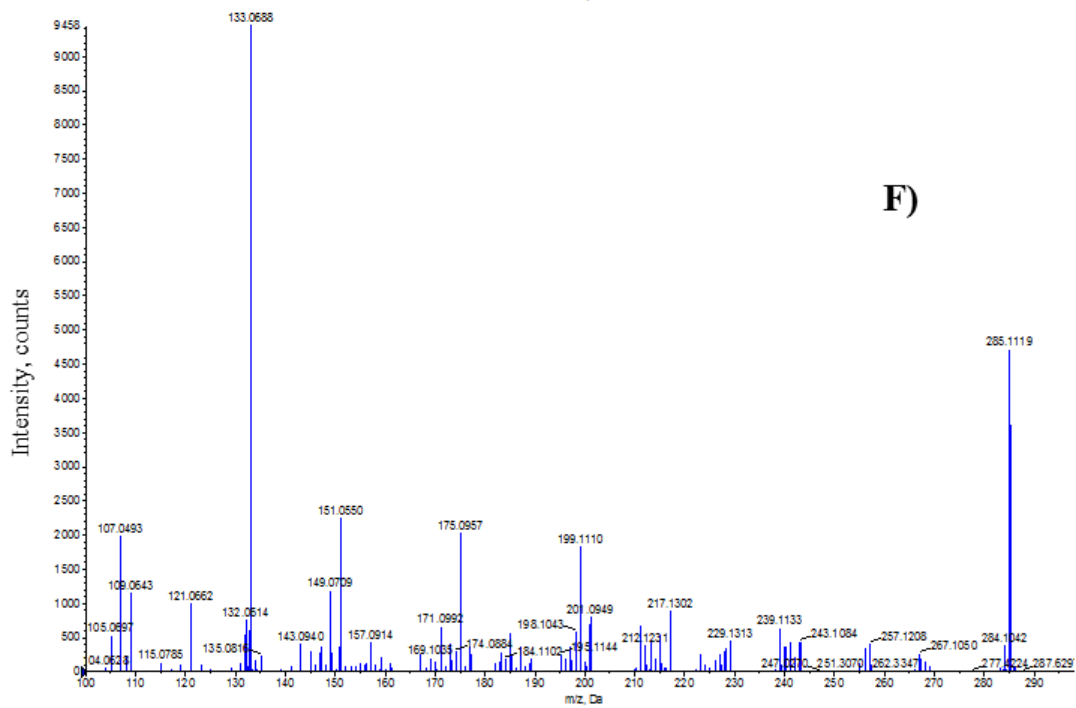


Figure 4.4: Continued.



E)



F)

Figure 4.4: Continued.

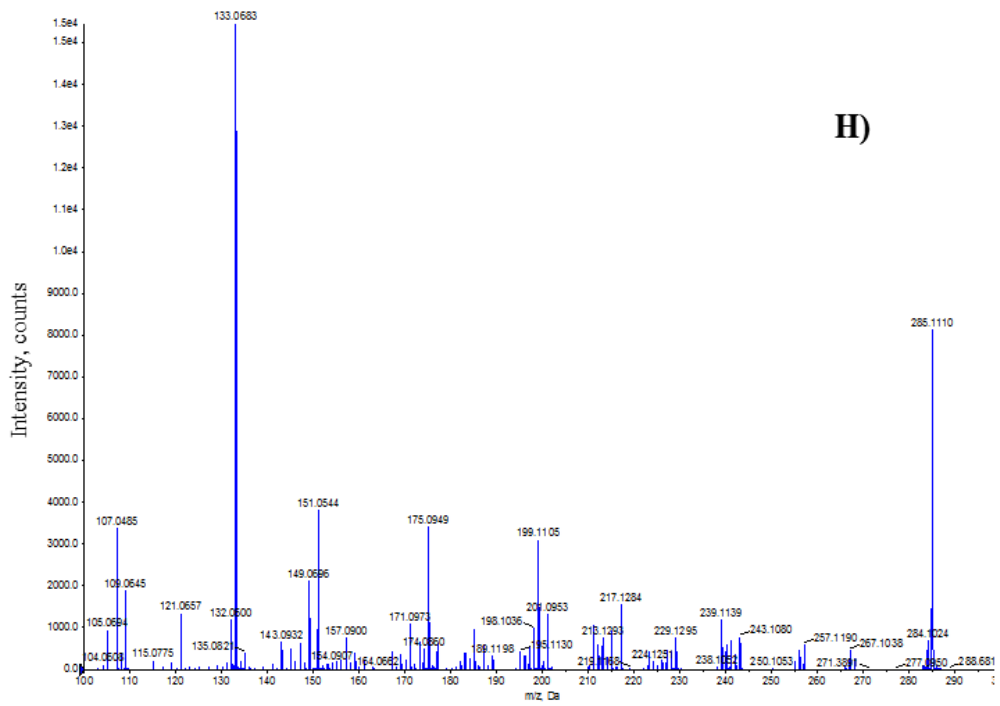
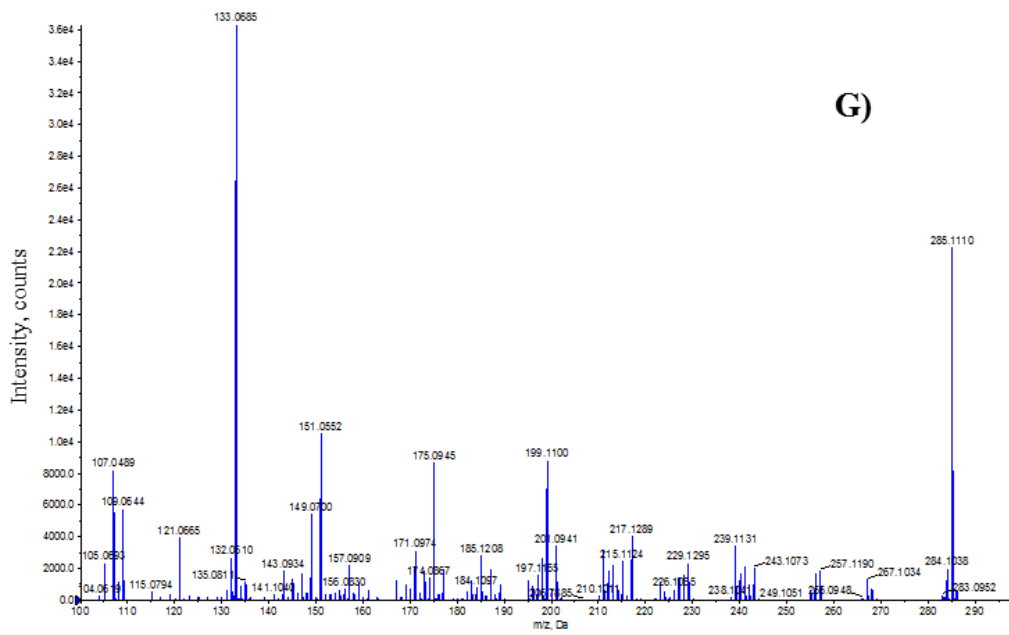


Figure 4.4: Continued.

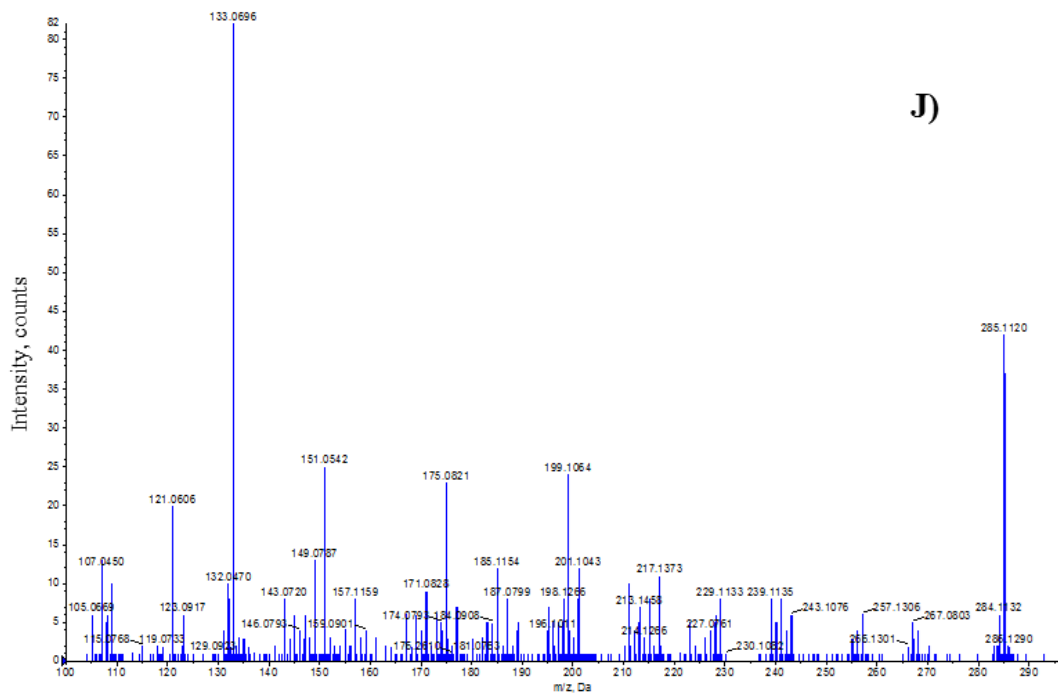
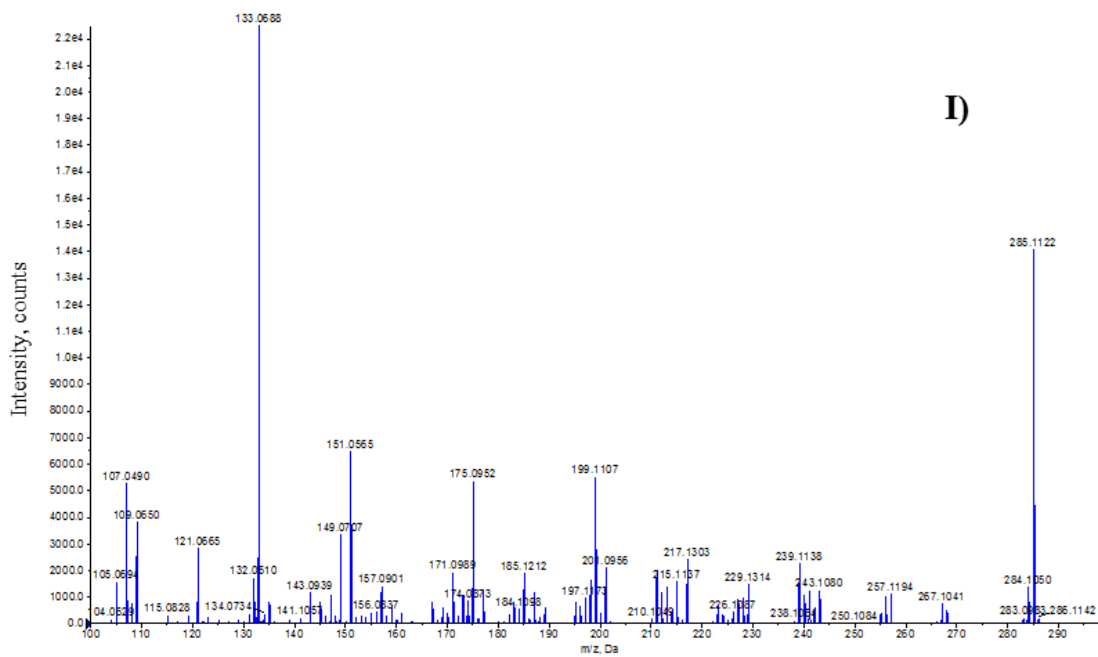


Figure 4.4: Continued.

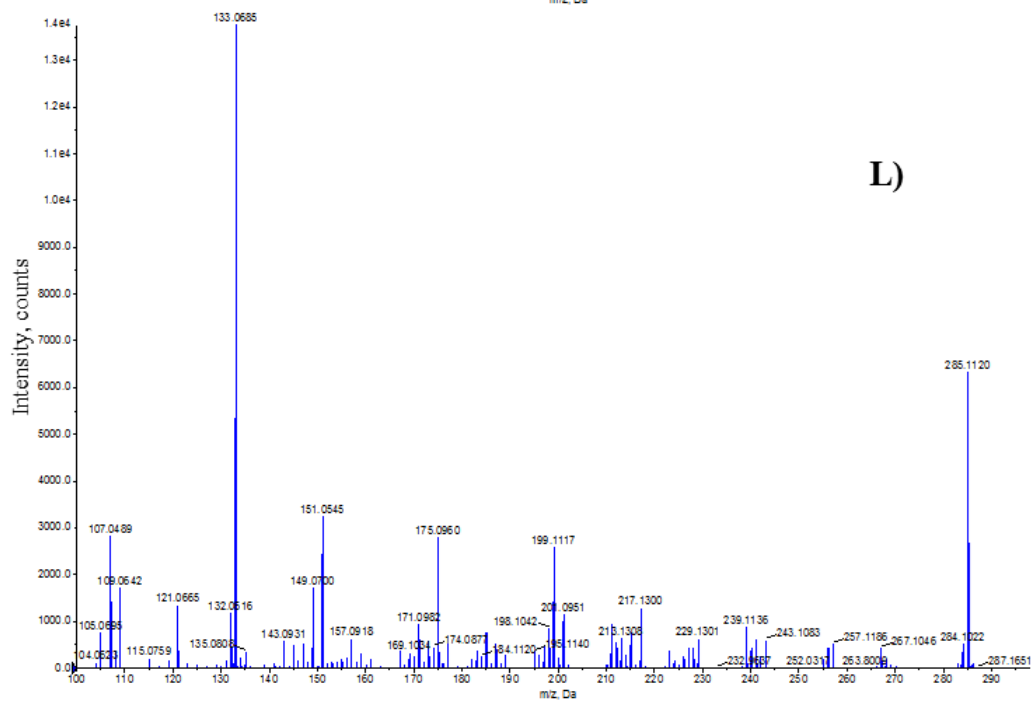
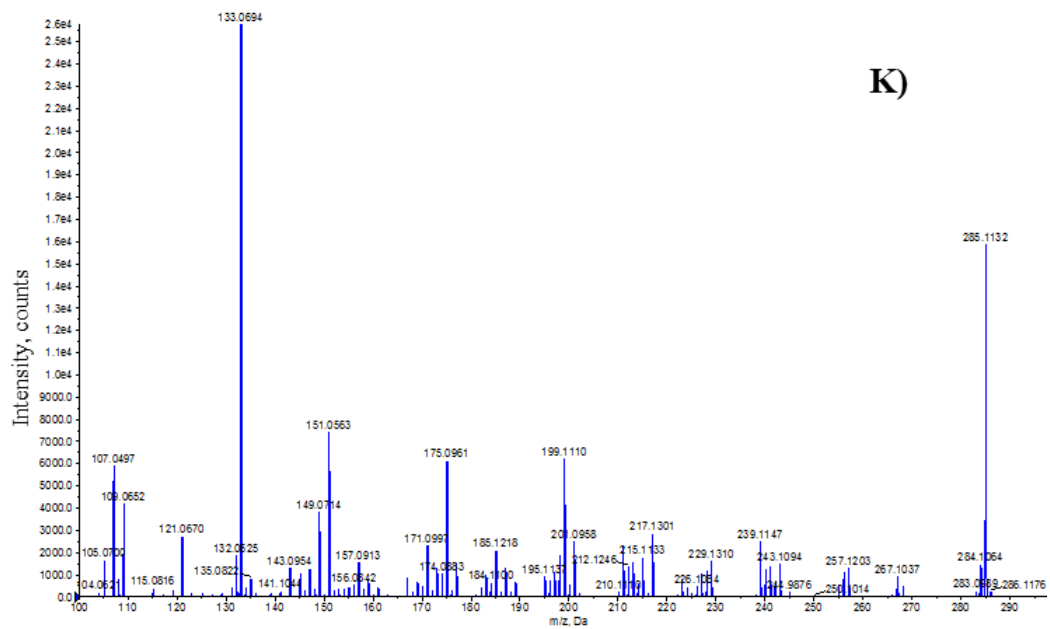
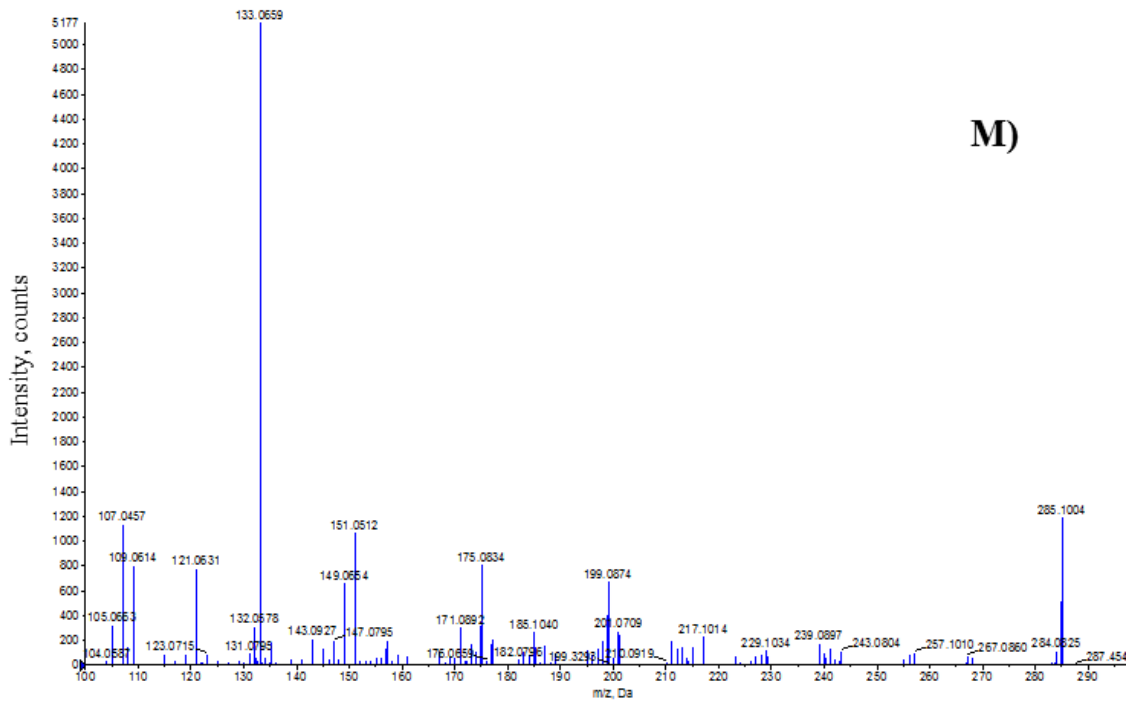
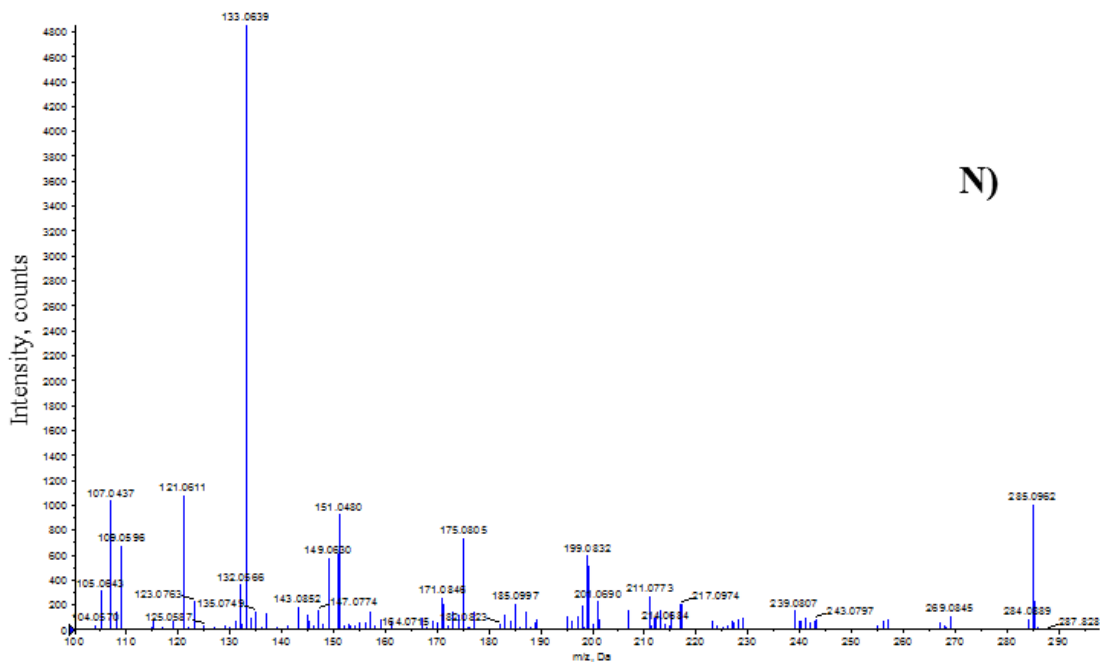


Figure 4.4: Continued.



M)



N)

Figure 4.4: Continued.

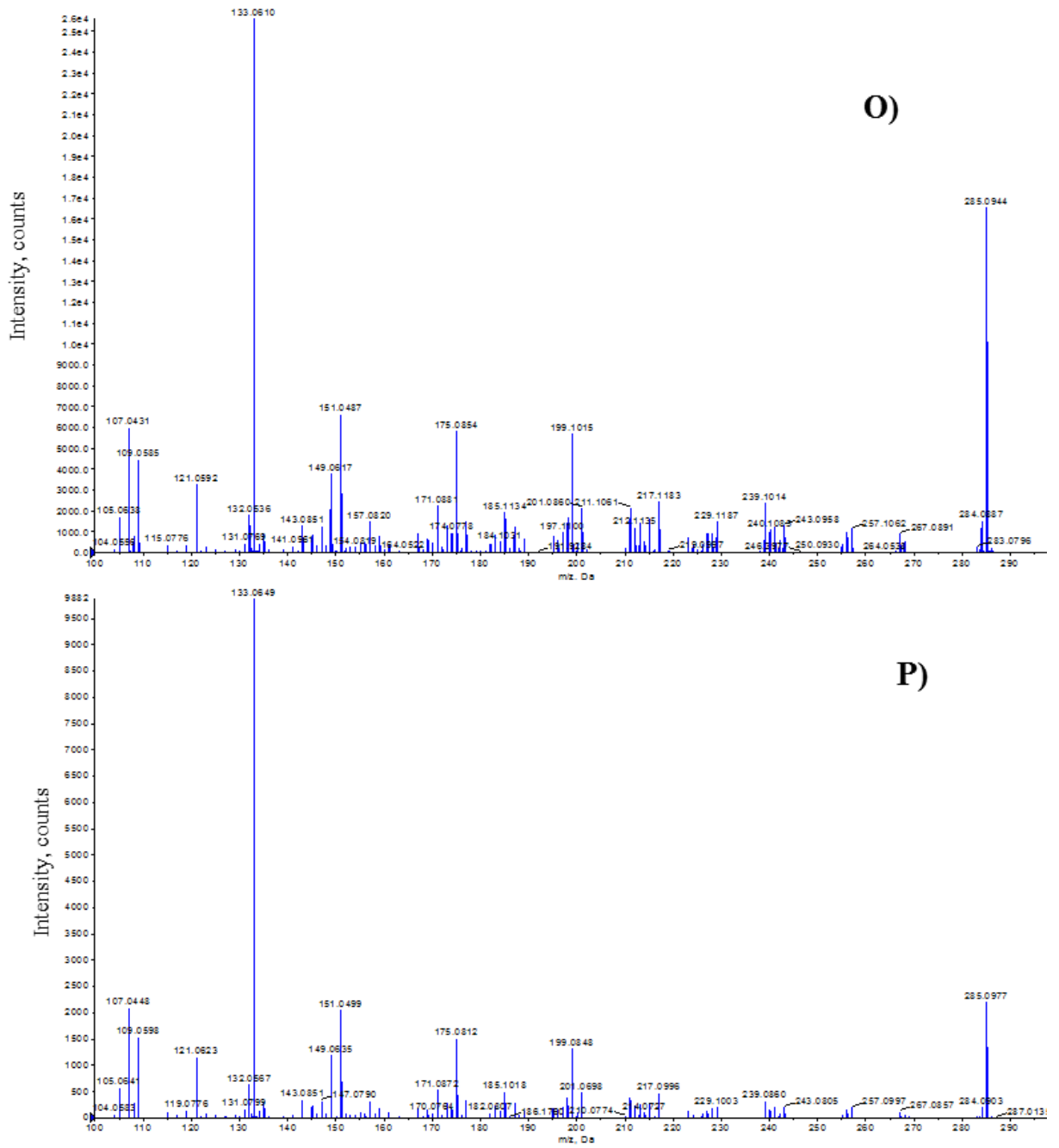


Figure 4.4: Continued.

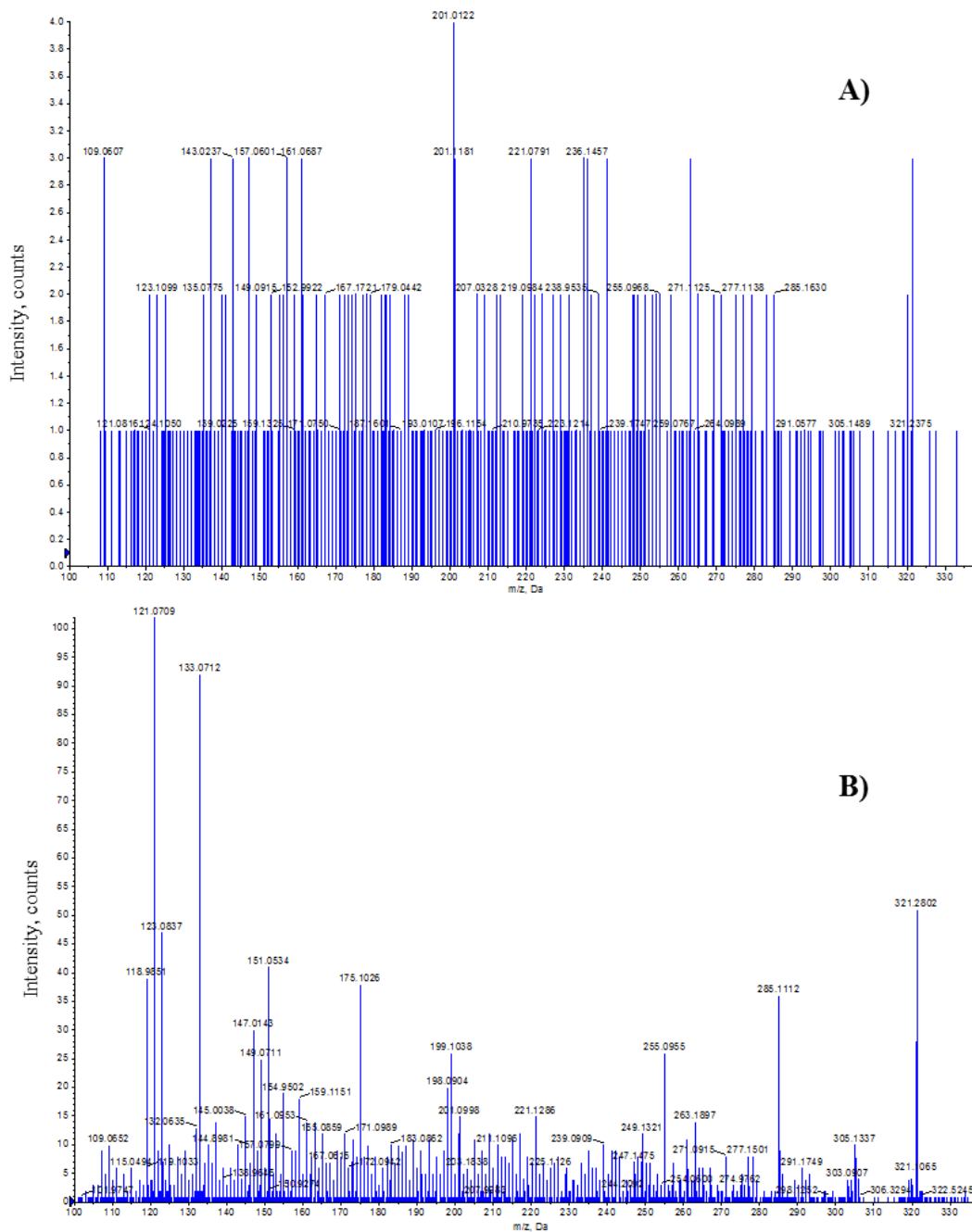
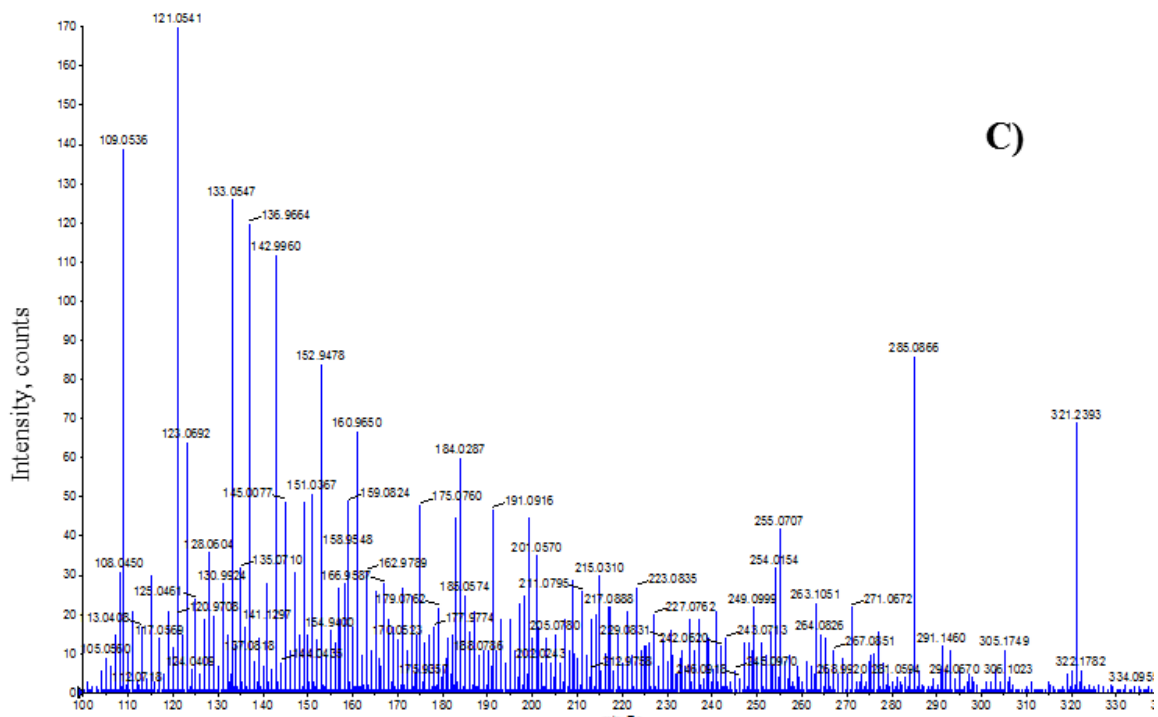
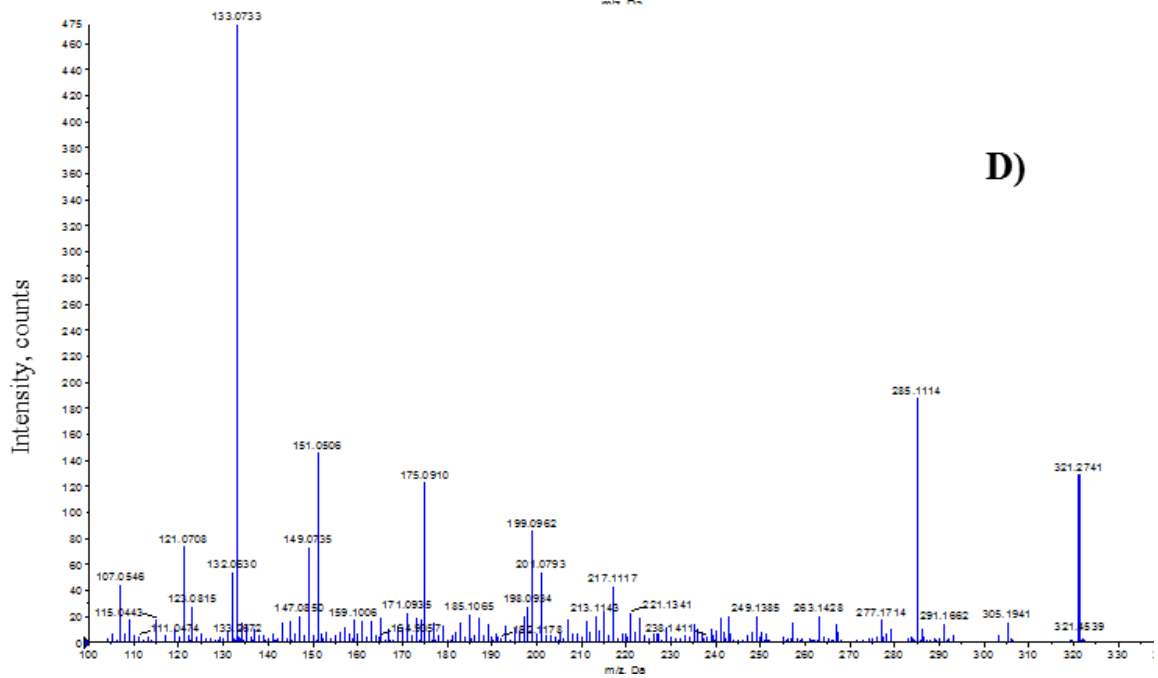


Figure A4.5: MS/MS fragmentation pattern of Cyanidin analysed in negative ESI mode. A) Cyanidin in heat shock & eCO₂ treatment, mature leaf, aqueous polar phase. B) Cyanidin in heat shock & eCO₂ treatment, mature leaf, organic polar phase. C) Cyanidin in heat shock treatment & eCO₂, new leaf, aqueous polar phase. D) Cyanidin in heat sock & eCO₂ treatment, new leaf, organic polar phase. E) Cyanidin in eCO₂ treatment, mature leaf, aqueous polar phase. F) Cyanidin in eCO₂ treatment, mature leaf, organic polar phase. G) Cyanidin in eCO₂ treatment, new leaf, aqueous polar phase. H) Luteolin in eCO₂ treatment, new leaf, organic polar phase. I) Cyanidin in heat shock treatment, mature leaf, organic polar phase. J) Cyanidin in heat shock treatment, mature leaf, organic polar phase. K) Cyanidin in heat shock treatment, new leaf, aqueous polar phase. L) Cyanidin in heat shock treatment, new leaf, organic polar phase. M) Cyanidin in control treatment, mature leaf, aqueous polar phase. N) Cyanidin in control treatment, mature leaf, organic polar phase. O) Cyanidin in control treatment, new leaf, aqueous polar phase. P) Cyanidin in control treatment, new leaf, organic polar phase.

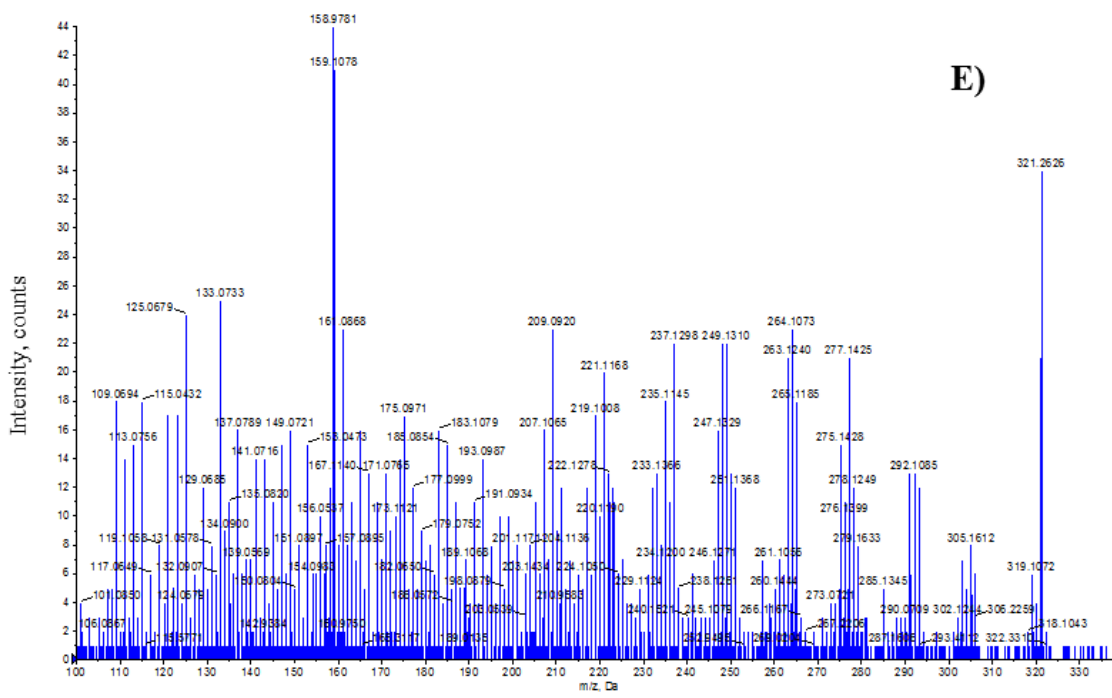


C)

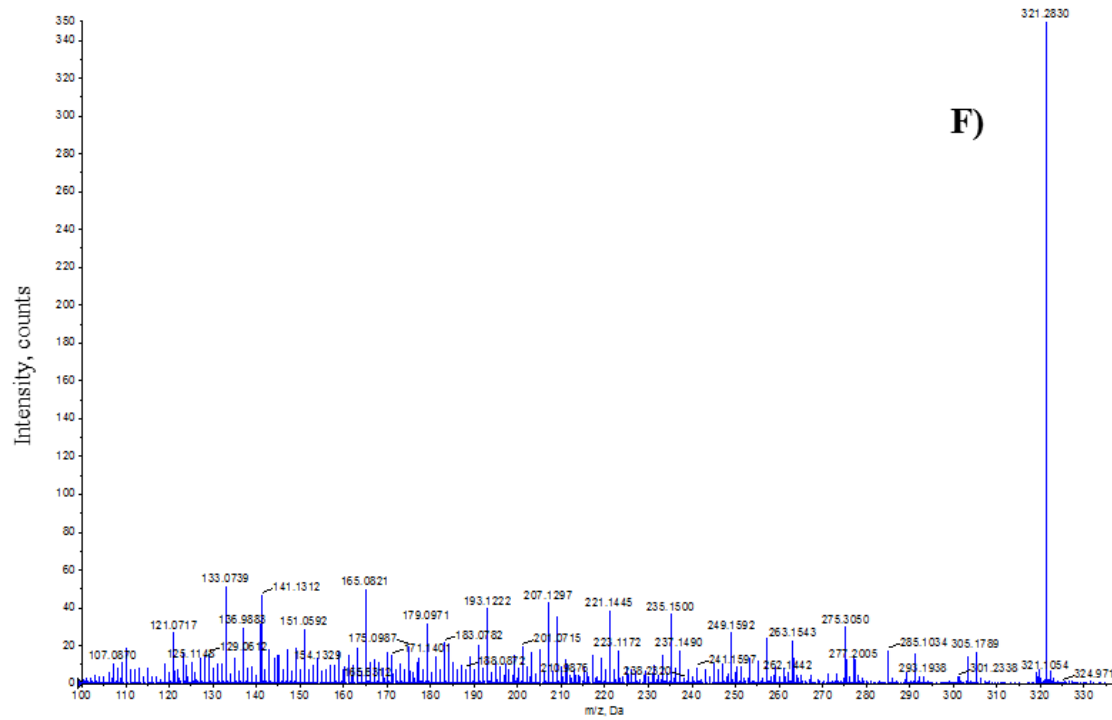


D)

Figure 4.5: Continued.



E)



F)

Figure 4.5: Continued.

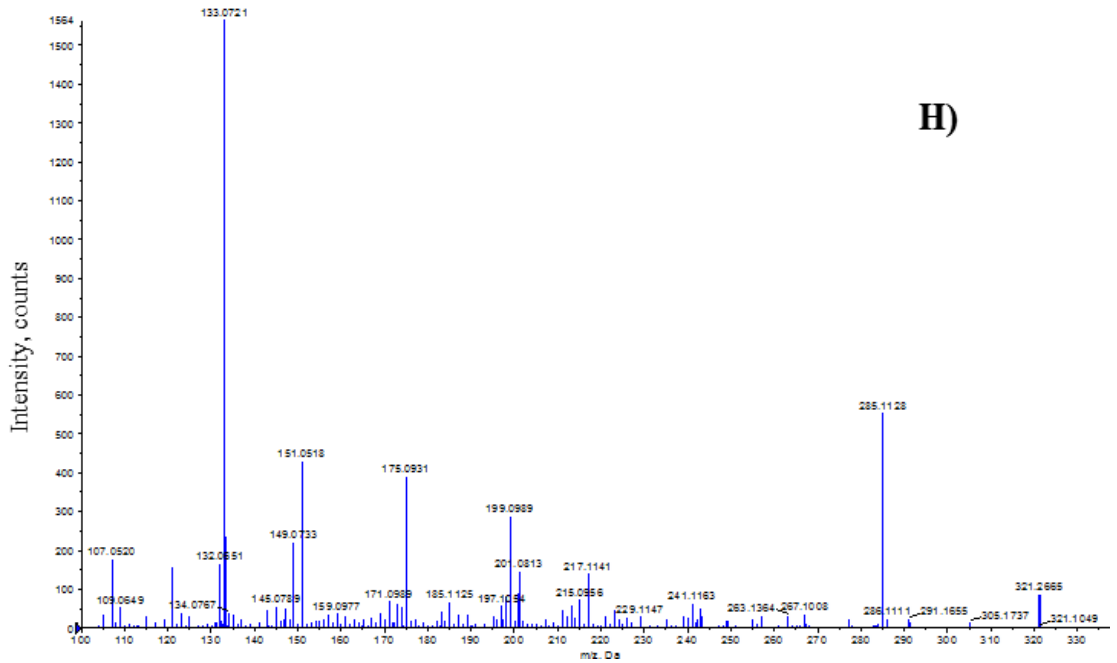
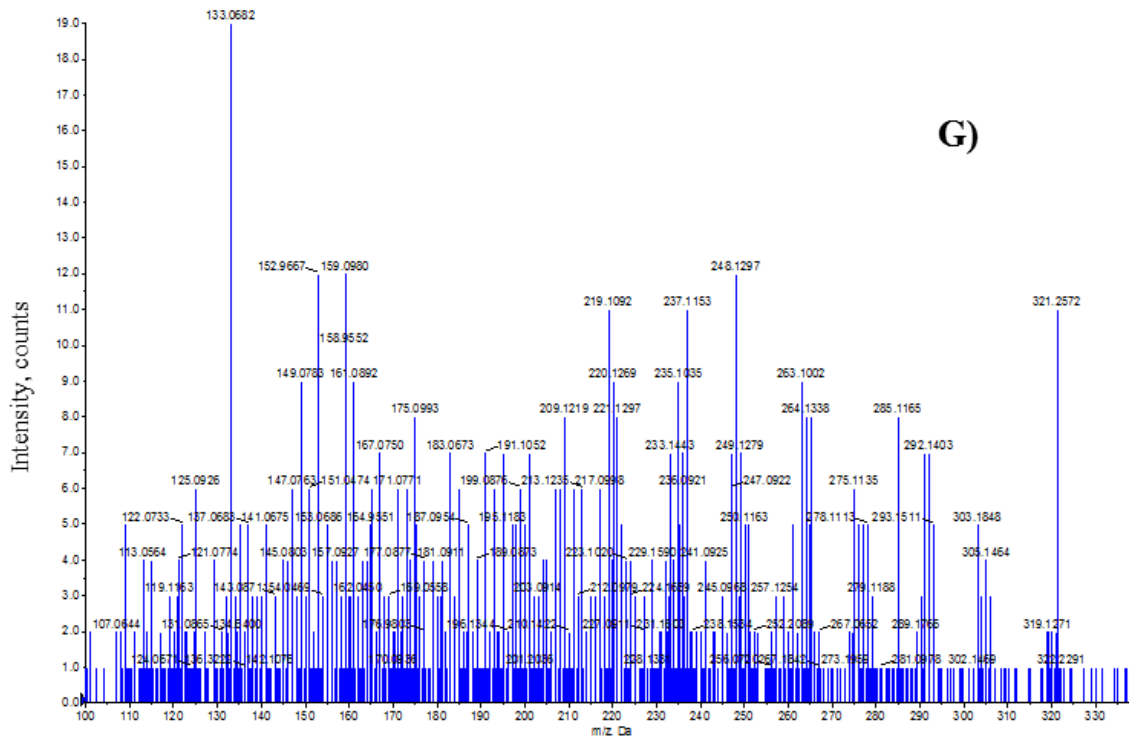
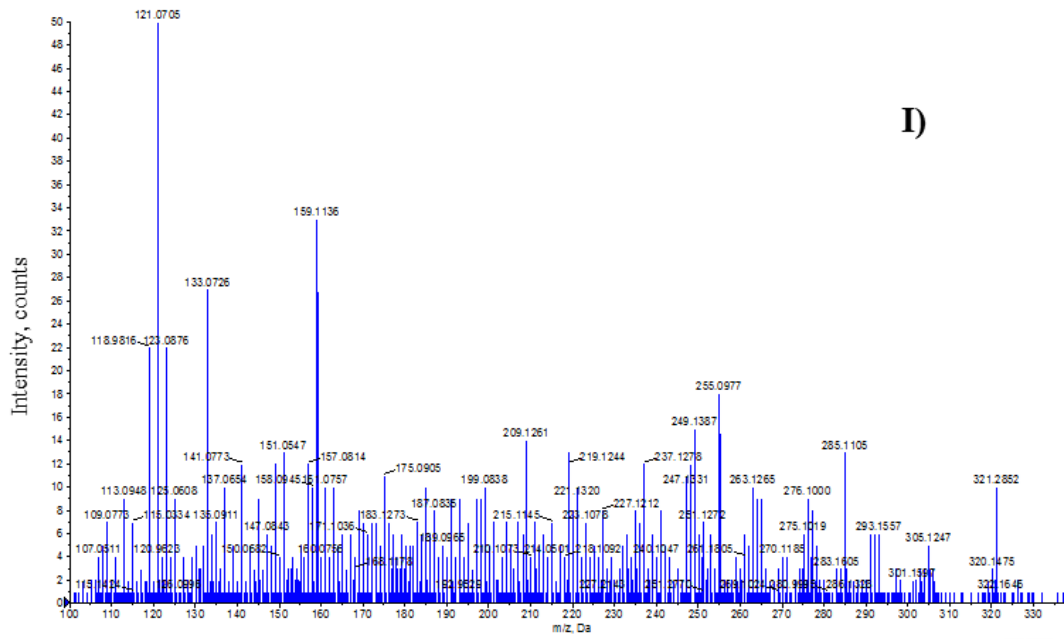
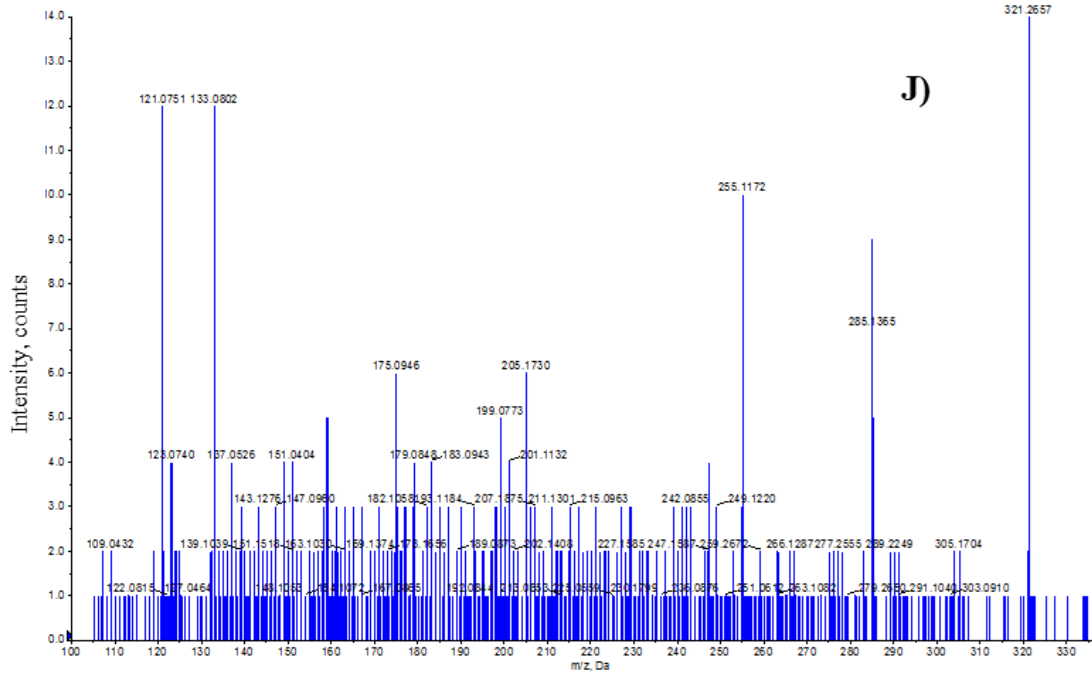


Figure 4.5: Continued.

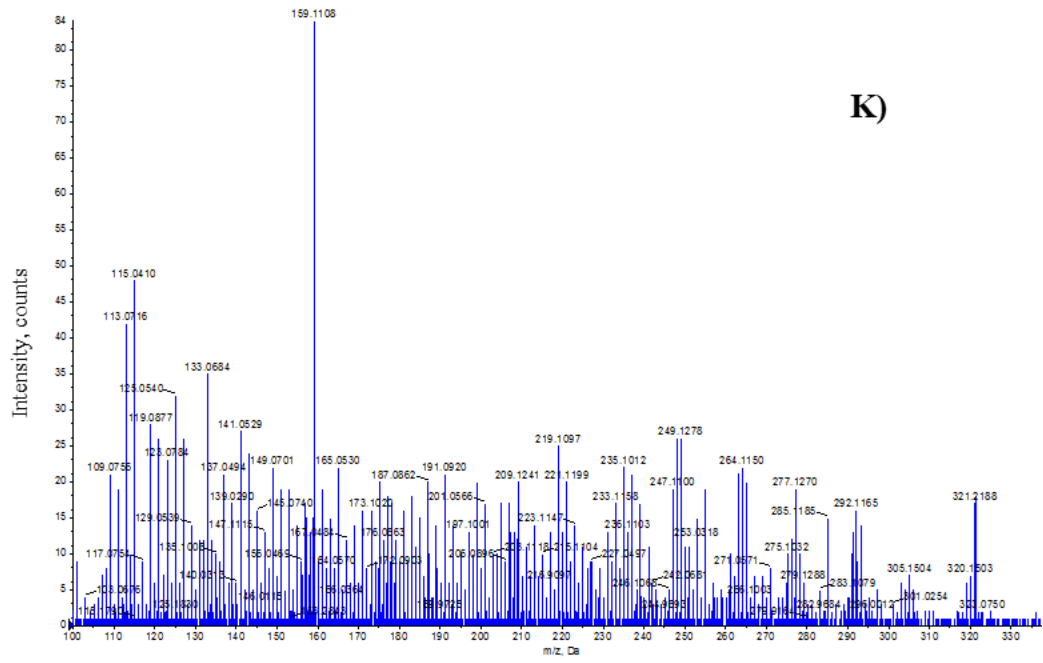


D

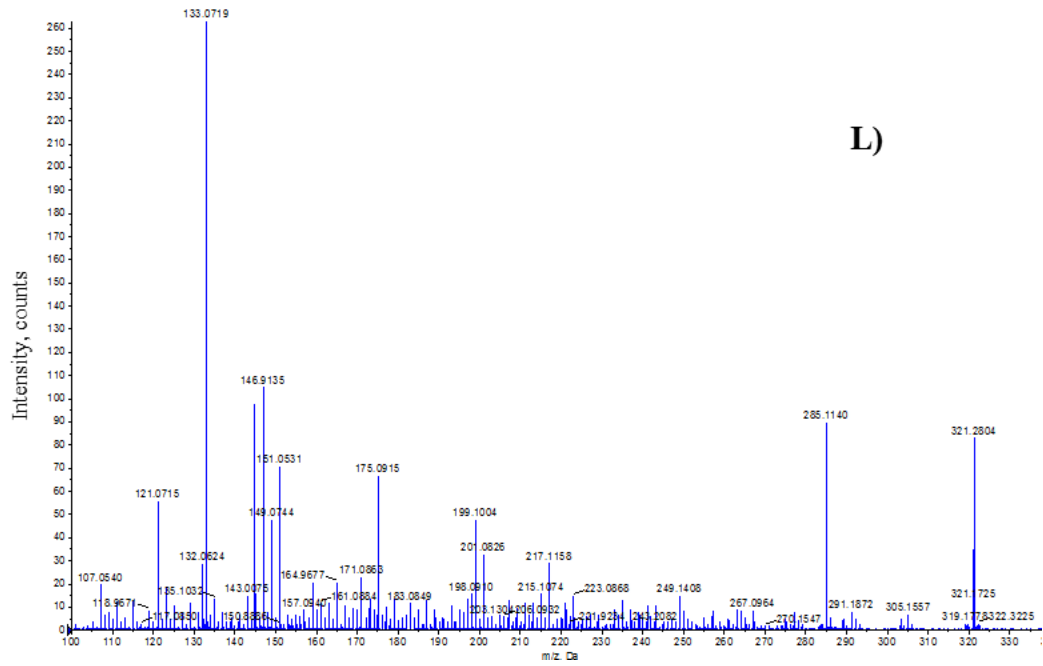


J

Figure 4.5: Continued.

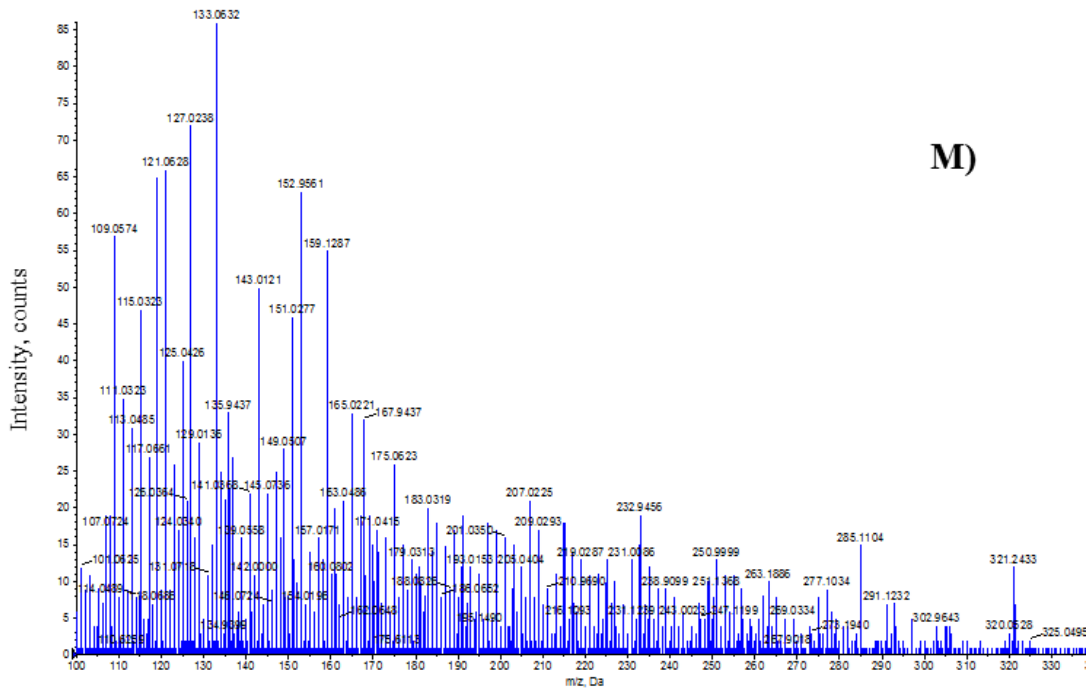


K)

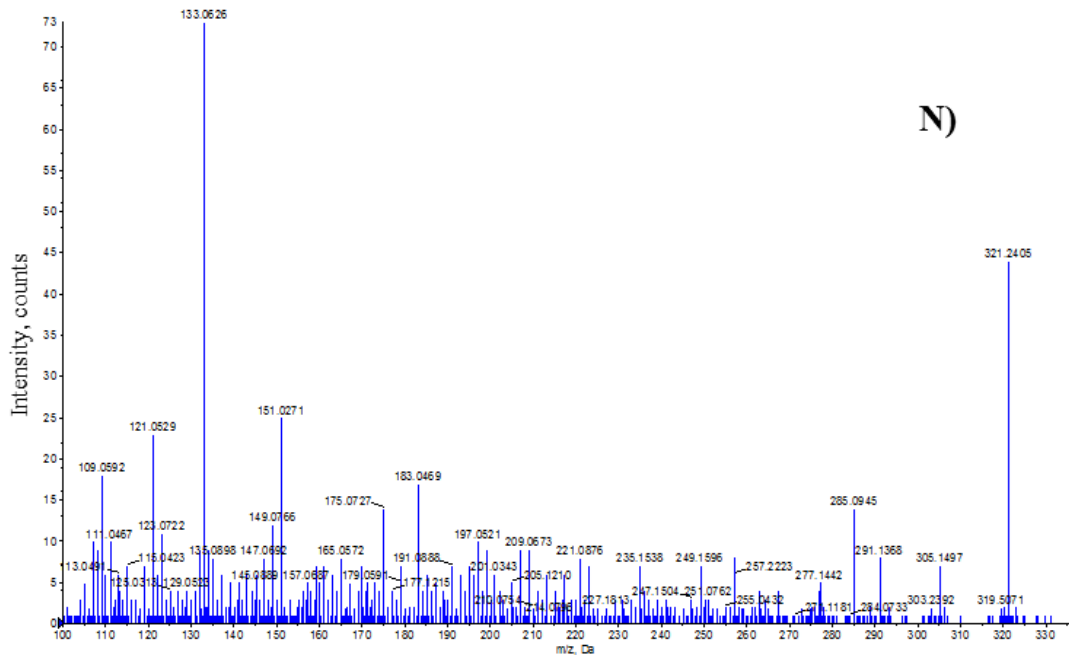


L)

Figure 4.5: Continued.



M)



N)

Figure 4.5: Continued.

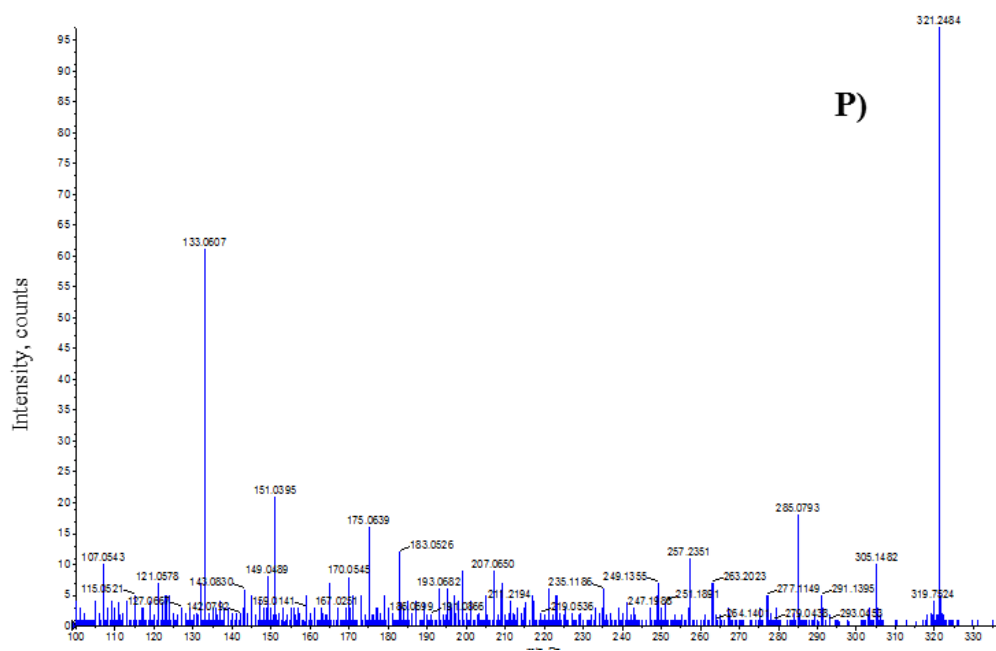
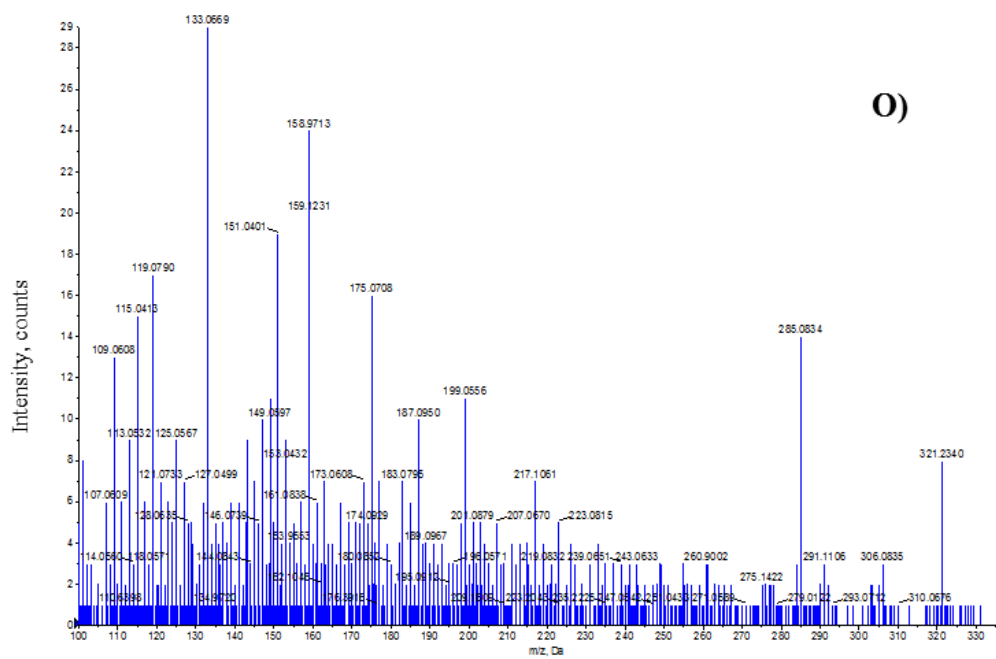


Figure 4.5: Continued.

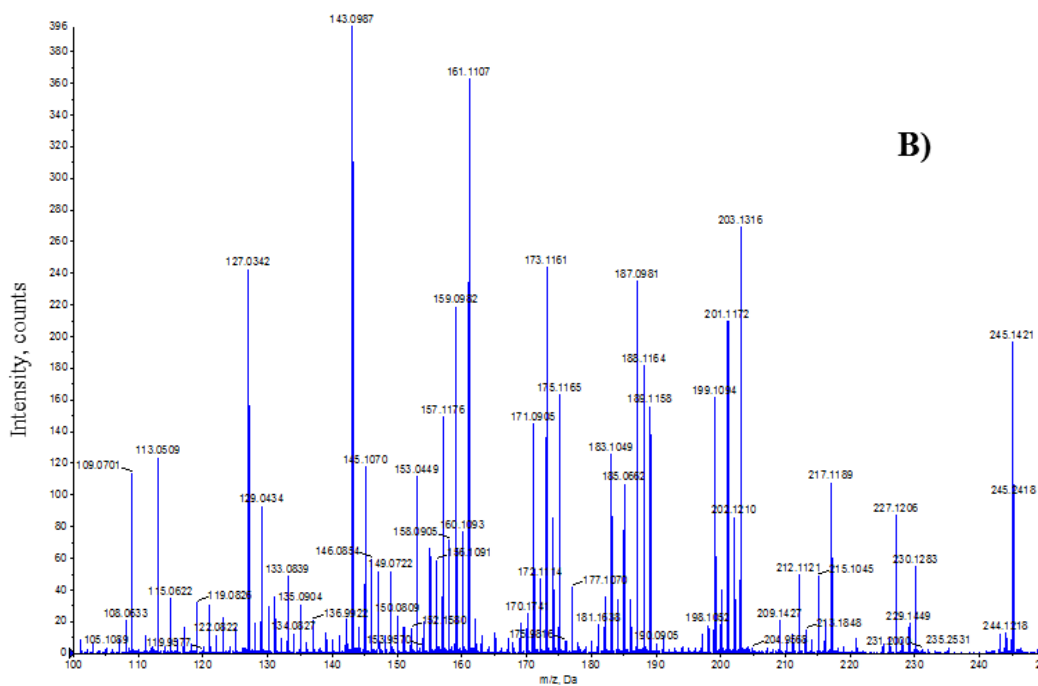
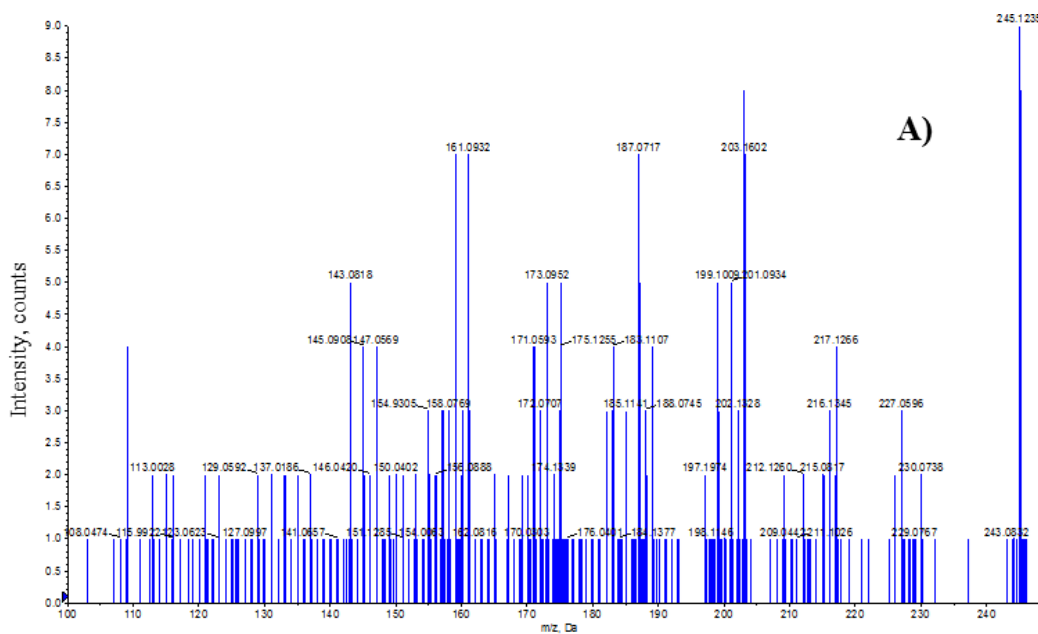


Figure A4.6: MS/MS fragmentation pattern of IPP analysed in negative ESI mode. A) IPP in heat shock & eCO₂ treatment, mature leaf, aqueous polar phase. B) IPP in heat shock & eCO₂ treatment, mature leaf, organic polar phase. C) IPP in heat shock treatment & eCO₂, new leaf, aqueous polar phase. D) IPP in heat shock & eCO₂ treatment, new leaf, organic polar phase. E) IPP in eCO₂ treatment, mature leaf, aqueous polar phase. F) IPP in eCO₂ treatment, mature leaf, organic polar phase. G) IPP in eCO₂ treatment, new leaf, aqueous polar phase. H) IPP in eCO₂ treatment, new leaf, organic polar phase. I) IPP in heat shock treatment, mature leaf, organic polar phase. J) IPP in heat shock treatment, mature leaf, organic polar phase. K) IPP in heat shock treatment, new leaf, aqueous polar phase. L) IPP in heat shock treatment, new leaf, organic polar phase. M) IPP in control treatment, mature leaf, aqueous polar phase. N) IPP in control treatment, mature leaf, organic polar phase. O) IPP in control treatment, new leaf, aqueous polar phase. P) IPP in control treatment, new leaf, organic polar phase.

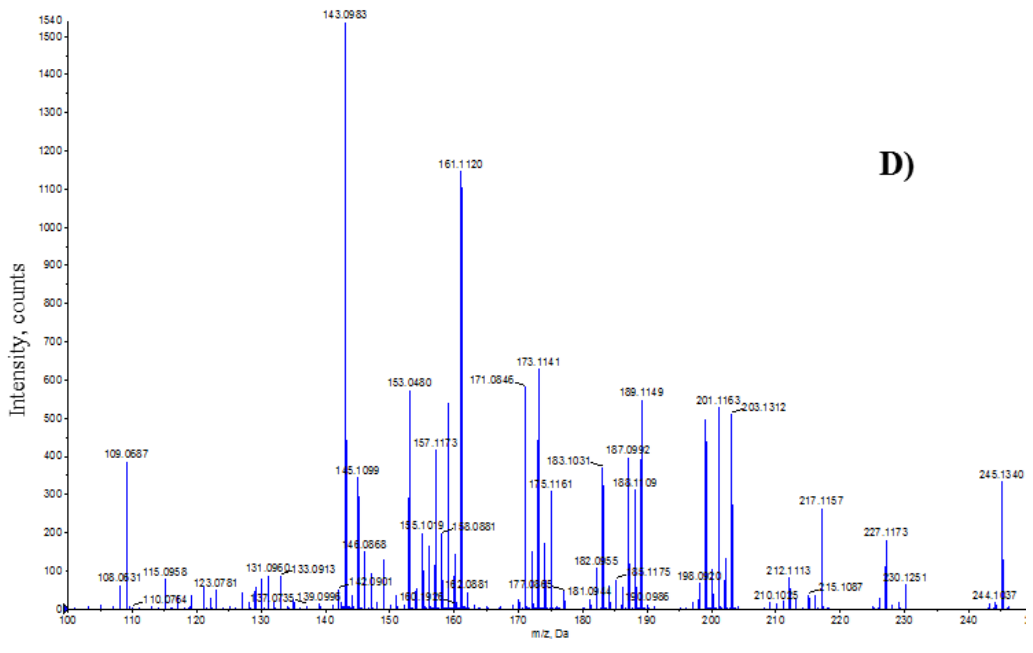
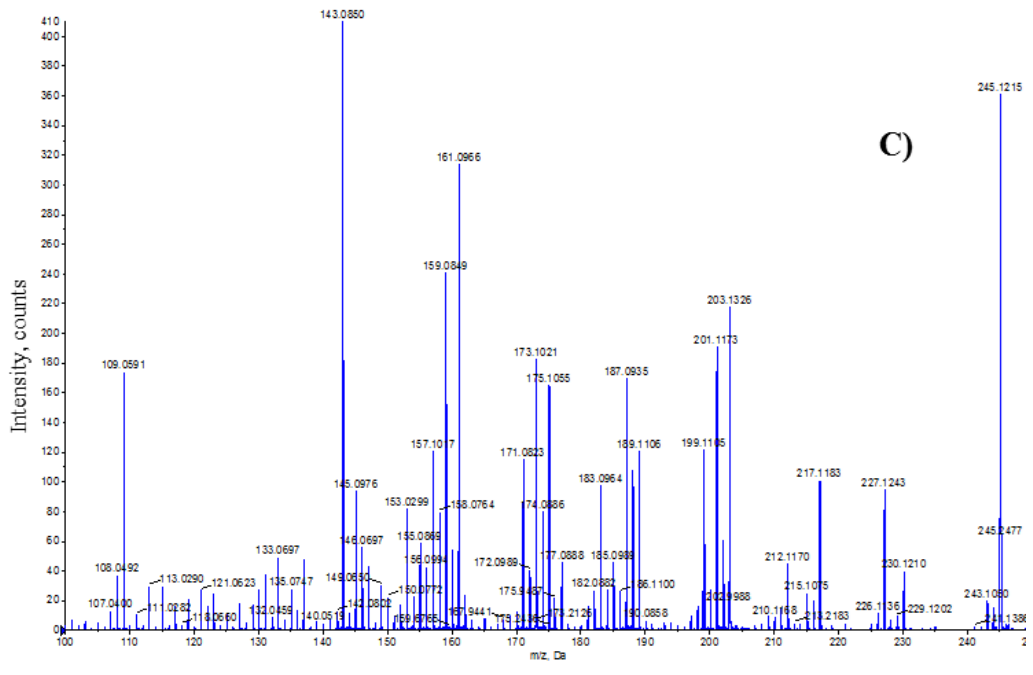


Figure 4.6: Continued.

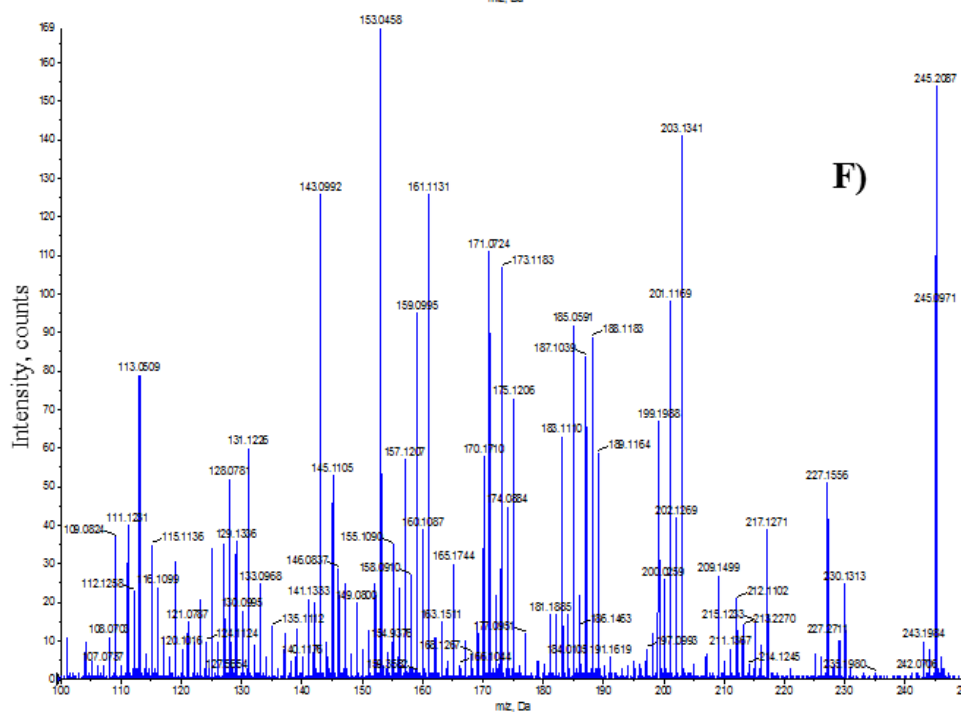
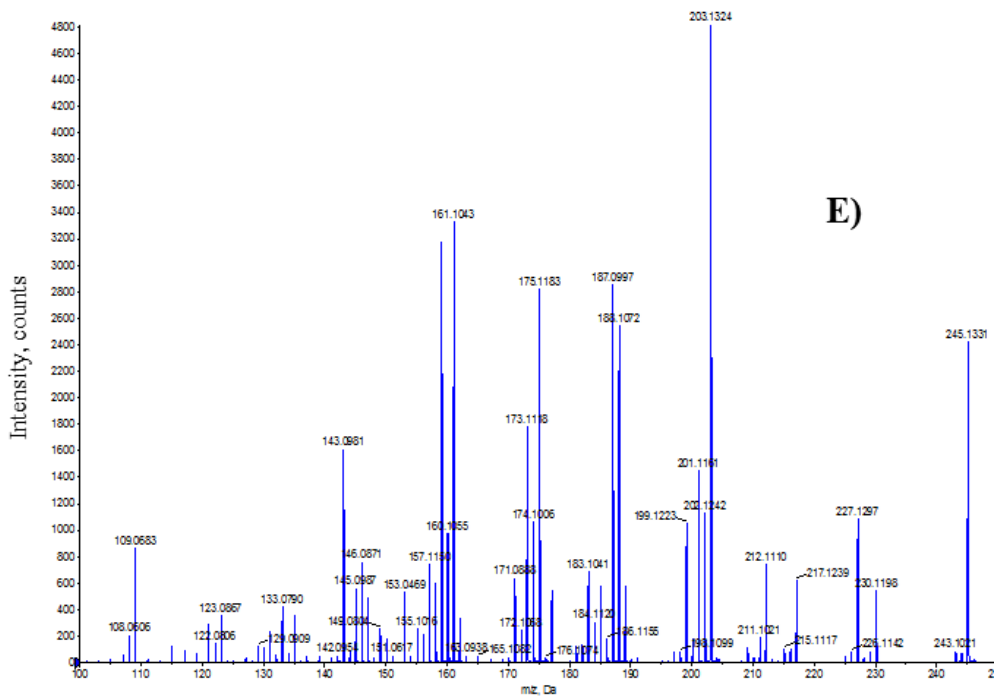


Figure 4.6: Continued.

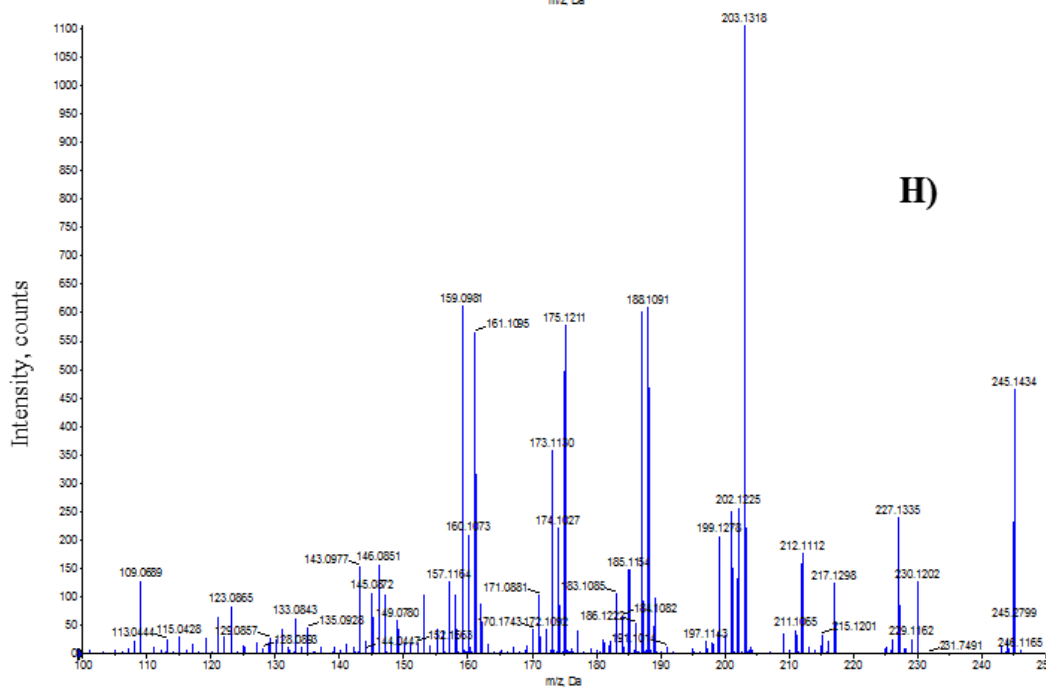
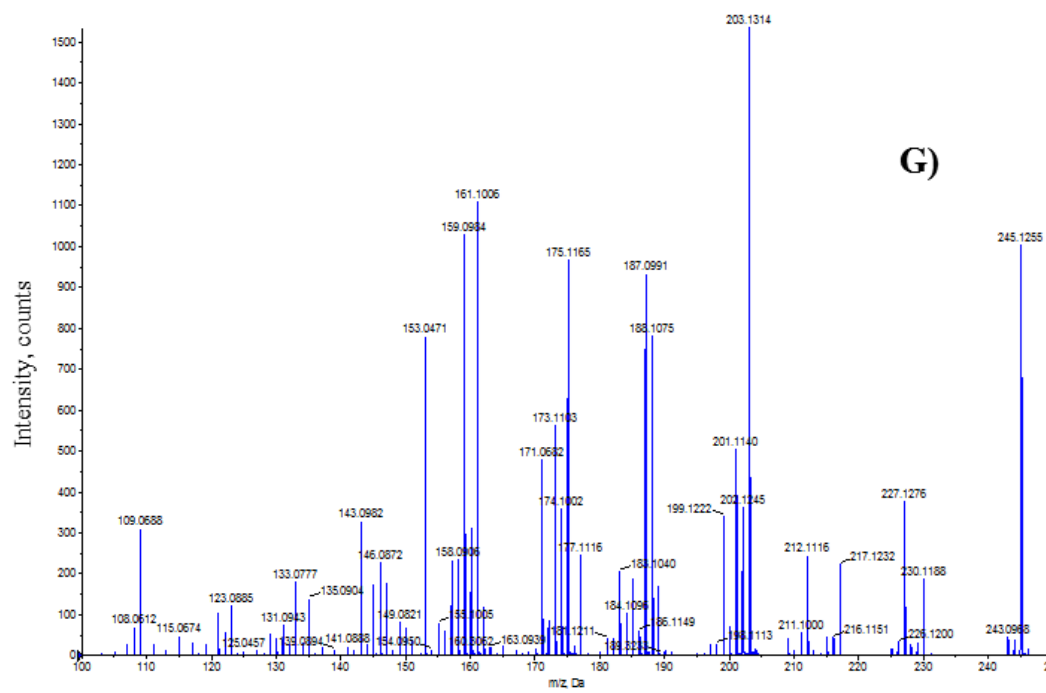


Figure 4.6: Continued.

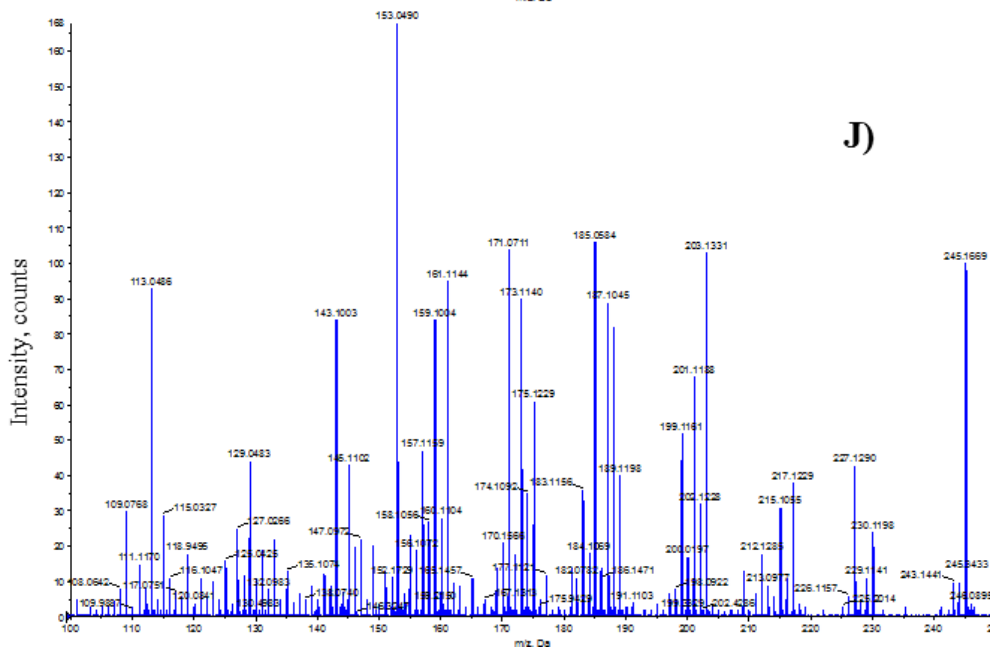
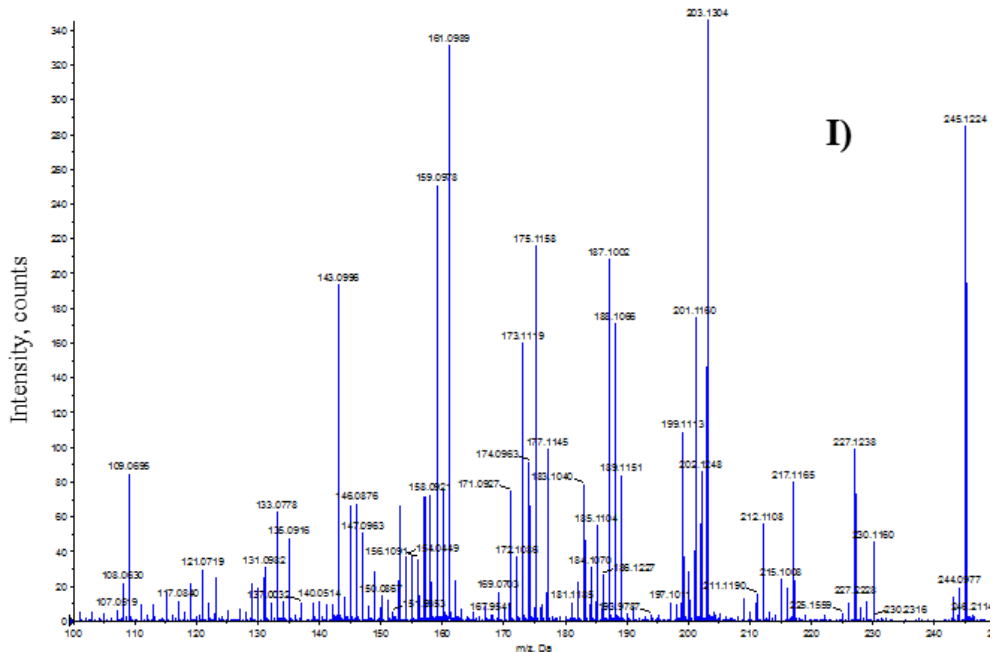


Figure 4.6: Continued.

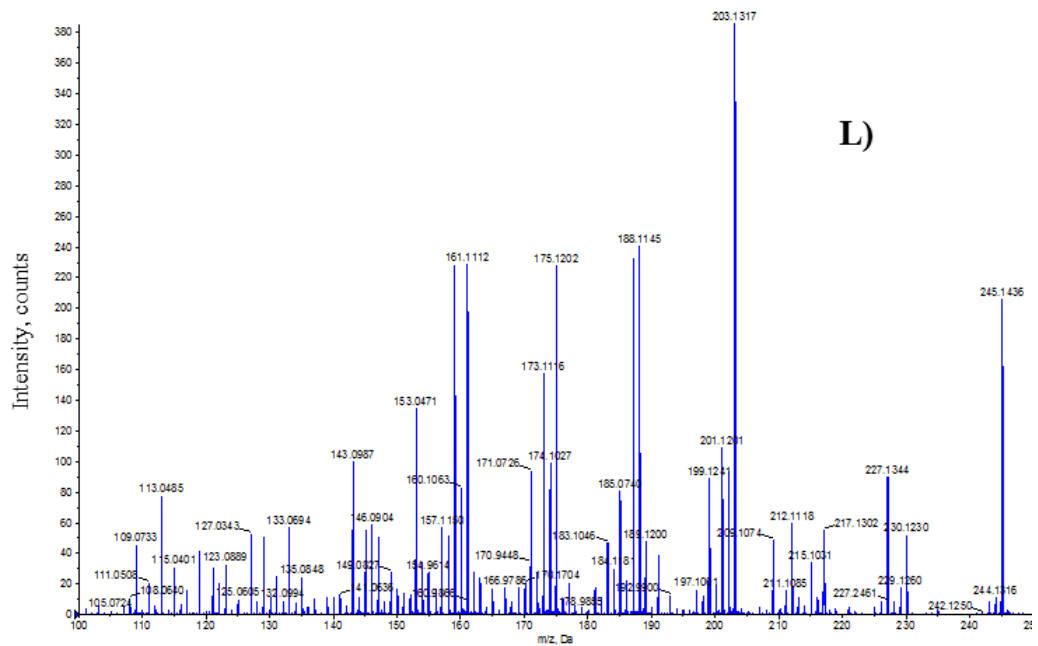
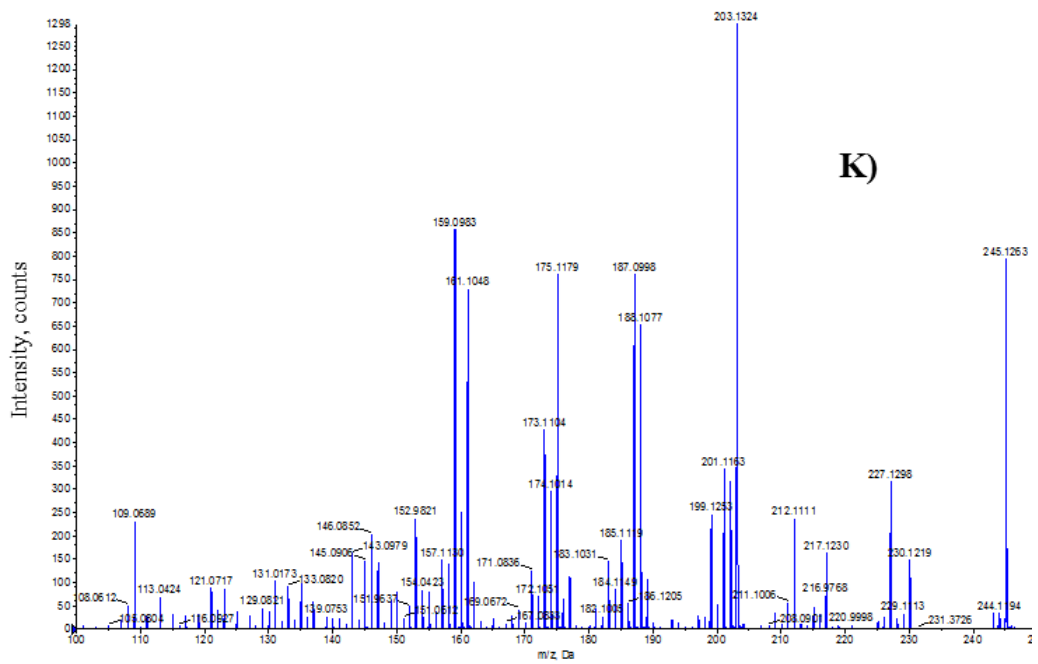
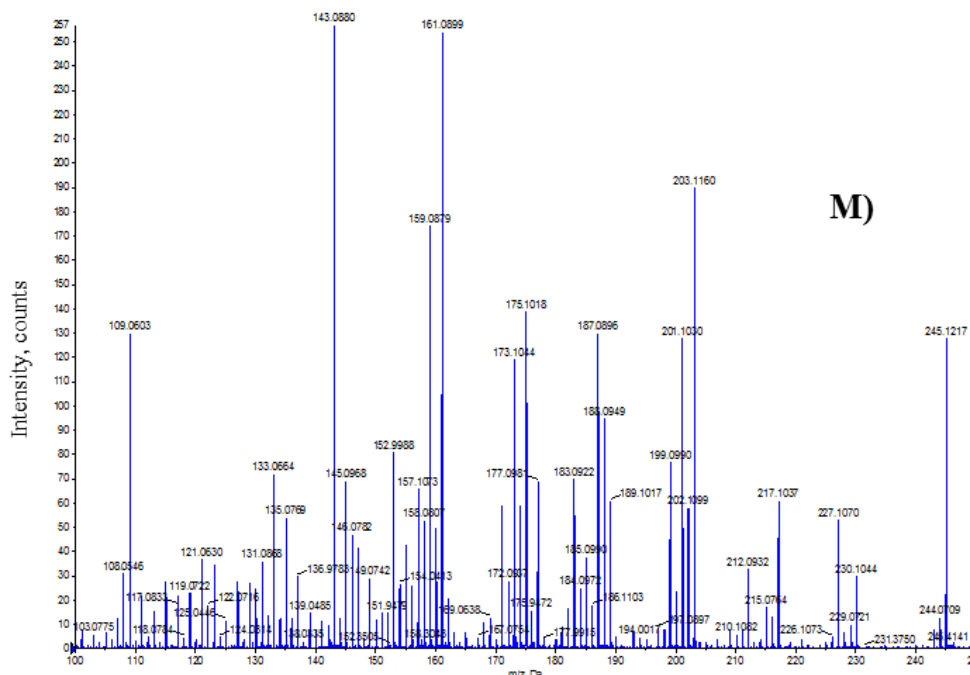
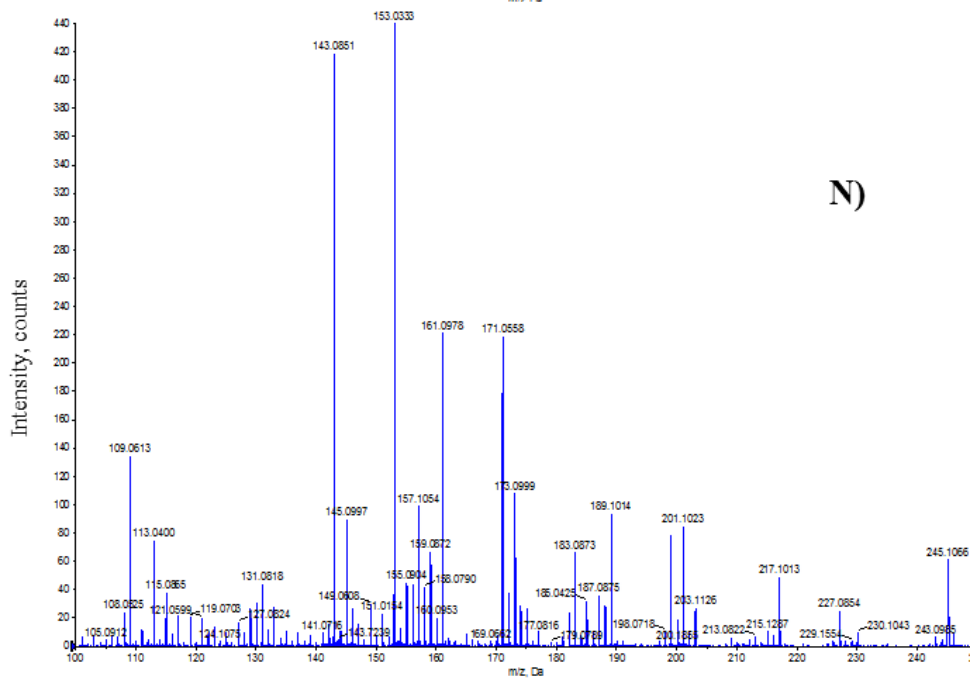


Figure 4.6: Continued.



M)



N)

Figure 4.6: Continued.

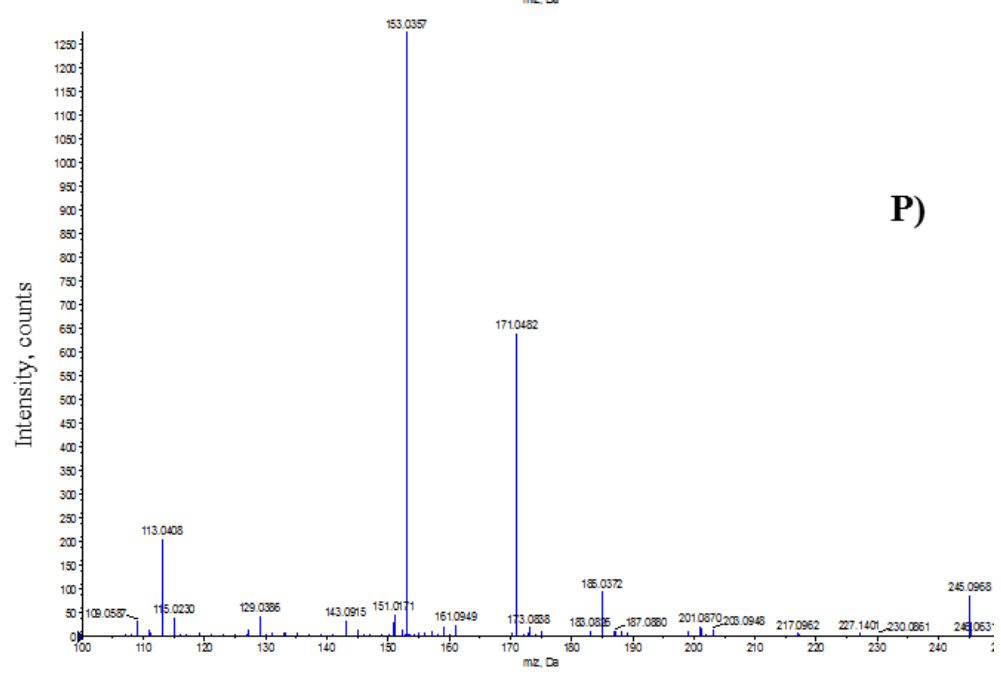
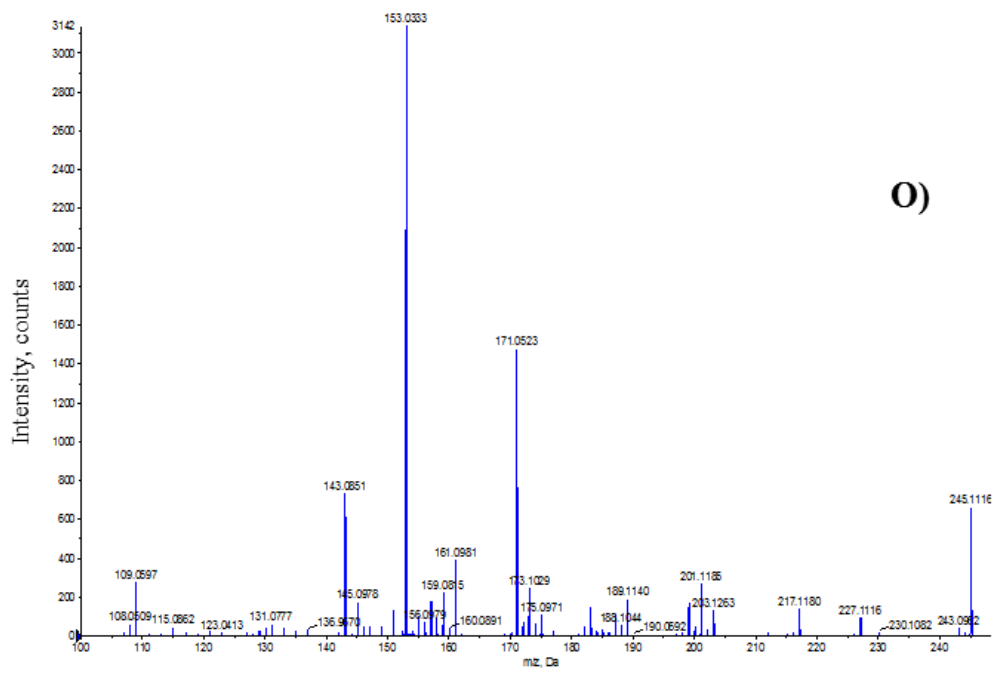


Figure 4.6: Continued.

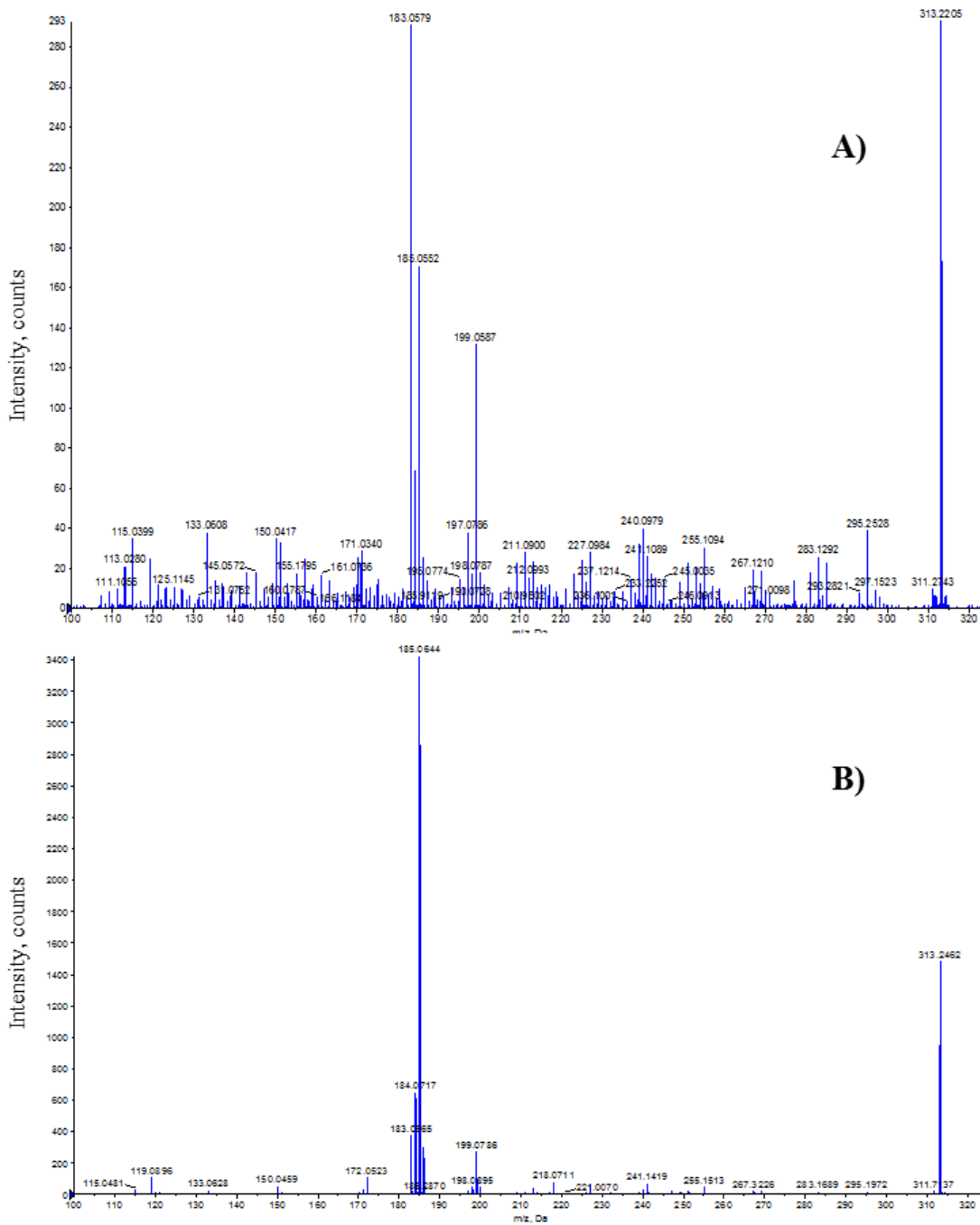


Figure A4.7: MS/MS fragmentation pattern of GPP analysed in negative ESI mode. A) GPP in heat shock & eCO₂ treatment, mature leaf, aqueous polar phase. B) GPP in heat shock & eCO₂ treatment, mature leaf, organic polar phase. C) GPP in heat shock treatment & eCO₂, new leaf, aqueous polar phase. D) GPP in heat sock & eCO₂ treatment, new leaf, organic polar phase. E) GPP in eCO₂ treatment, mature leaf, aqueous polar phase. F) GPP in eCO₂ treatment, mature leaf, organic polar phase. G) GPP in eCO₂ treatment, new leaf, aqueous polar phase. H) GPP in eCO₂ treatment, new leaf, organic polar phase. I) GPP in heat shock treatment, mature leaf, organic polar phase. J) GPP in heat shock treatment, mature leaf, organic polar phase. K) GPP in heat shock treatment, new leaf, aqueous polar phase. L) GPP in heat shock treatment, new leaf, organic polar phase. M) GPP in control treatment, mature leaf, aqueous polar phase. N) GPP in control treatment, mature leaf, organic polar phase. O) GPP in control treatment, new leaf, aqueous polar phase. P) GPP in control treatment, new leaf, organic polar phase.

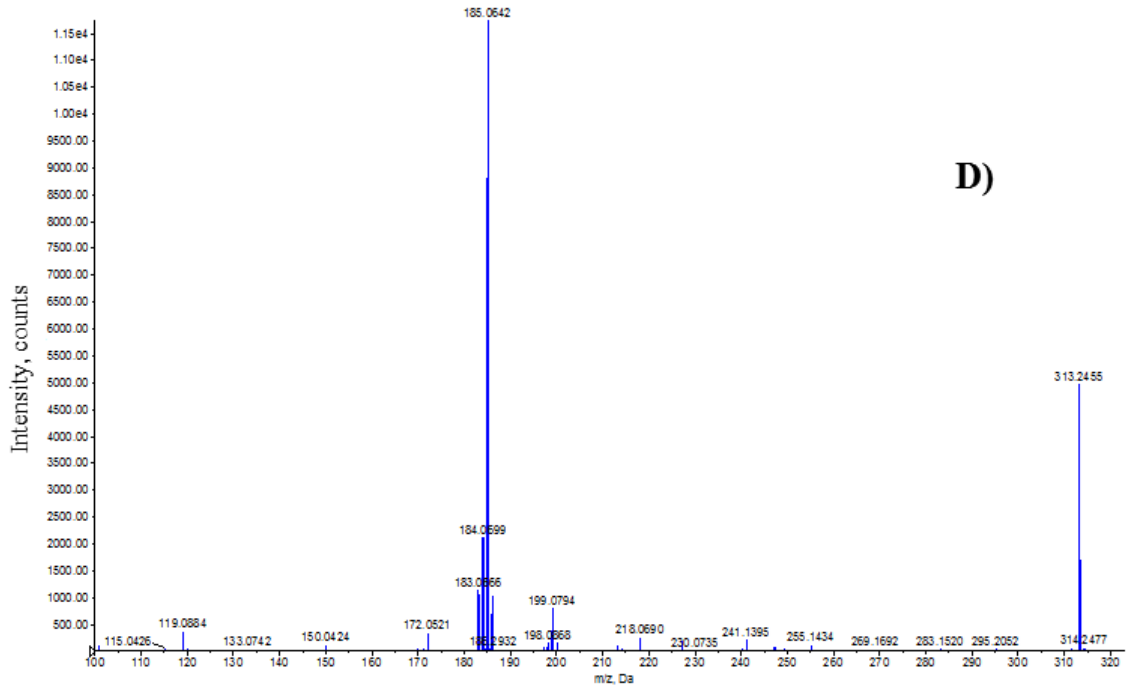
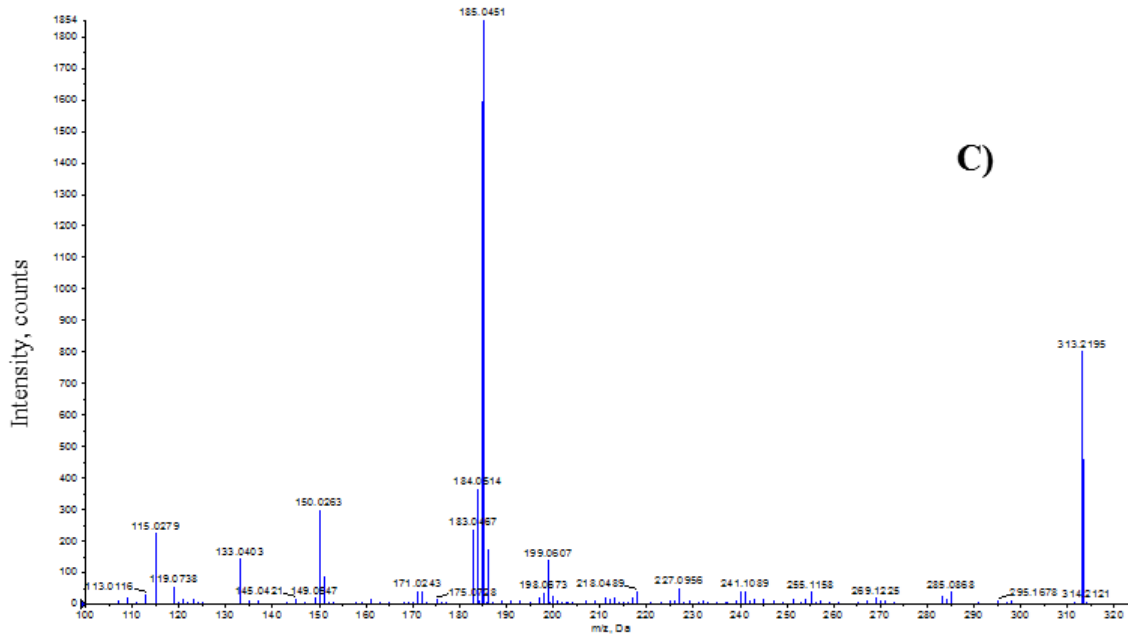
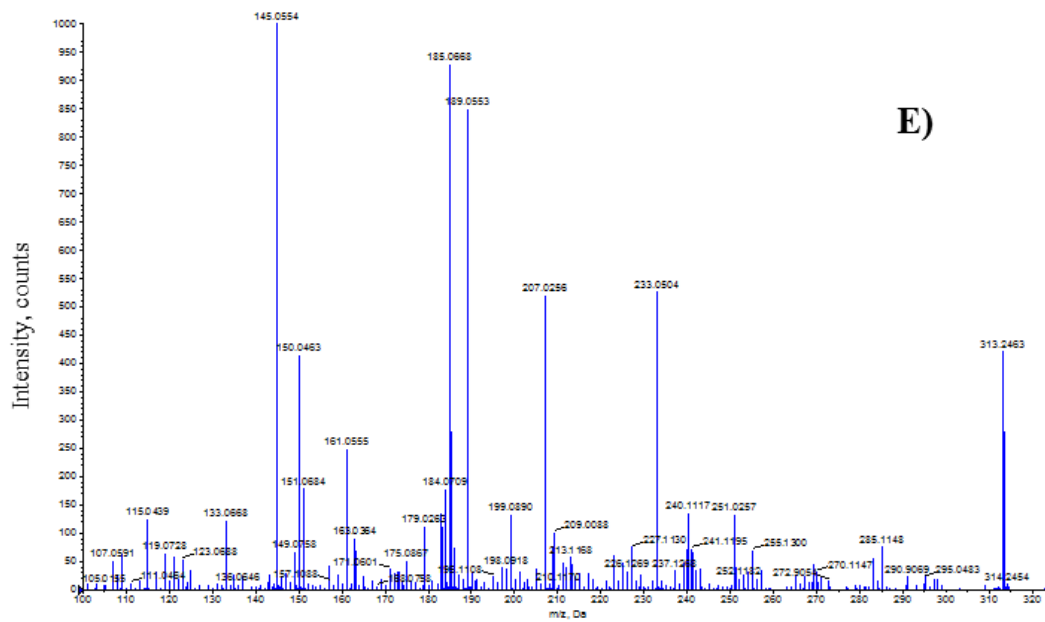
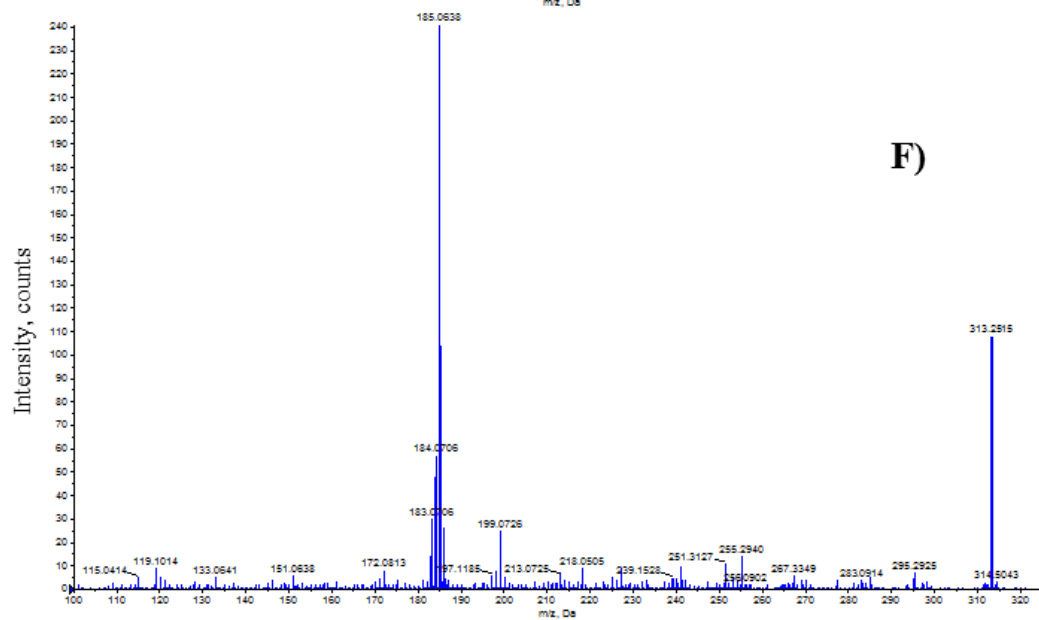


Figure 4.7: Continued.



E)



F)

Figure 4.7: Continued.

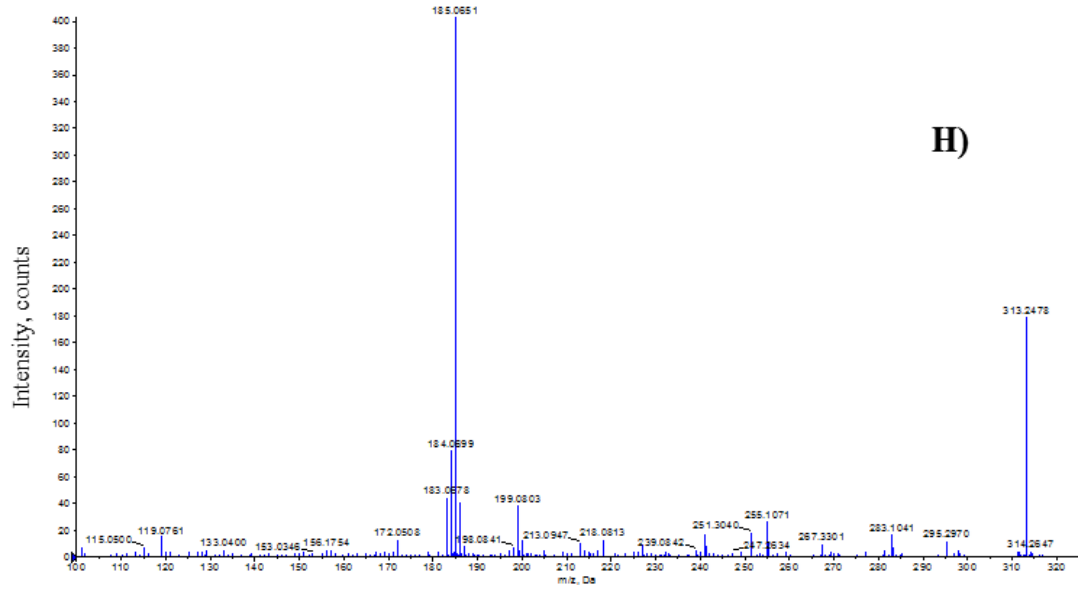
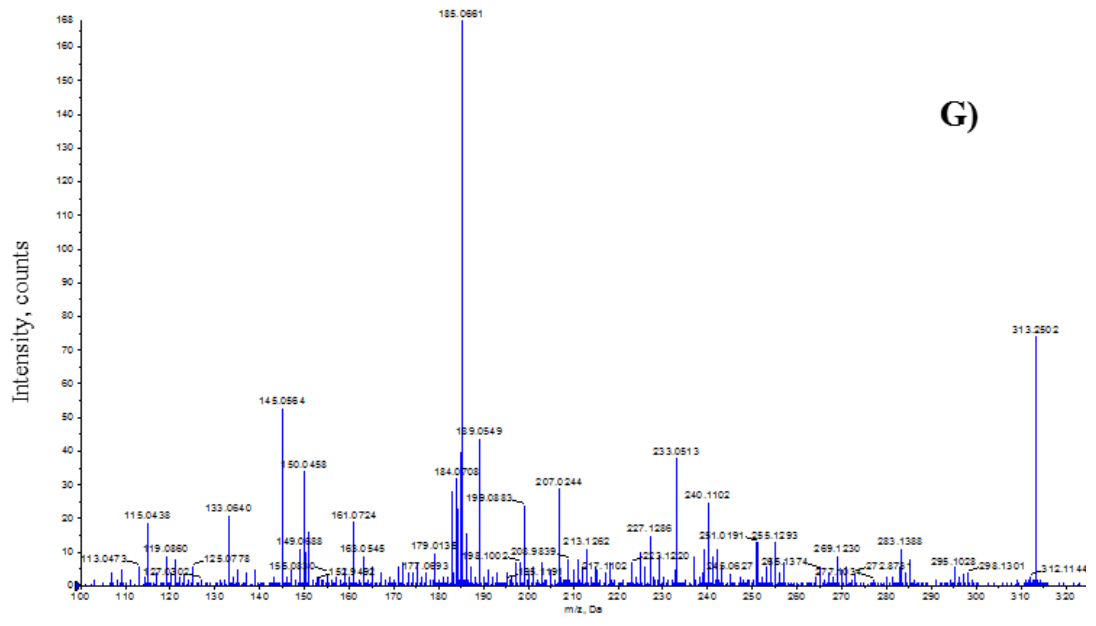
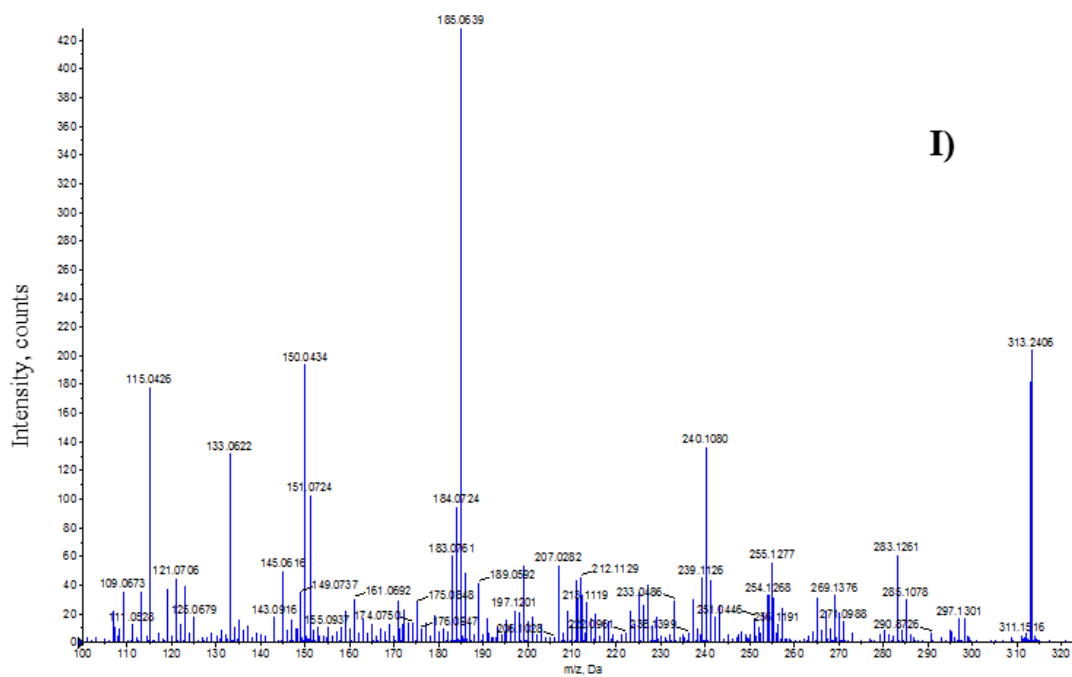
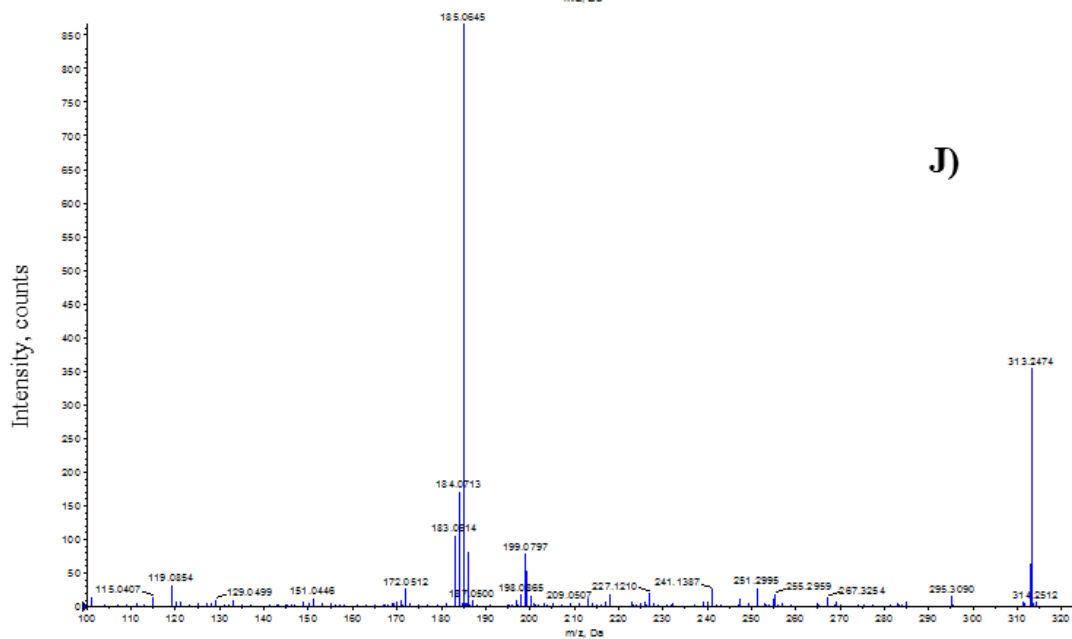


Figure 4.7: Continued.

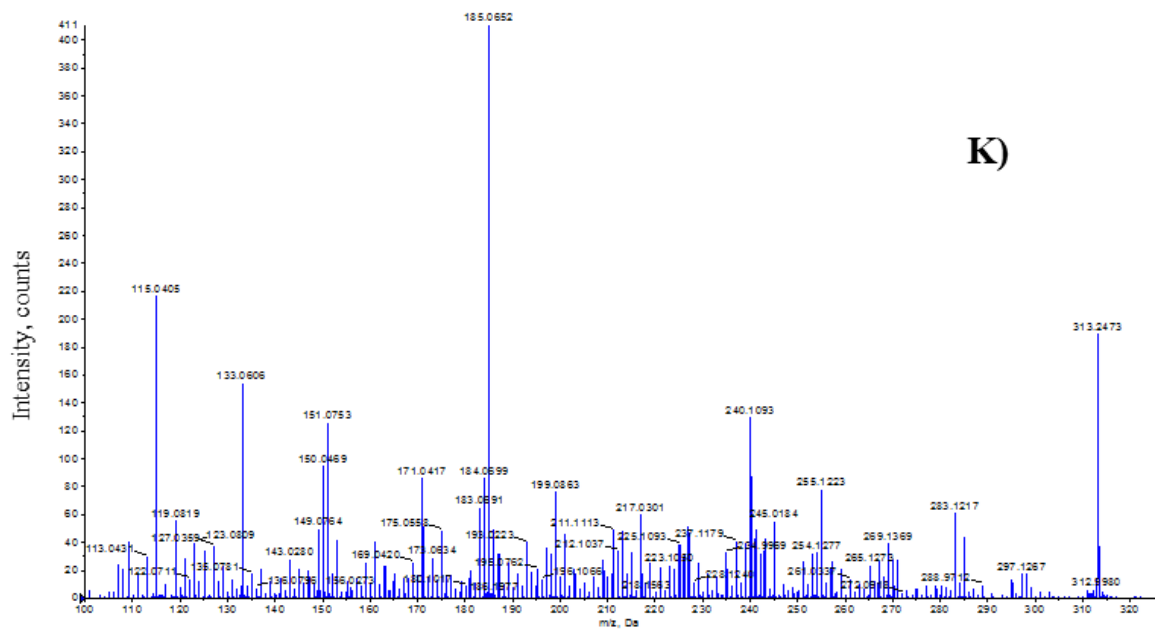


D

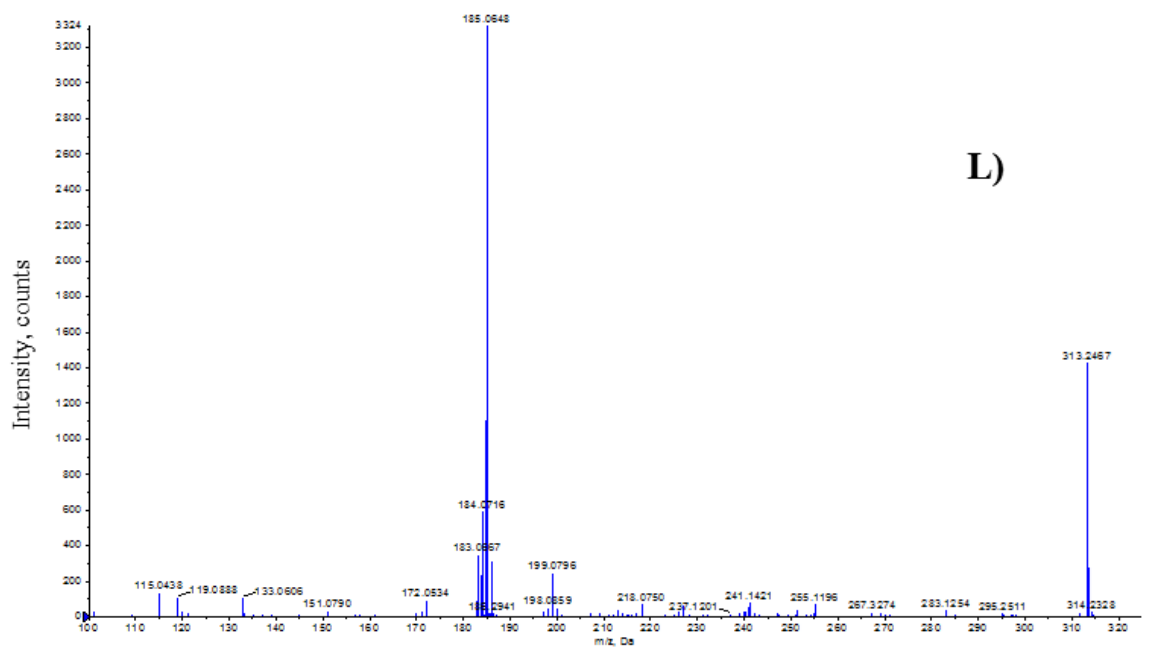


J

Figure 4.7: Continued.

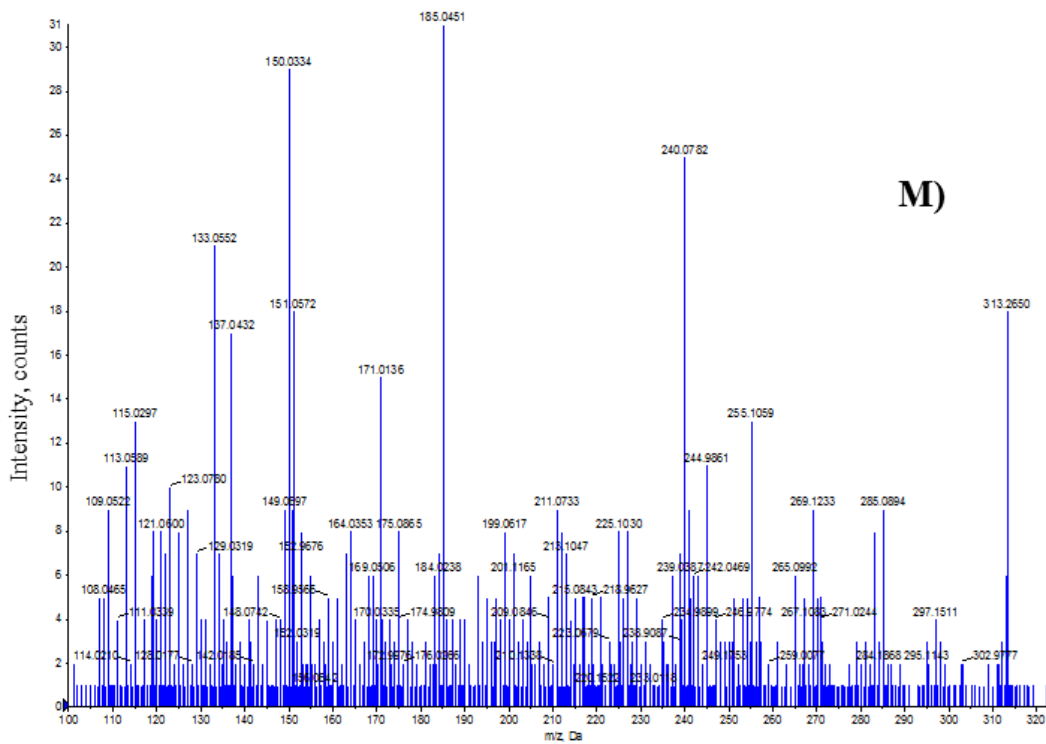


K)

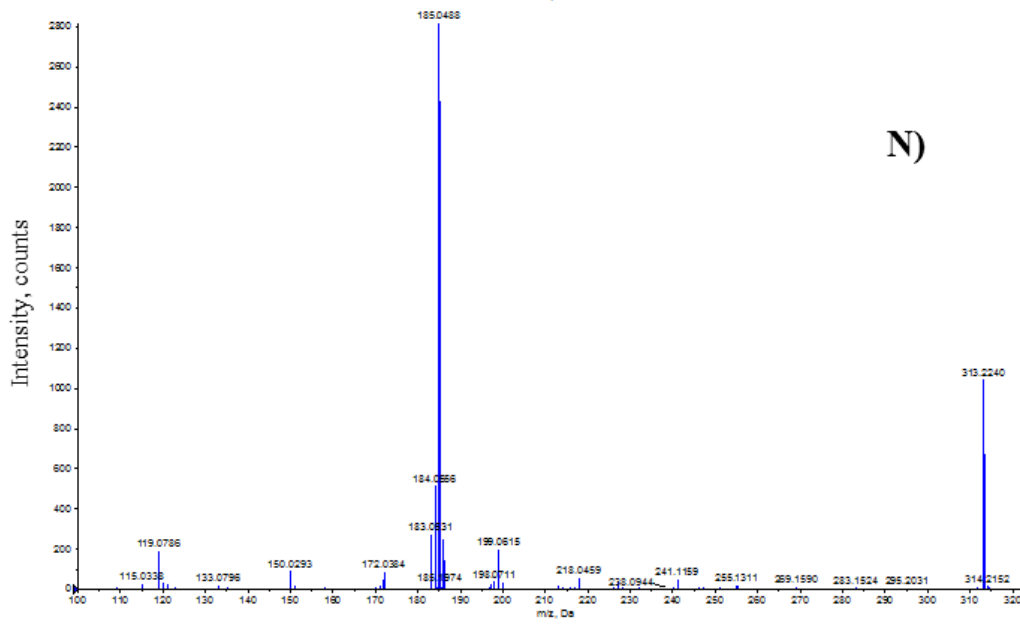


L)

Figure 4.7: Continued.

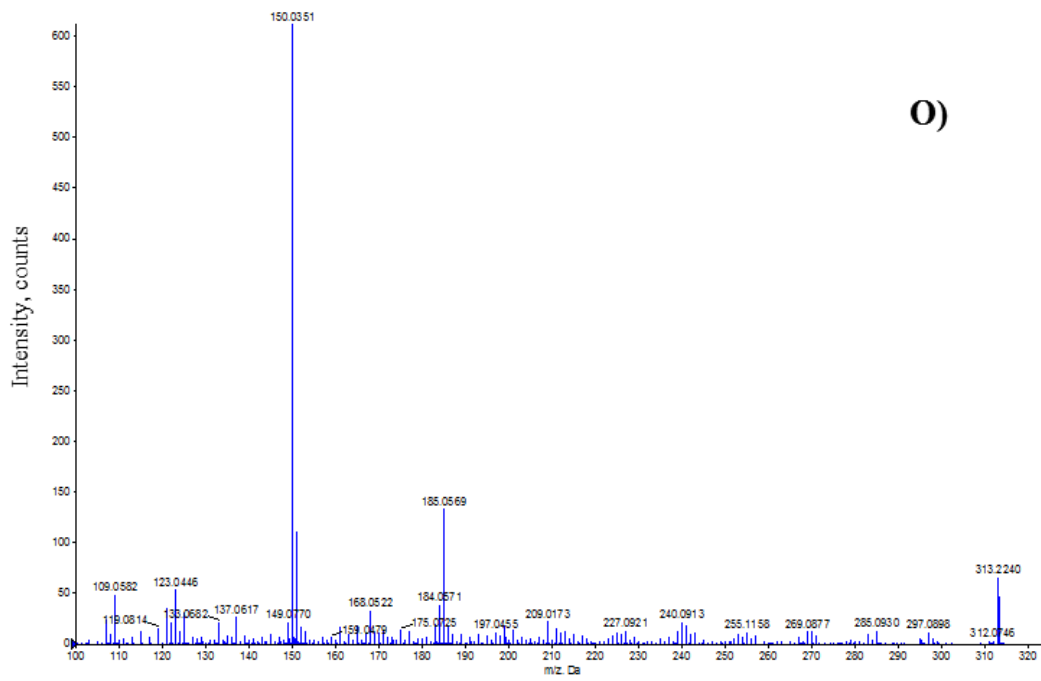


M)

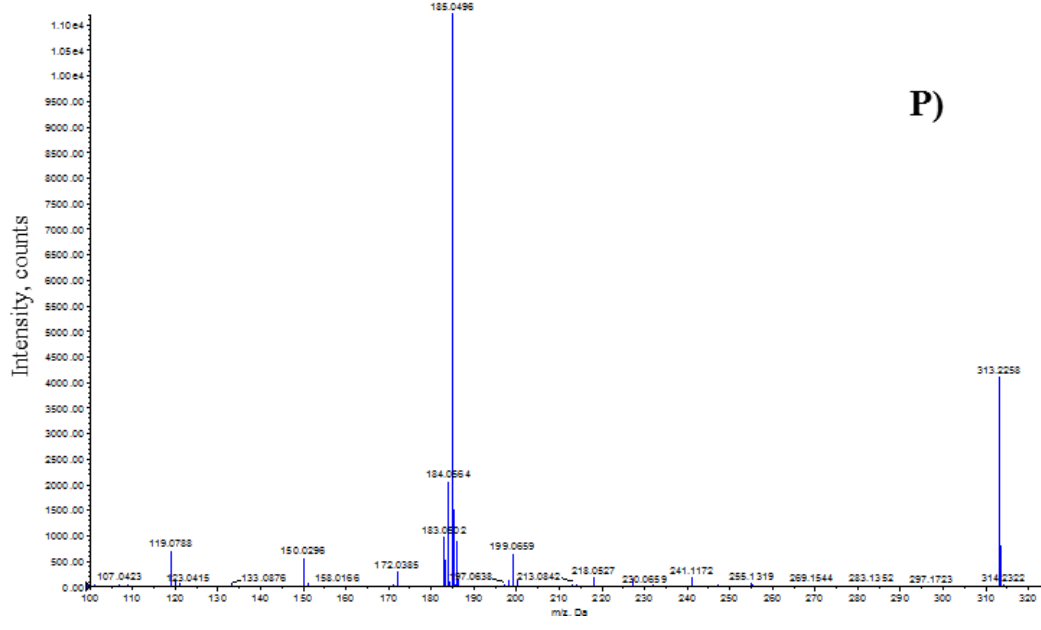


N)

Figure 4.7: Continued.



O)



P)

Figure 4.7: Continued.

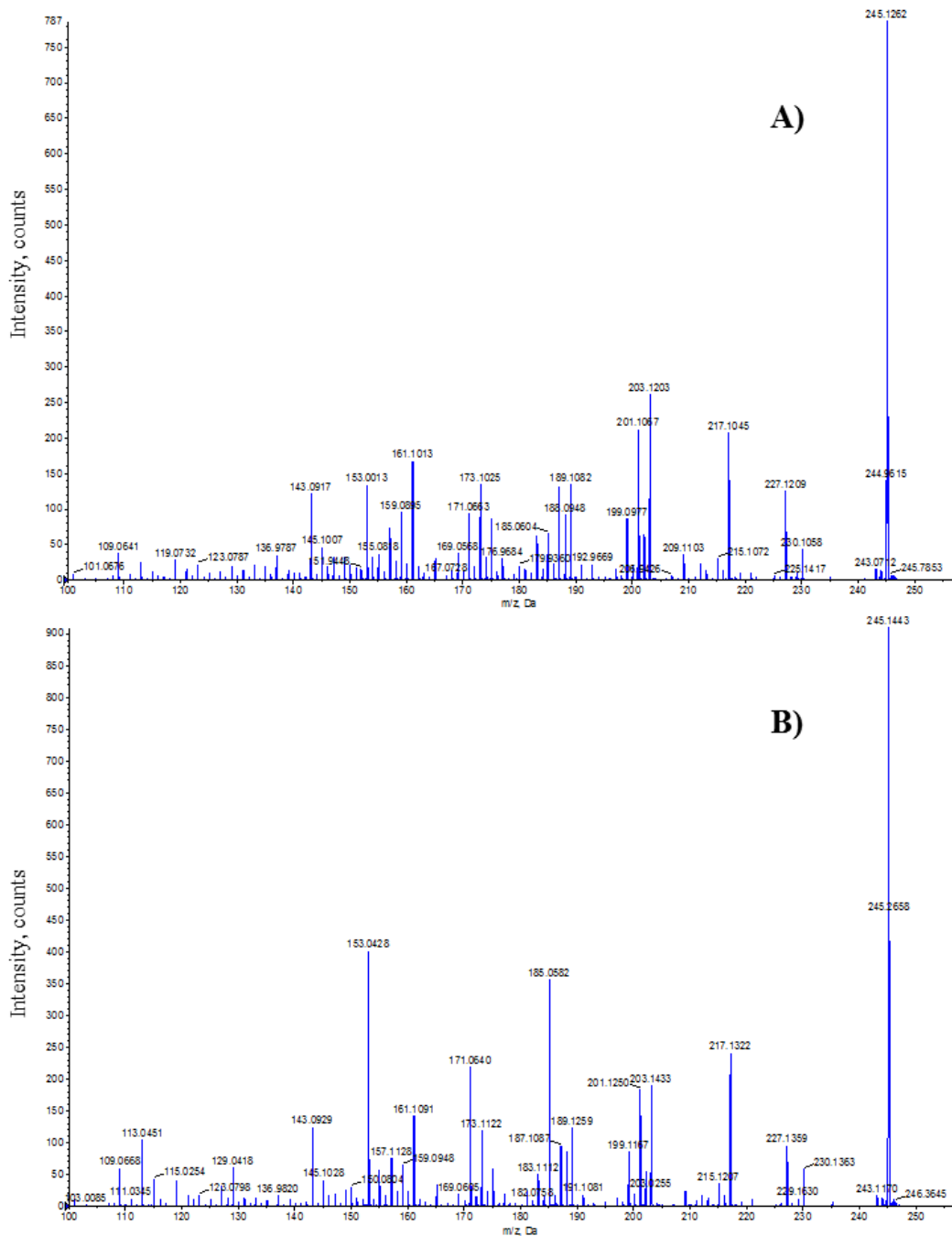


Figure A4.8: MS/MS fragmentation pattern of DMAPP analysed in negative ESI mode. A) DMAPP in heat shock & eCO₂ treatment, mature leaf, aqueous polar phase. B) DMAPP in heat shock & eCO₂ treatment, mature leaf, organic polar phase. C) DMAPP in heat shock treatment & eCO₂, new leaf, aqueous polar phase. D) DMAPP in heat sock & eCO₂ treatment, new leaf, organic polar phase. E) DMAPP in eCO₂ treatment, mature leaf, aqueous polar phase. F) DMAPP in eCO₂ treatment, mature leaf, organic polar phase. G) DMAPP in eCO₂ treatment, new leaf, aqueous polar phase. H) DMAPP in eCO₂ treatment, new leaf, organic polar phase. I) DMAPP in heat shock treatment, mature leaf, organic polar phase. J) DMAPP in heat shock treatment, mature leaf, organic polar phase. K) DMAPP in heat shock treatment, mature leaf, organic polar phase. L) DMAPP in heat shock treatment, new leaf, organic polar phase. M) DMAPP in control treatment, mature leaf, aqueous polar phase. N) DMAPP in control treatment, mature leaf, organic polar phase. O) DMAPP in control treatment, new leaf, aqueous polar phase. P) DMAPP in control treatment, new leaf, organic polar phase.

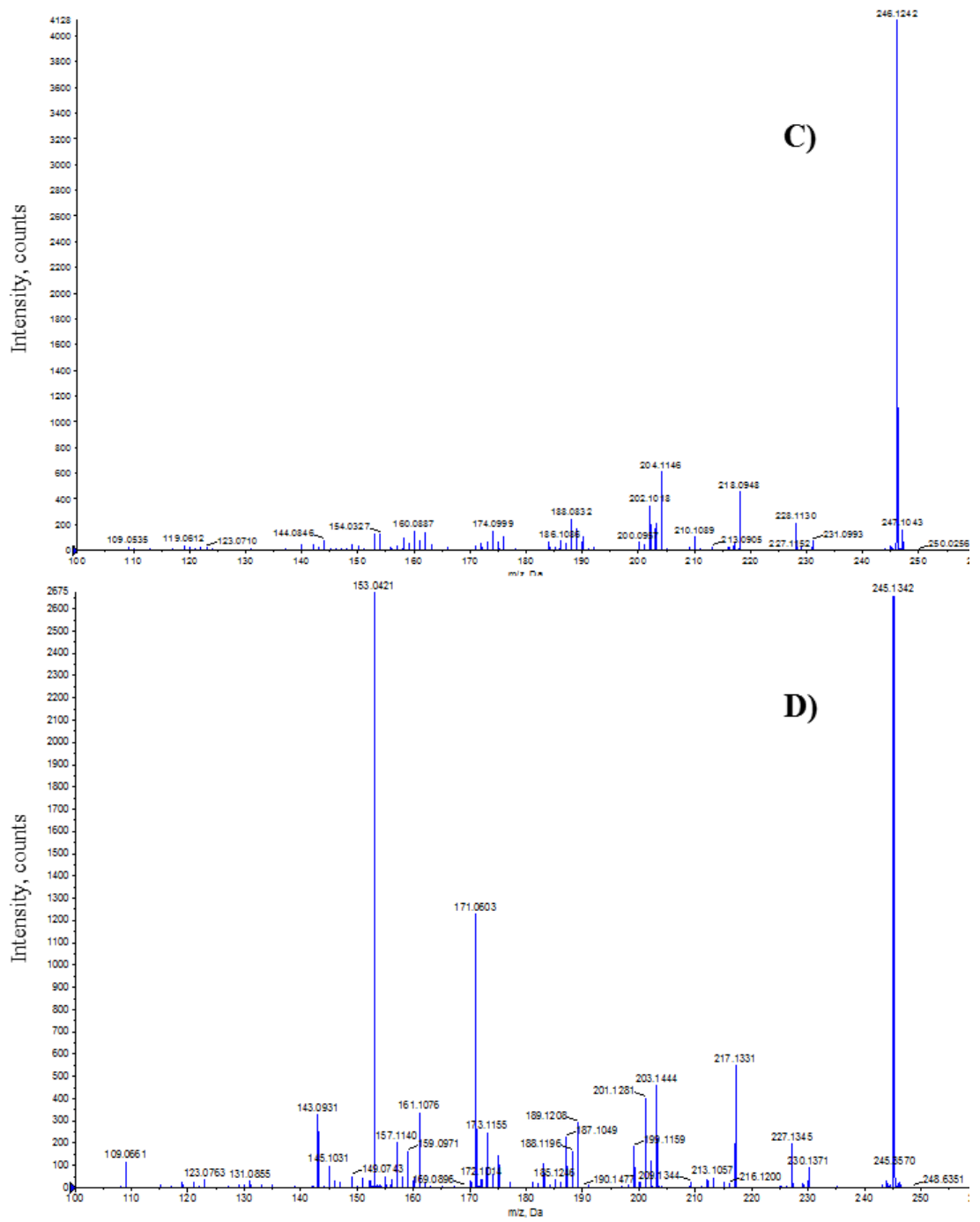


Figure 4.8: Continued.

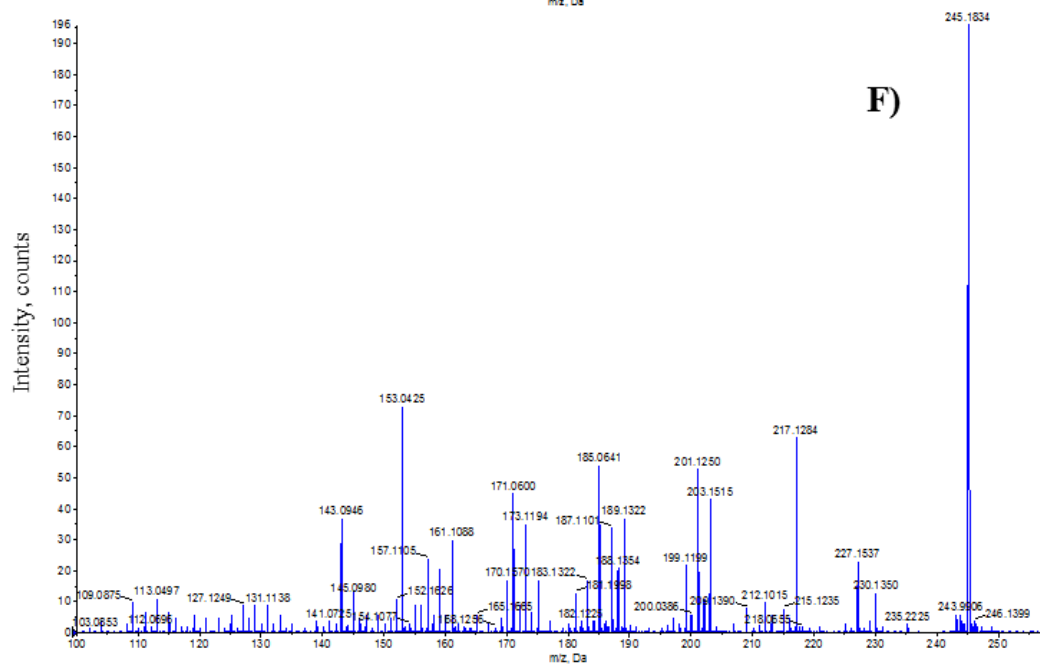
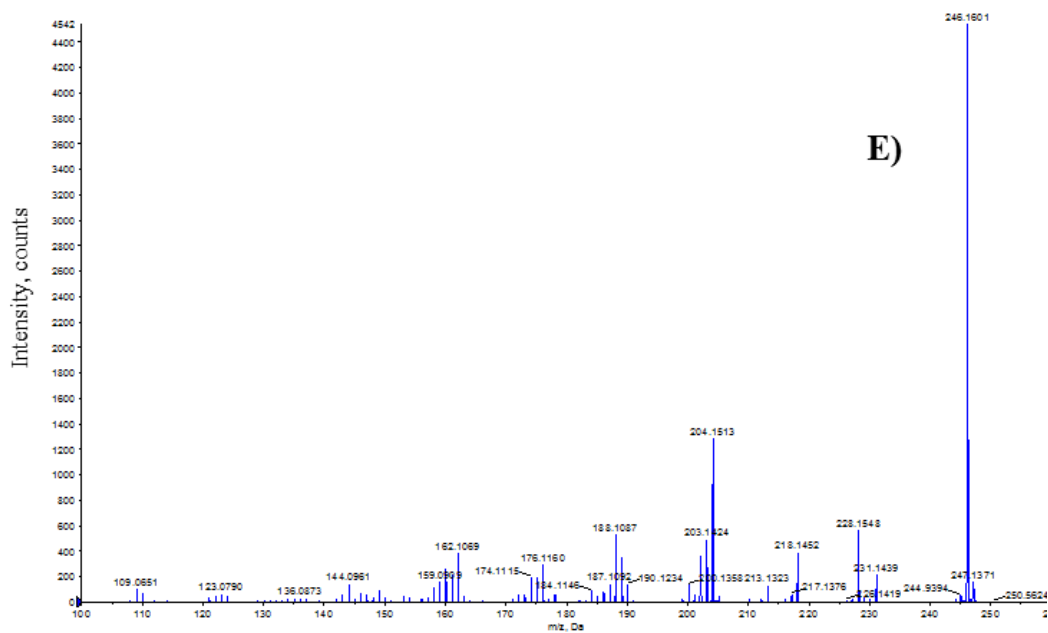


Figure 4.8: Continued.

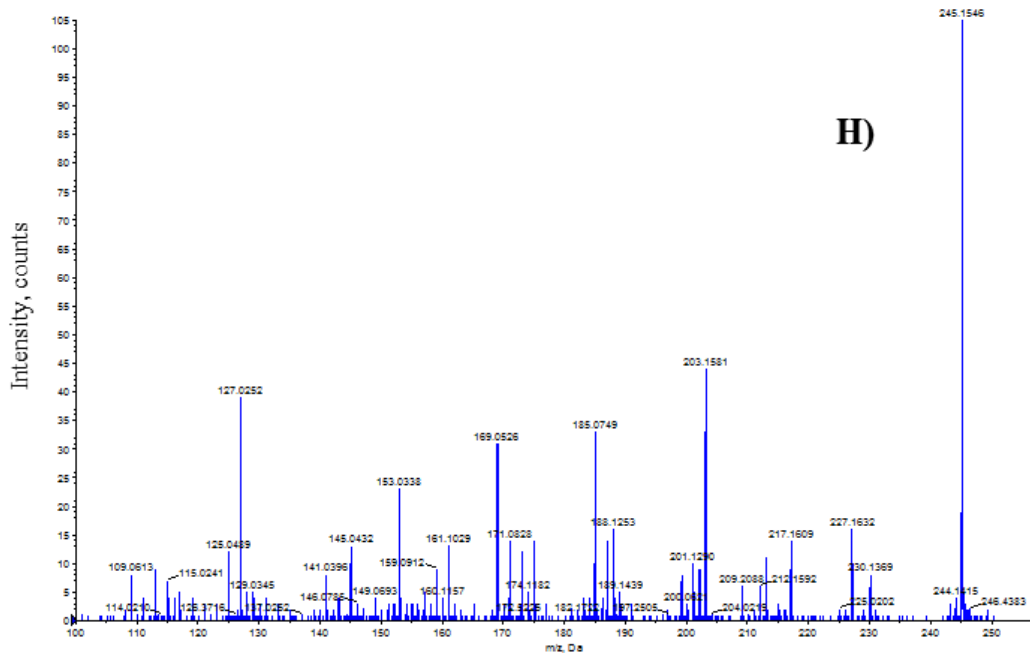
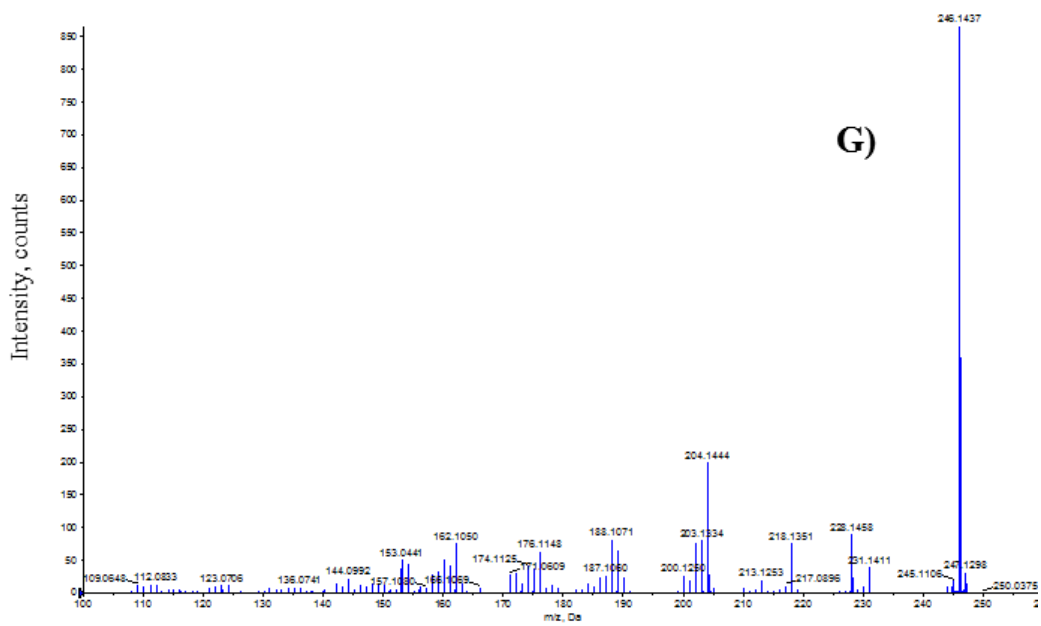


Figure 4.8: Continued.

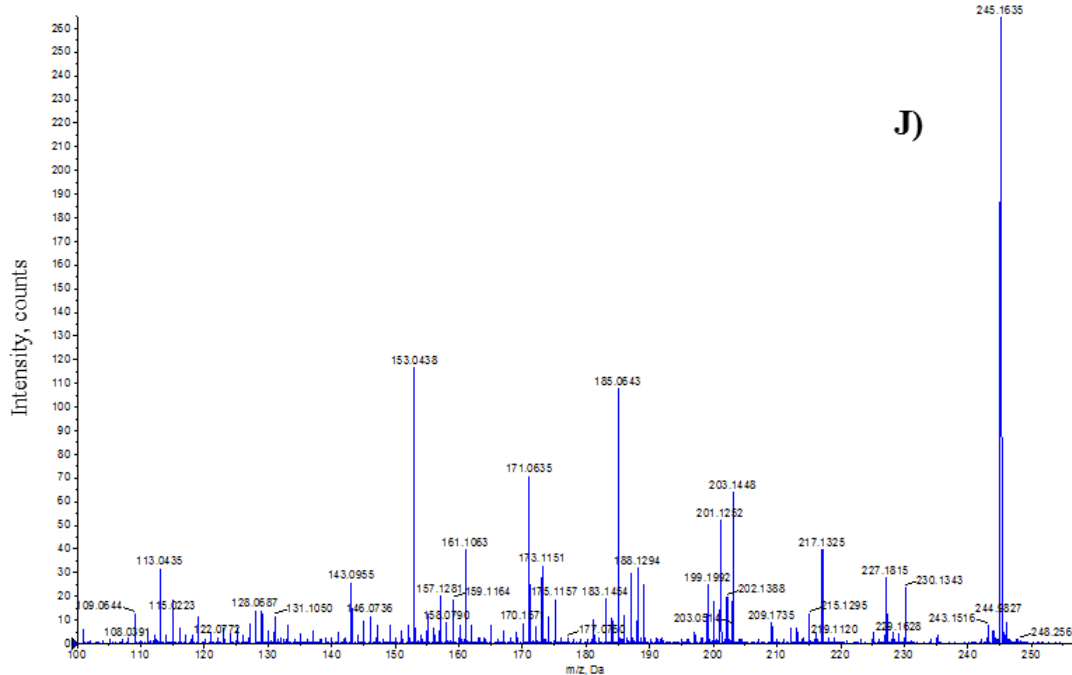
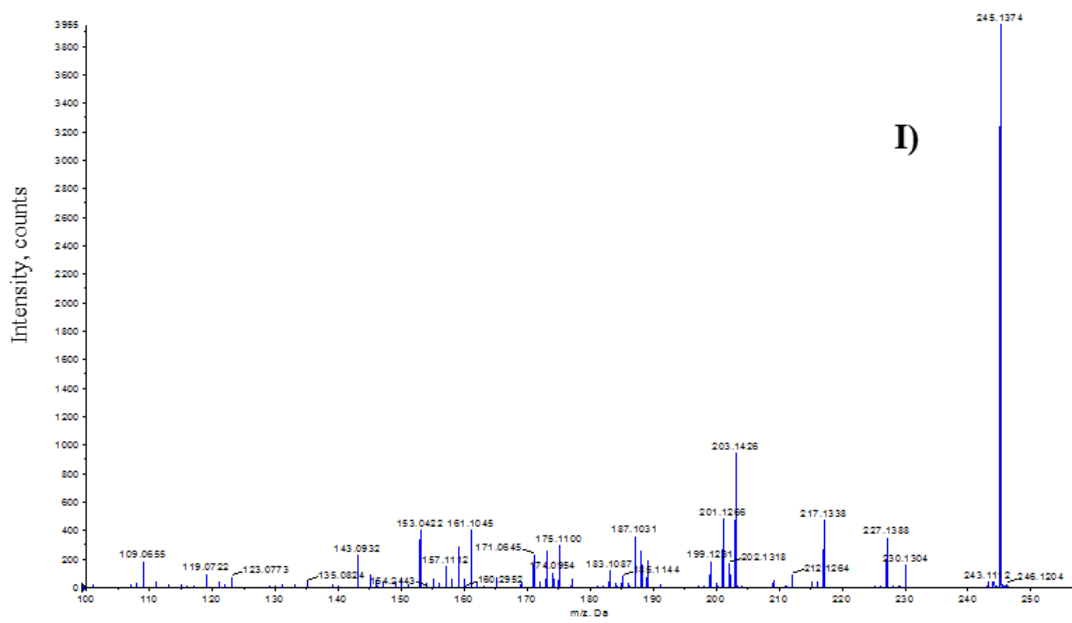


Figure 4.8: Continued.

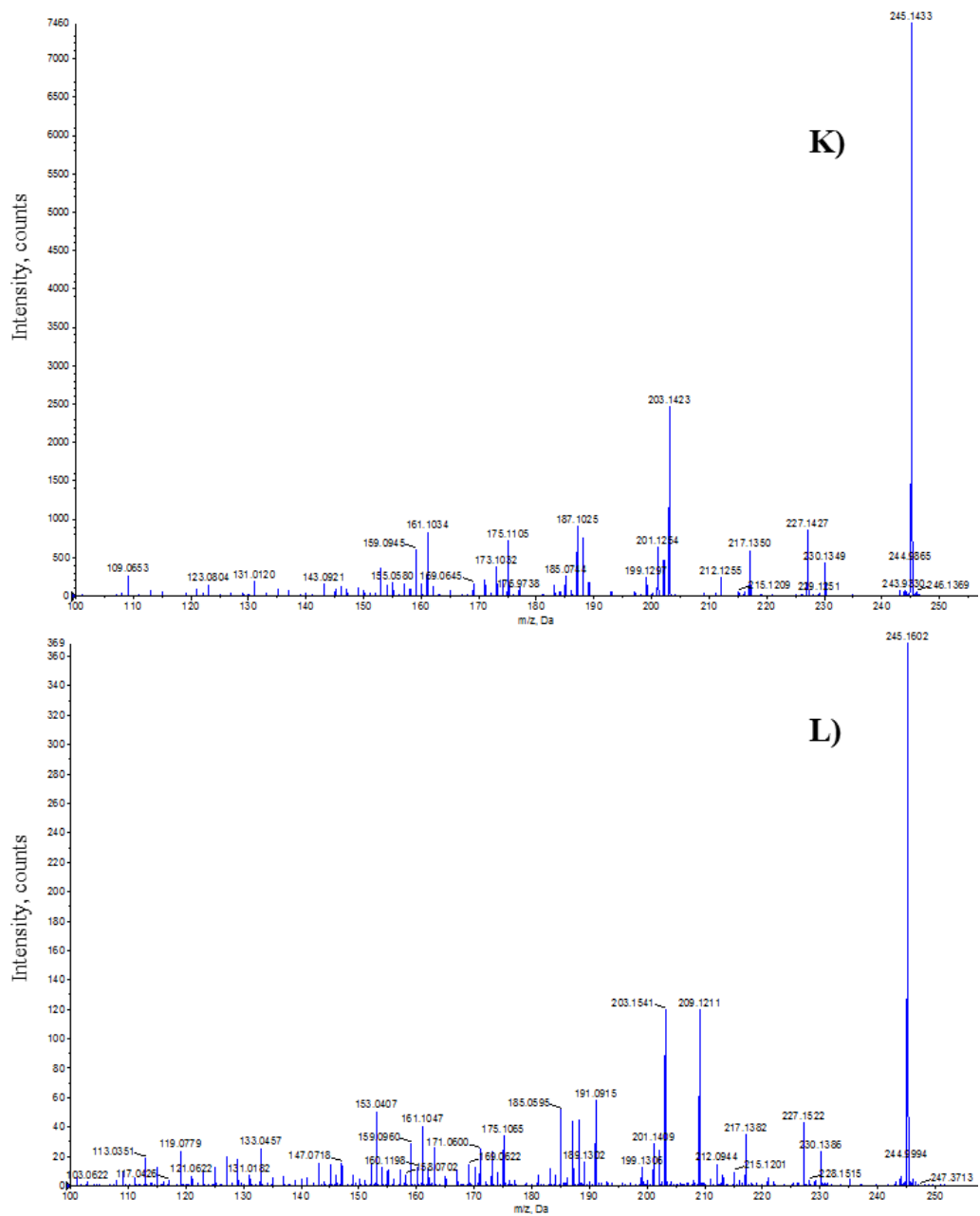


Figure 4.8: Continued.

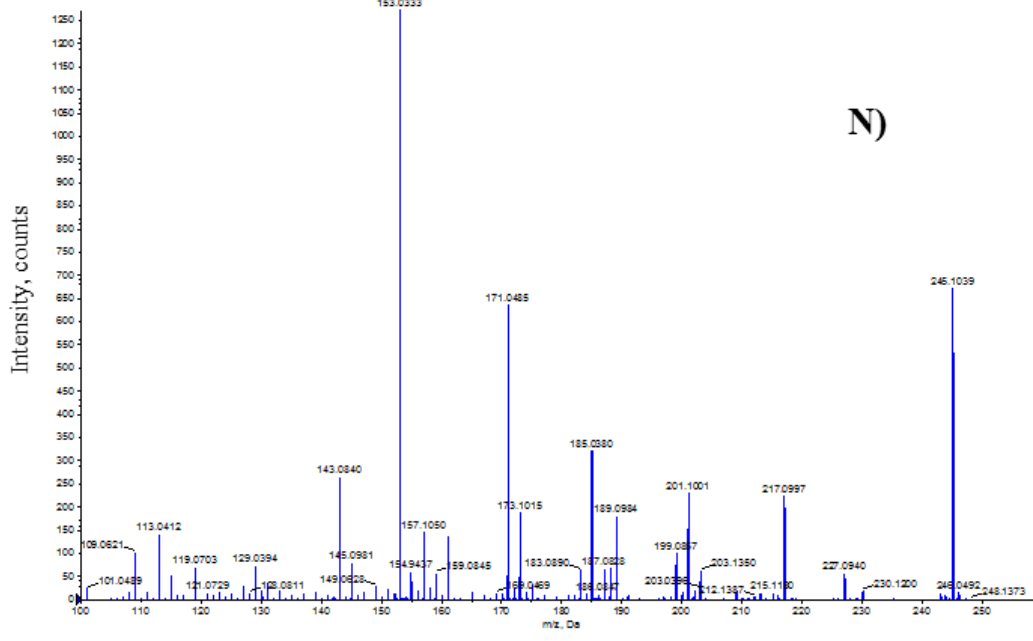
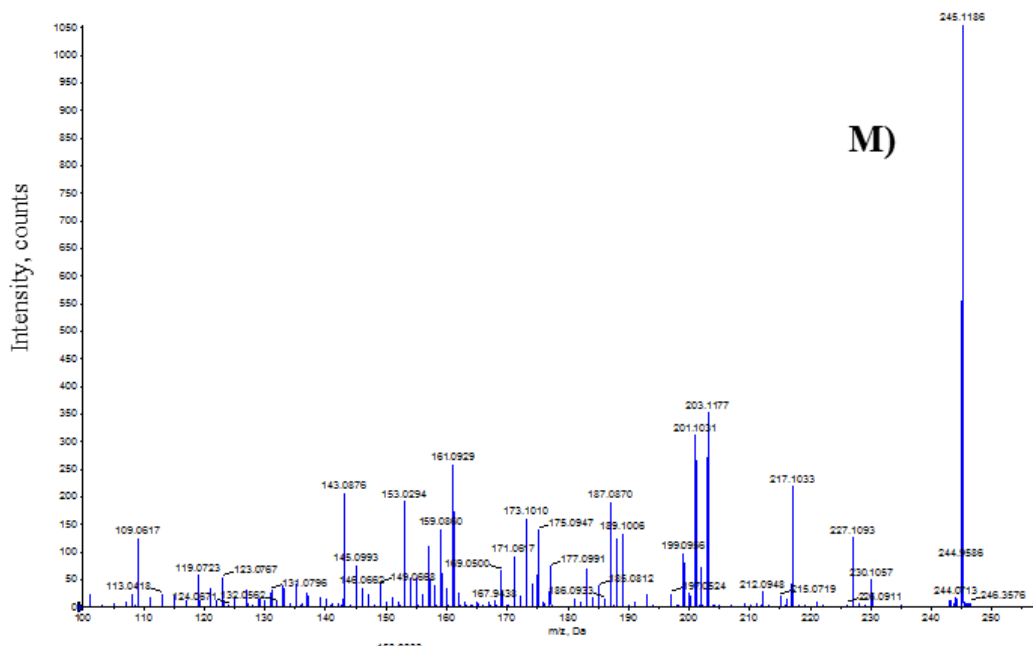


Figure 4.8: Continued.

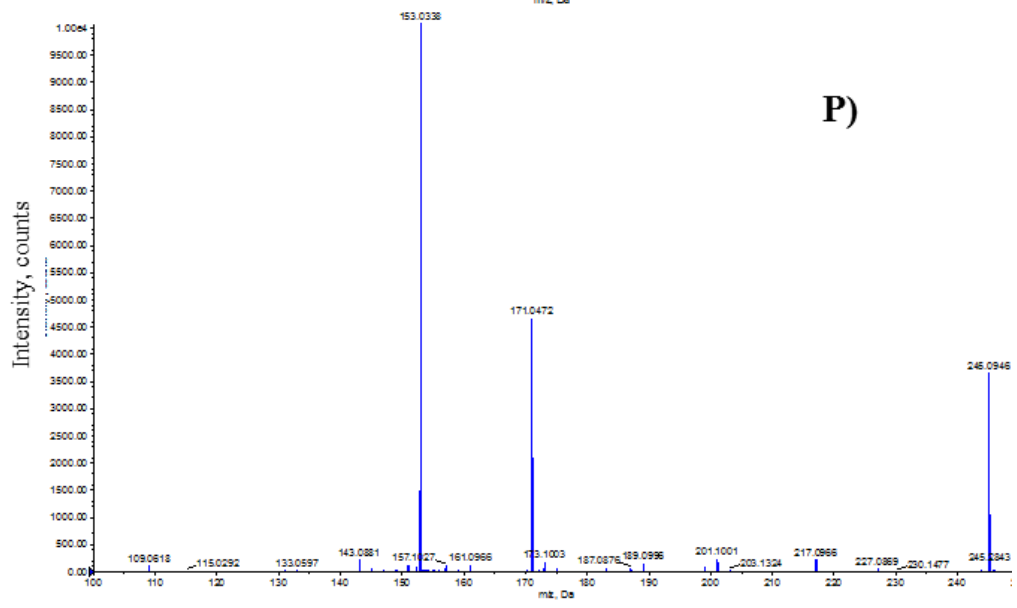
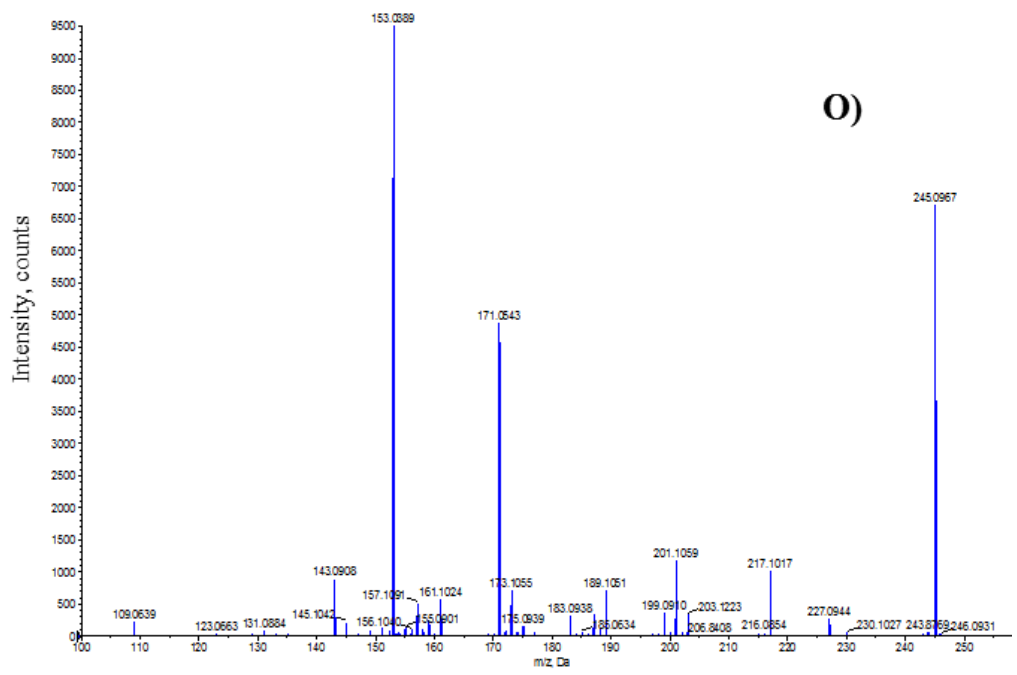


Figure 4.8: Continued.

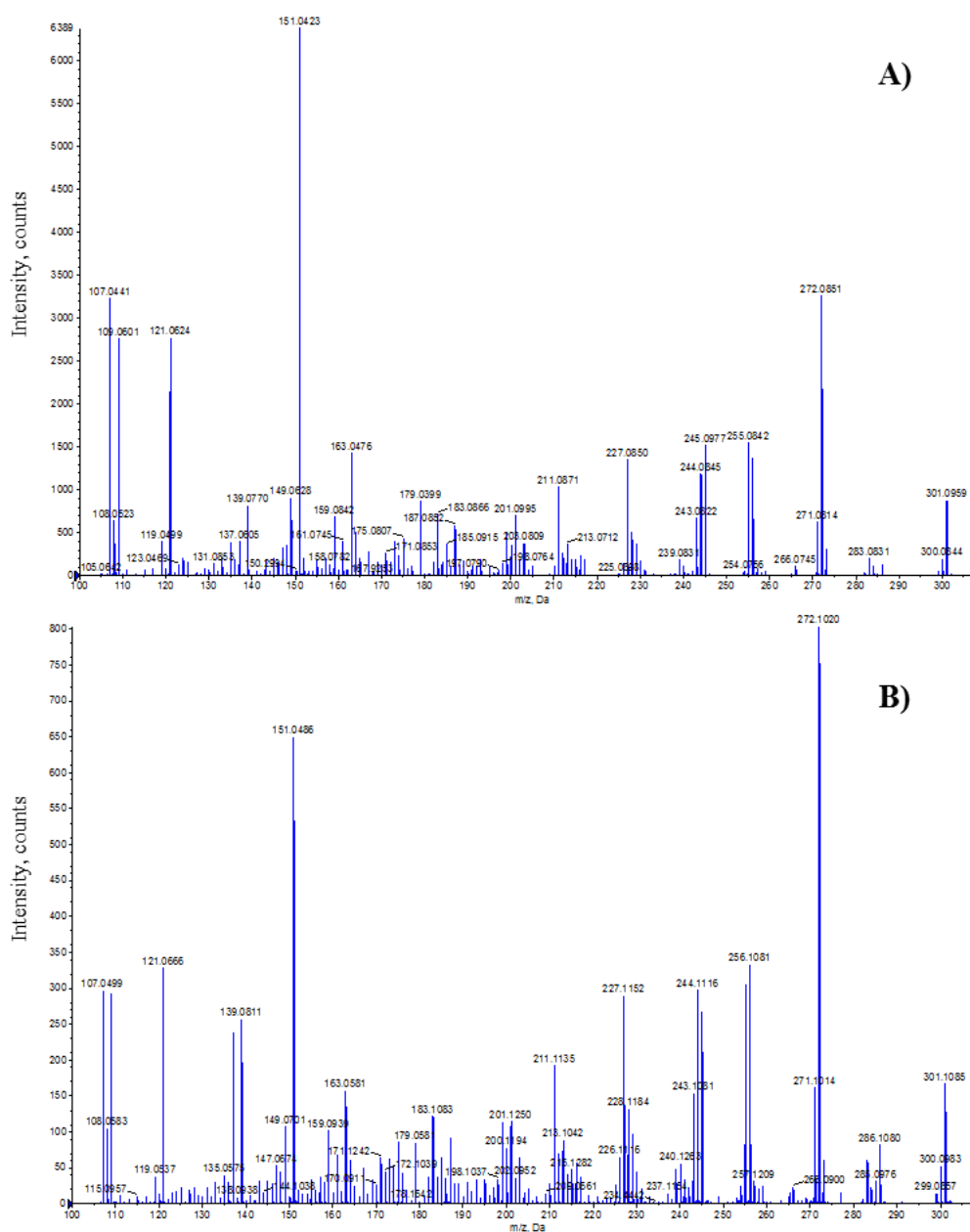


Figure A4.9: MS/MS fragmentation pattern of Quercetin analysed in negative ESI mode. A) Quercetin in heat shock & eCO₂ treatment, mature leaf, aqueous polar phase. B) Quercetin in heat shock & eCO₂ treatment, mature leaf, organic polar phase. C) Quercetin in heat shock treatment & eCO₂, new leaf, aqueous polar phase. D) Quercetin in heat sock & eCO₂ treatment, new leaf, organic polar phase. E) Quercetin in eCO₂ treatment, mature leaf, aqueous polar phase. F) Quercetin in eCO₂ treatment, mature leaf, organic polar phase. G) Quercetin in eCO₂ treatment, new leaf, aqueous polar phase. H) Quercetin in eCO₂ treatment, new leaf, organic polar phase. I) Quercetin in heat shock treatment, mature leaf, organic polar phase. J) Quercetin in heat shock treatment, mature leaf, organic polar phase. K) Quercetin in heat shock treatment, new leaf, aqueous polar phase. L) Quercetin in heat shock treatment, new leaf, organic polar phase. M) Quercetin in control treatment, mature leaf, aqueous polar phase. N) Quercetin in control treatment, mature leaf, organic polar phase. O) Quercetin in control treatment, new leaf, aqueous polar phase. P) Quercetin in control treatment, new leaf, organic polar phase.

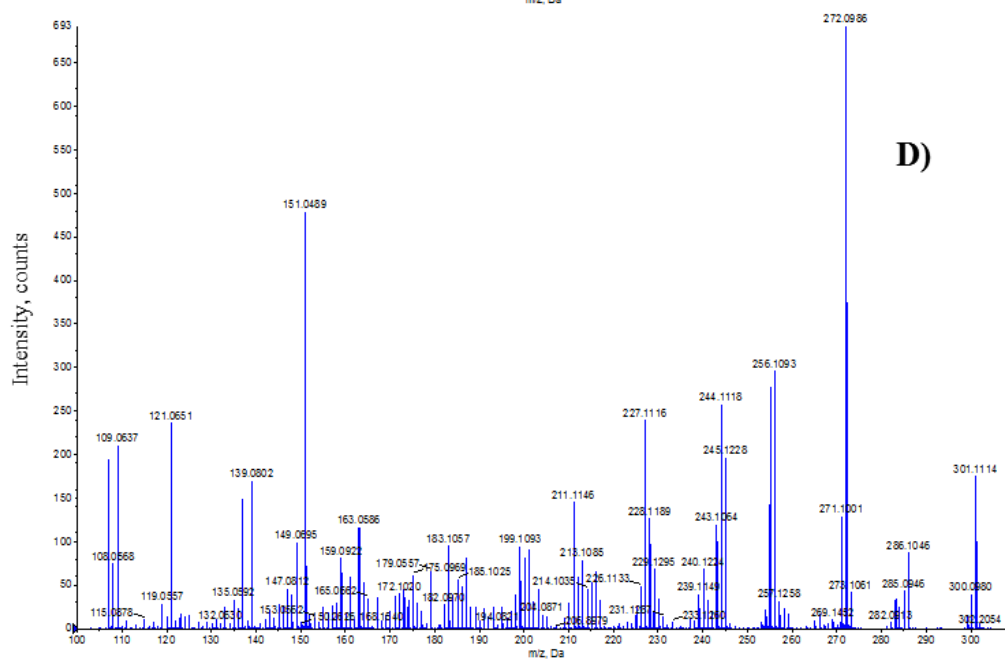
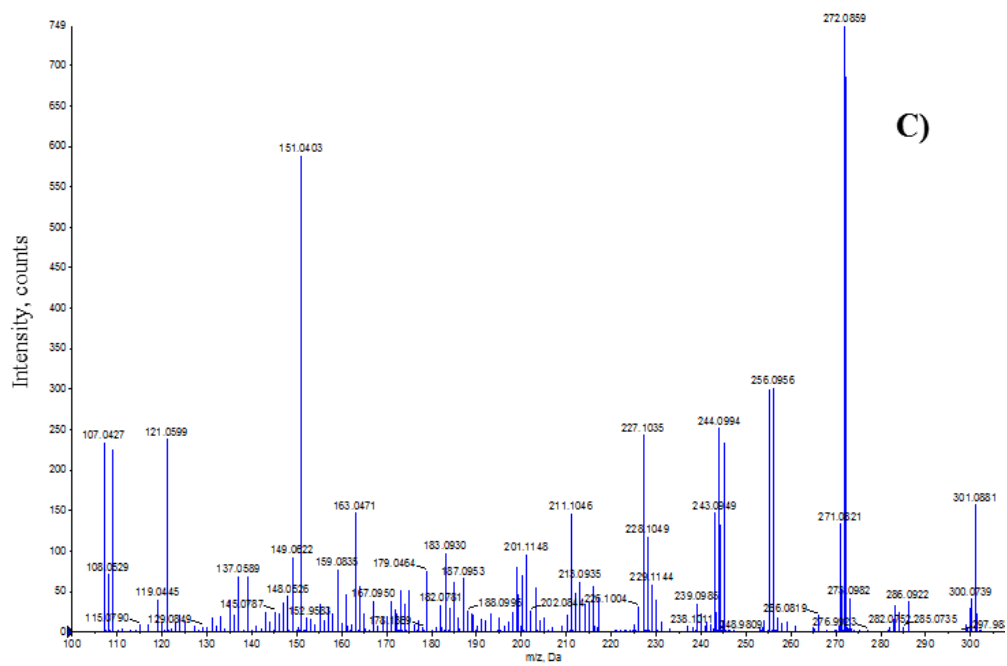


Figure 4.9: Continued.

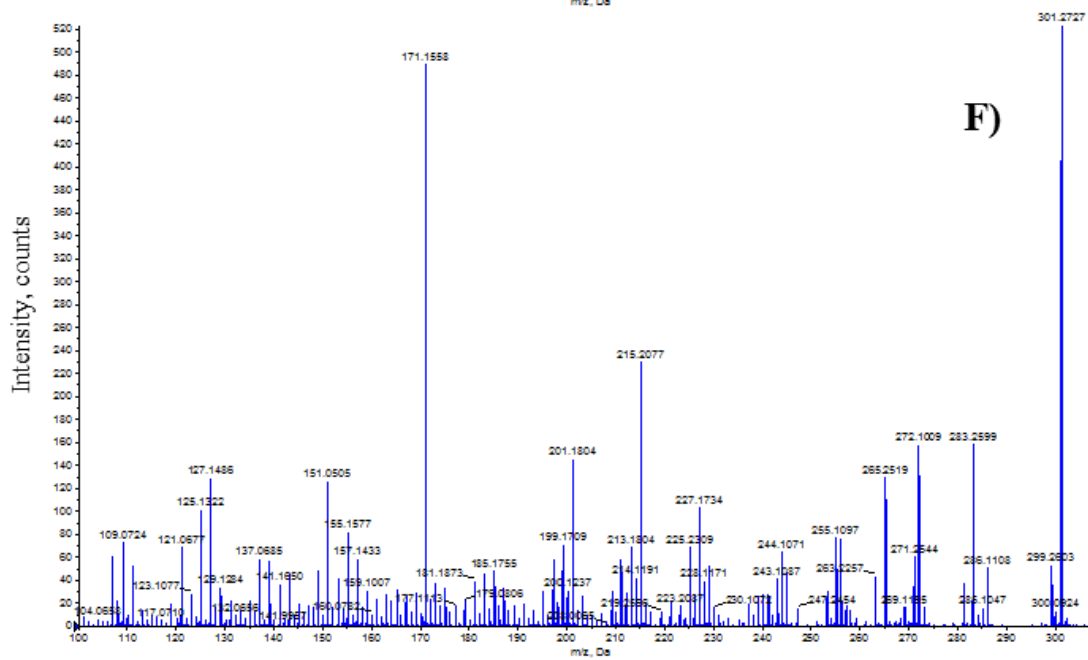
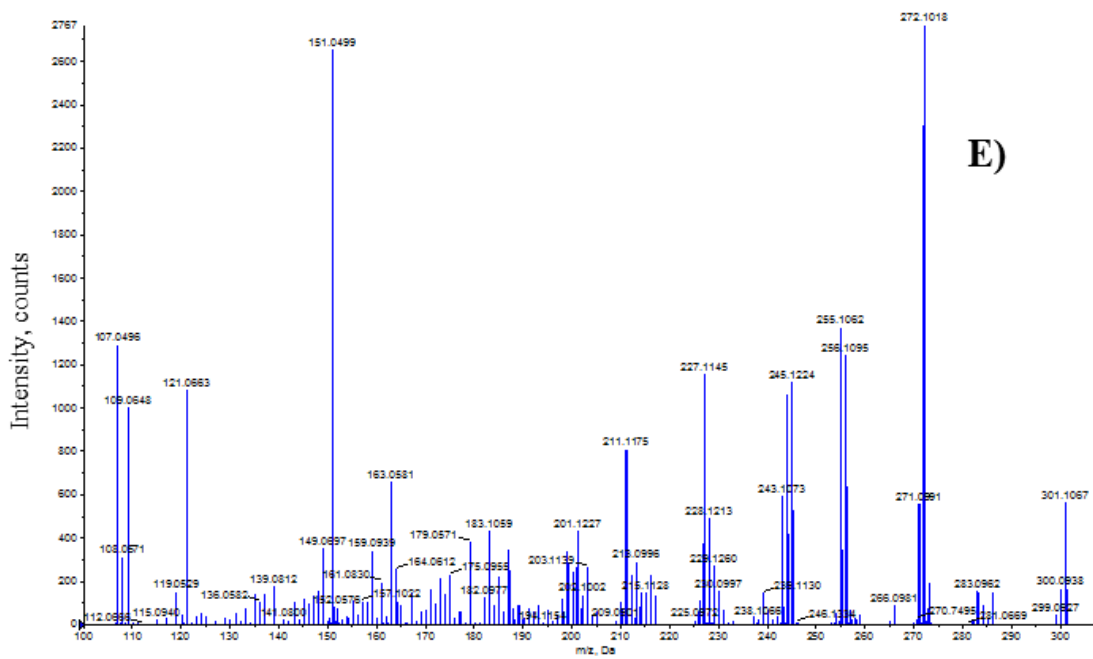


Figure 4.9: Continued.

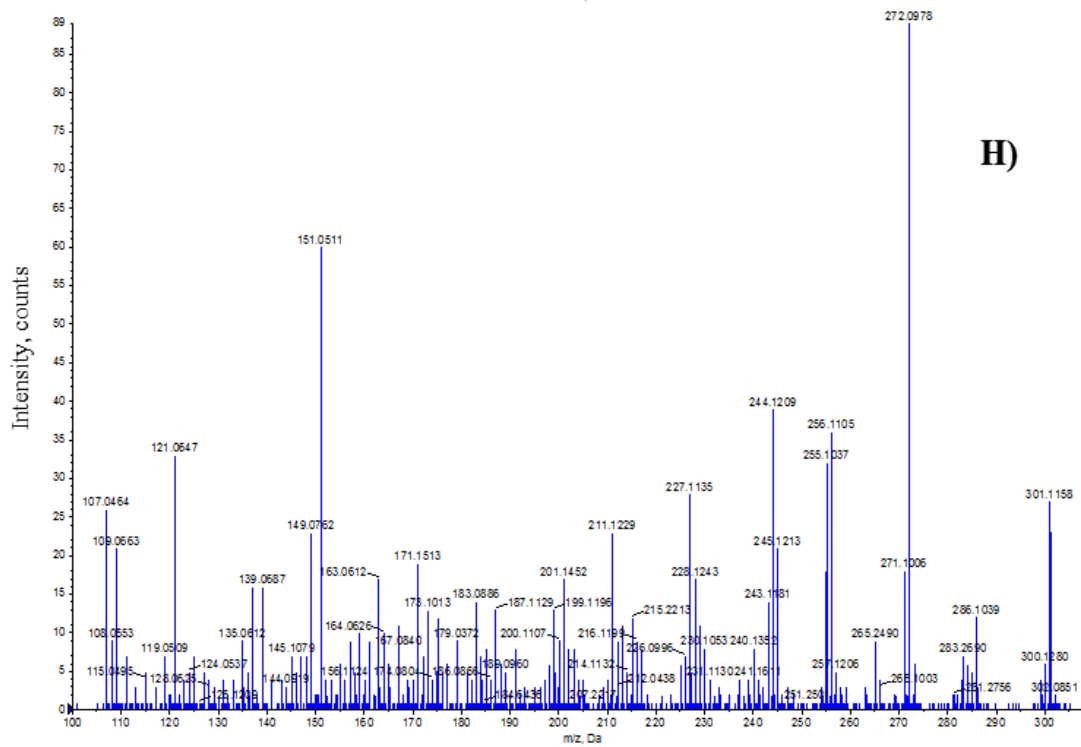
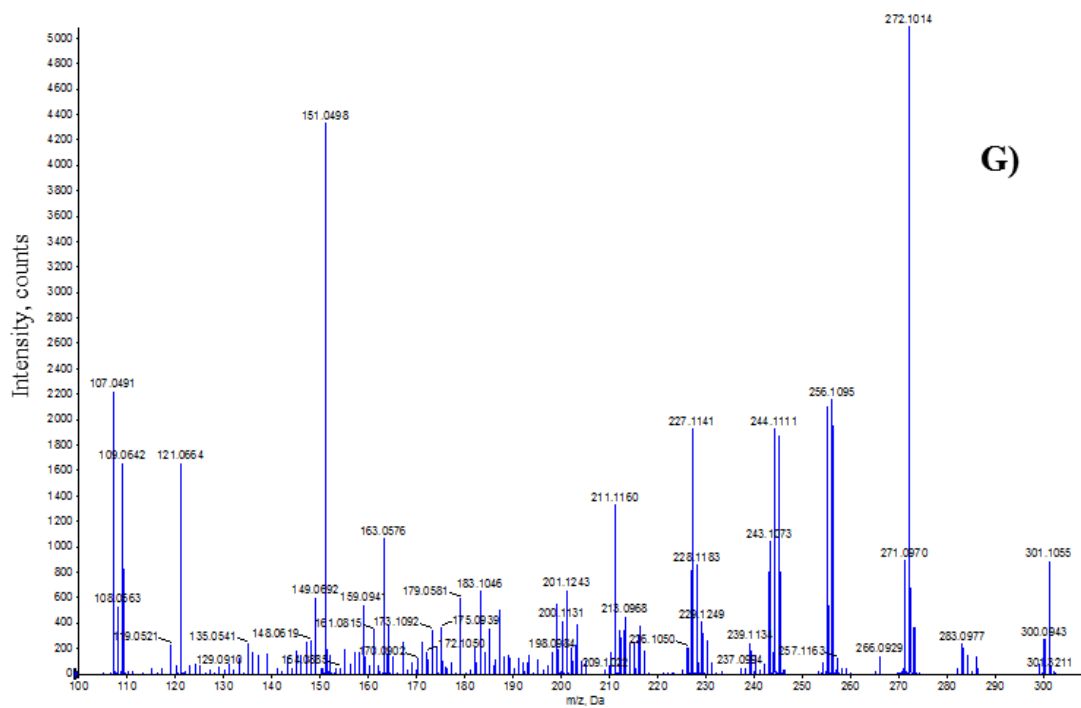


Figure 4.9: Continued.

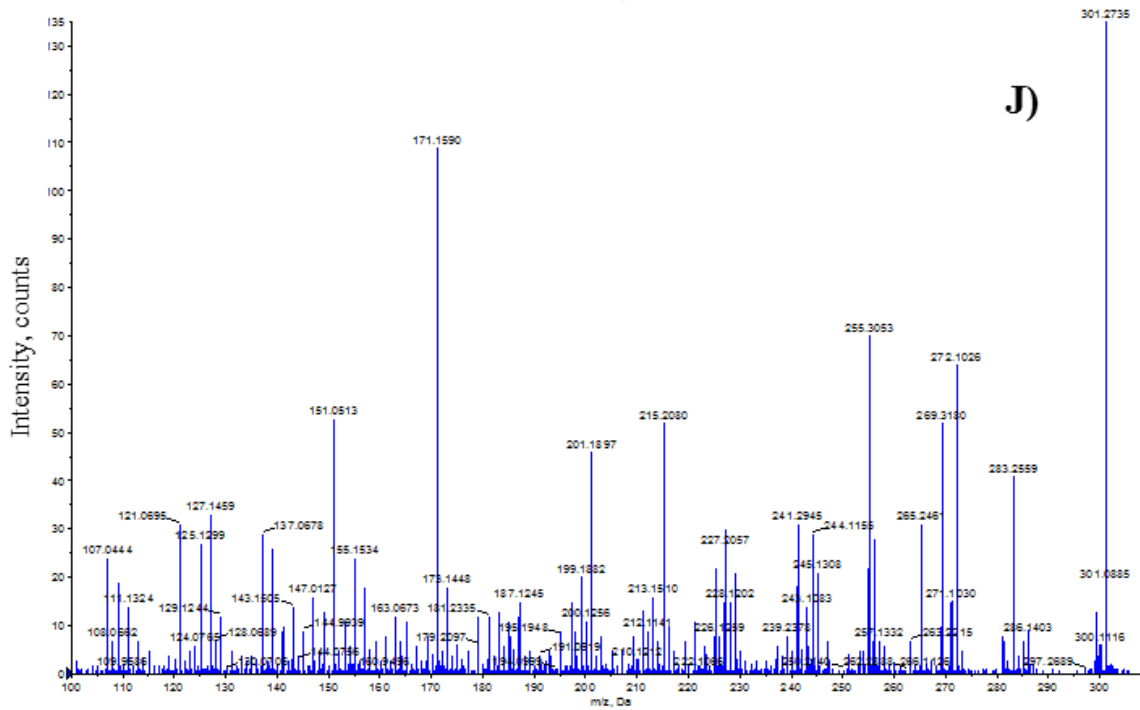
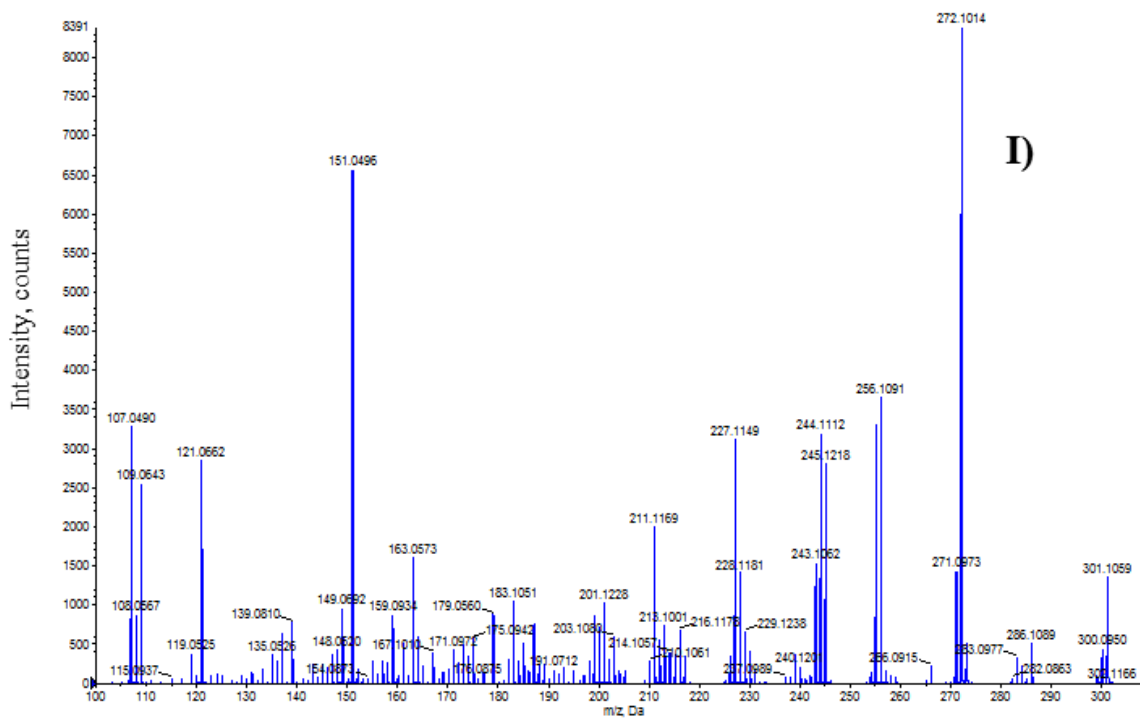


Figure 4.9: Continued.

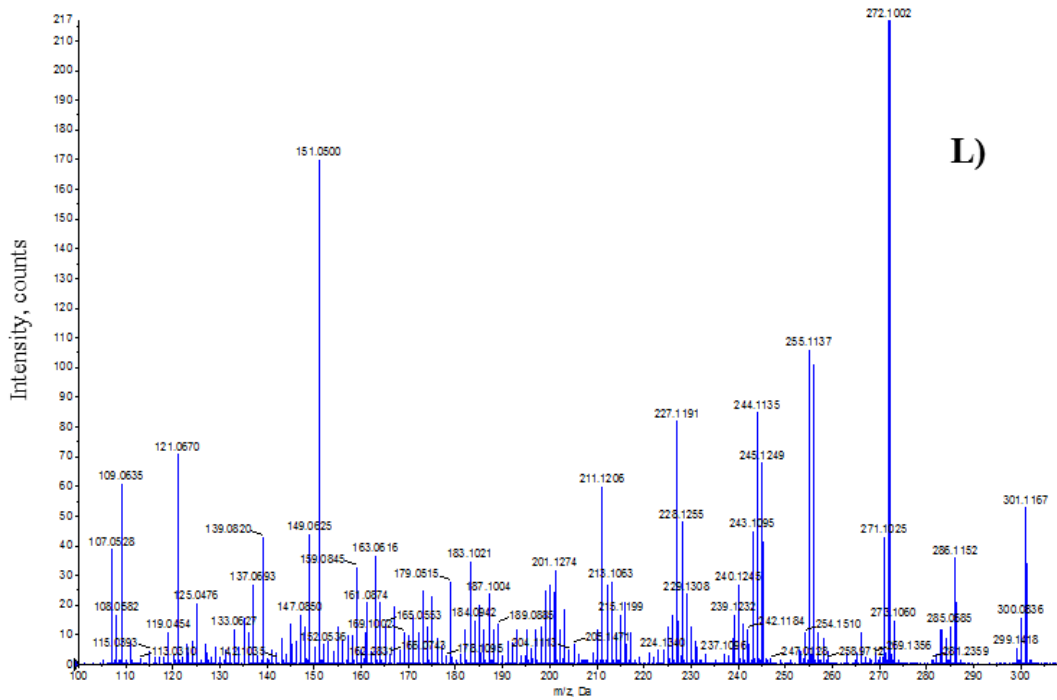
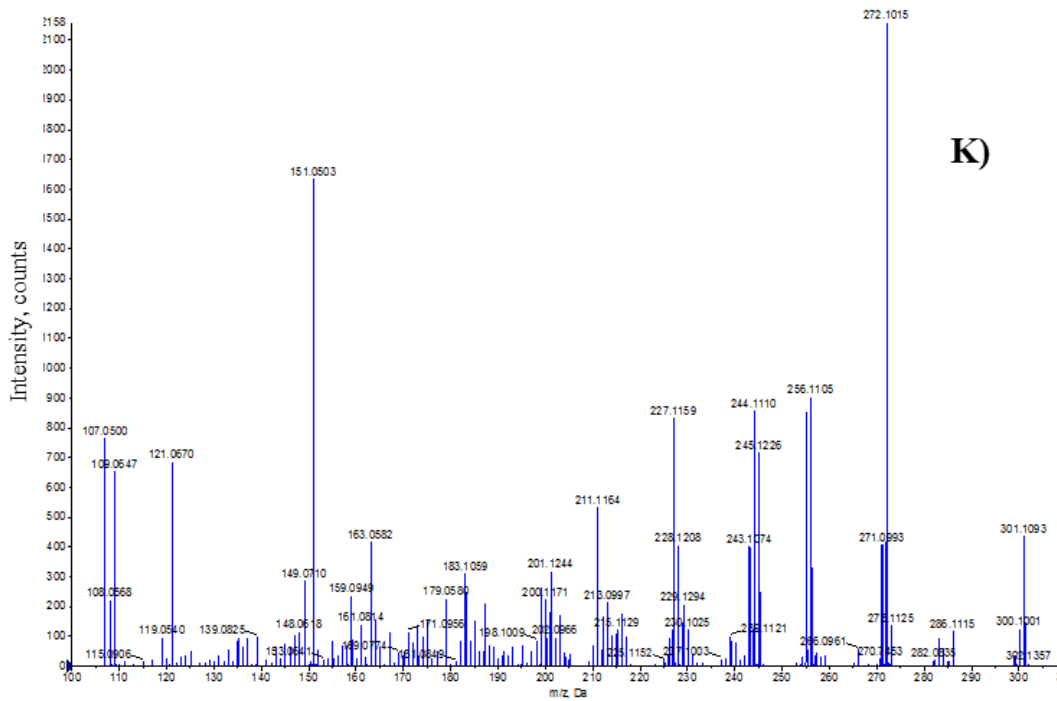
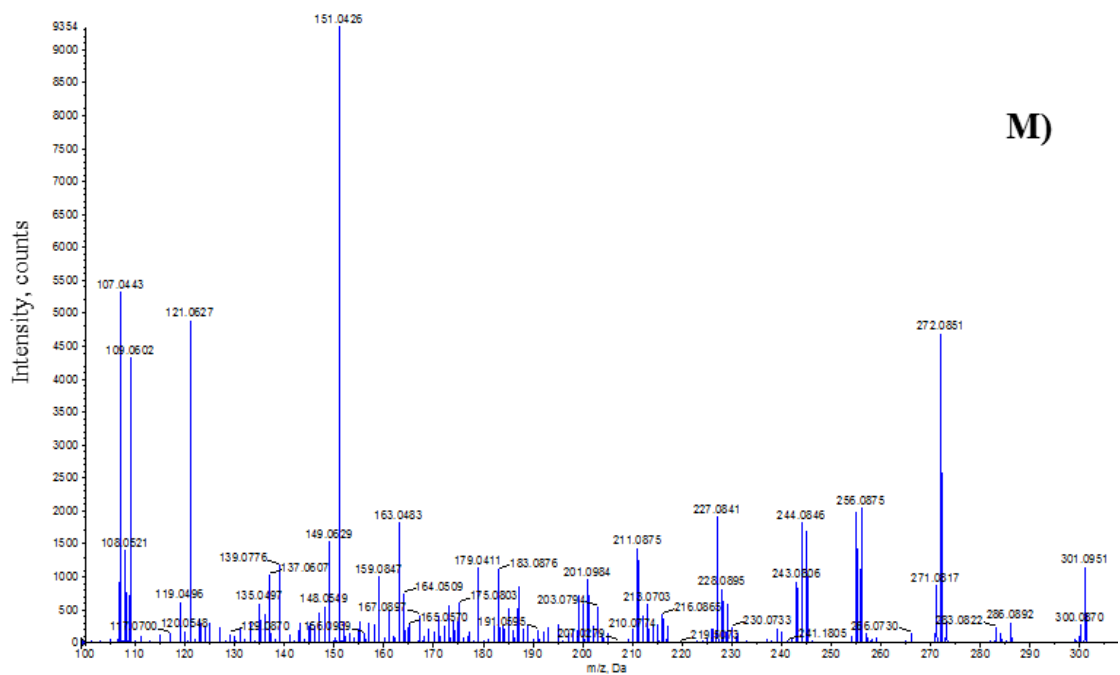
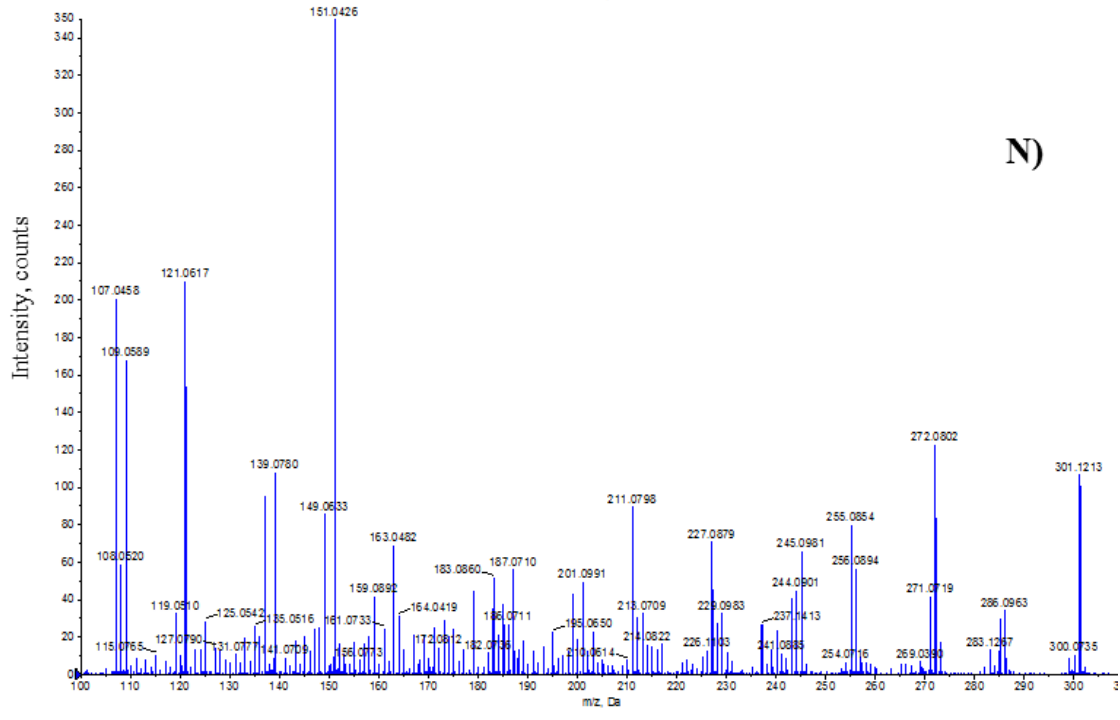


Figure 4.9: Continued.

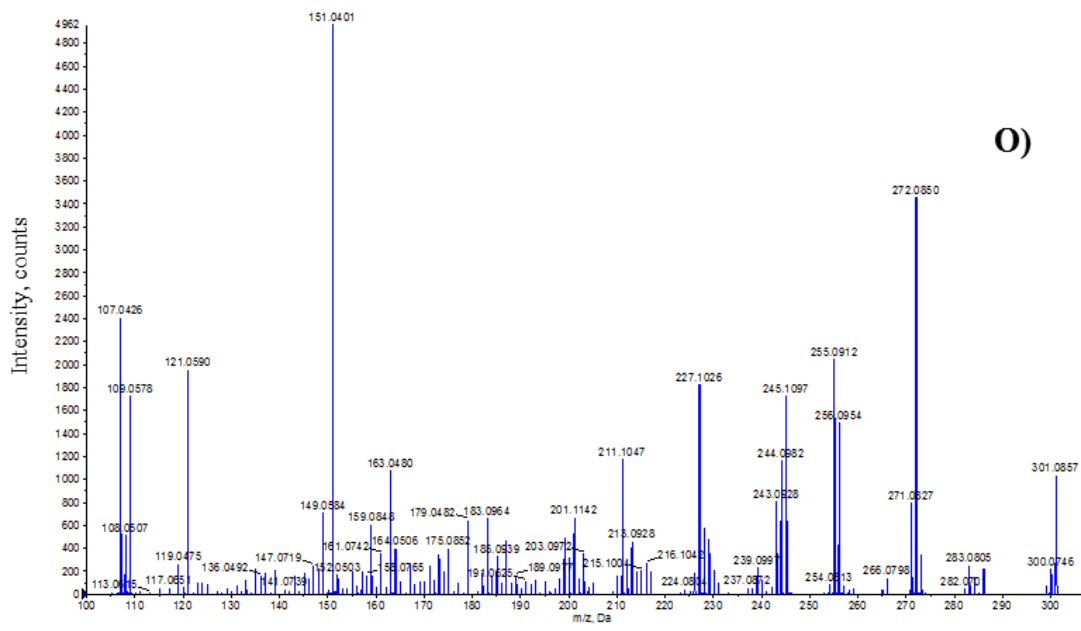


M)

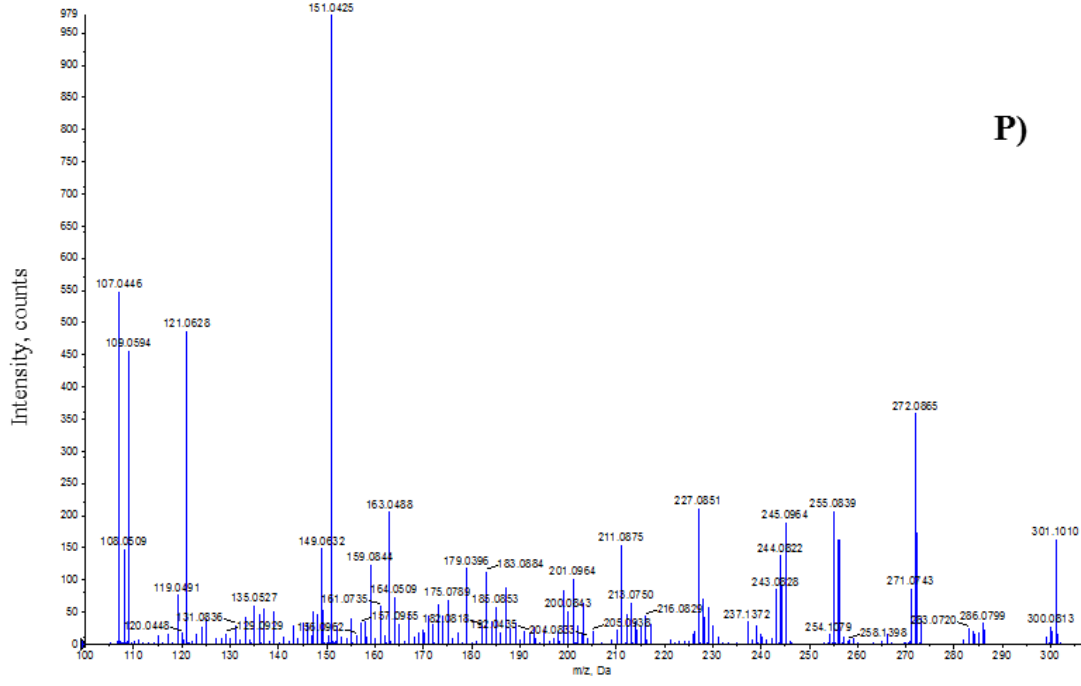


N)

Figure 4.9: Continued.



O)



P)

Figure 4.9: Continued.